SRC homology 2 (SH2) domain containing inositol polyphosphate 5-phosphatase 1 (SHIP1) – analysis of its structural and biochemical properties and its function in colorectal carcinoma (CRC)

Dissertationsschrift zur Erlangung eines Doktors der Naturwissenschaften (Dr. rer. nat.) zur Einreichung im Fachbereich Chemie der Universität Hamburg

vorgelegt von Nina Caroline Nelson aus Hamburg

2021

Vorblatt 1

1. Gutachter: Prof. Dr. Manfred Jücker, Institut für Biochemie und Signaltransduktion, Universitätsklinikum Hamburg-Eppendorf, Universität Hamburg

2. Gutachter: Prof. Dr. Andrew Torda, Zentrum für Bioinformatik Hamburg, Universität Hamburg

Vorblatt 2

Die Dissertation wurde vom 01.11.2017 bis 01.07.2021 am Institut für Biochemie und Signaltransduktion, Universitätsklinikum Hamburg-Eppendorf, Universität Hamburg durchgeführt. Teile der Arbeit wurden im Rahmen von Kooperationen am Zentrum für Bioinformatik Hamburg, Universität Hamburg, am Fraunhofer IME, Hamburg, sowie am EMBL und CSSB, Hamburg durchgeführt.
Datum der Disputation: 29.11.2021

I. Publikationsliste

- Nalaskowski, M.M., Ehm, P., Rehbach, C., Nelson, N., et al., 2018. Nuclear accumulation of SHIP1 mutants derived from AML patients leads to increased proliferation of leukemic cells. *Cell. Signal*., 2018, **49**, 87–94.
- Nelson, N., Wundenberg, T., Lin, H., Rehbach, C., et al., 2020. Characterization of the substrate specificity of the inositol 5-phosphatase SHIP1. *Biochem. Biophys. Res. Commun*., 2020, **524**, 366–370.
- Schaks, M., Allgoewer, K., Nelson, N., Ehm, P., et al., 2020. Ectopic Expression of Hematopoietic SHIP1 in Human Colorectal Cancer. *Biomedicines*, 2020, **8**, 215.
- Ehm, P.A.H., Lange, F., Hentschel, C., Jepsen, A., et al., 2019. Analysis of the FLVR motif of SHIP1 and its importance for the protein stability of SH2 containing signaling proteins. *Cell. Signal*., 2019, **63**, 109380.
- N. Nelson, A. Razeto, A. Gilardi, M. Grättinger, J. Kirchmair, M. Jücker, AKT1 and PTEN show the highest affinities among phosphoinositide binding proteins for the second messengers PtdIns(3,4,5)P3 and PtdIns(3,4)P2, *Biochem. Biophys. Res. Commun*. **568** (2021),110–115.https://doi.org/10.1016/j.bbrc .2021 .06.027.
- V. Ecker, M. Stumpf, L. Brandmeier, T. Neumayer, L. Pfeuffer, T. Engleitner, I. Ringshausen, N. Nelson, M. Jücker, S. Wanninger, T. Zenz, C. Wendtner, K. Manske, K. Steiger, R. Rad, M. Müschen, J. Ruland, M. Buchner, Targeted PI3K/AKT-hyperactivation induces cell death in chronic lymphocytic leukemia, *Nat. Commun*. **12** (2021) 1–17. https://doi.org/10.1038/s41467-021-23752-2.

II. Inhaltsverzeichnis

III. Abkürzungsverzeichnis

3' SIN-LTR	3' Self INactivating Long Terminal Repeat
4E-BP	Elongation factor 4E Binding Protein
ABI1	ABL Interactor 1
ABL	Abelson protein
Ac	Acidic domain
ACC	acetylCoA carboxylase
ACO2	aconitase 2
ADAM	A Disintegrin And Metalloproteinase
ADF	Actin Depolymerisation Factor
ADP	Adenosine Diphosphate
AGC kinase	Protein kinases A, G, C superfamily
AIEX	Anion Ion Exchange Chromatography
AKAP	A Kinase Anchoring Protein
AKT	RAC-alpha serine/threonine-protein kinase/Ak-strain 8 thyoma
ALL	acute lymphoide leukaemia
AML	Acute Myeloid Leukaemia
Amp	ampicillin
AMP	Adenosine Monophosphate
AMPK	Adenosyl Monophosphate (AMP) activated protein kinase
AMPK	AMP activated protein kinase
AP-1	Activator protein 1
APC/C	Anaphase Promoting Complex/Cyclosome
APE1	DNA-(apurinic or apyrimidinic site) endonuclease
AR	androgen receptor
ARC	Activity-Regulated Cytoskeleton-Associated Protein

ARF	ADP Ribosylation Factor
ARM	Armadillo Repeat
ARNO	ARF Nucleotide binding site Opener
ARP2/3	Actin Related Protein 2/3 complex
ARPC1-5	Actin Related Protein 2/3 Complex subunits 1-5
ARPIN	ARP2/3 Inhibitor
ATF1	Cyclic AMP-dependent transcription factor
ATM	Ataxia Telangiectasia Mutated
ATP	Adenosyl Triphoshate
ATP	Adenosine Triphosphate
ATR	Ataxia Telangiectasia Related
AVC	Angiogenic Vascular Cell
BAD	BCL-2 Antagonist of cell Death
BAK	BCL-2 homologous Antagonistic Killer
B-ALL	B-cell acute lymphoid leukaemia
BCL-2	B-cell Lymphoma 2
BCL-XL	B-Cell Lymphoma Extra Large
BCR	B-cell receptor
BCR/ABL	Breakpoint Cluster Region/Abelson
BER	Base Excision Repair pathway
BIM	Bcl2-interacting mediator of cell death
BLK	B lymphoid tyrosine kinase
BLNK	B-cell linker
BMX	BTK-like on X chromosome
b-PIX	b p21 activated kinase Interactive eXchange factor
BRCA1	Breast Cancer 1
BRCA2	Breast Cancer 2
BrdU	5-bromo-2'-deoxyuridine
BRK	Breast tumor kinase
BSA	bovine serum albumin
BTK	Bruton Tyrosine Kinase
C2	Ca2+ dependent lipid binding domain
CAF	Cancer Associated Fibroblast
CAK	Cyclin Dependent Kinase (CDK) Activating Kinase
CaM	Calmodulin
CAMK	Calcium/Calmodulin dependent protein kinase
cAMP	cyclic adenosine monophosphate
CAS	Crk-associated substrate family
CBG	corticosteroid binding globulin
CBP	CREB binding protein
CCDN3	cyclin 3
c-CRK	cellular CT10 Regulator of Kinase
CCY	cyclin Y
CD	Cluster of Differentiation
CDC25	Cell Division Cycle 25
CDC42	Cell Cycle Division Control 42
CDH1	Cell Division Cycle 20 (CDC20) Homologue 1
CDK	Cyclin Dependent Kinase
CDK5	Cyclin Dependent Kinase 5
CDKL	Cyclin Dependent Kinase Like
cDNA	complementary DNA
CED-12	Cell Death 12
CED-2	Cell Death 2
CED-5	Cell Death 5
CFTR	Cystic Fibrosis Transmembrane Conductance Regulator
cGMP	cyclic guanosine monophosphate
CG-NAP	centrosome and Golgi localized PKN-associated protein
CH	Calponin Homology domain
CHK	CSK homologue kinase
CHK1	G_2/M CHeckpoint Kinase 1
CHK1	Checkpoint kinase 1
ChREBP	Carbohydrate regulatory element-binding transcription factor
CIAP	Calf intestine alkaline phosphatase
c-IAP	cellular inhibitor of apoptosis
CIEX	Cation Ion Exchange Chromatography
c-JUN	Jun proto-oncogene, AP-1 transcription factor subunit
CK2	Casein Kinase 2
CKI	Cyclin Dependent Kinase (CDK) Inhibitor

CLL	Chronic lymphoid leukaemia
CML	Chronic myeloid leukaemia
CO_2	carbon dioxide
COAD	colorectal adenocarcinoma
COBL	Cordon Bleu WH2 repeat protein
COSMIC	Catalogue Of Somatic Mutations In Cancer
cPPT	central PolyPurine Tract
CRC	colorectal carcinoma
CREB	cAMP Responsive Element Binding transcription factor
CRISPR/Cas9	Clustered Regularly Interspaced Short Palindromic Repeat/CRISPR associated 9
CRK	v-crk avian sarcoma virus CT10 oncogene homolog
CSC	Cancer Stem Cell
CSK	c-SRC kinase
CTC	Circulating Tumour Cell
CTD	C-terminal domain
C-terminus	carboxy-terminus (protein)
CTMP	C-Terminal Modulator Protein
CV	column volume
CXCR4	CXC motif chemokine Receptor
D-3-PGDH	D-3-phosphoglycerate dehydrogenase
DAG	diacyl glycerol
DAPK	Death Associated Protein Kinase
DAPP1	Dual Adaptor for Phosphotyrosine and 3-Phosphoinositides 1
DBL	Diffuse B-cell Lymphoma subfamily of RHO-GEFs
DBS	DBL's Big Sister
DCAML2	Doublecortin-like and CaM kinase like 2
DDA	data dependent acquisition
ddH2O	doubly desalted water
DDR	DNA damage repair
DEP	Dishevelled, EGL-10, Pleckstrin domain
DH-PH	DBL Homology-Pleckstrin Homology tandem domain
DHR2/CZH2	DOCK Homology Region 2/CDM-Zizimin Homology 2 subfamily of RHO-GEFs
DMEM	Dulbecco's Modified Eagle Medium
DMSO	dimethyl-sulfoxide
DNA	dioxiribonucleic acid
DNA	deoxyribonucleic acid
DOCK	Dedicator of Cytokinesis protein family
DOK	Docking protein
DOPC	DiOleoylPhosphatidylCholine
DOPE	DiOleoylPhosphatidylEthanolamine
ds	double-stranded
DSG2	desmoglein 2
DTT	Dithiothreitol
DYRK2	Dual specificity tyrosine-phosphorylation-regulated kinase 2
$[E]_0$	initial enzyme concentration
E-Cadherin	Epithelial Cadherin
ECM	Extracellular Matrix
ECT2	Epithelial Cell Transforming 2
EDTA	Ethylen-diamino tetra acetic acid
EE	early endosome
EGF	Epithelial Growth Factor
EGF	epithelial growth factor
eGFP	enhanced green fluorescent protein
EGFR	Epithelial Growth Factor (EGF) Receptor
eIF-4A	eukaryotic transcriptional initiation factor 4A/helicase
eIF4E	eukaryotic transcriptional initiation factor 4E
ELISA	Enzyme-Linked Immunosorbent Assay
EMT	Epithelial Mesenchymal Transition
ENA/VASP	homologue of D. melanogaster Ena/Vasodillator Stimulated Phosphoprotein
ENaC	Epithelial Na(+) channel
ENAH1	Enabled Homologue of *Drosophila melanogaster* Ena
ER	estradiol receptor
ERK	Extracellular signal-regulated kinase
ETF1	eukaryotic translation termination factor 1
ETV1/ER81	ETS translocation variant 1
EVH	ENA/VASP Homology
EVL	ENA/VASP-like
f.c.	final concentration

FA	formic acid
FA	fatty acid
FACS	Fluorescent Activated Cell Sorting
FAK	Focal Adhesion Kinase
FANCE	FA Complementation Group E
FAS	tumor necrosis factor receptor superfamily, member 6
FAT	FRAP, ATM, TRRAP domain
FATC	FRAP, ATM, TRRAP, C-terminal domain
F-BAR	FCH-Bin, Amphiphysin and Rvs domains
FCS	fetal calf serum
$F_c\gamma RIII$	fragment crystallizable/constant gamma immunoglobulin receptor III
FDR	false discovery rate
FGR	feline Gardner-Rasheed sarcoma viral oncogene homolog
FITC	Fluorescein
FKBP12	FK506 Binding Protein, 12 kDa
FL	full length
FMLN2	Formin-Like 2
FOXO	Forkhead box O transcription factor
FRB	FKBP12-Rapamycin Binding domain
FRK	FYN Related Kinase
FSHR	Follicle-stimulating hormone receptor
fw	forward
FYVE	FAB1, YOTB/ZK632.12, VAC1, EEA1 lipid binding domain
G1 phase	Gap1 phase of the cell cycle
G2 phase	Gap2 phase of the cell cycle
G6PDH	Glucose-6-phosphate dehydrogenase
G-actin	globular actin
GAP	GTPase Activating Protein
GAPDH	Glyceraldehyde 3-phosphate dehydrogenase
GAS6	Growth arrest – specific 6
GDI	Guanine nucleotide Dissociation Inhibitors
gDNA	guide-DNA (CRISPR/Cas9)
GDP	Guanosine Diphosphate
GEF	Guanine nucleotide exchange factors
GLUT1	Gkucose Transporter 1
GLUT4	Glucose Transporter 4
GM-CSF	granulocyte-macrophage colony stimulating factor
GOI	gene of interest
GPCR	G-protein coupled receptor
GRB-2	Growth Factor Receptor Bound 2
GRB-4	Growth factor receptor-bound protein 4
GRK4	GPCR kinase 4
GSK3	Glycogen Synthase Kinase 3
GSK3	gylcogen synthase kinase 3
GST	glutathione-S-transferase
GTP	Guanosine Triphosphate
GuHCl	guanidinium hydrochloride
HA	Human influenza hemagglutinin
HABA	2-[4 -hydroxy-benzeneazo]benzoic acid
HADAG	Histone Deacetylase
H-bond	Hydrogen bond
HCC	hepatocellular carcinoma
HCD	higher energy collisional dissociation
HCK	hemopoietic cell kinase
HCl	hydrochloric acid
HEAT	Huntington, Elongation Factor 3 (EF3), Protein Phosphatase 2 (PP2A), TOR1 protein interaction repeat
HEF-1	Hemagglutinin-esterase-fusion glycoprotein 1
HEK-293T	Human Embryonic Kidney cells expressing large T-antigen
HEM1	Hematopoietic protein 1
HEPES	4-(2-hydroxyethyl)-1-piperazineethanesulfonic acid
HIF-1α	Hypoxia Induced Factor 1α
HIPK	Homeodomain Interacting Protein Kinase
HIST2HBE	histone 2 complex
HIV	Human Immunodeficiency Virus
HM	hydrophobic motif
HMEC	Human Mammary Epithelial Cells
HNSCC	Head and Neck Squamous Cell Carcinoma
HPA	hydrophobic alkanethiol sensor (SPR)

HR	homologous repair pathway
h-RAS	harvey RAS viral oncogene homologue
HRG	Heregulin
HRP	horseraddish peroxidase
HSC	Hematopoietic Stem Cell
HSC70	Heat-Shock chaperone, 70 kDa
HSP70	Heat-Shock protein, 70 kDa
HSPB1	heat shock protein family B (small) member 1
HSPC300	Hematopoietic Stem/Progenitor Cell protein 300
HUWE1	HECT, UBA and WWE containing 1
IAA	iodacetamide
IEX	Ion Exchange Chromatography
IFN	interferone
IIC	Infiltrating Immune Cell
IL	interleukin
INPP4A	Inositol polyphosphate-4-Phosphatase type I
INPP4B	Inositol polyphosphate-4-Phosphatase type II
INPP5B	Inositol polyphosphate-5-Phosphatase B
INPP5E	Inositol polyphosphate-5-Phosphatase E
IP4P	Inositol Polyphosphate-4-Phosphatase-like domain
IPTG	Isopropyl β- d-1-thiogalactopyranoside
ITAM	Immune receptor Tyrosine based Activating Motifs
ITAM	immunoreceptor tyrosine-based activation motif
ITIM	Immune receptor Tyrosine based Inhibitory Motifs
ITK	Interleukin-2 inducible T-cell Kinase
IYK	Intestine tyrosine kinase
JAK	Janus kinase
JMY	Junction Mediating and regulatory protein, p53 co-factor
JNK	c-Jun N-terminal kinase
Kann	kanamycine
k_{cat}	catalytic efficiency
KCl	potassium chloride
KD	knock-down
K_D	dissociation constant
KH_2PO_4	potassium hydrogen phosphate
KI	Knock-in
K_M	Menten constant
KO	knock-out
k-RAS	kirsten RAS viral oncogene homologue
LARG	Leukemia-associated RHO-GEF
LAT	linker for activation of T cells
LATS	Large tumor suppressor homolog 1
LB-agar	Luria Bertani agar for bacteria
LB-medium	Luria Bertani culture medium for bacteria
LCK	Lymphocyte Cell specific Kinase
LCK	Leukocyte C-terminal Src kinase
LC-MS/MS	liquid chromatography mass spectrometry/mass spectrometry
LFQ	Label-free Quantification
LIMK	LIM domain Kinases
LKB1	Liver kinase B1
LMTK	Lemur Tail Kinase
lncRNA	long non-coding RNA
LPA	Lysophosphatidic acid
LPD	Lamellipodin
LRP6	Low-density lipoprotein receptor-related protein 6
LRRC59	leucine rich repeat containing 59
LTR	Long Terminal Repeat
LUV	large unilamellar vesicle
LYN	v-yes-1 Yamaguchi sarcoma viral related oncogene homolog
M phase	mitosis phase of the cell cycle
m/z	mass-to-charge ratio
MAGE-A3/6	melanoma-associated antigen A3/6
MAGI-2	Membrane Associated Guanylate kinase Inverted 2
MAPK	Mitogen Activated Protein Kinase
MCCC2	methylcrotonoyl-CoA carboxylase 2
MCF-10A	Michigan Cancer Foundation-10 Attached cell line
MCL-1	Induced Myeloid Leukaemia Cell differentiation protein 1
MCM	minichromosome maintenance complex

MCT	monocarboxylate transporter
MDA-MB-231	MD Anderson-Metastatic Breast-231
mDia2	mammalian Diaphenous 2
MDM2	Mouse Double Minute 2
MDSC	Myeloid Derived Suppressor Cell
MEF	Mouse Embryonic Fibroblast
mELMO	mammalian Engulfment and cell Motility
MENA	Mammalian Enabled
MET	Mesenchymal Epithelial Transition
MFF	mitochondrial fission factor
MFN1	mitofusin 1
$MgCl_2$	magnesium chloride
MIM	Membrane Interacting Motif
miR	micro RNA
mLST8	Mammalian lethal with SEC13 protein 8
MMP	Matrix Metalloprotease
MOB	Mps one binder kinase activator-like
MOI	Multiplicity Of Infection
MOPS	3-(*N*-Morpholino)propano-sulfanic acid
MRD	Minimal Residual Disease
mRNA	messenger RNA
MS	mass spectrometry
MSA	multiple sequence alignment
MSK1	Mitogen and Stress-activated kinase 1
MT1-MMP	Membrane Type 1 Matrix Metalloprotease
mTORC1	Mammalian Target of Rapamycin Complex 1
mTORC2	Mammalian Target of Rapamycin Complex 2
Mw	molecular weight
MYC	Myelocytomatosis
MYO-GEF	Myosin Interacting Guanine nucleotide exchange factor
NaCl	sodium chloride
NADH	Nicotinamide adenine dinucleotide
NADH-DH	Nicotinamide adenine dinucleotide dehydrogenase
NADPH	Nicotinamide adenine dinucleotide phosphate
$NaHCO_3$	sodium hydrogen carbonate
$NaHPO_4$	sodium hydrogen phosphate
nano-ESI	nano-electrospray ionization
NaOH	sodium hydroxide
NAP1	Nucleosome Assembly Protein 1
NDMA	N-methyl-D-aspartate
NDR 1/2	Nuclear DBF2 Related kinase 1/2
NDRG1/2	N-myc downstream-regulated gene 1/2
NEDD4-1	Neural precursor cell expressed, Developmentally Downregulated 4-1
NEDD4L	Neural precursor cell expressed developmentally down-regulated protein 4-like
NES	nuclear export signal
NF2	Neurofibromin-2
NFAT	Nuclear factor of activated T-cells
NFDMB	non-fat dried milk bovine
NF-kB	nuclear factor 'kappa-light-chain-enhancer' of activated B-cells)
NHE3	sodium/hydrogen exchanger 3
NHEJ	Non-homologous end joining
NHERF	Na^+/H^+ Exchanger Regulatory Factor
NHR2	NERVY Homology Region 2
NIH-3T3	3-day transfer, inoculum 3×10^5 mouse fibroblasts
Ni-NTA	nickel-Nitrilotriacetic acid
NK	natural killer cell
NKCC1	bumetanide-sensitive sodium-(potassium)-chloride cotransporter 1
NLS	nuclear localization signal
NO	nitric oxide
NOS	nitric oide synthase
NP40	Nonidet-40
NPEPPS	aminopeptidase puromycin sensitive
NPF	Nucleation Promoting Factor
n-RAS	neuroblastoma RAS viral oncogene homologue
NSCLC	non-small cell lung carcinoma
NSG-mice	NOD scid gamma mice
NTD	N-terminal domain
N-terminus	amino-terminus (protein)

N-WASP	neural Wiskott–Aldrich Syndrome protein
OD600	optical density at 600 nm
Opti-MEM	optimized minimal essential medium
ORF	Open Reading Frame
OxPhos	oxidative phosphorylation
p130CAS	protein of 130 kDa, CRK associated Substrate
P4IM	4-phosphate Interacting Motif
p53	protein of 53 kDa
p70S6K	Small ribosomal subunit protein 6 Kinase
PAGE	polyacrylamide gel electrophoresis
PAK	p21 activated kinase
PBS	Protein Biosynthesis
PBS	Phosphate Buffered Saline
PBS-T	Phosphate Buffered Saline-Tween20
PCA	principal component analysis
pCG	Particulate guanylate cyclase
PCR	polymerase chain reaction
PDAC	Pancreatic ductal adenocarcinoma
PDB	Protein Data Base
PDCD4	programmed cell death protein 4
PDE	phosphodiesterase
PDGF	Platelet Derived Growth Factor
PDK1	phosphoinositide dependent kinase 1
PDK2	phosphoinositide dependent kinase 2
PDZ	PSD95, *Drosophila melanogaster* DLG1, ZO-1 domain
pen/strep	penicillin/streptomycine
PFKFB	phospho-fructo-2-kinase/fructo-2,6-bisphosphatase
PGC-1a	Peroxisome proliferator-activated receptor gamma coactivator 1-alpha
PH	Pleckstrin Homology lipid binding domain
PHGDH	D-3-phosphoglycerate dehydrogenase
PH-L	Pleckstrin Homology lipid binding-like domain
PHLPP	PH domain and Leucine rich repeat containing Protein Phosphatase
Pi	free phosphate ion
pI	isoelectric point
PI3K	Phosphoinositide-3-Kinase
PICK1	Protein Interacting with PRKCA 1
PICS	PTEN Induced Cellular Senescence
PIKFIVE	phosphoinositide kinase, FYVE-type zinc finger containing
PIPP	Proline rich Inositol Polyphosphate-5-Phosphatase
PIR121	p53 Inducible protein 121
PKA	Protein Kinase A
PKA	Protein Kinase A
PKB	Protein Kinase B
PKG2	Protein kinase G2
PKN2	Protein Kinase N2
PLA_2	phospholipase A2
PLC	Phospholipase C
PLD	phospholipase D
PLEC	plectin
PLO	Phospholipid Overlay Assay
PML	Promyelocytic leukemia protein
PMSF	phenylmethylsulfonyl fluoride
PP	Polypropylene
PP1a	Protein Phosphatase 1a
PP2A	Protein Phosphatase 2A
PPARg	Peroxisome Proliferator Activated Receptor g
PPase	Phosphatase domain
PPI	Protein Protein Interaction
PRAS-40	Proline Rich AKT Substrate, 40 kDa
P-REX	PtdIns(3,4,5)P_3 dependent RAC Exchanger
PROS1	Protein Seattle 1
PRR	Proline Rich Region
PTB	Phosphotyrosine Binding domain
PtdIns	Phosphatidyl inositol
PtdInsPx	Phosphatidyl inositol phosphate
PtdSer	Phosphatidyl Serine
PTEN	Phosphatase and Tensin homologue
PTENP1	PTEN Pseudogene 1

PTM	Posttranslational Modification
PTP	Protein Tyrosine Phosphatase
PTPL1	Protein Tyrosine Phosphatase Like
PX	PHOX lipid binding domain
pY	phospho tyrosine
QCM	Quick-Change Mutagenesis
RA	RAS Association domain
RAC	Ras-related C3 botulinum toxin substrate
RAL	RAS-related protein
RAPTOR	Regulatory Associated Protein of mTOR
RAS	Rat Sarcoma
Rat2	Rattus norvegicus fibroblast cell line
RB	Retinoblastoma protein
RbCl	rubidium chloride
RBD	RAS binding domain
RE	recycling endosome
REDD1	Regulated in Development and DNA damage 1
RHEB	RAS Homologue Enriched in Brain
RHO	RAS Homologue
RICTOR	Rapamycin insensitive companion of mTOR
RING domain	Really Interesting New Gene domain (superfamily)
RIPA	Radioimmunoprecipitation assay buffer
RNA	ribonucleic acid
ROCK1	RHO associated Coiled coil containing protein Kinase 1
ROS	Reactive Oxygen Species
ROS	radical oxygen species
rpm	revolutions per minute
r-RAS	related RAS viral oncogene homologue
RRE	rev Response Element
RT	room temperature
RTK	Receptor Protein Kinase
RU	resonance unit
rv	reverse
S phase	synthesis phase of the cell cycle
S-/T-kinase	serine-threonine kinase
S6K	small ribosomal subunit 6 protein Kinase
SALL4	SPALT Like 4
SAM	Sterile alpha domain
SAM68	Src-associated in mitosis 68 kDa protein
SAV1	Salvador homologue 1
SCID	severe combined immunodeficiency
SDC	sodium deoxycholate
SDS	Sodium Dodecyl Sulfate
sER	smooth endoplasmic reticulum
sGC	Soluble guanylate cyclase
SGK	serum and glucocorticoid regulated kinase
SGK	Serum and Glucocorticoid regulated Kinase
SH2	SRC homology 2 binding domain
SH3	SRC homology 3 binding domain
SHC	SH2 domain containing protein
SHIP1	SH2 domain containing inositol polyphosphate-5-phosphatase 1
SHIP2	SH2 domain containing inositol polyphosphate-5-phosphatase 2
shRNA	short hairpin RNA
SIN1	Stress-activated map kinase-interacting protein 1
SIP-110	Stem cell specific Inositol polyphosphate-5-Phosphatase, 110 kDa
SKIP	Skeletal muscle and Kidney enriched Inositol polyphosphate-5-phosphatase
SLC25A5	solute carrier family 25 member 5
SLP-76	SH2 domain-containing leukocyte protein of 76kD
SLUG	Zinc finger protein SLUG/SNA2
SMA	smooth muscle actin
SNAI1	Snail family transcriptional repressor 1
SNAIL	Zinc finger protein SNAIL/SNA1
SOS 1	Son of Sevenless 1
SOX9	SRY-Box Transcription Factor 9
SP1	Specificity Protein 1
SPAK	STE20/SPS1 homolog
SPIN90	SH3 domain containing Protein Interacting with NCK1, 90 kDa
SPIRE	homologue of D. melanogaster Spire

SPR	Surface Plasmon Resonance
SRA1	Steroid Receptor RNA Activator 1
SRC	Sarcoma (protein/protein family)
SREBP1c	Sterol regulatory element-binding transcription factor 1c
srGAP3	SLIT-ROBO Rho GTPase-activating protein 3
SRSF3	S-/R-rich splice factor 3
ss	single-stranded
SSR	SHIP Stem cell Recognition motif
STAT	Signal transducer and activator of transcription
SYK	spleen associated protein kinase
SYNJ	Synaptojanin
TAE	Tris-Acetate-EDTA buffer
TAGLN2	transgelin 2
TAL1	T-cell acute leukemia protein 1
T-ALL	T-lymphocyte Acute Lymhoid Leukaemia
TAM	Tumour Associated Macrophage
TAM	TYRO3, AXL, MERTK-protein receptor kinase superfamily
TAPP1	Tandem PH domain protein 1
TAPP2	Tandem PH domain protein 2
TAZ	Transcriptional coactivator with PDZ-binding motif
TBS	Tris Buffered Saline
TBS-T	Tris-Buffered Saline-Tween20
TC10	RAS-like protein TC10
TC21	TeratoCarcinoma 21
TCA	trichloric acid
TCR	T-cell receptor
TCTP	Translationally controlled tumour protein
TEA	Tri-ethanol amine
TEAB	triethylammonium hydrogen carbonate buffer
Tet	tetracycline
TGF-β	Transforming Growth Factor β
TGN	Trans-golgi network
TH	TEC homology
TIAM1	T-cell lymphoma Invasion And Metastasis 1
TM	transmembrane domain
TMA	Tissue Microarray
TMB	3,3',5,5'-Tetramethylbenzidine
TME	Tumour Microenvironment
TNFa	tumour necrosis factor alpha
TRAP1	TNF receptor associated protein 1
Treg	regulatory T-Lymphocyte
TRIM28	Tripartite motif-containing 28
TRIO	TRIple functional domain (PTPRF interacting)
Tris	(Tris-(hydroxymethyl)-aminomethan
TSC1	Tuberous sclerosis 1 protein (Hamartin)
TSC2	Tuberous sclerosis 2 protein (Tuberin)
TWIST	TWIST related protein
TYRO3	Protein Tyrosine Kinase Receptor 3
U	unit (enzyme activity)
ULA	Ultra Low Attachment
ULK1	Unc-51 Like Autophagy Activating Kinase 1
UPC	uncoupling protein
UPLC	Ultra performance liquid chromatography
UTR	Untranslated Region
UV	ultra-violet
V	voltage
VAMP7	Vesicle Associated Membrane Protein 7
VAV	Vav Guanine Nucleotide Exchange Factor
VEGF-A	Vascular Endothelial Growth Factor A
V_{max}	maximal velocity
v-SNARE	vesicle Soluble N-ethylmaleimide sensitive factor Attachment Receptor
VSV-G	Vesicular Stomatitis Virus-Glycoprotein
w./	with
w./o.	without
WASP	Wiskott–Aldrich Syndrome protein
WAVE	WASP family Verprolin homologous protein
WCA	WASP Homology 2 (WH2), Connecting/Central domain, Acidic domain
WIR	WAVE complex Interacting Regulatory motif

WNK4	WNK lysine deficient protein kinase 4
WNT	Wingless and Int-1 pathway
WPRE	*Woodchuck* hepatitis virus Post-transcriptional Regulatory Element
WRCH-1/2	Wnt-1 Regulated Cdc42 Homolog 1/2
WT	wildtype
XIAP	X-linked inhibitor of apoptosis
YAP	Yorkie homologue
YES	Yamaguchi sarcoma viral oncogene homolog
Y-kinase	tyrosine kinase
ZAP70	Zeta Chain Of T Cell Receptor Associated Protein Kinase 70
ZAP-70	zeta chain of T cell receptor associated protein kinase 70
ZEB-1	Zinc finger E-box-binding homeobox 1
α-SMA	α-Smooth Muscle Actin

IV. Zusammenfassung

SHIP1 ist ein Mitglied der Phosphoinositid-5-Phosphatase-Familie und im Gesunden spezifisch in hämatopoetischen Zellen exprimiert. In Leukämien wurde eine Funktion von SHIP1 als Tumorsuppressor in zahlreichen Studien bestätigt. Mechanistisch terminiert SHIP1 in diesen Zellen die PI3K/AKT/mTORC-Signaltransduktion durch Dephosphorylierung von PtdIns(3,4,5)P_3, was in einer verringerten Proliferation, Motilität, Zellwachstum und –überleben resultiert. Auf der anderen Seite konnte in initialen Experimenten unserer Arbeitsgruppe eine hohe Expression von SHIP1 in Karzinomen nachgewiesen werden, welche besonders stark in Kolorektalkarzinomen (CRC) beobachtet wurde. Im Rahmen dieser Arbeit wurde daraufhin die Funktion von SHIP1 in CRC genauer untersucht. Hierfür wurden zwei zelluläre Systeme (Überexpression von SHIP1 in der SHIP1-negativen CRC-Linie HCT-116 und *Knock-Down* von SHIP1 in den SHIP1-positiven Zelllinien SW-480 und HT-29) etabliert und die Funktion von SHIP1 im Hinblick auf Proliferation, Überleben, Migration/Invasion/Chemotaxis, Signaltransduktion, Proteom und Kinom *in vitro*, sowie im NSG-Mausmodell *in vivo* untersucht. Zusammenfassend lässt sich eine komplexe und kontextabhängige Funktion von SHIP1 in der Tumorigenese von CRC ableiten, wobei Argumente für eine Tumorsuppressor- und eine onkogene Funktion gefunden werden können. Eine solche duale Funktion in der Tumorigenese lässt sich auch für andere Phosphoinositid-5-Phosphatasen wie SHIP2 finden. Es ist im Rahmen der *Two-PIP*-Hypothese davon auszugehen, dass Phosphoinositid-5-Phosphatasen nicht wie beispielsweise PTEN das PI3K/AKT/mTORC-Signal notwendigerweise terminieren müssen, sondern eine alternative Aktivierung von Onkogenen wie AKT über das Produkt der Phosphoinositid-5-Phosphatase-Reaktion PtdIns(3,4)P_2 stattfinden kann. Im weiteren Verlauf der Arbeit wurden darüber hinaus patientenabgeleitete Mutanten der katalytischen Domäne von SHIP1 untersucht und gezeigt, dass die Mutationen die Eigenschaften von SHIP1 maßgeblich hinsichtlich der Phosphoinositidbindung und Katalyse, sowie der Expressionslevel, Stabilität und subzellulären Lokalisation beeinflussten und die Signaltransduktion durch die Mutationen verändert wurde. Im abschließenden Teil der Arbeit wurden die strukturellen (*in-silico*) und biochemischen Eigenschaften von SHIP1 mit einem speziellen Fokus auf die drei Phosphoinositid-Bindedomänen (PH-L, PPase, C2) analysiert. Von besonderer Bedeutung ist hierbei die Identifizierung von Ins(2,3,4,5)P_4 als alleiniges Substrat von SHIP1 und nicht von SHIP2. Darüber hinaus wurden die Phosphoinositidbindung und Katalyse der isolierten und kombinierten Phosphoinositid-Bindedomänen *in silico* und mithilfe biochemischer Assays untersucht. Im Rahmen dieser Untersuchung konnte die allosterische Aktivierung von SHIP1 durch die C2-Domäne verifiziert werden, wohingegen die PH-L-Domäne möglicherweise einen negativen Einfluss auf die SHIP1-Aktivität besitzt. Bezüglich der Bindung von PtdIns(3,4)P_2 und PtdIns(3,4,5)P_3 muss aufgrund der bisherigen Ergebnisse von einem komplexen Bindungsmodell ausgegangen werden, welches in weiterführenden Experimenten weiter untersucht werden soll. Perspektivisch wird die experimentelle Strukturanalyse von SHIP1 FL oder SHIP1 PHL-PPase-C2 angestrebt.

V. Abstract

SHIP1, a member of the phosphoinositide 5-phosphatase family is expressed specifically in hematopoietic cells in healthy individuals. Concerning leukaemia, a function of SHIP1 as a tumour suppressor was verified in several studies. Mechanistically, in those cells SHIP1 terminated the PI3K/AKT/mTORC signalling via dephosphorylation of PtdIns(3,4,5)P_3 resulting in reduced proliferation, motility, cell growth and survival. On the other hand, initial studies performed in our group could show high expression of SHIP1 in carcinoma, especially in colorectal carcinoma (CRC). Conclusively, the aim of this thesis was to elucidate the function of SHIP1 in CRC in more detail. For this, two cellular systems (overexpression of SHIP1 in the SHIP1-negative CRC line HCT-116 and *knock-down* of SHIP1 in the SHIP1-positive CRC lines SW-480 and HT-29) were established and the function of SHIP1 in CRC was analysed *in vitro* with regard to proliferation, survival, migration/invasion/chemotaxis, signal transduction, proteome and kinome as well as *in vivo* using an NSG mouse model. In summary, a complex and context-

dependent contribution of SHIP1 for the tumorigenesis of CRC could be concluded where SHIP1 seemed to have the general potential to fulfil a role of both a tumour suppressor or an oncogene. A similar dual function in tumorigenesis was also found for other phosphoinositide-5-phosphatases such as SHIP2. Taken into account the Two-PIP hypothesis one could suggest that phosphoinositide-5-phosphatases unlike e.g. PTEN did not necessarily have to terminate the PI3K/AKT/mTORC signalling but do open the possibility to an alternative activation of oncogenes such as AKT via the product of the phosphoinositide-5-phosphatase reaction PtdIns(3,4)P_2. In the further course of the thesis patient-derived mutations of the catalytic domain of SHIP1 were analysed and shown that those influenced the phosphoinositide binding and catalysis, stability and subcellular localization of SHIP1 as well as signal transduction. In the final part of the thesis, the structure (*in silico*) and biochemical properties of SHIP1 were studied with special focus on the three phosphoinositide binding domains (PH-L, PPase, C2). Of special interest was the identification of Ins(2,3,4,5)P_4 as a sole substrate of SHIP1 but not SHIP2. Further, the phosphoinositide binding and catalysis of SHIP1 FL and isolated and combined phosphoinositide binding domains were examined *in silico* regarding their mechanism and crucial residues and on a biochemical level. Here, the function of the C2 domain as an allosteric activator of SHIP1 could be verified whereas the PH-L domain might potentially negatively regulate SHIP1 activity. Regarding the accommodation of PtdIns(3,4)P_2 and PtdIns(3,4,5)P_3 into SHIP1 according to the results obtained so far one must suggest a complex binding model which should be analysed in more detail in the future. Prospectively, an experimental structure analysis of SHIP1 FL and/or SHIP1 PHL-PPase-C2 will be strived for.

Danksagung

Bei Prof. Dr. Jücker möchte ich mich für die Überlassung des Themas meiner Promotion, sowie die vielen fachlichen Anregungen bedanken. Desweiteren möchte ich mich bei der AG Jücker für die fachliche und experimentelle Unterstützung bedanken. Bei Dr. Susanne Witt und Phillip Lewe vom CSSB Hamburg möchte ich mich für die Zurverfügungstellung der experimentellen Ausstattung, sowie für fachliche und experimentelle Unterstützung bezüglich der Expression und Aufreinigung von SHIP1 bedanken, sowie bei Dr. Grättinger, Alessia Gilardi und Adelia Razeto vom Fraunhofer Screening Port Hamburg für die Unterstützung bei den SPR-Messungen, bei Tobias Lange und Hannah Maar (UKE Hamburg, Institut für Anatomie und experimentelle Morphologie) für die Durchführung der Mausexperimente, bei Konstantin Hoffer und Malte Kriegs von der Kinomics Core Facility des UKE Hamburgs für die Durchführung der PAMGENE-Messungen, bei Prof. Dr. Kirchmair und Christina de Bruyn Koops für die Unterstützung in bioinformatischen Fragestellungen und bei Prof. Dr. Schlüter, Hannah Voß und Paula Nissen für die Durchführung der Proteomik-Messungen. Zuletzt möchte ich mich bei Prof. Dr. Jücker und bei Prof. Dr. Torda für die Arbeit als Gutachter meiner Dissertation und bei Prof. Dr. Jücker, Prof. Dr. Schlüter und Dr. Perbandt für die Übernahme der Prüfungskomission meiner Disputation bedanken.

1. Introduction

1.1. Molecular mechanisms of tumorigenesis

1.1.1. General characteristics and classification of tumours

Tumours are defined as proliferative disorders originating from healthy cells. The observed phenotype of uncontrolled proliferation is typically achieved by successive acquisition of genetic or epigenetic alterations. The disease emanates from a single cell which adopts a selective advantage over its surrounding cells due to its modified phenotype (dominant clone). Most publications favour the view of a multi-step model of tumour progression meaning that the development from a healthy cell to a highly malignant tumour depends on the sequential or step-wise acquisition of alterations which favour tumour growth and are therefore positively selected (micro-evolution of tumour development). This process is dependent on both the tumour cell and the tumour microenvironment (TME) [1], [2]. Tumours are classified depending on the tissue type which they originated from. The most abundant tumour class is derived from epithelial cells and termed carcinoma (i.e. mammary carcinoma, colorectal carcinoma). Squamous carcinomas stem from covering epithelia (i.e. cervix carcinoma) and adenocarcinomas and adenomas spring from glandular epithelia (i.e. tumours of the stomach or colon mucosa). Sarcomas originate from ground tissue cells (mesenchymal cells such as fibroblasts, adipocytes, myocytes and osteoblasts). Hematopoietic tumours derive from the hematopoietic system and are further subdivided into leukaemia (single cell tumours) and lymphomas (solid tumours). Neuroectodermal tumours develop out of neuronal tissues (central and peripheral nervous system) and comprise gliomas, glioblastomas, neuroblastomas, schwannomas and medulloblastomas [1].
Cell proliferation or cell division is a highly regulated process which is subdivided in four phases:

1. G_1 (gap phase 1): cell growth and synthesis of building blocks needed for DNA replication and cytokinesis
2. S (synthesis phase): genome duplication
3. G_2 (gap phase 2)
4. M (mitosis phase): The M-phase is further subdivided into mitosis (nucleus division) and cytokinesis (cell body division). Mitosis comprises four steps: Within the prophase the chromosomes start to condense, and the spindle apparatus is formed at the cell poles. In the prometaphase the nuclear envelope is broken down and the chromosomes do attach to the spindle apparatus. Reaching the metaphase, the chromosomes align in the equatorial plane and the sister chromatids are pulled to the spindle poles for separation within the anaphase. The telophase is marked by reconstitution of the nuclear envelope and decondensation of the sister chromatids. Cytokinesis describes the actual process of cell division and is marked by the contraction of an actomyosin ring encompassing the cell body and subsequent budding off of the daughter cells as well as dispensation of the cellular organelles.

Cell cycle progression is controlled by three central binary (yes/no) check points which should prevent uncontrolled cell division and thus the development of proliferative disorders such as cancer.

1. G_1/S checkpoint: serves as a point to control if the extracellular environment and the general condition of the cell allows for cell division. Surmounting of this initial checkpoint is dictated by the presence or absence of extracellular cues such as mitogens. If cell cycle promoting signals are present cells will progress in cell cycle and if absent cells will either transit into a temporary resting state (G_0) or into apoptosis. The G_1/S checkpoint is also termed restriction point or *point of no return* as once this point is overcome extracellular signals cannot induce any reversion or otherwise said the cell starts to unroll a certain program which cannot be influenced by the cellular environment anymore.
2. G_2/M checkpoint: serves as a control point for correct and complete DNA replication (S-phase) and is paramount for transition into the M-phase. DNA damage or uncompleted DNA replication leads to cell cycle arrest or if severe to apoptosis mediated by the *gatekeeper* protein p53.
3. metaphase-to-anaphase checkpoint: serves as a control point for the correct attachment of the chromosomes to the spindle apparatus which is crucial for the synchronic dispensation of the sister chromatids to the daughter cells. The metaphase-to-anaphase checkpoint therefore prevents the occurrence of aneuploidies which are a common feature of cancer.

The cell cycle control system is based on the presence of a differential (cell cycle phase dependent) set of cyclin/CDK (Cyclin Dependent Kinase) complexes. CDKs are kinases which do steer various cell cycle related processes due to their ability to phosphorylate a wide set of target proteins. They become activated via association with cyclins and an activating phosphorylation which is catalysed by the CDK Activating Kinase (CAK). Cyclins are expressed in a cyclic (meaning cell cycle phase dependent) fashion. In addition of this transcriptional regulation mechanism, cyclin/CDK complexes may become inactivated by an inhibiting phosphorylation catalysed by the WEE1 kinase which may become reverted by the phosphatase CDC25 (Cell Division Cycle 25), or by CDK inhibitors

(CKIs). In eukaryotic cells four classes of cyclin/CDK complexes do exist which reflect the different phases of the cell cycle. The nomenclature used in the following listing is specific for human cells.

1. Cyclin D/CDK4 and CDK6 (G_1): activation of the expression of G_1/S cyclins in the late G_1 phase via phosphorylation of the transcriptional inhibitor protein RB (Retinoblastoma).
2. Cyclin E/CDK2 (G_1/S): crucial for overcoming the G_1/S checkpoint
3. Cyclin A/CDK1 and CDK2 (S): crucial for DNA replication
4. Cyclin B/CDK1 (M): crucial for overcoming the G_2/M checkpoint

Apart from the cyclin/CDK complexes mentioned the APC/C (Anaphase Promoting Complex/Cyclosome) complex is necessary for completion of the cell cycle. The APC/C complex is an E3 ubiquitin ligase complex activated in late mitosis, cytokinesis and early G_1 phase via association with CDH1 (Cell Division Cycle 20 (CDC20) Homologue 1) if chromosomes have attached correctly to the spindle apparatus. It induces the proteolysis of securin, a protein which tethers together the sister chromatids, as well as S- and M-cyclins. This is imperative to overcome the metaphase-to-anaphase checkpoint. The APC/C complex is inactivated in late G_1 phase by G1-cyclin/CDK complexes [3].

In tumour cells, the checkpoint system becomes out of control due to genetic aberrations. Genetic aberrations are commonly found in three classes of genes:

1. Activation of protooncogenes to oncogenes: Protooncogenes are genes which expression products facilitate tumour development (i.e. via the promotion of proliferation, migration, survival). Examples of oncogenes are growth factor receptors such as EGFR (Epithelial Growth Factor Receptor), intracellular signal transduction proteins such as onco-RAS (Rat Sarcoma) and transcription factors such as c-MYC (Myelocytomatosis). The transition of protooncogenes (=controllable) to oncogenes (=uncontrollable) may be realised by activating point mutations, deletions of regulatory domains, gene amplifications or chromosomal rearrangements leading to the formation of constitutively active fusion proteins.
2. Deactivation of tumour suppressor genes: tumour suppressor genes are genes which expression products negatively affect cell cycle progression. Classical tumour suppressor genes are RB and p53 (protein of 53 kDa). Inactivation of tumour suppressor genes may be achieved by inactivating point mutations, deletions, chromosomal translocations or epigenetic silencing (i.e. promotor hypermethylation).
3. Deactivation of DNA repair genes: The deactivation of DNA repair genes (i.e. Breast Cancer 1/2 (BRCA1/2)) is mechanistically similar to that observed in tumour suppressor genes. It promotes genetic instability which facilitates the acquisition of further genetic aberrations [1], [3].

1.1.2. Hallmarks and enabling characteristics of cancer

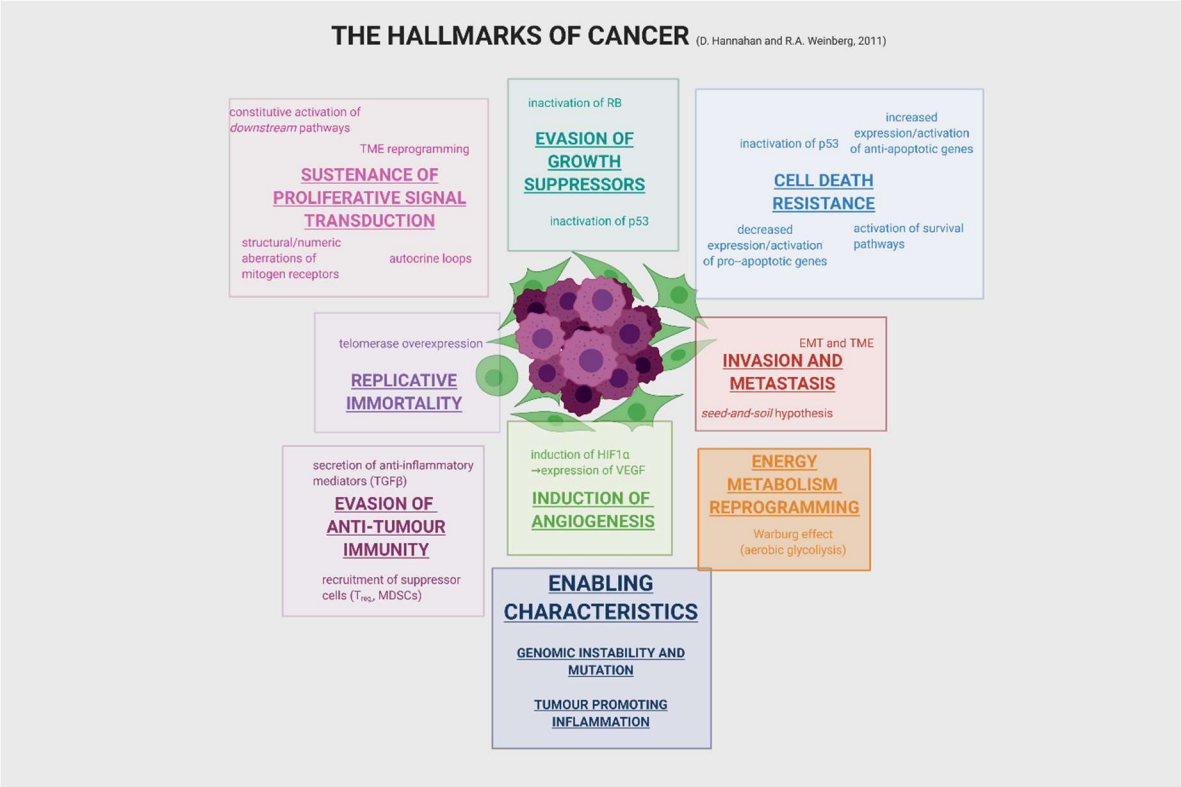

fig. 1: Hallmarks of cancer (adapted from [2]), details: see text

Cancer cells are marked by certain molecular abnormalities which were summarized by D. Hannahan and R.A. Weinberg in their essay *Hallmarks of Cancer: The next generation* [2]. They postulated that tumour cells would acquire more and more hallmark capabilities during their transition from a healthy cell to a highly malignant disorder due to genetic aberrations and changes in the TME. Eight hallmarks and two so-called enabling characteristics were suggested with focus on carcinoma development. The hallmarks of cancer were described as follows:

1. Sustenance of proliferative signal transduction: The constitutive proliferation of tumour cells is achieved due to constitutive (meaning independent from extracellular stimuli) activation of the cell cycle i.e. via autocrine loops, reprogramming of the TME with the aim to produce more mitogens, structural or numeric aberrations of mitogen receptors or constitutive activation of *downstream* signalling pathways i.e. due to inactivating mutations of PTEN (Phosphatase and Tensin homologue) or RAS GTPase Activating Proteins (GAPs) [2], [4], [5], [6].
2. Evasion of growth suppressors: This is mostly achieved by inactivation of RB and/or p53 [2]. RB suppresses cell cycle progression especially during the G_1 phase via transcriptional repression of G_1/S cyclins (*gatekeeper*) and acts in dependence of extracellular signals (i.e. presence/absence of mitogens) [7]. p53 senses DNA damage and other stress factors and induces either cell cycle arrest and subsequent DNA repair or in severe cases apoptosis [8].
3. Cell death resistance: Induction of apoptosis is a classical anti-tumour strategy realised either by the immune system or also by the application of anti-tumour drugs [9], [10], [11]. Tumor cells will typically develop mechanisms to circumvent apoptosis, i.e. inactivation of p53, enhanced expression and/or activation of anti-apoptotic proteins such as BCL-2 (B-Cell Lymphoma 2), BCL-XL (B-Cell Lymphoma extra Large) and signaling molecules promoting cell survival such as components of the PI3K/AKT/mTORC1 pathway, or downregulation of pro-apoptotic factors such as BAK (BCL-2 homologous Antagonistic Killer) and BAD (BCL-2 Antagonist of cell Death) [2].
4. Enablement of replicative immortality: Tumour cells do develop the potential of unlimited cell division capability due to telomerase overexpression (>90% of all cases of spontaneously developing tumours) [2]. In contrast, most healthy cells (with the exception of stem cells) do possess limited cell division capability and become senescent at the point of excess telomerase shortening. Some cells may overcome senescence but become apoptotic thereafter (*crisis*) [12], [13].
5. Induction of angiogenesis: In the rapidly growing tumour there is an enhanced demand for oxygen and nutrients as well as the elimination of CO_2 and metabolites which has to be covered by the vasculature. A tumour will depend on newly generated vessels (neoangiogenesis) to secure sufficient levels of oxygen and nutrients as soon as it reaches a diameter >2 mm. The most important pro-angiogenic factor is VEGF-A (Vascular Endothelial Growth Factor A) which is induced in the presence of hypoxia by the transcription factor HIF-1α (Hypoxia Induced Factor 1α). In tumour cells HIF-1α may also become induced by aberrant oncogenic signal transduction and is promoted by signals originating from the TME [14], [15], [16], [17], [18], [19]. The activation of neoangiogenesis is termed the *angiogenic switch*. In contrast to neoangiogenesis in healthy tissues (i.e. in the course of wound healing) tumour neoangiogenesis is not transient but constitutive [20]. Due to the uncontrolled hyperactivation of angiogenesis in tumours the tumour vasculature is aberrant, chaotic and highly permeable (*leaky*) which facilitates intravasation and metastasis [21], [22]. Of note, the angiogenic switch precedes the transition from non-invasive to invasive tumour behaviour [20], [23].
6. Invasion and metastasis: A local (primary) tumour may acquire the capability to become locally invasive or to generate metastases in distal tissues (secondary tumour). Carcinoma cells have to detach from the cell consortium before being able to migrate or invade. This is realised by transcriptional reprogramming termed the Epithelial Mesenchymal Transition (EMT). EMT is a developmental program orchestrated by master transcription factors (TWIST, SNAIL, SLUG). Cells having passed the EMT detach from the cell consortium due to the downregulation of cell-cell adhesions (i.e. E-cadherin, tight junction proteins), acquire a fibroblast-like appearance and migratory/invasive potential and are capable to survive outside the cell consortium (anoikis resistance) [24], [25], [26], [27], [28], [29], [30], [31], [32]. They invade through the Extracellular Matrix (ECM) using specialized actin-rich and matrix degrading structures (invadopodia) and break through the basement membrane. Breaking through the basement membrane marks the transition of a benign to a malignant tumour stage. The subsequent entering of tumour cells into blood or lymph vessels is called intravasation. Tumour cells move through the vasculature to distal tissues where they leave the vasculature (extravasation) and proliferate in the presence of an adequate microenvironment (colonisation, transition from a micrometastase to a macrometastase) [2], [33], [34]. For colonization, EMT is reversed, a process known as Mesenchymal Epithelial Transition (MET). Tumour

cells of a certain entity typically prefer certain sides for metastases generation and are attracted to them by the presence of soluble factors promising a favouring TME (*homing*, *seed-and-soil hypothesis*) [35], [36]. Dormant and circulating tumour cells (CTCs) form a severe problem in cancer therapy as they are typically highly therapy-resistant and capable of initiating post-therapy tumour growth (*relapse*) [36].

7. Energy metabolism reprogramming: Tumour cells show the unconventional characteristic of preferring glycolysis with subsequent generation of lactate out of pyruvate over oxidative carboxylation (citric acid cycle and respiratory chain) under normoxic conditions even, a phenomenon which is commonly known as aerobic glycolysis or Warburg effect [37], [38], [39]. It was hypothesized by different groups that tumour cells would use glycolysis intermediates to generate building blocks for the biosynthesis of amino acids and nucleic acids enabling them to grow and proliferate more rapidly [40], [41]. To compensate for the reduction in ATP gain glucose transporters are highly upregulated in tumour cells especially GLUT1 (Glucose Transporter 1) [42], [43], [44]. Oncoproteins (i.e. onco-RAS, onco-MYC) promote the sustenance of aerobic glycolysis i.a. via upregulation of HIF1α [42], [43], [45], [46], [47].
8. Evasion of anti-tumour immunity: The concept of immune surveillance states that newly generated tumour cells are detected and destroyed by the immune system and implies that visible (macro-)tumours must have developed the capacity to evade immune surveillance [2]. Anti-tumour immunity is mostly orchestrated by T-lymphocytes and natural killer cells [48], [49]. Tumour cells escape detection by the immune system i.a. via secretion of anti-inflammatory mediators such as TGF-β (Transforming Growth Factor β) or the recruitment of suppressor cells (T_{regs}(regulatory T-lymphocytes), MDSCs (Myeloid Derived Suppressor Cells) [50], [51], [52], [53].

The enabling characteristics are stated as

1. Genomic instability and mutation: Tumour cells gain a selective advantage due to the sequential acquisition of chance mutations or other genetic or epigenetic alterations. The mutational rate is typically enhanced in tumour cells via inactivation of so-called *caretaker* genes (DNA repair genes, p53 etc.) or increased sensitivity to DNA damaging substances [54], [55], [56].
2. Tumour promoting inflammation: Tumours become infiltrated with immune cells initially aiming to destroy the tumour but later being reprogrammed by the tumour to promote tumour progression [57], [58]. Tumour promoting immune cells are an essential pillar of the TME and provide i.e. growth factors, survival factors, EMT-inducing and matrix modifying signals [17], [58], [59], [60], [61].

1.1.3. Cancer Stem Cells (CSCs) and the Tumour Microenvironment (TME)

Recent evidence coming from the tumour biology research community suggest that tumours are not a mass of isolated tumour cells alone but rather a heterogeneous population of tumour cells, Cancer Stem Cells (CSCs) and the TME. CSCs show stem cell characteristics and are highly resistant to chemo- and radiotherapy. They are especially problematic due to their potential to foster Minimal Residual Disease (MRD). MRD is the re-initiation of tumours originating from few resistant cells having survived therapy [2].

The TME is essentially involved in tumour formation and progression due to the delivery of mitogens and anti-apoptotic and pro-angiogenic signalling molecules. The most decisive components of the TME are Cancer Associated Fibroblasts (CAFs), Angiogenic Vascular Cells (AVCs) and Infiltrating Immune Cells (IICs). The labelling characteristic of CAFs is the expression of α-SMA (α-Smooth Muscle Actin). They are increased in number in tumours and wounds and promote proliferation, invasion and metastasis. AVCs are endothelial cells and pericytes forming the tumour vasculature. The IICs are mainly assembled of T- and B-lymphocytes, Tumour Associated Macrophages (TAMs) and neutrophilic granulocytes and supply growth- and pro-angiogenic factors, pro-inflammatory cytokines and ECM degrading enzymes. In addition, tumour cells recruit suppressor cells to counteract anti-tumour immunity (see above) [2], [62].

1.1.4. Oncogenic signal transduction pathways: the role of phosphoinositides

Phosphoinositides are defined as a group of lipid-derived signalling molecules which are implicated in various cellular processes such as glucose homeostasis, immunity and tumorigenesis. The precursor molecule phosphatidyl inositol (PtdIns) is generated in the smooth endoplasmic reticulum (sER). It comprises a polar inositol head group in addition to its membranous acyl-chain originated in diacyl glycerol (DAG). Phosphatidyl inositol phosphates ($PtdInsP_x$) arise from PtdIns and may be converted into each other by combinatorial phosphorylation and dephosphorylation events [63], [64]. The known $PtdInsP_x$ species are as follows: PtdIns(3)P implicated in endosome function [65], PtdIns(4)P implicated in intracellular vesicle transport within the golgi apparatus and serving as a precursor for $PtdIns(4,5)P_2$ [66], [67], PtdIns(5)P, $PtdIns(4,5)P_2$ crucial for Ca^{2+} dependent signal transduction [67], [68], [69], $PtdIns(3,5)P_2$ functioning within endosomes in concert with PtdIns(3)P [70],

PtdIns(3,4)P_2 influencing various cellular processes such as immunity and tumorigenesis [71] and PtdIns(3,4,5)P_3 implicated in a variety of cellular outputs (immunity, tumorigenesis etc.) as well [72].
The functional impact of the individual PtdInsP_x species is dictated by the presence of PtdInsP_x specific lipid binding domains within *upstream* and *downstream* components of the signal transduction machinery i.e. FYVE (FAB1, YOTB/ZK632.12, VAC1, EEA1) and PX (PHOX) domains specifically recognize PtdIns(3)P whereas PH (Pleckstrin Homology) domains are specific for PtdIns(3,4)P_2 respectively PtdIns(3,4,5)P_3 [73].

1.2. The PI3K/AKT/mTORC1 signal transduction pathway

The protooncogenic PI3K(Phosphoinositide-3-Kinase)/AKT(Ak-strain 8 thyoma, also known as Protein Kinase B (PKB))/mTORC1 (mammalian Target Of Rapamycin Complex 1, also known as mTOR/RAPTOR ((mammalian Target Of Rapamycin/Regulatory Associated Protein of mTOR) complex) pathway is central in tumour progression as it positively regulates cell proliferation, cell growth and cell survival and also shares intensive *crosstalk* with migration and invasion promoting pathways as described in more detail in section 1.3. Deregulation of the PI3K/AKT/mTORC1 signal transduction pathway is frequently observed in tumour cells [63], [74].
The PI3K/AKT/mTORC1 pathway may become induced upon the presence of positive signals (i.e. mitogens, growth or survival factors) binding to adequate receptors (GPCRs or RTKs) in healthy tissues but tumour cells may find ways to circumvent the need for such extracellular stimuli i.e. making use of autocrine loops or displaying copy number variations or genomic aberrations (i.e. chromosomal rearrangements leading to fusion proteins). This leads to the activation of PI3KI isoenzymes at the plasma membrane and subsequent conversion of PtdIns(4,5)P_2 to PtdIns(3,4,5)P_3 [1], [72], [75]. PtdIns(3,4,5)P_3 serves as a *second messenger* for the recruitment of PtdIns(3,4,5)P_3 specific PH domain containing effector proteins to the plasma membrane [72]. Amongst them is the AGC kinase AKT. AKT becomes activated following its recruitment to the plasma membrane via phosphorylation at an invariant threonine and an invariant serine residue. Threonine phosphorylation is executed by Phosphoinositide Dependent Kinase 1 (PDK1) which also contains a PtdIns(3,4,5)P_3 specific PH domain and serine phosphorylation is dependent on a PDK2 enzyme which role can be filled in by multiple S-/T-kinases but mostly by the mTORC2 complex (also known as mTOR/RICTOR (mammalian Target Of Rapamycin/Rapamycin Insensitive Companion of mTOR) complex) [76], [77], [78], [79], [80]. Activated AKT positively regulates survival-, proliferation- and growth promoting pathways and therefore facilitates tumour progression [68]. PtdIns(3,4,5)P_3 degradation may be achieved by two independent pathways: (1) dephosphorylation of PtdIns(3,4,5)P_3 on position D3 by the phosphoinositide-3-phosphatase PTEN (Phosphatase and Tensin homologue) followed by dephosphorylation on position D5 by members of the phosphoinositide-5-phosphatase family i.e. INPP5E (Inositol polyphosphate-5-Phosphatase E), SKIP (Skeletal muscle and Kidney enriched Inositol polyphosphate-5-phosphatase), SHIP1 (SH2 domain containing Inositol polyphosphate-5-phosphatase 1), SHIP2 (SH2 domain containing Inositol polyphosphate-5-phosphatase 2) or PIPP (Proline rich Inositol Polyphosphate-5-Phosphatase) and (2) dephosphorylation on position D5 followed by dephosphorylation on position D4 by members of the phosphoinositide-4-phosphatase family i.e. INPP4A (Inositol polyphosphate-4-Phosphatase type I) and INPP4B (Inositol polyphosphate-4-Phosphatase type II) or on position D3 by PTEN [81], [82], [83]. Interestingly, the intermediate of this degradation pathway, PtdIns(3,4)P_2 may either confer oncogenic effects (i.e. activation of AKT) or abolish oncogenic signal transduction dependent on the cell type so that phosphoinositide-5-phosphatases do possess the potential to act both as an oncogene and a tumour suppressor protein which will be discussed in further depth in section 1.4.3. [84].

1.2.1. Components of the PI3K/AKT/mTORC1 pathway

As outlined in **fig. 2** the PI3K/AKT/mTORC1 pathway consists of three general levels of signal transduction [74].

1. PI3K: *upstream* events leading to the recruitment of PI3K to the plasma membrane, its activation and subsequent conversion of PtdIns(4,5)P_2 to PtdIns(3,4,5)P_3 which equals the generation of an oncogenic or protooncogenic *second messenger*
2. AKT: recruitment to the plasma membrane and activation
3. *downstream* signalling: regulation of *downstream* signalling pathways by activated AKT (phosphorylation and dephosphorylation events) preferentially in the cytoplasm and nucleus resulting in enhanced proliferation, cell growth and survival.

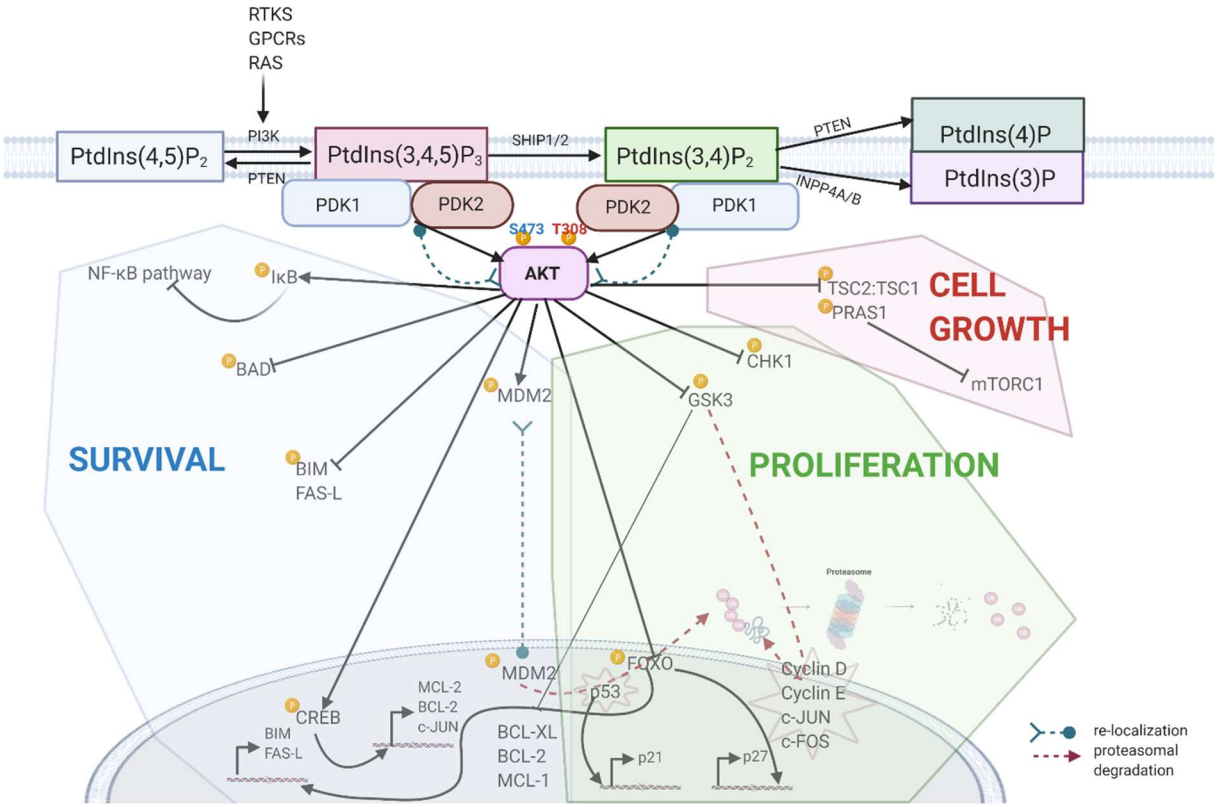

fig. 2: **overview of the PI3K/AKT/mTORC1 pathway.** The PI3K/AKT/mTORC1 pathway can be separated into three general levels of signal transduction: (1) activation of PI3K and generation of PtdIns(3,4,5)P_3, (2) recruitment and activation of AKT and (3) *downstream* signal transduction. PI3KI isoenzymes are activated upon binding of an agonist i.e. a growth or survival factor to the respective RTK or GPCR, or via small GTPases of the RHO or RAC family (not shown). Upon agonist binding the receptor becomes tyrosine phosphorylated leading to the recruitment of PI3K to the plasma membrane via the SH2 domain of the regulatory subunit p85 and abolishment of the basal inhibition of the catalytic subunit p110 by p85 (not shown). Subsequently, PtdIns(4,5)P_2 is converted into PtdIns(3,4,5)P_3 resulting in the recruitment of PtdIns(3,4,5)P_3 specific PH-domain containing effector proteins. Among them are the Ser/Thr kinases AKT and PDK1. AKT becomes activated by phosphorylation of an invariant threonine residue via PDK1 and an additional serine phosphorylation executed by a second Ser/Thr kinase commonly referred to as PDK2 (i.e. mTORC2). AKT activation promotes various *downstream* effects such as the inhibition of autophagy and apoptosis and the promotion of cell growth, proliferation, survival, cell cycle progression and glucose metabolism. PtdIns(3,4,5)P_3 may become degraded by two independent pathways, firstly via dephosphorylation on position D3 by the 3-inositol polyphosphate phosphatase PTEN and subsequent conversion of the resulting product PtdIns(4,5)P_2 to PtdIns(4)P through enzymes of the 5-phosphatase family; secondly via dephosphorylation on position D5 by 5-phosphatases INPP5E, SHIP1/2, SKIP and PIPP and subsequent dephosphorylation on position D4 by 4-phosphatases INPP4A or INPP4B. PtdIns(3,4)P_2 can serve as an additional *second messenger* in the context of AKT activation via recruitment of AKT and PDK1 and is implicated in the regulation of the cytoskeleton i.e. within the process of migration.

Of note, there are additional pathways *downstream* of PtdIns(3,4,5)P_3 apart from AKT mediated signal transduction i.e. SGK/mTORC2, RAC and BTK dependent signalling [85] but those will not be discussed in further detail.

1.2.1.1. Phosphoinositide-3-Kinase (PI3K)

The family of PI3K isoenzymes is characterized by their lipid kinase activity which enables them to phosphorylate phosphoinositides at position D3. Based on substrate specificity and domain architecture PI3K enzymes are subdivided in three main classes (I, II and III). The subclade of PI3KI is further differentiated into PI3KIA and PI3KIB [75]. A group of S-/T-kinases comprising i.a. mTOR, ATM (Ataxia Telangiectasia Mutated) and ATR (Ataxia Telangiectasia Related) is sometimes classified as PI3KIV, however they lack lipid kinase activity [86]. PI3KI and especially PI3KIA enzymes play a major role in tumorigenesis [75].

PI3KIA is a heterodimer built of a catalytic (p110) and a regulatory (p85) subunit. The catalytic subunit is specific for PtdIns(4,5)P_2 and therefore implicated in the activation of oncogenic signal transduction via PtdIns(3,4,5)P_3. There are three isoforms of the catalytic subunit (p110α encoded by *PIK3CA*, p110β encoded by *PIK3CB* and p110δ encoded by *PIK3CD*) and five isoforms of the regulatory subunit (p85α and its splicing variants p55α and p50α encoded by *PIK3R1*, p85β encoded by *PIK3R2* and p55γ encoded by *PIK3R3*). PI3KIB possesses a similar modular structure as PI3KIA and comprises the catalytic subunit p110γ (encoded by *PIK3CG*) with specificity for PtdIns(4,5)P_2 and either one of the regulatory subunits p101 (encoded by *PIK3R5*) or p87 (encoded by *PIK3R6*).

PI3KII isoenzymes are monomers and lack the regulatory subunit. They are specific for PtdIns. PI3KIIγ (encoded by *PIK3C2G*) is expressed in liver, prostate and mammary tissue whereas the expression pattern of PI3KIIα (encoded by *PIK3C2A*) and PI3KIIβ (encoded by *PIK3C2B*) is not restricted to certain tissues. PI3KIII is a heterodimer consisting of the catalytic subunit VPS34 specific for PtdIns and the regulatory subunit VPS15. It is implicated in autophagy and intracellular vesicle trafficking [75].
The activation of PI3KIA isoenzymes typically occurs via RTKs although activation via GPCRs is also possible for p110β containing enzymes. In contrast, PI3KIB is mostly activated by GPCRs but can be activated by RTKs if p87 is the regulatory subunit [87], [88], [89], [90], [91], [92], [93]. Following binding of an agonist to a receptor tyrosine kinase type-receptor and receptor transphosphorylation on conserved tyrosines, the SH2 domain of p85 is recruited to specified phospho-tyrosines within the consensus sequence PYXXM either of the respective RTK itself or of associated adaptor proteins. This concludes in the activation of p110 via (1) recruitment to the plasma membrane and its substrate PtdIns(4,5)P_2 and (2) relief of the autoinhibitory effect of the p85 iSH2 domain on the p110 C2 domain (basal inhibition) [94], [95], [96]. Alternatively, PI3KI members may be activated by small GTPases of the RAS superfamily. All p110 isoforms share a RAS Binding Domain (RBD) which is absent in PI3KII and PI3KIII [75]. The activation of p110α and p110δ occurs via k-RAS (kirsten RAS viral oncogene homologue), n-RAS (neuroblastoma RAS viral oncogene homologue), h-RAS (harvey RAS viral oncogene homologue) or onco-RAS [97], [98], [99], [100], [101]. From crystallographic data it was concluded that binding of RAS to the RBD induced the ordering of distinct loop structures in the RBD and that this conformational change was transferred to the C2 loop and the PtdIns(4,5)P_2 binding site located in the C-terminal lobe of the catalytic domain resulting in facilitated catalysis. Out of this reason, a role for RAS members as allosteric activators of PI3KI was proposed, however the observed activating effect might also be just the consequence of the RAS mediated recruitment of PI3KI to the plasma membrane [100]. Induction of p110δ in turn, is dependent on r-RAS (related RAS viral oncogene homologue) or TC21 (Teratocarcinoma 21, also known as r-RAS2) and the activation of p110β may be due to small GTPases of the RHO subfamily of RAS GTPases namely RAC (RAS related C3 botulinum toxin substrate) or CDC42 (Cell Cycle Division Control 42) [102], [103], [104].
PtdIns(3,4,5)P_3 dependent signal transduction pathways are frequently found to be hyperactivated in cancer due to

1. Loss of PTEN [105], [106].
2. Activating mutations in p110 typically found in either the catalytic domain (i.e. p110α H1047R) facilitating membrane recruitment and catalysis or in the helical domain (i.e. p110α E542K or E545K) weakening the autoinhibitory interaction with the p85 iSH2 domain [75].
3. Inactivating mutations of p85 i.e. within the iSH2 domain. A mutant variant of p85α termed p65α displayed complete loss of its autoinhibitory potential on p110 and was transforming in cell culture experiments. Mice harbouring T-cell specific overexpression of p65α developed lymphoproliferative disorders and when crossed with *trp53*$^{-/-}$ mice they developed lymphomas [75], [96], [107].
4. constitutive activation of *upstream* regulators (i.e. RAS, RTKs) [75], [96].

Of note, p110β was found to rather function as a tumour suppressor than as an oncogene. When overexpressed in a mammary carcinoma mouse model tumour progression was slowed due to decreased PI3K/AKT/mTORC signalling and it was hence suggested that the less catalytically active p110β might compete with p110α for pYXXM sites [108].

1.2.1.2. Ak-strain 8 thyoma (AKT)

The S-/T-kinase AKT belongs to the superfamily of AGC kinases named after their founding members protein kinases A, G and C [109]. It is the most prominent signalling component *downstream* of PtdIns(3,4,5)P_3 and comes in three distinct isoforms. AKT1 (PKBα) is the most abundantly expressed isoform in most tissues. In contrast, the expression of AKT2 (PKBβ) is most decisive in insulin sensitive tissues and the expression of AKT3 (PKBγ) is predominant in brain and testis [110], [111]. AKT comprises an N-terminal PH domain with specificity for PtdIns(3,4,5)P_3 and PtdIns(3,4)P_2, a centrally located kinase domain and a C-terminally located Hydrophobic Motif (HM) [110]. It is activated by two phosphorylation events [112], [113], [114], [115], [116]. Threonine phosphorylation (T308 in AKT1) by PDK1 results in a 100-fold increased catalytic activity [112]. Serine phosphorylation (S473 in AKT1) enhances the activity of AKT to another factor 5 to 10 and is executed by a second S-/T-kinase commonly referred to as PDK2 [76], [109]. mTORC2 was identified to be responsible for serine phosphorylation following extensive research. It was shown that loss of RICTOR or mTOR but not of RAPTOR reduced the activation status of AKT in several model organisms (*Drosophila melanogaster*, *Dyctiostelium discoideum*) as well as in human cancer cells and adipocytes [80], [117], [118]. Serine and threonine phosphorylation were furthermore demonstrated to be independent from each other. Threonine phosphorylation was not affected in *rictor*$^{-/-}$; *mlst8*$^{-/-}$ or *sin1*$^{-/-}$ MEFs (Mouse Embryonic Fibroblasts) and conversely, serine phosphorylation was not affected in *pdk1*$^{-/-}$

MEFs [119]. Crystallographic analysis of *in vitro* threonine phosphorylated AKT WT and the serine phosphorylation mimicking mutant AKT S474D revealed that serine phosphorylation induced a conformational change leading to the ordering of the αB and αC helices of the N-lobe which stabilized the activation loop containing the nucleotide binding pocket. Regarding AKT S474D the HM engaged in the formation of a hydrophobic groove at the interface covering the αB and the αC helices and the β4 and β5 strands of the central β-sheet. D474 was responsible for the stabilization of the hydrophobic groove realised by an H-bond to the side chain of Q220, a water-mediated contact to the main chain of Q220 and a *Van-der-Waals* contact to the side chain of F473 [109]. Data obtained from *rictor*$^{-/-}$; *mlst8*$^{-/-}$ or *sin1*$^{-/-}$ MEFS showed that serine phosphorylation was dispensable for the regulation of certain *downstream* targets of AKT (TSC2 S939 and T1462, GSK3α (Glycogen Synthase Kinase 3α) S9, GSK3β (Glycogen Synthase Kinase 3β) S21 and FOXO1/3 (FOrkhead Box O 1/3) S256) but not for others (FOXO3 T24 and T32) which offered the possibility of a regulatory or *fine-tuning* function of serine phosphorylation [120], [121], [122], [123]. However, other S-/T-kinases with similar substrate spectrum as AKT such as S6K (small ribosomal subunit 6 protein Kinase) or SGK (Serum and Glucocorticoid regulated Kinase) might have filled in for AKT in the described cases [124], [125], [126], [127]. The C-Terminal Modulator Protein CTMP prevents the phosphorylation events leading to the activation of AKT and overexpression of CTMP was observed to reverse the transforming potential of AKT overexpression [128]. AKT may become dephosphorylated by PP2A (Protein Phosphatase 2A) or PHLPP (PH domain and Leucine rich repeat containing Protein Phosphatase) [129], [130].
The substrate specificity of AKT is dictated by the presence of two conserved arginines at P(-5) and P(-3). Substrates containing a threonine at P(-2) and a bulky hydrophobic residue at P(+1) are preferred. The optimal substrate recognition sequence is RXXRXX(S/T)M where X stands for any amino acid and M is a bulky and hydrophobic residue. R(-3) is involved in a salt bridge to E236 and a hydrogen bond to D440 and R(-5) forms contacts with E279 and E342. T(-2) establishes a second hydrogen bond to E279 if present in the substrate which might explain a preference for threonine at this position [109].

1.2.1.2.1. TAPP1 and TAPP2 (Tandem PH domain proteins 1 and 2): Competition for PtdIns(3,4)P_2

TAPP proteins are adaptor proteins which are implicated in cell migration, adhesion and chemotaxis, responsiveness to insulin and B-cell activation [131]. TAPPs are expressed in a wide variety of tissues [132]. The N-terminal half of the protein is conserved amongst TAPP1 and TAPP2 as well as amongst TAPP proteins of different vertebrate species and includes two PH-domains in tandem arrangement [132]. By SPR (Surface Plasmon Resonance) and PLO (Phospholipid Overlay) assays the C-terminal PH-domain was shown to selectively bind PtdIns(3,4)P_2 and this was required for plasma membrane recruitment upon activation of PI3K whereas the N-terminal PH-domain did not participate in phosphoinositide binding [133], [134], [135]. The specificity of the C-terminal PH domain for PtdIns(3,4)P_2 with no apparent binding to PtdIns(3,4,5)P_3 was explained from crystal structure analysis of the TAPP1 PH domain in complex with citrate. Superposition of the obtained structure with the crystal structure of the PH domain of the related protein DAPP1 (Dual Adaptor for Phosphotyrosine and 3-Phosphoinositides 1) PtdIns(3,4,5)P_3/PtdIns(3,4)P_2 specific PH domain in complex with Ins(1,3,4,5)P_4 specified that A203 corresponding to G176 in DAPP1 sterically blocked access of the 5-phosphate and consistently, substitution of A203 with glycine resulted in specific binding to both PtdIns(3,4)P_2 and PtdIns(3,4,5)P_3 [136]. The *in vivo* significance of these findings was further supported by studies using fluorescence-labelled TAPP1 and PtdIns(3,4,5)P_3 specific PH domain comprising BTK. Upon activation of B-lymphoma cells TAPP1 became localized to the plasma membrane in a slow and sustained manner whereas recruitment of BTK was fast and transient correlating with the production respectively degradation kinetics of PtdIns(3,4)P_2 and PtdIns(3,4,5)P_3 [135], [137], [138]. Overexpression of SHIP1 or activation of SHIP1 by $F_c\gamma$RIII crosslinking negatively affected the membrane localization of BTK but enhanced the membrane localization of TAPP1 [138]. Similar observations were also made in T-cells [139]. The C-terminal half of TAPP proteins exhibits a higher level of divergence with the exception of a PDZ domain binding motif (S/T-X-V/I) [132], [140], [141]. The PDZ binding motif was shown to mediate the interaction with a set of PDZ domain containing proteins including syntrophins and PTPL1 (Protein Tyrosine Phosphatase Like 1) [142], [143]. Upon stimulation of NIH-3T3 cells with PDGF (Platelet Derived Growth Factor) and PI3K/SHIP dependent formation of PtdIns(3,4)P_2 syntrophins mediate the recruitment of TAPP1 to the plasma membrane at sites of membrane ruffles. Overexpression of TAPP1 in this setting negatively affected the formation of central but not peripheral ruffles and this was rescued by overexpression of syntrophin. It was speculated that syntrophins might be required for the correct localization of TAPP1 allowing TAPP1 to recruit positive regulators of membrane ruffling and that mislocalization of TAPP1 would favour recruitment of negative regulatory proteins. An alternative explanation would be competition of syntrophin and PTPL1 PDZ domains for the binding to TAPP1 [143]. PTPL1 is a negative regulator of growth factor receptor and PI3K signalling due to its function in dephosphorylating phosphotyrosines [142], [144], [145] and from *knock-down* studies in HEK-293T cells it was

suggested that TAPP1 might establish a negative *feedback* loop concerning PI3K signalling by sequestering PTPL1 to the plasma membrane [142]. TAPP2 was similarly found to be implicated in actin dynamics and migratory processes especially cell adhesion, cell polarization and chemotaxis [146]. TAPP2 expression was observed in CLL and was especially high in the ZAP-70$^+$ subgroup known for its strong migratory potential [147], [148]. To further analyse the *in vivo* function of TAPPs so-called TAPP KI mice were generated which bear point mutations in the phosphoinositide binding pocket preventing phosphoinositide binding [149], [150]. TAPP KI mice are characterized by hyperactivation of AKT cumulating in increased sensitivity to insulin and autoimmunity due to a hyperactivation of B-cells. From binding studies it was shown that TAPP proteins function as negative regulators of AKT by competing for binding to PtdIns(3,4)P_2 in addition to recruitment of PTPL1 [131], [142], [149].

1.2.1.3. Downstream signalling pathways

AKT is the starting point of numerous *downstream* signalling pathways which converge in enhanced proliferation, survival and cell growth [74].

1.2.1.3.1. Antiapoptotic effects

AKT is involved in the inhibition of apoptosis via direct phosphorylation of target proteins as well as impacting transcriptional processes. It phosphorylates and inactivates several pro-apoptotic proteins such as procaspase 9, BAD and GSK3 releasing anti-apoptotic proteins of the BCL-2 family, i.a. BCL-2, BCL-XL and MCL-1 (Induced Myeloid Leukaemia Cell differentiation protein 1) [151], [152], [153], [154], [155], [156], [157]. Furthermore, AKT sequesters the E3 ubiquitin ligase MDM2 (Mouse Double Minute 2) to the nucleus which enables it to induce the proteasomal degradation of p53 [158], [159]. On the transcriptional level AKT phosphorylates and inactivates FOXO transcription factors favoring the expression of pro-apoptotic genes (i.e. BIM (BCL-like protein 21), FAS ligand) and at the same time activates CREB (cAMP Responsive Element Binding) transcription factors promoting the expression of anti-apoptotic genes (i.e. MCL-1, BCL-2, c-JUN) [160], [161], [162], [163], [164], [165]. Finally AKT is involved in the activation of the anti-apoptotic NF-κB pathway by means of an activating phosphorylation of the IκB kinase [166], [167].

1.2.1.3.2. Cell growth promoting effects: The mTORC1 complex

The promotion of cell growth in permitting conditions (sufficient nutrients or the presence of growth factors) is centrally regulated by the mTORC1 complex [74]. mTORC1 serves as a signalling hub integrating various input signals [168]. It is a multiprotein complex consisting of the S-/T-kinase mTOR, the scaffold protein RAPTOR, mLST8 (mammalian Lethal with SEC13 8) and PRAS40 (Proline Rich AKT Substrate, 40 kDa) [169], [170], [171], [172], [173]. RAPTOR is a positive regulator of the mTORC1 complex as it facilitates substrate recruitment (scaffold function) [170], [174], [175] whereas PRAS40 negatively regulates the activity of mTORC1 via inhibiting the activation of the complex [169], [173]. mTOR belongs to the PI3K-related Kinase family [176] and comprises several HEAT (Huntington, Elongation Factor 3 (EF3), Protein Phosphatase 2 (PP2A), TOR1) repeats as landing sites for Protein Protein Interactions (PPIs) located at the N-terminus. The catalytic domain is found within the C-terminal part *downstream* of the FRB (FKBP12-Rapamycin Binding) domain. The FRB domain is named after its ability to negatively regulate the activity of mTOR in the presence of the FKBP12 (FK506 Binding Protein, 12 kDa):rapamycin complex [176], [177]. At the very C-terminus two FAT (FRAP, ATM, TRRAP) and a FATC (FRAP, ATM, TRRAP, C-terminal) domain can be found. In the presence of positive regulatory signals an interaction between FAT and FATC is induced which exposes the catalytic domain [178]. The redox sensitivity of mTORC1 can be explained by the presence of a disulphide bridge formed between two conserved cysteine residues of the FATC domain [179], [180].
mTORC1 can be activated by either nutrients (amino acids) or growth factors. Growth factors signal through RTKs and either the PI3K/AKT signal transduction pathway or the MAPK (Mitogen Activated Protein Kinase) cascade or both [181], [182], [183], [184]. AKT phosphorylates and inactivates TSC2 (Tuberin) at S939 and T1462. TSC2 is part of the TSC2:TSC1 (Hamartin)-RHEB (RAS Homologue Enriched in Brain)-GAP complex. Inactivation of TSC2:TSC1 by AKT allows GTP-loaded RHEB to activate mTORC1 [121], [123], [185], [186]. Tctp (Translationally controlled tumour protein) was identified as a RHEB-GEF in *Drosophila melanogaster*, however no homologue to Tctp has been found in human cells to date [176], [187]. AKT may bypass TSC2:TSC1 by means of an inactivating phosphorylation of PRAS40 at T246 [169], [188]. Amino acids especially branched chain ones such as leucine do positively impact the activity status of mTORC1 [168]. Regarding data obtained from *knock-out* and overexpression studies this seems to be independent on TSC2:TSC1 but dependent on RHEB (i.e. amino acid deprivation in *tsc2* cells still reduced the activity of the mTORC1 complex, overexpression of RHEB counteracted the amino-acid starvation induced reduction in mTORC1 activity and RNAi mediated *knock down* of RHEB resulted in decreased

activation of mTORC1 in the presence of amino acids) [189], [190]. Energy stress (AMP activated Kinase (AMPK)) and hypoxia (Regulated in Development and DNA damage 1 (REDD1)) serve as negative regulatory signals of mTORC1 activity. Both AMPK and REDD1 activate the TSC2:TSC1 complex [191].
The promotion of cell growth mediated by mTORC1 is due to its ability to enhance Protein Biosynthesis (PBS). Firstly, it phosphorylates the 4E Binding Protein (4E-BP) therefore liberating the eukaryotic transcriptional initiation factor eIF-4E, secondly it activates the protein kinase $p70^{S6K}$ (Small ribosomal subunit protein 6 Kinase) involved in the phosphorylation event leading to proteasomal degradation of PDCD4, a negative regulator of the helicase eIF-4A and lastly, it promotes ribosome biosynthesis [176], [192], [193], [194]. In *tsc2* cells hyperactivation of mTORC1 was transforming. The elevation of free eIF-4E was proposed to be crucial for this transforming potential as overexpression of eIF-4E led to accelerated tumour progression in a B-cell lymphoma mouse model phenocopying the overexpression of AKT1 and eIF-4E was demonstrated to exhibit a transforming potential itself when overexpressed in cell culture studies [195], [196], [197], [198].

1.2.1.3.3. Cell proliferation promoting effects

Cell proliferation is promoted by a synergistic interplay of i.a. the MAPK and the PI3K/AKT pathway [74]. AKT phosphorylates the CKIs p21 and p27 and sequesters them to 14-3-3 proteins in the cytosol [198]. In addition, the FOXO dependent expression of p27 and the p53 dependent expression of p21 become downregulated by AKT [158], [159], [199]. The AKT catalysed inactivating phosphorylation of GSK3 results in less proteasomal degradation of cell-cycle promoting proteins such as cyclins D and E, c-JUN (cellular v-JUN avian sarcoma virus 17 oncogene homologue) or c-MYC [200], [201], [202], [203]. The expression of c-MYC and cyclin D as well as further proliferation promoting proteins is also positively regulated by mTORC1 [204]. In addition, AKT inhibits the G_2/M Checkpoint Kinase 1 (CHK1). Hyperactivation of AKT achieved by loss of PTEN was shown to result in constitutive inactivation of CHK1 and constitutive cell cycle progression even in the presence of DNA damage leading to increased genomic instability further fuelling tumour progression [205], [206].

1.3. Regulation of invasion and metastasis: The interplay between Phosphoinositide-3-Kinase (PI3K) and small GTPases of the RAC family

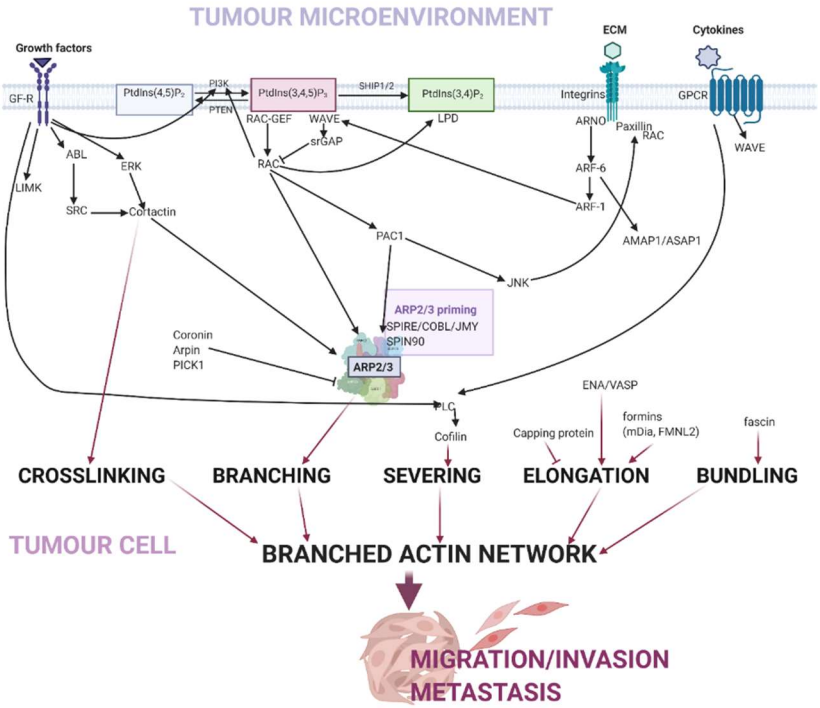

fig. 3: actin dynamics in the formation of migratory and invasive structures in tumour cells with focus on the lamellipodium leading edge. Lamellipodia formation is controlled by changes in gene expression in the course of the Mesenchymal Epithelial Transition (EMT) as well as signals form the extracellular matrix (ECM) via integrins, and the tumour microenvironment via growth factor receptors (GF-Rs) and G-protein coupled receptors (GPCRs). GF-R activation leads to the activation of PI3K and the generation of $PtdIns(3,4,5)P_3$ out of $PtdIns(4,5)P_2$. Subsequently, the nucleation promoting factor (NPF) WAVE and the small GTPase RAC are recruited to the plasma membrane and WAVE gets activated by synergistic action of $PtdIns(3,4,5)P_3$ and RAC leading to the binding and activation of the actin nucleator ARP2/3 via the WAVE WCA domain and the formation of branches within a given actin filament which are elongated by actin elongators ENA/VASP and formins. WAVE activation may also occur through lamellipodin (LPD) which is recruited to the leading edge

membrane via PtdIns(3,4)P_2 or RAC, or GPCRs. GF-R signalling additionally activates the tyrosine kinases ABL and SRC. SRC dependent phosphorylation of effector proteins such as the actin-crosslinking protein cortactin or the ARF-6 effector AMAP1/ASAP1 is a common regulatory feature of migratory/invasive structures. Cell adhesion executed by the interaction of integrins with ECM substrates induces the formation of migratory/invasive structures. This is achieved through activation of RAC via the adaptor protein paxillin (*outside-in-signalling*). RAC may enhance the activity of paxillin via a PAK1-JNK dependent signalling cascade (*inside-out signalling*). The actin severing protein cofilin was demonstrated to be crucial for directed actin polymerization at the leading edge and may also contribute to ARP2/3 priming which can be alternatively achieved via *de-novo* actin nucleation (SPIRE/COBL/JMY) or the SPIN90 protein.

The acquisition of hallmarks that equips tumour cells with the capability of invasion and metastasis marks the transition from a benign to a malignant tumour [2]. The generation of migratory and invasive structures in tumour cells of epithelial origin (carcinoma cells) depends on a developmental program termed the Epithelial Mesenchymal Transition (see also 1.1) which is orchestrated by intracellular signals (master transcription factors) as well as the ECM (integrins) and the TME (i.e. cytokines, growth factors) [207], [208], [209]. The process of EMT is associated with major changes in the gene expression profile of carcinoma cells which results in a fibroblast-like appearance of the respective cells and their ability to dissect from the cell community and form actin-rich invading or migratory structures (invadopodia, lamellipodia, membrane ruffles and filopodia) [207], [209]. Lamellipodia and invadopodia are highly similar in their capability to produce the force necessary to move the cell body forward but invadopodia do possess the additional potential of matrix degradation. Invasion through the ECM and subsequent intravasation therefore depends mostly on the formation of invadopodia. Of note, invadopodia are exclusively found in malignant tumour cells. Certain healthy cells (i.e. macrophages, dendritic cells and osteoclasts) establish so-called podosomes which permit matrix degradation as well but differ from invadopodia in certain aspects (i.e. morphology) [210], [211], [212], [213], [214]. Filopodia do not generate force but are involved in sensing biochemical or biophysical gradients (i.e. chemotaxis, haptotaxis, electrotaxis, durotaxis) and responding adequately to them (cell polarization and directed movement) [215], [216], [217]. Filopodia are thin and linear cell protrusions which originate from lamellipodia and are characterized by unbranched but bundled actin filaments. The formation of filopodia relies on actin elongation via ENA/VASP proteins (see below) and actin bundling via the actin bundling protein fascin [218], [219]. Fascin becomes upregulated during EMT and is highly expressed in invasion and metastasis establishment but undetectable in primary tumours, healthy tissues and established metastases [220], [221], [222]. The expression of fascin in carcinoma cells is associated with a poor prognosis [220], [223], [224], [225], [226], [227], [228].

Cell movement is a cyclic process of (1) integrin-mediated attachment of the cell front or leading edge (lamellipodia/invadopodia) to the ECM dependent on RAC or CDC42 members, (2) RHO-GTPase (RAS Homologue) induced contraction of the actomyosin stress fibres of the cell body (rear edge) and (3) deadhesion of the cell body and novel adhesion of the leading edge [229], [216]. Lamellipodia are flat highly branched structures whereas invadopodia are more finger-like in appearance to enable focused release of ECM degrading enzymes. Both structures are characterized by the presence of a branched actin-network including a set of actin regulatory proteins (the actin nucleator ARP2/3, nucleation promoting factors, small GTPases, actin elongators, integrin adaptor molecules and *upstream* regulatory proteins such as PI3K or RTKs) [209], [230], [231], [212], [213], [210], [211], [214].

Integrins signal to the actin cytoskeleton of lamellipodia and invadopodia through intracellular adaptor proteins such as paxillin. Paxillin coordinates the activity status of RAC (in lamellipodia) or CDC42 (in invadopodia) in a spatiotemporal manner [232], [233], [234], [235], [236], [237], [238]. RAC/CDC42 acts in concert with the PI3K dependent generation of PtdIns(3,4,5)P_3 to recruit the WAVE (in lamellipodia) respectively the WASP or N-WASP (in invadopodia) complex to the plasma membrane for activation [239], [240], [241], [242]. WAVE and WASP/N-WASP are highly homologous in their composition and their modes of activation and action and therefore only the WAVE complex will be discussed in detail. The WAVE (WASP family Verprolin homologous protein) complex is a heteropentamer comprising HSPC300 (Hematopoietic Stem/Progenitor Cell protein 300, also known as BRICK1), SRA1 (Steroid Receptor RNA Activator 1, also known as CYFIP1), PIR121 (p53 Inducible protein 121, also known as CYFIP2), NAP1 (Nucleosome Assembly Protein 1) or HEM1 (Hematopoietic protein 1) and WAVE-1, -2 or -3 [243], [244], [245], [246], [247]. WAVE possesses an ARP2/3 activating WCA (WASP Homology 2 (WH2), Connecting/Central domain, Acidic domain) in addition to its actin binding verprolin domain. In the resting state, the WCA domain is autoinhibited by SRA1 and the N-terminus of WAVE rendering the complex inactive and cytosolic [239], [248], [249]. Upon the presence of positive regulatory signals cells become enriched in RAC-GTP and PtdIns(3,4,5)P_3. RAC-GTP was shown to directly associate with SRA1 and WAVE albeit at low (µM) affinity which requires for the spatiotemporal enrichment of RAC-GTP by PtdIns(3,4,5)P_3 dependent RAC-GEFs (see 1.3.2.). i.e. P-REX1 (PtdIns(3,4,5)P_3 dependent RAC Exchanger 1) or VAV1 [230], [239], [241], [250]. Following its recruitment to the leading edge plasma membrane WAVE is phosphorylated at Y151 (WAVE-1, WAVE-3) respectively Y150

(WAVE-2) by ABL (Abelson) which exposes the WCA domain [239], [251], [252], [253]. Alternatively, WAVE may become activated by GPCRs, lamellipodin (LPD) or small GTPases of the ARF (ADP Ribosylation Factor) family. GPCRs exhibit a WIR (WAVE complex Interacting Regulatory) motif which associates with SRA1 [254]. LPD is recruited to the plasma membrane by PtdIns(3,4)P_2 or RAC in a PH domain or Ras Association (RA) domain dependent manner. It comprises a number of protein interaction motifs within its proline rich C-terminal region including eight SH3 binding PXXP motifs, three profilin binding motifs and six EVH1 binding motifs for the association with ENA/VASP proteins [255]. LPD directly interacts with the SH3 domain of the WAVE associated adaptor protein ABI1 (ABL Interactor 1) which is enhanced upon complex formation with RAC-GTP [256], [257], [258]. *knock-down* of *LPD* resulted in loss of directional migration and impaired lamellipodia formation in MDA-MB-231 breast cancer cells and Rat2 fibroblasts phenocopying *knock-down* of the WAVE complex [255], [259]. *lpd* mice are mostly unviable and surviving mice are reduced in size and miss ventral pigmentation due to defective migration of melanoblasts providing evidence for a crucial *in vivo* function of LPD in migration [131]. A role for LPD as a promotor of cell migration was concordantly found in *Xenopus laevis* and *Drosophila melanogaster* [255]. ARF-6, ARF-1 and the ARF-6 specific GEF ARNO (ARF Nucleotide binding site Opener) were demonstrated to localize to the leading edge of invadopodia and lamellipodia and to be crucial for their formation and function. Moreover, expression levels of ARF-1, ARF-6 and ARNO were increased in invasive cancer cells [260], [261], [262], [263], [264], [265], [266], [267]. Liposomes containing ARF-6 and ARNO recruited ARF-1 and the WAVE complex and it was concluded out of these experiments that ARNO would act as an *upstream* activator of ARF-6 which in turn would activate and recruit ARF-1 which would positively impact the WAVE complex [268].

The WAVE or WASP/N-WASP complex are responsible for activating the ARP2/3 (Actin Related Protein 2/3) actin nucleator complex and are therefore classified as Nucleation Promoting Factors (NPFs). In concert with the WAVE/WASP/N-WASP complex ARP2/3 associates with an existing actin filament imitating a 3 G-actin (globular actin) containing actin nucleation core. ARP2/3 dependent nucleation initiates the formation of new actin filaments branching from the main filament in an angle of 70° [269], [270]. Subsequently, these branches are elongated by actin elongators of the ENA/VASP family or the formins mDIA2 (mammalian Diaphenous 2) and FMNL2 (Formin-Like 2) [271], [272], [273], [274], [275], [276], [277], [278], [279], [280], [281]. The ENA/VASP proteins MENA (Mammalian Enabled, also known as ENAH (Enabled Homologue of *Drosophila melanogaster* ENA)), VASP and EVL (ENAH/VASP-Like) localize to the leading edge of lamellipodia and invadopodia and the tips of filopodia [282], [283], [284]. In addition, there are strongly upregulated in carcinoma cells whereas almost undetectable in healthy epithelial cells and this was linked to EGF (Epithelial Growth Factor) signalling in mammary carcinoma [285], [286], [287], [288]. ENA/VASP proteins promote the elongation of actin filaments through their protection from capping and recruitment of ATP-G-actin to profilin [271], [272], [273,289], [274], [275], [276], [289]. The ARP2/3 complex is a heteroseptamer of ARP2, ARP3 and ARPCs1-5 (Actin Related Protein 2/3 Complex subunits 1-5). It localizes to lamellipodia and invadopodia and is upregulated in malignant and invasive cancers [290], [231], [288], [291], [292], [293], [294], [295]. The delivery of actin filaments required for the formation of new branches is called *ARP2/3 priming*. Three mechanisms of *ARP2/3 priming* were described: (1) severing of pre-existing actin filaments by cofilin, (2) *de novo* nucleation of actin catalysed by the actin nucleators SPIRE, COBL (Cordon Bleu WH2 repeat protein) and JMY (Junction Mediating and regulatory protein, p53 co-factor) and (3) clustering of ARP2 and ARP3 mimicking a free actin (+) end and therefore promotion of ARP2/3 activation without the need for any pre-existing actin filaments mediated by SPIN90 (SH3 domain containing Protein Interacting with NCK1, 90 kDa) [296], [297], [270], [298]. The inactivation of the ARP2/3 complex requires either the presence of coronins or acidic-motif containing proteins. Coronins mediate the inhibition of ARP2/3 through active debranching, sequestration of inactive ARP2/3 complexes or decoration of existing actin filaments to hinder their accessibility to ARP2/3 [299], [300], [301]. Following the stimulation of cells with adequate growth factors, coronins become phosphorylated and inactivated and this is required for growth factor dependent cell motility [302], [303]. The acidic motif containing proteins ARPIN (ARP2/3 Inhibitor) and PICK1 (Protein Interacting with PRKCA 1) compete with the WCA domains of NPFs for the binding to ARP2/3 to reduce the pool of active ARP2/3 rather than actually inactivate the complex [304], [305], [306].

In cells exhibiting migratory or invasive characteristics, a carefully regulated balance concerning branching and elongation of actin is upheld and this is paramount for the rapid generation of new stable migratory or invasive structures in order to respond quickly to ingoing signals. Overactivation of branching (WAVE/WASP/N-WASP) over elongation (ENA/VASP, formins) results in stable but overly slowly forming structures whereas overactivation of elongation over branching leads to fast forming but highly unstable structures [230], [271]. The coordination of these processes may be achieved by LPD which is able to associate with both NPFs and ENA/VASP proteins [307], [308].

The Actin Depolymerisation Factor (ADF) cofilin is implicated in the severing of existing actin filaments, a process required for subsequent directed actin polymerization (re-distribution of the actin pool) and therefore migration [231], [309]. Cofilin is inhibited by PtdIns(4,5)P_2 which is abolished upon PLC (Phospholipase C) catalysed cleavage of PtdIns(4,5)P_2. In parallel with PLC mediated activation, cofilin is inhibited by a LIM domain Kinases 1 and 2 (LIMK1,-2) dependent phosphorylation on S3 which is reversed by PP1, -2A, -2B, slingshot or chromophin phosphatases [310], [311], [312], [313], [314], [315], [316], [317], [318], [319], [320]. The regulatory events leading to activation or inactivation of cofilin are tightly regulated in a spatiotemporal manner in order to allow a localized burst of new actin filaments at the leading edge [316], [321]. In concert with this proposition of a requirement for balanced cofilin activation and inactivation for migration/invasion stands the observation that overexpression of either LIMK or cofilin impaired the formation of migratory/invasive structures and reduced cell migration and invasion [322], [323].
The cortactin protein plays a role in actin crosslinking and stabilization and is a key player in lamellipodia and especially in invadopodia formation and function [231], [324], [325], [326], [327]. Cortactin comprises an N-terminal acidic domain binding to and weakly activating ARP2/3 via a conserved DDW motif and an actin binding motif [328], [324]. The cortactin gene *CTTN* was amplified in mammary carcinoma, bladder cancer and HNSCC (Head and Neck Squamous Cell Carcinoma) and this was correlated to enhanced invasiveness and metastasis and a poorer patient outcome [329], [330], [331].
The generation of a branched actin network in invadopodia and lamellipodia is regulated by *feedback* and *feed-forward* loops which mostly centre around RAC/CDC42 [230], [332], [333].

1. *feed-forward*: The activation of RAC/CDC42 is increased in the presence of F-actin the generation of which is positively influenced by RAC/CDC42. This ensures sustained actin polymerization [271], [289], [334], [335], [336], [337], [338].
2. *feed-forward*: interdependence of RAC/CDC42 and PI3K (PtdIns(3,4,5)P_3) leading to the sustained presence of PtdIns(3,4,5)P_3 and RAC/CDC42-GTP and sustained activation of NPFs and ARP2/3 [242], [339].
3. *feedback*: Hyperactivation of RAC/CDC42 results in disorganized migration/invasion without the characteristics for directional persistence [340]. Therefore, RAC/CDC42 are kept in check by negative *feedback* loops involving the LPD- and NPF-dependent activation of GAPs (i.e. srGAP3 in the case of RAC). srGAP3 was described as a RAC-specific GAP. It localizes to the leading edge membrane via its F-BAR domain and is recruited to the WAVE/LPD/RAC complex via its SH3 domain. In NIH-3T3 cells stimulated with PDGF (Platelet Derived Growth Factor) srGAP3 overexpression abolished the generation of lamellipodial protrusions and counteracted the effects of LPD overexpression and conversely *srgap3* MEFs displayed enhanced lamellipodia formation which was reversed by concomitant *knock-down* of *LPD*. The negative effects of srGAP3 on the WAVE/LPD/RAC complex were partly dependent and partly independent on its GAP activity [257], [341].

As drafted above, invadopodia differ from lamellipodia in their ability to secret matrix degrading enzymes [212], [210], [211], [213], [214]. ECM degradation mainly relies on Matrix Metalloproteases (MMPs) i.a. MT1-MMP (Membrane Type 1 Matrix Metalloprotease), members of the ADAM (A Disintegrin And Metalloproteinase) family i.a. ADAM12, -15 and -19 and the serine protease seprase [342]. Seprase was observed to be specifically upregulated in mammary carcinoma and melanoma cells but to be absent in healthy tissue and to be activated by β1-containing integrins in a collagen dependent manner [343], [344]. Similarly, the disintegrin domain of ADAMs associates with integrins (especially β1-containing integrins) [345]. The focused release of proteases or more specifically the directional targeting of proteases to the leading edge/to invadopodia was proposed to be dependent on cortactin and intracellular vesicle trafficking via the Golgi apparatus. In *time-lapse imaging* experiments the cortactin dependent formation of invadopodial core structures preceded the directed transport of proteases to the leading edge membrane and depletion of cortactin resulted in a reduction of the proteolytic activity of invadopodia [346]. With respect to intracellular trafficking processes, invadopodia typically localize close to the golgi apparatus and the brefeldin A induced inhibition of intracellular trafficking was shown to reduce the matrix degrading potential but not to affect the general structure of invadopodia [291], [347], [348]. Cholesterol-rich lipid rafts the generation of which being dependent on caveolin-1 may guide intracellular protease-containing vesicles to their place of destination [349]. The secretion of proteases may depend on the exocyst complex tethering exocytic vesicles to the plasma membrane or the v-SNARE (vesicle Soluble N-ethylmaleimide sensitive factor Attachment Receptor) VAMP7 (Vesicle Associated Membrane Protein 7) mediating vesicle fusion processes [350], [351], [352].

1.3.1. The RHO-GTPase family

RHO-GTPases are one of the clades of the RAS superfamily of small GTPases and are further subdivided into six classes: RAC (RAC1, RAC2, RAC3, RHO-G), RHO (RHO-A, RHO-B, RHO-C), CDC42 (CDC42, TC10, TCL,

CHP/WRCH-2, WRCH-1), RHO-BTB, RND and RHO-T [353]. The different subfamilies are implicated in different cellular functions i.e. regarding their influence on the actin cytoskeleton RAC-GTPases function in the formation of lamellipodia and membranous ruffles, CDC42 is involved in the formation of invadopodia, podosomes and filopodia and RHO plays a role in stress fibre generation [354], [355], [356], [357]. In addition, all RHO GTPase subfamilies are linked to the regulation of cell growth, survival, proliferation, metabolism and gene expression and also to tumorigenesis [358], [359].
Small GTPases are similar to heterotrimeric G-proteins in their capability to switch between an active (GTP-bound) and an inactive (GDP-bound) state [360]. The nucleotide binding site is located in the P-loop (Phosphate Binding loop) of the G1 domain. A conserved GXXXXGKS/T motif mediates the coordination of the Mg^{2+} stabilized γ- and β-phosphates [361], [362]. The transition between the GTP- (tense state) and GDP- (relaxed state) bound state is associated with a conformational change in the G1 domain which is transferred to the switch I and switch II region of the protein where the switch regions are responsible for the interaction with effector proteins. This is referred to as the *loading spring mechanism* [363], [364], [365], [361]. Transitory events between an active and an inactive state are described by the term GTPase cycle and are regulated by three key players.

1. Guanine nucleotide Exchange Factors (GEFs): facilitate the transition from a GDP- to a GTP-bound state by stabilizing the nucleotide free state (equal to the transitory state of the reaction) of the protein. The nucleotide-free state exhibits comparable affinities to GDP and GTP, however as the concentration of free GTP exceeds that of free GDP ~10-fold the incorporation of GTP is favoured [366], [367].
2. GTPase Activating Proteins (GAPs): induce the hydrolysis of GTP by activating the intrinsic GTPase activity of the small GTPase [368], [369], [370].
3. Guanine nucleotide Dissociation Inhibitors (GDIs): prevent the activation of small GTPases by masking their lipid moiety therefore forestalling their recruitment to GEF containing membranes and by actively recruiting inactive GTPases to the cytosol [371], [372].

Small GTPases are furthermore regulated by Posttranslational Modifications (PTMs) [362]. The addition of a lipid moiety to the GTPase is paramount for all GTPases as it enables their recruitment to membranes [373], [374]. The prenylation event is irreversible and catalysed by either farnesyl- or geranyl-geranyl transferases [362]. The lipid anchor is located at the very C-terminus of the protein at a conserved cysteine within the consensus sequence CAAX. Prenylation is typically followed by shedding of the AAX sequence and cysteine carboxymethylation and may be ensued by S-palmitoylation which was described to enhance the stability of the protein in some cases [375], [376], [377], [378], [379], [380]. Phosphorylation may have differential impacts depending on the localization of the PTM: Phosphorylation at the C-terminus may result in an altered subcellular localization whereas phosphorylation in the G1 domain or the switch regions may affect the GTPase cycling or the interaction with *downstream* effector proteins [362]. Other common PTMs are ubiquitination and sumoylation [362], [381], [382].

1.3.1.1. RAC (RAS related C3 botulinum toxin substrate)

The RHO-GTPase subclade RAC consists of ubiquitously expressed RAC1 and RHOG, hematopoietic RAC2 and neural RAC3 [250]. RAC1 was found to be overexpressed in numerous carcinoma entities (mammary, prostate, lung, gastric carcinomas) and this was correlated with enhanced aggressiveness, invasion and metastases and reduced patient overall survival [383], [384], [385], [386], [387]. The constitutively active splice variant of RAC1, RAC1b is marked by the additional exon 3b and was demonstrated to be abundantly expressed in cases of mammary or colorectal carcinoma but not in healthy tissue [388]. RAC1b exhibits a reduced affinity to GDIs as well as a heightened activity [389]. In a HNSCC mouse model, RAC1b was not sufficient to drive tumorigenesis on its own but to enhance the activity of the driver oncogene onco-k-RAS [390]. RAC1 P29S is a fast cycling mutant exhibiting faster GDP to GTP exchange but retaining its GTPase activity. The mutation is located in the switch I region [391], [392], [393], [394]. Equivalent mutations were found in RAC2 (P29L) and RAC3 (P29Q) [391], [394].
In addition to genetic alterations of the *RAC* gene itself, RAC may become hyperactivated by the misregulated expression and/or activation of *upstream* regulator proteins (i.e. overexpression of RAC-GEFs, downregulation or inactivation of RAC-GDIs or RAC-GAPs) [395], [396], [397], [398].

1.3.2. PtdIns(3,4,5)P_3 dependent Guanine Nucleotide Exchange Factors (GEFs)

As demonstrated in several independent pharmacological and genetic studies there is an interdependence of PI3K and small GTPases of the RHO family, especially the RAC subfamily of RHO-GTPases [399]. RHO-GTPases are positively influenced in their activity status by PtdIns(3,4,5)P_3 which is mainly due to the PtdIns(3,4,5)P_3 dependent recruitment of a number of RHO-GTPase specific GEFs to the plasma membrane [354]. The RHO-GTPase GEFs in question were demonstrated to associate with PtdIns(3,4,5)P_3 albeit at a low affinity. This suggests that additional

mechanisms may be required for the efficient membrane targeting of PtdIns(3,4,5)P_3 dependent GEFs i.e. Protein Protein Interactions [250], [400].
In general, there are two classes of RHO-GEFs: The DBL (Diffuse B-cell Lymphoma) family is characterized by a conserved DH-PH (DBL Homology-Pleckstrin Homology) tandem domain (see 1.3.2.1.) and in the atypical DHR2/CZH2 (DOCK Homology Region 2/CDM-Zizimin Homology 2) family the DH domain is replaced by a DHR2 or CZH2 domain (see 1.3.2.2.). The DH- respectively the DHR2/CZH2 domain is responsible for the RHO-GEF activity of the protein [401], [402], [403], [404].
RHO-GEFs are frequently classified as proto-oncogenes and implicated i.a. in the promotion of invasiveness and metastasis [398]. The DBL-RHO-GEF ECT2 (Epithelial Cell Transforming 2) was officially acknowledged as an oncogene in 2010 [405]. MYO-GEF (Myosin interacting GEF) was shown to enhance the invasiveness of mammary carcinoma cells [406]. β-PIX (β p21 activated kinase Interactive exchange factor) was found to be overexpressed in mammary carcinoma [407] and VAV1 was overexpressed in pancreatic, mammary and adenocarcinoma and this was linked to a poor prognosis [408], [409]. P-REX1 overexpression is common in cases of mammary carcinoma [410] and P-REX2 is frequently mutated in melanoma [411]. TIAM1 (T-cell lymphoma Invasion And Metastasis 1) impacts the invasive potential of T-cell lymphomas and the progression of mammary, prostate, lung and adenocarcinoma [385], [409], [412], [413], [414]. The cellular levels of TIAM1 inversely correlated with the expression levels of the TIAM1 specific E3-ubiquitin ligase HUWE1 (HECT, UBA and WWE containing 1) [414]. A role for RHO-GEFs in cancer progression was also confirmed in mouse models [415], [416], [417], [418], [419], [420], [421].

1.3.2.1. DBL family RHO-GEFs

The 69 members-comprising DBL family of RHO-GEFs is characterized by a central DH-PH tandem domain. The DH domain is responsible for the RHO-GEF activity whilst multiple functions for the PH domain have been proposed depending on the DBL-GEF in question [401]. DBL-GEFs stabilize the nucleotide free state of their target GTPases through disruption of the nucleotide binding pocket. This is achieved by extensive interactions between the DH domain of the DBL-GEF and the switch regions of the GTPase. Induced remodelling of the switch I region disorders the nucleotide binding site and conformational changes in the switch II region affect the Mg^{2+} coordination site [401]. Case-dependent, the PH domain is involved in assisting the DH domain in small GTPase binding (i.a. DBS (DBL's Big Sister), in serving as a membrane anchor (i.a. SOS1 (Son Of Sevenless 1), DBS, TIAM1, VAV1), in autoinhibition of the protein (i.a. SOS1 where the autoinhibition is relieved through binding of the PH domain to PtdIns(3,4,5)P_3), in the allosteric activation of the DH domain (i.a. DBL, P-REX1) or in protein protein interactions (i.a. TRIO (Triple functional domain (PTPRF interacting) and DBL) [401], [422], [423], [424], [425], [426], [427], [428], [429], [430], [431], [432].

1.3.2.1.1. VAV Guanine Nucleotide Exchange Factors

There are three members forming the VAV subfamily of DBL RHO-GEFs. VAV1 is hematopoietic-specific whereas VAV2 and VAV3 are ubiquitously expressed [433], [434]. The three VAV proteins share a common domain structure of a DH-PH domain, an SH3 domain, two SH2 domains and a proline rich domain and an autoinhibitory region at the N-terminus comprising an acidic (Ac) and a CH (Calponin Homology) domain [435]. The SH3 domain, the two SH2 domains and the proline rich domain are responsible for the mediation of protein protein interactions. In the inactive state the protein adopts a "closed" conformation with the RHO-GTPase binding pocket being blocked by a conserved tyrosine (Y174 in VAV1) [436]. The PH domain of VAV1 weakly associates with PtdIns(3,4,5)P_3 which was proposed to expose Y174 to suitable kinases of the LCK (Lymphocyte Cell specific Kinase) or the SRC (Sarcoma) family. Phosphorylation of Y174 results in a conformational change which reliefs autoinhibition [437]. First evidence for a putative role of VAV1 in promoting tumorigenesis came from studies identifying a VAV1 mutant truncated of 67 N-terminal amino acids to be constitutively active and transforming [438], [439]. Of note, hematopoietic VAV1 was found to be ectopically expressed in several carcinoma entities further underlining its oncogenic potential [408], [409].

1.3.2.1.2. Phosphatidyl inositol-3,4,5-trisphosphate dependent RAC Exchanger (P-REX)

The subfamily of P-REX DBL-GEFs holds specificity for RAC GTPases and comprises three members: P-REX1, P-REX2A and its splice variant P-REX2B. P-REX2A and P-REX1 share high sequence identity (56% at the protein level). P-REX2B is a shortened isoform lacking the C-terminal IP4P (Inositol Polyphosphate-4-Phosphatase-like) domain [429], [440], [441]. The expression of P-REX1 is especially high in neutrophils but expression is also observed in peripheral blood cells in general, endothelial cells, neurons and platelets. P-REX1 is most decisive in the regulation of inflammatory responses [429], [442], [443], [444], [445], [446], [447]. P-REX2A is mainly found in

the brain and less detectable in liver and adipose tissue [448], [449]. The expression of P-REX2B is restricted to endothelial cells and cardiac tissue [450], [451].
P-REX proteins contain the minimal DH-PH tandem domain in addition to two DEP (Dishevelled, EGL-10, Pleckstrin), two PDZ (PSD95, *Drosophila melanogaster* DLG1, ZO-1) and in the case of P-REX1 and P-REX2A an IP4P domain [429], [441], [450]. The DEP and the PDZ domains are responsible for the mediation of protein protein interactions. Furthermore, they confer autoinhibition to the DH domain [440], [452]. Although the IP4P domain was demonstrated to contain the crucial residues for inositol phosphate-4-phosphatase activity it does not seem to be catalytically active *in vivo*. Instead, a regulatory role for the IP4P domain is more likely [429], [451].
The activation of P-REX1 proteins is dependent on the synergistic signalling of PI3K ($PtdIns(3,4,5)P_3$) and GPCRs ($G_{\beta\gamma}$) which is unique in the RHO-GTPase specific GEF family [429], [440], [453]. The interaction between P-REX and $PtdIns(3,4,5)P_3$ relies on the DH-PH domain and that between P-REX and $G_{\beta\gamma}$ relies on the DH domain [452], [454]. $PtdIns(3,4,5)P_3$ increases the activity of the DH domain ~10-fold and in concert with $G_{\beta\gamma}$ ~50-fold [429]. It was suggested that this activating effect was due to an abrogation of the autoinhibitory state [452]. Comprehensively, $PtdIns(3,4,5)P_3$ and $G_{\beta\gamma}$ were approved to be both necessary and sufficient for the activation and also for the membrane recruitment of P-REX [429], [440], [453], [454], [455]. Regarding P-REX1 $PtdIns(3,4,5)P_3$ dependent activation was fully dependent on the GPCR stimulated p110 isoform p110γ [456]. Furthermore, P-REX1 was responsible for the transformation of mammary carcinoma cells following stimulation with the EGFR ligand HRG (Heregulin). Two mechanisms of an alternative activation of P-REX1 through RTKs were proposed: (1) transactivation of the GPCR CXCR4 (CXC motif chemokine Receptor 4) by HRG/EGFR and subsequent release of $G_{\beta\gamma}$ and (2) increase of the $PtdIns(3,4,5)P_3$ pool through direct activation of PI3KIA by EGFR dependent signal transduction [440], [456].
Another layer of P-REX regulation is via PTMs. P-REX proteins are target to an inactivating PKA (Protein Kinase A) dependent phosphorylation and an activating dephosphorylation catalysed by PP1α (Protein Phosphatase 1α) [453], [457], [458], [459]. P-REX1 purified from cytosol preparations exhibited a migratory behaviour similar to that observed for PKA phosphorylated P-REX1 whereas the migratory behaviour of P-REX1 purified from membrane preparations was comparable to PP1α dephosphorylated P-REX1. This culminated in the conclusion that the phosphorylation status of P-REX1 might dictate its intracellular localization or more specifically its access to membranous $PtdIns(3,4,5)P_3$ and $G_{\beta\gamma}$ [454], [459].
P-REX proteins are acknowledged for their role in cancerogenesis. Both P-REX1 and P-REX2 frequently show ectopic expression or mutation in cancers [460]. In healthy cells, the expression of P-REX1 is negatively regulated by the HDAC:SP1 (Histone DeACetylase: Specificity Protein 1) complex. The *P-REX1* promotor region is marked by the presence of an SP1 transcription factor binding site. Site-specific association of SP1 to the *P-REX1* promotor recruits HDAC which leads to histone H4 deacetylation and the repression of gene expression. Metastatic prostate carcinoma cells re-expressing P-REX1 contained less HDAC at the *P-REX1* promotor underlining the functional relevance for acetylation/deacetylation events in the regulation of P-REX1 expression [461]. Ectopic expression of P-REX1 is found in numerous cancers (i.e. thyroid, colorectal, prostate and kidney carcinoma) and most decisively in mammary carcinoma [410], [417], [456]. Immunohistological studies revealed an expression of P-REX1 in ~50% of the analysed mammary carcinoma samples whereas healthy breast tissue comprehensively stained negative for P-REX1. Of note, the expression of P-REX1 was restricted to the actual tumour cells but not found in the TME and enhanced in invasive and metastatic tumours [456]. miR-338 specifically suppresses the levels of P-REX2 and loss of miR-338 is common in several cancer entities amongst them gastric cancer and metastatic neuroblastoma [462], [463]. Data base analysis revealed mutations of the *P-REX2* gene in 14% of the tested melanoma samples (i.e. the confirmed oncogenic mutations K278*, E824*, G884D and Q1430*) [411]. Furthermore, P-REX2 was identified as a negative regulator of PTEN which was dependent on its DH-PH domain but independent on its RAC-GEF activity [448], [464]. Importantly, a synergistic interplay of PI3K and P-REX2 in the promotion of tumorigenesis (i.e. AKT phosphorylation and *downstream* signalling, RAC-dependent migration) was approved in PTEN expressing MCF-10 A cells but not in PTEN deficient BT-549 cells suggesting that the contribution of P-REX2 to tumorigenesis was dependent on the presence of PTEN [464].

1.3.2.2. DOCK Homology Region 2/CDM-Zizimin Homology 2 (DHR2/CZH2) RHO-GEFs

The DOCK family of atypical RHO-GEFs counts eleven members in humans which dispense to four subfamilies: DOCKA (DOCK180, DOCK2, DOCK5), DOCKB (DOCK3, DOCK4), DOCKC (DOCK6, DOCK7, DOCK8) and DOCKD (DOCK9, DOCK10, DOCK11) [465], [466]. DOCKA and DOCKB members are specific for RAC [404], [465], [467], [468], [469] and DOCKD proteins are specific for CDC42 [466], [470]. The substrate specificity of DOCKC is not known [465], [466].

DOCK proteins are widely expressed in the eukaryotic clade. In contrast to DBL family proteins DOCK proteins do not contain the classical DH domain but the DHR2 (CZH2) domain confers their GEF activity instead [404], [465], [466]. A working model for the function and regulation of DOCK proteins was first developed from studies performed in the model organism *Caenorhabditis elegans*. CED-12 (Cell Death 12), the homologue to human mELMO (mammalian Engulfment and cell Motility), CED-5 (Cell Death 5), the homologue to human DOCK180 and CED-2 (Cell Death 2), the homologue to human c-CRK (CT10 Regulator of Kinase) were identified as *upstream* regulators of CED-10 (Cell Death 10), the homologue to human RAC in the mediation of apoptotic cell engulfment and cell migration [471], [472], [473], [474], [475]. Later, it was shown that mELMO and c-CRK increased the DOCK180 dependent activation of RAC in human cell culture [404], [471], [476]. Mechanistically, c-CRK is an SH3/SH2 domain containing adaptor protein which is recruited to the leading edge membrane through the adaptor p130CAS (protein of 130 kDa, CRK associated Substrate) and assembles DOCK180 and mELMO [477], [478]. The multidomain scaffold protein mELMO is characterized by the presence of a number of Armadillo repeats (ARMs) which realise protein protein interactions, an atypical PH domain and a Proline Rich Region (PRR) [479]. mELMO is crucial for the activity of DOCK180 *in vivo* [404], [480]. For the *in vivo* function of mELMO a so-called bipartite GEF model was suggested stating that mELMO might contribute to the RAC-GEF activity of DOCK180 by (1) stabilizing the nucleotide free state of the DOCK180:RAC complex during the exchange reaction dependent on its PH domain, (2) relieving the SH3 domain dependent autoinhibitory state of DOCK180 through association of the mELMO PRR (PXXP motif) with the DHR2 domain and (3) facilitating the recruitment of DOCK180 to the plasma membrane through the interaction of its ARM repeats with membrane-associated RHO-G [476], [479], [480] [481], [482], [483], [484]. The DHR2 domain of DOCK180 associates with PtdIns(3,4,5)P_3 and this was identified as decisive for RAC-GEF activity *in vivo* but dispensable in *in vitro* experiments [485], [486]. A construct where the DHR2 domain was replaced by a canonical PH domain was equally efficient to mediate RAC dependent migration suggesting that PtdIns(3,4,5)P_3 contributed to the *in vivo* activation of DOCK180 due to its functional role in recruiting DOCK180 to the plasma/leading edge membrane but did not act as an allosteric regulator of DOCK180 [479], [486].

1.4. Phosphoinositide phosphatases

Phosphoinositide and inositol phosphate dependent signal transduction is highly dynamic and the levels of the different signalling molecules are regulated by a vast pool of enzymes i.e. phospholipases (i.a. PLC), phosphoinositide/inositol phosphate kinases (i.a. PI3K) and phosphoinositide/inositol phosphate phosphatases (i.a. PTEN, SHIP1, SHIP2, INPP4A, INPP4B). The ability to rapidly convert members of the phosphoinositide/inositol phosphate family into each other and thus to shift the balance of the existing phosphoinositide/inositol phosphate pool is paramount to rapidly adapt to varying extracellular conditions and to adequately respond to them. The enzymes in question are also often targets of (genetic) alterations or misregulation in cancers [63], [64].

1.4.1. Phosphatase and Tensin Homologue (PTEN)

PTEN is a phosphoinositide-3-phosphatase and a highly prominent tumour suppressor [105], [487], [488]. The tumour suppressor function of PTEN is mostly attributed to its ability to convert the oncogenic *second messenger* PtdIns(3,4,5)P_3 into PtdIns(4,5)P_2 but also its protein phosphatase activity and its impact on p53 may be of relevance [489], [490], [491]. PTEN is found amongst the most frequently altered tumour suppressor proteins in spontaneously developing cancers in addition to p53 and RB [492], [493] and germline mutations of *PTEN* are associated with a number of heritable syndromes marked by their enhanced susceptibility to tumour acquisition (i.e. Bannayan-Zonana syndrome, Cowden syndrome) [494], [495].
PTEN is a dual specificity phosphatase which specificity for PtdIns(3,4,5)P_3/PtdIns(3,4)P_2 (lipid phosphatase activity) and acidic peptides (protein phosphatase activity) [489], [490]. The lipid and the protein phosphatase activity are executed by the same domain (phosphatase domain) [490], [496], [497]. The phosphatase domain comprises a Protein Tyrosine Phosphatase (PTP) signature motif of the consensus sequence HCXXGXXR where X represents any amino acid. Compared to conventional PTPs, the consensus motif of PTEN is unusually basic which explains its specificity for acidic lipids and peptides. Furthermore, the binding pocket of PTEN is markedly wide helping to accommodate PtdIns(3,4,5)P_3. In a previous publication, Ins(1,3,4,5)P_4 was modelled into the crystal structure of PTEN in complex with L(+)-tartrate. T167 and Q171 residing in the TI loop were identified to putatively interact with the D4 and the D5 phosphate, K125 and K128 of the HCXXGXXR motif to interact with the D1 and the D5 phosphate and H93 within the WPD loop to contact the D5 phosphate. Mutating any of this candidate residues significantly affected the lipid phosphatase activity towards PtdIns(3)P, PtdIns(3,4)P_2 and PtdIns(3,4,5)P_3 but substituting K128 with a methionine (K128M) or H93 with an alanine (H93A) specifically reduced the activity of PTEN towards PtdIns(3,4,5)P_3 further solidifying the proposal of H93 and K128 being implicated in the recognition

of the D5 phosphate [498], [497]. The protein phosphatase activity of PTEN seems to influence multiple signal transduction pathways attributed to cancerogenesis. A PTEN mutant lacking protein phosphatase activity but retaining lipid phosphatase (G129E) activity negatively affected cell migration but not cell proliferation whereas a mutant lacking both activities (C124) failed in regulating neither migration nor proliferation. Out of this it was concluded that the protein phosphatase activity of PTEN was decisive in cell migration but dispensable for cell proliferation [499], [498], [500]. Due to electrostatic interactions the basic protein PTEN is recruited to acidic membranes enriched in PtdIns(4,5)P_2 and phosphatidyl serine (PtdSer) [498], [501], [502], [503], [504], [505], [506] which enhances the absolute activity level of the PTEN pool towards its main substrate PtdIns(3,4,5)P_3 by sequestering them away from the cytosol and to the plasma membrane and by additional allosteric activation of PTEN by PtdIns(4,5)P_2 [498], [501], [502], [503], [504], [505], [506]. In addition to its catalytic domain PTEN comprises a C2 domain and a C-terminal domain. The C2 domain is halfway segmented by a flexible loop region [498]. The C-terminal region comprises a PDZ domain, two PEST motifs and several putative phosphorylation sites. It is majorly implicated in the regulation of the function and subcellular localization of PTEN [489].
PTEN is regulated in a complex manner regarding its expression, localization and activity. Levels of regulation are genetic alterations, epigenetic silencing, post-transcriptional regulation by small non-coding RNAs, PTMs and protein-protein or protein-lipid interactions [496]. Somatic mutations scatter along the entire PTEN gene with no *hotspot* mutations regarding individual cancer entities [492], [496]. Of note, there is a number of PTEN mutants which retain their enzymatic activity but are marked by decreased stability due to C-terminal truncations (see below) [507]. PTEN is epigenetically silenced in many cancers through methylation of its promotor but also through SALL4 (Spalt Like 4) dependent histone deacetylation [508], [509]. Furthermore, transcription factors positively (p53, PPARγ (Peroxisome Proliferator Activated Receptor γ)) [510], [511] or negatively (SNAIL, c-JUN, c-MYC) [496], [512], [513] affect the expression of PTEN. A clade of miRNAs (microRNAs) displays seed complementarity to the 3`UTR (Untranslated Region) of the *PTEN* gene [514]. Those include the miR-17 to miR-92 cluster in lymphoproliferative disorders, miR-19 in Cowden syndrome and miR-21 in numerous entities of spontaneously developing cancers [515], [516], [517], [518], [519]. The miRNAs are antagonized by the PTENP1 (PTEN Pseudogene 1) transcript which serves as a decoy sequestering the miRNAs away from PTEN transcripts [520]. Loss of PTENP1 is a common feature of prostate and mammary carcinomas correlating with decreased levels of PTEN despite no epigenetic or genetic alterations [520], [521]. With regard to PTMs ubiquitination and phosphorylation are most relevant [496]. The C-terminal region may become phosphorylated at T366/S370 by Casein Kinase 2 (CK2) and GSK3 and at a cluster of S380, T382, T383 and S385 by CK2 [522], [523], [524], [525]. Phosphorylation events at the 380-385 cluster resulted in a reduction of the enzymatic activity of PTEN and its membrane localization but enhanced its stability [524], [525]. The suggestion originating out of these observations was that the C2 domain interacted with the C-terminal region in a phosphorylation state dependent fashion in a way that phosphorylation of the 380-385 cluster resulted in the adoption of a “closed” conformation impeding substrate access, protein-lipid interactions and protein-protein interactions [524], [525]. Most importantly, the interaction between PTEN and the E3 ubiquitin ligase NEDD4-1 (Neural precursor cell expressed, Developmentally Downregulated 4-1) possibly was affected by this phosphorylation event which would favour the stability of phosphorylated PTEN. NEDD4-1 executes poly- and monoubiquitination of PTEN at K13 and K289. Monoubiquitination was demonstrated to shift the balance of cytosolic vs. nuclear localization of the cytosol-nucleus shuttling protein PTEN towards its nuclear localization. Of note, both K13 and K289 are susceptible to mutational events in spontaneously developing cancers and Cowden syndrome [526]. Furthermore, PTEN is regulated by the cellular redox status. It comprises two conserved cysteines (C71 and C124) engaging in a disulphide bond upon oxidation i.e. in the presence of Reactive Oxygen Species (ROS) which disrupts the active site. Typically, ROS levels are elevated in cancer cells which provides an additional level of downregulating the levels of active PTEN [527], [528]. The localization, activity status and stability is also shaped by protein protein interactions i.e. NHERF (Na^+/H^+ Exchanger Regulatory Factor) [529], [530] and MAGI2 (Membrane Associated Guanylate kinase Inverted 2) [531] associate which the PDZ domain and this was reported to increase the catalytic activity of PTEN, interaction of the C2 domain with ROCK1 (RHO associated Coiled coil containing protein Kinase 1) increased the stability of PTEN [532] whereas the PI3KIA subunit p85 negatively impacted the lipid phosphatase activity of PTEN thereby potentiating PI3KI dependent signal transduction and promoting tumour progression [524], [533].
PTEN and p53 do intensively communicate with each other in order to prevent tumour formation [489]. p53 transcriptionally upregulates the expression of PTEN and conversely p53 is stabilized by its association with PTEN in a *feed-forward* loop [510], [534], [535], [536]. p53 is called a *dormant gatekeeper* as it is almost undetectable in non-stressed healthy cells but strongly upregulated in stress situations i.e. DNA damage to prevent the acquisition of potentially dangerous genetic aberrations [489], [537], [538]. In contrast, PTEN is constitutively expressed in healthy cells to counteract unhealthily strong activation of PI3K dependent signal transduction events and found

downregulated in cancer cells (*default gatekeeper*) [489], [539], [540]. Of note a *fail-safe* mechanism to compensate for the loss of PTEN in early steps of tumorigenesis was identified: Loss of PTEN was described to trigger the expression of p53 via CHK1 substituting for the lost *gatekeeper* function of PTEN [541]. In consistence with this, complete loss of PTEN resulted in PICS (PTEN Induced Cellular Senescence) which is a special case of tumour suppressor induced cellular senescence and this state was upheld until concomitant loss of p53 [542], [543].

1.4.2. INPP4A/B

The related phosphoinositide-4-phosphatases INPP4A and INPP4B are critical regulators of intracellular phosphoinositide homeostasis by converting PtdIns(3,4)P_2 to PtdIns(3)P. Both molecules possess distinct *second messenger* capacities as will be described below [131].
INPP4A (107 kDa) and INPP4B (105 kDa) share a common domain architecture comprising an N-terminal lipid-binding C2 domain, a central stretch and the C-terminal phosphatase domain [544], [82], [545], [546]. The C2 domain mediates recruitment of INPP4 to the plasma membrane. The C2 domain of INPP4A was demonstrated to preferentially associate with PtdIns(3,4)P_2 and PtdInsSer to a lesser extent [547]. From studies of the murine INPP4B C2 domain it was deduced that the human INPP4B C2 domain would most likely bind to phosphatidic acid and PtdIns(3,4)P_2 [546]. The INPP4A central domain holds a PEST motif for its degradation by calpain which was not described for INPP4B [82], [548], [549]. In INPP4B an NHR2 domain (NERVY Homology Region 2) was identified as potential realisator of protein protein interactions and oligomerization [550], [551], [552]. The phosphatase domain comprises a CKSAKDRT motif conserved in dual specificity phosphatases. INPP4B was shown to possess both lipid- and protein tyrosine phosphatase activity. By mutational studies the cysteine residue was demonstrated to be essential for the lipid phosphatase activity of INPP4B. AKT Y176 was identified as target of the protein phosphatase activity. A number of studies provided evidence of AKT Y176 phosphorylation as a positive regulator for AKT activating mechanisms (T308/S473 phosphorylation and recruitment to the plasma membrane). Therefore, INPP4B would negatively impact the activity status of AKT in this context [83], [553].
INPP4B expression shows a wide tissue distribution whereas expression of INPP4A is mainly restricted to the brain [546]. INPP4A is a critical determinant of brain development and function by counteracting the PtdIns(3,4)P_2 dependent enhanced susceptibility of neuronal cells to the endotoxic component glutamate. *inpp4a weeble* (expressing a truncated form of INPP4A) or *inpp4a knock-down* mice develop severe neurodegenerative disorders [554], [555], [556].
INPP4B is implicated in osteoclast differentiation and most decisively in cancer development [557]. From studies having aimed to analyse the role for INPP4B in tumorigenesis there is evidence for both a potential oncogenic and tumour suppressor function dependent on the context [558]. Speaking in favour for a tumour suppressor role of INPP4B loss or decreased expression of INPP4B was verified in several cancer entities including prostate cancer, mammary carcinoma, ovarian carcinoma and melanoma [557]. In all cases loss of INPP4B correlated with poorer patient outcome, increased cell proliferation, motility, EMT and AKT activation in cell culture and enhanced tumorigenic and metastatic potential in xenograft mouse models. The observed phenotype was highly reminding on the characteristic phenotype of PTEN loss arguing for a catalysis dependent mode of tumour suppression mainly due to depletion of PtdIns(3,4)P_2 resulting in decreased AKT activation [83], [557], [558], [559], [560]. Interestingly, double *knock out* of *PTEN* and *INPP4B* in Human Mammary Epithelial Cells (HMEC) led to high levels of cellular senescence which could be rescued by concomitant loss of *p53* [83]. In controversy with the before mentioned findings some groups provided evidence for an oncogenic role of INPP4B in breast cancer and AML. In a subset of breast cancer amplification of the *SGK3* gene was found in line with overexpression of INPP4B and INPP4B was shown to contribute to the activation of SGK3 by its PtdIns(3)P/SGK3 PX domain dependent recruitment to the plasma membrane or endomembranes bringing it in close proximity to its substrates. SGK3 is marked by a substrate profile similar to AKT and might therefore compensate for reduced AKT activation in INPP4B overexpressing cancers. In *pi3kca* breast cancer cells SGK3 was identified as essential for cell proliferation and survival providing further evidence for a possible oncogenic INPP4B/SGK3 axis [561]. With concern to AML ectopic expression of INPP4B resulted in poor patient survival and enhanced drug resistance however, conflicting evidence was given concerning the dependency of INPP4B oncogenesis on its lipid phosphatase activity [562], [563].

1.4.3. SH2 domain containing Inositol polyphosphate-5-phosphatases 1 and 2 (SHIP1 and SHIP2) and their dual role in carcinogenesis

SHIP1 and SHIP2 belong to the family of phosphoinositide-5-phosphatases. The expression of SHIP1 (encoded by *INPP5D*) is traditionally restricted to hematopoietic cells and it influences differentiation processes in the hematopoietic lineage as well as the function of the immune system. SHIP2 (encoded by *INPPL1*) is more widely expressed and plays a role in upholding glucose homeostasis [564], [565], [566], [567], [568]. The primary targets

of SHIP1/-2 are the D5 phosphate of PtdIns(3,4,5)P_3 and Ins(1,3,4,5)P_3 with the latter effecting calcium dependent signal transduction pathways [564], [569], [570], [571], [572]. In a recent study published by our group we measured the substrate specificity of SHIP1 towards a panel of commercially available InsPs and identified several substrates shared with SHIP2, amongst them Ins(1,3,4,5)P_4 and most interestingly, we observed Ins(2,3,4,5)P_4 to be exclusively hydrolysed by SHIP1 but not SHIP2. The activity of SHIP1 towards Ins(2,3,4,5)P_4 was reduced 3-fold with regard to Ins(1,3,4,5)P_4 and by comparing the pattern of phosphate positions in identified substrates to our enzymatic data we would conclude that the presence of a 6- and the absence of a 3- and 4-phosphate might reduce the catalytic turnover of InsPs. Using GLIDE docking we found that the novel substrate Ins(2,3,4,5)P_4 would form several contacts with SHIP1 within the expected binding pocket which will provide a basis for further mutational studies [573].

Phosphoinositide-5-phosphatases with specificity for PtdIns(3,4,5)P_3 (i.e. SHIP1, SHIP2, SYNaptoJanin (SYNJ) 1, SYNJ 2) affect tumorigenesis in a highly worthwhile way as due to their enzymatic activity they have the potential to fulfil the role of an oncogene *or* a tumour suppressor dependent on the cellular context or cell type. As outlined in section 1.2. both PtdIns(3,4,5)P_3 (substrate) and PtdIns(3,4)P_2 (product) exhibit an oncogenic potential (*Two PIP Hypothesis)* and it is with regard to the individual cell type which *second messenger* dominantly contributes to (proto-)oncogenic outputs [574].

Looking at genetic studies performed in mouse or cell models *SHIP1*$^{-/-}$ mice are impaired in the development and function of the hematopoietic system and display lymphoproliferative and most obviously myeloproliferative disorders. The life span of *SHIP1*$^{-/-}$ mice is significantly reduced with a massive infiltration of the lung with myeloid cells and subsequent respiratory failure as the major death cause. This is due to increased levels of pro-inflammatory molecules triggering the proliferation of myeloid cells. In addition, they suffer from massive osteoporosis due to a hyperactivation of osteoclasts, splenomegaly, neutrophil granulocyte and monocyte hyperactivation, reduction of the B-lymphocyte pool and impaired HSC (Hematopoietic Stem Cell) differentiation and function. Interestingly, a shift of T-lymphocyte and myeloid cell differentiation from effector to suppressor cell is also featured and this was proposed as a measure to compensate for the highly proinflammatory environment. In summary, *SHIP1*$^{-/-}$mice develop myeloproliferative disorders similar to human CML (Chronic Myeloid Leukaemia) [575], [576], [577], [578], [579], [580], [581], [582], [583], [584], [585]. Downregulation of SHIP1 is thus a common feature of human CML. In most cases SHIP1 levels are reduced by ABL or BCR/ABL (Breakpoint Cluster Region/Abelson) dependent SRC kinase mediated phosphorylation and subsequent proteasomal degradation of SHIP1 [586], [587]. Furthermore, SHIP1 inactivating mutations (i.e. V684Q), deletions leading to truncated proteins or loss of *INPP5D* are frequent in T-ALL (T-lymphocyte Acute Lymphatic Leukaemia) and AML (Acute Myeloid Leukaemia) being in favour with a role for SHIP1 as a tumour suppressor in the hematopoietic system [588], [589], [590]. On the other hand, recent data from our laboratory may support an oncogenic function of SHIP1 in carcinomas. In more detail, we found ectopic expression of SHIP1 in several carcinoma entities especially in carcinomas of the intestinal tract. For example, high or moderate expression of SHIP1 was found in 60% of the colorectal carcinoma samples analysed. Furthermore, the expression and activity of SHIP1 was confirmed in selected carcinoma cell lines and SHIP1 expression could be linked to WNT signalling and clinical parameters [591] (see also 4.1.). SHIP2 is most decisive in glucose sensitive tissues (liver, skeletal muscle, adipose tissue) and is associated with the regulation of glucose homeostasis. It counteracts the AKT dependent translocation of the insulin sensitive glucose transporter GLUT4 to reduce glucose uptake and the AKT dependent inhibition of GSK3β to reduce glycogen synthesis [592], [593]. *SHIP2*$^{-/-}$ mice are hypersensitive to insulin and suffer from hypoglycaemia and massive underweight and in contrast *SHIP2* overexpressing mice are marked by insulin resistance. Of note, *SHIP2*$^{-/-}$ *mice* fail to gain weight under a high-fat died and display decreased levels of cholesterol, triglycerides and free fatty acids. This makes SHIP2 a valuable target for the targeted treatment of high impact civilization diseases such as diabetes and obesity [594], [595], [596], [597]. An oncogenic potential for SHIP2 was demonstrated in mammary carcinoma development. SHIP2 was ectopically expressed in mammary carcinoma cells but undetectable in healthy breast tissue. Moreover, loss of the *INPPL1* gene in the mammary carcinoma cell line MDA-231 reduced their proliferation as well as their tumour and metastases developing capability in nude mice [598]. Conversely, SHIP2 seems to act as a tumour suppressor in HCC (Hepatocellular Carcinoma) as SHIP2 levels were found to be commonly decreased in this tumour entity [599].

Conclusively, the effects of SHIP enzymes on cancerogenesis were proposed to be strictly context dependent. Ambivalent findings regarding the issue of SHIP enzymes being a tumour suppressor or an oncogene may be explained by the fact that 5-phosphateses in contrast to the 3-phosphatase PTEN do not simply revert the PI3K reaction but rather create a new *second messenger*, PtdIns(3,4)P_2 which acts in a quite similar fashion to PtdIns(3,4,5)P_3 [84]. It was shown that the PH domains of AKT and PDK1 were able to bind to PtdIns(3,4)P_2 with equally high affinity as to PtdIns(3,4,5)P_3 which might provide an alternative mode of AKT activation. Binding to and

subsequent activation of lamellipodin by PtdIns(3,4)P_2 additionally promotes cell migration, invasion and metastasis [600]. Therefore, SHIP enzymes may exhibit oncogenic effects in cell types relying more strongly on PtdIns(3,4)P_2 than PtdIns(3,4,5)P_3 and tumour suppressor effects in the situation vice versa [84]. Adding an additional layer of complexity, SHIP1 is also implicated in the regulation of the anti-tumour immune response i.e. SHIP1 deficiency promotes the formation of suppressor cells as explained above and this may ultimately lead to a reprogramming of the immune system respectively the tumour microenvironment from an anti-tumour to a tumour promoting one [601].

SHIP1 exists in different isoforms. The canonical isoform is termed SHIP1α and exhibits a molecular weight of 145 kDa. It comprises five functional domains implicated in protein-protein and protein-lipid interactions as well as catalysis (**fig. 4**). For amino acid numbering the Caucasian isoform (isoform 2) was used as a reference which differs from the Asian isoform (isoform 1) by missing V117.

1. SH2 (SRC Homology 2) domain (aa 5-101): responsible for the association with phosphotyrosines (pY). Phosphotyrosines are critical cellular signals typically occurring early in a signal transduction cascade (receptor or adaptor protein level) and serve as docking sites for *downstream* components (here: SHIP1). Conserved tyrosine residues of RTKs (i.e. growth factor receptors, ITIMs (Immune receptor Tyrosine based Inhibitory Motifs), ITAMs (Immune receptor Tyrosine based Activating Motifs)) or RTK associated adaptor proteins (i.e. SHC (SH2 domain Containing) or DOK-3 (Docking protein 3)) get phosphorylated upon ligand binding recruiting SH2 domain containing intracellular signalling molecules to the plasma membrane (i.e. to their respective substrate or to regulatory molecules). In SHIP1, the SH2 domain mainly serves for guiding SHIP1 to plasma membrane located PtdIns(3,4,5)P_3 following PI3K activation [564], [565], [566], [602], [603], [604], [605], [601], [606], [607].
2. PH-L (Pleckstrin Homology 2-Like) domain (aa 294-403): shown to associate with PtdIns(3,4,5)P_3 [608].
3. catalytic (5'-PPase) domain (aa 403-709): highly conserved domain responsible for substrate accommodation and catalysis [609]. Several crystal structures of the catalytic domain of phosphoinositide-5-phosphatases are available (i.e. SHIP2, yeast synaptojanin, INPP5B). The catalytic domain of the prototypical 5'-PPase INPP5B displays a catalytic core consisting of two stacked β-sheets and a set of peripheral α-helices. The active site is located at the upper edge of the β-core and composed of α-helices and loop structures. An additional Membrane Interacting Motif (MIM) anchors the 5'-PPase into the membrane due to electrostatic and hydrophobic interactions. Electrostatic interactions are between basic residues of the protein (H314, K308, R376 and R410 in INPP5B) and the negatively charged headgroups of acidic lipids and hydrophobic interactions are between hydrophobic residues of the protein (F311, F312, F313, I373, M374 and M377 in INPP5B) and the aliphatic hydrocarbon chains of membrane-composing lipids. The substrate is recognized by the stereospecific arrangement of the phosphate groups. The presence of a phosphate moiety at position D4 is preliminary for substrate recognition. The D4 phosphate is bound by a so-called P4 Interacting Motif (P4IM) consisting of K503, K516, R518 and Y502 within a loop structure in INPP5B. In SHIP enzymes the P4IM loop is expanded by seven residues allowing for a conserved arginine to interact with the D3 phosphate [186]. Furthermore, the D1 phosphate is recognized by N379 and K380 (in INPP5B). Following correct substrate accommodation, the D5 phosphate is hydrolysed in an acid-base catalysis. An invariable acidic residue (D447 in INPP5B) serves as a base activating an uncaged water molecule which subsequently starts a nucleophilic attack on the D5 phosphate. The resulting pentavalent intermediate is highly negative in charge and stabilized by a coordinated Mg^{2+} ion. Finally, the D5 phosphate is released by protonation of the O^- moiety where the proton is provided by D447-H^+ (here serving as an acid) [610], [611], [612], [613]. For a more detailed view on the structure of the catalytic domain see also the result section 4.3.1.
4. C2 (Protein Kinase C Conserved region 2) (aa 710-862): associating with the reaction product PtdIns(3,4)P_2. This was described to result in the allosteric activation of SHIP1 in one publication [614].
5. PRR (Proline Rich Region) (aa 863-1188): serving as a platform for protein protein interactions. The PRR comprises two NPXY (INPY and ENPLY) motifs associating with PTB (Phosphotyrosine Binding) domains of i.e. SHC, DOK-1, DOK-2 and several PXXP motifs associating with SH3 domains of i.e. GRB2 (Growth factor Receptor Bound 2) [569], [564].

fig. 4: domain structure of SHIP1.

In addition to SHIP1α further isoforms were described. SHIP1β is the result of alternative splicing and lacks the INPNY and several PXXP motifs due to a C-terminal truncation [568], [615]. The stem-cell specific isoform SIP-110 (Stem cell specific Inositol polyphosphate-5-Phosphatase, 110 kDa) is expressed from an internal promotor located in between introns 5 and 6 and lacks the SH2 domain. Instead, it is marked by a unique N-terminal SHIP Stem cell Recognition (SRR) sequence of 44 bp [616], [617]. SHIP2 (142 kDa) shares the general domain structure of SHIP1 but for an additional C-terminal SAM (Sterile Alpha Motif) domain [568].

2. Preliminary work and objectives of the thesis

2.1. Preliminary work

Phosphoinositide-5-phosphatases are remarkable players in carcinogenesis due to their potential to fulfil both tumour suppressing and oncogenic roles depending on the cell type. An oncogenic role for SHIP2 and SYNJ2 was confirmed in mammary carcinoma by other groups. This opened the possibility for SHIP1 which has since then ostensibly acknowledged as a tumour suppressor in proliferative disorders of the hematopoietic system to act as an oncogene as well.
Initial Tissue Microarray (TMA) data conducted in our group showed a moderate or high expression of hematopoietic SHIP1 in a vast panel of carcinoma entities. The percentage of SHIP1 positive samples was especially high in colorectal carcinoma (~60%). SHIP1 expression was additionally verified on the protein level in a panel of patient-derived carcinoma cell lines by Western Blot analysis [591]. Overexpression of SHIP1 in the human colorectal cancer cell line HCT116 resulted in enhanced migration when compared to the empty vector control. (Schaks et al., 2015, unpublished data). Furthermore, based on data base (COSMIC-Catalogue Of Somatic Mutations In Cancer) research, somatic mutations of the *INPP5D* gene were found in a number of listed carcinoma samples (i.e. in 5.4% of cancers in the large intestine). Those results pointed to a functional role of SHIP1 in carcinomas, especially in CRC.
With regard to the structural, biochemical and biophysical properties of SHIP1 focused on the three PtdInsP binding domains (PH-L, PPase, C2) there was sparse knowledge available especially concerning the PH-L and the C2 domain. For the PPase domain research had been performed for SHIP1 and also for other 5-PPases which can be in part applied to SHIP1 due to the high level of conservation concerning this domain.

2.2. Objectives

2.2.1. SHIP1- a player in Colorectal Carcinoma (CRC)?

To analyse the function of SHIP1 in CRC in more depth, two model systems will be established by lentiviral transduction (overexpression of SHIP1 WT in the SHIP1-negative CRC line HCT-116 vs. LeGO vector control and *knock-down* of SHIP1 in the SHIP1-positive CRC lines SW-480 and HT-29 vs. SCR control). The function of SHIP1 will then be analysed in cell culture regarding invasion/migration/chemotaxis, proliferation, apoptosis and tumoroid behaviour. Furthermore, the impact of SHIP1 on the kinome, proteome and signal transduction will be investigated. Lastly, the results found *in vitro* will be aimed to be confirmed *in vivo* using an NSG mouse xenotransplant model.

2.2.2. The role of patient-derived SHIP1 mutations of the catalytic domain

Selected patient-derived mutations of the SHIP1 catalytic domain (according to the COSMIC database) will be induced by side-directed mutagenesis and stable H1299 cells overexpressing SHIP1 WT, SHIP1 mutants or a LeGO vector control will be established. The impact of the mutations on protein level and stability, sub-cellular localization, phosphatase activity and signal transduction will be analysed and structural alterations by those mutations will be predicted by computational modelling. The function of SHIP1 (mutants) will be further investigated in the context of the so-called phosphoinositide-trapping hypothesis.

2.2.3. Structural, biochemical and biophysical analysis of SHIP1

Structure models of SHIP1 PtdInsP binding domains will be generated and investigated *in situ* and the structure of SHIP1 binding domains will be aimed to be solved experimentally. SHIP1 and its PtdInsP binding domains will be expressed in *E. coli* and analysed regarding its phosphoinositide binding, substrate specificity and catalysis to better elucidate the individual roles of those domains and their interplay.

3. Materials and methods

3.1. Materials

3.1.1. Devices

autoclave *EVO 120*	MediTech Service GmbH
bath sonicator *Sonofier 450*	Branson Ultraschall
casting stand for agarose gel electrophoresis	Peqlab
casting stand for SDS-polyacrylamide gel electrophoresis (mini)	BioRad
casting stand for SDS-polyacrylamide gel electrophoresis *SE 600*	Hoefer
clean bench for bacterial cultures type 20229	MDH
cooling centrifuge *RC-5B*	Sorvall
cooling centrifuge *Varifuge 3.OR*	Heraeus
extruder LiposoFast	Avestin
electrophoresis chamber for agarose gels	MWG Biotech
electrophoresis chamber for SDS-polyacrylamide gels (mini)	BioRad
electrophoresis chamber for SDS-polyacrylamide gels *SE 600*	Hoefer
glass syringe, gas-tight for extruder	Hamilton
ice machine	Scotsman
incubator for bacterial cultures	Memmert
Life Cell Imaging system IncuCyte Zoom	Essen Bioscience
magnetic stirrer	Heidolph
micropipette *Research* 0.1-2.5 µL	Eppendorf
micropipette *Research* 0.5-10 µL	Eppendorf
micropipette *Research* 2-20 µL	Eppendorf
micropipette *Research* 10-100 µL	Eppendorf
micropipette *Research* 100-1000 µL	Eppendorf
microtiter plate reader *MultiScan Fc*	Thermo Scientific
microwave	Sharp
pH meter *CG 820*	Schott
photometer BioPhotometer	Eppendorf
pipetting aid *Pipetus-akku*	Hirschmann Laborgeräte
power supply for agarose gel electrophoresis *PowerPack P25*	Biometra
power supply for SDS-polyacrylamide gel electrophoresis *Powerpac 1000*	BioRad
precision scales *AUW 320*	Shimadzu
probe sonicator *Sonophos GM 70*	Bandelin
scales *PM 2000*	Mettler
shaking incubator for bacterial cultures *G 25*	New Brunswick Sc. Co. Inc
spectral photometer *NanoDrop 2000c*	Thermo Scientific
surface plasmon resonance analysing machine *MASS-1*	SierraSensors
thermocycler *T3*	Biometra
thermomixer *5436*	Eppendorf
table centrifuge *5415D*	Eppendorf
table centrifuge *Minispin*	Eppendorf
transfer chamber	BioRad
UV-table BioDoc Analyzer	Biometra
vortexer MS2 Minishaker	IKA

3.1.2. Consumables

cell culture flasks for adherent cells, 75 mm^2 CELLSTAR	Greiner
cell culture flasks for adherent cells, 175 mm^2 CELLSTAR	Greiner
cell culture plates, 6-well CELLSTAR	Greiner
cuvettes polystyrene	Sarstedt
microtiter plates, 96-well, round bottom CELLSTAR	Greiner
microtiter plates, 96-well, flat bottom CELLSTAR	Greiner
microtiter plates, 96-well, flat bottom, *Image Lock*	Essen Bioscience

microtiter plate sealers, 96 well	SierraSensors
petri dishes, 10 cm	Sarstedt
reagent glasses	Th. Geyer GmbH & Co.KG
sample tubes, type falcon, PP, conical, 50 mL	Sarstedt
sample tubes, type falcon, PP, conical, 15 mL	Sarstedt
sample tubes, type falcon, PP, conical for ultrafiltration *Amicon Ultra-4*	Millipore
sample tubes, type falcon, PP, conical for ultrafiltration *Amicon Ultra-15*	Millipore
sample tubes, type eppendorf, PP, 1.5 mL	Sarstedt
sample tubes, type eppendorf, PP, 2 mL	Sarstedt
sample tubes, PP, 0.2 mL, thin-walled for PCR	Sarstedt
sensor chips for surface plasmon resonance *Affinity Sensor High Capacity Amine*	SierraSensors
sensor chips for surface plasmon resonance *Affinity Sensor Hydrophobic*	SierraSensors
serological pipettes, PP, 5 mL	Sarstedt
serological pipettes, PP, 10 mL	Sarstedt
serological pipettes, PP, 25 mL	Sarstedt
tips for micropipettes, all sizes	Sarstedt

3.1.3. Chemicals

If not specified otherwise all chemicals were purchased from Merck, Fluka, Sigma-Aldrich, BioRad, Thermo Fisher and Serva. Materials for the *Strep-Tactin* affinity chromatography resins were purchased from IBA. Phospholipids and phosphatidyl inositol phosphates were purchased from Echelon. Reagents for use with the *IncuCyte Zoom* were purchased from Essen Bioscience.

3.1.4. Kits

Amine Coupling kit I, 10 mL	SierraSensors
Immobilization buffer kit I	SierraSensors
NucleoBond Xtra Midi	Macherey-Nagel
NucleoSpin Gel and PCR clean-up	Macherey-Nagel
NucleoSpin Plasmid	Macherey-Nagel
Super Signal West Pico chemiluminescence substrate kit	Thermo Scientific
Super Signal West Dura chemiluminescence substrate kit	Thermo Scientific
Q5 mutagenesis kit	New England Bioscience

3.1.5. Enzymes

Esp3I (10 U/µL)	Thermo Scientific
HindIII (10 U/µL)	Thermo Scientific
LguI (5 U/µL)	Thermo Scientific
Phusion HS II (2 U/µL)	Thermo Scientific
T4-DNA-Ligase (1 U/µL)	Thermo Scientific
XbaI (10 U/µL)	Thermo Scientific
BamHI (10 U/µL)	Thermo Scientific
EcoRI (10 U/µL)	Thermo Scientific
DpnI (10 U/µL)	Thermo Scientific
CIAP Calf Intestine Alkaline Phosphatase (1 U/µL)	Thermo Scientific
KpnI (10 U/µL)	Thermo Scientific
DNAseI (RNAse free) (1 U/µL)	Thermo Scientific

3.1.6. Resins and bead material for the purification and enrichment of proteins

Ni-NTA Superflow	IBA
Strep-Tactin Superflow XT	IBA
Pierce SXT cation exchange spin columns	Thermo Scientific
Pierce SAX anion exchange spin columns	Thermo Scientific
Protein G Sepharose 4 Fast Flow	GE

3.1.7. Bacterial strains

BL21(DE3)pLysSpREP4 (F $^-$ ompT gal dcm lon hsdS_B(r_{B^-} m_{B^-})λ(DE3) pLysS(Cam^R) pREP4(Kan^R))

TOP10 (F-mcrA (mrr-hsdRMS-mcrBC) 80lacZ M15 lacX74 recA1 ara 139 (ara-leu)7697 galU galK rpsL (StrR) endA1 nupG)
XL1-blue (recA1 endA1 gyrA96 thi-1 hsdR17 supE44 relA1 lac [F'proAB lacIqZDM15 Tn10 (Tet^R)])
DH10B (F–mcrAΔ(mrr-hsdRMS-mcrBC) Φ80 lacZ ΔM15 ΔlacX74 recA1endA1araD139Δ(araleu) 7697galU galK rpsL nupG λ–)
Rosetta2(DE3) (F$^-$ ompT hsdSB(rB^- mB^-) gal dcm (DE3) pRARE2 (Cam^R))
BL21(DE3) F^- ompT $hsdS_B$ (r_B^- m_B^-) gal dcm (DE3)

3.1.8. Primers

3.1.8.1. Primers for the mutagenesis of SHIP1

NN_QCM E452K fw	CGGCACCCAAAAGGACCCCCTG
NN_QCM E452K rv	CAGGGGGTCCTTTTGGGTGCCG
MN 597 (R673Q fw)	ACTTGCCTTCCTGGTGTGACCAAGTCCTCTGGAAGTCTTATCC
MN 598 (R673Q rv)	GGATAAGACTTCCAGAGGACTTGGTCACACCAGGAAGGCAAGT
R577C_vor	AGTCCCTTTAACATCACTCACTGCTTCACGCACCTTTTCTGGTTTGGGGATCTTAAC
R577C_rück	GTTAAGATCCCCAACCAGAAAAGGTGCGTGAAGCAGTGAGTGATGTTAAAGGGACT
MN 585 (R551Q fw)	GACTTCAGGAAGTGAAAAGAAGCTTAGGCAAAACCAAAACTATATGAACAT
MN 586 (R551Q rv)	ATGTTCATATAGTTTTGGTTTTGCCTAAGCTTCTTTTCACTTCCTGAAGTC
QCM_NcoI_FW	TCACCCATCATGGGGAGTT
QCM_NcoI_RV	TCACCCATCATGGGGAGT
SHIP1domain_9	GGAGTCACTTCCCAGTTTGTCTC
SHIP1domain_10	CATGTCGGGCTCCGGCTG

3.1.8.2. Primers for Stargate and restriction cloning

All primers for the Stargate cloning method were purchased as 3' PTO (Phosphorothioate) oligos to prevent their degradation by the *Phusion HS II* 3´ → 5' *proofreading* function.

NN_SG SHIP1 fw	AGCGGCTCTTCAATGGTCCCCTGCTGGAACCATG
NN_SG SHIP1 rv	AGCGGCTCTTCTCCCCTGCATGGCAGTCCTGCC
TAPP1_fw	AGCGGCTCTTCAATGCCTTATGTGGATCGTCAGAAT
TAPP1_rv	AGCGGCTCTTCTCCCCTTTGGAAGCTGGTTCTCTTG
TAPP2_fw	AGCGGCTCTTCAATGCCTTATGTGGATCGGCAGAA
TAPP2_rv	AGCGGCTCTTCTCCCCACATCAGAGGTCCGTATGT
NN_SG AKT1 fw	AGCGGCTCTTCAATGAGCGACGTGGCTATTGTGAA
NN_SG AKT1 rv	AGCGGCTCTTCTCCCGGCCGTGCCGCTGGCC
NN_SG PTEN fw	AGCGGCTCTTCAATGACAGCCATCATCAAAGAGATC
NN_SG PTEN rv	AGCGGCTCTTCTCCCGACTTTTGTAATTTGTGTATGCT
NN_SG PREX-1 fw	AGCGGCTCTTCAATGGAGGCGCCCAGCGGCAG
NN_SG PREX1 rv	AGCGGCTCTTCTCCCGAGGTCCCCATCCACCGG
NN_SG VAV1 fw	AGCGGCTCTTCAATGGAGCTGTGGCGCCAATGC
NN_SG VAV1 rv	AGCGGCTCTTCTCCCGCAGTATTCAGAATAATCTTCC
PHL_fw	AGCGGCTCTTCAATGTCCCTTATCCCTCCAGTCAC
PHL_rv	AGCGGCTCTTCTCCCCATGTCGGGCTCCGGCTG
PPase_fw	AGCGGCTCTTCAATGATGATCACCATCTTCATCGGC
PPase_rv	AGCGGCTCTTCTCCCCTCAAATGTGGCAAAGACAGG
C2_fw	AGCGGCTCTTCAATGGCAGGAGTCACTTCCCAGT
C2_rv	AGCGGCTCTTCTCCCCTCCCTCGTCTTGCCCTG
SHIP1_PPase_398-712_fw	AGCGGCTCTTCAATGCCGGAGCCCGACATGATC

SHIP1_PPase_398-712_rv	AGCGGCTCTTCTCCCAGTGACTCCTGCCTCAAATG
PHLPPaseC2short_fw	TAAGCAGGTACCGGCCCTCCCTTATCCCTCC
PHLPPaseC2short_rv	TGCTTAAAGCTTTTAGGTCTGCAGCTTGATCTCCCCC

3.1.8.3. Sequencing primers

SHIP-FP 594-617	TTCCTCGTGCGTGCCAGCGAGTCC
SHIP-RP 751-727	TCCAGCTTGGTGAAGAACCTCATGG
SHIP-FP 933	GAGGTTCCTTTTTCAAACGAGAATC
SHIP-FP 1205	GTCTCTGCAGAGGTTATTTGACCAG
SHIP-FP 1906-30	AACACTCCCTGCAAGAAATCACCAG
SHIP-FP 2294-2318	TACCTGGGAGGCAGAAACCATCATC
SHIP-FP 2964-87	TGCATTGCCCTTCGGTTAGAGGCC
SHIP-FP 3516-40	ACGCTGCCTCAGGAGGACCTGCCGC
ASG-Primer -for	GAGTTATTTTACCACTCCCT
ASG-Primer-rev	CGCAGTAGCGGTAAACG
ENTRY-Primer-for2	GCGAAACGATCCTCGAAG
ENTRY-Primer-rev	CCCCTGATTCTGTGGATAACCG
PSG-Primer for	TAATACGACTCACTATAGGG
PSG-Primer rev	TAGTTATTGCTCAGCGGTGG
pASK-IBA5plus fw	GAGTTATTTTACCACTCCCT
pASK-IBA5plus rv	CGCAGTAGCGGTAAACG
EGFP-C-for	GTCCTGCTGGAGTTCGTG
pETM30seq_GST	GAAATCCAGCAAGTATATAGC
pETM30seq_T7terminator	CCCAAGGGGTTATGC

3.1.9. Plasmids

pENTRY-IBA51
pASG-IBA105
pASG-IBA3
pASG-IBA5
pASG-IBA5plus-SHIP1 wt
pLeGO-iG2-Puro(+)-HA-SHIP1 wt_dUTR
pLeGO-iG2-Puro(+)-OneStrep-SHIP1 wt_dUTR
pLeGO-iG2-Puro(+)
pCMV-VSV-G
pMDLg/pPE
pRSV-REV
pEGFP-C1
p.LKO1 SHIP1 shRNA:

TRCN0000039895	NM_005541.2-3413s1c1	SHCLNG08011621MN	INPP5D
TRCN0000010362	NM_005541.x-281s1c1	SHCLNG08011621MN	INPP5D
TRCN0000039896	NM_005541.2-2387s1c1	SHCLNG08261603MN	INPP5D
TRCN0000039897	NM_005541.2-3878s1c1	SHCLNG08261603MN	INPP5D
TRCN0000039893	NM_005541.2-4480s1c1	SHCLNG08261603MN	INPP5D

pET47b(+)
pETM-30
LeGO empty vectors were a gift of the group of Prof. Fehse (UKE Hamburg) [618]. pLeGO-iG2-Puro(+)-OneStrep-SHIP1 wt_dUTR was cloned by Marcus Nalaskowski (AG Itzen, UKE Hamburg) .Lentiviral vectors were a gift of Carol Stocking. pASG-IBA vectors were purchased from IBA. pET47b(+) was purchased from Merck. pLKO.1 vectors were purchased from Sigma Aldrich.

3.1.10. Molecular weight standards

GeneRuler 1 kb DNA ladder, ready-to-use	MBI Fermentas
GeneRuler 100 bp DNA ladder, ready-to-use	MBI Fermentas
HyperLadder 1 kb DNA ladder, ready-to-use	Bioline

Spectra Multicolor Broad Range Protein Ladder, prestained	Thermo Scientific
RotiMark Tricolor, prestained protein standard	Roth

3.1.11. Buffers and solutions

3.1.11.1. Buffers and solutions for the generation of chemically competent bacteria

RF I	100 mM RbCl, 50 mM $MnCl_2$ x 4 H_2O, 30 mM KAc, 10 mM $CaCl_2$ x 2 H_2O, 15% (v/v) glycerol adjust to pH 5.8 with acetate, sterile-filter and store at 4°C.
RF II	10 mM MOPS, 10 mM RbCl, 75 mM $CaCl_2$ x 2 H_2O, 15% (v/v) glycerol adjust to pH 6.8 with acetate, sterile-filter and store at 4°C.

3.1.11.2. Buffers and solutions for the cultivation of bacteria

LB-medium (Luria-Bertani)	1% bacto-tryptone, 0.5% yeast extract, 1% NaCl pH 7.2, autoclave
LB-agar (Luria-Bertani)	1% bacto-tryptone, 0.5% yeast extract 1% NaCl, 1.5% bacto-agar, pH 7.2, autoclave

The respective antibiotic was added to a final concentration of 10 µg/mL (tetracycline), respectively 50 µg/mL (ampicillin or kanamycin). In order to perform *blue white screening* X-Gal was added to a final concentration of 50 µg/mL in addition to the respective antibiotic.

3.1.11.3. Buffers and solutions for agarose gel electrophoresis

TAE-buffer	40 mM tris-acetate, 1 mM EDTA, pH 8
6x DNA-loading dye	30% (v/v) glycerol, 0.1% (w/v) bromophenol blue, 0.1% (w/v) xylene cyanol

3.1.11.4. Buffers and solutions for the Ni-NTA and Strep-Tactin based purification of recombinant proteins and for SDS polyacrylamide gel electrophoresis (SDS-PAGE)

buffer W (wash- and equilibration buffer for *Strep-Tactin-Superflow XT*, IBA Cat. 2-1003-100)	100 mM Tris/Cl, 150 mM NaCl, 1 mM EDTA, pH 8
buffer BXT (elution buffer for *Strep-Tactin-Superflow XT*, IBA Cat. 2-1041-250)	100 mM Tris/Cl, 150 mM NaCl, 1 mM EDTA, 50 mM biotin, pH 8
buffer R (regeneration buffer for *Strep-Tactin-Superflow-Macroprep* und *–Sepharose*, may be used in order to survey the regeneration process of *Strep-Tactin-Superflow XT* resins, IBA Cat. 2-1002-100)	100 mM Tris/Cl, 150 mM NaCl, 1 mM EDTA, 1 mM HABA, pH 8
Ni-NTA lysis buffer	50 mM $NaHPO_4$, 300 mM NaCl, 10 mM imidazole, pH 8
Ni-NTA wash buffer	50 mM $NaHPO_4$, 300 mM NaCl, 20 mM imidazole, pH 8
Ni-NTA elution buffer	50 mM $NaHPO_4$, 300 mM NaCl, 250 mM imidazole, pH 8
Ni-NTA regeneration buffer	6 M GuHCl, 0.2 M acetic acid
4x sample buffer for SDS-PAGE	200 mM Tris/Cl, 5.4% mercaptoethanol, 0.04% bromophenol blue, 8.8% SDS, 15% glycerol, pH 6.8
4x separating gel buffer for SDS-PAGE	1.5 M Tris/Cl, 0.4% SDS, pH 8.8
4x stacking gel buffer for SDS-PAGE	500 mM Tris/Cl, 0.4% SDS, pH 6.8
running buffer for SDS-PAGE according to Lämmli	25 mM Tris/Cl, 192 mM Glycine, 0.1% SDS
Coomassie Brilliant Blue staining solution	0.5% *Coomassie blue*, 9% acetoacetate, 45% methanol
Coomassie Brilliant Blue destaining solution	8% acetoacetate, 25% ethanol

3.1.11.5. Buffers and solutions for Surface Plasmon Resonance (SPR)

All solutions were 0.2 µm filtered and degassed prior to use.

SPR running buffer (*Amino coupling*)	20 mM HEPES, 200 mM NaCl, 0.05% (v/v) Tween-20, pH 7.0

SPR running buffer for LUVs	20 mM HEPES, 200 mM NaCl, pH 7.0
desorb solution #1	0.5% (w/v) SDS
desorb solution #2	50 mM glycine, pH 9.5
sanitize solution	2% (v/v) NaClO
EDTA solution	50 mM EDTA, pH 8.0
acetic acid solution	1% (v/v) acetic acid
sodium bicarbonate solution	200 mM $NaHCO_3$

3.1.11.6. Buffers and solutions for Phospholipid Overlay Assay (PLO)

blocking buffer (anti-Strep-mAB-HRP)	PBS supplemented with 3% (w/v) fatty-acid free BSA and 0.5% (v/v) Tween-20
enzyme dilution buffer (anti-Strep-mAB-HRP)	PBS supplemented with 0.2% (w/v) BSA and 0.1% (v/v) Tween-20
PBS-T	PBS supplemented with 0.1% (v/v) Tween-20
PBS	4 mM KH_2PO_4, 16 mM Na_2HPO_4, 115 mM NaCl, pH 7.4
biotin blocking buffer (IBA, Cat. 2-0501-002)	dilute stock solution 1:1000 in PBS-T
blocking buffer	TBS supplemented with 5% non-fat dried milk bovine (NFDMB) and 0.05% Tween-20
washing buffer	TBS supplemented with 2.5% NFDMB and 0.05% Tween-20
TBS-T	TBS supplemented with 0.05% Tween-20
TBS	10 mM Tris, 144 mM NaCl, pH 7.8

3.1.11.7. Buffers and solutions for the phosphatase assay

2x assay buffer	40 mM TEA, 200 mM KCl, 5 mM $MgCl_2$, pH 7.2
working solution (BioAssay Systems, Cat. POMG-25H)	mix 100 volumes of reagent A with 1 volume of reagent B, stable for at least 1 day at RT according to the manufacturer

3.1.11.8. Buffers and solutions for cell culture

maintenance medium	DMEM supplemented with 10% FCS and 1% pen/strep
maintenance medium for HEK293T cells	DMEM supplemented with 10% FCS, 1% pen/strep, 2 mM glutamine, 1 mM sodium pyruvate and 20 mM HEPES
selection medium	DMEM supplemented with 10% FCS, 1% pen/strep and 1-4 µg/mL puromycin
starvation medium	DMEM supplemented with 0.1% sterile-filtered BSA
PBS	4 mM KH_2PO_4, 16 mM Na_2HPO_4, 115 mM NaCl, pH 7.4, autoclave
freezing medium	90% FCS, 10% DMSO

3.1.11.9. Buffers and solutions for the cell lysis and Western Blot analysis

1x loading buffer w./o. DTT, w./o. bromophenol blue	0.0625 M Tris/HCl, pH 8.8, 3% SDS, 10% glycerol
3x loading buffer (complete)	0.18 M Tris/HCl, pH 8.8, 6% SDS, 30% glycerol, 0.03% bromophenol blue, add fresh: 0.3 M DTT
1x running buffer	25 mM Tris/HCl, 192 mM glycine, 0.1% SDS
1x transfer buffer	25 mM Tris/HCl, 192 mM glycine, 0.1% SDS, 20% methanol
TBS-T	TBS supplemented with 0.05% Tween-20
TBS	10 mM Tris, 144 mM NaCl, pH 7.8
blocking solution	5% non-fat dried milk powder in TBS-T
washing solution	2.5% non-fat dried milk powder in TBS-T
NP40 buffer	50 mM Tris/Cl, 150 mM NaCl, 1% NP40, pH 8
M-PER buffer	proprietary detergent in 25mM bicine buffer (pH 7.6), purchased by Thermo Scientific

GST-PAK lysis/wash buffer	50 mM Tris HCl, pH 7.2, 150 mM NaCl, 10 mM $MgCl_2$, 1% Triton X-100, 10 µg/ml Leupeptin, 10 µg/ml Aprotinin, 0.1 mM PMSF
RAC-RIPA buffer	50 mM Tris HCl, pH 7.2, 150 mM NaCl , 10 mM $MgCl_2$, 1% Triton X-100, 0.5% Sodium-Deoxycholat, 0.1% SDS, 10 µg/ml Leupeptin, 10 µg/ml Aprotinin, 0.1 mM PMSF

3.1.12. Antibodies

StrepMAB Classic, HRP conjugate	IBA
anti-SHIP1 P1C1 mouse IgG	Santa Cruz Biotechnology
anti-GST, mouse monoclonal	Sigma Aldrich
anti-Strep-MAb-Immo	IBA
anti-HA High Affinity rat IgG	Roche
anti-pAKT S473 rabbit IgG	Cell Signalling
anti-panAKT rabbit IgG	Cell Signalling
goat-anti-rat-HRP	Santa Cruz Biotechnology
anti-mouse-HRP	Cell Signalling
anti-rabbit-HRP	Cell Signalling
anti-GAPDH mouse IgG	Santa Cruz Biotechnology
anti-pan-SRC	Cell Signalling
anti-P-pan-SRC D49G4 Y416	Cell Signalling
anti-p-p44/42 MAPK (Erk1/2) T202/Y204 rabbit IgG	Cell Signalling
anti-SHIP1 P290 (specific for human, in-house validated)	Cell Signalling
anti-HSP70 D1M6J (specific for human, in-house validated)	Cell Signalling
anti-PHGDH (D8F3O)	Cell Signalling
anti RAC1 mouse IgG	BD
anti-SRC (36D10)	Cell Signalling
anti-P-SRC Y527	Cell Signalling
anti-G6PDH (D5D2)	Cell Signalling
anti- Tyro3 (D38C6)	Cell Signalling
anti-P-Axl(Tyr698)/Mer(Tyr749)/Tyro3(Tyr681) (D6M4W)	Cell Signalling
anti-P-EGFR Y1068	Cell Signalling

3.1.13. Software

AIDA Image Analyser 3.44	fujifilm
BioDoc Analyze 266.3.31	Biometra
Bioedit 7.2.5	Tom Hall
Pymol	Schrödinger Inc.
GraphPad Prism 3.03	GraphPad Software
Image Reader LAS-3000 1.1	fujifilm
IncuCyte Zoom	Essen Bioscience
MASS-1 Control Software M1	Sierra Sensors
NanoDrop 2000c	Thermo Scientific
ScanIT for multiscan fc	Thermo Scientific
Sierra Analyser 3.1.3.0	Sierra Sensors
SnapGene 3.3	GSL Biotech LLC
UCSF Chimera	Resource for Biocomputing, Visualization and Informatics (RBVI)
Biorender	Biorender (website-based)

3.2. Methods

3.2.1. Microbiological methods

3.2.1.1. Generation of chemically competent bacteria

Chemically competent bacteria were generated by use of the rubidium chloride method, an optimized variant of the calcium chloride method. The day before, 5 mL LB-medium containing an adequate antibiotic was inoculated with 10 µL of the desired bacterial strain and incubated for 18 to 20 hours at 37°C and 220 rpm. The day after, 50 mL LB-medium with an appropriate antibiotic added was inoculated with 500 µL of the overnight culture and incubated at 37°C and 220 rpm until an OD_{600} ≈0.6 was reached. The bacterial culture was transferred into a 50 mL sterile conical sample tube, type falcon and allowed to chill on ice for 15 minutes. Subsequently, it was centrifuged for 15 minutes at 3000 g and 4°C and the supernatant was discarded. The pellet was resuspended in 16.7 mL ice-cold RFI and incubated on ice for 15 minutes. The culture was centrifuged for 15 minutes at 3000 g and 4°C and the supernatant was discarded. The pellet was resuspended in 4 mL ice-cold RFII and incubated for 15 minutes on ice. The bacteria were then aliquoted into 100 µL portions, immediately shock-frozen in liquid nitrogen and stored at -80°C.

3.2.1.2. Transformation of chemically competent bacteria

The incorporation of foreign DNA into chemically competent bacteria (transformation) was induced by heat shock. A 100 µL aliquot of the desired chemically competent strain was partly thawed on ice and 50-100 ng of the desired plasmid DNA was added and mixed carefully by swirling the solution with the pipet tip. The solution was incubated for 30 minutes on ice. Heat shock was performed for one minute at 42°C. If the respective plasmid contained an ampicillin resistance the bacteria were shortly chilled on ice and directly plated on LB-Amp or LB-Amp/X-Gal agar plates for *blue white screening* purposes and incubated for ~20 hours at 37°C. In case of a kanamycin resistance 900 µL LB-medium containing no antibiotic was added after heat shock and the bacteria were incubated at 37°C and 450 rpm for 45 minutes to induce the expression of the encoded kanamycin resistance before being plated on LB-Kan or LB-Kan/X-Gal agar plates for *blue white screening* purposes and incubated for ~20 hours at 37°C. Plates containing bacterial colonies could be stored for up to one month at 4°C.

3.2.2. Molecular biological methods

3.2.2.1. Generation of destination vectors for recombinant protein expression using the Stargate cloning system

The *Stargate* cloning system was developed by IBA to facilitate the *screening* process required to assess optimal conditions for protein expression and purification. It offers vectors (1) equipped with different tags (i.e. Strep, TwinStrep, His_6, GST) or combinations of tags, (2) equipped with different (inducible) promotor systems (i.e. T7, tet), (3) suitable for different hosts (i.e. bacteria, mammalian and insect cells) and (4) for either intracellular localization or secretion of the protein of interest. The central part of the cloning system is the generation of a so-called donor vector containing the GOI (Gene Of Interest) which can be conveniently cloned into the full range of acceptor vectors to yield the desired destination vector for expression. Briefly, the GOI is amplified with primers equipped with the *LguI* combinatorial and recognition site and cloned into the entry vector pENTRY-IBA51 in an *LguI* based reaction yielding the donor vector. In the second step, the GOI is transferred from the donor vector to an acceptor vector of choice in an *Esp3I* based reaction yielding the desired destination vector for protein expression.
In more detail, primers are designed for the amplification of the GOI from a given template (i.e. purchased cDNA) and elongation of the amplified sequence with the combinatorial site AATG and the *LguI* recognition site.
For instance, to amplify a GOI with a given sequence 5'-ATGTTGACCTGCAACAGCTGCATAGCC-3' the fw primer would be AGCGGCTCTTC**AATG**TTGACCTGCAACAGCTGCATAGCC containing the *LguI* recognition site (underlined) and the *upstream* combinatorial site (in bold) and the rv primer would be AGCGGCTCTTC**TCCC**GGCTATGCAGCTGTTGCAGGTCAA containing the *LguI* recognition site (underlined) and the reverse complement of the *downstream* combinatorial site GGGA (in bold).
Subsequently, the PCR product is cloned into pENTRY-IBA51 using *LguI*. This reaction is orientation-specific which is due to the presence of the two combinatorial sites. The lacP/Z gene of the entry vector becomes replaced by the GOI enabling for *blue white screening*. The resulting product is called the donor vector.
For the generation of a destination (=expression) vector of choice, the GOI is cloned from the donor to a desired acceptor vector which is mediated by *Esp3I*. The correct orientation of the GOI is dictated by combinatorial sites in both the donor and the acceptor vector and the acceptor/destination vector system is also capable of *blue white screening*.

3.2.2.1.1. Donor vector generation

In order to generate a donor vector carrying the GOI of choice, the GOI was amplified from a cDNA or plasmid DNA template by PCR using the *proof read* polymerase *Phusion HSII*. Primers were designed as described above using the *StarPrimer D'Signer* (IBA) tool. The reaction mixture for the PCR is shown in **table 1** and the PCR program is shown in **table 2**.

Table 1: donor vector generation by means of the *Stargate* cloning method (reaction mixture for the amplification of the GOI via PCR using *Stargate* compatible primers)

component	volume/ amount
HF-/GC buffer (5x)	10 µL
dNTPs (10 mM)	1 µL
primer fw (10 µM)	2.5 µL
primer rv (10 µM)	2.5 µL
DMSO	1.5 µL
Phusion HSII (2 U/mL	0.5 µL
template plasmid	200 pg
ad. ddH_2O	50 µL

Table 2: donor vector generation by means of the *Stargate* cloning method (PCR program)

step	temperature [°C]	time [s]	
1. initial denaturation	98	30	
2. denaturation	98	10	
3. annealing	variable, default: 55 or 60	30	
4. elongation	72	variable, 30/kb	go to 2., 19x
5. final elongation	72	480	
6. pause	4	∞	

The PCR was analysed by 0.8% agarose gel electrophoresis and specific bands were extracted using the NucleoSpin *Gel and PCR CleanUp* kit (Macherey-Nagel). The concentration of the extracted amplification product was determined by *NanoDrop* and the amplification product was diluted to 2 nM final concentration for cloning into pENTRY-IBA51. The cloning protocol is shown in **table 3**.

Table 3: donor vector generation by means of the *Stargate* cloning method (reaction mixture for the recombination of the amplified GOI and the entry vector pENTRY-IBA51)

component	volume [µL]
pENTRY-IBA51 (0.67 ng/µL)	7.5
PCR product (2 nM)	12
ATP (12.5 mM)	1
T4-DNA ligase (1 U/µL)	1
LguI (5 U/µL)	1
buffer Tango (10x)	2.5

The reaction mixture was pipetted into a 0.2 mL thin walled PCR-tube and incubated for 1 hour at 30°C. 10 µL were then used for transformation into *E. coli TOP10* (see 3.2.1.2.) and plated on LB-Kan/X-Gal agar plates. The day after, 3 white colonies were picked and overnight cultures were prepared in 2 mL LB-Kan medium each. The plasmid DNA was extracted by DNA Miniprep using the *NucleoSpin Plasmid* kit (Macherey Nagel) and the DNA concentration was determined by *NanoDrop*. The vector was verified by sequencing (*Seqlab* sequencing service) using ENTRY-primer rev and ENTRY-primer for2. Verified donor vectors were stored at -20°C.

3.2.2.1.2. Destination vector generation

For destination vector generation the donor vector carrying the GOI of choice was diluted to 2 ng/µL and the GOI was cloned from pENTRY-IBA51 GOI into the desired acceptor vector according to **table 4**.

Table 4: destination vector generation by means of the *Stargate* cloning method (reaction mixture for the recombination of the GOI-containing donor vector and the acceptor vector of choice).

component	volume [µL]
acceptor vector of choice (0.67 ng/µL)	7.5
250 mM DTT/12.5 mM ATP	1
T4-DNA ligase (1 U/µL)	1
Esp3I (10 U/µL)	0.5
buffer Tango (10x)	2.5
donor vector (pENTRY-IBA51 GOI) (2 ng/µL)	12.5

The reaction mixture was pipetted into a 0.2 mL thin walled PCR-tube and incubated for 1 hour at 30°C. 10 µL were then used for transformation into *E. coli TOP10* (see 3.2.1.2.) and plated on LB-Amp/X-Gal agar plates. The day after, 3 white colonies were picked and overnight cultures were prepared in 2 mL LB-Amp medium each. The plasmid DNA was extracted by DNA Miniprep using the *NucleoSpin Plasmid* kit (Macherey Nagel) and the DNA concentration was determined by *NanoDrop*. The vector was verified by sequencing (*Seqlab* sequencing service) using the adequate sequencing primer pairs (i.e. ASG-for and ASG-rev for pASG-IBA vectors). Verified destination vectors were stored at -20°C.

3.2.2.2. Classic (restriction) cloning

For the restriction cloning method, either the insert was directly cutted out of the entry vector using the restriction enzymes of choice and ligated into the linearized vector of choice using T4 DNA ligase or the insert of choice was amplified by PCR using primers bearing the desired restriction sites plus 3-6 extra bases to increase the restriction efficiency and eventually extra nucleotides to ensure that the insert is cloned in-frame , the PCR was evaluated by agarose gel electrophoresis and extracted using the NucleoSpin *Gel and PCR CleanUp* kit (Macherey-Nagel). The restriction was typically performed with 1 U restriction enzyme per µg DNA for 1-2 hours at 37°C. If necessary (only one enzyme used for linearization), following restriction the linearized vector was treated with Calf Intestine Alkaline Phosphatase (CIAP) directly after linearization for 30 minutes at 37°C and CIAP was inactivated by heat (15 minutes at 65°C). For ligation, T4 DNA ligase (5 Weiß-U per reaction) was utilized and the ligation was performed either for 1-2 hours at RT or overnight at 15°C. Following ligation, the reaction was transformed into chemically competent *E. coli XL-1 blue* or *DH10B*. The day after, typically 2-4 colonies were picked and overnight cultures were prepared in 2 mL LB medium supplemented with the required antibiotic each. The plasmid DNA was extracted by DNA Miniprep using the *NucleoSpin Plasmid* kit (Macherey Nagel) and the DNA concentration was determined by *NanoDrop*. The vector was verified by sequencing (*Seqlab* sequencing service).

3.2.2.3. Mutagenesis

3.2.2.3.1. Quick Change Mutagenesis (QCM)-insertion of point mutations

Quick Change Mutagenesis (QCM) was originally developed by *Stratagene* as a means to conveniently introduce mutations into a vector of choice. The protocol comprises three general steps:

1. Generation of the mutant strand (PCR): The dsDNA (plasmid) template is amplified by PCR using complementary primers which hybridize to exactly the same site on the *sense*- and *antisense* strand and both harbour the desired mutation. To minimize the risk of secondary mutations a *proofread* polymerase i.e. *Pfu* or *Phusion* is used.
2. Digestion of the template DNA by *DpnI*: *DpnI* is a methylation sensitive restriction enzyme (recognition sequence Gm^6ATC) which selectively cleaves the template plasmid DNA harvested from methylation competent strains but not the unmethylated mutant strand (PCR product).
3. Transformation of the mutant strand into *E. coli XL1-blue* for *nick* repair

For the generation of the mutant strand two reactions (one containing the fw and one containing the rv primer) were set as shown in **table 5**.

Table 5: Quick-Change Mutagenesis (reaction mixture for the amplification of the template vector). Two reactions were prepared for each mutation, one harbouring the respective fw and the other one the respective rv primer.

component	volume [µL]
ddH_2O	13
GC-buffer (5x)	5
dNTPs (10 mM)	0.5
primer fw/rv (10 µM)	1
target vector (10 ng/µL)	5
Phusion HSII (2U/µL)	0.5

The PCR program depicted in **table 6** was run for 12 cycles. Afterwards, the two reactions were unified and the program was run for another 15 cycles.

Table 6: Quick-Change Mutagenesis (PCR program). The two reaction mixtures containing the fw respectively the rv primer were amplified for 12 cycles, unified and amplified for another 15 cycles.

step	temperature [°C]	time [s]	
1. initial denaturation	98	30	
2. denaturation	98	15	
3. annealing	55	60	
4. elongation	72	225 (pASK-IBA5plus SHIP1) 255 (pEGFP-C1 HA-SHIP1)	go to 2., 11x respectively 14x
5. final elongation	72	120	
6. pause	4	∞	

Following amplification 1.25 µL *DpnI* (10 U/µL) was added and the reaction was incubated for at least one hour at 37°C. 10 µL of the digested PCR product was used for transformation into chemically competent *E. coli XL1 blue* (see 3.2.1.2.). The remaining product was stored at -20°C. The day after, overnight cultures were prepared in 2 mL LB medium containing an appropriate antibiotic and the plasmid DNA was extracted using the *NucleoSpin Plasmid* kit (Macherey-Nagel). The concentration and purity of the plasmid DNA was determined by *NanoDrop* and the presence of the mutation was validated by sequencing (*Seqlab* sequencing service) using adequate sequencing primers.

3.2.2.3.2. Deletion of domains

For domain deletions, the *Q5 mutagenesis kit* (New England Bioscience) was used according to the instructions of the manufacturer.

3.2.3. Protein biochemical methods

3.2.3.1. Recombinant expression of Strep tagged proteins under the control of the inducible tet promotor system

The tet promotor is an inducible promotor system which usually allows for lower yields in comparison to the strong T7 promotor system but enhanced solubility of the protein of interest in some cases. In addition, the tet promotor is completely repressed in the absence of an inducing agent (tetracycline or tetracycline derivates) which prevents "leaky expression" events as typically found in the case of the T7 promotor. In relation to tetracycline anhydrotetracycline exhibits a ~200-fold higher affinity for the tet promotor allowing for efficient induction of protein expression at antibiotically non-effective concentrations (200 ng/mL).
For the expression of Strep-tagged proteins the vector of choice was transformed into chemically competent *E. coli BL21(DE3)pLysSpREP4* according to 3.2.1.2. The next day, an overnight culture was prepared in LB-medium containing the appropriate antibiotic and incubated for 16-18 hours at 37°C and 220 rpm. The day of expression, an adequate volume of LB medium (i.e. 500 mL as a starting volume for a column volume of 0.2 mL) was inoculated 1:100 to 1:50 with the overnight culture and incubated at 37°C and 220 rpm until and OD_{600}≈0.6 was reached. The culture was either allowed to cool down for 30 minutes at RT followed by induction of expression with 200 ng/mL f.c. anhydrotetracycline for 3-4 hours at RT and shake or allowed to cool down for 10 minutes on ice followed by induction of expression with 200 ng/mL f.c. anhydrotetracycline for 20 hours at 12°C and shake to improve the solubility of the protein if necessary. Following expression, bacteria were harvested by centrifugation for 10 minutes at 4065.9xg and 4°C and resuspended in 1/100 of the initial culture volume of the purification buffer of choice. With regard to the volume of purification buffer used for resuspension of the bacteria 1/5 volume of Triton X-100 (10%), 1/50 volume of benzamidine (0.1 M), 1/25 volume of PMSF (0.1 M) and 1/250 volume of DTT (1 M) was added to improve bacterial lysis and to minimize proteolytic effects. The bacteria were lysed by ultrasonication (3-4 times 45 seconds with one minute pause on ice in between) using a probe sonicator. Cellular debris was removed by centrifugation for 30 minutes at 19200xg and 4°C. The supernatant (=lysate) was used for protein purification.

3.2.3.2. Chromatographic purification of Strep tagged proteins

3.2.3.2.1. Ion Exchange chromatography (IEX)

3.2.3.2.1.1. Pre-purification of bacterial lysates by Ion Exchange chromatography (IEX) for subsequent Strep-Tactin affinity chromatography

IEX is a method to separate proteins according to their charge at a given pH value that is to say dependent on their isoelectric point (pI). An ion exchange resin contains negatively (for Cation Exchange, CIEX) or positively (for Anion Exchange, AIEX) charged functional groups which can associate with complementary charged ions (charged proteins). The binding strength is dependent on the charge strength which is in turn determined by the pI and the pH value of the purification buffer. Proteins charged the same as the resin or being uncharged at the given pH value do not bind to the resin (flow-through). For the elution of bound proteins the buffer conditions are changed (i.e. by increasing the salt strength (linear NaCl gradient) or by altering the pH value). The higher the interaction strength between the resin and the protein the later the protein will elute.
For IEX the *Pierce Strong Ion Exchange Spin columns mini* (Thermo Scientific) were utilized. AIEX columns (Q) contain immobilized quaternary ammonium functional groups and CIEX columns (S) contain sulphonic acid functional groups. The Column Volume (CV) is 0.5 mL. Purification buffers were selected according to the pI of the protein and the buffering capacity of available buffer systems at the desired pH value (i.e. 50 mM Na-citrate/citric acid, pH 5.0 for CIEX or 50 mM Tris/Cl, pH 8.5 for AIEX). The column was equilibrated with 1 CV purification buffer by centrifugation for 5 minutes at 2000xg and 4°C and the bacterial lysate (see 3.2.3.1.) was loaded on the column in as many steps as necessary by centrifugation for 5 minutes at 2000xg and 4°C. The column was washed twice with 1 CV purification buffer by centrifugation for 5 minutes at 2000xg and 4°C. Elution was performed in four fractions of 1 CV each using increasing salt concentrations (250 mM, 500 mM, 750 mM and 1000 mM NaCl in purification buffer). The elution fractions were analysed by SDS-PAGE according to 3.2.3.3. and fractions containing the protein of interest were pooled and used for *Strep-Tactin* purification (see 3.2.3.2.2.).

3.2.3.2.1.2. Post-purification of Strep-Tactin eluates by Ion Exchange chromatography (IEX)

Protein of interest containing *Strep-Tactin* eluates originating from a 0.5 mL CV resin were pooled and directly used for AIEX as described in 3.2.3.2.1.1. The elution fractions were analysed by SDS-PAGE according to 3.2.3.3. and fractions containing the protein of interest were pooled, shock-frozen in liquid nitrogen and stored at -80°C in 10 µL aliquots.

3.2.3.2.2. Strep-Tactin affinity purification

The *Strep-Tactin*/Strep tag system makes use of the high affinity between biotin and avidin or streptavidin. It comprises the Strep-tag mimicking the streptavidin binding site of biotin and *Strep-Tactin*, a modified streptavidin. The system was improved by the introduction of *Strep-Tactin XT*/TwinStrep tag allowing for almost covalent binding conditions (low nM range) and enabling more stringent washing and improved yields.
Buffer W (100 mM Tris, 150 mM NaCl, 1 mM EDTA, pH 8.0) was used as purification buffer and could be modified by the addition of NaCl or Tween-20 for more stringent washing. The bacterial lysate (see 3.2.3.1.) was loaded onto a 0.2 mL CV (for a culture volume of 500 mL) *Strep-Tactin superflow XT* resin and allowed to flow through at reduced flow rate (~0.5-1 mL/min). The resin was washed with 10 CV buffer W and proteins were eluted in three fractions by the addition of 0.6 CV/1.6 CV/0.8 CV buffer BXT (100 mM Tris/Cl, 150 mM NaCl, 1 mM EDTA, 50 mM biotin, pH 8.0). The elution fractions were analysed by SDS-PAGE according to 3.2.3.3. Fractions containing the protein of interest (typically fractions 2 and 3) were pooled shock-frozen in liquid nitrogen and stored at -80°C in 10 µL aliquots or were used for post-purification using AIEX (see 3.2.3.2.1.2.). The resin was regenerated by the addition of 10-20 CV 20 mM NaOH. Regeneration was verified by adding 1 CV buffer R (100 mM Tris/Cl, 150 mM NaCl, 1 mM EDTA, 1 mM HABA) which would turn from yellow to an orange shade of red if regeneration was successful. Remaining NaOH and HABA was removed by 10-20 CV buffer W and the resin was stored in buffer W at 12°C. Resins could be reused up to 6 times according to the manufacturer.

3.2.3.2.3. Concentration of purified proteins by ultrafiltration

In cases of low protein yields (i.e. Strep-SHIP1) further concentration of the purified protein was necessary. To this aim, the purified protein was applied to an *Amicon Ultra* sample tube of an appropriate molecular weight *cut-off* and centrifuged at 3500xg and 4°C until the desired rate of concentration was reached (typically between 5 and 15 minutes). The concentrate was transferred to a fresh sample tube and analysed by SDS-PAGE according to 3.2.3.3. The concentrated protein was shock-frozen in liquid nitrogen and stored at -80°C in 10 µL aliquots.

3.2.3.3. Sodium Dodecyl Sulphate Polyacrylamide Gel Electrophoresis (SDS-PAGE)

For SDS-PAGE (*BioRad mini* system) a 10-14% separating gel and a 4.8% stacking gel was used. An appropriate sample volume was mixed with 3x loading dye, vortexed and incubated for 10 minutes at 95°C. The samples were shortly centrifuged to remove condense water and loaded onto the gel. The gel was let run for 30-45 minutes at 200 V until the leading front reached the end of the separating gel. The gel was stained for 20 minutes in *Coomassie Brilliant Blue R-250* staining solution and washed twice with ddH_2O to remove residual *Coomassie*. The gel was then destained using *Coomassie* destaining solution until background staining was totally removed. The destaining solution was changed several times within the process.
For densitometric concentration determination, appropriate volumes of the sample were loaded (i.e. 1, 2, 4 µL) in addition to a BSA standard (600, 1200, 2400 ng). The band intensity was evaluated using the *AIDA Image Analyser 3.44* software. The BSA-standard intensities were plotted against the amount of BSA and a linear regression curve was calculated which was used for the quantification of the protein of interest.

3.2.3.4. Phosphatase assay (recombinant SHIP1)

The phosphatase assay is a colorimetric assay used to evaluate the enzymatic activity of phosphoinositide phosphatases and is based on the reaction

$$ci8 - PtdInsP_n \xrightarrow{PPase} ci8 - PtdInsP_{n-1} + P_i$$

The liberated P_i is proportional to the amount of hydrolysed substrate and can be detected by complex formation with malachite green which shifts its colour from yellow to green-blue. This is measured at a wavelength of 620 nm. For an assay the following reaction mixture was pipetted into a 1.5 mL sample tube with the exception of the substrate and pre-incubated for 5 minutes at 37°C. The substrate was added and 90 µL aliquots were taken at adequate time points depending on the velocity of the reaction and stopped by adding 31.5 µL 0.1 M EDTA.

200 µL 2x assay buffer
x µL phosphatase
x µL ci8-$PtdInsP_x$
ad. ddH_2O to 400 µL

All measurements were done in threefold determination.
80 µL of each sample and 80 µL of a $NaHPO_4$ standard (0, 0.5, 1, 3, 5, 10, 30, 50 µM) were pipetted into a 96-well plate and 20 µL working solution was added to each well. The reaction was incubated for 30 minutes at RT and measured at 620 nm using a microplate reader. The concentration of liberated phosphate was determined following calculation of the $NaHPO_4$ standard linear regression curve. As the reaction was stopped with EDTA the phosphate concentration had to be multiplied by the factor 1.3. To assess the specific enzymatic activity, the difference of the measured phosphate concentrations between two time points of the linear range of the reaction was divided through the time lying between those points (µM/min), multiplied with 0.1 (nmol/min or mU) and divided through the amount of enzyme used (mU/mg). For the determination of kinetic parameters, the enzymatic activity was assessed for different substrate concentrations (0, 5, 10, 20, 50, 100, 300 µM) and plotted against the substrate concentration. The K_M value and V_{max} were calculated by hyperbolic regression (*One site binding hyperbola*, *GraphPad Prism 3.03*) and k_{cat} was calculated by $k_{cat}=V_{max}/[E]_0$. The enzymatic efficiency was k_{cat}/K_M.

3.2.4. Surface Plasmon Resonance (SPR): Lipid monolayer measurements

SPR is a label-free technique to analyse the strength of ligand-analyte interactions based on a resonance phenomenon between surface plasmons and a polarized light beam originated evanescent wave.
In an SPR experimental setting, the ligand would be immobilized on an adequate sensor consisting of a glass (prism) and a thin (~50 nm) metal layer (typically gold). The sensor may be derivatized by functional groups used to capture the ligand (i.e. hydrophobic groups for lipid-derived ligands). The analyte is solved in an aqueous phase and let flown over the sensor bearing the immobilized ligand.

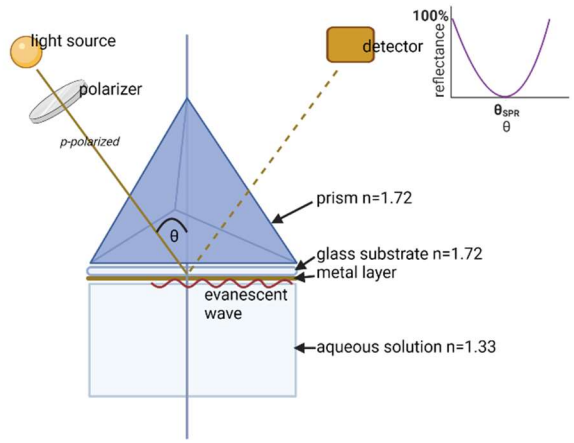

fig. 5: general principle of Surface Plasmon Resonance (SPR). SPR is utilized to measure the interaction between a ligand immobilized on a sensor and an analyte which is let flown over the sensor in an aqueous solution. The sensor consists of a glass and a metal layer. Surface plasmons are electromagnetic fields which oscillate between the aqueous phase and the metal phase. The sensor is subjected to p-polarized light which becomes totally reflected in order to generate an evanescent wave when crossing the interface from the sensor (high refractive index) to the aqueous phase (low refractive index). Resonance between the surface plasmons and the evanescent wave occurs at a specific incident angle θ_{SPR} at which the wave vector of the surface plasmons is equal to that of the evanescent wave. The detected reflectance signal is minimal at θ_{SPR} as the energy of the evanescent wave is partly absorbed by the surface plasmons. Binding of a ligand to the sensor or analyte to the immobilized ligand results in a shift of θ_{SPR} in a way that a mass shift of 1 pg/mm^2 equals a shift of θ_{SPR} of 0.0001° or a resonance signal of 1 RU (Resonance Unit)

Surface plasmons are electromagnetic fields oscillating between an aqueous and a metallic phase and exhibiting successive decrease in energy in a gradient perpendicular to the interface.

$$E = E_0(\hat{x} + i\hat{z})\mathrm{e}^{i(kx-\omega t)}\mathrm{e}^{-k|z|} \quad (1)$$

E_0=initial amplitude, k=wave vector, ω=angular frequency, $\hat{x}$ and $\hat{z}$=unit vectors, E=resulting amplitude

A *p*-polarized light beam directed towards the sensor surface becomes totally reflected at the transition from a phase of a higher (prism, n=1.72) to a lower (aqueous phase, n=1.33) optical density which results in the generation of an evanescent electromagnetic field of the form

$$E = E_0(\hat{x} + i\hat{z})\mathrm{e}^{i\left(k_t x \sin\theta \frac{n_i}{n_t} - \omega t\right)}\mathrm{e}^{-\beta|z|} \quad (2)$$

β=wave vector in the transmitted (aqueous) phase, θ=incident angle, n_i=refractive index of the incident (prism) phase, n_t=refractive index of the transmitted phase

Surface Plasmon Resonance basically describes the excitation of surface plasmons by an evanescent field and will occur if the wave vector of the evanescent wave equalizes that of the surface plasmons (resonance condition).

$$\boldsymbol{k_{SP}} = \frac{\omega}{c}\sqrt{\frac{\varepsilon_m n^2}{\varepsilon_m + n^2}} = \sin\theta\frac{n_i}{n_t} \quad (3)$$

k_{SP}=wave vector of surface plasmons, ε_m=dielectric constant of the metallic phase, n=refractive index of the bordering phase, c=light velocity (vacuum)

Reasoning out of **eq. 3** surface plasmon excitation is dependent on the incidence angle of the evanescent wave θ and can be observed only at a specific incidence angle θ_{SPR} for which the resonance condition is fulfilled. This corresponds to a drop of the amplitude of the outgoing wave (reflectance signal) as a portion of its energy is transferred to the surface plasmons, which is detected. Mass/area changes at the sensor surface (i.e. binding of a ligand or analyte) shifts θ_{SPR} and the extend of this shift depends on Δpg/mm^2 where a mass shift of 1 pg/mm^2 equalizes a shift of θ_{SPR} of 0.0001° or a resonance signal of 1 RU (Resonance Unit).

3.2.4.1. Generation of Large Unilamellar Vesicles (LUVs)

For LUV generation DiOleoylPhosphatidylCholine (DOPC), DiOleoylPhosphatidylEthanolamine (DOPE) and the ci16-PtdInsP$_x$ of interest dissolved in chloroform were mixed in a reagent glass in a molar ratio of 20:77:3 (DOPE:DOPC:PtdInsP$_x$) or 20:80 (DOPE:DOPC) for the generation of control surfaces in amounts to reach a final lipid concentration of 10 mM in 500 µL. The lipids were dried under N_2(g) and the lipid film was resuspended in

500 µL SPR running buffer for LUVs and vortexed for 5 minutes. The mixture was sonicated for 30 seconds, constant, full power in a bath sonicator and passed 15 times through an extruder bearing a 100 µm polycarbonate membrane. The LUVs could be stored for up to three days at 4-8°C.

3.2.4.2. Coating of HPA sensors with LUVs (lipid monolayer generation)

A hydrophobic (HPA) sensor was used for lipid coating. Previously, it was noted that LUVs formed lipid monolayers upon contact with the hydrophobic sensor surface with the acyl chains associating with the sensor surface and the head groups orientated to the outside. This mimics the inner leaflet of a plasma- or endomembrane. The protocol for coating is shown in **table 7**.

Table 7: coating of HPA sensors with Large Unilamellar Vesicles (LUVs). LUVs containing lipids at a molar ratio of 20:80 (DOPE:DOPC, control vesicles) or 20:77:3 (DOPE:DOPC:PtdInsP$_x$) were diluted in running buffer for LUVs to the desired final concentration. Prior to docking of the HPA sensor the system was primed 5 times with ddH_2O and 2 times with running buffer for Luvs. Prior to the experiment a *Prime-Main Degas-Prime* step was included.

sample	spot	flow rate [µL/min]	volume [µL]	dissociation [s]
10 mM NaOH/1 M NaCl	A/B	30	10	1
0,1 M HCl	A/B	30	10	1
10 mM NaOH/1 M NaCl	B	30	10	1
0,1 M HCl	B	30	10	1
10 mM NaOH/1 M NaCl	A	30	10	1
0,1 M HCl	A	30	10	1
40 mM ocytl-glucoside	A+B	15	60	1
ddH_2O	A+B	15	45	1
40 mM ocytl-glucoside	A+B	15	60	1
LUVs	B	12.5	75	1
10 mM NaOH	A+B	10	10	1
0.1 mg/mL BSA	A+B	5	25	1
10 mM NaOH	A+B	10	10	1

3.2.4.3. Assay

The protein of interest (analyte) was serially diluted 1:2 starting from a concentration of 37.5 nM (initial) or lower if necessary and let flown over the ligand coated HPA sensor at a flow rate of 20 µL/min, a volume of 60 µL and a dissociation time of 180 seconds (spots A+B). All measurements were done in triple determination.

3.2.4.4. Data evaluation

For data evaluation the raw data (.sdf) file was opened in the *Sierra Analyser* software and an overlay was created. The data were grouped *by channel*, *control channel assignment* was B-A and *reference channel assignment* was *inter injection event closest* for double subtraction. Spikes were removed by the *smooth curve* option. To determine the lipid coating level the *post injection stop* points were assigned for the capture step (injection 10) in the panel *report point table*. For the evaluation of the assay data the *pre injection stop* points were assigned in the panel *report point table* and plotted against the corresponding analyte concentration. Curves were fitted by hyperbolic regression (*One site binding hyperbola*, *GraphPad Prism 3.03*) to obtain the K_D value.

3.2.5. Phospholipid Overlay (PLO) assay and COVA-PIP Array assay

For the PLO assay and COVA-PIP array assay membranes or plates coated with the phosphoinositide of interest were purchased from Echelon Bioscience. The protein of interest was diluted to 0.5, 1.0 or 1.5 µg/mL in blocking buffer (3% BSA, 0.5% Tween in PBS) and 100 µL/well was pipetted into the COVA-PIP plate and incubated for 1 h at RT and gentle shake respectively the membrane was incubated in 5 mL of the protein solution. The protein solution was discarded and the plate or membrane was washed 3 times for 3 minutes with wash buffer (0.1% Tween-20 in PBS) after which Strep-Mab classic-HRP (1:10000 diluted according to the manufacturer) was added and incubated for 1 h at RT and gentle shake. The plate was washed as described above and additionally 3 times for 3 minutes with PBS and bound protein was detected by developing the plate for 30 minutes with 100 µL/well TMB in the dark and measuring the absorbance at 650 nm (COVA-PIP Array) or by chemiluminescence (PLO assay) using the LAS imager system.

3.2.6. Cell culture methods

3.2.6.1. General cell culture techniques

3.2.6.1.1. Culturing and subculturing (splitting) of cells

Cells were cultured at 37°C and 5% CO_2. H1299, HCT-116, HT-29, SW-480, SCKHA-1, NIH-3T3 and HepG2 cells were cultured in DMEM, 10% FCS, 1% p/s. HEK-293T cells were cultured in DMEM, 10% FCS, 1% pen/strep, 2 mM glutamine, 1 mM sodium pyruvate, 20 mM HEPES. M1 cells were cultured in RPMI, 10% FCS, 1% p/s. For adherent cells, for media change the old medium was removed and the cells were washed once with PBS if wanted. Depending on the type of culture vessel an adequate amount of fresh medium was added (i.e. 12 mL for a 75 mm^2 flask, 8 mL for a 25 mm^2 flask, 20 mL for a 175 mm^2 flask or 4 mL for a 6-well plate). To detach cells (i.e. for splitting) the medium was removed and cells were washed once with PBS. An appropriate amount (usually 1-5 mL depending on the type of culture vessel) was added and the cells were incubated for 5 minutes at 37°C and 5% CO_2. Proper detachment of the cells was verified by phase contrast microscopy. The detachment reaction was stopped by the addition of an adequate amount of medium. For splitting, the desired volume of the cell suspension was left in the culture vessel or was transferred to a new culture vessel and an adequate volume of fresh medium was added. For suspension cells, cells were suspended with a pipette and the desired amount of cell suspension was left in the flask and fresh medium was added to an appropriate volume.

3.2.6.1.2. Thawing and freezing of cells

For long-term storage cells were freezed. For freezing, cells of a fully confluent 75 mm^2 flask were detached as described in 3.2.6.1.1. (for adherent cells) or for suspension cells directly transferred into a 15 mL conical sample tube, type falcon. Cells were centrifuged for 5 minutes at 1400xg and RT and the supernatant was discarded. The cell pellet was resuspended in 1 mL freezing medium and 500 µL each of the suspension was transferred into a 2 mL cryo tube which was put into a freezing help device filled with isopropanol up to the marking line immediately afterwards. The freezing help device was stored over night at -80°C. The next day, cells were transferred into liquid nitrogen.
For thawing of freezed cells 6 mL medium each was pipetted into a 15 mL conical sample tube, type falcon and a 75 mm^2 cell culture flask. Cells of one cryo tube were pipetted into the sample tube and centrifuged for 5 minutes at 1400xg and RT. The supernatant was discarded and cells were resuspended in 6 mL medium and transferred to the culture flask. Cells were cultivated at 37°C and 5% CO_2 according to 3.2.6.1.

3.2.6.2. Lentiviral transfection of HEK-293T cells and subsequent transduction of target cells

Lentiviral transduction was used for stable overexpression or *knock-down* of a protein of interest in mammalian cell culture. *Lentivirae* are able to infect both dividing and quiescent cells which broadens their range of application. The system is based on the infection cycle of *lentivirae* (i.e. Human Immunodeficiency Virus (HIV)). Those viruses attach to a host cell through the association of their surface envelope proteins to a suitable host cell receptor which releases the nucleocapsid into the cytosol. The ssRNA genome is transcribed into dsDNA by the viral reverse transcriptase and translocated to the nucleus where it becomes integrated into the host genome (provirus, latent state of infection). The integration is mediated by Long Terminal Repeats (LTRs) which do flank the viral genome. In the lytic state the provirus becomes transcribed and eventually translated by the host machinery yielding the structural proteins and the viral genome, and the viral particles are assembled before being released from the host by cell lysis. The lentiviral genome comprises several overlapping ORFs. The most decisive genes are *env* encoding the envelope protein, *gag* encoding the matrix, capsid and nucleocapsid proteins, *pol* encoding the reverse transcriptase and integrase, *rev* which gene product facilitates the nuclear export of partially spliced or unspliced transcripts by associating with the rev Response Element (RRE) and *tat* encoding the transactivator protein. For laboratory use, two systems are routinely utilized. Regarding the second generation system the genes are splitted over three plasmids: the envelope plasmid (*env*, i.e. VSV-G (Vesicular Stomatitis Virus-Glycoprotein) is used as envelope protein), the packaging plasmid (*gag*, *pol*, *tat*, *rev*) and the transfer plasmid (GOI and the packaging signal Ψ flanked by LTRs, may additionally contain a selection marker (i.e. puromycin resistance) and/or a fluorescence reporter). In the third-generation system the packaging plasmid is further splitted into *rev* and *gag/pol* which provides an extra level of security. The 5' LTR is fused to a constitutive and strong promotor which dispenses the dependence of high-level GOI expression on *tat*. For improved transduction results the transfer genes *cPPT* (central PolyPurine Tract) specifying the recognition site for proviral DNA synthesis and enhancing the transduction efficiency and expression of the GOI, WPRE (*Woodchuck* hepatitis virus Post-transcriptional Regulatory Element) increasing the nuclear export and expression of the GOI and the *rev* binding site RRE are included.

Lentiviral particles are produced by transfecting the producer cell line HEK-293T with the envelope, packaging and transfer plasmids. The generated lentiviral particles are released into the medium and are replication incompetent due to the presence of a 3' Self Inactivating Long Terminal Repeat (3' SIN-LTR). The virus containing medium (supernatant) is harvested and used for the transduction of the target cell line. Cells can then be selected by culturing them in an appropriate selection medium.
For the transfection of HEK-293T cells, cells were cultured for ~2 weeks prior to transfection. The afternoon before transfection, cells were plated in a density of $6x10^5$ cells/well in a 6-well plate and allowed to adhere overnight. Cells should be ~70% confluent the day of transfection. The reaction mixture for the transfection is shown in **table 8**. All reagents with the exception of lipofectamine 3000 and P3000 reagent were pipetted into a 1.5 mL sample tube. The P3000 reagent was added and mixed carefully by snipping. Next, the lipofectamine 3000 reagent was added and mixed again carefully by snipping. The reaction was incubated for 15 minutes at RT. During the incubation time, the medium of the HEK-293T cells was changed. The final volume of medium had to be 2 mL/well. The transfection mixture was pipetted dropwise to the cells and mixed by carefully swivelling the plate. Cells were incubated overnight at 37°C and 5% CO_2.Target cells were plated at a density of 1-$2x10^5$/well in a 6-well plate.

Table 8: transfection of HEK293T cells for the production of lentiviral particles. Cells were plated in a 6-well plate at a count of $6x10^5$ cells/well the day before transfection and should be 70% confluent at the day of transfection

component	volume/amount
pCMV-VSV-G	0.4 µg
pMDLg/pPE	2 µg
pRSV-Rev	1 µg
target plasmid	2 µg
P3000 reagent	5 µL
Lipofectamine 3000 reagent	7 µL
Opti-MEM	ad. 300 µL

The desired target cell line was transduced with the respective viral supernatants harvested 24 hours and 48 hours post-transfection. For harvesting of viral supernatants the medium of the HEK-293T cells transfected with the desired construct was transferred into a 15 mL conical sample tube, type Falcon and filtered through a 0.22 µm filter device. An appropriate aliquot was transferred into a 1.5 mL sample tube and subjected to one cycle of freeze and thaw. In the meantime, the medium of the target cells was changed to 2 mL/well medium supplemented with 8 µg/mL f.c. polybrene. The supernatant was then titrated on the target cell using suitable volumes (i.e. ranging from 0.001 µL to 100 µL in a first approach). The cells were centrifuged for 30 minutes at 2000 rpm and 20°C and incubated for three to four days at 37°C and 5% CO_2. The remaining viral supernatant was stored at -80°C in 300 µL aliquots. If possible (presence of a fluorescent reporter), the percentage of transduced cells was determined by FACS analysis and should lie in the range of 5% to 19% eGFP-positive cells if aimed for single integration. Otherwise, the transduction should be repeated with the remaining viral supernatant using adjusted volumes. The Multiplicity Of Infection (*MOI*) was calculated using the formula:

$$MOI = \frac{x_{\text{plated}} * (\frac{x_{\text{eGFP+}}}{x_{\text{plated}}})}{V_{\text{viral supernatant}}} \quad (4)$$

MOI=Multiplicity of Infection [mL^{-1}], x_{plated}=number of plated cells, x_{eGFP+}=number of eGFP-positive cells, $V_{viral\ supernatant}$=volume of viral supernatant [mL]

A rate of eGFP-positive cells of ~5% should be used for the calculation of the titre.
Adequately transduced cells were selected with puromycin starting 3-4 days after transduction (f.c. dependent on the cell line and determined by a puromycin killing curve) for a minimum of ~3-4 days and analysed by FACS if possible (fluorescent-dye containing vectors). For FACS analysis cells were detached as described in 3.2.6.1.1., washed once with PBS and resuspended in 1 mL PBS. Cells were gated into the living population (P1) by forward and sideward scatter and P1 was further gated into the eGFP positive population (P2) by the FITC channel plotted against the forward scatter using the respective parental cells as negative sample. The percentage of eGFP-positive cells should be >90% in case of a successful selection. If necessary eGFP-positive cells were sorted using the *FACS Aria IIIu* or *FACS Aria Fusion* at the UKE FACS Core Facility. The selected (and sorted) cells were frozen and stored in liquid nitrogen.

3.2.6.3. Stimulation of cells

Cells were stimulated with EGF or LPA in order to assess the functional impact of a genetic alteration i.e. SHIP1 overexpression on the signalling pathways in question. For a stimulation experiment cells were seeded at an appropriate density in a cell culture vessel of choice (i.e. $3x10^6$ cells/10 cm dish) and allowed to attach for 18-20 hours in normal culture medium (i.e. DMEM+10% FCS). The medium was removed and cells were washed once with PBS. Cells were the starved for 24 hours in starvation medium (i.e. DMEM+0.1% BSA) and stimulated for the desired period of time (i.e. 10 or 30 minutes) with EGF (50 ng/mL f.c. in starvation medium) or LPA (100 ng/mL f.c. in starvation medium) and lysed by TCA or NP40 lysis for Western Blot analysis.

3.2.6.4. Determination of the half life time of SHIP1 proteins (cycloheximide treatment of cells)

To determine the half life time of individual SHIP1 proteins cells were treated with the ribosome inhibitor cycloheximide. Cells were seeded at a density of $3x10^5$/well in a 6-well plate and allowed to attach for 24 hours. One well was lysed immediately after the attachment period (t=0 control). For the remaining wells the medium was changed to medium containing either cycloheximide (750 µM f.c. solved in DMSO) or an equal volume of DMSO (DMSO control) and incubated for the desired period of time (i.e. 0.25, 0.5, 1, 2, 3, 4, 6, 8 hours) after which cells were lysed by NP40 lysis and the lysates were analysed by Western Blot using SHIP1 P1C1 mouse monoclonal antibody for detection (threefold determination). The band intensity was quantified and normalized to Ponceau staining and the mean intensity at t=0 and the half-life time was calculated using the formula $y = Bottom + (Top - Bottom) * \left(1 - \mathrm{e}^{-k*x_0}\right)$ or $y = Span * \mathrm{e}^{-kx} + Plateau$ where the half-life was x_0+0.69/k or 0.69/k.

3.2.6.5. MG-132 treatment

MG-132 is a well-known proteasome inhibitor and used to determine if a given protein is target of enhanced proteasomal degradation. For MG-132 treatment cells were seeded in a 6-well plate in an appropriate density the day before treatment so that they would reach 70-80% confluence at the day of treatment. The medium was changed to medium containing 1 µM or 10 µM MG-132 or an equal volume of DMSO and incubated for 5-8 hours at 37°C and 5% CO_2. One well was left untreated. Cells were then lysed by NP-40 lysis and SHIP1 levels were monitored by Western Blot using SHIP1 P1C1 mouse monoclonal antibody and normalized to HSC70 levels.

3.2.6.6. TCA lysis

For the TCA lysis of cells an appropriate amount of cells was seeded into an adequate cell culture vessel (i.e. a 6-well plate or a 10 cm dish) and incubated as desired (i.e. overnight) at 37°C and 5% CO_2. Cells were washed once with PBS and placed on ice. 500 µL ice-cold 0.15 M NaCl/well was added and cells were detached using a cell scraper and transferred to a 1.5 mL sample tube. Cells were centrifuged for 2 minutes at 2000xg and 4°C, the supernatant was discarded and the pellet was resuspended in 500 µL 0.15 M NaCl. The washing step was repeated. After washing, cells were resuspended in 500 µL 0.15 M NaCl and 50 µL 99% TCA was added. Cells were incubated for 30 minutes on ice followed by centrifugation for 5 minutes at 13148xg and 4°C and discarding of the supernatant. The pellet was resuspended in 100 µL1x loading dye w./o. bromophenol blue w./o. DTT and 1/10 volume 1 M Tris/HCl, pH 8.8 was added for neutralization. The volumes of loading dye and Tris/HCl could be adjusted depending on the expected amount of protein. The suspension was sonicated 2 times for 30 seconds, constant, max. energy using a bath sonicator. If the pellet was still visible, additional rounds of sonication were included. The whole protein concentration of the lysate was determined by the *BioRad DC* assay according to the manufacturer. For the calculation of the protein concentration from the absorption values a BSA standard was used (0, 0.125, 0.25, 0.5, 0.75, 1, 1.25 and 1.5 mg/mL in 1x loading dye w./o. bromophenol blue w./o. DTT). For Western Blot analysis, an appropriate amount (typically between 20 and 50 µg) of the lysate was mixed with 1x loading dye w./o. bromophenol blue with DTT to a final volume of 20-30 µL (final volume could be adjusted if necessary) and 0.5 µL 1% bromophenol blue was added. If the solution turned yellow, 1 M Tris/HCl, pH 8.8 would be added until the colour would shift from yellow to bright blue. The sample was vortexed shortly, incubated for 10 minutes at 95°C and centrifuged shortly. It was then ready for Western Blot analysis.

3.2.6.7. NP40 lysis

For the NP40 lysis of cells, cells were washed once with ice-cold PBS and immediately transferred on ice. An appropriate volume of NP40 buffer was added (i.e. 300 µL for a 6-well plate or 800 µL for a 10 cm dish) and cells were detached using a cell scraper and transferred into a 1.5 mL sample tube. Cells were centrifuged for five minutes at 11000 g and 4°C and the supernatant (NP40 cell lysate) was transferred into a fresh sample tube and

could be stored at -80°C. The whole protein concentration of the lysate was determined by the *BioRad DC* assay according to the manufacturer. For the calculation of the protein concentration from the absorption values a BSA standard was used (0, 0.125, 0.25, 0.5, 0.75, 1, 1.25 and 1.5 mg/mL in 1x loading dye w./o. bromophenol blue w./o. DTT). For Western Blot analysis, an appropriate amount (typically between 20 and 50 µg) of the lysate was mixed with ½ volume of 3x loading dye with bromophenol blue and with DTT. The sample was vortexed shortly, incubated for 10 minutes at 95°C and centrifuged shortly. It was then ready for Western Blot analysis

3.2.6.8. Western Blot

For Western Blot samples were prepared according to 3.2.6.6. or 3.2.6.7. and loaded onto a 10% SDS-PAGE gel (Hoefer system). The gel was let run at 100-120 V in the stacking gel and at 150 V in the separating gel or overnight at 20 V. For the transfer (wet blot) all components were soaked in transfer buffer. The 0.45 µm nitrocellulose membrane was equilibrated for 5 minutes in ddH_2O before soaking it in transfer buffer. The blot was mounted in an air-bubble free manner and under the avoidance of any component becoming dry and transferred into a transfer chamber filled with transfer buffer. A small stirring fish was added and the chamber was put onto a magnetic stirrer localized in the cold room and stirred at low frequency. The transfer was performed for 2 hours at 70 V (const. voltage) in the cold room. The membrane was blocked in an appropriate blocking buffer according to the manufacturer (i.e. 3% BSA, 0.5% Tween-20 in PBS or 5% non-fat dried milk powder, 0.5% Tween-20 in TBS) for 1 hour at RT and gentle shake. The primary antibody was diluted in washing buffer (i.e. 0.1% Tween-20 in PBS or 2.5% non-fat dried milk powder, 0.5% Tween-20 in TBS) according to the manufacturer and incubated over night at 12°C and gentle shake. The next day, the membrane was washed 3 times for 10 minutes in washing buffer. The secondary antibody was diluted 1:5000 in washing buffer and incubated for 1 hour at RT. Subsequently, the membrane was washed 4 times 15 minutes with PBS, 0.1% Tween-20 or TBS, 0.5% Tween-20 and twice for 15 minutes with PBS or TBS depending on the buffer system used. In case of a directly HRP-coupled antibody the membrane was washed 4 times 15 minutes with PBS, 0.1% Tween-20 or TBS, 0.5% Tween-20 and twice for 15 minutes with PBS or TBS depending on the buffer system used following primary antibody incubation. For detection, the *Super Signal West Pico* or *Super Signal West Dura chemiluminescence substrate kit* (Thermo Scientific) was used according to the instructions of the manufacturer. Signal strength was evaluated using the *AIDA Image Analyser 3.44* software.

3.2.6.9.. IncuCyte Zoom

The *IncuCyte Zoom* is a *Life Cell Imaging* system which allows for the evaluation of cells using 96- or 384-well plates. This makes it a valuable *screening* system i.e. to test the influence of compounds on cellular traits (proliferation, apoptosis/survival, cytotoxity, migration, invasion).

3.2.6.9.1. Proliferation assay

For the proliferation assay cells were seeded in an adequate density (i.e. 2500 cells/well) in a 96-well plate and placed into the *IncuCyte Zoom*. *Basic Analyser* was set as *Scan Type* and phase contrast and if desired red or green fluorescence was selected as image channel. Proliferation was monitored every two hours for an appropriate amount of time (typically until confluence reached a plateau). For data evaluation 6-10 representative images were selected as training set for the generation of a confluence mask. The images should cover different time points and conditions/cell lines. The default confluence mask was generated automatically by the *IncuCyte Zoom* software and refined by the user with regard to pixel size, background/cell ratio, eccentricity, size, hole fill and pixel size. The mask was applied to all images taken in the course of the experiment. The confluence at *t=x* was normalized to the confluence at t_0 and the doubling time was calculated by fitting the curves to $confluence_t = confluence_{t_0} * \mathrm{e}^{kt}$ with the doubling time being defined as $t_\mathrm{d} = \ln 2/k$

3.2.6.9.2. Apoptosis assay

Apoptosis was detected either by using *Annexin V red/green* or *Caspase 3/7 red/green* reagent (Essen Bioscience). The desired reagent was mixed with medium as instructed by the manufacturer: *Annexin V red/green* reagent was solubilized in 100 µL medium or PBS and diluted 1:200 in medium for the assay. *Caspase 3/7 red/green* reagent was diluted 1:1000 in medium. For the apoptosis assay cells were seeded in an adequate density (i.e. 2500 cells/well) in a 96-well plate and placed into the *IncuCyte Zoom*. *Basic Analyser* was set as *Scan Type* and phase contrast and red or green fluorescence was selected as image channel. Apoptosis was monitored every two hours for an appropriate amount of time. For data evaluation 6-10 representative images were selected as training set for the generation of a confluence or fluorescence mask. The images should cover different time points and conditions/cell lines. The default confluence and red/green fluorescence mask were generated automatically by the

IncuCyte Zoom software and refined by the user with regard to pixel size, background/cell ratio, eccentricity, size, hole fill and pixel size. The masks were applied to all images taken in the course of the experiment. The fluorescence confluence (*Annexin V red/green*) normalized to the phase contrast confluence or the fluorescent object count (*Caspase 3/7 red/green*) was determined as a measure of apoptosis.

3.2.6.9.3. Migration assay

For the migration assay, the day before cells were seeded in an adequate density (i.e. 40000 cells/well) in a 96-well *Image Lock* plate and allowed to adhere overnight. Cells should have reached ~100% confluence at the day of the assay. The day of the assay cells were wounded making use of the *Woundmaker* (Essen Bioscience) and washed twice with medium and 100 µL medium/well was added. The plate was then placed into the *IncuCyte Zoom* and the *Scan Type* was set to *Scratch wound* and phase contrast. Migration was monitored every two hours for an appropriate amount of time. For data evaluation 6-10 representative images were selected as training set for the generation of a scratch wound mask. The images should cover different time points and conditions/cell lines. The default confluence mask, initial wound mask and wound mask were generated automatically by the *IncuCyte Zoom* software and refined by the user with regard to pixel size, background/cell ratio, eccentricity, size, hole fill and pixel size. The slope of wound width/time in the linear range of the curve was taken as a measure for the migratory speed.

3.2.6.9.4. Invasion assay

For the invasion assay, a 96-well *Image Lock* plate was coated with *Matrigel Basement GF-reduced* (0.1 mg/mL in medium) and incubated over night at 37°C and 5% CO_2. The next day, cells were seeded in an adequate density (i.e. 40000 cells/well) so that they were ~100% confluent and allowed to adhere for 4-22 h at 37°C and 5% CO_2. Cells were wounded making use of the *Woundmaker* (Essen Bioscience), washed twice with medium and chilled for 5 minutes on ice. The medium was then discarded and the cells were layered with 50 µL/well *Matrigel Basement GF-reduced* (8 mg/mL in medium). The plate was incubated for 30 minutes at 37°C and 5% CO_2 and 50 µL medium/well was added and subsequently the cells were placed into the *IncuCyte Zoom.* The *Scan Type* was set to *Scratch wound* and phase contrast. Invasion was monitored every two hours for an appropriate amount of time. For data evaluation 6-10 representative images were selected as training set for the generation of a scratch wound mask. The images should cover different time points and conditions/cell lines. The default confluence mask, initial wound mask and wound mask were generated automatically by the *IncuCyte Zoom* software and refined by the user with regard to pixel size, background/cell ratio, eccentricity, size, hole fill and pixel size. The slope of wound width/time in the linear range of the curve was taken as a measure for the invasion speed.

3.2.6.9.5. Chemotaxis (Boyden Chamber) assay

For the chemotaxis assay the day before, cells were starved for 22 hours in DMEM, 0.2% BSA, 1% p./s. and 1000 cells/well in 60 µL/well were seeded in the top vessel of a *IncuCyte ClearView* 96-well plate and DMEM, 10% FCS, 1% p./s. was used for the bottom vessel (reservoir plate, 200 µL/well). Cells were placed into the *IncuCyte Zoom.* The *Scan Type* was set to *Chemotaxis* and phase contrast. Chemotaxis was monitored every two hours for an appropriate amount of time. For data evaluation 6-10 representative images were selected as training set for the generation of a scratch wound mask. The images should cover different time points and conditions/cell lines. The default masks (top/bottom) were generated automatically by the *IncuCyte Zoom* software and refined by the user. The number of migrated cells was plotted against the time and fitted using the one phase exponential association option of *GraphPad Prism* $y = y_{max} * (1 - \mathrm{e}^{-kx})$ where k is the chemotaxis rate.

3.2.6.10. BrdU ELISA proliferation assay

To determine the proliferation rate of cells the *Cell Proliferation ELISA, BrdU (colorimetric)* kit (Roche) was utilized according to the instructions of the manufacturer. Briefly, cells were seeded at an appropriate density into a flat-bottomed 96-well plate and cultured for an adequate period of time. The synthetic base analogue 5-bromo-2'-deoxyuridine (BrdU) was added to the cells and allowed to be incorporated for two hours. Incorporation of BrdU reflects the level of cell division. Following the incorporation step cells were fixed and the DNA was partially denatured. BrdU was then detected in a colorimetric reaction using a peroxidase coupled BrdU specific antibody.

3.2.6.11. Phosphatase assay using whole cell lysates

The phosphatase assay is a colorimetric assay used to evaluate the enzymatic activity of phosphoinositide phosphatases (for the principle of the phosphatase assay see 3.2.3.4.). For an assay, cells were seeded at a density of i.e. $5x10^6$/10 cm dish and incubated as desired i.e. for 24 h in standard culture medium. Cells were then

lysed by NP40 lysis (see 3.2.5.6.) and the protein concentration was determined by the *BioRad DC* assay according to the manufacturer. For one measurement in threefold determination 150 µL of *a Protein G Sepharose 4 FastFlow* (GE) bead suspension was transferred into a 1.5 mL sample tube and centrifuged for 30 seconds at 11000 g and 4°C. The supernatant was discarded and 300 µL NP40 buffer were added and mixed by inversion of the tube. The beads were centrifuged again for 30 seconds at 11000 g and 4°C. The supernatant was discarded and 300 µL NP40 buffer were added and mixed by inversion of the tube. The washing step was repeated once more. The beads were then resuspended in 300 µL NP40 buffer and 30 µL SHIP1 P1C1 mouse monoclonal antibody was added (stock: 200 ng/µL) and the beads were incubated for 4-6 hours at 12°C and overhead rotation. The beads were centrifuged as described above and washed once with NP40 buffer. The supernatant was discarded and 1 mg of the whole cell lysate was added in a final volume of 800 µL and incubated over night at 12°C and overhead rotation. For an assay the following reaction mixture was pipetted into a 1.5 mL sample tube with the exception of the substrate and pre-incubated for 5 minutes at 37°C. The substrate was added and 90 µL aliquots were taken at adequate time points depending on the velocity of the reaction and stopped by adding 31.5 µL 0.1 M EDTA.
200 µL 2x assay buffer
x µL phosphatase
50 µL ci8-PtdInsP$_x$ (1 mM corresponding to 20 µM f.c.)
ad. ddH_2O to 400 µL
All measurements were done in threefold determination.
80 µL of each sample and 80 µL of a $NaHPO_4$ standard (0, 0.5, 1, 3, 5, 10, 30, 50 µM) were pipetted into a 96-well plate and 20 µL working solution was added to each well. The reaction was incubated for 30 minutes at RT and measured at 620 nm using a microplate reader. The concentration of liberated phosphate was determined following calculation of the $NaHPO_4$ standard linear regression curve. As the reaction was stopped with EDTA the phosphate concentration had to be multiplied by the factor 1.3. To assess the specific enzymatic activity, the difference of the measured phosphate concentrations between two time points of the linear range of the reaction was divided through the time lying between those points (µM/min), multiplied with 0.1 (nmol/min or mU) and divided through the amount of enzyme used (mU/mg). The amount of enzyme used was determined by Western Blot using a recombinant SHIP1 standard curve.

3.2.6.12. Kinome analysis (PAMGENE system)

For the analysis of the kinome the PAMGENE system was used according to the instructions of the manufacturer. The kinome measurements of M-PER lysates were performed at the group of Malte Kriegs (UKE Hamburg).

3.2.6.13. Proteome analysis (differential quantitative proteomics)

For the proteome analysis cells were seeded into 10 cm plates for biological triplicates and at 70-80% confluence cells were trypsinated, the cell pellets were washed 5 times with PBS and shock-frozen in liquid nitrogen. The sample preparation and data analysis was performed by Hannah Voß and Paula Nissen (UKE MS Core facility/AG Schlüter).

3.2.6.13.1. Tryptic digestion for mass spectrometric analysis

Cell pellets were lysed in triethylammonium hydrogen carbonate buffer (TEAB, Thermo Fisher) with 1% w/w sodium deoxycholate (SDC, Sigma Aldrich), boiled at 95°C for 5 min and sonicated 5 times at 30% using a probe sonicator to destroy DNA/RNA. The protein concentration of denatured proteins in deparaffinized, reversed formalin fixed human MB samples was determined by the Pierce TM BCA Protein assay kit following the manufacturer's instructions. For a higher quantification accuracy, the protein concentration was determined in duplicates. 20 µg protein were used for tryptic digestion. Disulfide bridges were reduced in the presence of 10 mM dithiothreitol (DTT, Sigma Aldrich) at 60°C for 30 min and alkylated with 20 mM iodoacetamide (IAA, Sigma Aldrich) for 30 min in the dark at 37°C. Trypsin (sequencing grade, Promega) was added at a 1:100 ratio (enzyme to protein) and digestion was performed overnight at 37°C. The reaction was quenched and SDC was precipitated using 1% formic acid (FA, Fluka). Samples were centrifuged for 10 min at 14'000 x g, the supernatant was transferred into a new tube and lyophilized using a SpeedVac™ vacuum concentrator.

3.2.6.13.2. Mass spectrometric measurements and data analysis

Prior to mass spectrometric analyses, peptides were resuspended in 0.1% FA to a final concentration of 1 µg/µl. LC-MS/MS measurements were performed on a quadrupole- orbitrap mass spectrometer (QExactive, Thermo Fisher) coupled to a nano-UPLC (Dionex Ultimate 3000 UPLC system, Thermo Fisher). 1 µg of tryptic peptides were injected into the chromatographic system via an autosampler, purified and desalted using a reversed phase

trapping column (Acclaim PepMap 100 C18 trap; 100 µm x 2 cm, 100 Å pore size, 5 µm particle size; Thermo Fisher) and transferred to a reversed phase column for chromatographic separation (Acclaim PepMap 100 C18; 75 µm x 25 cm, 100 A pore size, 2 µm particle size, Thermo Fisher). Trapping was done for 5 min at a flow rate of 15 µl/min with 99% solvent A (0.1% FA) and 1% solvent B (0.1% FA in ACN). Separation and elution of peptides were achieved by a linear gradient from 1 to 30% solvent B in 70 min at a flow rate of 3 µl/min. Eluted peptides were ionized using a nano-electrospray ionization source (nano-ESI) with a spray voltage of 1800, transferred into the mass spectrometer and analysed in data dependent acquisition (DDA) mode. For each MS1 scan, ions were accumulated for a maximum of 120 milliseconds or until a charge density of $2x10^5$ ions (AGC Target) was reached. Fourier-transformation-based mass analysis of the data from the orbitrap mass analyzer was performed covering a mass range of 400-1300 m/z with a resolution of 120.000 at m/z = 200. Peptides with charge states between 2+ - 5+ above an intensity threshold of 1000 were isolated within a 1.6 m/z isolation window in Top speed mode for 3 seconds from each precursor scan and fragmented with a normalized collision energy of 30% using higher energy collisional dissociation (HCD). MS2 scanning was performed using an orbitrap mass analyser, covering a mass range of 380-1500 m/z with a orbitrap resolution of 15'000 at m/z = 200 and accumulated for 60 ms or to an AGC target of $1x10^5$. Dynamic exclusion of fragmented peptides was applied for 15 seconds after precursor selection.
Raw data obtained from LC-MS/MS measurements was processed with MaxQuant in the version 1.6.2.10 (Max Plank Institute for Biochemistry, Version 1.6.2.10) using the integrated Andromeda algorithm. For protein identification, measured MS2 spectra were searched against theoretical fragment-spectra of tryptic peptides, generated from a reviewed murine Swissprot FASTA database obtained in February 2020, containing 17015 entries. All samples were handled as individual experiments.
The Carbamethylation of cysteine residues was set as a fixed modification. Methionine oxidation, protein N-terminal acetylation, removal of the initiator methionine at the protein N-terminus and the conversion of glutamine to pyroglutamate were set as variable modifications. Peptides with a minimum length of 6 amino acids and a maximum mass of 6000 Da were identified with a mass tolerance of 10 ppm. Only peptides with maximum of two missed trypsin cleavage sites were considered. For peptide identification, matching between runs was included, using a match time window of 0.7 minutes and an alignment time window of 20 minutes between individual runs. The error tolerance was set to 20 ppm for the first precursor search and to 4.5 ppm for the following main search. Fragment spectra were matched with 20 ppm error tolerance. A false discovery rate (FDR) value threshold <0.01, using a reverted decoy peptide databases approach was set for peptide identification. Label free quantification was performed with an LFQ minimum ratio count of 1. For quantification, all identified razor and unique peptides were considered. The label minimum ratio count was set to 1.

3.2.6.13.3. Statistical analysis

For mass spectrometric analysis, the ProteinGroups.txt result file from MaxQuant was loaded into Perseus software (Max Plank Institute for Biochemistry, Version 1.5.8.5). The quantitative LFQ Intensity values for protein groups were used as main columns. The relative protein abundance for each protein was transformed into $\log_2$ values and normalized by subtraction of the median, for each column. Protein lists were filtered for proteins, quantifiable in at least 2 samples of each compared group. Pearson correlation based unsupervised clustering as well as principal component analysis was performed to estimate the distinguishability of compared groups and for the identification of potential outliners. Individual student's t-test were performed to identify statistically differential abundant proteins between Parental cells, SCR samples and SHIP1 *knockdown* cell lines as well as matching EGFR stimulated samples after 22 hours of starvation for SW-480 Cells (p-value <0.05). Equal settings were applied for the comparison of HCT-116 parental, LeGO transduced and SHIP1 overexpressing cells.
For further analysis, only proteins, whose abundance difference exceeded an 1.5 foldchange difference between compared conditions were considered. For enrichment analysis and protein-protein interaction visualisation of regulated proteins the STRING Database was used. For each analysis a full network was displayed. Experiments, Curated Databases, Co-Expression and Co-Occurrence were used as active interaction sources. A minimum confidence level of medium confidence (Confidence > 0.4) was required. For enrichment analysis a minimum FDR < 0.01 was applied. Principle component analysis as well as group specific abundance distributions of potential biomarker candidates were visualized using PRISM Graph Path in the version 5.

3.2.6.14. Tumoroid assay

In order to form spheroids cells were seeded in serial dilution (ranging from 2000 to 32 cells or 1000 to 16 cells) into ULA (Ultra Low Attachment) 96-well plates and centrifuged for 5 minutes at 900 rpm. ULA plates are coated with a hydrogel layer which prevents cells from attaching to the surface and enabling tumoroid formation which is accelerated by centrifugation. Tumoroid formation was assayed by microscopy or by Alamar Blue assay.

3.2.6.15. RAC-GTP assay

In the RAC-GTP assay active (GTP-bound) RAC was detected due to its association with GST-PAK. GST-PAK was expressed from the vector pGEX-2TK-GST-PAK [PBD] in *E.coli BL21(DE3)pLysSpREP4*. The main culture of 1 L total volume was inoculated with the overnight pre-culture and allowed to let grow at 37°C and 220 rpm to an OD_{600} of 0.6. Expression was induced by adding 0.1 mM IPTG for 4 hours at RT. Bacteria were harvested by centrifugation and resuspended in 40 mL PAK lysis-/wash buffer supplemented with 10 mg/mL lysozyme and incubated for 5 minutes on ice after which bacteria were sonicated for total lysis. The sonicated bacteria were centrifuged for 20 minutes at 12000 rpm and 4°C to remove cell debris. The supernatant (lysate) was subjected to a test-purification cycle. For this, 50, 100 and 200 µL lysate was mixed with 25 µL *Glutathione Sepharose 4B* beads each and incubated for 45 minutes at 4°C in the overhead-shaker. The beads were washed four times with 300 µL PAK lysis-/wash buffer and the beads were then resuspended in 25 µL 1xloading buffer supplemented with bromophenol blue and DTT and incubated for 5 minutes at 95°C. The beads were centrifuged for 5 minutes at 13000 rpm and the supernatant was loaded onto a 12.5% SDS-PAGE gel together with a BSA standard and analysed by *Coomassie* staining. For the pulldown, the day before cells were seeded into a 10 cm plate and allowed to adhere overnight. All steps of the pulldown were performed on ice and with pre-chilled consumables. 25 µL *Glutathione Sepharose 4B* beads were washed twice with 300 µL RAC-RIPA buffer (centrifugation 1 minutes at 5000 rpm and 4°C). 200 µL GST-PAK was added to the beads and the beads were rotated for 30-45 minutes at 4°C. During the incubation time, cells were washed once with ice-cold TBS and lysed with 500 µL RAC-RIPA buffer. The cells were transferred to pre-chilled 1.5 eppendorf tubes and centrifuged for 5 minutes at 14000 rpm and 4°C. The supernatant was transferred to a fresh eppendorf tube and can either be freezed at -80°C or directly used in the pulldown. The concentration of the lysate was determined by Lowry assay. The beads were washed once with RAC-RIPA buffer and 1.5 mg lysate was loaded to the beads and the volume was filled up to 500 µL with RAC-RIPA buffer and rotated for 45 minutes at 4°C. The beads were then washed five times with 300 µL RAC-RIPA buffer each and resuspended in 25 µL 1xloading buffer supplemented with bromophenol blue and DTT and incubated for 5 minutes at 95°C. The beads were centrifuged for 5 minutes at 13000 rpm and the supernatant as well as 40 µg of the lysates was loaded onto a 12.5% SDS-PAGE gel and RAC1 levels were determined by Western Blot using RAC1 mouse monoclonal antibody.

3.2.6.16. NSG-mouse experiments

SW-480 SCR and SHIP1 KD2 cells were injected subcutaneously into NSG-mice. 15 mice were used per group. The overall survival of the mice was monitored for the generation of Kaplan-Meyer curves and follow-up analysis was performed using alu-PCR and Western Blot of NP40 lysates generated out of tumour tissues. For the Western Blot analysis human-specific antibodies were used (anti-HSP70 D1M6J and anti-SHIP1 P290, purchased by Cell Signalling).

3.2.7. Bioinformatic methods

3.2.7.1. Structure modelling of the SHIP1 catalytic domain

The catalytic domain of SHIP1 (res. 403-709) was modelled using *PRIME 4.7.* (homology modelling, embedded in *Maestro 11*) and several webservers for complementation.
The query sequence was

>SHIP1 Caucasian variant catalytic domain aa 403-709 (uniprot identifier: Q92835-2)
ITIFIGTWNMGNAPPPKKITSWFLSKGQGKTRDDSADYIPHDIYVIGTQEDPLSEKEWLEILKHSLQEITSVTFKTVAIHTLWNIRIVVLAKPEHE
NRISHICTDNVKTGIANTLGNKGAVGVSFMFNGTSLGFVNSHLTSGSEKKLRRNQNYMNILRFLALGDKKLSPFNITHRFTHLFWFGDLNYRV
DLPTWEAETIIQKIKQQQYADLLSHDQLLTERREQKVFLHFEEEEITFAPTYRFERLTRDKYAYTKQKATGMKYNLPSWCDRVLWKSYPLVHV
VCQSYGSTSDIMTSDHSPVFATFEA

Homology modelling is based on structural or evolutionary relationship of the query sequence to templates available in the Protein Database (PDB). In general terms, the query sequence is aligned with a set of template sequences or by a single template sequence and the alignment is then used for model building. Homology modelling was performed using the structure prediction wizard embedded in *PRIME*. To introduce mutations into a built model, the residue of interest was selected and mutated using the *mutate* function within *Maestro 11*. The residue of interest was substituted with the desired amino acid and the free energy of the residue in question was minimized using the minimize selected atoms tool. Subsequently, the surrounding residues (5 Å) were equally minimized.

3.2.7.2. Docking

For docking the *GLIDE* inlet of *Maestro 11* was used.

3.2.7.3. Visualization and analysis of protein structures

For the visualization and analysis of protein structures *Maestro 11* and *PYMOL* were used applying the protein structure and sequence alignments tools as well as the determination of intra-protein and protein-ligand interactions and the determination of distances and angles.

3.2.8. Protein structure determination

3.2.8.1. Domain boundary determination

For the determination of cognate domain boundaries sequence and structure alignments of homologous structures derived from the Protein Database (PDB) and evaluation of secondary structure elements (performed in *PYMOL* and *Clustal 2.1*.) and secondary structure prediction analysis (*PHYRE2, PSIPRED*) as well as literature research was used.

3.2.8.2. Cloning and expression

The initial construct PHL-PPase-C2_long was cloned into pETM30 using an *EcoRI/NcoI* strategy. The respective cDNA was synthesized by Integrated DNA technology with the silent mutation c.C2517→T (H839H) to remove an internal *NcoI* cleavage site. The construct PHL-PPase-C2_short was cloned into the expression vector pET47b(+) using a *KpnI/NcoI* strategy. Both constructs were expressed in *E. coli* varying bacterial strains, IPTG concentration and expression temperature for 22 h and harvested by centrifugation and lysed by sonication. For expression analysis a 1 mL sample of the bacteria was taken before and after the expression, pelleted and reconstituted in ddH_2O to an OD_{600}=0.1. The whole cell bacteria samples were analysed together with the pellet and the lysate by SDS-PAGE and Coomassie staining as well as Western Blot. In a mammalian expression system, pLeGO(iG2)-Puro(+)-TwinStrep-SHIP1_dUTR was transduced into H1299 (see 3.2.6.2.) and NP40 lysates were subjected to *StrepTactin XT* test purification or the same vector was transfected in HEK-293F cells (see 3.2.8.2.1.). All trial expressions with the exception of mammalian expression in H1299 and purifications were performed at the CSSB Hamburg with the support of Philipp Lewe and Susanne Witt.

3.2.8.2.1. Expression of TwinStrep-SHIP1 FL in HEK-293F cells

HEK-293F cells are a variant of HEK cells which have been adapted to grow in serum-free suspension culture using a shaking incubator. HEK-293F cells were purchased from Thermo Fischer and cultured according to the protocol of the manufacturer.

3.2.8.2.1.1. Thawing, freezing and general handling of HEK-293F cells

Cells were cultured at 37 °C, 8 % CO_2 and 130 rpm. For the establishment of a fresh culture an aliquot of HEK-293F cells ($1x10^7$ cells in 1 mL 90% FreeStyle 293F expression medium, 10 % DMSO) was quick-thawed in a 37 °C water bath and transferred in a pre-prepared 125 mL flask containing 17 mL of pre-warmed FreeStyle 293F expression medium. After 3-5 days a small aliquot of cells was transferred into a 1.5 mL Eppendorf tube and vortexed to avoid cell clusters. Cells were mixed 1:1 with trypan blue and the cell density and viability were determined using a Neubauer counting chamber. Cells were diluted to $1\text{-}3x10^5$/mL in a total volume of 30 mL. This refers to one passage. Prior to transfection cells were passaged for at least two additional times and should reach a cell viability of >90 %. To freeze cells, cells were counted as described and diluted to $5\text{-}8x10^6$/mL in freshly prepared freezing medium (90% FreeStyle 293F expression medium, 10 % DMSO, sterile-filtered, keep on ice until use). Cells were aliquoted to 1 mL per cryo-tube and transferred into a freezing help device filled with isopropanol till the filling line. The freezing help device was stored at -80 °C for at least 24 hours after which the cells could be transferred to the liquid nitrogen tank.

3.2.8.2.1.2. Transfection of HEK-293F cells with 293fectin

For transfection cells were counted and $3x10^7$ cells were transferred into a 50 mL falcon tube and centrifuged for 5 minutes at 100xg. The cell pellet was resuspended in 28 mL pre-warmed Freestyle 293F expression medium and transferred into a 125 mL flask. The transfection mixture was prepared in two Eppendorf tubes:

Tube 1: 30 µg plasmid DNA (95 % plasmid of interest (pLeGO-iG2-Puro(+)-TwinStrep-SHIP1FL_dUTR), 5 % GFP transfection control), pre-warmed OptiMEM I ad. 1 mL, mix gently by snipping

Tube 2: 60 µL 293fectin, 1940 µL pre-warmed OptiMEM I, mix gently by snipping

Both tubes were incubated for 5 minutes at RT after which they were unified and incubated for another 20-30 minutes at RT. The transfection mixture was then transferred drop-wise and whilst shaking the flask to the cells and incubated for 24-96 hours. To analyse the transfection at desired time-points and before transfection (negative

control) 1 mL aliquots were taken and the total and GFP-positive cells were counted in a Neubauer counting chamber. The cells were centrifuged for 2 minutes at 13000 rpm and the supernatant was filtered through a 0.2 µm filter and transferred to a fresh Eppendorf tube. Supernatant (portion of secreted proteins) and cell pellet (portion of intracellular protein) were freezed separately in liquid nitrogen and stored at -20 °C until use. For the analysis via SDS-PAGE and Western Blot the samples were thawed on ice and the cell pellets were resuspended in 1 mL PBS and lysed by sonication (30 seconds, full speed) and centrifuged for 10 minutes at full speed to remove cell debris. 10 µL/lane of the supernatant (cell medium/secreted proteins) and the amount of cell lysate corresponding to $1x10^4$ cells/lane (i.e. preparing a stock solution of $1x10^6$ cells/mL in PBS, 10 µL/lane) was loaded onto a 10 % SDS-PAGE gel and analysed by *Coomassie Brilliant Blue* staining and Western Blot as described in 3.2.6.8.

4. Results

4.1. SHIP1 is a player in the tumorigenesis of colorectal carcinoma (CRC)

4.1.1. SHIP1 in CRC-Indications from clinical samples

SHIP1 expression in healthy tissue is restricted to hematopoietic cells, however previous Tissue Microarray (TMA) studies performed in our lab identified moderate to strong expression of SHIP1 in a number of cancer entities of mesenchymal and epithelial origin. This was most pronounced in colorectal carcinoma (54% of analysed samples) (**fig. 7**). According to the COSMIC ((Catalogue Of Somatic Mutations In Cancer) database [619] mutant forms of SHIP1 were observed in several carcinoma entities. For instance, in cancers of the large intestine 5.65% of 2547 samples tested were found to be mutated (date of access: 07.12.2020) with mostly missense or synonymous substitutions as shown in **fig. 6A**. As depicted in **fig. 6B** with regard to missense substitutions no apparent hotspot mutations were found, however mutations were most dense in the catalytic domain of SHIP1.

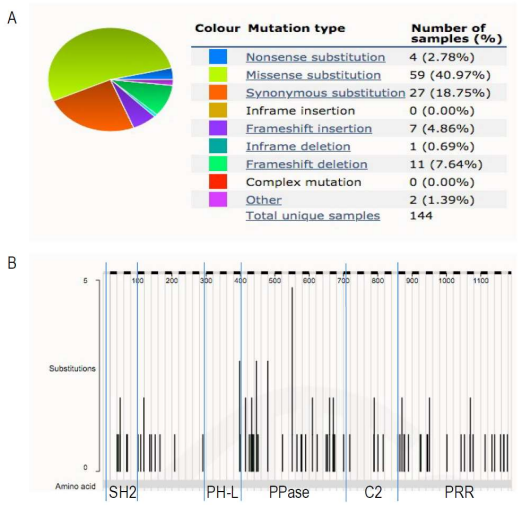

fig. 6: Analysis of the mutational spectrum of SHIP1 (*INPP5D*) in large intestine cancer. Panel A shows the distribution of mutation types. Panel B shows the distribution of missense substitutions over the five SHIP1 domains. Data were obtained from the COSMIC database [619].

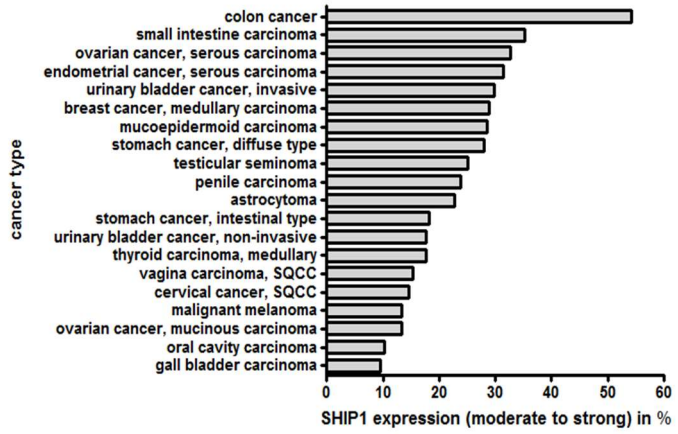

fig. 7: Tissue Microarray of a panel of tumour samples to test for SHIP1 expression ([591]; Data by Matthias Schaks)

Western Blot analysis was performed to validate SHIP1 expression in selected carcinoma cell lines. The hepatocellular carcinoma cell line HepG2, the cholangiocarcinoma cell line SKCHA-1 and the two colorectal carcinoma cell lines HT-29 and SW-480 were proven to be SHIP1 positive (**fig. 8**) and further experiments showed that expressed SHIP1 was enzymatically active but activity was significantly reduced in HT-29 hinting at a possible mutation of SHIP1 in this cell line (**fig. 9**).

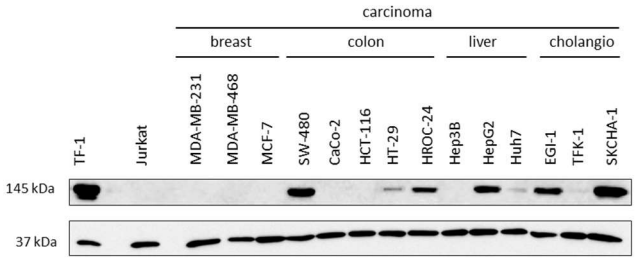

fig. 8: Western Blot analysis of a panel of carcinoma cell lines of various origin to test for SHIP1 expression. SHIP1 levels were detected using SHIP1 P1C1 mouse monoclonal antibody and normalized to GAPDH. TF-1 (positive) and Jurkat (negative) cells were used as control [591] (Data by Matthias Schaks).

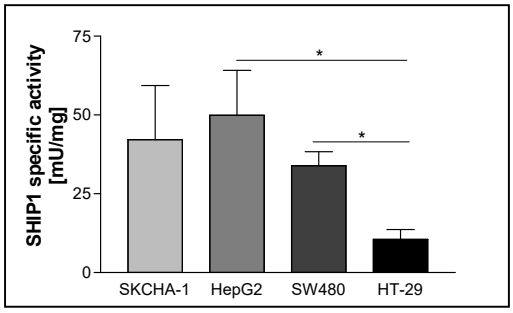

fig. 9: SHIP1 enzymatic activity in selected carcinoma cell lines. Cells were lysed by NP40 lysis and SHIP1 was immunoprecipitated using SHIP1 P1C1 mouse monoclonal antibody coupled to G sepharose beads. SHIP1 activity was assessed using a malachite green based phosphatase assay. The level of immunoprecipitated SHIP1 per reaction was determined by Western Blot using a recombinant SHIP1 standard curve in order to calculate the specific activity. Error bars indicate standard deviations. Significances were determined by t-test. n=3 [591]

Further database research using the tnmplot server ([620], date of access 17.03.2021) based on GeneChip data revealed ectopic expression of SHIP1 in primary CRC which was further pronounced in metastatic CRC (**fig. 10**). Of note, SHIP1 was ectopically expressed in cancers of the digestive system as well as pancreatic, renal and testis cancer and downregulated in others such as breast, prostate or uterus cancer. In all carcinoma entities SHIP1 expression was relatively low compared to hematopoietic tissues (AML) (**fig. 11**).

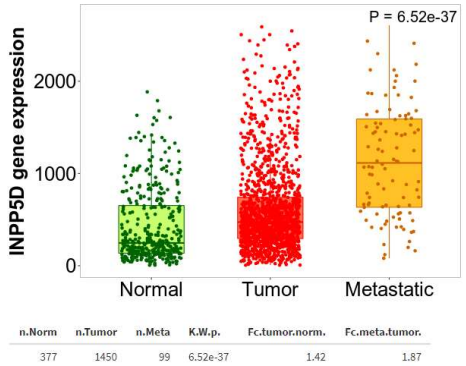

fig. 10: SHIP1 expression in healthy colorectal tissue compared to primary and metastatic CRC based on GeneChip data. Data were obtained from the tnmplot server. Error bars indicate standard deviations. P-values were determined by Kruskal-Wallis test. [620].

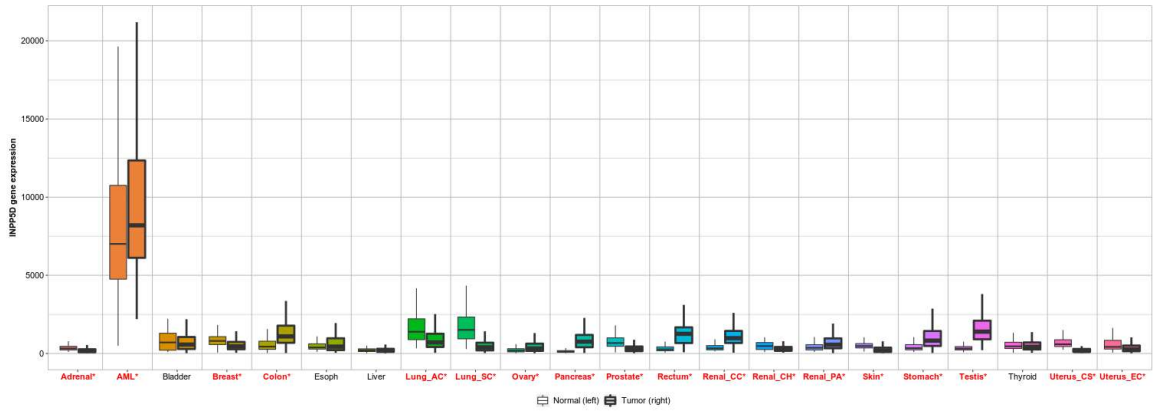

fig. 11: SHIP1 expression in healthy vs. tumour tissues of various origin. Data were obtained from the tnmplot server [620]. Error bars indicate standard deviations.

Using the UALCAN server ([621], date of access 16.03.2021) a comparable result was found for colon adenocarcinoma (COAD) using TCGA data. SHIP1 expression was highest in cancer stages 1 and 4 and slightly enhanced in metastatic tumours compared to primary COAD. Moreover, ectopic expression of SHIP1 in COAD was linked to the egalization of promotor hypermethylation (beta-value 0.592 in healthy tissue, where a beta-value of 0.5-0.7 indicates hypermethylation and a beta-value of 0.25-0.3 indicates hypomethylation of a promotor [622], [623]) but the median beta-value was not <0.3 in neither tumour or metastatic stage as shown in **fig. 12**.

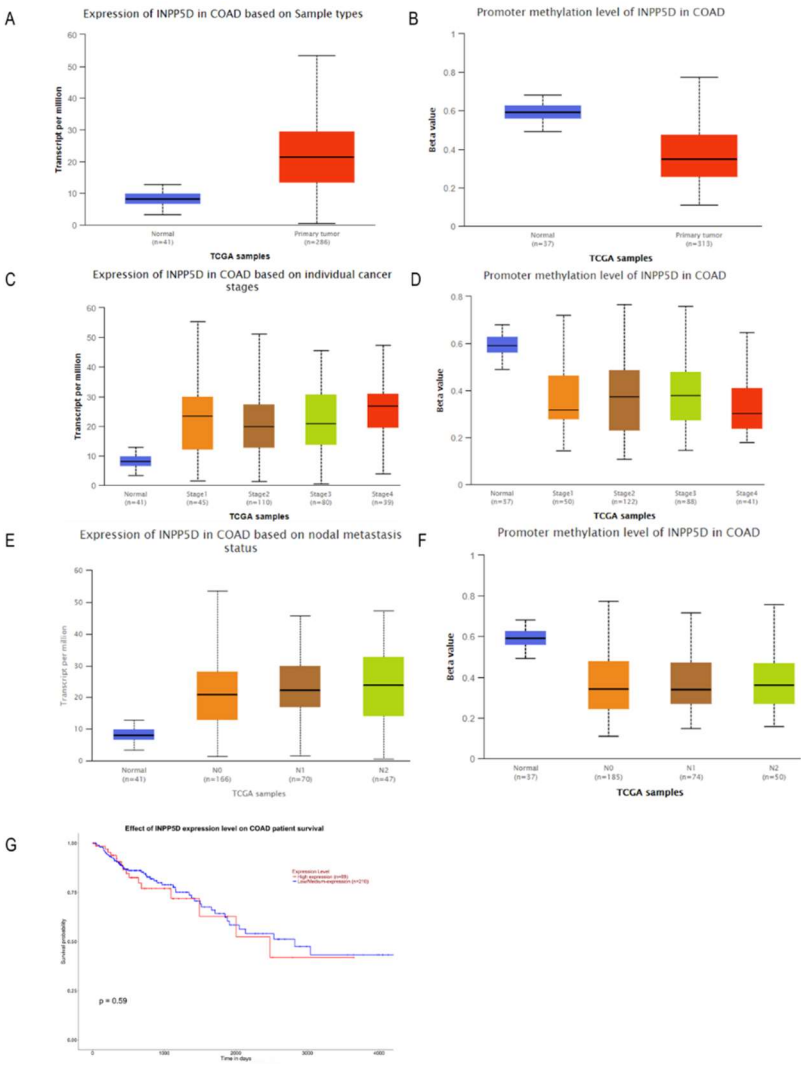

fig. 12: SHIP1 expression, promotor methylation status and impact of SHIP1 on patient survival in COAD. Panel A and B show the expression and methylation status of SHIP1 in COAD compared to healthy tissue based on TCGA data, panels C/D and E/F show the expression and methylation level of SHIP1 in dependence on the cancer or metastatic stage and panel G shows the Kaplan Meier curve of

high compared to low SHIP1 expression with the P-value determined by log rank test. Data were obtained from the UALCAN server [621]. Error bars indicate standard deviations.

In conclusions, those clinical data supported a possible oncogenic function of SHIP1 in CRC (or COAD) which is of special interest as SHIP1 have traditionally been categorized as a tumour suppressor (in malignancies of hematopoietic origin). However, as described in 1.4.3. due to the Two PIP hypothesis an oncogenic function would be rationale in certain contexts.
In the following it will be aimed to investigate the function of SHIP1 in more detail. For this, two complementary strategies will be pursued as shown in **fig 13**.

1. Overexpression of SHIP1 in the SHIP1 negative CRC cell line HCT-116
2. Downregulation (*Knock-Down* (or *Knock-Out*)) of SHIP1 in the SHIP1 positive CRC cell lines HT-29 and SW-480

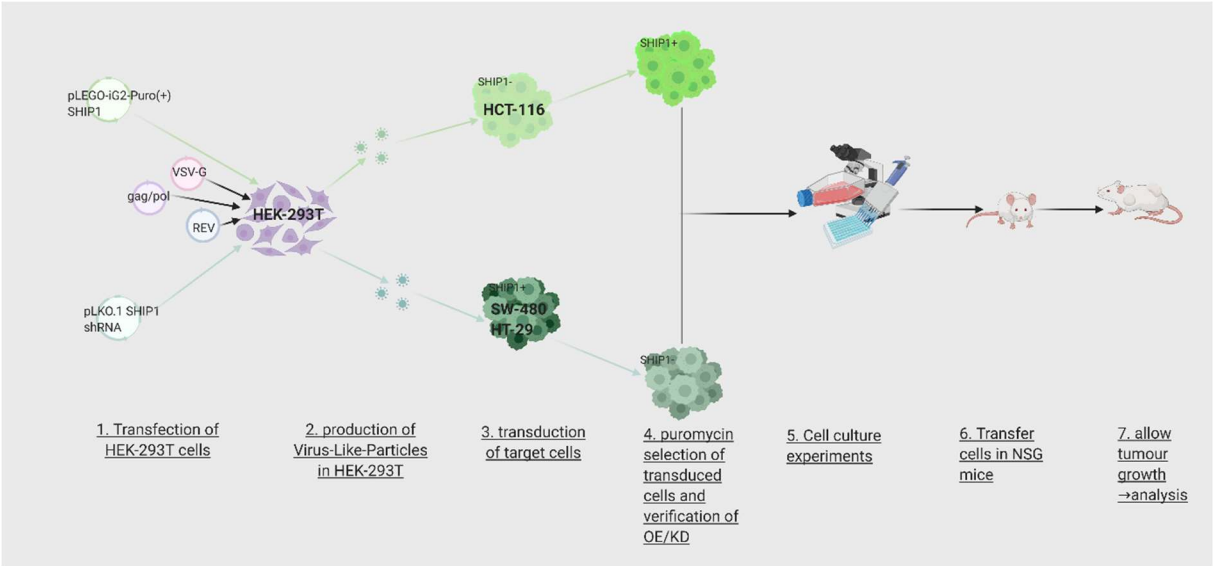

fig. 13: Examination of the function of SHIP1 in CRC (workflow). For the investigation of SHIP1 in CRC two complementary approaches were pursued: (1) Overexpression of SHIP1 WT in the SHIP1 negative CRC cell line HCT-116 and (2) Downregulation of SHIP1 in the SHIP1 positive cell lines HT-29 and SW-480. For this, cells were transduced using lentiviral transduction, selected with puromycin and the overexpression or downregulation of SHIP1 was verified by Western Blot. In the following, the function of SHIP1 was investigated in cell culture and NSG mice.

On a mechanistic level the function of SHIP1 in CRC will be investigated in cell culture with regard to cellular behaviour and signal transduction. Furthermore, the *in vivo* function of SHIP1 will be examined in an NSG mouse model with regard to primary tumour development and metastasis.
In the second part it will be focused on SHIP1 mutants especially of the catalytic domain as a significant part of SHIP1 found in CRC was shown to bear mutations (see above) and those were most pronounced in the catalytic domain. Selected mutants will therefore be analysed regarding their binding to PtdIns(3,4,5)P_3 and PtdIns(3,4)P_2, their catalytic activity, localization, cellular behaviour and signal transduction. In this context, the working hypothesis of a phosphoinositide trapping model will also be discussed.

4.1.2. Establishment of cell lines

In the first approach SHIP1 was overexpressed in the SHIP1 negative CRC cell line HCT-116. HCT-116 cells were transduced with either SHIP1 WT or a LeGO empty vector control aiming for single integration (5-19% eGFP-positive cells 3 days after transduction as analysed by FACS). Successfully transduced cells were selected for 10 days with 1.5 µg/mL puromycin and sorted for eGFP-positive cells. SHIP1 overexpression was verified by Western Blot using NP40 lysates prepared under standard growth conditions (DMEM, 10% FCS, 70-80% confluence). SHIP1 P1C1 mouse monoclonal antibody was used for detection and total protein levels were normalized to HSC70 as depicted in **fig 14**.

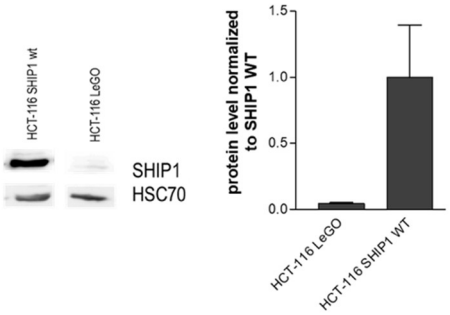

fig. 14: determination of the SHIP1 levels of HCT-116 SHIP1 WT vs. HCT-116 LeGO. Cells were stably transduced using a lentiviral system and selected with puromycin and sorted for eGFP positive cells. The transduction was verified by Western Blot analysis of NP40 lysates using SHIP1 P1C1 monoclonal antibody. Error bars indicate standard deviations. n=3

In the second approach it was aimed to downregulate SHIP1 levels in the endogenously SHIP1 expressing CRC lines SW-480 and HT-29 (1) by *knock-down* using shRNA and (2) by *knock-out* using CRISPR/CAS9.
For the *knock-down* approach two shRNA constructs were purchased and tested as specified below.

TRCN0000010362 NM_005541.x-281s1c1 SHCLNG08011621MN KD2
TRCN0000039896 NM_005541.2-2387s1c1 SHCLNG08261603MN KD3
shRNA2: CCGGAATTGCGTTTACACTTACAGCTCGAGCTGTAAGTGTAAACGCAATTCTTTTTG
shRNA3: CCGGGCAGAAGGTCTTCCTACACTTCTCGAGAAGTGTAGGAAGACCTTCTGCTTTTTG

In order to generate stable *knock-down* cell lines a third generation lentiviral transduction system was utilized and positive cells were selected with puromycin and SHIP1 expression was monitored by Western Blot using anti-SHIP1 P1C1 mouse monoclonal antibody and normalized to HSC70 levels and SCR control (**fig. 15**).

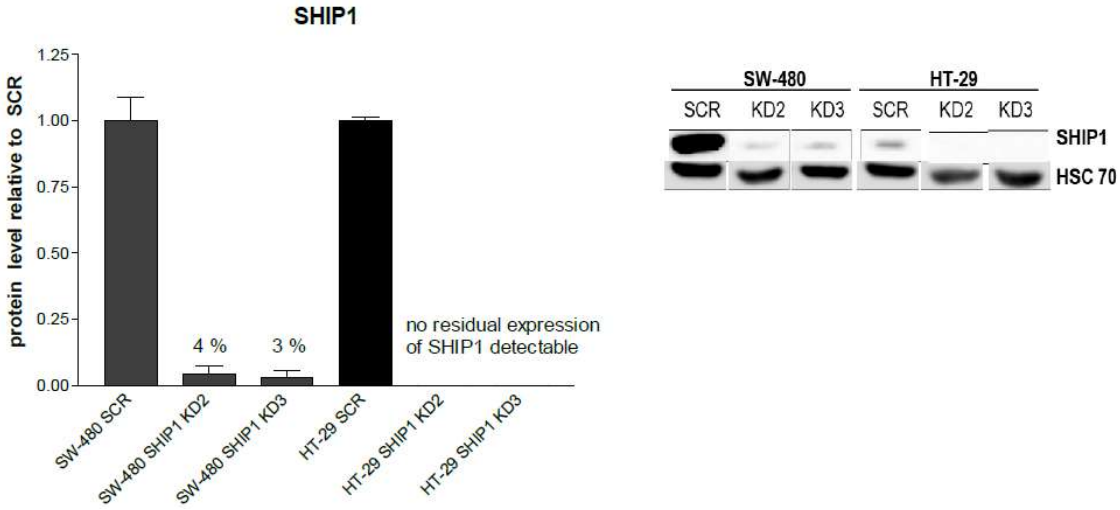

fig. 15: *Knock-down* of SHIP1 in SW-480 and HT-29. Cells were transduced with two SHIP1 shRNAs (KD2 and KD3) or a SCR control using a lentiviral transduction system and selected with puromycin. The *knock-down* was verified by Western Blot analysis of NP40 lysates using SHIP1 P1C1 mouse monoclonal antibody and HSC70 as loading control. Error bars indicate standard deviations. n=3

In both cell lines *knock-down* of SHIP1 was highly efficient. For SW-480 residual expression of SHIP1 was 4% respectively 3% of SCR control whereas in HT-29 no residual expression of SHIP1 was detectable possibly because of the overall low expression level of SHIP1 in this cell line.
Due to Western Blot analysis performed in the course of KD cell line establishment which showed that SHIP1 *knock-down* cells were prone to loss of the KD over a limited amount of passages it was aimed to generate a stable downregulation of SHIP1 by CRSIPR/CAS mediated *knock-out*. For the *knock-out* the *all-in-one system* purchased by Sigma Aldrich was used. Two gDNAs were selected using the *Custom CRISPR Design Tool* based on position, specificity, efficiency and number of predicted *off-target* sites (**table 9**). The gDNAs were ordered inserted in the lentiviral vector pLVO.1 containing eGFP and puromycin resistance. All experiments were done with SW-480 cells only.

Table 9: KO of SHIP1 in SW-480, selection of gDNAs. The gDNAs were selected using the *Custom CRISPR Design Tool* of Sigma Aldrich based on position, specificity, efficiency and number of predicted *off-target* sites

	knock-out 1	***knock-out 2***
Start Coordinate	233198228	233060562
Chromosome	2	2
Species	Human	Human
Gene ID	3635	3635
Gene Symbol	INPP5D	INPP5D
RefseqId/Target mRNA Exon	NM_001017915/25 NM_005541/25 XM_017004004/25	NM_001017915/1 NM_005541/1
# Transcripts Hit (Selected 3 /Total 3)	3	2
# of Sites in genome that are 3 nt different from Target Sequence	0	2
# of Sites in genome that are 2 nt different from Target Sequence	0	0
# of Sites in genome that are 1 nt different from Target Sequence	0	0
# of Perfect Matches in the Genome	1	1
Specificity	100.0	99.45
Efficiency	54.98	61.67
Sense(+) AntiSense(-)	+	-
PAM	AGG	AGG
Target Sequence:5'-3' (does not include with PAM)	AGCTACGACCAGCCGC CCA	GGACTCGCTGGCACGCACG
Target ID/Clone Name	HS0000055026	HS0000055008

For the generation of *knock-out* cells SW-480 cells were transduced with the respective *knock-out* vectors using a second generation lentiviral system containing a deficient integrase (D64V) to prevent stable integration of the gDNA. 48 hours following transduction cells were either selected for eGFP positive cells or with puromycin. To determine the minimal concentration of puromycin needed to kill the parental cells a puromycin killing curve was done ranging from 0 µg/mL to 1.5 µg/mL. The minimal puromycin concentration was found to be 0.5 µg/mL for SW-480. Cells were cultured in the respective puromycin containing medium for 24 hours after which puromycin was removed from the cells and they were cultured from there on in puromycin-free medium. Single clones were placed into individual wells of a 96-well plate using the *FACS Aria Fusion* (live gate) and allowed to grow until a sufficient number of cells was reached for Western Blot analysis. Concerning eGFP selection cells were gated for eGFP positive cells and single clones were placed into individual wells of a 96-well plate using the *FACS Aria Fusion* and allowed to grow until a sufficient number of cells was reached for Western Blot analysis. As shown in **fig. 16** eGFP fluorescence was very low in intensity which was due to the transduction system used.

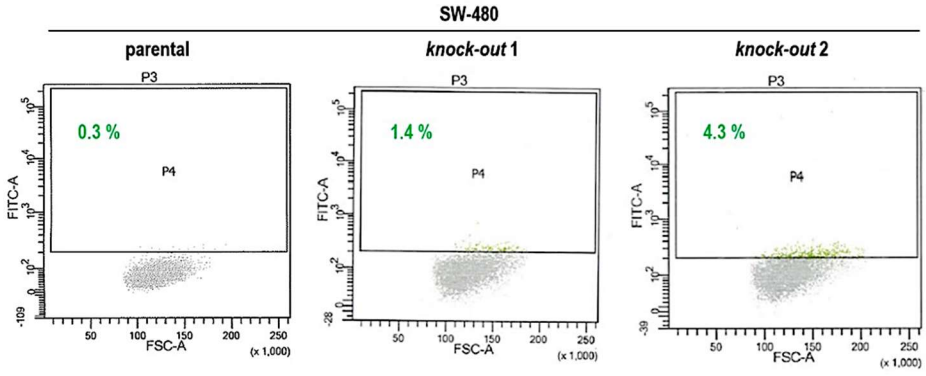

fig. 16: Generation of SW-480 *knock-out* cells. Cells were transduced with p.LVO.1 KO1 or KO2 using lentiviral transduction and single clones were selected with puromycin (not shown) or by eGFP fluorescence.

For Western Blot-based *screening* of clones cells were harvested at ~70-80% confluence and lysed in NP40 buffer. Lysates were tested in one-fold determination for the expression of SHIP1 using SHIP1 P1C1 mouse monoclonal antibody and SHIP1 expression was normalized to HSC70 and the average SHIP1 expression of parental clones. The four most promising clones resulting out of the screening were then re-analysed in three-fold determination for quantification which is shown in **fig. 17.** Remarkably, all four clones had been selected with puromycin which might

indicate that FACS assisted selection for eGFP-positive cells was not feasible in this set-up (especially due to the low expression of eGFP and difficulties in clearly distinguishing negative and positive cells).

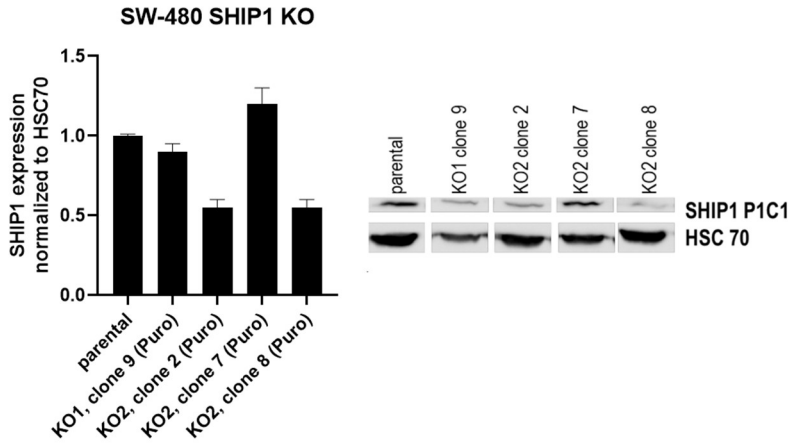

fig. 17: Generation of SW-480 *knock-out* cells, Western Blot analysis of SHIP1 expression in selected promising clones. Cells were transduced with p.LVO.1 KO1 or KO2 using lentiviral transduction and single clones were selected with puromycin or by eGFP fluorescence. Clones with promising results obtained in the screening were analysed by Western Blot (n=3) to determine the exact efficiency of the KO using SHIP1 P1C1 and HSC70 as a loading control. Error bars indicate standard deviations.

As shown, KO2 clones 2 and 8 (Puro) displayed a 50% (heterozygous) KO of SHIP1. Unfortunately, further experiments with those clones to achieve a full (homozygous) KO failed.
In a second approach, instead of transducing the SW-480 cells they were transfected with p.LVO1 SHIP1 KO1 or KO2 (2 µg plasmid for $4x10^5$ cells/well in a 6-well plate) and after 24 hours were selected with 1.5 µg/mL puromycine for 24 hours after which single clones were seeded into 96-well plates using FACS (live gate) and for each construct, 6 clones were transferred to 6-well plates after 3-4 weeks culturing time and let grow until there were sufficient cells for Western Blot analysis. SW-480 SHIP1 KO2, clone 4 turned out to display a complete *knock-out* of SHIP1. To ensure that this would be stable over several passages, this clone was cultured for another 12 passages (6 weeks) and analysed again for SHIP1 expression which was still not detectable as shown in **fig. 18**. This indicated that the SHIP1 KO seemed to be stable (at least in the time range observed). Due to time limitations, most further experiments were done with the SW-480 SHIP1 KD cells during the thesis but shall be also performed with the SW-480 SHIP1 KO cells in the future.

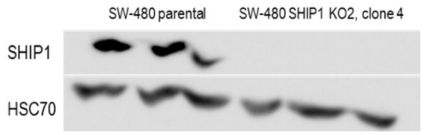

fig. 18: Generation of SW-480 *knock-out* cells, Western Blot analysis of SHIP1 KO2, clone 4 after 12 passages culturing time. Cells were transfected with p.LVO.1 KO1 or KO2 and single clones were selected with puromycin. For each construct, six clones were analysed by Western Blot for SHIP1 expression using SHIP1 P1C1 and HSC70 as a loading control (not shown) and SHIP1 KO2, clone 4 showed a complete loss of SHIP1 which was verified after 12 passages (shown). n=3.

4.1.3. Analysis of the cellular behaviour (proliferation, apoptosis, migration, invasion and chemotaxis)

In HCT-116 LeGO vs. SHIP1 WT cell proliferation/cell viability was assessed using Alamar Blue assay and phase confluence assessment (*IncuCyte Zoom*). For the Alamar Blue assay, cells were plated in a density of 2000 cells/well in a 96-well plate and allowed to grow for 24 hours. Alamar Blue fluorescence intensity was measured two hours after reagent addition and normalized to HCT-116 LeGO. For the *IncuCyte Zoom* based assay cells were plated in a density of 2500 cells/well and phase confluence was monitored every two hours. Phase confluence was plotted against the time and resulting growth curves were fitted in the initial (exponential) growth phase by $y = Start * e^{xk}$ in order to determine the doubling time. As shown in **fig. 19** proliferation was not significantly influenced by SHIP1 expression.

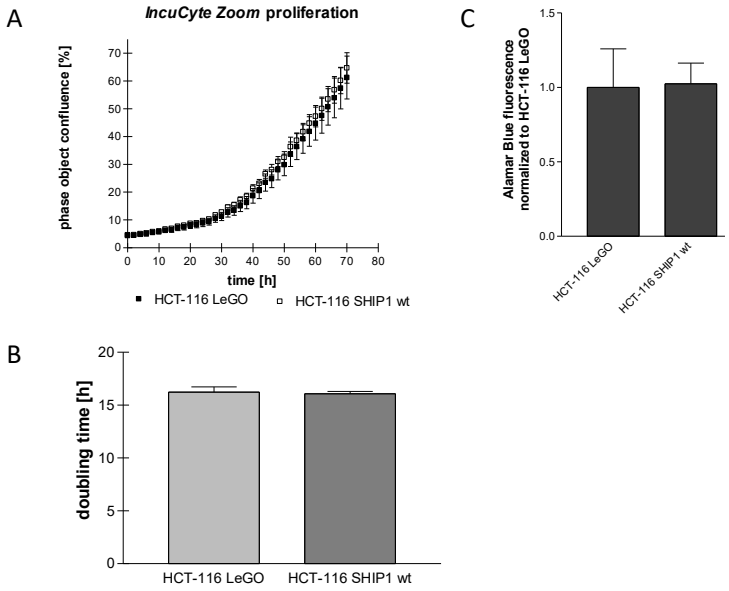

fig. 19: proliferation of HCT-116 SHIP1 WT vs. LeGO. The proliferation was accessed either by the *IncuCyte Zoom* (phase object confluence) (panels A and B) or by Alamar Blue assay (panel C). Error bars indicate standard deviations. Significances were determined by t-testing. n=5

For the migration and invasion assay the *IncuCyte Zoom* was used. Cells were plated in a density of 90000 cells/well in a 96-well *ImageLock* plate and allowed to adhere for ~4 hours. Cells were wounded using the *Woundmaker* system and for the invasion assay the scratch was additionally filled with *Matrigel Basement, Growth Factor reduced* and a top layer of medium. Plates were placed into the IncuCyte Zoom and monitored every two hours. The average wound width was determined per time point and the migration/invasion velocity was calculated. As depicted in **fig. 20** both migration and invasion velocity was significantly enhanced in HCT-116 SHIP1 WT which was in accordance with previous results of our group (unpublished results). Invasion of HCT-116 SHIP1 WT was enhanced 1.3-times and migration 1.2 times relative to HCT-116 LeGO.

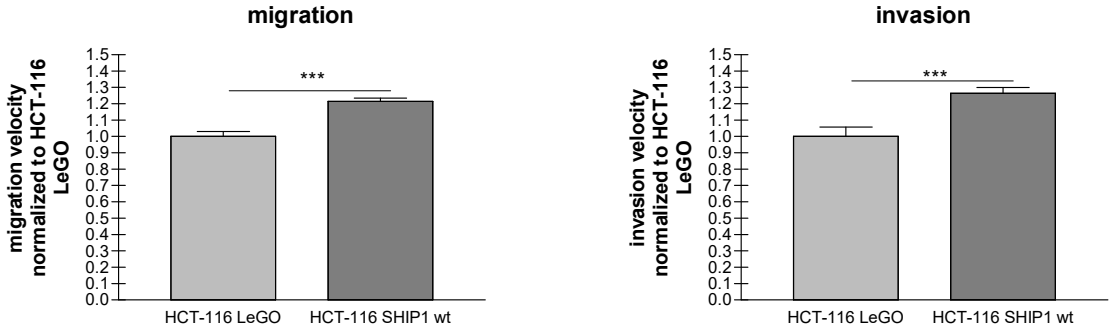

fig. 20: migration and invasion assay of HCT-116 SHIP1 WT vs. HCT-116 LeGO. The assays were performed using the *IncuCyte Zoom.* The migration/invasion velocity was determined as change in wound width (μm/h). Error bars indicate standard deviations. Significances were determined by t-testing. n=5.

In SW-480 and HT-29 SRC vs. SHIP1 KD proliferation was analysed using the *IncuCyte Zoom* (phase confluence) however no clear effect on proliferation was found over four replications of the experiment (**fig. 21**).

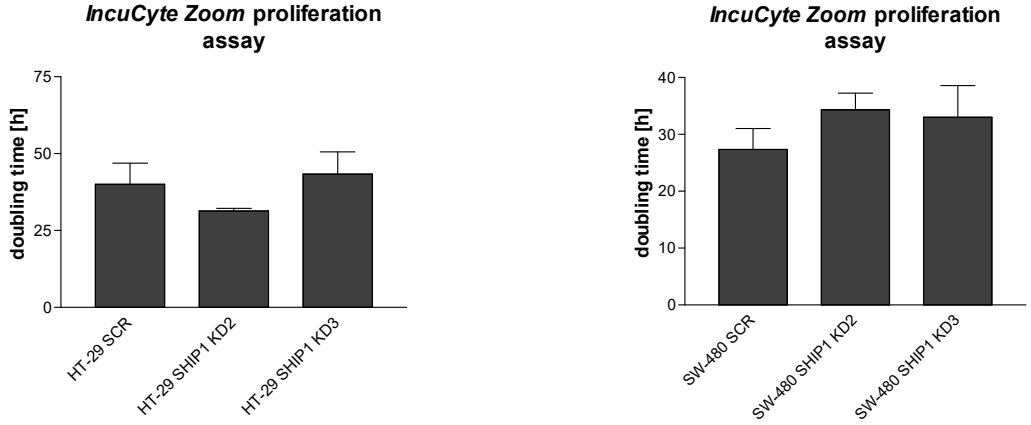

fig. 21: *IncuCyte Zoom* based proliferation assay of SW-480 and HT-29 SCR and SHIP1 KD cells. Cells were seeded in a density of 2500 cells/well and proliferation as measured by phase confluence was monitored every 2 hours. The doubling time was calculated over the exponential growth phase. Error bars indicate standard deviations. Significances were determined by t-testing. n=5

In order to analyse the migrative potential of SW-480 it was aimed to use the standard migration assay, however due to technical problems reliable data could not be obtained for SW-480 even after several optimization approaches regarding the protocol (number of seeded cells, attachment time, scratch technique). Therefore, a Boyden chamber chemotaxis assay was applied which could also be performed in the *IncuCyte Zoom* according to the protocol of the manufacturer (**fig. 22**). For the assay the day before, cells were starved for 22 hours in DMEM, 0.2% BSA, 1% p./s. and 1000 cells/well were seeded in the top vessel of a 96-well *IncuCyte ClearView* plate and DMEM, 10% FCS, 1% p./s. was used for the bottom reservoir vessel. The number of migrated cells was plotted against the time and fitted using the one phase exponential association option of *GraphPad Prism* $y = y_{max} * (1 - \mathrm{e}^{-kx})$ where k is the chemotaxis rate.

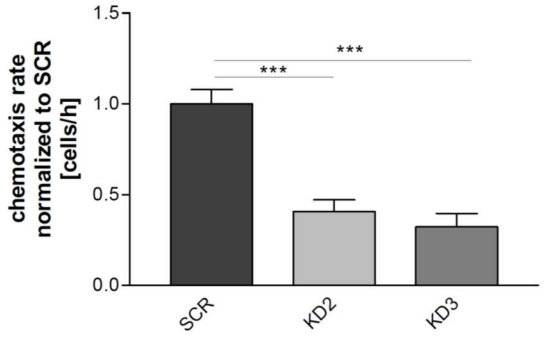

fig. 22: Boyden Chamber assay of SW-480 SCR, SHIP1 KD2 and SHIP1 KD3. The assay was performed according to the standard protocol of the manufacturer using a 0% FCS to 10% FCS gradient. Error bars indicate standard deviations. Significances were calculated by t-testing. n=5

As depicted, KD of SHIP1 highly significantly reduced the chemotaxis rate in both KD constructs. Therefore, a positive role of SHIP1 in the regulation of chemotaxis/cell movement could be proposed.
For HT-29 cells both the standard migration assay and the chemotaxis assay were performed as shown on **fig. 23**. The chemotaxis assay was performed as described above for SW-480 cells. For the migration assay the day before cells were seeded at 25000 cells/well in a 96-well *Image Lock plate* (Essen Bioscience) and allowed to attach for 18-22 h. The scratch was done using the *WoundMaker*. Pictures were taken every 2 hours for 22 h and the wound width was evaluated. For the calculation of the migration velocity the change in wound width from 0-22 h was taken.

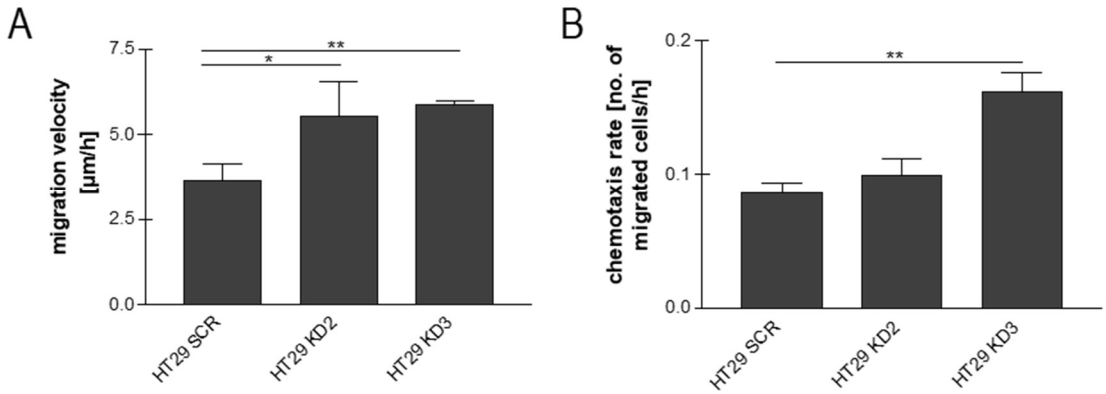

fig. 23: Migration and chemotaxis assay of HT-29 SCR, SHIP1 KD2 and KD3 cells. For the migration assay (panel A) cells were seeded at 25000 cells/well in a 96-well *Image Lock* plate and allowed to attach for 18-22 h. The scratch was done using the *Woundmaker* according to the general protocol. Pictures were taken every 2 hours for 22 h and the wound width was evaluated. For the calculation of the migration velocity the change in wound width from 0-22 h was taken. The chemotaxis (Boyden Chamber) assay (panel B) was performed according to the standard protocol of the manufacturer using a 0% FCS to 10% FCS gradient. Error bars indicate standard deviations. Significances were calculated by t-testing n=5

In contrast to SW-480 in HT-29 both KDs showed (significantly) increased chemotaxis rates which were in accordance to increased migration velocities. Therefore, in this scenario SHIP1 seemed to have a negative impact on cell migration/chemotaxis.
Apoptosis was assessed by Neubauer chamber cell counting and trypan blue staining. As indicated in **fig. 24** as for proliferation also apoptosis was not significantly altered by SHIP1.

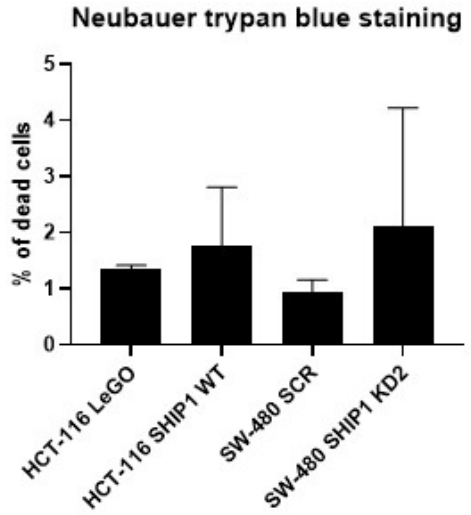

fig. 24: apoptosis assay of HCT-116 LeGO and SHIP1 WT and SW-480 SCR and SHIP1 KD2. The percentage of dead cells was determined by Neubauer chamber cell counting and trypan blue staining. Error bars indicate standard deviations. Significances were determined by t-testing. n=2

Conclusively, taken into account the results obtained in approaches 1 (HCT-116) and 2 (SW-480 and HT-29) a cell-line dependent effect of SHIP1 on the migration/chemotaxis of CRC cell lines could be suggested whereas SHIP1 did not have a significant impact on cell proliferation and survival.

4.1.3.1. Behaviour in 3D culture (tumoroid assay)

In order to achieve a biologically more relevant model for the examination of SHIP1 in CRC tumorigenesis a 3D cell culture model (tumoroid/spheroid model) was utilized. Spheroids represent tumours in a much more realistic way than 2D culture systems and it was described for several cases that results obtained from 2D-culture studies were not always transferrable to 3D culture. Furthermore, using co-culture techniques i.e. with fibroblasts or immune cells the tumour microenvironment can be depicted [624].

4.1.3.1.1. Establishment of a 3D spheroid culture and co-culture system in H1299 LeGO

In order to form spheroids cells were seeded in serial dilution (ranging from 2000 to 32 cells or 1000 to 16 cells) into ULA (Ultra Low Attachment) 96-well plates and centrifuged. ULA plates are coated with a hydrogel layer which prevents cells from attaching to the surface and enabling tumoroid formation which is accelerated by centrifugation. Tumoroid formation was assayed by microscopy.
Different conditions were tested as listed below:

1. DMEM, 10% FCS
2. DMEM, 10% FCS mixed 1+1 with *Matrigel Basement, Growth Factor Reduced* (stock concentration 9.6 mg/mL)
3. DMEM, 0.1% BSA (starvation medium)
4. starvation medium, 1000 ng/mL LPA
5. starvation medium, 500 ng/mL EGF
6. starvation medium, 1000 ng/mL LPA, 500 ng/mL

Cells were either starved for 24 hours prior to the experiment or left unstarved. Representative pictures at day 2 and day 5 are shown in **fig. 27**.
The reason behind those conditions used was that tumour formation is dependent on extracellular signals provided by the TME or autocrine loops. FCS is a highly complex mixture containing several of those stimuli and therefore it is difficult to exactly determine the critical factors leading to tumour (and in this case tumoroid) formation. Therefore, in besides FCS two candidate factors (EGF and LPA) were also taken into account in addition to the negative control condition (DMEM, 0.2% BSA).
The EGFR signalling pathway is found frequently altered in cancers and promotes cell proliferation, cell survival and cell growth. Upon binding of EGF to the EGFR receptor transphosphorylation is induced at multiple sites including Y1068. Adaptor and effector proteins are then attracted to said pY residues via their SH2 domains. They cover kinases of the SRC and JAK family, PI3K and the adaptor protein GRB2 which is part of the MAPK signalling cascade. *Downstream* signal transduction is mainly dependent on various activating and inactivating phosphorylation events and affects proteins residing in the cytosol and the nucleus (transcription factors) which is summarized in **fig. 25**. The pathways mentioned also show extensive crosstalk concerning each other [1].

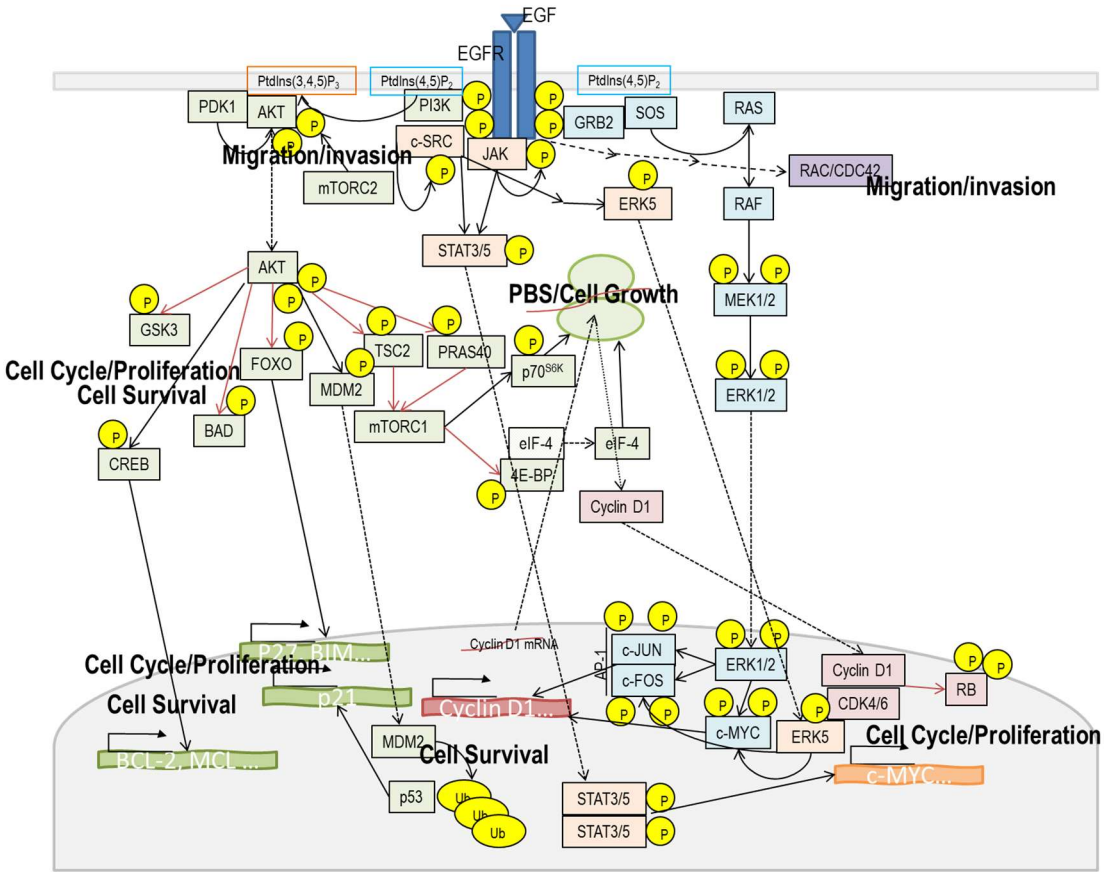

fig. 25: overview on the EGFR signalling pathway.

LPA (Lysophosphatidic Acid) is a phospholipid-type signalling molecule which acts to promote migration, invasion, proliferation and survival mediating pathways amongst others [625], [626]. It is found in all tissues with especially high levels in blood plasma (sub-µM range) [627]. LPA comes in different forms due to its complex metabolism. Two major pathways of LPA production out of phospholipids were described: (1) intracellular via phospholipase D (PLD) and phospholipase A_2 (PLA_2) and (2) extracellular via PLA_2 and the lysoPLD ATX [627]. ATX was proposed to be responsible for the bunch of LPA production in blood plasma as heterozygous *atx*$^{+/-}$ mice displayed halved plasma levels of LPA whereas *atx*$^{-/-}$ mice died at mid-gestation due to an essential function of LPA during embryo development [628], [629]. LPA acts through binding to cognate rhodopsin-like GPCRs (type I) termed LPA_1 to LPA_6 (LPA_6 not shown) culminating in the activation of distinct heterotrimeric G-protein subclasses and their associated *downstream* pathways. Given to the broad combinatorial spectrum of LPA receptor expression LPA signalling displays a high level of complexity and signalling outcomes may differ in different tissue/cell types. LPA_1 and LPA_2 do act on $G_\alpha12/13$ initiating RHO-A/ROCK dependent signal transduction pathways especially affecting the actomyosin cytoskeleton, $G_\alpha q/11$ activating phospholipase C (PLC) and Ca^{2+} dependent signalling pathways, and $G_\alpha i/o$ activating the MAPK and PI3K/AKT/mTORC1 pathway as well as PLC and inactivating adenylate cyclase (AC). LPA_3 acts on $G_\alpha12/13$ and $G_\alpha i/o$. LPA_4 activates $G_\alpha12/13$, $G_\alpha q/11$, $G_\alpha i/o$ and $G_\alpha s$ (activating adenylate cyclase/cAMP/PKA dependent signal transduction) subclasses and LPA_5 acts on $G_\alpha i/o$ and $G_\alpha s$ [627]. In addition, LPA can induce EGFR transactivation through shedding of membrane-bound EGFR ligands as a result of i.e. ADAM protease upregulation [630]. LPA was shown to promote tumorigenesis in various cancer entities (mammary carcinoma, gastrointestinal cancer, prostate cancer, ovarian carcinoma, lung cancer, glioma and mesothelioma) due to its positive effect on survival, proliferation, migration, invasion/MMP production, angiogenesis (production of VEGF, IL-6 and IL-8) and chemoresistance as well as metastasis. As plasma levels of LPA are way over the cognate K_D values of LPA receptors to LPA also in healthy individuals the tumour promoting effect of LPA seems to be mainly due to LPA receptor upregulation. Especially LPA_2 but also LPA_1 and LPA_3 are frequently found to be upregulated in cancers and genetic or pharmacological downregulation of those receptors reversed the positive impact of LPA on tumour development in cell culture studies and mouse models [627]. LPA signalling is summarized in **fig. 26**.

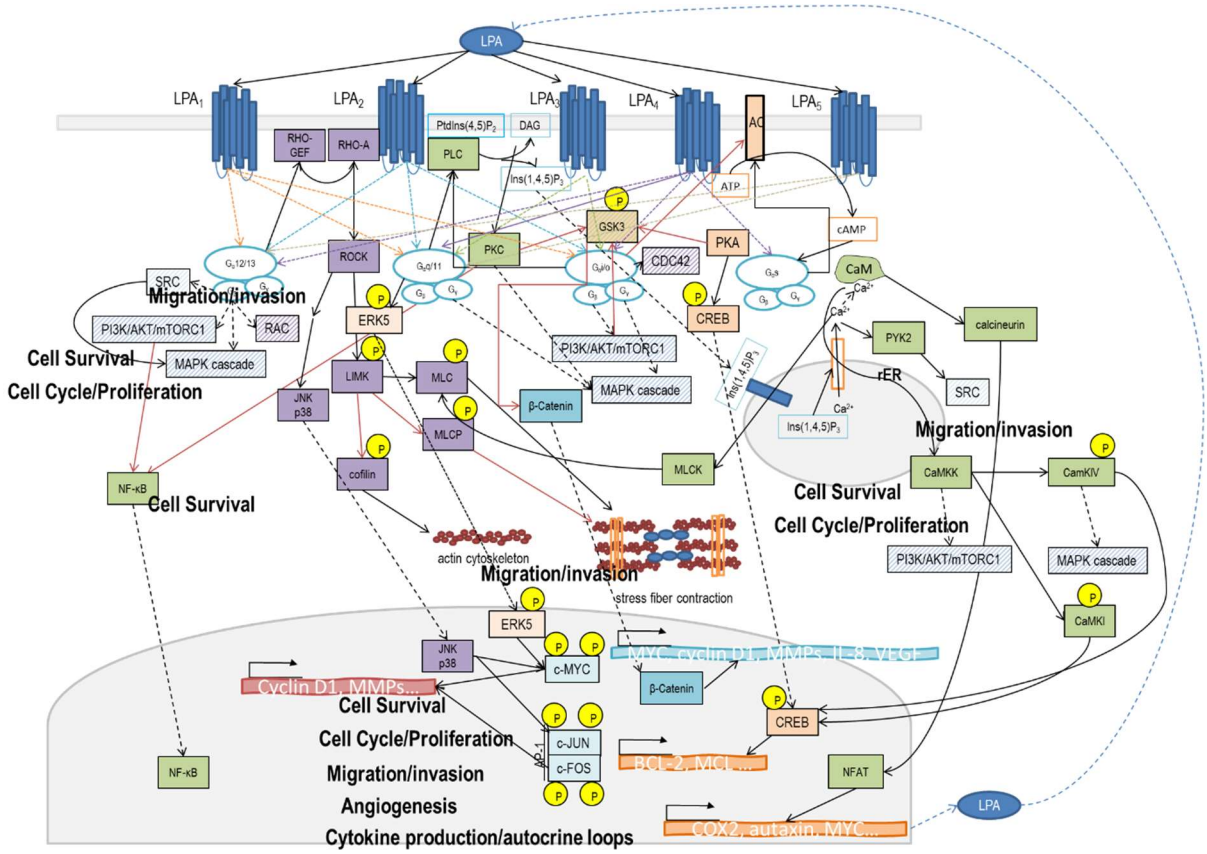

fig. 26: Overview on LPA signalling.

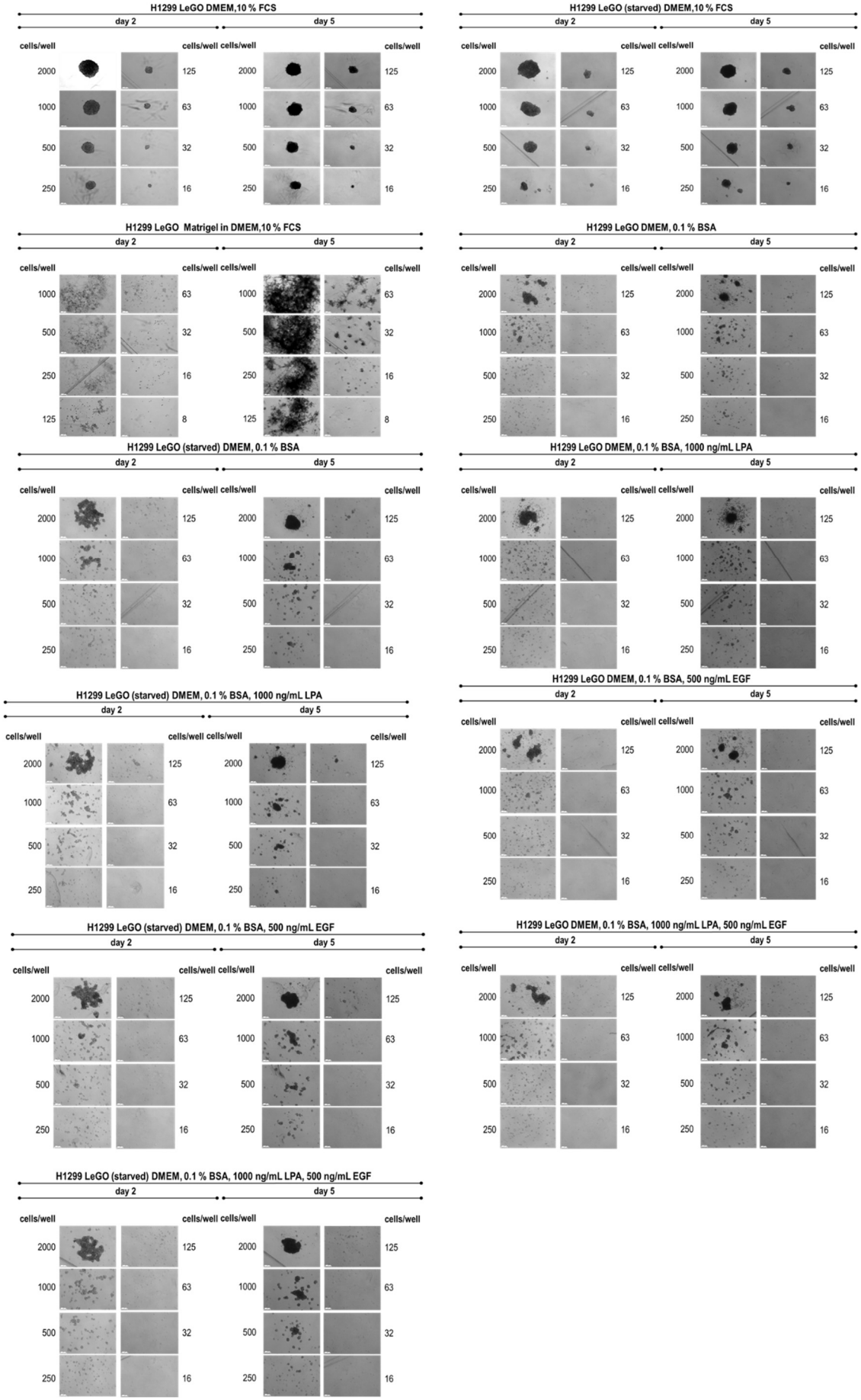

fig. 27: establishment of a 3D-tumoroid/spheroid system in H1299 LeGO. Tumoroid formation assay was assayed by phase microscopy and representative images are shown. n=3 (details see text).

As shown, tumoroids were formed well and fast (within 2 days) only in DMEM, 10% FCS for all cell numbers applied and starving prior to the assay did not affect tumoroid formation. Tumoroids did not form in DMEM, 0.2% BSA and application of either LPA or EGF or both was not sufficient to enable full tumoroid formation efficiency as seen for DMEM, 10% FCS. In those conditions, tumoroid formation was delayed to five days and the critical number of cells to form tumoroids was 2000 whereas in DMEM, 10% tumoroids formed at a number of as low as 16 cells. Tumoroid formation in Matrigel/DMEM, 10% FCS was strongly delayed compared to tumoroid formation in medium probably due to the fact that the cells had to overcome the matrix barrier prior to tumoroid formation.
To analyse if metabolic effects might influence tumoroid formation, tumoroid formation was evaluated in (1) DMEM (4.5 mg/mL glucose, +glutamine, -sodium pyruvate), 10% FCS (control), (2) DMEM (w./o. glutamine), 10% FCS, (3) DMEM (w./o. glucose), 10% FCS and (4) MEM (reduced medium), 10% FCS. However, tumoroid formation was similar for all conditions (not shown).
To establish a co-culture system of H1299 LeGO with human fibroblasts (IMR-90) deriving from the same organ (the lung) three different strategies were tested:

1. 500 cells/well of each cell line were mixed prior to plating. Tumoroids were analysed after 2 days.
2. H1299 LeGO was plated alone at 500 cells/well and tumoroids were allowed to form for 18 hours. The medium was then carefully removed and 500/well IMR-90 cells were added carefully either resuspended in medium or *Matrigel, Basement, Growth-Factor reduced* (1:1 in medium, f.c. 4.8 mg/mL). Tumoroids were analysed 3 days after addition of IMR-90.

As shown in **fig. 28** comparing the incident light image to the fluorescence (GFP-filter) image there was clear impression that IMR-90 (non-fluorescence) did not participate in tumoroid formation but rather stayed at the surrounding of the tumour in all three cases which would reflect the physiological situation of tumour vs. TME/soft tissue.

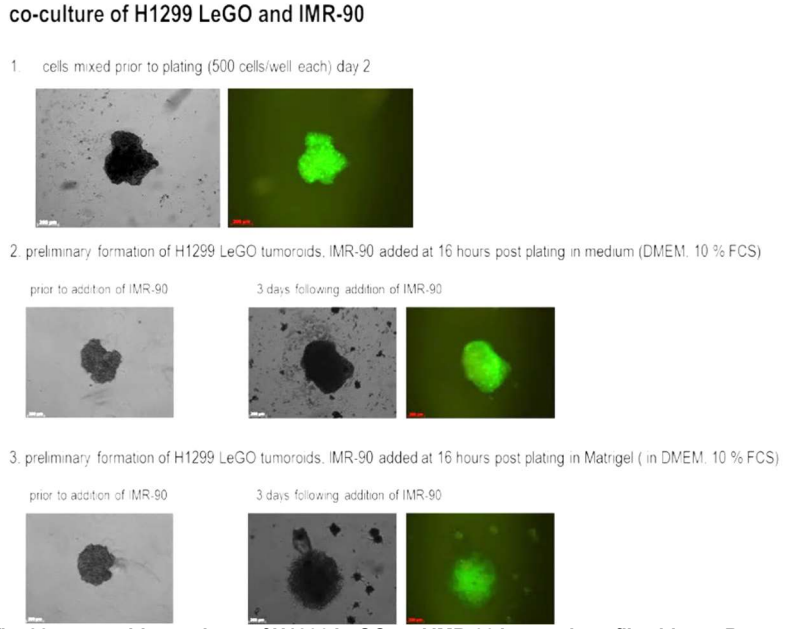

fig. 28: tumoroid co-culture of H1299 LeGO and IMR-90 human lung fibroblasts. Representative images (phase and green fluorescence) are shown. n=3 (details: see text)

4.1.3.1.2. Comparison of spheroids formed out of HCT-116 SHIP1 WT vs. LeGO and SW-480 SCR vs. SHIP1 KD

To form spheroids cells were seeded in serial dilution in DMEM,10% FCS (ranging from 2000 to 1 cells into ULA 96-well plates and centrifuged. Tumoroid formation was evaluated 5 days post-plating by phase microcopy. Cell viability was compared 5 days post-plating using the Alamar Blue assay. Alamar Blue fluorescence intensity was determined after 4 hours and plotted against the number of cells/well. As shown for HCT-116, SHIP1 did not affect tumoroid formation or morphology and cell viability was correlated to the number of cells plated per well. Qualitatively, HCT-116 SHIP1 WT showed lower viability than HCT-116 LeGO in one repetition of the experiment but in the other no major differences between the two cell lines were found (**fig. 29**).

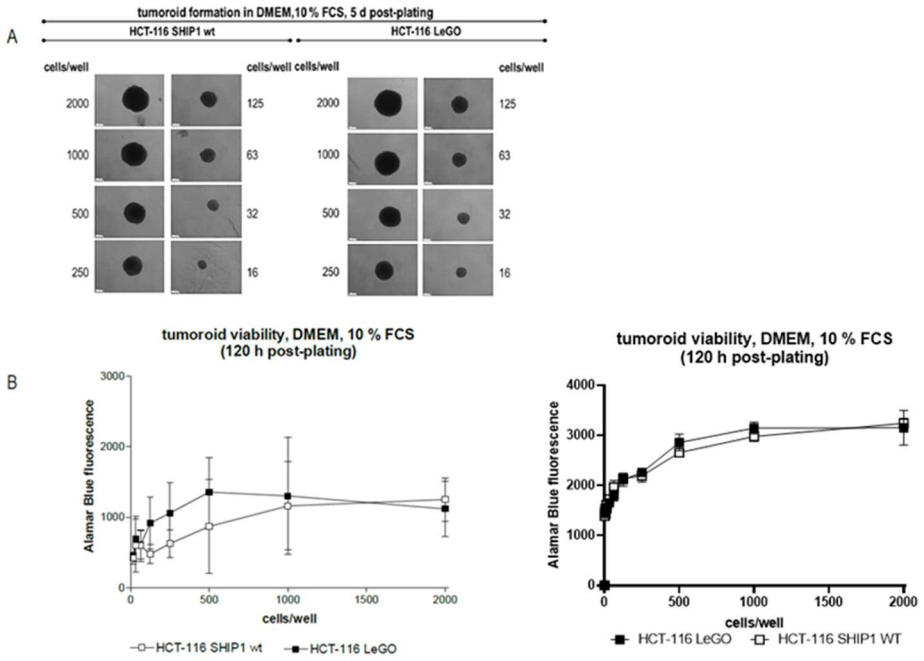

fig. 29: Tumoroid formation and viability of HCT-116 SHIP1 WT and HCT-116 LeGO. For the tumoroid assay cells were seeded in serial dilution (ranging from 2000 to 1 cells in DMEM, 10% FCS) into ULA 96-well plates and centrifuged. Tumoroids were allowed to form over a time range of 120 hours and documented by microscopy (panel A). Cell viability of HCT-116 SHIP1 WT and HCT-116 LeGO derived tumoroids was compared using the Alamar Blue assay in two repetitions (panel B, left and right). For the assay fluorescence intensity was determined after 4 hours and plotted against the number of cells/well. Error bars indicate standard deviations. n=3 per repetition.

Regarding SW-480 cells, SW-480 SHIP1 KD2-derived tumoroids displayed higher viability in the first repetition but lower viability in the second repetition of the experiment and on the morphological level those tumoroids appeared less compact than those derived from SW-480 SCR (**fig. 30**)

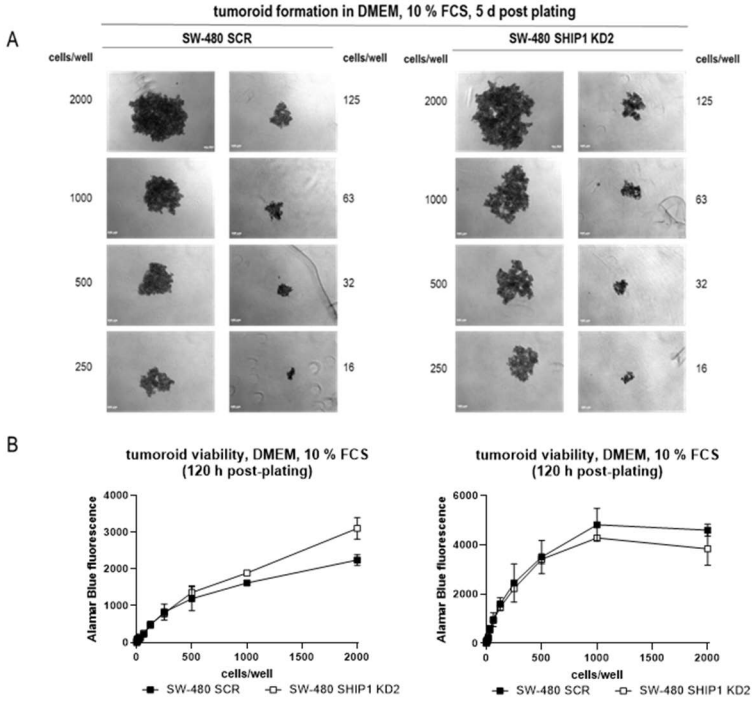

fig. 30: Tumoroid formation and viability of SW-480 SHIP1 KD2 and SW-480 SCR. For the tumoroid assay cells were seeded in serial dilution (ranging from 2000 to 1 cells in DMEM, 10% FCS) into ULA 96-well plates and centrifuged. Tumoroids were allowed to form over a time range of 120 hours and documented by microscopy (panel A). Cell viability of SW-480 SCR or SHIP1 KD2 derived tumoroids was compared using the Alamar Blue assay in two repetitions (panel B, left and right). For the assay fluorescence intensity was determined after 4 hours and plotted against the number of cells/well. Error bars indicate standard deviations. n=3 per repetition

Conclusively, in both cases SHIP1 expression overall showed no uniform impact on tumoroid viability and in the case of SW-480 but not in the case of HCT-116 it altered the overall morphological appearance of the tumoroids. This was in general accordance to the results obtained in 2D-culture (no impact on cell proliferation/viability observed).

4.1.4. Signal transduction analysis

Signal transduction was assessed by Western Blot using NP40 lysates prepared under standard growth conditions (DMEM, 10% FCS, 70-80% confluence). For the analysis of the PI3K/AKT/mTOR pathway P-AKT S473 rabbit monoclonal antibody was used and for the analysis of the MAPK pathway P-p44/42 MAPK T202/Y204 rabbit monoclonal antibody was used (**fig. 31**). For SW-480 SHIP1 KO2, clone 4 the PI3K/AKT/mTOR pathway apart from P-AKT S473 was analysed in more detail (P-mTOR S2481 and P-S6 S240/S244).

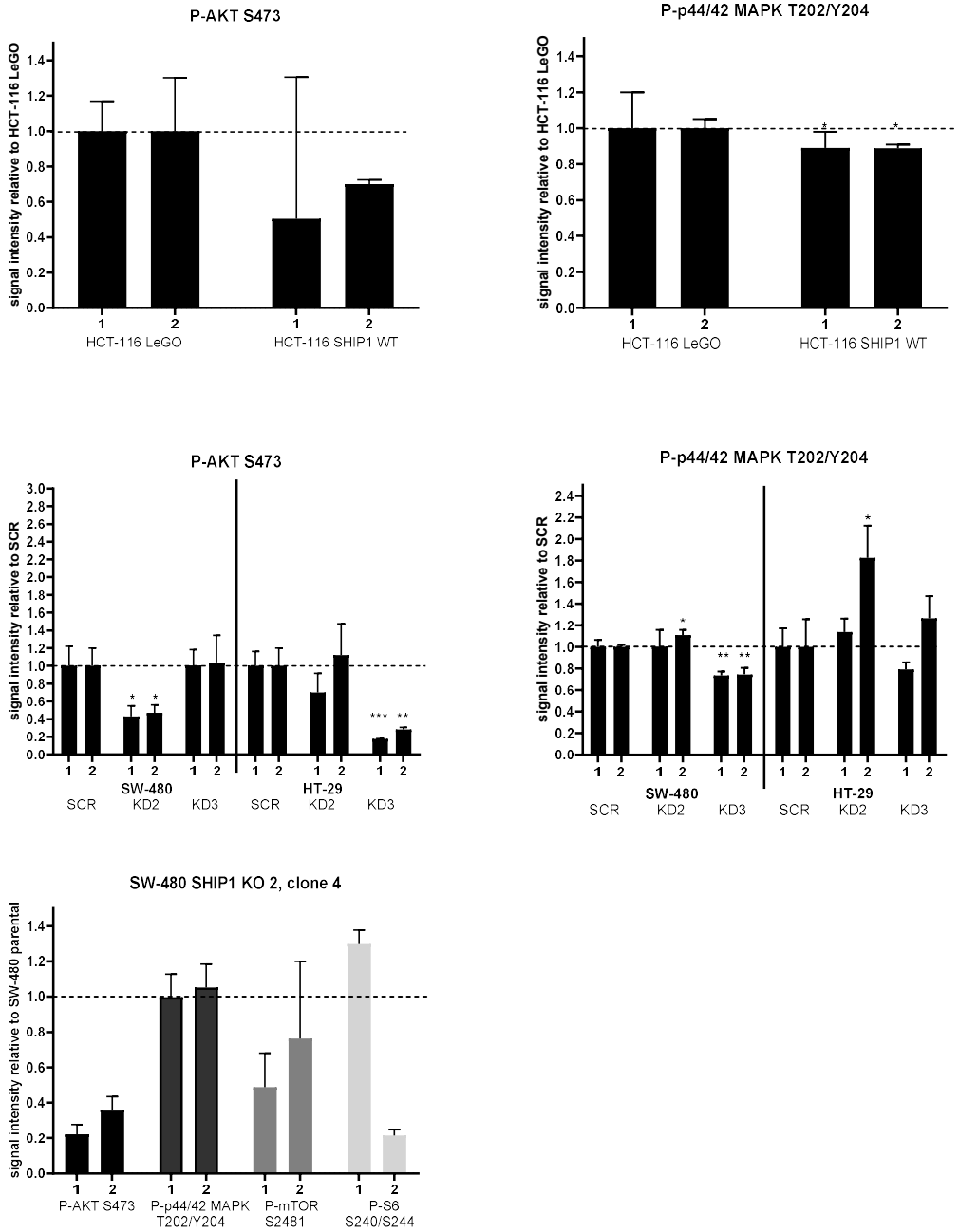

fig. 31: analysis of the impact of SHIP1 on signal transduction in HCT-116, SW-480 and HT-29. Cells were lysed by NP40 lysis at maintenance conditions and 70-80% confluence and signal transduction was analysed by Western Blot. Error bars indicate standard deviations. Significances were determined by t-testing. n=3 per repetition (repetitions indicated by numbering 1-2 on x-axis).

In HCT-116 SHIP1 negatively impacted both the PI3K/AKT/mTORC and the MAPK signalling pathway. In SW-480 and HT-29 the two KDs impacted signal transduction in a varying way. Regarding the PI3K/AKT/mTORC pathway, in SW-480 KD2 showed a negative impact and KD3 showed no significant impact and in HT-29 KD2 showed no significant and KD3 showed a negative impact. Regarding the MAPK pathway in SW-480 KD2 displayed no strong effect and KD3 a rather negative impact and in HT-29 KD2 showed a positive and KD3 no significant effect. SW-480 SHIP1 KO2, clone 4 behaved similar to SW-480 SHIP1 KD2 (negative impact on P-AKT S473 and weak to no impact on P-MAPK T202/Y204) and the negative impact on SHIP1 KO on PI3K/AKT/mTOR signalling was also reflected in the levels of P-mTOR S2481 and at least for repetition 2 those of P-S6 S240/S244. Conclusively, a strongly cell-line dependent effect of SHIP1 on signal transduction could be concluded. While in HCT-116 SHIP1 expression rather negatively impacted PI3K/AKT/mTORC1 signalling in SW-480 and HT-29 SHIP1 rather positively impacted it. The MAPK pathway was overall less strongly affected by SHIP1 expression and in HCT-116 rather negatively and in SW-480 and HT-29 ambiguously affected by SHIP1.

4.1.4.1. RAC1-GTP Pulldown

To analyse the observed enhanced migration of HCT-116 SHIP1 WT versus HCT-116 LeGO and SW-480 SCR vs. SHIP1 KD2 on a mechanistic level, RAC1-GTP pulldown assays were performed. The assay is based on the principle that RAC1-GTP but not RAC1-GDP is able to associate with its effector protein PAK. In the assay PAK is used as GST-PAK and immobilized on GSH sepharose beads to precipitate active RAC1 from whole cell lysates. The level of GTP-RAC1 is then normalized to the level of total RAC1 to determine the relative amount of GTP-RAC1 in the respective cell sample.
RAC1 is activated upon positive regulatory signals and promotes cell migration. Therefore, enhanced RAC1-GTP levels would hind at enhanced migratory capacity.

4.1.4.1.1. Establishment of the assay in H1299 cells

4.1.4.1.1.1. Expression of GST-PAK

GST-PAK was expressed from pGEX-2TK-GST-PAK(PDB) in *E.coli BL21(DE3)pLysSpREP4*. Expression was induced by addition of 0.1 mM IPTG for 3.5 hours at RT. GST-PAK1 was then test-purified using GSH-sepharose beads and eluted by denaturation. For the test-purification, different volumes of GST-PAK lysate (50, 100, 200 µL) were loaded onto the beads and analysed by SDS-PAGE. This is shown in **fig. 32**.

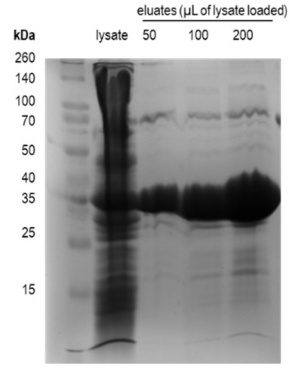

fig. 32: Expression and purification of GST-PAK. GST-PAK was expressed in *E.coli BL21(DE3)pLysSpREP4* for 3.5 hours at RT and GST-PAK lysates were purified using GSH-sepharose beads loading 50, 100 or 200 µL of lysate. The lysate and eluates were analysed by 10% SDS, page, *Coomassie Brilliant Blue* staining.

GST-PAK was present at high levels in the lysate and able to be purified by GSH-sepharose beads. The amount of purified GST-PAK correlated to the amount of lysate loaded. In the following, a volume of 200 µL GST-PAK was used for the assay.

4.1.4.1.1.2. Pulldown

To establish the assay, several control experiments were performed as can be seen in **fig. 33**.

- H1299 SHIP1 WT, no GST-PAK loaded (GST-PAK control)
- H1299 SHIP1 WT, no lysate (lysate control)
- H1299, transfected with dominant negative mutant pEGFP-C3-RAC1 N17
- H1299, transfected with constitutively active mutant pEGFP-C3-HA-RAC1 V12

- H1299 SHIP1 WT, treated with GTPγS (0.1 mM f.c.)
- H1299 SHIP1 WT, treated with GDP (1 mM f.c.)
- H1299 SHIP1 WT (Ctrl)

Pulldowns and lysates were analysed by Western Blot using anti-RAC1 monoclonal antibody.

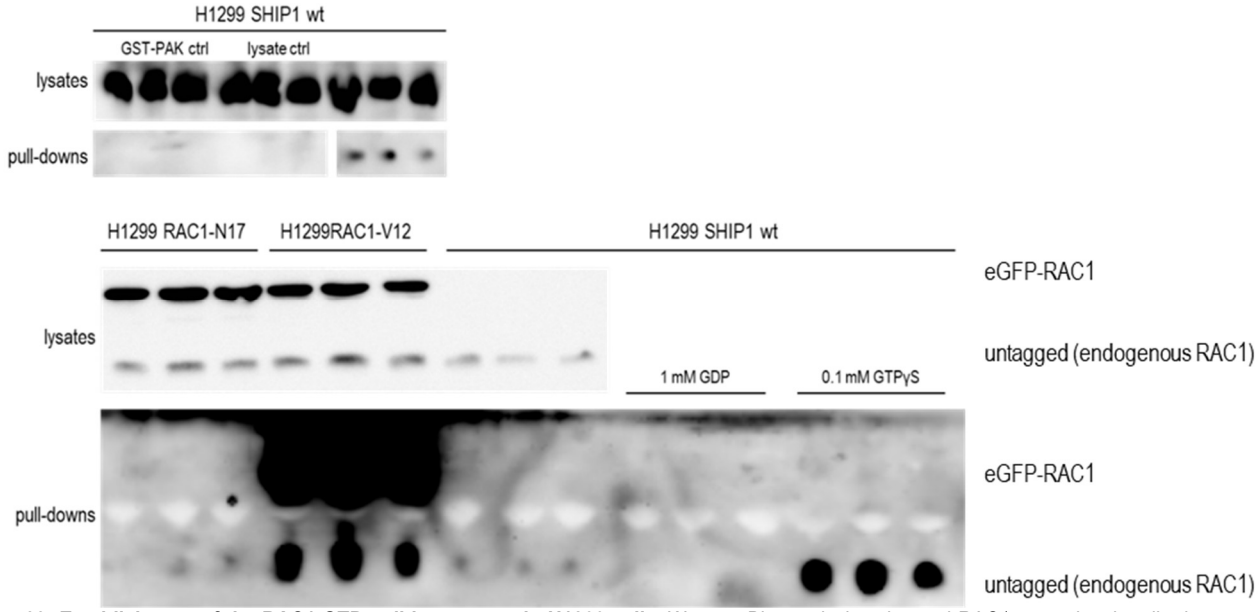

fig. 33: Establishment of the RAC1-GTP pulldown assay in H1299 cells. Western Blot analysis using anti-RAC1 monoclonal antibody (for details: see text).

As can be seen, all negative controls (GST-PAK and lysate control, H1299 RAC1-N17 and H1299 SHIP1 WT treated with GDP) were negative whereas the positive controls (H1299 RAC1-V12 and H1299 SHIP1 WT treated with GTPγS) showed strong signals in the pulldowns. Of note, also the signal strength of endogenous RAC1 was increased in H1299 RAC1-V12.

4.1.4.1.1.3. Comparison of relative RAC1-GTP levels of H1299 SHIP1 wt and H1299 LeGO

For the comparison of RAC1-GTP levels in H1299 SHIP1 WT and H1299 LeGO lysates were prepared under maintenance conditions (DMEM, 10% FCS) and loaded on GSH-sepharose beads containing immobilized GST-PAK. Active RAC1 (RAC1-GTP) was precipitated and analysed by Western Blot. Band intensity was normalized to RAC1 levels in the whole cell lysates and GST-PAK1 levels in the eluates detected by anti-GST. This is shown in **fig. 34**.

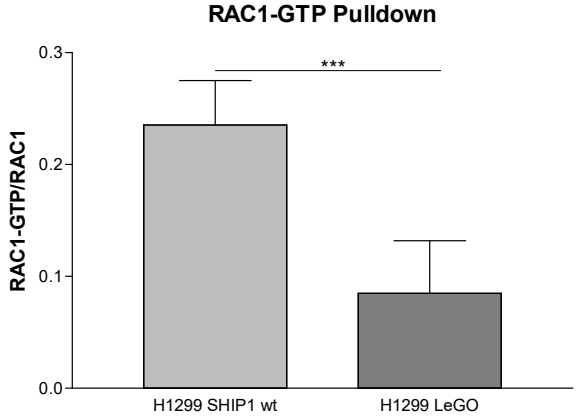

fig. 34: RAC1-GTP pulldown of H1299 SHIP1 WT and H1299 LeGO. Lysates were prepared of cells held in DMEM, 10% FCS and the relative amount of RAC1-GTP was determined by RAC1-GTP pulldown assay. Lysates and pulldowns were analysed by Western Blot analysis using anti-RAC1 or anti-GST for the detection of GST-PAK. Band intensities of RAC1 signals in the pulldowns (RAC1-GTP) were normalized to total RAC1 content in the lysates and GST-PAK1 content. Error bars indicate standard deviations. n=5.

The relative amount of RAC1-GTP was very significantly enhanced in H1299 SHIP1 WT (0.24±0.04) with regard to H1299 LeGO (0.09±.0.05) which was in accordance with the observed phenotype. Therefore, enhanced activation of RAC1 seems to contribute to the observed increased migratory potential of H1299 SHIP1 WT.

4.1.4.1.2. Comparison of relative RAC1-GTP levels in HCT-116 SHIP1 WT vs. HCT-116 LeGO and SW-480 SCR vs. SHIP1 KD

The RAC-GTP pulldown of HCT-116 SHIP1 WT vs. LeGO and SW-480 SHIP1 KD2 vs. SCR was performed as established for H1299. Unfortunately, RAC1-GTP levels for SW-480 were below the detection limit. For HCT-116, RAC1-GTP levels were not significantly altered by SHIP1 (**fig. 35**).

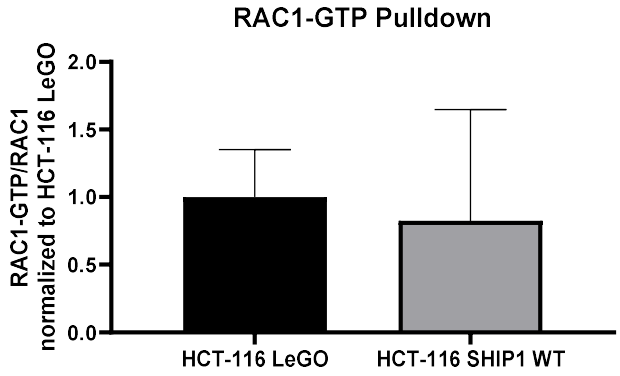

fig. 35: RAC1-GTP pulldown of HCT-116 SHIP1 WT and HCT-116 LeGO. Lysates were prepared of cells held in DMEM, 10% FCS and the relative amount of RAC1-GTP was determined by RAC1-GTP pulldown assay. Lysates and pulldowns were analysed by Western Blot analysis using anti-RAC1 or anti-GST for the detection of GST-PAK. Band intensities of RAC1 signals in the pulldowns (RAC1-GTP) were normalized to total RAC1 content in the lysates and GST-PAK1 content. Error bars indicate standard deviations. n=3.

4.1.5. Kinome analysis

For the kinome analysis the PAMGENE system was used. PAMGENE is an array-based analysis tool which screens a variety of S-/T- or Y-kinase target sequences in order to generate an estimated activity profile for cellular kinases [631]. Of note, the generated profile should be taken with certain care as direct kinase activity is not monitored but only indirectly concluded out of the phosphorylation pattern of the target sequences immobilized to the array.

4.1.5.1. S-/T-kinases

For the PAMGENE analysis cells were seeded in a 10 cm plate in DMEM, 10% FCS and lysed at 70-80% confluence using M-PER buffer as proposed by the manufacturer. PAMGENE analysis was done by the group of Malte Kriegs, UKE Hamburg (**fig. 36** and **fig. 38**).

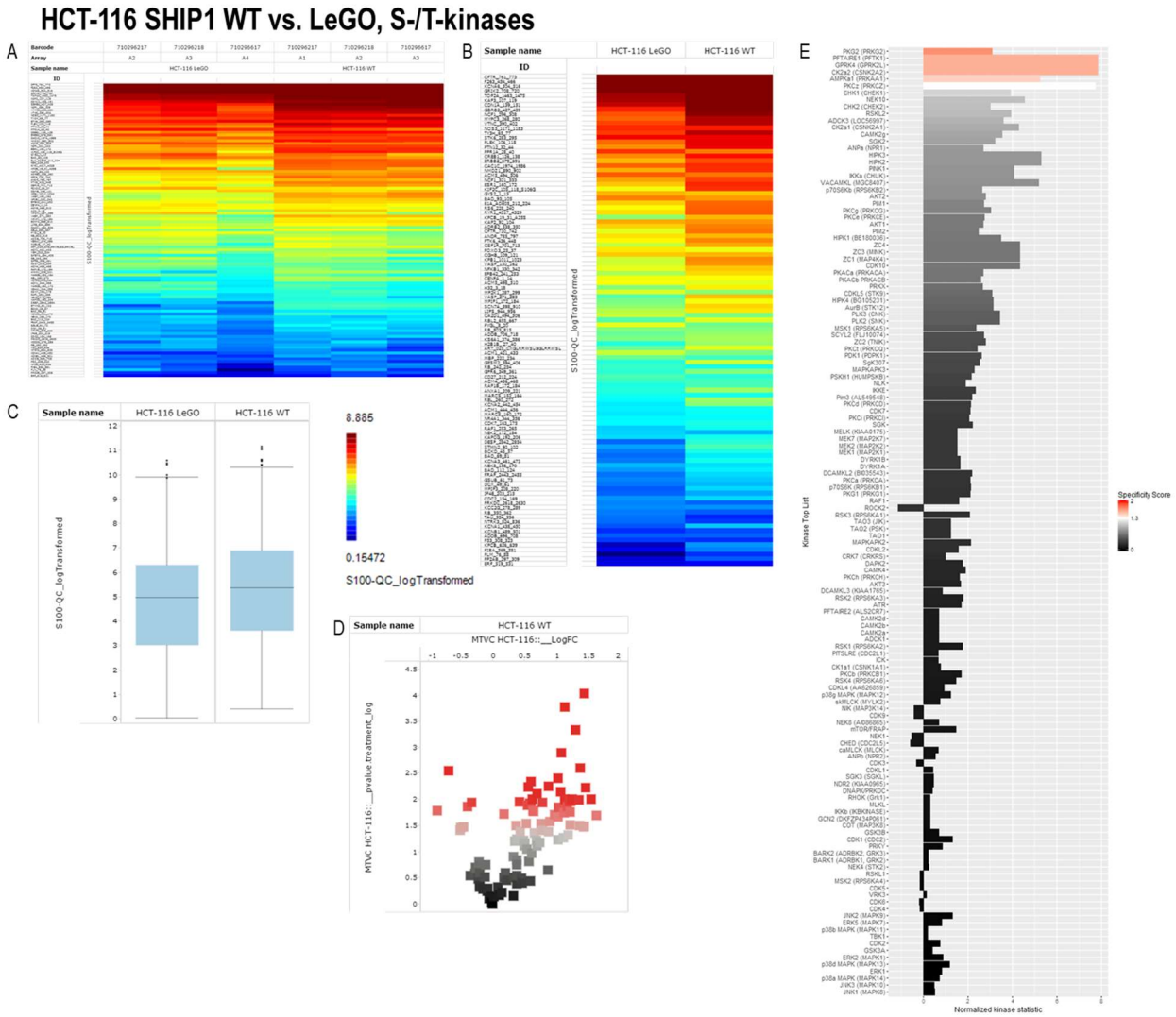

fig. 36: PAMGENE S-/T- analysis of HCT-116 SHIP1 WT vs. HCT-116 LeGO. Cells grown in DMEM, 10% FCS were lysed at 70-80% confluence in M-PER buffer and analysed for S-/T-kinase activity using the PAMGENE assay kit. Panel A depicts the heat map of individual triplicates and panel B depicts the heat map of averaged samples. Panel C shows the total kinase activity and panel D depicts the volcano plot of HCT-116 SHIP1 WT kinase activity normalized to HCT-116 LeGO and panel E depicts the normalized kinase statistic (log_2) of HCT-116 SHIP1 WT kinase activity normalized to HCT-116 LeGO. The PAMGENE analysis was performed by the group of Malte Kriegs, UKE Hamburg. n=3

The proposed significantly upregulated kinases in HCT-116 SHIP1 WT compared to HCT-116 LeGO (normalized kinase statistic >1, specificity score ≥1.3) were identified as PKG2, AMPKa1 (PRKAA1), PKCz, PFTAIRE1 (PFTK1), GPRK4 (GPRK2L), CK2a2 and CHK1.
The biological functions of said kinases is summarized in **fig. 37** and described in more detail below.

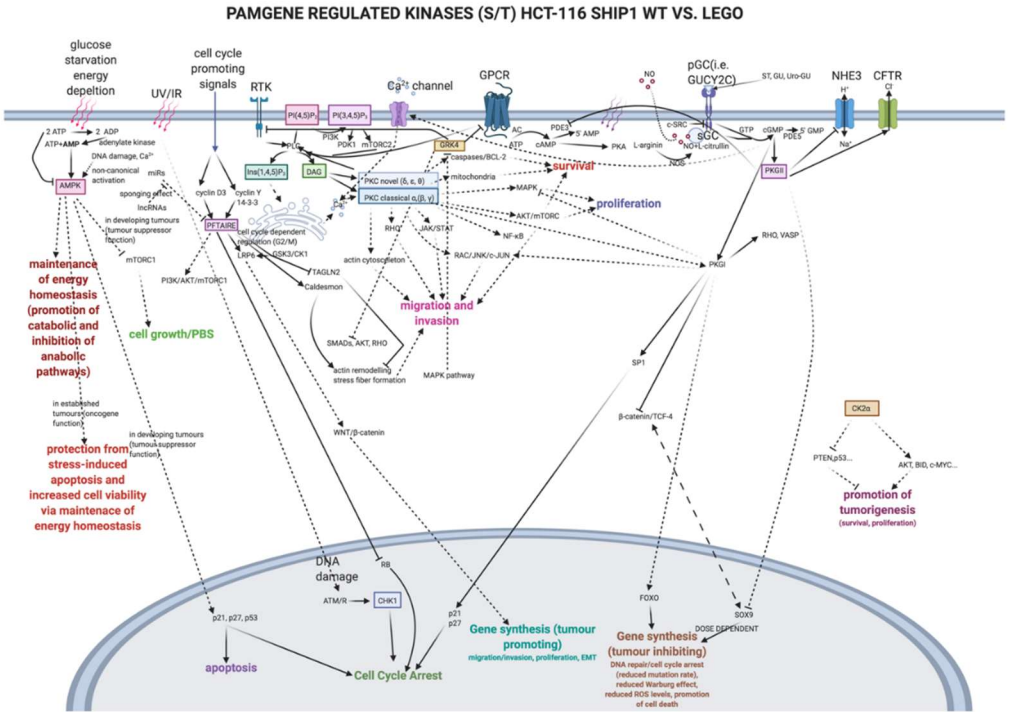

fig. 37: PAMGENE regulated S-/T-kinases in HCT-116 SHIP1 WT vs. HCT-116 LeGO (normalized kinase statistic >1, specificity score ≥1.3). Details: see text

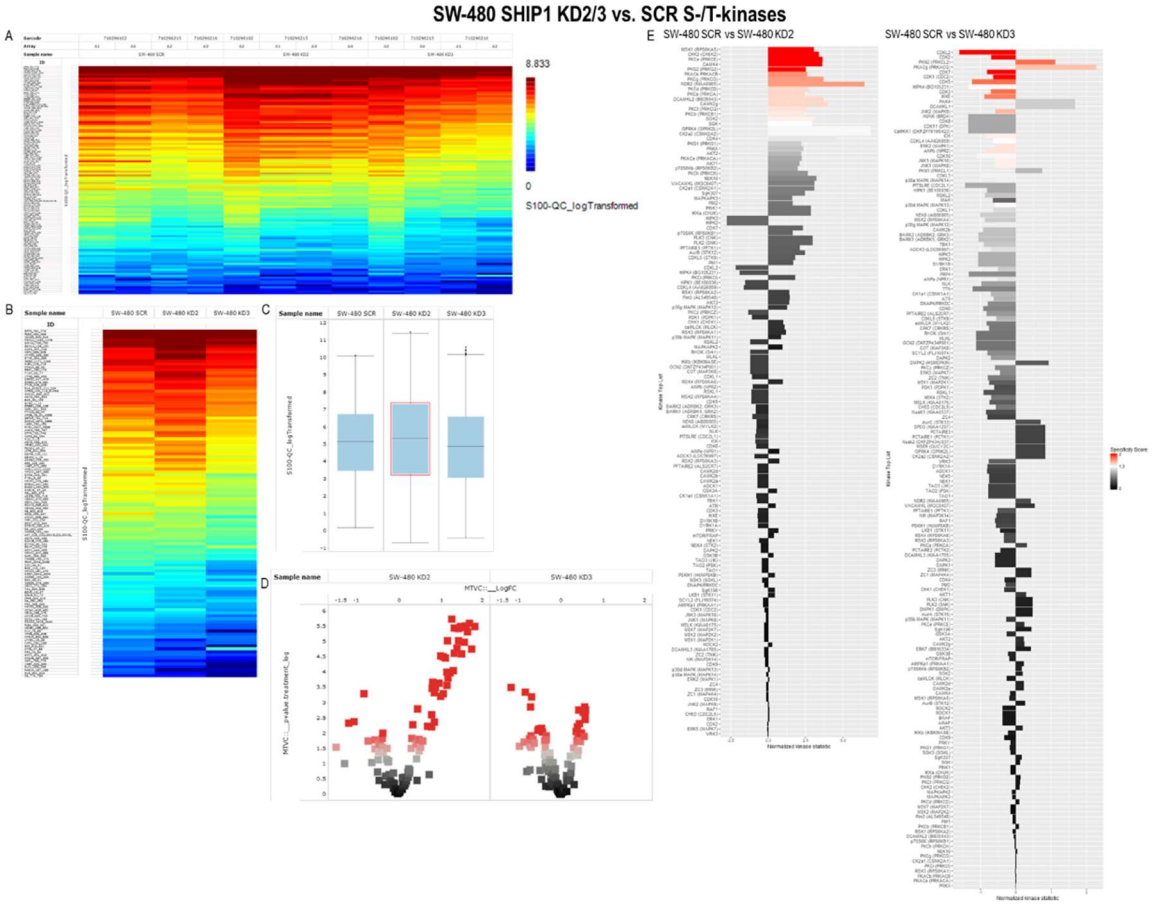

fig. 38: PAMGENE S-/T- analysis of SW-480 SCR vs. SW-480 KD2/KD3. Cells grown in DMEM, 10% FCS were lysed at 70-80% confluence in M-PER buffer and analysed for S-/T-kinase activity using the PAMGENE assay kit. Panel A depicts the heat map of individual quadruplicates and panel B depicts the heat map of averaged samples. Panel C shows the total kinase activity and panel D depicts the volcano plot of SW-480 SHIP1 KD2/3 kinase activity normalized to SW-480 SCR and panel E depicts the normalized kinase statistic (log_2) of SW-480 SHIP1 KD2/3 kinase activity normalized to SW-480 SCR. The PAMGENE analysis was performed by the group of Malte Kriegs, UKE Hamburg. n=4.

The proposed significantly upregulated kinases in SW-480 KD2 vs. SCR (normalized kinase statistic >1, specificity score ≥1.3) were MSK1, CHK2, PKCs (ε, β, γ, δ, α, θ), CAMK4, PKG2, PKACb, NDR2, DCAMKL2, CAMK2γ, SGK2, GPRK4 and CK2a2. The proposed significantly upregulated kinases in SW-480 KD3 vs. SCR were PKN2 and PKACg and downregulated kinases were CDKL2, CDK5 and HIPK4.
The biological functions of said kinases is summarized in **fig. 39** and **fig. 40** and described in more detail below.

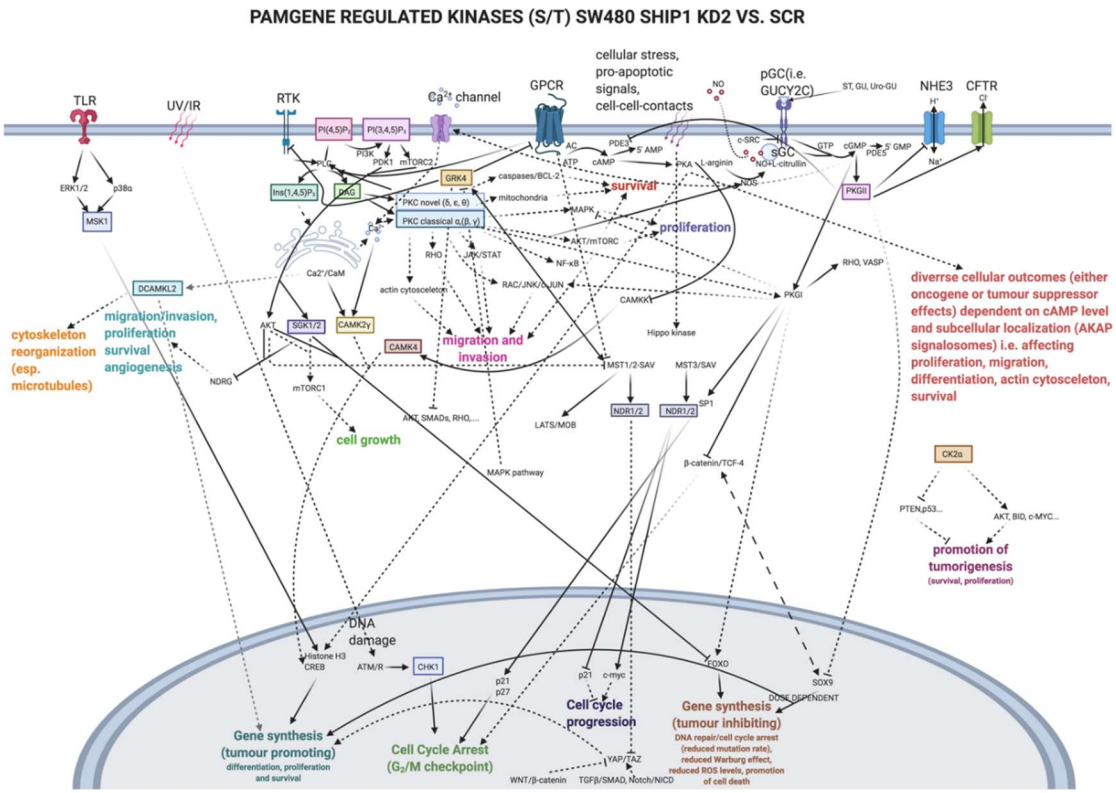

fig. 39: PAMGENE regulated S-/T-kinases in SW-480 SHIP1 KD2 vs. SW-480 SCR (normalized kinase statistic >1, specificity score ≥1.3). Details: see text

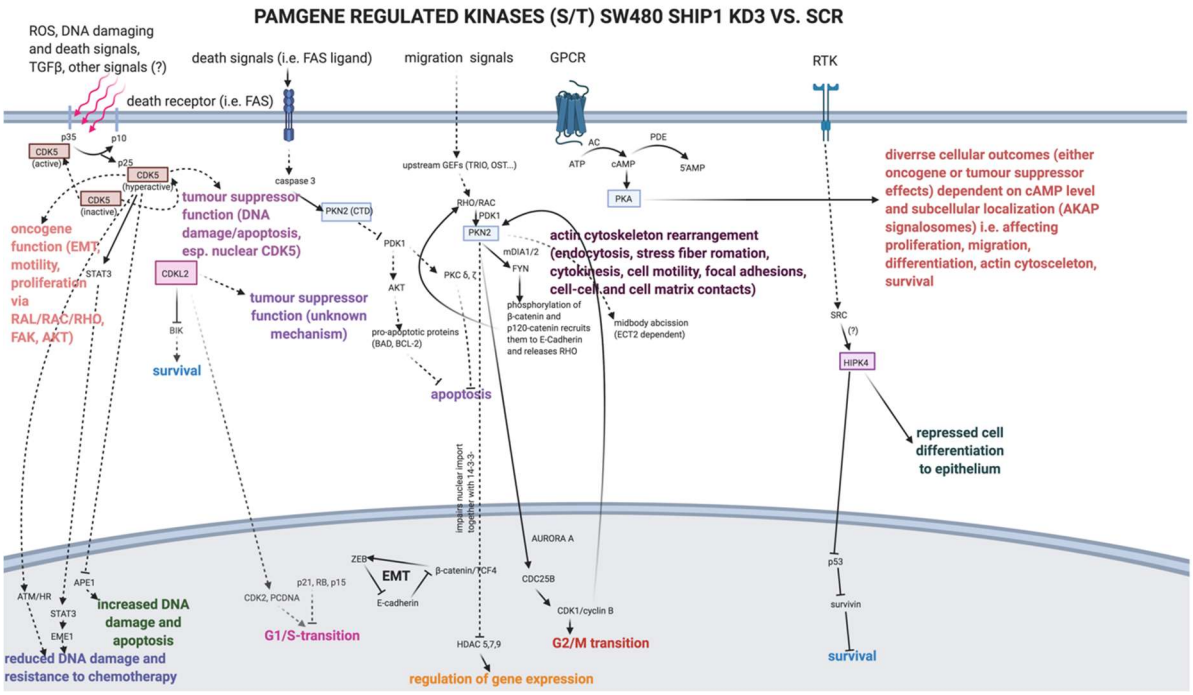

fig. 40: PAMGENE regulated S-/T-kinases in SW-480 SHIP1 KD3 vs. SW-480 SCR (normalized kinase statistic >1, specificity score ≥1.3). Details: see text

CHK1 (Checkpoint kinase 1)

CHK1 is a checkpoint kinase involved in cell cycle arrest in response to DNA damage or incomplete respectively faulty DNA replication. It is activated in a RAD17/ATR dependent manner in the presence of UV irradiation or in an ATM dependent manner in the presence of ionizing irradiation. Both ATM and ATR phosphorylate CHK1 at S317 and S345. Phosphorylation of S345 is necessary for consistent nuclear localization of CHK1 during the DNA damage repair process and phosphorylation of S317 leads to its activation and liberates the FBOX06 binding site resulting in ubiquitination of K436. CHK1 promotes DNA damage repair and cell cycle arrest by phosphorylating a panel of targets. Phosphorylation of CDC25A-C promotes their recruitment to 14-3-3 proteins or their proteolytic or proteasomal degradation and results in the inhibition of cyclin/CDK complexes. Cell cycle arrest is further supported by CHK1 mediated activation of p53 and RB. CHK1 participates in DNA damage repair by enhancing the chromatin binding capacity of RAD51 and activating FANCE. Additionally, it contributes to the epigenetic regulation of gene expression via phosphorylation of histone H3.1 [632].

PKC (Protein Kinase C)

The PKC family of AGC kinases comprises three subfamilies which are classified upon their domain structure and activation mode: Classical PKCs (α, βI/II, γ) require DAG and Ca^{2+} for their activation which are typically produced following activation of PLC. Novel PKCs (δ, ε, θ, η) dependent on lipids (PtdIns(3,4,5)P_3, DAG, PS) but not on Ca^{2+} for their activation. Atypical PKCs ($\zeta$and ι/λ) are activated independently on lipids/DAG and Ca^{2+} [633], [634]. For full activation and maturation of PKCs they require PDK1 dependent phosphorylation of three conserved S-/T-residues residing in the catalytic domain (i.e. T566, T710 and S729 in PKCε) [635]. This occurs while PKCs remain bound to the anchor/adaptor protein CG-NAP. Phosphorylated PKC is then released from CG-NAP and recruited to different cellular compartments to fulfil their various functions [636]. They promote survival, proliferation and migration/invasion via activation of the MAPK pathway, p38α, NF-κb, RAC/JNK/c-JUN and JAK/STAT as well as crosstalk with the PI3K/AKT/mTORC1 pathway [633], [634], [637]. The strongest oncogenic potential is given for PKCε. It is sufficient for cell transformation predominantly via the MAPK pathway and overexpressed in several cancers such as breast cancer, colorectal cancer, prostate cancer, stomach cancer and lung cancer but only minimally expressed in most healthy tissues. Overexpression of PKCε is correlated with a poor prognostic outcome as well as lower respondance to therapeutic intervention [633], [634], [637].

PKG (Protein kinase G)

Protein kinase G members PKG1 and PKG2 belong to the family of AGC kinases. They are activated by cGMP and regulate multiple signalling pathways necessary to maintain homeostasis and counteract tumorigenesis. cGMP is produced by guanylate cyclase enzymes which are separated into two classes. Particulate guanylate cyclase (pGC) is a transmembrane receptor cyclase and is activated by ligand binding. Soluble guanylate cyclase (sGC) is a cytosolic enzyme and activated by nitric oxide (NO). NO can either be produced by neighbouring cells and diffuse through the plasma membrane into the cytoplasm of the target cell or it can be produced out of L-arginine by members of the NOS (NO synthase) family. Guanylate cyclases catalyse the formation of cGMP out of GTP. cGMP is degraded to 5'GMP by phosphodiesterases (PDEs) in order to halt cGMP dependent signalling [638]. In CRC silencing of cGMP signalling was found to contribute to tumorigenesis. cGMP signalling in the intestine is mainly dependent on the pGC GUCY2C. In a homeostatic state GUCY2C is activated either by uroguanylin/guanylin, tissue hormones produced by the enterocytes and acting in an autocrine or paracrine fashion, or by the enterotoxic *E. coli* derived ST peptide resulting in the accumulation of cGMP and activation of PKG1 and PKG2. In this state, proliferation is reduced in favour to cell differentiation, DNA stability is increased, tight junctions/barrier function is intact, the stroma milieu is in a quiescent and anti-inflammatory state, the microbiome is balanced and mucus secretion as well as metabolism is healthy. In an oncogenic state, reduced cGMP signalling results in uncontrolled hyperproliferation, increased inflammation (increased levels of TNFα and IFNγ), induction of the Warburg effect, DNA instability, leaky barrier, gut dysbiosis, thinning mucus and increased neoangiogenesis and metastasis [639]. Mechanistically, silencing of cGMP signalling in the intestine is realized by multiple pathways:

- upregulation of PDEs such as PDE5 in CRC or PDE10 in APC [640], [641], [642], [643]
- overexpression of c-SRC; c-SRC is responsible for the phosphorylation of GUCY2C at Y820 suppressing the activation of GUCY2C [644]
- removal of GUCY2C from the plasma membrane by endocytosis and translocation to other compartments. A function of GUCY2C in compartments other than the plasma membrane has not been examined [645].
- reduced levels of GUCY2C ligands (paracrine hormone hypothesis): Uroguanylin and guanylin belong to the top reduced targets in CRC. For instance, in a study comprising 300 CRC patients >85% displayed loss of guanylin on both the mRNA and protein level. Moreover, using a mouse model *knock down* of

guanylin led to crypt hyperplasia and readministration of guanylin either by feeding or genetic manipulation opposed crypt hyperplasia [646], [647], [648], [649], [650].

- Importantly, the expression of GUCY2C itself is not silenced [645], [648], [651], [652].

The oncogenic phenotype observed for reduction of cGMP seems to be mainly mediated trough reduced activity of PKG1 and PKG2. PKG1 contributes to tumour suppression mainly via inhibition of β-catenin/TCF-4. β-catenin/TCF-4 induces the expression of c-MYC promoting proliferation and angiogenesis and cyclin D promoting G_1/S progression. Furthermore, it activates the CKIs p21 and p27 and FOXO transcription factors and counteracts RHO/VASP and MAPK signalling reducing migration/invasion and proliferation. PKG1 is downregulated in CRC and in APC_{min} xenografts overexpression of PKG1 induced apoptosis and reduced cell motility and *knock-down* of PKG1 resulted in enhanced tumour load and metastasis. The exact function of PKG2 in CRC has not been examined yet, however as for PKG1 levels of PKG2 are downregulated in CRC. PKG2 contributes to fluid and ion homeostasis by inhibiting the Na^+/H^+ exchanger NHE3 and activating the Cl^- channel CFTR. It is proposed that its anti-tumour effect is mediated mostly through inhibition of SOX9 mediated cell proliferation. Of note, SOX9 expression is dependent on β-catenin/TCF-4 and vice versa suggesting that PKG1 and PKG2 act in concert to maintain intestine homeostasis and prevent tumorigenesis [638].

CK2 (Casein Kinase 2)

CK2 was shown to be a constitutively active kinase with wide tissue distribution and to promote cellular transformation and tumorigenesis, especially the development of aggressive tumours [653], [654], [655]. Overexpression of CK2 was found in several cancer entities including breast, kidney, lung, prostate and head and neck cancer [655], [656], [657], [658], [659]. In mouse models of T-cell leukaemia and breast carcinoma an oncogenic function of CK2 was verified [657], [660] and it was shown that overexpression of CK2 acted in concert with downregulation of tumour suppressor proteins (p53) or overexpression of oncogenes (c-MYC, TAL1) to promote tumour progression (synergistic effect) [660], [661], [662]. CK2 does mediate oncogenesis via different mechanisms:

- CK2 inactivates or destabilizes tumour suppressor proteins: Phosphorylation of PML S517 leads to increased proteasomal degradation of PML. Phosphorylation of PTEN by CK2 stabilizes its inactive conformation resulting in reduced activity of PTEN [663], [664], [665].
- CK2 activates and stabilizes oncogenes such as c-MYC, c-JUN, c-MYB, NF-κB or β-catenin [666], [667], [668], [669], [670], [671], [672], [673].
- CK2 cross-activates AKT by phosphorylating it on S129 rendering it constitutively active and indirect by inactivation of PTEN (see above) [674].
- a special focus has been laid on the antiapoptotic function of CK2: As indicated above, CK2 positively regulates anti-apoptotic pathways such as WNT, NF-κB or PI3K/AKT/mTORC1. Furthermore, it phosphorylates pro-apoptotic proteins such as BID to mask them from caspase-cleavage mediated activation, it inhibits the activation of pro-caspases (i.e. procaspase 2) by cleavage or activation of the caspase inhibitor ARC (i.e. concerning procaspase 8). In cell models CK2 was demonstrated to be crucial for protection of cells from intrinsic or extrinsic apoptosis. In HT-29 cells *knock-down* of CK2 increased TRAIL induced apoptosis, DISC complex formation and the levels of active caspase 8 and BID as well as it downregulated anti-apoptotic proteins (XIAP, c-IAP). In HeLa cells *knock-down* of CK2 increased apoptosis in response to IR. In HCT-116 and HeLa cells CK2 protected those from intrinsic apoptosis induced by 6-TG mediated DNA damage. These properties are of special interest as they qualify CK2 to render cells resistant to anti-tumour therapy [653], [675], [676], [677], [678], [679].

AMPK (AMP activated kinase)

AMPK is a highly sensitive cellular energy sensor protein [680], [681], [682]. It comprises three subunits which come in different isoforms; namely the catalytic α-subunit (α1 or α2), the regulatory/scaffolding β-subunit (β1 or β2) and the regulatory autoinhibitory γ-subunit (γ1, γ2 or γ3) [683]. Upon energy depletion (increased AMP:ATP ratio) AMPK gets activated [683]. In more detail, when cells are reduced in energy ATP is consumed for energy production and the AMP is formed out of ADP by the adenylate kinase reaction [684]. AMP then binds to the γ-subunit of AMPK (CBS3) and the resulting conformational switch is transferred to the α-subunit which releases the kinase domain from autoinhibition and exposes T172 [685], [686]. T172 is then phosphorylated mainly by the *upstream* kinase and tumour suppressor protein LKB1 which leads to full activation of AMPK [687], [688]. Additionally, AMP prevents the dephosphorylation of T172 once AMPK is activated [689]. Thus, LKB1 and AMP act synergistically on the activation of AMPK. Non-canonical activation of AMPK by Ca^{2+}, DNA damage or reduced glucose levels was also described [690], [691], [692], [693].

The main function of AMPK is to maintain energy homeostasis and cell viability by reducing ATP consuming and favouring ATP producing processes. In general, catabolic metabolism is enhanced and anabolic metabolism is inhibited as described in the following [683].

- activation of catabolic pathways/ATP production: AMPK promotes the uptake of glucose via GLUT4 and GLUT1 [694], [695], [696], [697], [698]. In proliferating cells, it stimulates the glycolytic degradation of glucose via activation of PFKFB2/3 (phospho-fructo-2-kinase/fructo-2,6-bisphosphatase) which synthesizes Fru-2,6-P_2. Accumulated Fru-2,6-P_2 then allosterically activates the glycolysis enzyme 6-phospho-fructo-1-kinase. Of note, PFKFB is typically overexpressed in tumours to realize the Warburg effect [699], [700], [701]. In quiescent cells AMPK rather favours the degradation of glucose via oxidative phosphorylation by activation of acetyl-coA carboxylase (ACC) [41]. In this term, also fatty acid breakdown is stimulated [702]. Furthermore, oxidative phosphorylation of carbohydrates and fatty acids is increased by AMPK mediated promotion of healthy mitochondria count (mitochondria biogenesis (via PGC-1α), mitochondria fission (via MFF) and removal of defect mitochondria/mitophagy (via ULK1 and DAPK/Beclin-1)) [703], [704], [705], [706], [707], [708], [709], [710], [711].
- deactivation of anabolic pathways/ATP consumption: AMPK inactivates ACC1 and HMGR thus reducing the synthesis of fatty acids and sterols [712], [713]. Furthermore, the SREBP1c and ChREBP dependent expression of ACC and fatty acid synthase complex is inhibited [714], [715]. In muscle and liver AMPK negatively regulates the glycogen synthase [716], [717]. The synthesis of nucleotides and NADPH (via PRPS1/2) and protein biosynthesis (via mTORC1) is also inhibited [718], [719], [720], [721].

Consistent with the described impacts of AMPK on cellular metabolism and energy homeostasis AMPK favours cell cycle arrest. In more detail, it activates p53, it induces the expression of p53 and p21 and stabilizes p27 [722], [723].

The function of AMPK on tumorigenesis was extensively studied in mouse models. As a global *knock-out* of both α-isoforms was proven to be lethal and tissue specific *knock-outs* are complex and time-consuming hematopoietic cells were preferentially used as they exclusively express AMPKα1 [724], [725]. Using an Eμ-MYC B-lymphoma mouse model *knock-out* of AMPKα1 accelerated lymphoma progression and this effect was stronger in homozygous compared to heterozygous *knock-outs*. Mechanistically, the effect of AMPKα1 *knock-down* was tracked down to mTORC1 hyperactivation and increased synthesis of biointermediates by aerobic glycolysis. In order to rule out indirect effects of the global AMPKα1 *knock-out*, in a following experiment mice were irradiated to destroy the hematopoietic system and replenished with homozygous or heterozygous AMPKα1 *knock-out* or control (WT) B-cells to generate a tissue-specific *knock-out* [726]. In a tissue specific inducible LCK/CRE-*knock-out* system of T-ALL *knock-out* of PTEN alone was sufficient to induce T-ALL and *knock-out* of AMPKα1 alone did not have any effect but in combination with *knock-out* of PTEN tumour progression was accelerated compared to single *knock-out* of PTEN [727]. As re-expression of the AMPKα1 specific ubiquitin ligase complex MAGE-A3/6-TRIM28 was observed in tumours in mouse models of breast, prostate and colorectal carcinoma *knock-out* of either MAGE-A3/6 or TRIM28 led to accumulation of AMPKα1 and inhibition of mTORC1 as well as delayed cancer progression [728]. Similarly, *knock-out* of AMPKα2-specific ubiquitin ligase UBE20 delayed tumour progression which was rescued by *knock-out* of AMPKα2 [729].

Interestingly, a tumour promoting role of AMPK in established tumours was proposed. Using a T-ALL model and a tamoxifen-inducible AMPKα1 *knock-out* T-ALL was allowed to develop and mice were then treated with tamoxifen to induce the AMPKα1 knock-out. Of note, *knock-out* of AMPK reduced the viability of established T-ALL cells and increased the overall survival of said mice [730]. This tumour promoting role of AMPK in established T-ALL was in contrast with its tumour suppressor role in developing T-ALL as discussed above. In a comparable inducible model of AML AMPKα1/2 was similarly required to maintain the glycolytic flux/Warburg metabolism, cell viability and tumour load in established AML [731]. Furthermore, stress induced apoptosis was more pronounced in established tumour cell lines displaying a *knock-out* of either AMPKα1 or LKB-1 therefore, a protective function of AMPK during cellular stress (such as tumour therapy conditions) was suggested [732], [733]. In an established lung carcinoma model *knock-out* of AMPKα1/2 reduced the tumour load especially in *p53*$^{-/-}$ cells and consistent with that AMPKα1 amplification was frequently found in human carcinomas and especially in those with loss of p53 suggesting a protective role of AMPKα1 from genotoxic stress in the absence of p53 [734], [735].

PFTAIRE1 (PFTK1/CDK14)

PFTAIRE is a protein of the CDK family and positively regulates cell cycle progression by interacting with cyclins D3 and Y (CCDN3 and CCNY) [736], [737], [738], [739], [740], [741]. Specifically, it promotes G_2/M progression via the WNT signalling pathway [741], [742]. During WNT signalling LRP6 acts as an *upstream* receptor. For its

activation phosphorylation of the cytoplasmic PPPSP motifs is required. It was found that phosphorylation of S1490 by CCNY/PFTAIRE1 primed LRP6 for subsequent GSK3/CK1-mediated full activation. CCNY is a membrane-tethered cyclin and necessary for the translocation of PFTAIRE to plasma membrane residing LRP6. Genetic studies showed that WNT signalling peaked at G_2/M and was dependent on the expression of CCNY during that phase of the cell cycle [742]. Furthermore, in a HCC cell culture study PFTAIRE1 promoted migration. Mechanistically, phosphorylation of caldesmon by PFTAIRE1 dissociated it from actin resulting in actin remodelling processes that favoured migration [743].

The role of PFTAIRE1 has been studied in several cancer moieties. In HCC PFTAIRE1 is frequently overexpressed and positively impacts cell motility. Using a 2D-PAGE-MS approach to scan for phosphoproteins affected by PFTAIRE1 expression β-actin and transgelin 2 (TAGLN2) were identified as top regulated targets. Reduced phosphorylation of those proteins in PFTAIRE1 *knock-down* cells was associated with reduced actin dynamics and cell motility. The tumour suppressor protein TAGLN2 suppresses actin dynamics in its dephosphorylated state by tight binding to actin and by PFTAIRE1 mediated phosphorylation of TAGLN2 its affinity to actin is significantly reduced allowing for actin dynamics [744]. In mammary carcinoma and NSCLC PFTAIRE1 was found to be frequently overexpressed and this was correlated with tumour grade and a poor prognosis [745], [746]. In cell culture studies of mammary carcinoma *knock-down* of PFTAIRE1 reduced cell proliferation, migration and invasion and anchorage-independent growth as well as the WNT/β-catenin dependent expression of cyclin D, MMP-9 and HEF-1 [746]. In gastric and epithelial ovarian cancer ectopic expression of PFTAIRE1 correlated with lymph node status and tumour grade and increased proliferation, invasion and migration in cell culture studies [747], [748]. In pancreatic cancer PFTAIRE1 promoted proliferation, invasion and migration and EMT via the PI3K/AKT/mTORC1 axis [749]. *Knock-down* of PFTAIRE1 reduced migration and invasion, EMT and proliferation in CRC and the reduction of EMT was linked to reduced Hedgehog signalling [750], [751]. Generally, ectopic expression of PFTAIRE1 was linked to reduced levels of certain miRs or overexpression of buffering/sponging lncRNAs in several cancer entities (i.e. in osteosarcoma, mammary carcinoma, glioma, prostate cancer, ovarian carcinoma, pancreatic cancer and NSCLC) [752], [753], [754], [755], [756], [757], [758], [759], [760], [761], [762]. In mammary carcinoma expression levels of PFTAIRE1 were also observed to be controlled via the DYRK2/AR axis [763].

GRK4 (GPCR kinase 4)

GRKs phosphorylate the cytosolic domains of active GPCRs inducing their desensitization and internalization and therefore negatively regulate GPCR signalling [764]. The expression of GRK4 is generally very low and mainly restricted to the myometrium, brain, testis, ovaries and kidney [765]. Very little is known about the biological relevance of GRK4. GRK4 was found to target the GPCRs AT-1 and FSHR [766], [767], [768]. Moreover, it was downregulated in malignant ovary carcinoma compared to benign ovary carcinoma and this was correlated to increased FSHR activity in malignant ovary carcinoma which may provide a link between GRK4 and tumour development [768].

MSK1 (Mitogen and Stress activated Kinase 1)

MSK1 is a S-/T-kinase that is induced by mitogens or stress such as EGF, ROS and UV irradiation. For its activation phosphorylation of three conserved residues (S360, S376, T581 and T700) in the CTKD (C-terminal Kinase Domain) by either ERK1/2 or p38α is required to release the CTKD from its inhibitory loop and to allow the CTKD to subsequently phosphorylate S212, S376 and S381 in the NTKD. The activated NTKD then is able to phosphorylate *downstream* substrates [769]. In particular, it regulates transcription factors CREB, ATF1, STAT3, RELA and ETV1/ER81 resulting in repression of pro-inflammatory and activation of anti-inflammatory cytokines. Gene expression is also regulated by histone phosphorylation. Phosphorylation of S1 on histone H2 and S10 on histone H3 by MSK1 induces the expression of proto-oncogenes c-JUN and c-FOS [770].

CAMKIIγ and CAMKIV (Ca2+/CaM dependent signalling)

CAMKs are activated in response to Ca^{2+}/CaM. CAMKII exists in four isoforms (α, β, γ, δ) which differ in their tissue distribution [771]. CAMKIIγ is predominantly expressed in muscle and neuronal tissue under physiological conditions [771]. Following association of CAMKII with Ca^{2+}/CaM via its regulatory domain it gets phosphorylated on T287 (β, γ, δ) or T286 (α) which enhances its affinity to Ca^{2+}/CaM over 1000-fold and prevents its switch to its autoinhibited stage even when Ca^{2+}/CaM is dissociated from the complex [772], [773], [774]. Deactivation is mediated by designated protein phosphatases [773]. Alternative modes of activation comprise glycosylation, nitrosylation or oxidation [772], [775], [776]. CAMKII contributes to cancer progression by enhancing cell proliferation, survival and migration/invasion in several cancer incidences [777], [778], [779], [780], [781], [782]. However, a tumour suppressor function of CAMKII was also reported in some cases (see below) [783].

In an osteosarcoma cell culture and mouse model pharmacological inhibition using the CAMKII inhibitor KN-93 decreased cell proliferation and tumour growth and this correlated with increased expression of p21 [784].

Hyperproliferation of CML cells specifically depended on CAMKIIγ and was mediated via the MAPK pathway, STAT3/5 and GSK3β/β-catenin activation [785]. Additionally, CAMKII impacts cell proliferation by directly regulating cell cycle progression. In colon adenocarcinoma it activates ERK which leads to proteasomal degradation of p27 and promotes G_2/M progression [786]. In osteosarcoma CAMKIIα represses the expression of p21 via TIAM/RAC [784] and in breast carcinoma the BRCA1 mediated expression of p21 is reduced and the cyclin D1 expression is increased which promotes G_1/S progression [787]. In contrast, cell cycle progression was found to be negatively regulated by CAMKII in lung and breast cancer subtypes and in this case p53 levels were elevated because CAMKII inactivated the RING-H2 E3 ubiquitin ligase by phosphorylation [783]. Of note, it was shown that the impact of CAMKII on cell proliferation might depend on its phosphorylation state. Overexpression of CAMKII WT or a CAMKII T286 phosphomimic mutant increased and overexpression of a T253 phosphomic mutant reduced proliferation in a breast carcinoma and neuroblastoma model [788]. In breast carcinoma apoptosis was reduced due to CAMKII mediated suppression of caspase signalling [789], [790]. Concerning cell motility, CAMKIIα was found to be upregulated in osteosarcoma and in further experiments *knock-down* of CAMKIIα reduced and overexpression increased osteosarcoma cell migration in a scratch assay [791]. In HNSCC CAMKII activation was coupled to HA-CD44 mediated signalling via LARG, RHOA and PLCε induced Ca^{2+} influx and active CAMKII phosphorylated actin-bound filamin causing its release from actin filaments which resulted in increased migration [792]. CAMKIV is activated via CAMKK which is in turn activated by Ca^{2+}/CaM. PKA inhibits CAMKK. Like CAMKII it promotes tumorigenesis as it activates CREB family transcription factors as well as MAPK1/ERK, MAPK8/JNK and MAPK14/p38 [793]. Furthermore, it links Ca^{2+} signalling to microtubule dynamics [794]. Overexpression of CAMKIV was observed in ovarian carcinoma, small lung cell carcinoma and hepatocellular carcinoma and correlated with prognostic outcome, stage and histological grade in ovarian carcinoma [795].

Protein kinase A (PKA)

PKA is involved in the regulation of various processes *downstream* of cAMP signalling such as proliferation and cell cycle progression, metabolism, regulation of the actin cytoskeleton and survival [796]. In the inactive state it is found in its tetrameric form composed of two catalytic (CATα and CATβ) and two regulatory (REGα and REGβI in PKAI or REGα and REGβII in PKAII) subunits. The subcellular localization of PKA enzymes is dependent on the type of regulatory subunit. PKA can either be localized to the cytoplasm or attached to various organelles such as mitochondria, cytoskeleton or endosomes by AKAP family (A Kinase Anchoring Protein) proteins [797]. cAMP is the main activator of PKA. Upon binding of cAMP to the regulatory subunits their affinity to the catalytic subunits is reduced which releases the catalytic part of PKA and allows it to phosphorylate its *downstream* targets [798]. cAMP independent activation of PKA was also described i.e. via I-κb, SMAD3/4 or PDK1 [799], [800], [801], [802].

PKA mediated signalling may differ dependent on the type of stimulus. It seems that different stimuli only activate a fraction of PKA localized to a specific cellular compartment (i.e. only cytosolic PKA) [796]. One major target of PKA are CREB (cAMP responsive element) transcription factors and the cAMP/PKA/CREB axis is altered in many cancers [796], [803]. PKAI is typically overexpressed in tumours and especially in endocrine tumours [804], [805]. PKA CATβ was found to be positively regulated on the transcriptional level by c-MYC and implicated in c-MYC mediated cellular transformation [806]. In breast and ovarian carcinoma PKAI contributes to cell migration and invasion by regulating the actin cytoskeleton (via phosphorylation of actin, VASP, integrin, myosin, RHO, c-SRC and others) [807], [808], [809] and in lung carcinoma PKAI is upregulated by HIF1α and contributes to hypoxia induced EMT, invasion and migration [810]. Of note, while PKAI contributes to tumorigenesis PKAII displays a tumour suppressor function. As PKAI shows high affinity to cAMP and mediates activation of PKA at low levels of cAMP and PKAII shows low affinity to cAMP and mediates activation of PKA at high levels of cAMP the effect of PKA on tumorigenesis seems to depend on the level of cAMP and furthermore, on its subcellular localization which is dictated by the regulatory subunit [796].

SGK (Serum and Glucocorticoid regulated Kinase)

SGK kinases are of special interest in tumour formation as they show striking similarities to AKT [811], [812], [813]. There are three SGK isoenzymes which differ in tissue distribution and transcriptional regulation. SGK2 and SGK3 are constitutively expressed, however the expression of SGK2 is restricted to liver, pancreas, brain and kidney [812], [813]. In contrast, SGK1 expression is found in all tissues but is tightly regulated [814]. Upon appropriate stimuli such as growth factors, glucocorticoids, cytokines and stress (hyperosmosis, heat stress, UV irradiation or oxidative stress) expression of SGK1 is induced [815], [816], [817], [818], [819] and SGK1 is rapidly degraded by proteasomal degradation which a half life time of 20-30 minutes [820], [821]. As AKT SGK is activated by the PI3K/PDK1/mTORC2 axis. It gets phosphorylated at T256 in the activation loop by PDK1 (homologous to T308 in AKT) and S422 in the hydrophobic loop by mTORC2 (homologous to S473 in AKT) [812], [822], [823]. Opposed to AKT where the two phosphorylation events occur largely independent from each other in the case of SGK serine

phosphorylation conformationally primes it for subsequent threonine phosphorylation [824], [825], [825], [826], [827]. Overexpression of SGK is a common feature in cancer (i.e. in two independent studies overexpression of SGK1 was shown in 31% respectively 48% of breast carcinoma patient samples) [828], [829]. The function of SGK1 with respect to tumorigenesis was elusively shown in mouse models. In a CRC model, *sgk1*$^{-/-}$ mice showed a 50% reduction in chemical induced tumour load compared to WT mice and this was coupled to increased levels of pro-apoptotic proteins BIM and FOXO3A [830]. T-cell specific deletion of SGK1 reduced the number of lung metastasis in a melanoma mouse model underlining a function of SGK1 in the regulation of anti-tumour immunity [831]. In HCC overexpression of SGK3 is more common than overexpression of AKT and implicated in cell proliferation, anchorage-independent growth, migration and angiogenesis [832]. AKT and SGK share the same optimal target motif RXRXXS/T and overlapping target specificity [812], [813]. Of note, AKT and SGK can compensate for each other in case one kinase is genetically or pharmacologically silenced [812], [833], [834]. SGK mediates resistance to both PI3K and AKT inhibitors. When breast carcinoma cell lines displaying high levels of SGK1 are treated with a PI3K inhibitor SGK1 is able to activate residual activity of mTORC1 by direct phosphorylation of TSC2, however the mechanism of PI3K independent SGK1 activation remains unclear [835]. Furthermore, in those cells SGK1 can also mediate resistance to AKT inhibitors [836]. Prolonged treatment with either PI3K or AKT inhibitor resulted in transcriptional upregulation of SGK3 and resistance to the treatment program [837]. In the absence of active AKT SGK is able to phosphorylate common AKT targets such as before mentioned TSC2, GSK3 or FOXO3 [812], [833]. Other verified shared targets of SGK and AKT are NEDD4L ubiquitin ligase (regulates the levels of several plasma membrane proteins) [838], [839], [840] and PIKFIVE (regulates the endosomal trafficking of ion and amino acid transporters) [841], [842]. Confirmed unique targets of SGK but not AKT are NDRG1/2, the Na^+/H^+ exchanger NHE3 or the Na^+ channel ENaC [843], [844], [845], [846]. It is suggested that SGK target far more proteins than those mentioned however those has not been verified yet [811].

NDR1/2 (Nuclear DBF2 Related kinase 1/2)

NDR kinases belong to the HIPPO pathway. The classical HIPPO pathway is activated in response to mechanical tension, stress or increased cellular density/cell-cell contacts and mediates adequate stress responses as well as being implicated in tumour suppression. Diverse *upstream* HIPPO kinases such as FAT, NF2 or TAO activate the HIPPO core consisting of MST kinase, SAV1, LATS kinase and MOB in the canonical version. MST kinases in concert with SAV1 do activate LATS kinase. The active state of LATS is further stabilized by binding to MOB. Active LATS kinase then phosphorylates designated *downstream* targets such as the transcriptional co-activators YAP and TAZ resulting in reduced activation of oncogenic outcomes (see below) [847], [848]. As LATS1/2 also NDR1/2 are targets of MST kinases and MOB. Association of MOB to NDR1/2 facilitates autophosphorylation on S281/282 (T-loop) which is then followed by Ca^{2+} dependent phosphorylation on T444/442 (NTR domain) by MST1/2/3 [849], [850], [851]. The regulation of NDR1/2 activity is probably more complex and may involve membrane targeting and other PTMs such as mono-ubiquitination or acetylation besides its phosphorylation status [852]. NDR kinases regulate several *downstream* effects such as DNA damage response, stress response, autophagy, apoptosis and cell cycle progression, however most effects have not been evaluated in detail [853]. Of interest, NDR kinases seem to fulfil a dual role in tumorigenesis dependent on the *upstream* kinase. The MST1/NDR pathway promotes apoptosis, centrosome duplication and in general tumour suppression [854], [855], [856] and the MST2/NDR pathway regulates chromosome alignment during mitosis [857]. In contrast, MST3/NDR positively contributes to tumour progression (oncogenic function of NDR) [858]. Mechanistically, in the case of MST1/NDR mediated tumour suppression both LATS1/2 and NDR1/2 can phosphorylate YAP1 on S127 resulting in cytoplasmic retention and subsequent degradation of YAP1 and reduced proliferation and survival. In mice, overexpression of YAP1 was shown to be transformative and deletion of MST1/2 from the colon or liver resulted in tissue hyperplasia which was not dependent on LATS1/2 but on NDR1/2. Loss of NDR1/2 in the colon of mice reduced phosphorylation of YAP1 on S127 and increased their sensitivity to chemically induced cancer. Moreover, in human CRC samples an inverse correlation of NDR2 and YAP1 levels was observed [859]. Regarding the oncogenic MST3/NDR pathway MST3 was found to exclusively activate NDR kinases in the G_1 phase of the cell cycle and subsequent phosphorylation of p21 on S146 reduced the stability of p21 and promoted G_1/S progression. Furthermore, kinase-independent stabilization of c-MYC by NDR kinases was reported, however in *knock-down* experiments the positive effect of MST3/NDR on cell cycle progression was dependent only on destabilization of p21 but not on stabilization of c-MYC [858].

DCAMKL2 (Doublecortin-like and CaM kinase like 2)

DCAMKL2 is a minor studied protein kinase. It consists of a N-terminal doublecortin-like domain which may contribute to the stabilization of microtubules, a S-/P-rich domain which may confer protein-protein interactions and a C-terminal kinase domain with similarity to Ca^{2+}/CaM dependent kinases but less dependence and affinity to Ca^{2+}/CaM which may inhibit CREB dependent gene expression and nuclear translocation of CREB [860], [861].

CDKL2 (Cyclin Dependent Kinase Like 2)

The CDKL family consists of five members (CDKL1-5). They show similarities to CDKs, however they do not bind to cyclins and probably display a distinct functional branch from classical CDKs [862]. CDKL2 is a mostly cytoplasmic protein with low levels present in the nucleus [862]. It is highly expressed in the brain and associated with learning [863], [864]. CDKL proteins are linked to tumorigenesis and have been shown to exhibit a dual context dependent role as either oncogene or tumour suppressor. In the case of CDKL2 the *Oncomine* database revealed downregulation of CDKL2 in brain, colorectal, kidney, lung and mammary carcinoma [865]. However, a study of breast cancer patients showed increased expression of CDKL2 in breast carcinoma compared to healthy tissue and this was linked to decreased disease-free survival [866]. In cell culture and mice xenografts overexpression of CDKL2 promoted EMT, cell proliferation and cell migration/metastasis via a positive *feed forward* loop consisting of the transcriptional repressor ZEB-1 which mediated reduced expression of E-Cadherin and release of E-cadherin associated β-catenin and β-catenin/TCF induced expression of ZEB-1. In line with this, overexpression of CDKL2 was more common in mesenchymal compared to epithelial breast carcinoma [866]. On the other hand, downregulation of CDKL2 was reported in gastric cancer and this was correlated with decreased survival and increased staging. In gastric carcinoma cell culture experiments, overexpression of CDKL2 reduced proliferation and invasion [865].

PKN2 (Protein Kinase N2)

PKN2 is a member of the PKC related PKN family comprising PKN1, 2 and 3. It consists of an N-terminal HR1 domain, a central HR2 domain and a C-terminal kinase domain. The HR1 domain contains three repeats of a GAEN motif combined with a leucine-zipper motif which was found to bind to RHO or RAC. The HR2 domain is a regulatory domain which confers autoinhibition in the resting state [867]. Autoinhibition is released by RHO/RAC or caspase cleavage [868], [869], [870]. Furthermore, the HR2 displays a proline rich motif which binds to adapter proteins NCK-1 and GRB4 (NCK-2) [871]. PKN2 mediates (1) apoptosis *downstream* of caspase-3 and (2) various effect *downstream* of RHO/RAC [867], [872]. Upon treatment of Jurkat cells with FAS-ligand, staurosporine or etoposide cleavage of PKN2 at D117 and D700 was observed followed by release of the kinase domain and induction of apoptosis. Mechanistically, the kinase domain of PKN2 associated with AKT preventing its phosphorylation at T308 and S473 and reducing the AKT-dependent activation of BAD, and it inhibits PKCζ and PKCδ. This effect was abolished when cells were treated with caspase inhibitor and cleavage of PKN2 was also demonstrated when it was incubated with recombinant caspase-3 [868], [869], [873]. For the latter, PKN2 was identified as a target of both RHOA and RAC. Albeit they also mediate distinct *downstream* signalling RHO and RAC have been demonstrated in the last years to share overlapping functions and *downstream* targets and the GEFs TRIO and OST were shown to activate both RHOA and RAC. By genetic experiments actin stress fibre formation and adhesion was dependent on the RHO/PKN2 axis but not on RAC. Cell cycle progression, cytokinesis, receptor mediated endocytosis and membrane ruffling was mediated by both RHOA and RAC *upstream* of PKN2 [867]. For instance, in keratinocytes, focal cell adhesion was linked to RHOA/PKN2/FYN. Activation of RHOA was sufficient to activate FYN mediated phosphorylation of β-catenin and p120 and subsequent formation of focal adhesions as well as elevated RHOA activation via a *feed-forward* loop. This phenotype was mimicked by activation of PKN2. Of note, upon treatment of keratinocytes with Ca^{2+} the levels of active RHOA, PKN1, PKN2 and FYN were increased 1 h after starting the stimulation while at later time points, RHOA and FYN activity further increased, PKN1 activity decreased to basal levels and PKN2 activity remained constant. From this, it was suggested that other mechanisms besides PKN2 may be necessary for prolonged activation of FYN. mDia1/2 were proposed as candidate proteins as they display a SRC binding domain which induces a conformational change but no activation of SRC proteins upon association. Therefore, mDia1/2 may prime FYN for PKN2 mediated activation [872]. With regard to cell cycle progression and cytokinesis, deletion of PKN2 led to a defect in cytokinesis/midbody abscission and delayed G_2/M progression in HeLa S3 cells. The function of PKN2 during cytokinesis was dependent on the RHO-GEF ECT2 while the function of PKN2 in mitosis was independent on ECT2. During G_2/M progression PKN2 was necessary for the activation of CDC25B and subsequent activation of CDK1/Cyclin B. Genetic deletion of CDC25B phenocopied that of PKN2 (cytokinesis defect and G_2/M delay) and *knock-down* of centrosome-associated AURORA-A kinase reduced the level of active CDK1/Cyclin B, therefore AURORA-A may act *downstream* of or in parallel with PKN2 in the activation of CDK1/Cyclin B. Furthermore, by application of a CDK inhibitor reduced activation of PKN2 was observed which may hind to the presence of a *feed-forward* loop in which PKN2 is initially activated by RHOA and PKN2 activity is then sustained via phosphorylation of PKN2 by CDK1/Cyclin B [874].

CDK5 (Cyclin Dependent Kinase 5)

CDK5 was originally examined in neurons. Under normal conditions, it gets transiently activated by recruitment to membrane bound and unstable protein p35. When neurons are exposed to cell death signals however, the intracellular Ca^{2+} level is increased through activation of NMDA receptors leading to the activation of calpain which

cleaves p35 to membrane bound p10 and cytosolic and stable p25. CDK5 is then bound to p25 resulting in its hyperactivation and translocation of the p25-CDK5 complex to the nucleus where it induces apoptosis [875]. In neurons, CDK5 activity is negatively regulated by cyclins E and D [876], [877].
In contrast, in most cancers CDK5 shows an oncogenic function and is either overexpressed or hyperactivated or both [875]. In lung cancer CDK5 was positively regulated by cyclin G1 and expression of CDK5 was linked to clinical staging and a poorer prognosis [878]. In prostate and thyroid cancer CDK5 promoted cell survival vie the FAK/AKT axis [879], [880], [881]. In head and neck cancer and mammary carcinoma overexpression of CDK5 was linked to enhanced EMT and metastatic potential [882] and in HCC CDK5 hyperactivation and overexpression led to enhanced proliferation [883]. In pancreas carcinoma inhibition of CDK5 reduced the activation of RAL-A, RAL-B, RHO and RAC and RHO/RAC mediated metastasis as well as RAS/RAL mediated neoplasia. In pancreatic cancer cells expressing a dominant negative CDK5 mutant overexpression of constitutively active RAL-A or RAL-B was able to rescue the proliferation defect. In these cells CDK5 induced cell proliferation was also linked to the activation of AKT and STAT3 [884]. However, in some cancers i.e. in gastric cancer downregulation of both p35 and CDK5 was observed [749].
In addition to its function in apoptosis, motility/EMT and proliferation CDK5 was also linked to the DDR (DNA Damage Repair) pathway. In one study CDK5 was shown to activate STAT3 mediated expression of EME1 in response to topoisomerase I inhibitor treatment [885], [886]. In neurons, CDK5 activates ATM in the presence of DNA damage thereby promoting homologous repair (HR) responses [887]. In contrast, in response to oxidative stress CDK5 was found to inactivate the BER (Base Excision Repair) protein APE1 and BER was rescued through inhibition of CDK5 [888].

HIPK4 (Homeodomain Interacting Protein Kinase 4)

HIPK4 is a cytosolic protein kinase with expression in lung and white adipose tissue. It shows low similarity to the other members of the HIPK family (HIPK1-3) with the exception of the catalytic domain [889]. HIPKs are activated in the presence of stress signals and require autophosphorylation of a conserved Y within the activation loop as demonstrated by the examination of designated Y→F mutants [890]. HIPK4 function is poorly understood with the exception of one study demonstrating that it phosphorylated p53 at S9 which reduced the activity of p53-repressed surviving promotor whereas the BCL-2 promotor was not affected [889].

Of note, a panel of S-/T- kinases (PKG2, PKC, GPRK4, CK2a2 and CHK1) was regulated both in HCT-116 SHIP1 WT/LeGO and SW-480 KD2/SCR. However, in both cases the indicated kinases were upregulated in HCT-116 SHIP1 WT compared to LeGO as well as in SW-480 SHIP1 KD2 compared to SCR which was not expected given that SHIP1 overexpression was expected to have contrary effects to SHIP1 downregulation. Therefore, cell-line dependent effects of SHIP1 on kinase regulation are most likely. In all other cases there are no overlaps in kinase regulation.
The PAMGENE analysis was verified by Western Blot using PKG2 and P-PKG2 S126 and MSK1 and P-MSK1 S376 as depicted in **fig. 41**. PKG2 was shown to be autophosphorylated at various serine residues including S126 and the phospho-mimicking mutant PKG2 S126E was rendered constitutively active [891]. As described above, phosphorylation of MSK1 on S376 was shown to be activating.

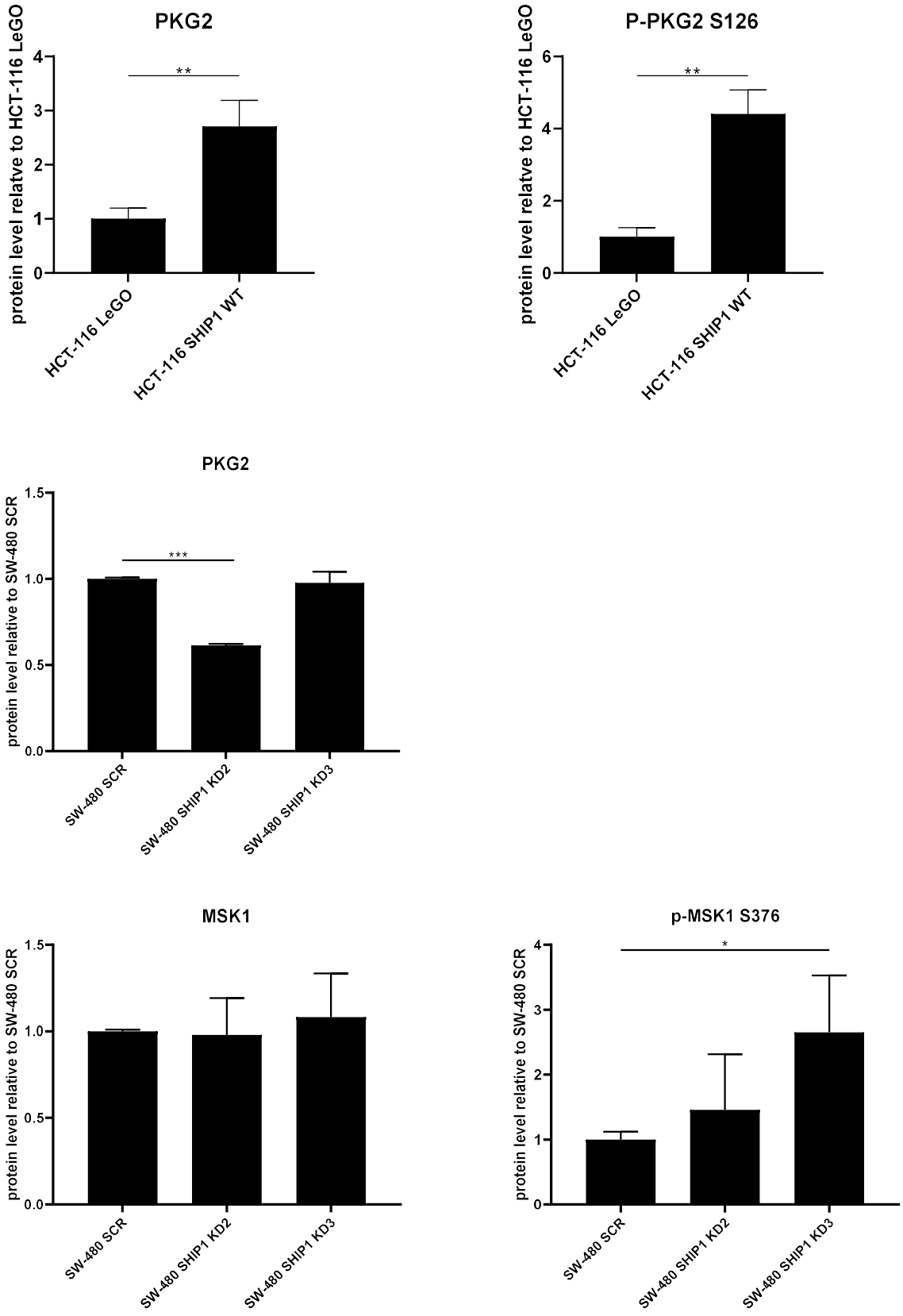

fig. 41: Western Blot analysis for the verification of the PAMGENE S/T- data in HCT-116 and SW-480. Error bars indicate standard deviations. Significances were determined by t-testing. n=3

As depicted, in HCT-116 both the overall and phosphorylated level of PKG2 were significantly elevated in HCT-116 SHIP1 WT with regard to HCT-116 LeGO which was in accordance with the data obtained for the PAMGENE

measurements. In SW-480, no P-PKG2 was detected and the levels of unphosphorylated PKG2 did not reflect those expected from the PAMGENE measurements. For MSK1 both KD lines showed upregulated levels of P-MSK1 S376 which was in accordance with the data obtained from the PAMGENE measurements for KD2.

4.1.5.2. Y-kinases

The analysis of the Y-kinome was as described for the S-/T- kinome (4.1.5.1.). The analysis was performed by the group of Malte Kriegs and depicted in **fig. 42** and **fig. 44**.

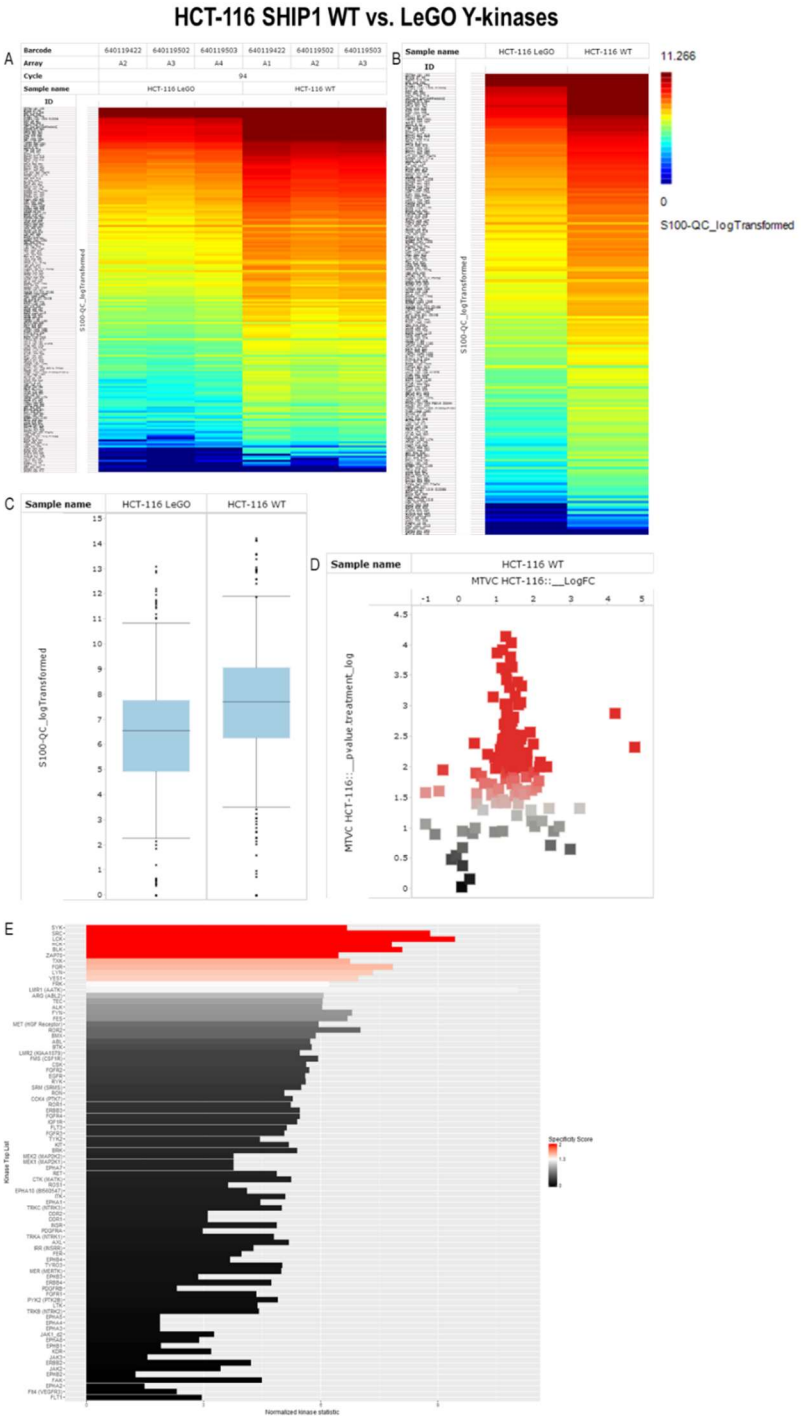

fig. 42: PAMGENE Y- analysis of HCT-116 SHIP1 WT vs. HCT-116 LeGO. Cells grown in DMEM, 10% FCS were lysed at 70-80% confluence in M-PER buffer and analysed for S-/T-kinase activity using the PAMGENE assay kit. Panel A depicts the heat map of individual triplicates and panel B depicts the heat map of averaged samples. Panel C shows the total kinase activity and panel D depicts the volcano plot of HCT-116 SHIP1 WT kinase activity normalized to HCT-116 LeGO and panel E depicts the normalized kinase statistic (log_2) of HCT-116 SHIP1 WT kinase activity normalized to HCT-116 LeGO. The PAMGENE analysis was performed by the group of Malte Kriegs, UKE Hamburg. n=3

Upregulated Y-kinases of HCT-116 compared to HCT-116 LeGO were identified as SRC Kinases (SRC, YES, FGR, LCK, HCK, BLK, LYN), SYK, ZAP70, TXK and LMTK1 (LMR1 (AATK)) as depicted in **fig. 43** and described below.

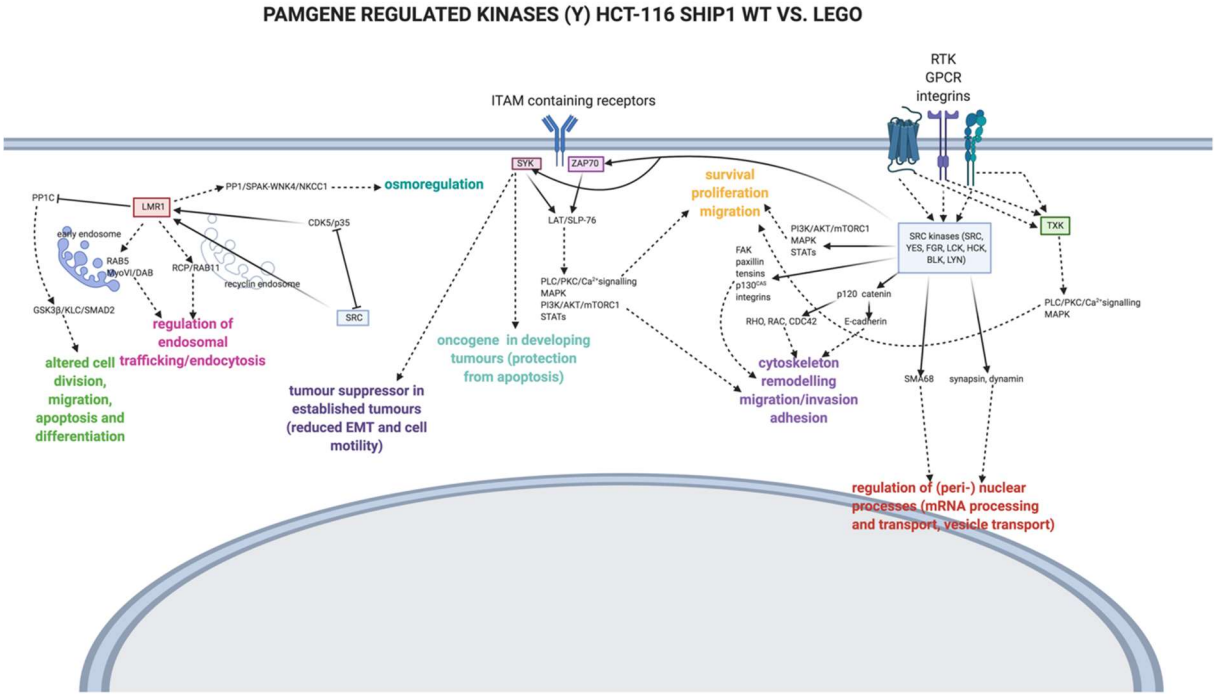

fig. 43: PAMGENE regulated S-/T-kinases in HCT-116 SHIP1 WT vs. HCT-116 LeGO (normalized kinase statistic >1, specificity score ≥1.3). Details: see text

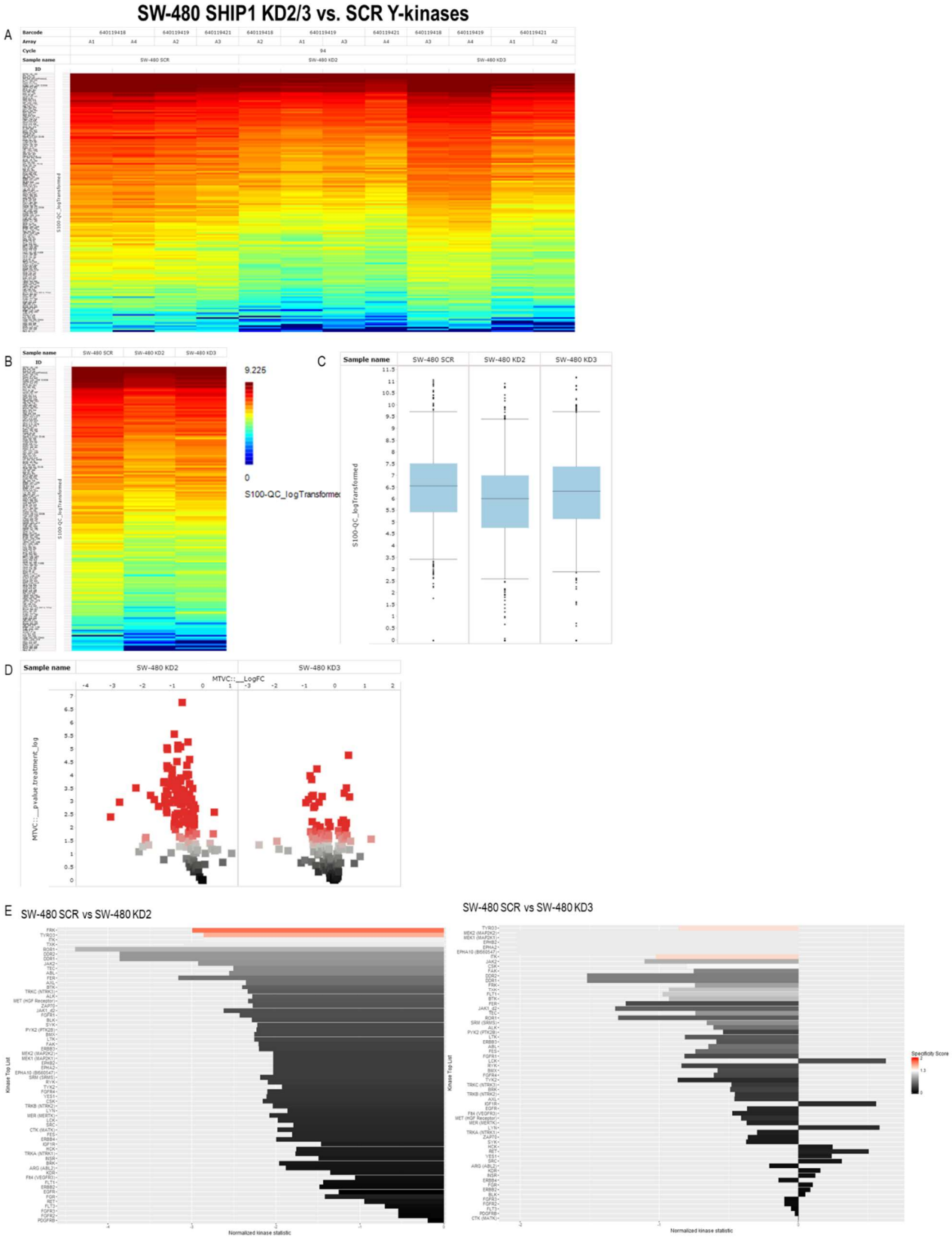

fig. 44: PAMGENE Y-analysis of SW-480 SCR vs. SW-480 KD2/KD3. Cells grown in DMEM, 10% FCS were lysed at 70-80% confluence in M-PER buffer and analysed for S-/T-kinase activity using the PAMGENE assay kit. Panel A depicts the heat map of individual quadruplicates and panel B depicts the heat map of averaged samples. Panel C shows the total kinase activity and panel D depicts the volcano plot of SW-480 SHIP1 KD2/3 kinase activity normalized to SW-480 SCR and panel E depicts the normalized kinase statistic (log_2) of SW-480 SHIP1 KD2/3 kinase activity normalized to SW-480 SCR. The PAMGENE analysis was performed by the group of Malte Kriegs, UKE Hamburg. n=4.

The proposed downregulated kinases in SW-480 KD2 vs. SCR were FRK and TYRO3 and in SW-480 KD3 vs. SCR ITK and TYRO3. This is shown in **fig. 45** as an overview and described in more detail below.

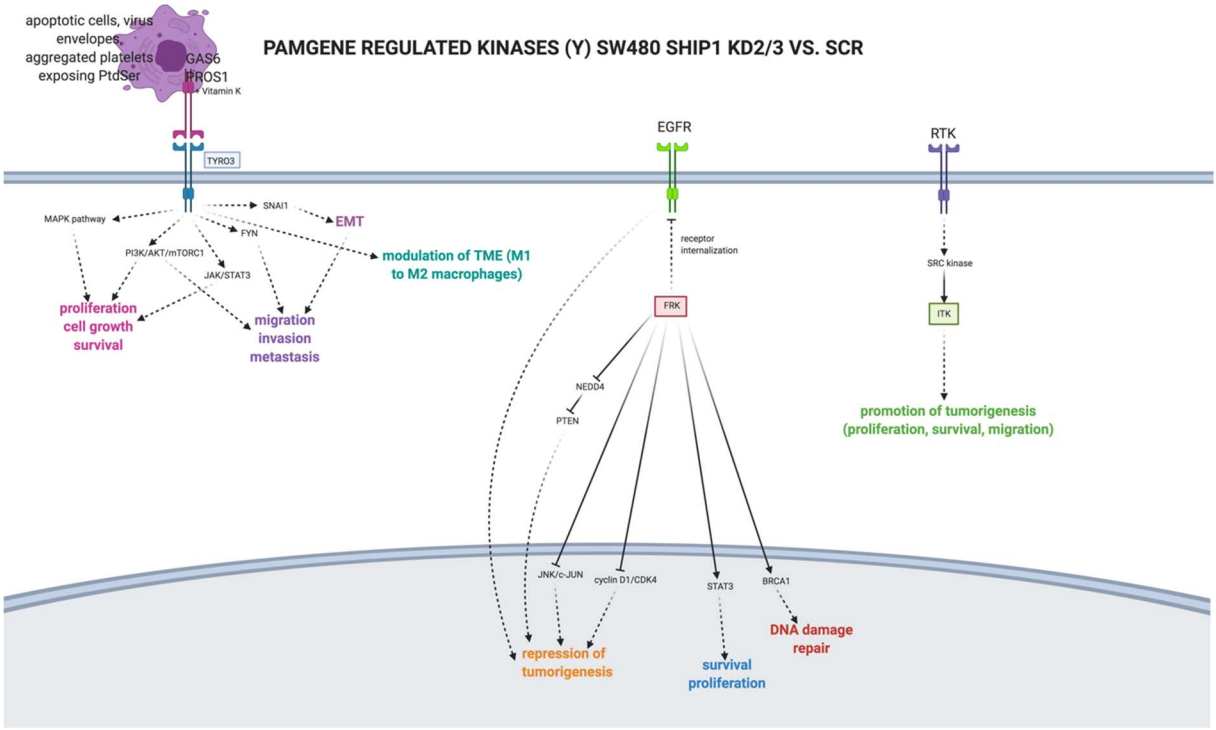

fig. 45: PAMGENE regulated Y-kinases in SW-480 SHIP1 KD2/3 vs. SW-480 SCR (normalized kinase statistic >1, specificity score ≥1.3). Details: see text

TYRO 3 (Protein Tyrosine Kinase Receptor 3)

TYRO 3 is a receptor tyrosine kinase of the TAM group comprising of TYRO 3, AXL and MERTK. It is activated by its ligands GAS 6 and PROS 1 followed by dimerization and autophosphorylation of dedicated tyrosine residues within the intracellular domain (i.e. Y681) [892], [893], [894]. Classically, two TYRO 3 monomers are found to form homodimers but heterodimerization with AXL has also been described [895], [896], [897], [898]. Moreover, at a sufficiently high density of TYRO 3 at the cell surface spontaneous homodimerization and activation of TYRO 3 is possible independent of ligand binding [899]. GAS 6 and PROS 1 are bound to exposed PtdSer residues on the surface of apoptotic cells, enveloped viruses or aggregated platelets after vitamin K dependent γ-carboxylation and exposure of their lipid binding domain [892], [893], [894]. TYRO 3 promotes tumorigenic traits using different pathways. It promotes cell proliferation, growth, survival and migration/invasion via the PI3K/AKT/mTORC pathway [898], [900], [901], [902], [903], [904], [905], [906] and proliferation via the MAPK pathway [898], [907], [908], [909], [910], [911]. It activates the SRC kinase FYN which leads to increased migration as well as cross-activation of AKT [901], [906]. Further oncogenes are positively regulated via the JAK/STAT 3 pathway [909], [912]. In addition, TYRO 3 induces the transcriptional regulator SNAI1 which represses epithelial genes such as *E-cadherin* and *β-catenin* and activates the expression of mesenchymal markers such as *N-cadherin* and *α-SMA* promoting Epithelial Mesenchymal Transition (EMT) and increasing cell motility, migration/invasion and metastasis [913]. Non-canonical functions of a nuclear resided fragment of TYRO 3 lacking the NTD were described. Nuclear TYRO 3 was detected in CRC samples and cell culture studies comparing TYRO 3 mutants lacking the NLS with TYRO 3 WT showed an altered cell morphology and increased apoptosis in cells expressing the TYRO 3ΔNLS mutant. Furthermore, expression of nuclear TYRO 3 fragment in CRC correlated with a poor outcome pointing to a relevant role of nuclear TYRO 3 in tumorigenesis [914]. Of note, TYRO 3 also influences the Tumour Microenvironment (TME). In more detail using a murine CRC model expression of TYRO 3 on tumour cells was able to induce GAS 6 or PROS 1 on the surface of macrophages via TYRO 3 mediated secretion of IL-10 or GM-CSF which further favours tumorigenesis in a paracrine loop manner. In said model GAS6 was strongly upregulated in TAMs compared to other macrophages and *knock down* of GAS6 significantly impaired tumour growth [915], [916], [917]. On the other hand, expression of PROS1 is induced in tumour cells in response to pro-inflammatory M1 macrophage cytokines such as IFNγ which then induces TYRO 3 in TME macrophages and switches their phenotype from M1 to M2 thus silencing the anti-tumour immunity. Mechanistically, PROS1 stimulation of macrophages resulted in a

predominance of inhibiting p38γ/c-JUN over activating p38α/c-JUN complex and consequently reduced expression of pro-inflammatory cytokines IL-1 and IL-6 [918].
Overexpression and/or hyperactivation of TYRO 3 was found in several cancer entities including colorectal carcinoma, breast carcinoma, hepatocellular carcinoma and melanoma [919], [920], [921]. shRNA or antibody mediated reduction of TYRO 3 resulted in enhanced apoptosis and reduced proliferation in cell culture and reduced tumour volume and tumour incidence in mouse models of different tumour entities [896], [909], [910], [915], [922], [923], [924], [925], [926], [927], [928] and expression of a chimeric construct composed of the extracellular domain of the EGFR and the intracellular domain of TYRO 3 induced anchorage independent growth and transformation as well as increased tumour growth in mouse models of various kinds following EGF stimulation [893], [901], [929], [930]. In HCT-116 and HT-29 shRNA mediated downregulation of TYRO 3 reduced migration, invasion and EMT and converse effects were observed in cells overexpressing TYRO 3 [926], [929]. In a mouse model metastasis was significantly higher in mice having been injected with HCT-116 SCR control cells compared with TYRO 3 *knock-down* cells and in CRC patient samples TYRO 3 positively correlated with the expression of mesenchymal marker proteins and negatively correlated with epithelial marker proteins confirming a positive role of TYRO 3 in EMT and cell motility/metastasis in CRC [931]. Furthermore, TYRO 3 was shown to confer resistance to chemotherapy or targeted therapeutic approaches in cancer. HCT-116 TYRO 3 *knock-down* cells displayed higher sensitivity to 5-fluorouracil, paclitaxel and oxaliplatin as shown in increased apoptosis rates. Similar results were obtained in primary CRC cells and mouse models displaying reduced TYRO 3 activity by use of an anti-TYRO 3 monoclonal antibody [915], [929]. TYRO 3 overexpression also conveyed acquired resistance to chemotherapy in breast carcinoma MCF10A and ovarian carcinoma SKOV3 and A2780 cells [925], [932] and resistance to targeted therapy in Huh7 (sorafenib) and breast carcinoma (lapatinib) cells [926], [933].
Summarizing, TYRO 3 is a proven oncogene which promotes tumorigenesis increasing survival, proliferation and migration/invasion/metastasis, inducing EMT, providing resistance to therapeutic treatments and manipulating the TME.

FRK (FYN Related Kinase)

FRK is an intracellular tyrosine kinase related to BRK and IYK. As BRK and IYK it comprises three domains (SH3, SH2, kinase). Its activity is mediated by its phosphorylation status. Phosphorylation of Y387 in the activation loop is activating and phosphorylation of Y497 in the CTD is inhibiting. The active conformation is possibly stabilized by a conserved tryptophan (W227) which has been shown so far only for the homologous W184 in BRK. In addition, an NLS is present, however FRK is not exclusively nuclear but seems to shuttle between nucleus and cytosol. Both oncogene and tumour suppressor functions have been proposed for FRK probably dependent on the context. Advocating for an oncogene function is especially the presence of active FRK (FRK pY387) in liver, breast, lung, cervix, ovarian and stomach carcinoma. Moreover, FRK is able to activate STAT3 mediated expression of (proto-) oncogenes. Speaking for a tumour suppressor function, FRK can phosphorylate PTEN to protect it from NEDD4 mediated ubiquitination and subsequent proteasomal degradation. It induces the internalization of EGFR and represses cyclin D1/CDK4 and JNK/c-JUN mediated gene expression. Further, it phosphorylates BRCA1 to protect it from UBE2 mediated ubiquitination and degradation thereby fostering HR/NHEJ DNA damage response preventing the accumulation of tumour promoting mutations [934].

ITK (Interleukin-2 inducible T-cell Kinase)

ITK is a member of the TEC kinase family and predominantly expressed in hematopoietic cells. In T-cells following activation of the TCR and accumulation of PtdIns(3,4,5)P_3 by the PI3K ITK is recruited to the plasma membrane resided TCR signalosome by its PH domain and gets activated by LCK mediated phosphorylation of Y511 [935]. It mediates the influx of Ca^{2+} in concert with PLC and the activation and nuclear translocation of transcription factors such as AP-1 and NFAT and expression of cytokines [935]. Of note, hypomethylation of the *ITK* promotor was found in melanoma and the level of promotor hypomethylation and ITK protein increased with tumour progression or melanoma stage. Pharmacological (B1 10N ITK inhibitor) or genetic downregulation of ITK in melanoma cell lines resulted in cell cycle arrest at the G_1/S checkpoint and reduced cell proliferation. In mouse xenografts tumour load was decreased when mice were treated with B1 10N. The exact mechanism on how ITK would fulfil its oncogenic driver function in melanoma has not been elucidated yet however an impact of ITK on the expression of p53 or cyclins was suggested [936].

SRC kinases

The SRC kinase family comprises nine members. SRC, YES, FYN and FGR belong to the SRCA subfamily and LCK, HCK, BLK and LYN belong to the SRCB subfamily. The nuclear FRK stands unique [937], [938]. SRC kinases are activated by RTKs, GPCRs, FAK, integrins or steroid receptors and regulate cell growth and differentiation, morphology, migration/invasion, survival and proliferation, cell-cell and cell-matrix adhesion, cytoskeleton dynamics and gene expression and promote tumorigenesis [938], [939], [940], [941] with the exception of FRK which was

found to display tumour suppressor properties in breast cancer [942]. SRC kinases share a domain structure comprising an N-terminal myr anchor, an SH3 domain, an SH2 domain, a linker, a Y-kinase domain and a C-terminal regulatory domain [943], [944], [945], [946]. FRK contains an NLS instead of the myr anchor [947], [948]. SRC kinases are typically overactivated in cancers which is most often due to dysregulated *upstream* signalling [940]. Mechanistically, in the resting state the Y-kinase domain of SRC kinases are autoinhibited by the CTD. The autoinhibited state is maintained by phosphorylation of Y527 via CSK (c-SRC kinase) or CHK (CSK homologue kinase) [949], [950], [951], [952]. In this context, a negative regulatory *feedback loop* was described in which active SRC phosphorylated the lipid raft signalling hub protein CBP which then recruits CHK/CSK to SRC preventing hyperactivation or constitutive activation of SRC [953], [954]. Phosphorylation of Y530 is reversed by protein tyrosine phosphatases such as PTPα, PTPγ, SHP1/2 or PTP1B [955], [956], [957], [958]. Those proteins are typically overexpressed in cancers. For activation, SRC proteins are typically recruited to *upstream* regulators such as EGFR or FAK via their SH2 domain to get phosphorylated at the activating site Y416 [959], [960], [961], [962]. It positively regulates STAT signalling, MAPK, PI3K/AKT/mTORC1 or cytoskeleton dynamics [940], [941]. In more detail, activated SRC associates with actin via its SH3 domain and recruits a bunch of signalling proteins associated with cell motility and adhesion such as RHO family members, paxillin, p130/CAS or FAK [963]. Furthermore, they were found to associate to endosomal/lysosomal membranes and microtubules to regulate intracellular trafficking [964], [965]. In malignant cells, SRC kinases frequently associate with nuclear and perinuclear membranes which is absent in healthy cells [966], and were linked to the regulation of mRNA splicing and transport (via SAM68) [967] as well as perinuclear/TGN transport (via synapsin and dynamin) [968], [969], [970].

ZAP-70 and SYK

ZAP-70 is a T-cell protein implicated in cytokine expression and secretion and therefore immune response modulation, T-cell proliferation, survival and development. Upon activation of the TCR it gets recruited to doubly phosphorylated ITAMs via its tandem SH2 domain and gets phosphorylated and activated by the SRC kinase LCK which released its autoinhibition of the C-terminal kinase domain [971], [972], [973]. Mechanistically, ITAM association partially opens the closed conformation of ZAP-70 and LCK-mediated phosphorylation of ZAP-70 residues Y315, Y319 and Y493 in the interdomain B/activation loop leads to its full activation [974], [975]. ZAP-70 is negatively regulated by the protein phosphatases STS1/2 [976], [977], [978]. ZAP-70 displays a narrow substrate specificity composed of the scaffolding proteins LAT and SLP-76 which positively regulate the RAS/MAPK pathway, PLCγ/PKC/Ca^{2+}, NFAT dependent transcription of i.e. cytokines and cytoskeleton dynamics [971], [979], [980], [981]. ZAP-70 substrates are enriched in negative residues (DYE motif) which contrasts the substrate profile of SRC kinases/LCK (enriched in positive residues) with the consequence that ZAP-70 substrates cannot be phosphorylated by SRC kinases and vice versa [982], [983], [984]. Furthermore, ZAP-70 acts as a phosphoprotein adaptor independent of its catalytic activity [985], [986]. In more detail, it protects ITAMs from dephosphorylation [987], it stabilizes LCK via Y319 [988], [989] and via Y315 it recruits the RHO-GEF VAV to mediate cytoskeleton dynamics [990] and CRK/CBG/RAP to Y319 to mediate cell adhesion and integrin signalling [991], [992].

SYK is the closest homologue of ZAP-70 and expressed in hematopoietic cells such as B-lymphocytes [993], [994]. As ZAP-70 it comprises a tandem SH2 domain (SH2-linker A-SH2), a linker B domain and a C-terminal kinase domain [995]. The tandem SH2 domain associates with doubly phosphorylated ITAMs (of BCR, NK cell receptors, integrins and others) and the protein is then activated by SRC family kinases relieving the autoinhibition [996], [997], [998]. Substrates of SYK are adaptor or scaffold proteins such as BLNK, LAT and SLP-76, lipid kinases, phospholipases and GEFs which ultimately activate *downstream* signalling pathways such as PI3K/AKT/mTORC1, MAPK, PLCγ/PKC/Ca^{2+}/NFAT and NF-κB to promote the activation of immune cells [996], [997], [998]. Apart from hematopoietic cells SYK is also present at low levels in epithelial cells [999], [1000].

Of note, SYK was designated as both a tumour promotor and suppressor dependent on the context [1001]. In B-CLL SYK promotes tumorigenesis [1002], [1003], [1004]. In cell culture and mouse models of carcinomas SYK was demonstrated to protect cells from apoptosis aroused from uncontrolled activation of oncogenes (K-RAS) or loss of tumour suppressors (RB) in earlier stages of tumorigenesis whereas in later stages SYK was dispensable as tumour cells had developed alternative mechanisms to protect themselves from apoptosis such as loss of PTEN or overactivation of AKT [1001], [1005], [10], [1006]. Increased levels of SYK were found in several carcinoma entities such as brain, kidney, colon, ovary and lung carcinoma [1007]. In ovarian carcinoma aberrant expression of SYK correlated with tumour grade [1007] and in squamous Head and Neck cancer it was associated with a poor prognosis [1008]. In contrast, SYK was found to be a tumour suppressor in B-ALL [1009]. With regard to carcinomas SYK is often highly expressed in earlier stages displaying low metastasis and a high level of differentiation as outlined above and lost in later more malignant stages displaying a low level of differentiation and a highly aggressive and metastasising phenotype and re-expression of SYK in those cells reduced cell motility, invasive growth, motility and metastasis in cell culture and mouse models of HCC, CRC, melanoma and PDAC [1010],

[1011], [1012], [1013], [1014]. Mechanistically, SYK was demonstrated to promote an epithelial phenotype and cell-cell-contacts by regulating the actin cytoskeleton and protein substrates such as E-cadherin, α-tubulin and α-catenin and loss of SYK promoted EMT (motility, expression of mesenchymal marker genes such as MMP-9, suppression of epithelial marker genes such as E-cadherin and fibroblast-like morphology) in cell culture models of breast carcinoma and PDAC [1014], [1015]. Of note, SYK exists in two alternative splice variants, FL SYK (SYK(L)) and the less active SYKB lacking 23 amino acids in linker B [1016]. Whereas SYK(L) is typically downregulated in invasive carcinomas SYKB is re-expressed in those and was demonstrated to promote EMT, motility and tumour growth in HCC [1017]. In earlier stages of ovary carcinoma high expression of SYK(L) promoted tumorigenesis and protected the cells from c-JUN induced apoptosis whereas overexpression of SYKB led to apoptosis [1018]. The opposite effects of SYK(L) and SYKB are most likely due to differential localization patterns (SYK(L) in the cytoplasm and nucleus and SYKB in the cytoplasm only) [1017], [1018].

LMTK1 (LMR1, Lemur Tail Kinase 1)

The LMTK family comprises three members (LMTK1, 2, 3) which are predominantly expressed in neurons [1019]. They share a common domain structure of an N-terminal domain containing a signal peptide for endosomal (early and recycling endosomes; EE and RE) localization, a transmembrane (TM) domain, a short linker, a Y-kinase domain and a long C-terminal tail. LMTK2/3 contain an NLS signal which is absent in LMTK1 [1019], [1020]. LMTK1 is expressed in two alternative splice variants. LMTK1B contains the TM domain which is absent in LMTK1A. In LMTK1A the protein is tethered to endosomal membranes via palmitoylated cysteines [1019]. LMTKs regulate endosomal trafficking [1019]. LMTK2 phosphorylates and inactivates PP1C which modulates membrane receptor turnover [1021] and LMTK3 regulates the RCP/RAB11 axis of recycling endosomes [1022]. There are no verified substrates of LMTK1 but it is likely that the substrate specificity of LMTKs would be overlapping [1019]. LMTK1 and LMTK2 were shown to be autophosphorylated [1023]. LMTK1 hyperphosphorylation was found when cells were confronted with apoptosis and this was suppressed in S480A, S558A and S566 mutants. LMTK1 was hypophosphorylated in depolarized cells [1019]. Apart from its catalytic function LMTKs can act as scaffolding proteins, i.e. LMTK1 mediates osmoregulation by scaffolding the PP1/SPAK/WNK4/NKCC1 complex independent on its kinase activity [1019]. The most important cellular function of LMTKs is to prime targets for endosomal trafficking [1019]. For example, LMTK2 regulates the trafficking of SMAD2 and LMTK2/3 regulate the transport of nuclear receptors (ERα or AR) via Myosin VI [1019], [1024], [1025], [1026]. Of note, LMTKs were shown to be regulated in an opposite manner by p35/CDK5 and SRC dependent phosphorylation and both *upstream* regulators are implicated in endocytosis as well [1019], [1027]. The role of LMTKs in cancer is rather unclear due to the low number of studies and the fact that most studies are based on mRNA data only [1019]. In metastatic melanoma SRC and LMTK1 levels were shown to be inversely correlated and loss of LMTK1 was associated with increased migration and proliferation and reduced apoptosis [1019]. In prostate carcinoma LMTK2 downregulation was found [1028]. On the other hand, LMTK3 was a survival factor in several carcinomas and positively regulated WNT signalling [1023], [1029], [1030], [1031], [1032]. In breast cancer, it was linked to increased cell motility [1033]. Nuclear LMTK3 was identified as a regulator of chromatin structure in complex with KAP1 and PP1α and promoted the expression of DNA damage repair, survival and drug resistance proteins [1034].

TXK (protein tyrosine kinase TXK)

TXK is a member of the TEC kinase family comprising ITK, RLK/TXK, TEC, BTK and BMX and is implicated in T-cell signalling. TEC kinases are activated by different receptors such as antigen receptors, cytokine and chemokine receptors, TLRs, GPCRs and integrins. They regulate PLCγ/PKC/Ca^{2+} and MAPK signalling and shape immune responses by regulating the expression and secretion of certain cytokines and chemokines. ITK, RLK/TXK and TEC are expressed in T-cells where ITK is most relevant and KO mice display defects in T-cell development and function. They comprise a C-terminal Y-kinase domain, an SH2 and SH3 domain, a TH (TEC homology) domain comprising 2 PRRs for SH3 domain interaction and an N-terminal PH domain (in the case of ITK and TEC) or palmitoylated cysteines (in the case of TXK) for membrane localization. TXK is expressed also in an alternative splice variant lacking the palmitoylated cysteines. Interestingly, upon activation of the TCR the majority of TXK is localized to the nucleus therefore, a predominantly nuclear function of TXK can be proposed [1035].

Regarding the Y-kinome there were no kinases regulated in both HCT-116 SHIP1 WT vs. LeGO and SW-480 SHIP1 KD vs. SCR further supporting the hypothesis that the kinome is most probably highly dependent on the cell line (see also the S-/T- kinome).

The results of the PAMGENE measurements were verified by Western Blot analysis (**fig. 46**). For HCT-116 panSRC/P-pan SRC Y416 and SRC/P-SRC Y527 were used. As described above, phosphorylation of SRC kinases at Y416 activates and phosphorylation at Y527 inhibits them. For SW-480, TYRO3/P-TYRO3 Y681 and P-DDR1/2

Y796/Y740 were used. Outlined above, phosphorylation of TYRO3 at Y681 within the activation loop is required for its full activation. Phosphorylation of DDR1/-2 on Y796/Y740 was shown to be activating [1036].

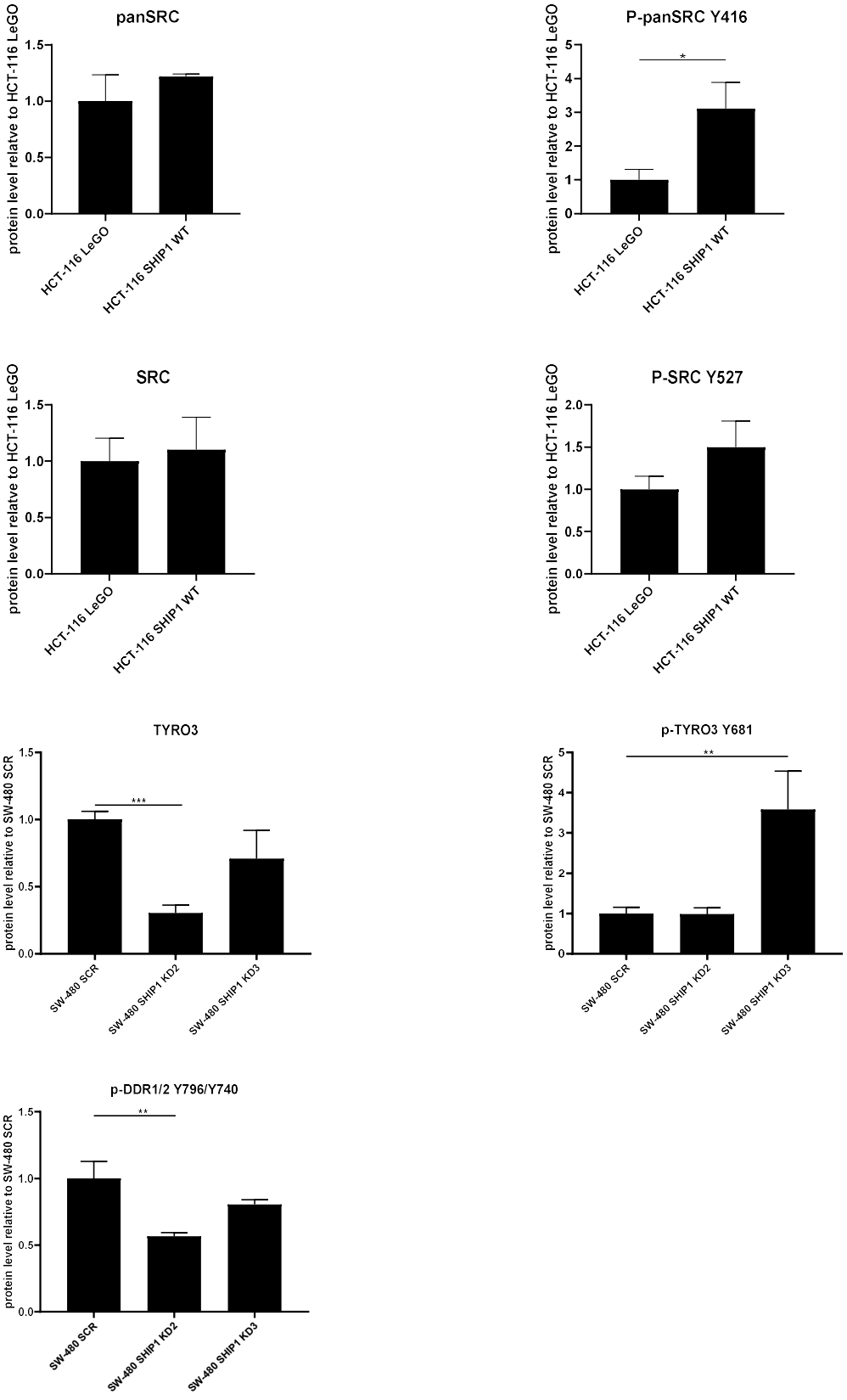

fig. 46: Western Blot analysis for the verification of the PAMGENE Y- data in HCT-116 and SW-480. Error bars indicate standard deviations. Significances were determined by t-testing. n=3

In HCT-116 the levels of unphosphorylated panSRC or SRC were comparable between HCT-116 LeGO and HCT-116 SHIP1 WT, but P-panSRC Y416 was significantly enhanced in HCT-116 SHIP1 WT to around 3.5-fold the level found in HCT-116 LeGO whereas P-SRC Y517 was not significantly altered which pointed to enhanced activity of SRC kinases in HCT-116 SHIP1 WT as expected. In SW-480 concerning SW-480 SHIP1 KD2 there were no significant differences in P-TYRO3 Y681 levels with regard to SW-480 SCR but the P-TYRO3/TYRO3 level was enhanced around 2.5-fold. In SW-480 SHIP1 KD3 P-TYRO3 levels were also strongly enhanced compared to those found in SW-480 SCR. In both cases, this was not expected. However, one has to be taken into account that the P-TYRO3 antibody used was also described to detect P-AXL and P-MERTK. On the other hand, the activating phosphorylation of P-DDR1/2 Y796/Y740 was enhanced in SW-480 SCR which was in accordance with the results obtained from the PAMGENE analysis.

4.1.6. Proteome analysis

The proteome of SW-480 parental, SHIP1 KD2, KD3 and SCR and HCT-116 parental, SHIP1 WT and LeGO was determined by differential quantitative proteomics. Sample preparation and measurements were performed by Hannah Voß (MS Core facility/AG Schlüter, UKE Hamburg). The data evaluation was performed by Hannah Voß and Paula Nissen (MS Core/AG Schlüter, UKE Hamburg).
For HCT-116 cells were held in DMEM, 10% FCS (maintenance conditions), pelleted and frozen in liquid nitrogen before being prepared for the analysis. For SW-480 cells, in addition to the maintenance conditions the influence of SHIP1 downregulation under EGF stimulation (starvation for 22 h, stimulation with 50 ng/mL f.c. EGF for 0 h (unstimulated control), 10 minutes and 22 h) was analysed.

4.1.6.1. Influence of the transduction procedure on the proteome

Surprisingly, the transduction procedure was found to significantly affect the proteome as shown when SW-480 parental and SCR respectively HCT-116 parental and LeGO were compared. As shown in **fig. 47** in the unstimulated state the proteome of SW-480 SCR and parental SW-480 differed markedly which was less pronounced when cells were stimulated with EGF over a long time (22 h). Due to the long stimulation time it can be proposed that EGF stimulation affected the transcription/translation of certain genes and from the differential quantitative proteomics data it was concluded that the transduction procedure induced similar transcriptional/translational alterations as EGF stimulation. The PCA analysis (not depicted) conclusively showed that the samples taken under maintenance conditions clustered in-between the unstimulated and the 22 h EGF-stimulated samples. In summary, 314 proteins were found to be significantly regulated between SW-480 SCR and parental in the unstimulated samples, mostly regulating transcription and translation. As indicated in the STRING analysis (**fig. 48** and **fig. 49**) mRNA splicing factors and superoxide-dismutases as well as apoptosis-inducing factors (below the *cut-off*) were upregulated in SW-480 SCR and several ribosomal translation factors and MCM complex proteins were downregulated. The EGF stimulation of SW-480 parental partly mimicked that of the translation procedure. In more detail, EGF-stimulation also upregulated mRNA splicing factors and downregulated ribosomal translation factors and MCM complex proteins (**fig. 50**)

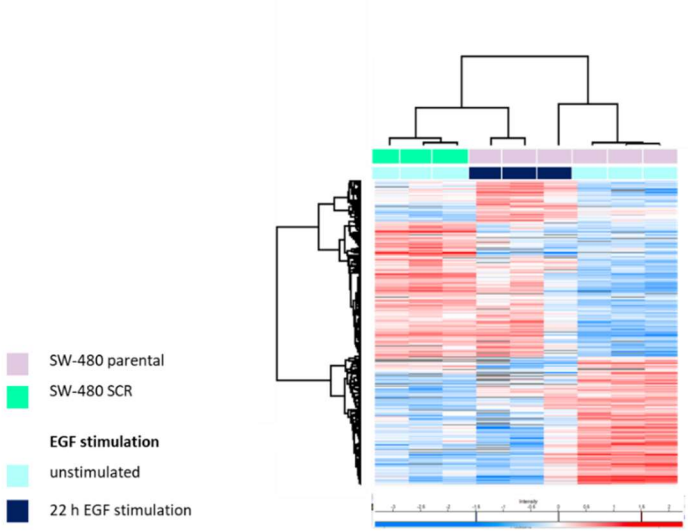

fig. 47: Heat map of the differential quantitative proteomics analysis of SW-480 SCR vs. parental. Differential quantitative proteomics and data evaluation were performed by Hannah Voß and Paula Nissen (MS Core/AG Schlüter, UKE Hamburg). n=3

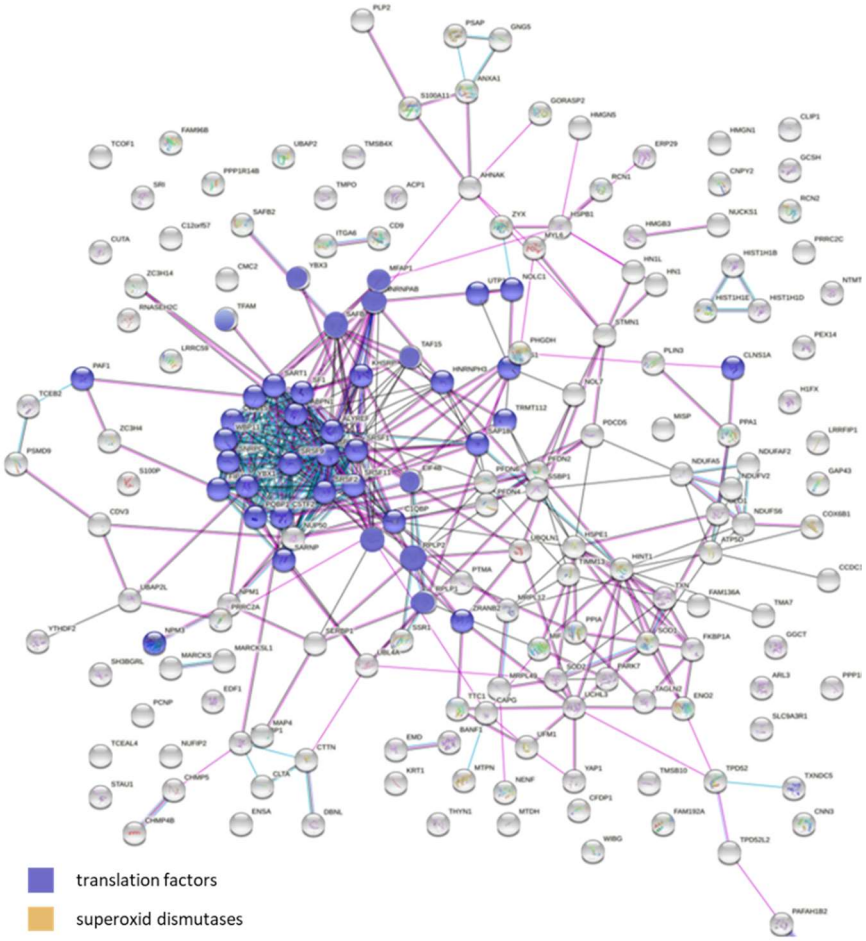

fig. 48: Network of the proteins being upregulated in the proteome of SW-480 SCR vs. SW-480 parental under unstimulated conditions. Network analysis was performed with the algorithm STRING. Differential quantitative proteomics and data evaluation were performed by Hannah Voß and Paula Nissen (MS Core/AG Schlüter, UKE Hamburg). n=3.

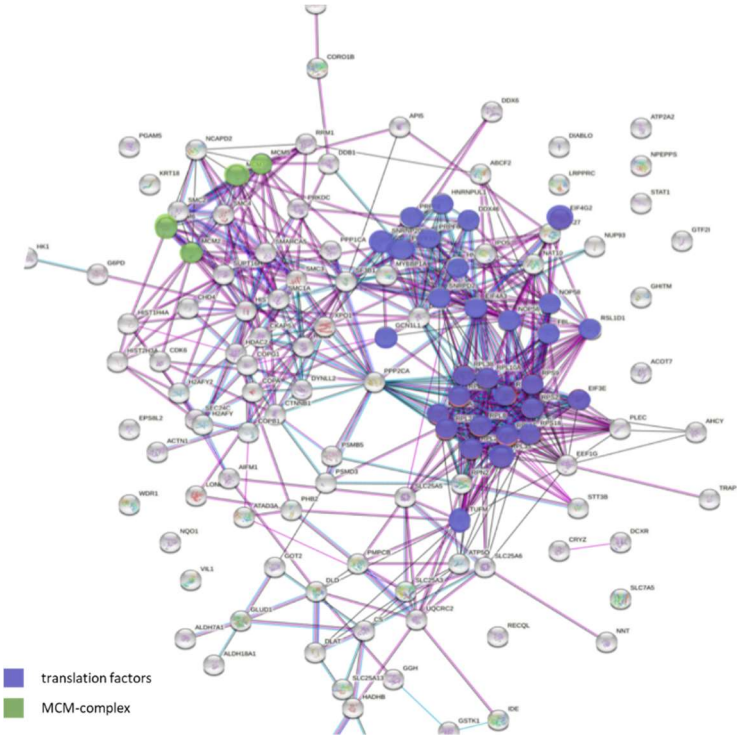

fig. 49: Network of the proteins being downregulated in the proteome of SW-480 SCR vs. SW-480 parental under unstimulated conditions. Network analysis was performed with the algorithm STRING. Differential quantitative proteomics and data evaluation were performed by Hannah Voß and Paula Nissen (MS Core/AG Schlüter, UKE Hamburg). n=3.

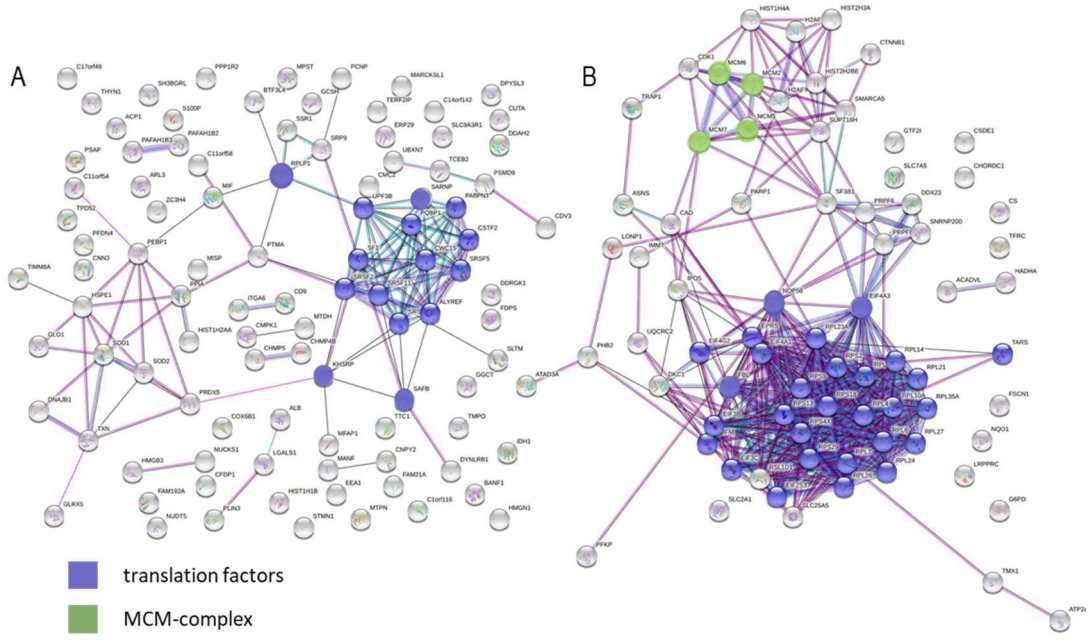

fig. 50: Network of the proteins being differentially regulated in the proteome of SW-480 parental after 22 h EGF stimulation. Panel A shows the proteins upregulated by EGF-stimulation and panel B shows the proteins downregulated by EGF-stimulation. Network analysis was performed with the algorithm STRING. Differential quantitative proteomics and data evaluation were performed by Hannah Voß and Paula Nissen (MS Core/AG Schlüter, UKE Hamburg). n=3.

In HCT-116 LeGO vs. parental only 23 proteins were found to be significantly regulated (**fig. 51**). Congruent with SW-480 vs. parental some transcription factors and ribosomal proteins and apoptosis-inducing factors were upregulated due to the transduction procedure, however with regard to the differential regulation of transcription and translation mostly mRNA splicing factors were affected in this scenario. Also, ATP- and glucose transporters were upregulated in HCT-116 LeGO compared to HCT-116 parental but not in SW-480 SCR compared to SW-480 parental (**fig. 52**). With regard to proteins downregulated by the transduction procedure there was little overlap of SW-480 SCR vs. parental and HCT-116 LeGO vs. parental. Whereas transcription- and translation regulating

proteins were downregulated in SW-480 SCR vs. parental as described above in HCT-116 LeGO vs. parental transport- and folding proteins, hormone-induced transcription and translation and DNA repair proteins were downregulated (**fig. 53**).

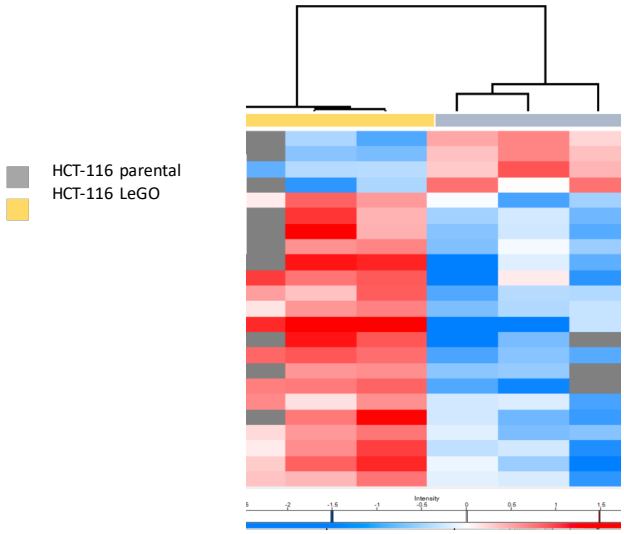

fig. 51: Heat map of the differential quantitative proteomics analysis of HCT-116 LeGO vs. parental under maintenance conditions. Differential quantitative proteomics and data evaluation were performed by Hannah Voß and Paula Nissen (MS Core/AG Schlüter, UKE Hamburg). n=3

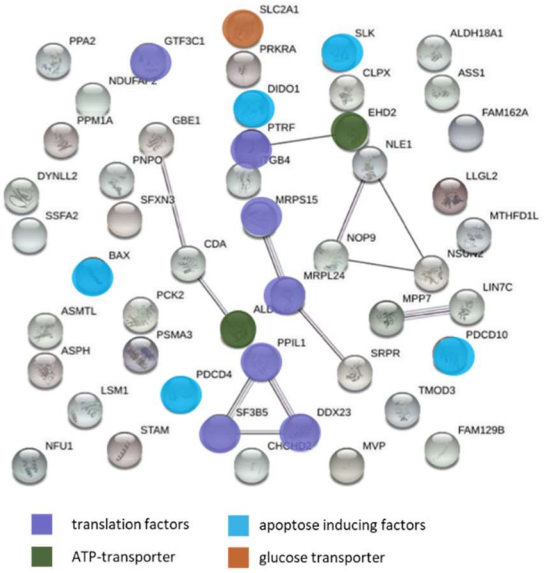

fig. 52: Network of the proteins being upregulated in the proteome of HCT-116 LeGO vs. parental under maintenance conditions. Network analysis was performed with the algorithm STRING. Differential quantitative proteomics and data evaluation were performed by Hannah Voß and Paula Nissen (MS Core/AG Schlüter, UKE Hamburg). n=3.

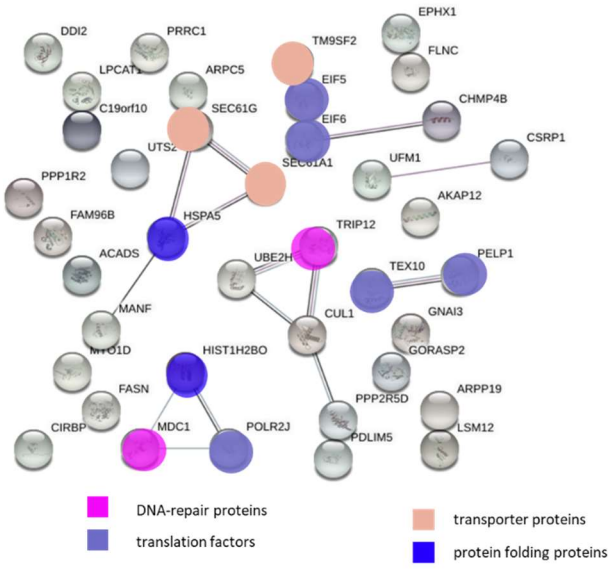

fig. 53: Network of the proteins being downregulated in the proteome of HCT-116 LeGO vs. parental under maintenance conditions. Network analysis was performed with the algorithm STRING. Differential quantitative proteomics and data evaluation were performed by Hannah Voß and Paula Nissen (MS Core/AG Schlüter, UKE Hamburg). n=3

4.1.6.2. Influence of SHIP1 on the proteome

For SW-480 the analysis mainly concentrated on unstimulated cells and cells stimulated with EGF for 22 h due to the PCA analysis showing that the maintenance condition again clustered in-between the unstimulated and the 22 h EGF stimulated samples for all cell lines (SW-480 SCR, KD2 and KD3). The heat maps for unstimulated and 22 h EGF stimulated cells showed that SW-480 SCR significantly differed from both KD lines whereas the KD lines were highly homologous. In general, 151 (unstimulated) or 60 (22 h EGF-stimulation) proteins were found to be regulated by the SHIP1 KD (**fig. 54**). Of note, the difference between SW-480 SCR vs. KD was less pronounced in the 22 h EGF stimulated samples. A possible conclusion from that result could be that SHIP1 influenced the EGF stimulation ability of the cells on the level of the EGFR or *downstream* signalling and that EGF stimulation partly reversed the effect of the SHIP1 KD.

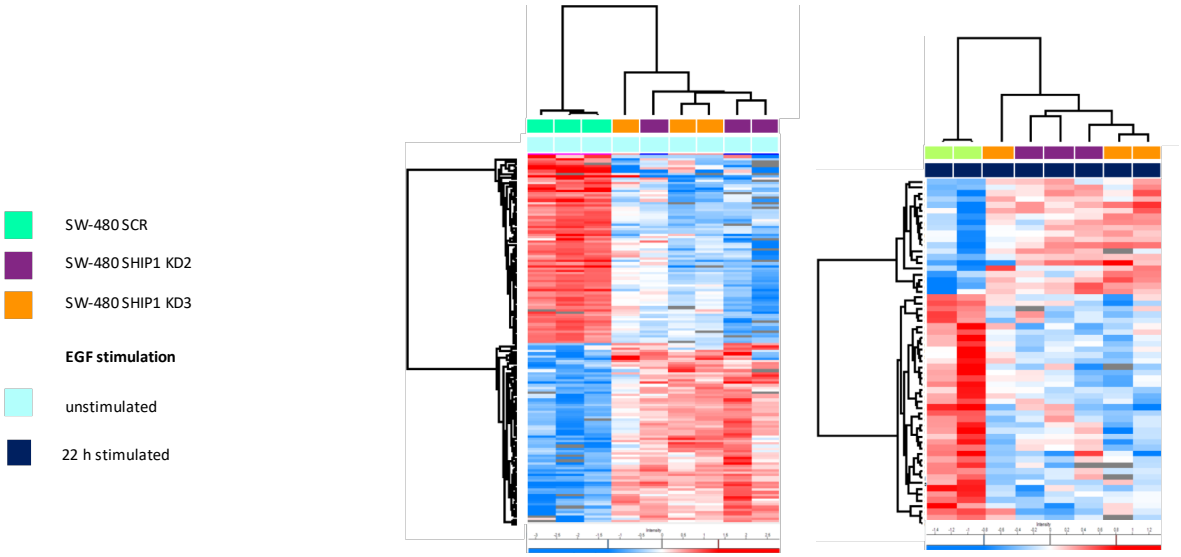

fig. 54: Heat map of the differential quantitative proteomics analysis of SW-480 KD2/-3 vs. SCR. Differential quantitative proteomics and data evaluation were performed by Hannah Voß and Paula Nissen (MS Core/AG Schlüter, UKE Hamburg). n=3

The STRING analysis (**fig. 55-58**) revealed that for the unstimulated condition ribosomal translation factors, mRNA splicing factors, ADP/ATP transporters and MCM complex proteins were upregulated and NADH-DH, histones (especially linker histones) and splicing factors (especially S-/R- rich ones) were downregulated by the SHIP1 KD. In the 22 h EGF stimulated condition histones and NADH-DH were downregulated. MCM proteins and transcription-

/translation factors were upregulated by the SHIP1 KD under both conditions. No splicing factors or ADP-/ATP-transporters were regulated in the 22 h stimulated samples.

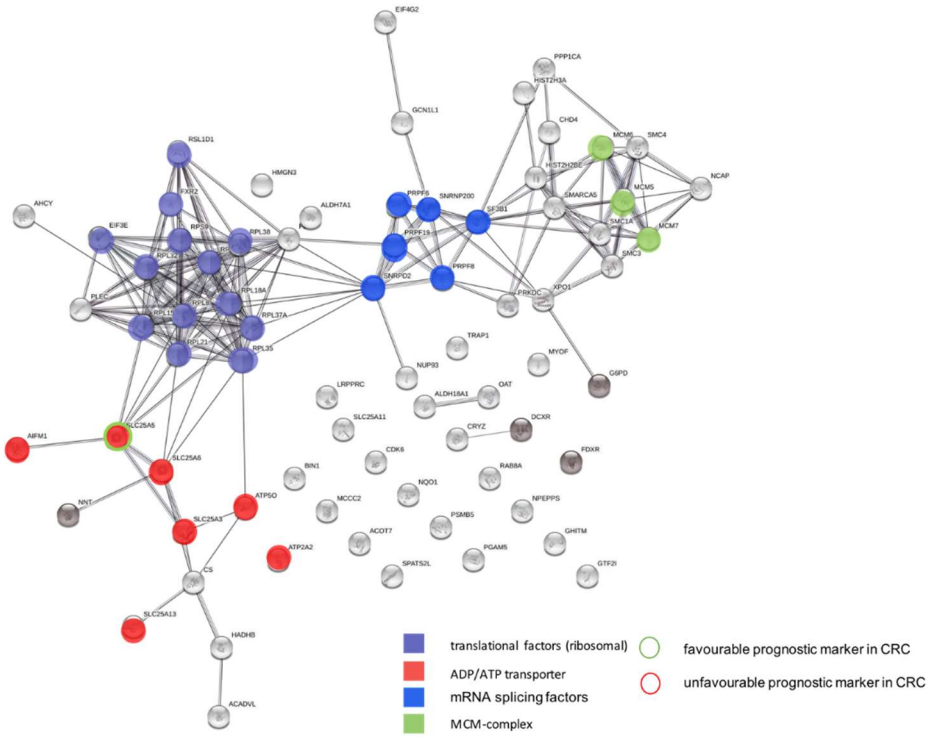

fig. 55: Network of the proteins being upregulated in the proteome of SW-480 SHIP1 KD2/KD3 vs. SCR under unstimulated conditions. Network analysis was performed with the algorithm STRING. Differential quantitative proteomics and data evaluation were performed by Hannah Voß and Paula Nissen (MS Core/AG Schlüter, UKE Hamburg). n=3

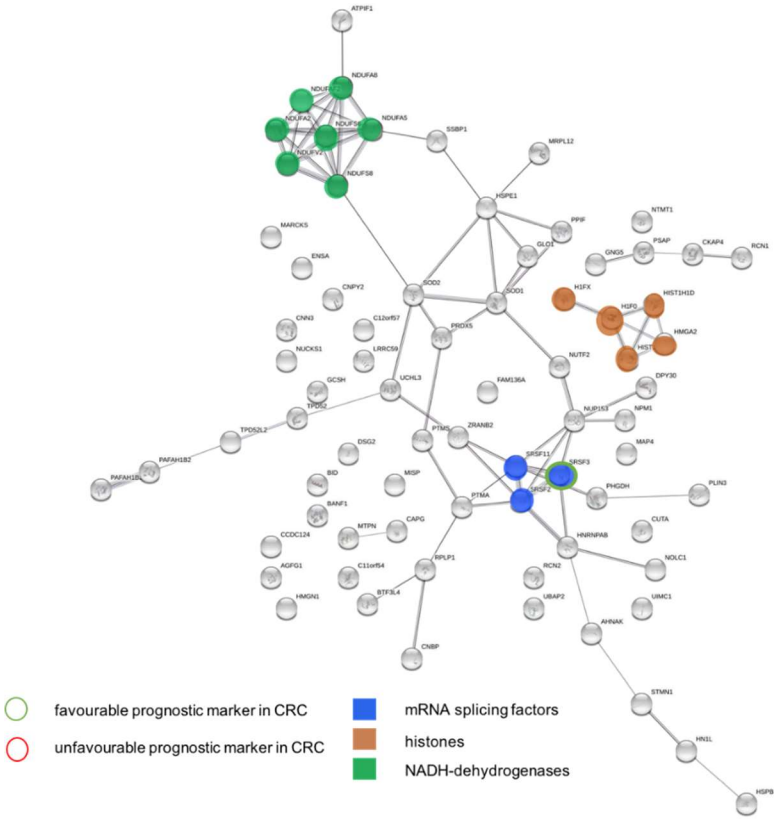

fig. 56: Network of the proteins being downregulated in the proteome of SW-480 SHIP1 KD2/KD3 vs. SCR under unstimulated conditions. Network analysis was performed with the algorithm STRING. Differential quantitative proteomics and data evaluation were performed by Hannah Voß and Paula Nissen (MS Core/AG Schlüter, UKE Hamburg). n=3

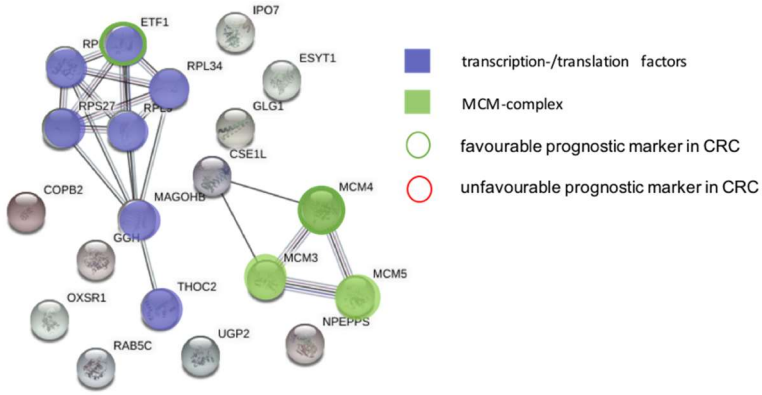

fig. 57: Network of the proteins being upregulated in the proteome of SW-480 SHIP1 KD2/KD3 vs. SCR after 22 h EGF stimulation. Network analysis was performed with the algorithm STRING. Differential quantitative proteomics and data evaluation were performed by Hannah Voß and Paula Nissen (MS Core/AG Schlüter, UKE Hamburg). n=3

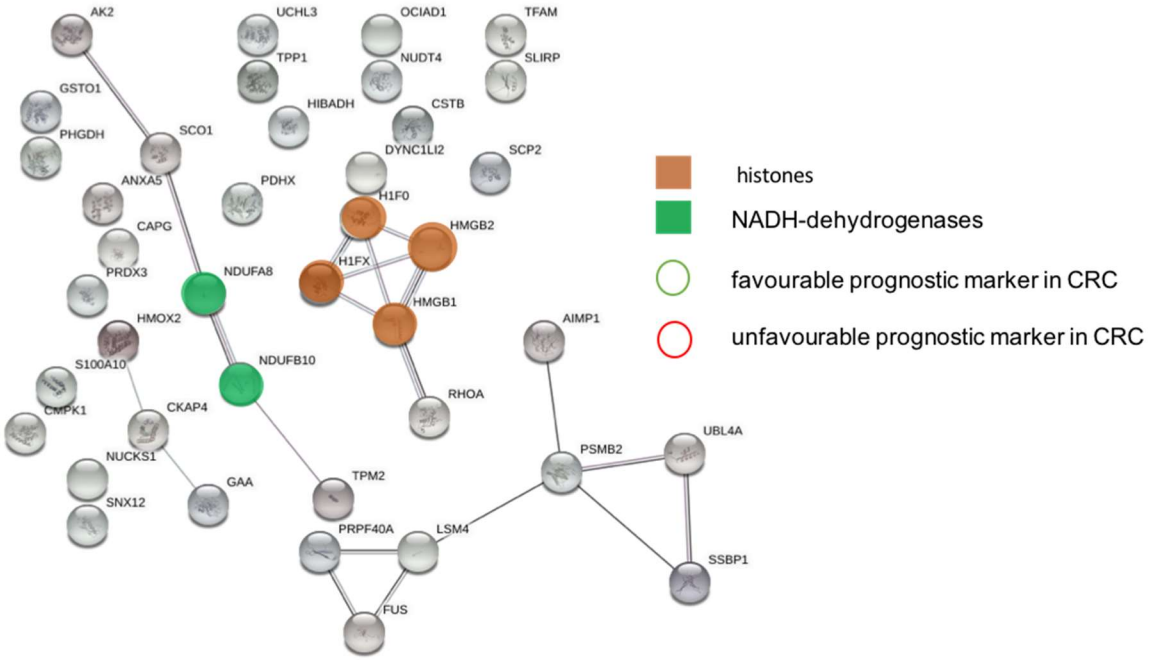

fig. 58: Network of the proteins being downregulated in the proteome of SW-480 SHIP1 KD2/KD3 vs. SCR after 22 h EGF stimulation. Network analysis was performed with the algorithm STRING. Differential quantitative proteomics and data evaluation were performed by Hannah Voß and Paula Nissen (MS Core/AG Schlüter, UKE Hamburg). n=3

Using the human protein atlas [1037] the significantly regulated proteins (included in STRING analysis or fold-change >2) in the 22 h EGF-stimulated condition were mapped to the clinical prognosis (no prognostic marker, favourable or unfavourable) which is summarized in **table 10**.

Table 10: mapping of significantly regulated proteins SW-480 SCR vs. SHIP1 KD, 22 h EGF-stimulation to the clinical prognosis in CRC. The prognostic relevance was derived from the human protein atlas. Analysed proteins were included in the STRING analysis or showed a fold-change >2.

upregulated in KD		
ETF1	transcription and translation	favourable
MCM4	DNA replication	favourable
NPEPPS	aminopeptidase, cell viability and cell growth	favourable
TRAP1	function and polarization of mitochondria, repression of OxPhos	favourable
SLC25A5	ATP/ADP exchange (mitochondrion-cytosol)	favourable
MCCC2	catabolism of leucine and isovaleric acid	favourable

HIST2HBE	histone	unfavourable
PLEC	actin binding protein, MT-actin linker, cell-adhesion	unfavourable
downregulated in KD		
HSPB1	chaperone, maintains denatured proteins in a folding-competent state, stress response	unfavourable
SRSF3	S-/R-rich splice factor, alternative splicing and mRNA export	favourable
LRRC59	nuclear import of FGF1, anti-apoptotic function	favourable
DSG2	cell-cell junction (desmosome)	favourable

With regard to the impact of SHIP1 overexpression on the proteome (HCT-116 SHIP1 WT vs. LeGO, maintenance conditions) there were only 31 proteins found to be significantly regulated (**fig. 59**). In general, SHIP1 KD and SHIP1 OE affected the proteome in an opposite way as expected, however it has to be taken into account that the two systems are not 100% comparable as they are based on two different cell lines. Mitochondrial transporters, cytochrome C and glycolysis-/gluconeogenesis proteins were downregulated by the overexpression of SHIP1 while upregulated by the SHIP1 KD. SHIP1 OE most prominently upregulated replication and cell cycle proteins but no histones which were strongly downregulated by the SHIP1 KD.

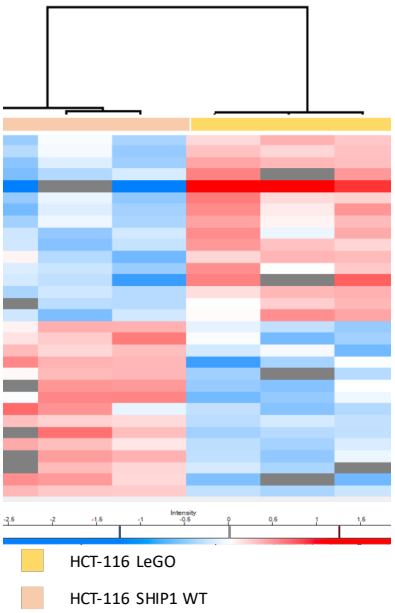

fig. 59: Heat map of the differential quantitative proteomics analysis of of HCT-116 SHIP1 WT vs. LeGO. Differential quantitative proteomics and data evaluation were performed by Hannah Voß and Paula Nissen (MS Core/AG Schlüter, UKE Hamburg). n=3

As indicated in **fig. 60** SHIP1 KD partly reversed the effect of the transduction procedure in SW-480 as the KD lines clustered more strongly with SW-480 parental than SW-480 SCR. This was not the case for the SHIP1 overexpression (HCT-116) which clustered more strongly with HCT-116 LeGO than with HCT-116 parental.

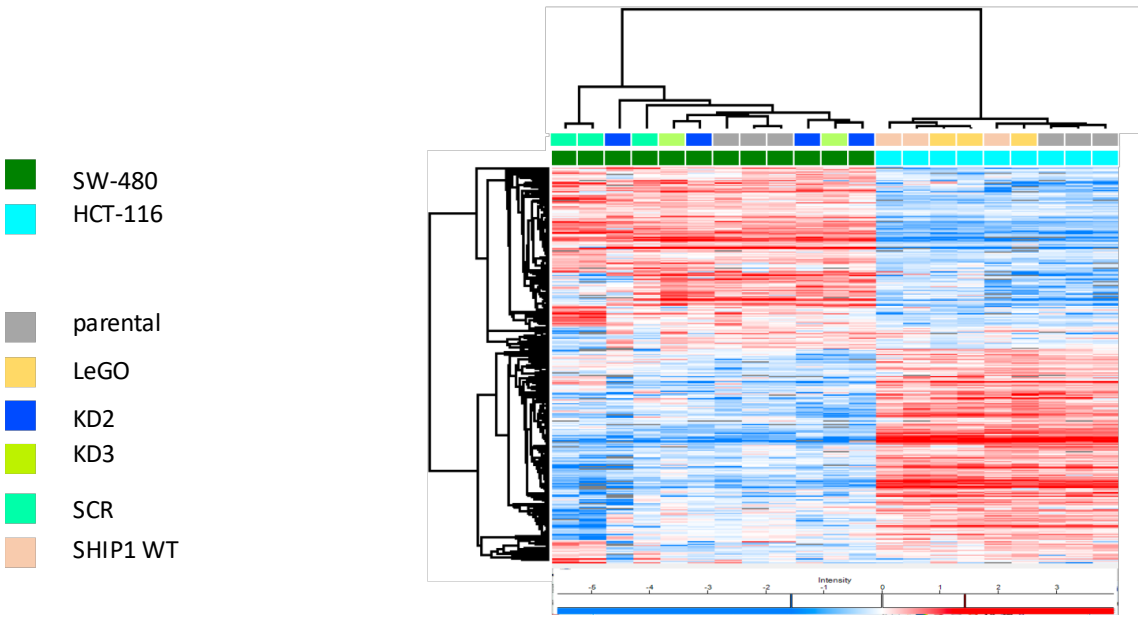

fig. 60: Heat map of the differential quantitative proteomics analysis of of HCT-116 SHIP1 WT vs. LeGO vs. parental and SW-480 SHIP1 KD2/-3 vs. SCR vs. parental under maintenance conditions. Differential quantitative proteomics and data evaluation were performed by Hannah Voß and Paula Nissen (MS Core/AG Schlüter, UKE Hamburg). n=3

The reliability of the differential quantitative proteomics analysis was verified by WB of selected targets exemplarily for SW-480 SHIP1 KD2/-3 vs. SCR and 22 h EGF stimulation. For the differential quantitative proteomics analysis PGDH and G6PDH were used due to their significant regulation concerning SHIP1 KD vs. SCR (**fig. 61** and **fig. 62**).

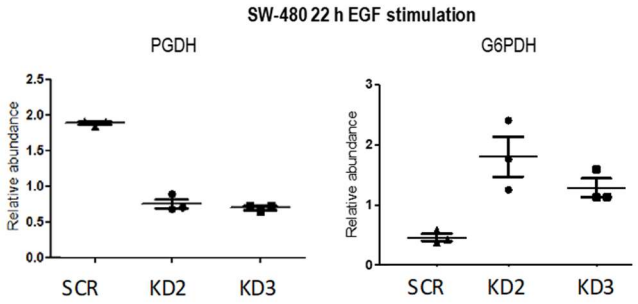

fig. 61: Differential quantitative proteomics analysis of SW-480 KD2/-3 vs. SCR, 22h EGF stimulation-selection of targets for Western Blot verification. The relative abundance diagrams of the targets selected for the WB verification are depicted. Differential quantitative proteomics measurements and data evaluation were performed by Hannah Voß and Paula Nissen (MS Core/AG Schlüter, UKE Hamburg). Error bars indicate standard deviations. n=3

fig. 62: Western Blot verification of the reliability of the differential quantitative proteomics analysis of SW-480 KD2/-3 vs. SCR, 22 h EGF stimulation. The protein levels of G6PDH and PGDH were determined by Western Blot relative to HSC70 and SW-480 SCR. Error bars indicate standard deviations. Significances were calculated by t-testing. n=3

4.1.7. *in vivo* analysis of the function of SHIP1 in CRC (SW-480 SCR vs. KD2 in NSG-mice)

To analyse the *in vivo* function of SHIP1 in CRC NSG-mice injected with SW-480 KD2 and SCR were compared. The experiment was performed by the group of Prof. Schumacher, institute for anatomy, UKE with the exception of the Western Blot analysis of tumour tissues.
A xenograft mouse model of CRC using SW-480 was described previously by Li et al. [1038]. In this paper they found significantly higher metastasis of SW-480 stably overexpressing HIF1α compared to control cells following intraperitoneal injection in nude mice (metastasis was measured as number of nodules found in the intestinal wall). However, no metastasis of SW-480 was found in a study of Schumacher et al. using SCID mice and subcutaneous injection [1039]. In order to determine if SW-480 would possibly metastasize in NSG mice a pre-experiment was performed using a cohort of five NSG mice injected with SW-480 SCR. In the pre experiment metastasis of SW-480 in NSG was successfully shown (metastasis in the lung 5 out of 5) (**fig. 63**).

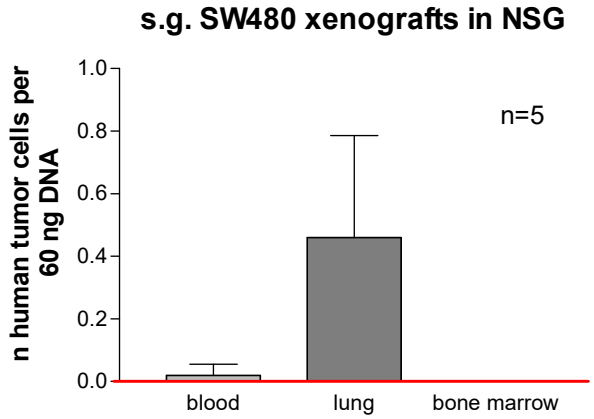

fig. 63: Analysis of human DNA in blood, lung and bone marrow of NSG mice after subcutaneous growth of SW-480 colorectal cancer cells. Alu PCR was performed on DNA extracted from blood, lungs and bone marrow of NSG mice after subcutaneous injection of SW-480 cells and tumor growth. The number of human cells in each organ/tissue was normalized to 60 ng DNA. The red line is indicating the detection limit of the Alu PCR (0.002 human cells per 60 ng DNA). In 3 out of 5 mice low amounts of human DNA were detected in the blood whereas in 5 out of 5 mice distinct amounts of human DNA was detectable in the lungs. In the bone marrow, human DNA was not detectable in any of the mice. Error bars indicate standard deviations. The experiment was performed in the group of Prof. Schumacher, UKE Hamburg.

Following this, for each group 15 mice were subcutaneously injected with SW-480 SCR or KD2. During the course of the experiment most mice had to be sacrificed due to ulci except for 5 mice of the KD2 group which developed larger tumours due to the longer lifespan (**table 11**). The Kaplan Meier curve indicated significantly higher survival of SW-480 KD2 mice compared to SCR (**fig. 64**) which pointed to an oncogenic function of SHIP1 *in vivo*.

Table 11: Lifespan and tumour mass of NSG-mice subcutaneously injected with SW-480 KD2 or SCR. The experiment was performed in the group of Prof. Schumacher, UKE Hamburg.

SW480 SCR					**SW480 SHIP1 KD2**			
T-Base No.	histo-no.	lifepan [d]	tumour mass [g]		T-Base No.	histo-no.	lifespan[d]	tumour mass [g]
2493	422-1-20	29	1,63		2420	423-1-20	29	1,71
2494	422-2-20	29	1,85		2423	423-2-20	29	1,19
2460	422-3-20	29	1,61		2472	429-1-20	30	1,11
2459	428-1-20	30	1,86		2473	429-2-20	30	1,71
2482	428-2-20	30	0,98		2478	429-3-20	30	1,01
2483	428-3-20	30	1,54		2419	436-1-20	31	0,55
2484	428-4-20	30	0,91		2421	436-2-20	31	1,4
2486	428-5-20	30	0,98		2422	436-3-20	31	1,3
2487	428-6-20	30	0,78		2475	440-1-20	32	0,65
2461	435-1-20	31	0,9		2477	440-2-20	32	0,97
2462	435-2-20	31	1,56		2414	460-1-20	43	3,21
2485	439-1-20	32	1		2415	460-2-20	43	0,63
2488	439-2-20	32	2,73		2416	460-3-20	43	3,09
2491	439-3-20	32	1,45		2417	460-4-20	43	2,45
2492	439-4-20	32	1,71		2418	460-5-20	43	2,01
			MW					MW
			1,432666667					1,532666667

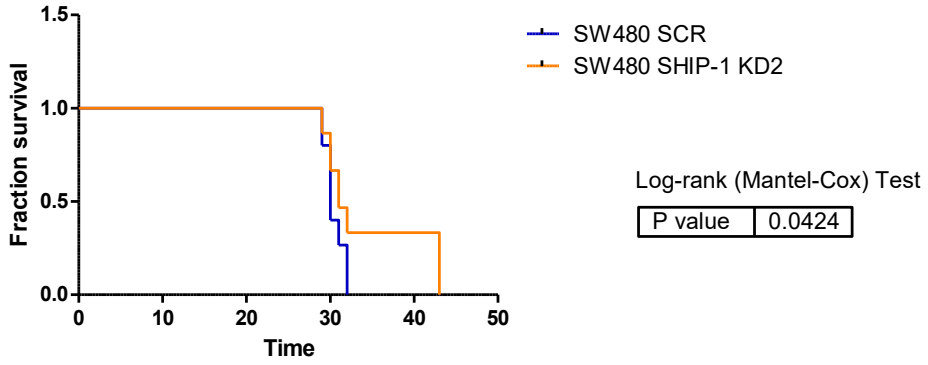

fig. 64: Kaplan-Meier curves of NSG-mice subcutaneously injected with SW-480 SCR or SHIP1 KD2. 15 mice were used per group. The experiment was performed in the group of Prof. Schumacher, UKE Hamburg.

As the *in vitro* data pointed to a positive impact of SHIP1 on the migratory potential but not on the proliferation of SW-480 cells the *in vivo* data would be most plausibly explained by a positive impact of SHIP1 also on tumour metastasis. To test this, alu-PCR of blood, lung, bone marrow and liver was performed. However, in neither case significant amounts of human DNA could be identified (not shown).
The tumours derived from the sacrificed mice were analysed for the expression of human SHIP1 by Western Blot. To discriminate between human and murine tissue, human-specific antibodies for SHIP1 and HSP70 were utilized which had been validated in-house by the manufacturer and also validated during the experiment using lysates of M1 (murine, SHIP1-positive), NIH-3T3 (murine, SHIP1-negative), SW-480 SCR (human, SHIP1-positive) and SW-480 SHIP1 KD2 (human, SHIP1-negative) (not shown). The result of the Western Blot is depicted in **fig. 65**.

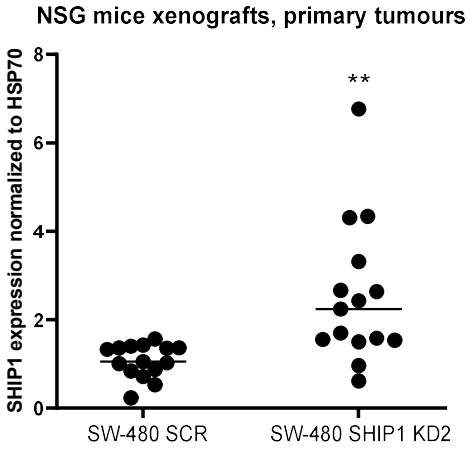

fig. 65: Determination of human SHIP1-levels in primary tumours derived from NSG-mice subcutaneously injected with SW-480 SCR or SHIP1 KD2 by Western Blot. Significances were determined by t-testing. n=15.

As can be seen, general SHIP1 levels in tumours derived from mice injected with SW-480 SHIP1 KD2 were significantly higher than those of tumours derived from mice injected with SW-480 SCR indicating a loss of the SHIP1 KD and potentially (compensatory) higher expression of the SHIP1-expressing cells that outgrew the SHIP1 KD cells. Of note, SHIP1 levels were highly heterogeneous in the tumours derived from SW-480 SHIP1 KD2. Further analysis showed a correlation of SHIP1 expression and lifespan in SW-480 SHIP1 KD2 injected mice (**fig. 66**) and would point to a potential overcompensation of the SHIP1 KD over time (the longer the lifespan, the higher the SHIP1 expression).

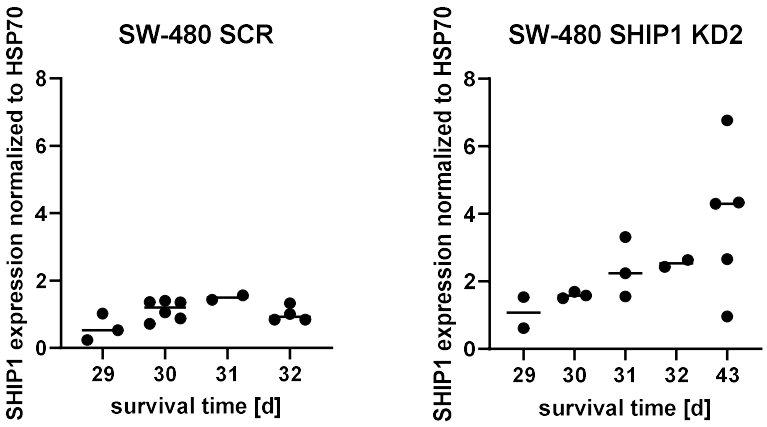

fig. 66: Correlation of SHIP1 expression and lifespan in NSG-mice. SHIP1 was detected in primary tumours by Western Blot and SHIP1 expression levels were plotted against the lifespan of designated NSG-mice injected with SW-480 SCR or SW-480 SHIP1 KD2.

4.2. Patient-derived mutations of the SHIP1 phosphatase domain impact its catalytic activity, phosphoinositide binding specificity, stability and subcellular localization and signal transduction capabilities and may alter its role in tumorigenesis

4.2.1. Determination of the cellular impact of ectopic expression of SHIP1 WT and selected patient derived SHIP1 mutants of the catalytic domain in model carcinoma cell lines (H1299, HCT-116 and WM-164)

As indicated in 4.1.1. a significant portion of SHIP1 found in carcinoma samples was shown to bear mutations and this was especially pronounced within the phosphatase domain. In this section selected patient-derived mutations of the SHIP1 phosphatase domain were examined regarding their catalytic activity, binding specificity to phosphoinositides, stability, subcellular localization and impact on signal transduction. For the analysis either stably transduced carcinoma cells (4.2.1.) or recombinant SHIP1 (4.2.2.) were used. The selected SHIP1 mutants were obtained from the COSMIC database [619] and are summarized in **table 12**.

Table 12: Overview of selected SHIP1 patient derived mutants of the phosphatase domain. Data were obtained from the COSMIC database [619]

E452K (c.1354G>A)	Liver carcinoma (2x) CRC
R551Q (c.1652G>A)	CRC (4x) CNS glioma Malignant melanoma Endometrium carcinoma
R577C (c.1729C>T)	Malignant melanoma (4x)
R673Q (c.2018G>A)	Malignant melanoma Endometrium carcinoma

To analyse the function of SHIP1 mutants compared to SHIP1 WT the SHIP1 mutants obtained from the COSMIC database were inserted into the lentiviral transduction vector pLeGO-iG2-Puro(+)-SHIP1 WT by *QuickChange Mutagenesis* and the carcinoma cell line of choice (mostly H1299) was transduced with SHIP1 WT, SHIP1 mutants or an empty vector control. It was aimed for single integration of the GOI (transduction rate between 5% and 19%). Transduced cells were selected using puromycin and sorted to obtain a maximally homogenous population. The transduction was verified by Western Blot and verified cell lines were analysed regarding their protein expression level/stability, subcellular localization, catalytic activity and impact on signal transduction. A special focus was laid on the mutation R673Q. The workflow is shown in **fig. 67**.

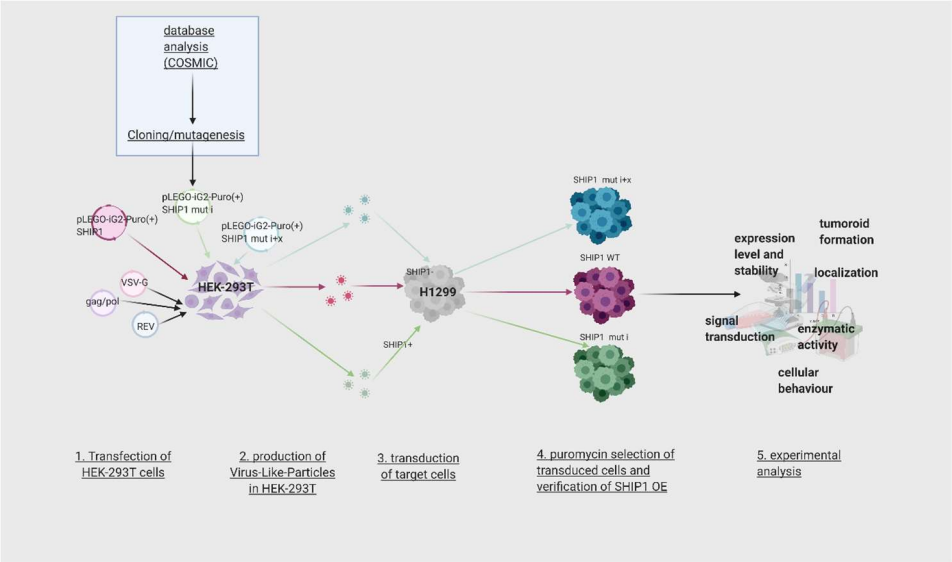

fig. 67: Workflow for the analysis of the impact of SHIP1 mutants of the phosphatase domain on the behaviour of H1299 cells. Mutants were obtained from the COSMIC database and introduced into pLeGO-iG2-Puro(+) SHIP1 by *QuickChange Mutagenesis*. Cells were transduced with SHIP1 WT, SHIP1 mutants or an empty vector control, selected with puromycin and sorted. The transduction was verified by an anti-SHIP1 Western Blot and cells were analysed with regard to different cellular features.

4.2.1.1 Expression, subcellular localization and stability

To access the expression levels of SHIP1 proteins NP40 lysates were prepared and analysed by Western Blot using anti-SHIP1 P1C1 mouse monoclonal antibody for detection. This is shown in **fig. 68** and **fig. 69**.

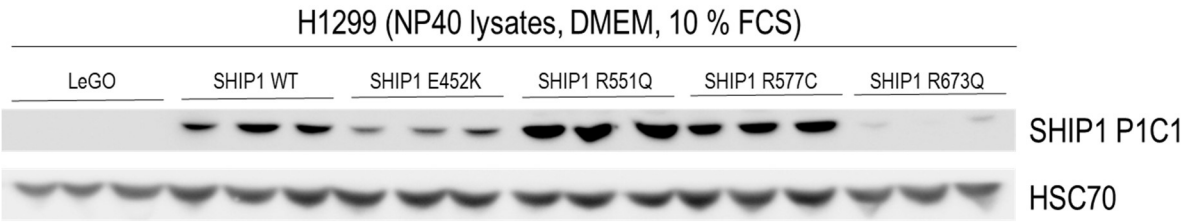

fig. 68: analysis of the expression level of SHIP1 proteins in H1299 cells. Cells were lysed by NP40-lysis and SHIP1 expression was detected by Western Blot using anti-SHIP1 P1C1 mouse monoclonal antibody.

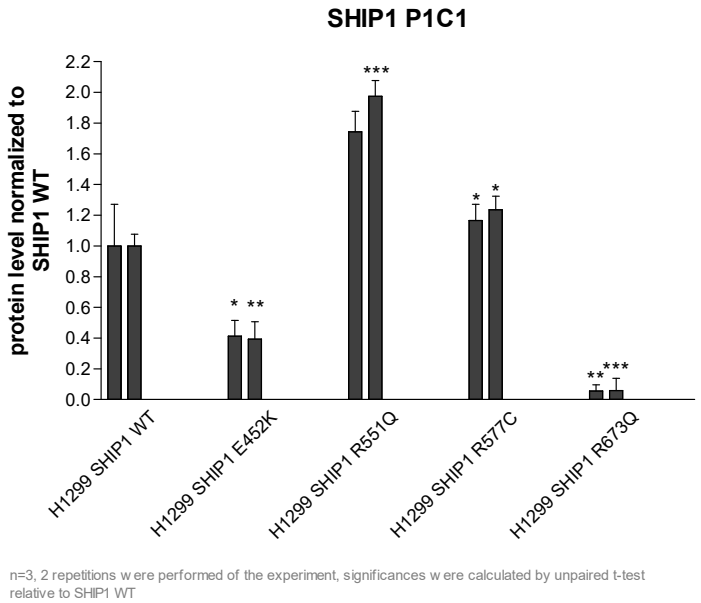

fig. 69: analysis of the expression level of SHIP1 proteins in H1299 cells (data evaluation). Cells were lysed by NP40 lysis and SHIP1 expression was detected by Western Blot using anti-SHIP1 P1C1 mouse monoclonal antibody and normalized to HSC70 and SHIP1 level in H1299 SHIP1 WT. Error bars indicate standard deviations. Significances were determined by t-test. n=3 per repetition.

In both repetitions the expression levels of SHIP1 E452K (around 40% of SHIP1 WT) and SHIP1 R673Q (around 2-5% of SHIP1 WT) were reduced whereas the expression of SHIP1 R551Q and R577C were increased to around 200% respectively 140% of SHIP1 WT.
Of note, strongly reduced expression of SHIP1 R673Q was also found in HCT-116 and WM-164 cells whereas SHIP1 E452K was reduced in HCT-116 but enhanced in protein level in WM-164 cells. (**fig. 70**).

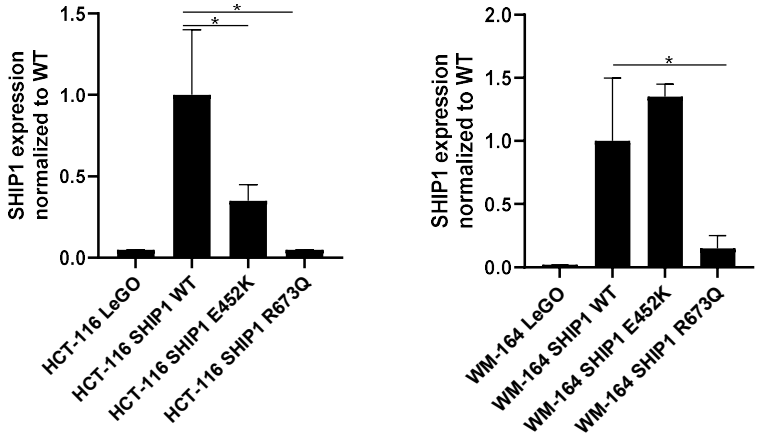

fig. 70: analysis of the expression level of SHIP1 proteins in HCT-116 and WM-164 cells. Cells were lysed by NP40 lysis and SHIP1 expression was detected by Western Blot using anti-SHIP1 P1C1 mouse monoclonal antibody and normalized to HSC70 and SHIP1 level in HCT-116/WM-164 SHIP1 WT. Error bars indicate standard deviations. Significances were determined by t-test. n=3

Due to the cell line-concordant significant reduction of SHIP1 R673Q maintenance protein level in comparison to SHIP1 WT it was aimed to examine the mechanisms behind this finding in more detail. In general, the reduced protein level of SHIP1 R673Q could be explained by either reduced expression or reduced stability of this mutant. In the following, only the latter aspect will be analysed. First, the half-life time of SHIP1 R673Q and SHIP1 WT was determined. For this, H1299 SHIP1 WT and H1299 SHIP1 R673Q cells were treated with 750 µM cycloheximide for 0.25 to 8 hours or a DMSO control and SHIP1 levels were analysed by Western Blot using anti-SHIP1 P1C1 mouse monoclonal antibody and normalized to Ponceau staining. To calculate the half life time band intensities were plotted against the time and curves were fitted using the equation $y = Span * \mathrm{e}^{-kx} + Plateau$ or $y = IF(x < x_0, Plateau, Bottom + (Plateau - Bottom) * \mathrm{e}^{-k*(x-x_0)}$ were the half life time $t_{1/2}$ is 0.69/k. This is depicted in **fig. 71**.

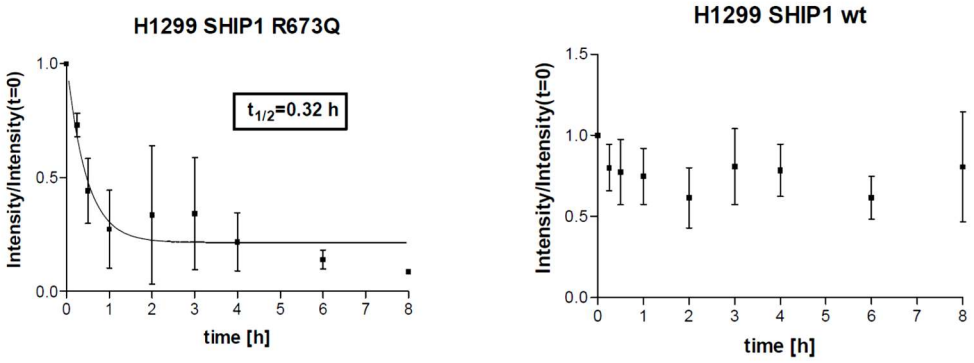

fig. 71: analysis of the half life-time of SHIP1 WT and SHIP1 R673Q in H1299 cells. Cells were seeded at a density of $3x10^5$/well in a 6-well plate and incubated for 48-72 hours. Cells were then treated with 750 µM cycloheximide or an equal volume of DMSO for control purposes and lysed by NP40 lysis at the indicated time points. SHIP1 expression was detected by Western Blot using anti-SHIP1 P1C1 mouse monoclonal antibody. Band intensities were normalized by Ponceau staining and normalized band intensity at t=0. Normalized band intensities were plotted against the time and curves were fitted using the equation Y=Span*exp(-K*X)+Plateau or Y=IF(X<X0, Plateau, Bottom+(Plateau-Bottom)*exp(-k*(X-X0))) were the half life time $t_{1/2}$ is 0.69/K. Error bars indicate standard deviations. n=3

Compared to SHIP1 WT which showed no significant decrease in protein level during the course of the experiment the half life time of SHIP1 R673Q was highly reduced for SHIP1 R673Q ($t_{1/2}$<30 min) which correlated with the low observed level of protein expression of this mutant. Regarding the DMSO controls no such decay was visible (not shown). In an additional experiment using time points ranging from 0 h to 32 h the half life-time of SHIP1 WT was shown to be in the range of 24-32 h but could not be exactly determined due to curve fitting problems (**fig. 72**).

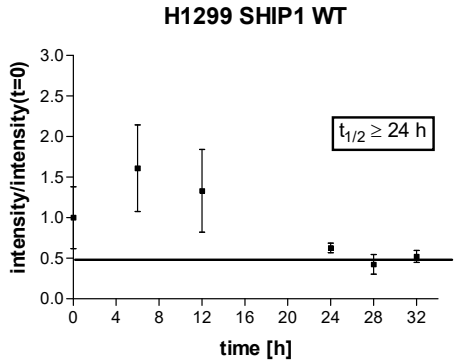

fig. 72: analysis of the half life-time of SHIP1 WT in H1299 cells. Cells were seeded at a density of $3x10^5$/well in a 6-well plate and incubated for 48-72 hours. Cells were then treated with 750 µM cycloheximide or an equal volume of DMSO for control purposes and lysed by NP40 lysis at the indicated time points. SHIP1 expression was detected by Western Blot using anti-SHIP1 P1C1 mouse monoclonal antibody. Band intensities were normalized to HSC70 and normalized band intensity at t=0 and plotted against the time. Error bars indicate standard deviations. n=3.

Furthermore, it was examined if the observed decreased stability was due to enhanced proteolytic degradation. Hence, H1299 SHIP1 R673Q cells were treated with 1 or 10 µM of the proteasome inhibitor MG-132 or a DMSO control for 8 hours and lysed by TCA lysis. The amount of SHIP1 R673Q was then determined by Western Blot using SHIP1 P1C1 mouse monoclonal antibody and normalized to HSC70. For both concentrations of MG-132 the level of SHIP1 R673Q was significantly increased with regard to the DMSO control and the effect of MG-132 was visibly albeit not significantly concentration dependent (**fig. 73**). Therefore, it was concluded that SHIP1 R673Q was target of enhanced proteasomal degradation.

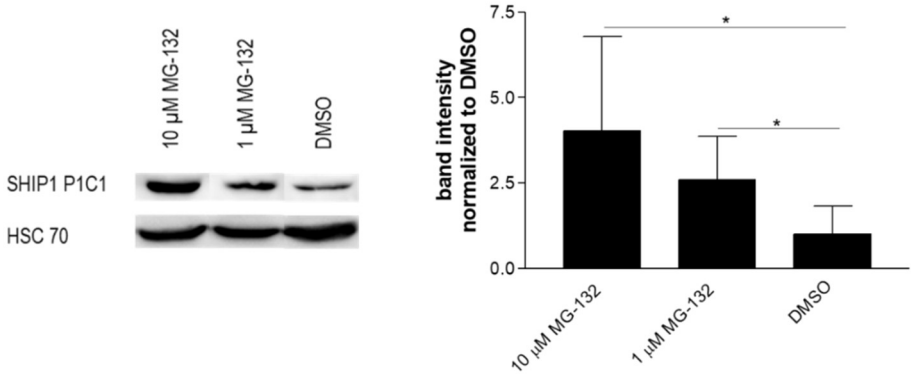

fig. 73: MG-132 treatment of H1299 R673Q cells. Cells were treated with 1 or 10 µM of the proteasome inhibitor MG-132 or a DMSO control for 8 hours and lysed by TCA lysis. SHIP1 levels were detected by Western Blot using SHIP1 P1C1 mouse monoclonal antibody and normalized to HSC70. Error bars indicate standard deviations. Significances were determined by t-test. n=3.

Another possibility which could cause the reduced stability of SHIP1 R673Q could be an alteration regarding its subcellular localization. Of particular interest would be a reduction of its membrane localization as SHIP1 can be stabilized by interaction with other membrane-bound proteins such as GRB2 (not published). To determine the subcellular localization of the SHIP1 proteins the membranous (P200) and cytosolic (S200) fraction of SHIP1 transduced H1299 cells were separated by differential ultracentrifugation at 200,000xg and the amount of SHIP1 was determined by Western Blot using anti-SHIP1 P1C1 mouse monoclonal antibody. Blotting against EGFR (membrane) or GAPDH (cytosol) was used to verify that fractions were properly separated (not shown). The P200/S200 ratios of SHIP1 WT and SHIP1 R673Q are depicted in **fig. 74**. As can be seen, SHIP1 WT was equally distributed to the membranous and the cytosolic fraction (P200/S200=1) whereas SHIP1 R673Q was enriched 10-fold in the cytoplasmic fraction compared to the membrane fraction.

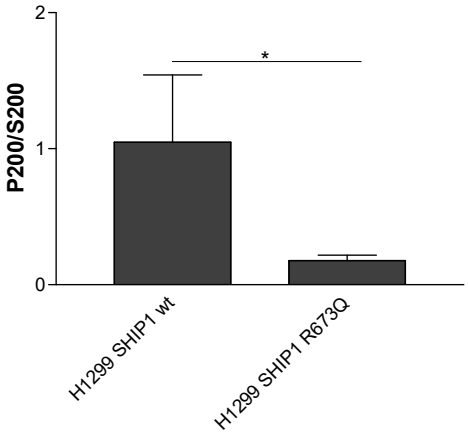

fig. 74: analysis of the subcellular localization of SHIP1 WT and R673Q proteins stably transduced in H1299 (differential centrifugation). The membranous (P200) and cytosolic (S200) fraction were separated by differential ultracentrifugation at 200,000xg and the amount of SHIP1 was determined by Western Blot using anti-SHIP1 P1C1 mouse monoclonal antibody and normalized to Ponceau staining. Error bars indicate standard deviations. Significances were determined by t-test. n=3.

4.2.1.2. Signal transduction

For the signal transduction analysis cells were lysed at maintenance conditions (DMEM, 10% FCS, 70-80% confluence) by NP40 lysis and examined by Western Blot using P-AKT S473 and P-p44/42 MAPK T202/Y204 in order to determine the impact of SHIP1 WT and SHIP1 mutants on the PI3K/AKT/mTORC and the MAPK pathway. This is shown in **fig. 75** and **fig. 76**.

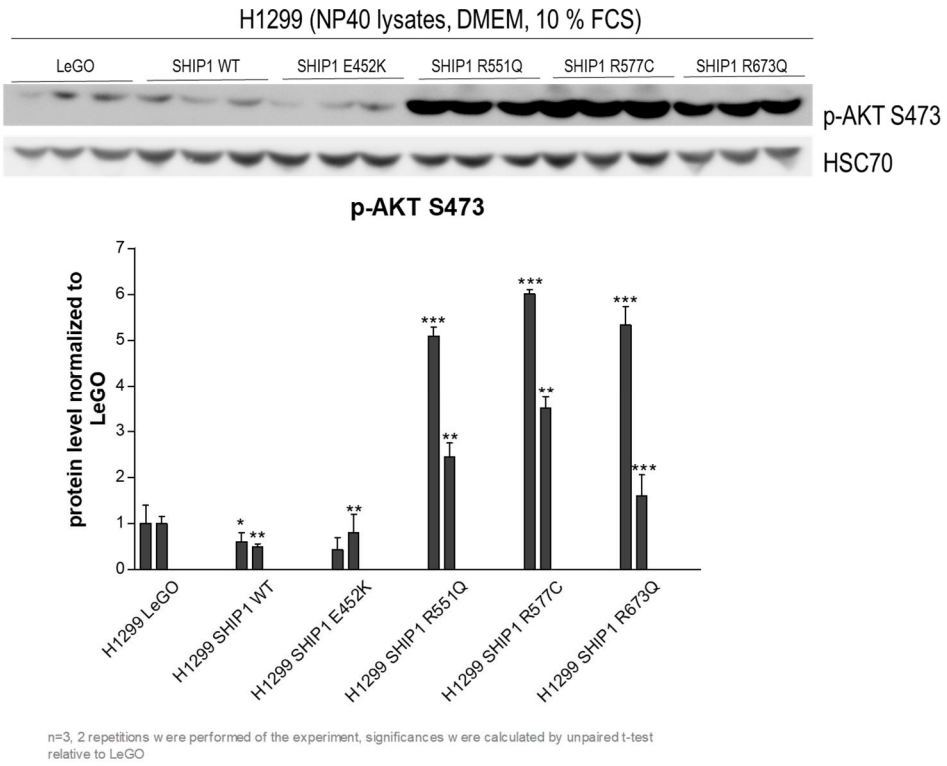

fig. 75: Analysis of the impact of SHIP1 WT and selected patient-derived SHIP1 mutants of the phosphatase domain on the PI3K/AKT/mTORC pathway. H1299 cells stably transduced with SHIP1 WT, SHIP1 mutants or a LeGO control were lysed by NP40 lysis and examined by Western Blot using P-AKT S473. Error bars indicate standard deviations. Significances were determined by t-testing. n=3 per repetition

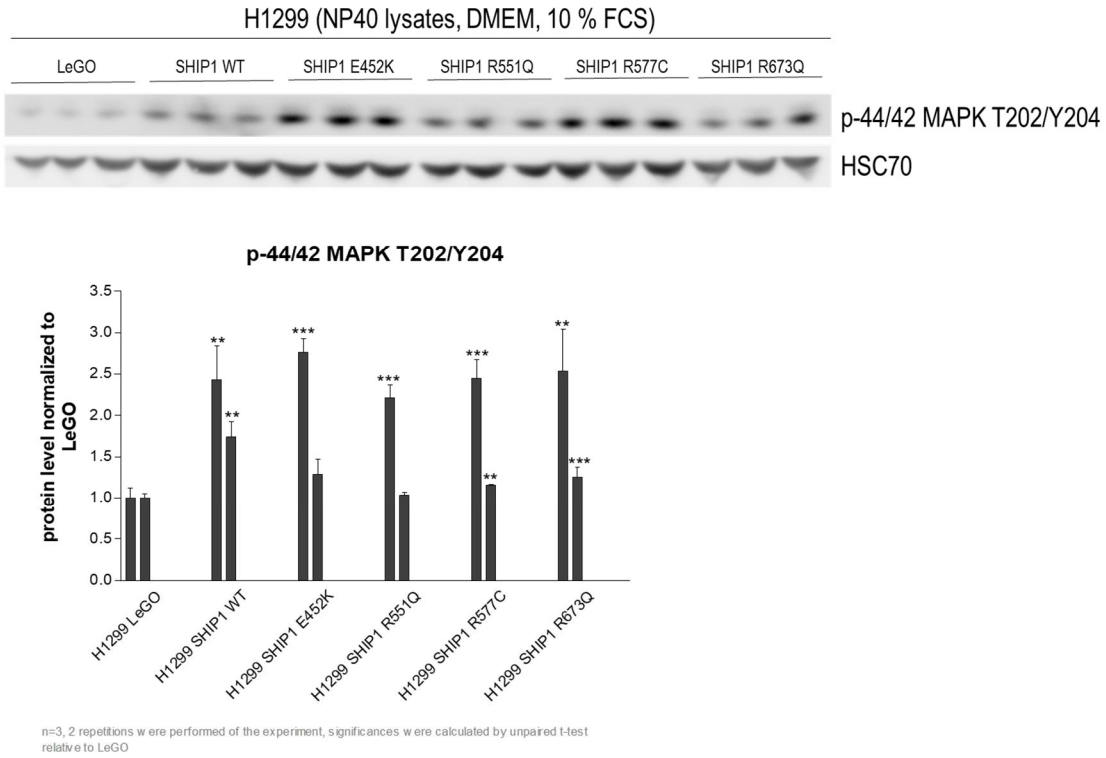

fig. 76: Analysis of the impact of SHIP1 WT and selected patient-derived SHIP1 mutants of the phosphatase domain on the MAPK pathway. H1299 cells stably transduced with SHIP1 WT, SHIP1 mutants or a LeGO control were lysed by NP40 lysis and examined by Western Blot using P-p44/42 MAPK T202/Y204. Error bars indicate standard deviations. Significances were determined by t-testing. n=3 per repetition

As shown, SHIP1 WT and SHIP1 E452K negatively impacted the PI3K/AKT/mTORC1 pathway whereas this pathway was enhanced for the remaining SHIP1 mutants. In contrast, all SHIP1 proteins positively influenced the MAPK pathway.

4.2.1.3. Catalytic activity of SHIP1 immunoprecipitated from H1299 SHIP1 WT/mutant transduced lysates

The catalytic activity of SHIP1 proteins was assessed using a phosphatase assay which is based on the malachite green mediated detection of phosphate released in the course of the SHIP1 catalysed reaction.
For the assay, cells were seeded in a density of 2-3x10^6 cells/10 cm dish and incubated overnight so that around 70-80% confluence was reached the next day. Cells were lysed by NP40 lysis (non-denaturing) and 1-1.5 mg protein lysate was used for immunoprecipitation of SHIP1 using SHIP1 P1C1 mouse monoclonal antibody coupled to G-sepharose beads. Immunoprecipitated SHIP1 was subject to the malachite-green based phosphatase assay using ci8-PtdIns(3,4,5)P_3 as substrate (f.c. 20 µM). Released phosphate was measured photometrically using a phosphate standard curve. The amount of released phosphate was plotted against the time (shown exemplarily for H1299 SHIP1 WT, **fig. 77A**) and the initial velocity was calculated (equalizing the enzymatic activity in mU). A separate aliquot of immunoprecipitated SHIP1 was employed for Western Blot in order to determine the amount of immunoprecipitated SHIP1 in the reaction using a recombinant SHIP1 standard and to calculate the specific enzymatic activity in mU/mg (shown for one example experiment in **fig. 77B**).

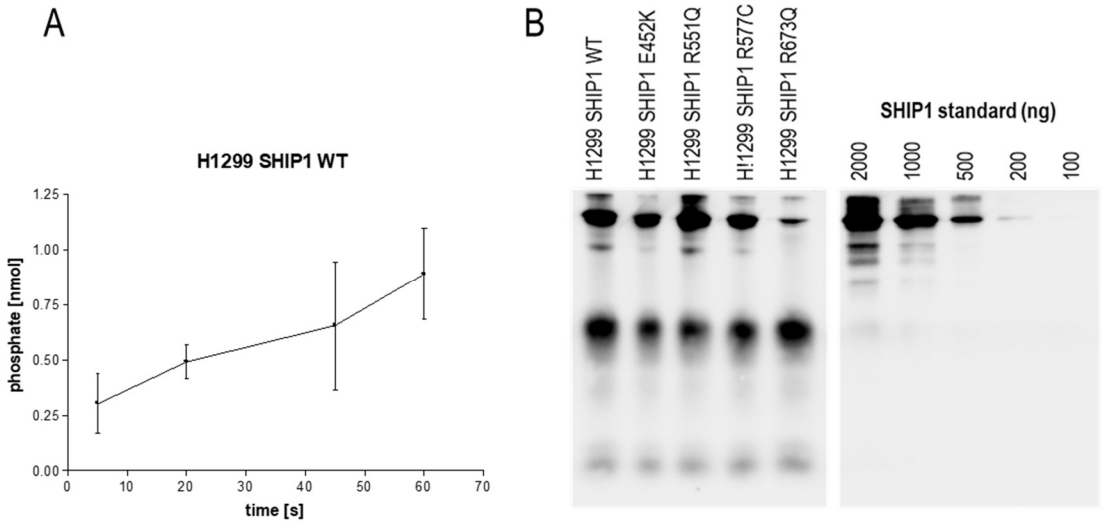

fig. 77: SHIP1 phosphatase assay using SHIP1 immunoprecipitated from stably transduced H1299 cells and ci8-PtdIns(3,4,5)P_3 as substrate (experimental setup). Panel A shows an example of the enzymatic reaction (amount of released phosphate detected by complex formation with malachite green against the reaction time) for H1299 SHIP1 WT. Panel B shows an example Western Blot for the assessment of mg protein/assay and specific enzymatic activity. Error bars indicate standard deviations. n=3

As depicted in **fig. 78** the R673Q mutation resulted in a complete loss of enzymatic activity and the R551Q mutation in a nearly complete loss of enzymatic activity in both repetitions whereas the mutation E452K did rather positively affect and the mutation R577C may reduce enzymatic activity albeit at a lower level compared to R551Q or R673Q at utilized substrate concentration. These findings were in accordance with previous experiments done in our lab respectively the medical student practical course.

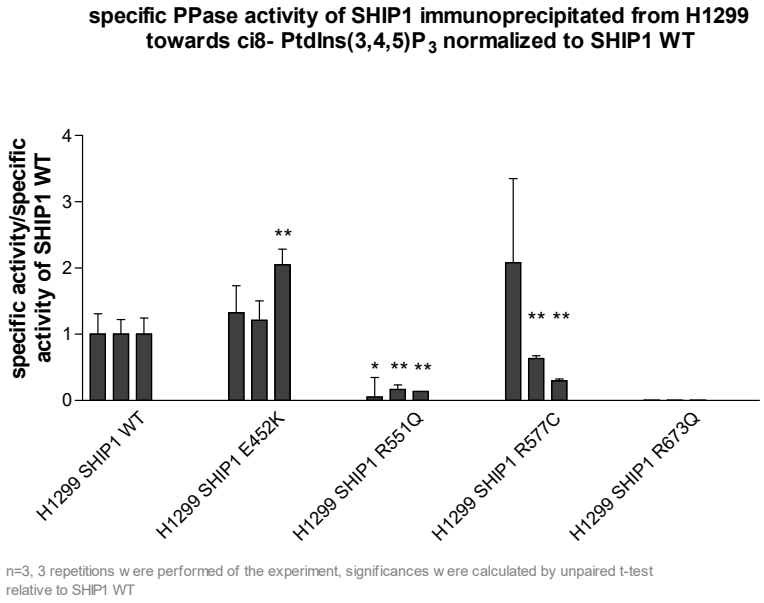

fig. 78: SHIP1 phosphatase assay using SHIP1 immunoprecipitated from stably transduced H1299 cells and ci8-PtdIns(3,4,5)P_3 as substrate. Error bars indicate standard deviations. Significances were determined by t-test. n=3 per repetition.

In addition, the SHIP1 inhibitor 3-AC was applied to SHIP1 WT immunoprecipitated from H1299 SHIP1 WT. As 3-AC had been reported to possess an IC_{50} value of 10 µM concerning SHIP1 WT (as opposed to >1 mM for SHIP2 and PTEN) [1040] 3-AC concentrations of 0, 5, 20 and 50 µM were tested. SHIP1 specific activity at 0 µM 3-AC was 525.6±7.3 mU/mg and 3-AC exhibited a clear inhibitory effect on SHIP1 specific activity. Due to lack of enough data points, an actual IC_{50} value could not be determined, however the theoretical 3-AC concentration needed to reduce the catalytic activity to 50% of the control value (calculated by exponential fitting of the form $y = SPAN * e^{-kx} + PLATEAU$ was 2.985 µM (**fig. 79**).

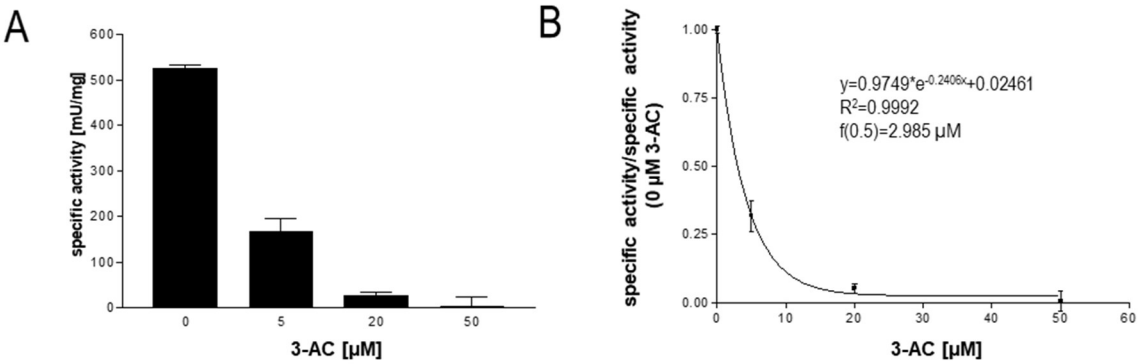

fig. 79: treatment of SHIP1 WT immunoprecipitated from H1299 cells with 3-AC. SHIP1 WT was immunoprecipitated from stably transduced H1299 cells using SHIP1 P1C1 monoclonal antibody coupled to G-sepharose beads and the inhibitory effect of 3-AC was tested for 20 µM PtdIns(3,4,5)P_3 and 0,5, 20 or 50 µM 3-AC using a malachite-green phosphatase assay. The amount of SHIP1 per assay was determined by Western Blot using a recombinant SHIP1 standard to calculate the specific activity. The IC_{50} value was approximated by exponential fitting. Error bars indicate standard deviations. n=3

4.2.1.4. in-silico structure analysis

In summary, all tested patient-derived mutations influenced the behaviour (localization and/or expression/stability and/or enzymatic activity) of SHIP1 in H1299 cells. In order to define possible molecular mechanisms for this finding indicated residues were evaluated in *Maestro 11* using the structure of SHIP1 PPase-C2 (PDB 6IBD) and BiPh(2,3',4,5',6)P5 of the structure of SHIP2 PPase-C2 (PDB 4A9C_B) superposed to PDB 6IBD to better clarify the substrate binding pocket. **fig. 80** shows a general overview of the distribution of residues R577, R673, E452 and R551. As can be seen, especially E452 and R551 are located in close proximity of the substrate whereas R673

is rather orientated in the closer surroundings of the substrate binding pocket and may not be a direct part of it. R577 on the other hand is clearly located outside the substrate binding pocket.

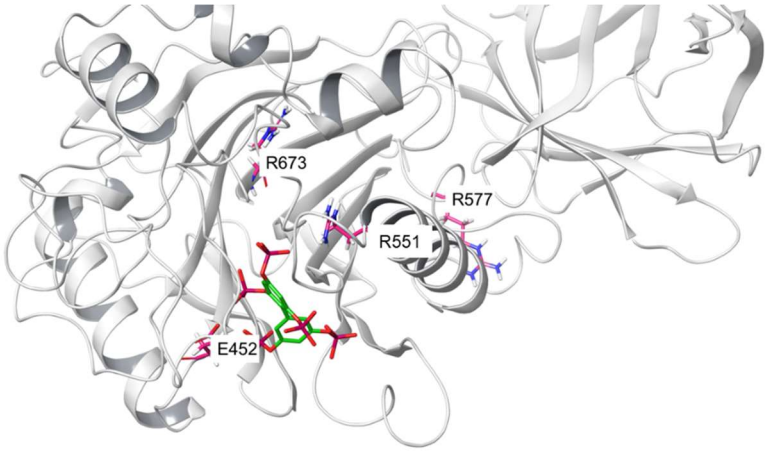

fig. 80: *In silico* analysis of the localization of SHIP1 residues E452, R673, R551 and R577 within the SHIP1 PPase domain. The crystal structure of SHIP1 PPase-C2 (PDB 6IBD) is shown in light grey and BiPh(2,3',4,5',6)P5 of the structure of SHIP2 PPase-C2 (PDB 4A9C) superposed to PDB 6IBD is shown in green. Residues of interest are coloured in raspberry and labelled. The image was generated in *Maestro 11*.

Next, residues of interest were looked at in more detail focusing on putative side chain mediated interactions which may be disturbed by the patient derived mutations (**fig. 81**). The main chain of E452 would form a hydrogen bond to N414 and the side chain with N411. By mutating the glutamate to lysine the side chain interaction with N411 would be abolished due to conversion of charge but would be replaced by a novel salt bridge of K452 to D699. R551 would form hydrogen bonds to the main chains of G544 and Q618. Conversion of the arginine to glutamine would lead to a 1C shorter side chain, loss of the positive charge and conversion of an H-donor (=NH_{ε}) to an H-acceptor (=O_{δ}) and loss of the side chain interaction. R673 would contact E634 and D617 via salt bridges. The R673Q mutation would result in changes of the interaction pattern (loss of side chain interactions) as explained for R551Q. The main chain of R577 would make contact S533 and I547 and the side chain would contact the main chains of F572, L564 and L569. The main chain interactions would be in place in the R577C mutant but the side chain interactions would be abolished by the R577C mutation due to a shorter chain length, loss of positive charge and conversion of an H-donor to an H-acceptor (SH). In addition, residues E452 and R673 were found to lie in conserved motifs of SHIP1 (see 4.3.1.) indicating that they are very likely be functional relevant. In addition, especially R551Q and E452K would most likely impact substrate accommodation and catalysis due to their intimate proximity to relevant residues and the substrate itself (see also section 4.3.1.).

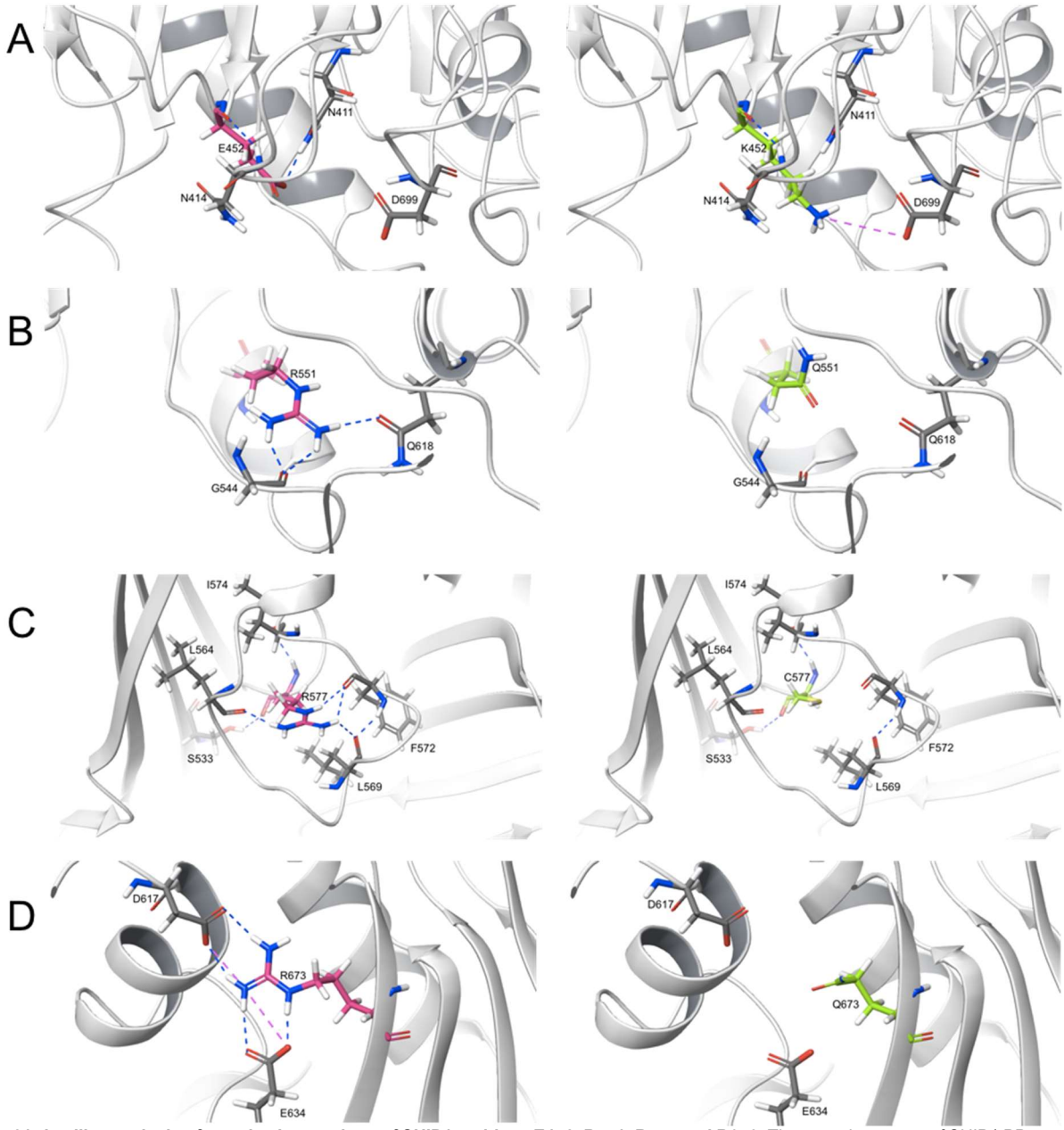

fig. 81: *in silico* analysis of putative interactions of SHIP1 residues E452, R551, R577 and R673. The crystal structure of SHIP1 PPase-C2 (PDB 6IBD) is shown in light grey. Residues of interest are coloured in raspberry and mutated residues in green and labelled and interacting residues are labelled. Salt bridges are shown in lilac dashed lines and H-Bonds in blue dashed lines. Images were generated in *Maestro 11*.

4.2.2. SHIP1 WT and SHIP1 mutants in the context of phosphoinositide binding proteins-the phosphoinositide trapping model

The phosphoinositide trapping model summarized in **fig. 82** and published in [1041] is one possible model to explain putative oncogenic effects of SHIP1 WT and patient-derived SHIP1 mutants in carcinoma. Ectopic expression of SHIP1 WT or SHIP1 mutants may protect phosphoinositides implicated in oncogenic signal transduction ($PtdIns(3,4,5)P_3$ and $PtdIns(3,4)P_2$) from degradation by phosphoinositide phosphatases thereby increasing their concentration. Accumulation of $PtdIns(3,4,5)P_3$ and/or $PtdIns(3,4)P_2$ may then recruit and activate $PtdIns(3,4,5)P_3$ and/or $PtdIns(3,4)P_2$ binding effector proteins replacing SHIP1 which would stimulate oncogenic outputs such as increased proliferation, survival and/or migration. This would ultimately result in enhanced tumour proliferation and /or metastasis of carcinoma cells. The prerequisite for phosphoinositide trapping would be K_D (phosphatases) > K_D (SHIP1) > K_D (effector proteins). Moreover, SHIP1 proteins protecting $PtdIns(3,4,5)P_3$ (substrate) would have to be ideally catalytically dead or at least exhibit reduced catalytic activity as otherwise $PtdIns(3,4,5)P_3$ would become degraded instead of trapped. Concerning $PtdIns(3,4)P_2$ SHIP1 proteins could be either active or inactive and

trapping of PtdIns(3,4)P_2 by active SHIP1 proteins might be even more efficient as they would be capable to enhance the pool of PtdIns(3,4)P_2 in parallel. As SHIP1 is allosterically activated by PtdIns(3,4)P_2 this would further enable a *feed-forward* loop amplifying the accumulation of PtdIns(3,4)P_2 and resulting oncogenic signal transduction pathways.
Conclusively, the following parameters have to be considered when aiming to evaluate the phosphoinositide trapping model in total: (1) binding and enzymatic properties of SHIP1 proteins, (2) binding (and enzymatic) properties of phosphoinositide phosphatases and (3) binding properties of effector proteins.
To this end, the proteins in question were recombinantly expressed and purified by appropriate chromatographic techniques. The K_D values for PtdIns(3,4)P_2 and PtdIns(3,4,5)P_3 were then quantified by Surface Plasmon Resonance (SPR) and in future experiments the enzymatic properties of SHIP1 and phosphoinositide phosphatases should be determined by means of a malachite green based colorimetric phosphatase assay (not included in the thesis).

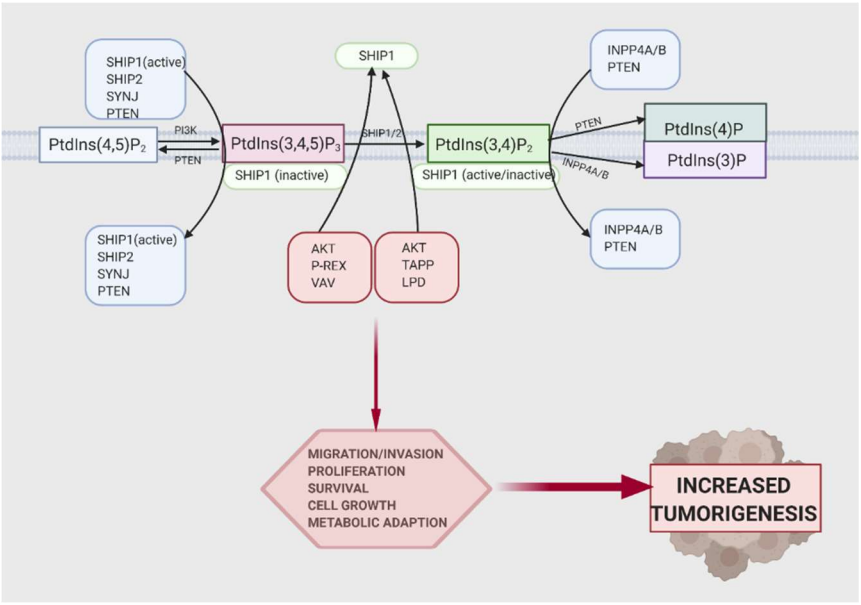

fig. 82: overview of the phosphoinositide trapping model. In this model, ectopic expression of SHIP1 WT or SHIP1 mutants would protect phosphoinositides implicated in oncogenic signal transduction (PtdIns(3,4,5)P_3 and PtdIns(3,4)P_2) from degradation by phosphoinositide phosphatases (PTEN, INPP4A/B, active SHIP1, SHIP2) thereby increasing their concentration. Accumulation of PtdIns(3,4,5)P_3 and/or PtdIns(3,4)P_2 would then recruit and activate PtdIns(3,4,5)P_3 and/or PtdIns(3,4)P_2 binding effector proteins (AKT, P-REX, VAV, LPD, TAPP) replacing SHIP1 which would stimulate oncogenic outputs such as increased proliferation, survival and/or migration. This would ultimately result in enhanced tumour proliferation and /or metastasis of carcinoma cells. The prerequisite for phosphoinositide trapping would be K_D (phosphatases) > K_D (SHIP1) > K_D (effector proteins). SHIP1 proteins protecting PtdIns(3,4,5)P_3 (substrate) would have to be ideally catalytically dead or exhibit reduced catalytic activity as otherwise PtdIns(3,4,5)P_3 would become degraded instead of trapped. Concerning PtdIns(3,4)P_2 SHIP1 proteins could be either active or inactive and trapping of PtdIns(3,4)P_2 by active SHIP1 proteins might be even more efficient as they would be capable to enhance the pool of PtdIns(3,4)P_2 in parallel. As SHIP1 is allosterically activated by PtdIns(3,4)P_2 this would further enable a *feed-forward* loop amplifying the accumulation of PtdIns(3,4)P_2 and resulting oncogenic signal transduction pathways [1041].

4.2.2.1. Recombinant expression and purification of SHIP1 proteins and PtdIns(3,4,5)P_3 and/or PtdIns(3,4)P_2 specific phosphoinositide phosphatases and effector proteins

4.2.2.1.1. Expression and purification of SHIP1

SHIP1 was expressed as an N-terminal tagged Strep fusion protein. To this end, SHIP1 was cloned into pASG-IBA5 using the *Stargate* protocol. The verified (sequenced) vectors were then transformed into the expression strain *E. coli BL21(DE3)pLysSpREP4*. Expression was under the control of the inducible tet promotor system and induced by the addition of anhydrotetracycline (200 ng/mL) for 3 h at RT. Bacteria were harvested in washing buffer (buffer W, 100 mM Tris/Cl, 150 mM NaCl, 1 mM EDTA, pH 8.0) and lysed by ultrasonication. The lysate was purified by *Strep-Tactin* affinity chromatography using *Strep-Tactin XT* resins due to their superiority over the classical *Strep-Tactin* material regarding capacity, washing stringency and binding strength. Following loading of the lysate to the resin, the resin was washed with 10 CV washing buffer (buffer W) and the protein was eluted using 0.6/1.6/0.8 CV elution buffer (buffer BXT, 100 mM Tris/Cl, 150 mM NaCl, 1 mM EDTA, 50 mM biotin, pH 8.0). The eluates were analysed by 10% SDS-PAGE and *Coomassie Brilliant Blue R-250* staining which is depicted in **fig. 83**. In addition,

SHIP1 expression was verified by Western Blot using SHIP1 P1C1 mouse monoclonal antibody and a Strep-tag specific antibody. Following purification fractions 2 and 3 were pooled and 10x-concentrated by means of ultrafiltration.
In previous experiments SHIP1 expression and purification was aimed to be optimized however not successfully (Nelson, 2017, unpublished).

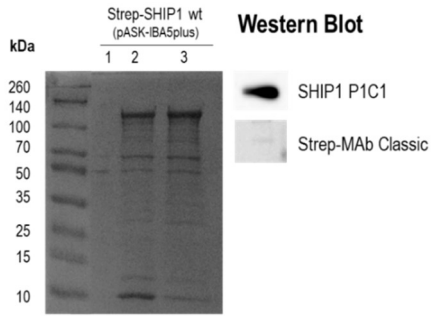

fig. 83: expression and purification of Strep-SHIP1. pASG-IBA5 SHIP1 was transformed into the expression strain *E coli BL21(DE3)pLysSpREP4.* SHIP1 was expressed as Strep-SHIP1 under the control of the tet promotor for 3 hours at RT in a culture volume of 0.5 L and purified by *Strep-Tactin XT* affinity chromatography (0.2 mL CV). Elution was performed in three fractions (0.6/1.6/0.8 CV buffer BXT) and the elution fractions were analysed by 10% SDS and *Coomassie Brilliant Blue R-250* staining. Elution fractions 2 and 3 were pooled and SHIP1 expression was verified by Western Blot using SHIP1 P1C1 mouse monoclonal antibody and a Strep-tag specific antibody (Strep-Mab classic).

4.2.2.1.2. Expression and purification of PtdIns(3,4,5)P_3 and/or PtdIns(3,4)P_2 specific phosphoinositide phosphatases

4.2.2.1.2.1. PTEN

PTEN was expressed as Strep-fusion protein. To this end, PTEN was cloned into pASG-IBA3 (PTEN-Strep) or pASG-IBA5 (Strep-PTEN) using the *Stargate* protocol. The verified (sequenced) vectors were then transformed into the expression strain *E.coli BL21(DE3)pLysSpREP4*. Expression was under the control of the inducible tet promotor system and induced by the addition of anhydrotetracycline (200 ng/mL) at RT. Bacteria were harvested in washing buffer (buffer W, 100 mM Tris/Cl, 150 mM NaCl, 1 mM EDTA, pH 8.0) and lysed by ultrasonication. The lysate was purified by *Strep-Tactin* affinity chromatography using *Strep-Tactin XT* resins due to their superiority over the classical *Strep-Tactin* material regarding capacity, washing stringency and binding strength. Following loading of the lysate to the resin, the resin was washed with 10 CV washing buffer (buffer W) and the protein was eluted using 0.6/1.6/0.8 CV elution buffer (buffer BXT, 100 mM Tris/Cl, 150 mM NaCl, 1 mM EDTA, 50 mM biotin, pH 8.0). The eluates were analysed by 10% SDS-PAGE and *Coomassie Brilliant Blue R-250* staining which is depicted in **fig. 84**. In addition, PTEN expression was verified by Western Blot using two PTEN specific antibodies directed against different epitopes of the protein (PTEN A2B1 directed against aa 388-400 and PTEN F-1 directed against aa 3-29) and a Strep-tag specific antibody.

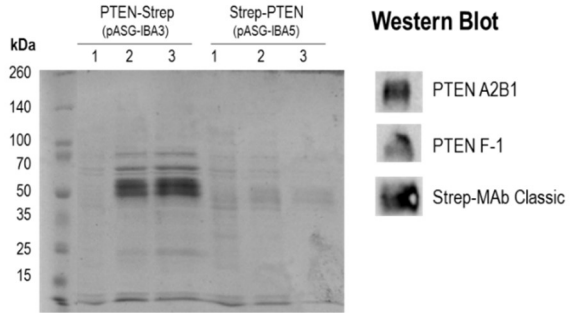

fig. 84: expression and purification of PTEN. pASG-IBA3 PTEN or pASG-IBA5 PTEN were transformed into the expression strain *E coli BL21(DE3)pLysSpREP4.* PTEN was expressed as PTEN-Strep or Strep-PTEN under the control of the tet promotor for 3 hours at RT in a culture volume of 0.5 L and purified by *Strep-Tactin XT* affinity chromatography (0.2 mL CV). Elution was performed in three fractions (0.6/1.6/0.8 CV buffer BXT) and the elution fractions were analysed by 10% SDS and *Coomassie Brilliant Blue R-250* staining. PTEN-Strep elution fractions 2 and 3 were pooled and PTEN expression was verified by Western Blot using two PTEN specific antibodies directed against different epitopes of the protein (PTEN A2B1 directed against aa 388-400 and PTEN F-1 directed against aa 3-29) and a Strep-tag specific antibody (Strep-Mab classic).

As shown, PTEN was successfully expressed as PTEN-Strep (pASG-IBA3) but not as Strep-PTEN (pASG-IBA5). The concentration of pooled PTEN-Strep eluates 2 and 3 typically was ~100 ng/µL. However, significant impurities remained. Therefore, buffers were either supplemented with 0.1% Tween-20 or 500 mM NaCl to enhance the washing stringency with no significant optimization of the result (not shown).
Next, it was aimed to combine the *Strep Tactin* affinity chromatography with Ion Exchange chromatography (IEX). As for IEX the choice of buffer pH is dependent on the pI of the protein of interest, the theoretical pI for PTEN-Strep was calculated as 5.99 using the *ExPASy Compute pI/Mw* tool. For Cation Exchange (CIEX, *Pierce* Strong Ion Exchange Spin Column S (sulphonic acid functional groups)) 50 mM Na-citrate/citric acid, pH 5.0 was selected as buffer system and for Anion Exchange (AIEX, *Pierce* Strong Ion Exchange Spin Column Q (quaternary ammonium functional groups)) 50 mM Tris/Cl, pH 7.5 or pH 8.5 was chosen as buffer system. Expression of PTEN-Strep was as described above and bacteria were resuspended in the desired purification buffer after having been harvested. Following binding of the lysate to the resin the resin was washed with 2 CV of the respective purification buffer and elution was performed in four steps applying increasing concentrations of NaCl (250 mM, 500 mM, 750 mM and 1000 mM NaCl; 1CV each for elution) to the respective purification buffer. The elution fractions were analysed by 10% SDS-PAGE and *Coomassie Brilliant Blue R-250* staining (not shown). Elution fractions 1 and 2 (AIEX) or 2 (CIEX) containing the majority of PTEN were diluted 1:10 in *Strep-Tactin* washing buffer (buffer W) and applied to a *Strep-Tactin XT* resin. In relation to IEX the column volume was downscaled 1:0.4 for further concentration of PTEN. The resin was washed with 10 CV washing buffer (buffer W) and the protein was eluted using 0.6/1.6/0.8 CV elution buffer (buffer BXT). The elution fractions were analysed by 10% SDS-PAGE and *Coomassie Brilliant Blue R-250* staining. However, this improvement strategy was also not observed to be successful (not shown).
Next, post-purification of Strep eluates by AIEX was attempted. To this aim, PTEN-Strep was expressed for 3 hours at RT and purified by *Strep-Tactin XT* chromatography. Elution fractions 2 and 3 were pooled and loaded onto a *Pierce* Strong Ion Exchange Spin Column Q resin equilibrated with buffer BXT. The resin was washed twice with buffer BXT and elution was performed in four fractions by applying 1 CV each of buffer BXT supplemented with 100 mM, 300 mM, 500 mM and 700 mM NaCl (NaCl step gradient) to the column. The purification was analysed by 10% SDS-PAGE and *Coomassie Brilliant Blue R-250* staining. Strep+AIEX elution fraction 1 showed a higher grade of purity compared to Strep purification alone; however, the overall yield of PTEN was significantly reduced (not shown). To increase the concentration of PTEN in the Strep+AIEX eluates (1) PTEN was expressed overnight at 12°C aiming to increase the amount of soluble protein and (2) the culture volume was doubled at standard expression conditions (3 h at RT). The purification was performed as described above and analysed by 10% SDS-PAGE and *Coomassie Brilliant Blue R-250* staining which is shown in **fig. 85**.

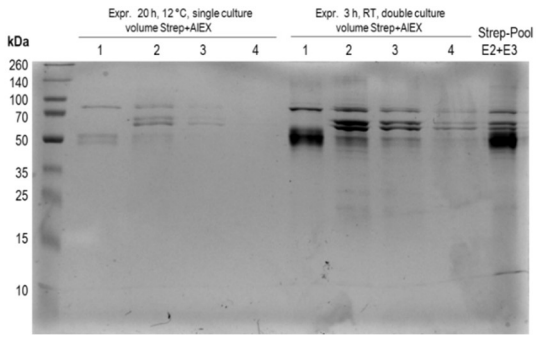

fig. 85: optimization of the expression and purification of PTEN (*Strep-Tactin*+AIEX). pASG-IBA3 PTEN was transformed into the expression strain *E coli BL21(DE3)pLysSpREP4*. PTEN was expressed as PTEN-Strep under the control of the tet promotor for 3 hours at RT in a culture volume of 2 L or for 20 hours at 12°C in a culture volume of 1 L and pre-purified by *Strep-Tactin XT* affinity chromatography (1 mL respectively 0.5 mL CV). Elution was performed in three fractions (0.6/1.6/0.8 CV buffer BXT). Elution fractions 2 and 3 were pooled and loaded onto a *Pierce* Strong Ion Exchange Spin Column Q (0.4 mL CV) resin equilibrated with buffer BXT. The resin was washed twice with buffer BXT and elution was performed in four fractions by applying 1 CV each of buffer BXT supplemented with 100 mM, 300 mM, 500 mM and 700 mM NaCl (NaCl step gradient) to the column. The purification was analysed by 10% SDS-PAGE and *Coomassie Brilliant Blue R-250* staining.

PTEN was not strongly expressed at 12°C and 20 h resulting in the observed low concentration of PTEN in the corresponding Strep+AIEX eluates. In contrast, doubling of the culture volume resulted in a comparable concentration but increased purity of PTEN in the Strep-AIEX elution fraction 1 than in the Strep purification alone. Therefore, this strategy resulted in an overall improvement of the purification protocol for PTEN. In an attempt to further enhance the purity of PTEN a size exclusion pre-purification step was included using Superdex 200 prep

grade. However, this strategy was not successful (not shown). Therefore, Strep+AIEX elution fraction 1 was used for further experiments.

4.2.2.1.2.2. INPP4B

INPP4B was expressed as Strep-fusion protein. To this end, INPP4B was cloned into pASG-IBA3 (INPP4B-Strep) or pASG-IBA5 (Strep-INPP4B) using the *Stargate* protocol. The verified (sequenced) vectors were then transformed into the expression strain *E. coli BL21(DE3)pLysSpREP4*. Expression was under the control of the inducible tet promotor system and induced by the addition of anhydrotetracycline (200 ng/mL) at RT. Bacteria were harvested in washing buffer (buffer W, 100 mM Tris/Cl, 150 mM NaCl, 1 mM EDTA, pH 8.0) and lysed by ultrasonication. The lysate was purified by *Strep-Tactin* affinity chromatography using *Strep-Tactin XT* resins due to their superiority over the classical *Strep-Tactin* material regarding capacity, washing stringency and binding strength. Following loading of the lysate to the resin, the resin was washed with 10 CV washing buffer (buffer W) and the protein was eluted using 0.6/1.6/0.8 CV elution buffer (buffer BXT, 100 mM Tris/Cl, 150 mM NaCl, 1 mM EDTA, 50 mM biotin, pH 8.0). The eluates were analysed by 10% SDS-PAGE and *Coomassie Brilliant Blue R-250* staining which is depicted in **fig. 86**. In addition, INPP4B expression was verified by Western Blot.
INPP4B expression was observed for both vectors used, however the elution fractions obtained for INPP4B-Strep showed a higher grade of purity. INPP4B-Strep E2 and E3 showed the highest grade of purity and were therefore pooled and used for further experiments.

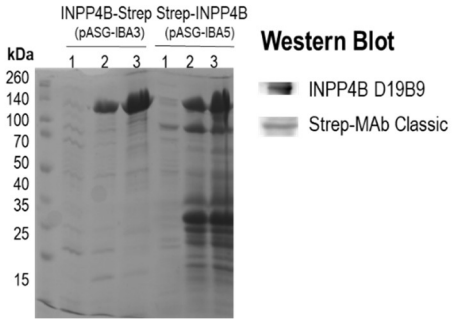

fig. 86: expression and purification of INPP4B. pASG-IBA3 INPP4B or pASG-IBA5 INPP4B was transformed into the expression strain *E. coli BL21(DE3)pLysSpREP4.* INPP4B was expressed as INPP4B-Strep or Strep-INPP4B under the control of the tet promotor for 3 hours at RT in a culture volume of 0.5 L and purified by *Strep-Tactin XT* affinity chromatography (0.2 mL CV). Elution was performed in three fractions (0.6/1.6/0.8 CV buffer BXT) and the elution fractions were analysed by 10% SDS and *Coomassie Brilliant Blue R-250* staining. INPP4B-Strep elution fractions 2 and 3 were pooled and INPP4B expression was verified by Western Blot using an INPP4B specific antibody and a Strep-tag specific antibody (Strep-Mab classic)

4.2.2.1.3. Expression and purification of PtdIns(3,4,5)P_3 and/or PtdIns(3,4)P_2 specific effector proteins

4.2.2.1.3.1. AKT1

AKT1 was expressed as Strep-fusion protein. To this end, AKT1 was cloned into pASG-IBA3 (AKT1-Strep) or pASG-IBA5 (Strep-AKT1) using the *Stargate* protocol. The verified (sequenced) vectors were then transformed into the expression strain *E.coli BL21(DE3)pLysSpREP4*. Expression was under the control of the inducible tet promotor system and induced by the addition of anhydrotetracycline (200 ng/mL) at RT. Bacteria were harvested in washing buffer (buffer W, 100 mM Tris/Cl, 150 mM NaCl, 1 mM EDTA, pH 8.0) and lysed by ultrasonication. The lysate was purified by *Strep-Tactin* affinity chromatography using *Strep-Tactin XT* resins due to their superiority over the classical *Strep-Tactin* material regarding capacity, washing stringency and binding strength. Following loading of the lysate to the resin, the resin was washed with 10 CV washing buffer (buffer W) and the protein was eluted using 0.6/1.6/0.8 CV elution buffer (buffer BXT, 100 mM Tris/Cl, 150 mM NaCl, 1 mM EDTA, 50 mM biotin, pH 8.0). The eluates were analysed by 10% SDS-PAGE and *Coomassie Brilliant Blue R-250* staining (not shown). No specific bands for AKT1 were detectable in the *Coomassie Brilliant Blue R-250* staining, however using the more sensitive Western Blot technique, eluates 2 and 3 stained weakly positive for anti-AKT1 C73H10 (not shown).
To enhance the solubility and yield of AKT1 expression was performed for 20 h at 12°C. Bacteria were harvested, lysed by ultrasonication and the lysate was utilized for *Strep-Tactin XT* purification as described above. The eluates were analysed by 10% SDS-PAGE and *Coomassie Brilliant Blue R-250* staining which is depicted in **fig. 87**. In addition, AKT1 expression was verified by Western Blot using the AKT1 specific antibody AKT1 C73H10 and a Strep-tag specific antibody.

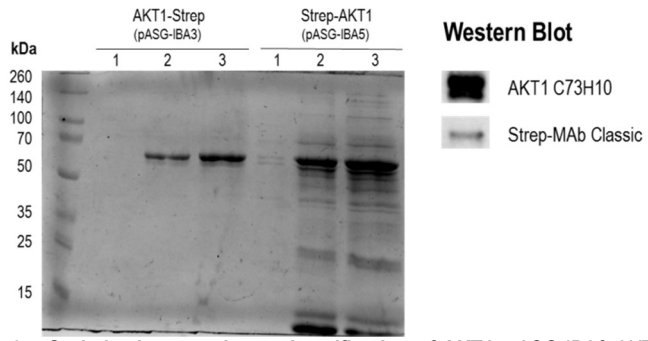

fig. 87: Optimized expression and purification of AKT1. pASG-IBA3 AKT1 or pASG-IBA5 AKT1 was transformed into the expression strain *E. coli BL21(DE3)pLysSpREP4.* AKT1 was expressed as AKT1-Strep or Strep-AKT1 under the control of the tet promotor for 20 hours at 12°C in a culture volume of 0.5 L and purified by *Strep-Tactin XT* affinity chromatography (0.2 mL CV). Elution was performed in three fractions (0.6/1.6/0.8 CV buffer BXT) and the elution fractions were analysed by 10% SDS and *Coomassie Brilliant Blue R-250* staining. AKT1-Strep elution fractions 2 and 3 were pooled and AKT1 expression was verified by Western Blot using AKT1 C73H10 monoclonal antibody and a Strep-tag specific antibody (Strep-Mab classic).

Specific bands were detected for both constructs; however, AKT1-Strep eluates were found to be significantly purer and therefore were used for further experiments.

4.2.2.1.3.2. VAV1

VAV1 was expressed as Strep-fusion protein. To this end, VAV1 was cloned into pASG-IBA3 (VAV1-Strep) or pASG-IBA5 (Strep-VAV1) using the *Stargate* protocol. The verified (sequenced) vectors were then transformed into the expression strain *E. coli BL21(DE3)pLysSpREP4*. Expression was under the control of the inducible tet promotor system and induced by the addition of anhydrotetracycline (200 ng/mL) at RT. Bacteria were harvested in washing buffer (buffer W, 100 mM Tris/Cl, 150 mM NaCl, 1 mM EDTA, pH 8.0) and lysed by ultrasonication. The lysate was purified by *Strep-Tactin* affinity chromatography using *Strep-Tactin XT* resins due to their superiority over the classical *Strep-Tactin* material regarding capacity, washing stringency and binding strength. Following loading of the lysate to the resin, the resin was washed with 10 CV washing buffer (buffer W) and the protein was eluted using 0.6/1.6/0.8 CV elution buffer (buffer BXT, 100 mM Tris/Cl, 150 mM NaCl, 1 mM EDTA, 50 mM biotin, pH 8.0). The eluates were analysed by 10% SDS-PAGE and *Coomassie Brilliant Blue R-250* staining which is depicted in **fig. 88** In addition, VAV1 expression was verified by Western Blot.

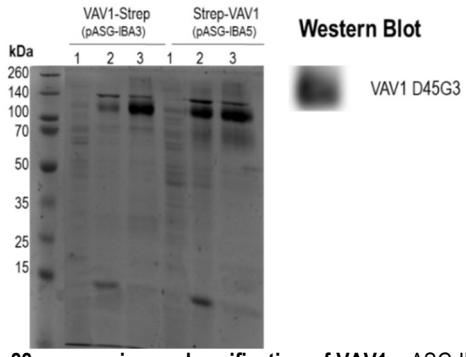

fig. 88: expression and purification of VAV1. pASG-IBA3 VAV1 or pASG-IBA5 VAV1 was transformed into the expression strain *E coli BL21(DE3)pLysSpREP4.* VAV1 was expressed as VAV1-Strep or Strep-VAV1 under the control of the tet promotor for 3 hours at RT in a culture volume of 0.5 L and purified by *Strep-Tactin XT* affinity chromatography (0.2 mL CV). Elution was performed in three fractions (0.6/1.6/0.8 CV buffer BXT) and the elution fractions were analysed by 10% SDS and *Coomassie Brilliant Blue R-250* staining. VAV1-Strep elution fractions 2 and 3 were pooled and VAV1 expression was verified by Western Blot using a VAV1 specific antibody.

VAV1 expression was observed for both vectors used, however the elution fractions obtained for VAV1-Strep showed a higher grade of purity. As VAV1-Strep E3 showed the highest grade of purity it was selected for further experiments.

4.2.2.1.3.3. P-REX1

P-REX1 was expressed as Strep-fusion protein. To this end, P-REX1 was cloned into pASG-IBA3 (P-REX1-Strep) or pASG-IBA5 (Strep-P-REX1) using the *Stargate* protocol. The verified (sequenced) vectors were then transformed into the expression strain *E. coli BL21(DE3)pLysSpREP4*. Expression was under the control of the

inducible tet promotor system and induced by the addition of anhydrotetracycline (200 ng/mL) at RT. Bacteria were harvested in washing buffer (buffer W, 100 mM Tris/Cl, 150 mM NaCl, 1 mM EDTA, pH 8.0) and lysed by ultrasonication. The lysate was purified by *Strep-Tactin* affinity chromatography using *Strep-Tactin XT* resins due to their superiority over the classical *Strep-Tactin* material regarding capacity, washing stringency and binding strength. Following loading of the lysate to the resin, the resin was washed with 10 CV washing buffer (buffer W) and the protein was eluted using 0.6/1.6/0.8 CV elution buffer (buffer BXT, 100 mM Tris/Cl, 150 mM NaCl, 1 mM EDTA, 50 mM biotin, pH 8.0). The eluates were analysed by 10% SDS-PAGE and *Coomassie Brilliant Blue R-250* staining which is depicted in **fig. 89**. In addition, P-REX1 expression was verified by Western Blot.

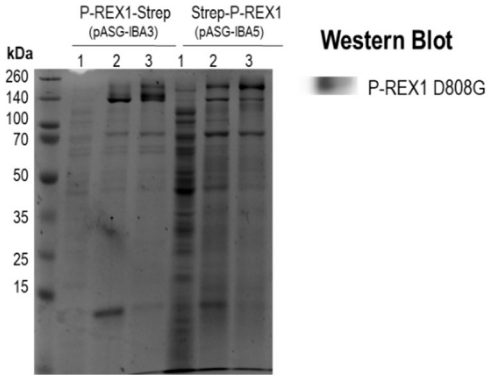

fig. 89: expression and purification of P-REX1. pASG-IBA3 P-REX1 or pASG-IBA5 P-REX1 was transformed into the expression strain *E coli BL21(DE3)pLysSpREP4.* P-REX1 was expressed as P-REX1-Strep or Strep-P-REX1 under the control of the tet promotor for 3 hours at RT in a culture volume of 0.5 L and purified by *Strep-Tactin XT* affinity chromatography (0.2 mL CV). Elution was performed in three fractions (0.6/1.6/0.8 CV buffer BXT) and the elution fractions were analysed by 10% SDS and *Coomassie Brilliant Blue R-250* staining. P-REX1-Strep elution fractions 2 and 3 were pooled and P-REX1 expression was verified by Western Blot using a P-REX1 specific antibody.

P-REX1 expression was observed for both vectors used, however the elution fractions obtained for P-REX1-Strep showed a higher grade of purity. As P-REX1-Strep E3 showed the highest grade of purity it was selected for further experiments.

4.2.2.1.3.4. TAPP1

TAPP1 was expressed as Strep-fusion protein. To this end, TAPP1 was cloned into pASG-IBA3 (TAPP1-Strep) or pASG-IBA5 (Strep-TAPP1) using the *Stargate* protocol. The verified (sequenced) vectors were then transformed into the expression strain *E. coli BL21(DE3)pLysSpREP4*. Expression was under the control of the inducible tet promotor system and induced by the addition of anhydrotetracycline (200 ng/mL) at RT. Bacteria were harvested in washing buffer (buffer W, 100 mM Tris/Cl, 150 mM NaCl, 1 mM EDTA, pH 8.0) and lysed by ultrasonication. The lysate was purified by *Strep-Tactin* affinity chromatography using *Strep-Tactin XT* resins due to their superiority over the classical *Strep-Tactin* material regarding capacity, washing stringency and binding strength. Following loading of the lysate to the resin, the resin was washed with 10 CV washing buffer (buffer W) and the protein was eluted using 0.6/1.6/0.8 CV elution buffer (buffer BXT, 100 mM Tris/Cl, 150 mM NaCl, 1 mM EDTA, 50 mM biotin, pH 8.0). The eluates were analysed by 10% SDS-PAGE and *Coomassie Brilliant Blue R-250* staining which is depicted in **fig. 90**. In addition, TAPP1 expression was verified by Western Blot.
TAPP1 expression was observed only in the case of Strep-TAPP1 however with significant impurities. It was tried to express TAPP1-Strep where a higher grade of purity was expected (see other proteins) over night at 12°C, however expression was still not observed. Next, it was aimed to use a post-purification step of Strep-TAPP1 E2 and E3 applying AIEX as described for PTEN. However, no binding to the AIEX resin could be observed. In the end, Strep-elution fraction E2 was used for further experiments as it was slightly purer than E3.

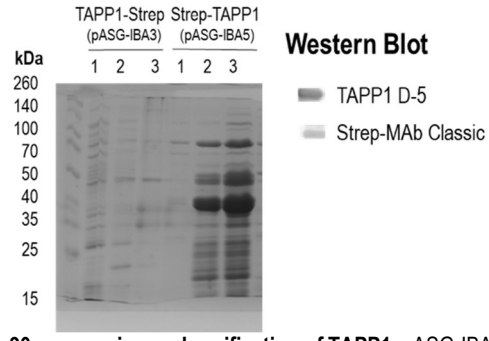

fig. 90: expression and purification of TAPP1. pASG-IBA3 TAPP1 or pASG-IBA5 TAPP1 was tranformed into the expression strain *E coli BL21(DE3)pLysSpREP4.* TAPP1 was expressed as TAPP1-Strep or Strep-TAPP1 under the control of the tet promotor for 3 hours at RT in a culture volume of 0.5 L and purified by *Strep-Tactin XT* affinity chromatography (0.2 mL CV). Elution was performed in three fractions (0.6/1.6/0.8 CV buffer BXT) and the elution fractions were analysed by 10% SDS and *Coomassie Brilliant Blue R-250* staining. TAPP1-Strep elution fractions 2 and 3 were pooled and TAPP1 expression was verified by Western Blot using a TAPP1 specific antibody and a Strep-tag specific antibody (Strep-Mab classic).

4.2.2.1.3.5. TAPP2

TAPP2 was expressed as Strep-fusion protein. To this end, TAPP2 was cloned into pASG-IBA3 (TAPP2-Strep) or pASG-IBA5 (Strep-TAPP2) using the *Stargate* protocol. The verified (sequenced) vectors were then transformed into the expression strain *E.coli BL21(DE3)pLysSpREP4*. Expression was under the control of the inducible tet promotor system and induced by the addition of anhydrotetracycline (200 ng/mL) at RT. Bacteria were harvested in washing buffer (buffer W, 100 mM Tris/Cl, 150 mM NaCl, 1 mM EDTA, pH 8.0) and lysed by ultrasonication. The lysate was purified by *Strep-Tactin* affinity chromatography using *Strep-Tactin XT* resins due to their superiority over the classical *Strep-Tactin* material regarding capacity, washing stringency and binding strength. Following loading of the lysate to the resin, the resin was washed with 10 CV washing buffer (buffer W) and the protein was eluted using 0.6/1.6/0.8 CV elution buffer (buffer BXT, 100 mM Tris/Cl, 150 mM NaCl, 1 mM EDTA, 50 mM biotin, pH 8.0). The eluates were analysed by 10% SDS-PAGE and *Coomassie Brilliant Blue R-250* staining which is depicted in **fig. 91**. In addition, TAPP2 expression was verified by Western Blot.
TAPP2 expression was observed for both vectors used, however the elution fractions obtained for Strep-TAPP1 showed a higher grade of purity. As TAPP2-Strep E2 showed the highest grade of purity it was selected for further experiments.

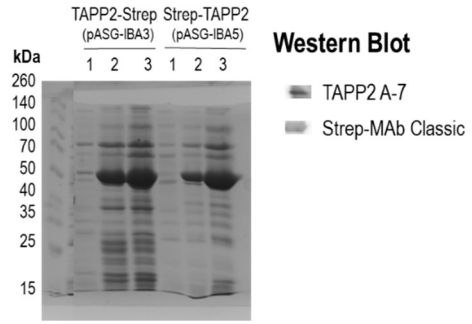

fig. 91: expression and purification of TAPP2. pASG-IBA3 TAPP2 or pASG-IBA5 TAPP2 was transformed into the expression strain *E. coli BL21(DE3)pLysSpREP4.* TAPP2 was expressed as TAPP2-Strep or Strep-TAPP2 under the control of the tet promotor for 3 hours at RT in a culture volume of 0.5 L and purified by *Strep-Tactin XT* affinity chromatography (0.2 mL CV). Elution was performed in three fractions (0.6/1.6/0.8 CV buffer BXT) and the elution fractions were analysed by 10% SDS and *Coomassie Brilliant Blue R-250* staining. TAPP2-Strep elution fractions 2 and 3 were pooled and TAPP2 expression was verified by Western Blot using a TAPP2 specific antibody and a Strep-tag specific antibody (Strep-Mab classic).

4.2.2.2. SPR (Surface Plasmon Resonance)

Surface Plasmon Resonance was used to determine the affinity of expressed and purified SHIP1 proteins (SHIP1 WT, SHIP1 E452K and SHIP1 R673Q), effector proteins and phosphoinositide phosphatases towards PtdIns(3,4)P_2 and/or PtdIns(3,4,5)P_3. The results are already published in [1041]. Lipid monolayers containing either one of the two phosphoinositides or a control surface were used as a ligand and the proteins of choice were used as analytes in appropriate concentration ranges. As can be seen in **fig. 92-97** and summarized in **table 13** all proteins showed specific binding (K_D values in the nM range) towards their respective binding partner with the exception of binding

of VAV1 and P-REX1 to PtdIns(3,4,5)P_3 which was in accordance with results from other groups showing that PtdIns(3,4,5)P_3 specific GEFs displayed low affinity towards PtdIns(3,4,5)P_3. Especially, the affinity of AKT1 and PTEN towards both phosphoinositides (K_D value in the pM range), of INPP4B towards both phosphoinositides (K_D values in the sub-nM range) and of TAPP1 and SHIP1 E452K towards PtdIns(3,4)P_2 (K_D values in the sub-nM or pM range) was remarkable. The order of K_D values was

- P-REX1>>>VAV1>>>SHIP1 E452K=SHIP1 R673Q>SHIP1 WT>INPP4B>>PTEN>>AKT1 for PtdIns(3,4,5)P_3
- SHIP1 WT=SHIP1 R673Q>TAPP2>>TAPP1=INPP4B>>SHIP1 E452K>AKT1>>PTEN for PtdIns(3,4)P_2

No specific binding was observed when control surfaces were used.

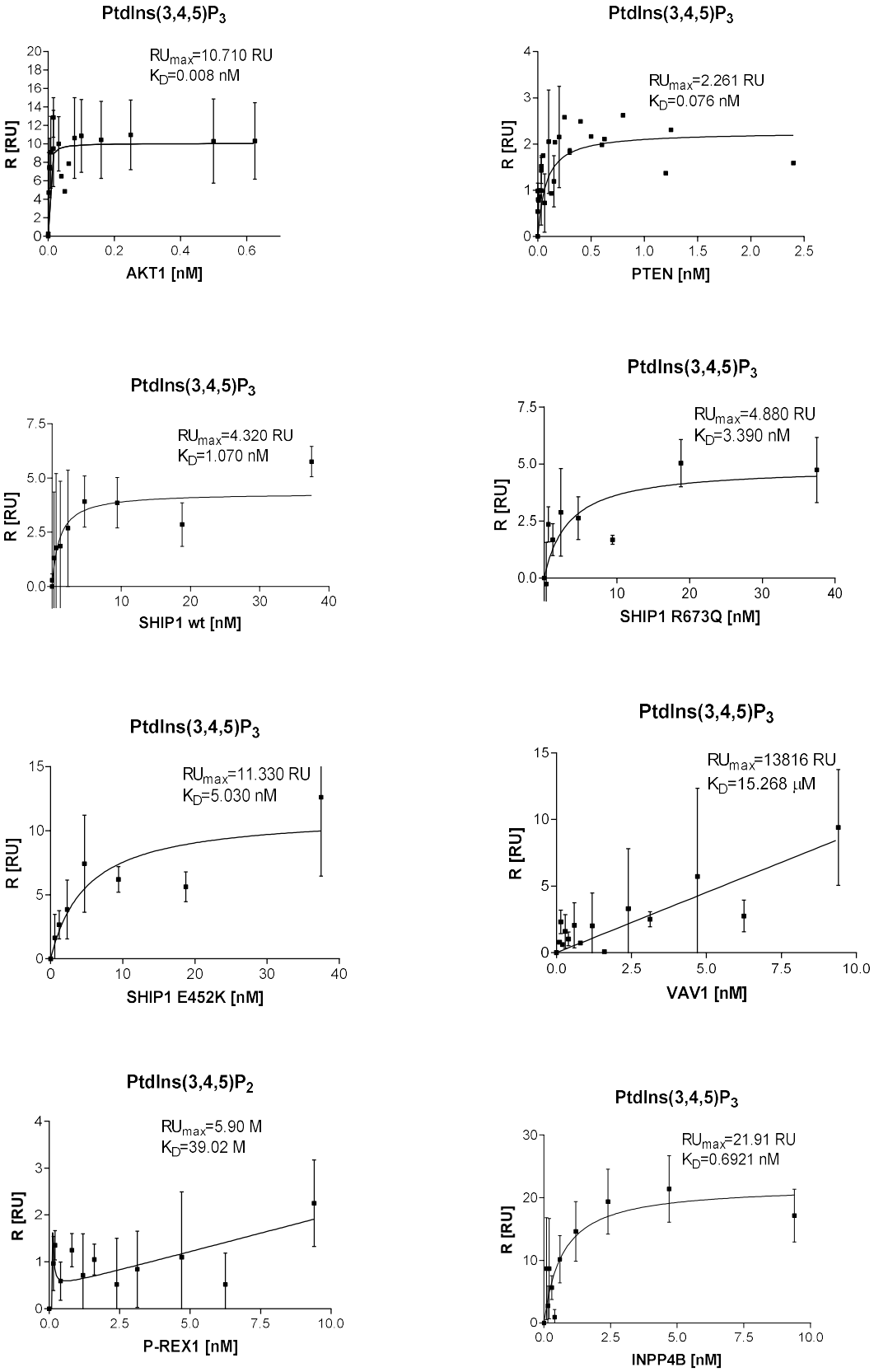

fig. 92: Surface Plasmon Resonance (SPR) analysis of the affinity of phosphoinositide binding proteins towards PtdIns(3,4,5)P_3. Lipid monolayers containing PtdIns(3,4,5)P_3 or a control surface were used as a ligand and the proteins of choice were used as analytes in appropriate concentration ranges. Measurements were performed at the MASS-1 (Sierra Sensors). For calculation of K_D values measured RU values were plotted against the concentration of the analyte and fitted by hyperbolic regression. Error bars indicate standard deviations. n=3.

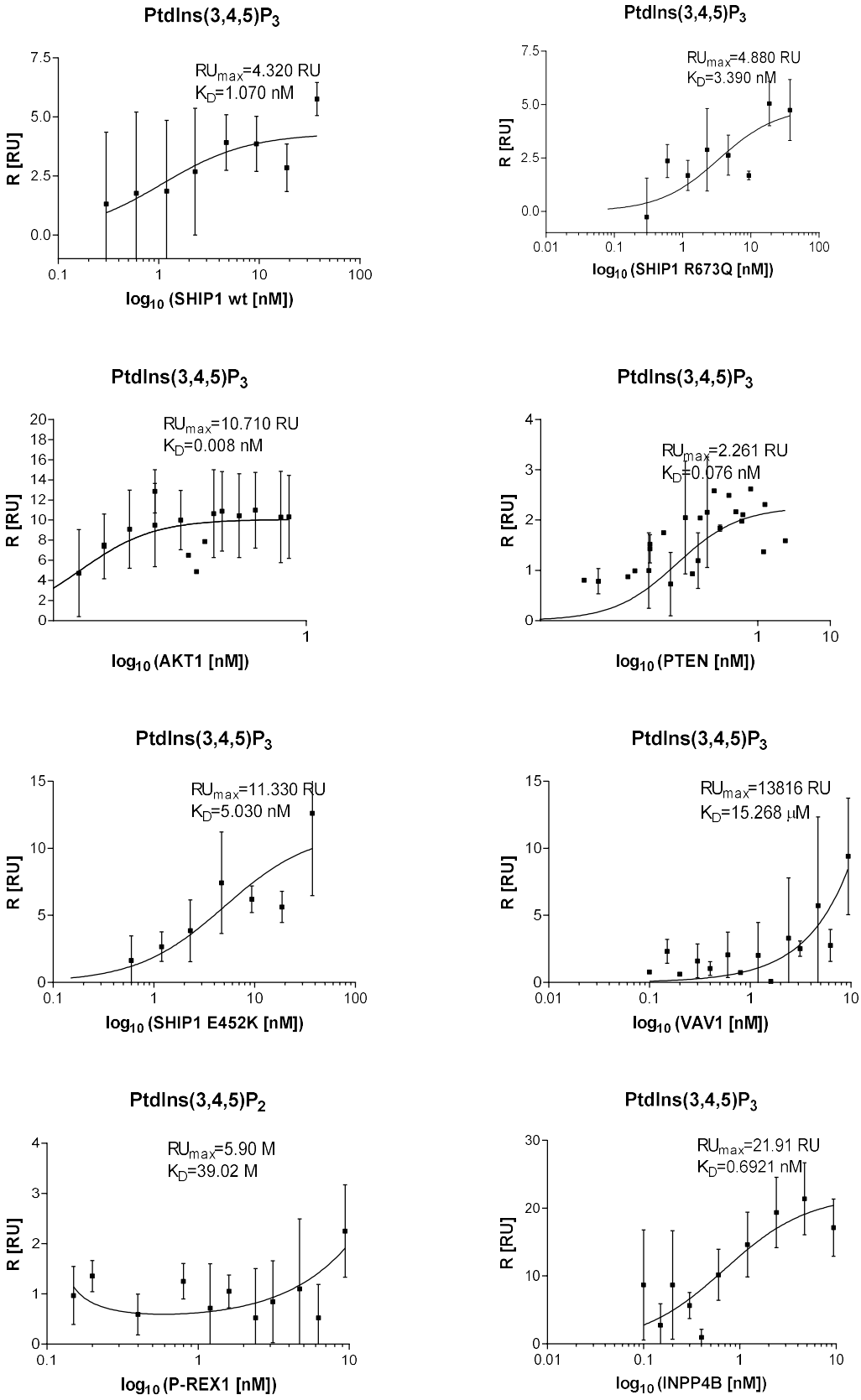

fig. 93: Surface Plasmon Resonance (SPR) analysis of phosphoinositide binding proteins towards PtdIns(3,4,5)P_3 (log_{10} representation). Lipid monolayers containing PtdIns(3,4,5)P_3 or a control surface were used as a ligand and the proteins of choice were used as analytes in appropriate concentration ranges. Measurements were performed at the MASS-1 (Sierra Sensors). For calculation of K_D values measured RU values were plotted against the concentration of the analyte and fitted by hyperbolic regression. The log_{10} representation is shown. Error bars indicate standard deviations. n=3 [1041].

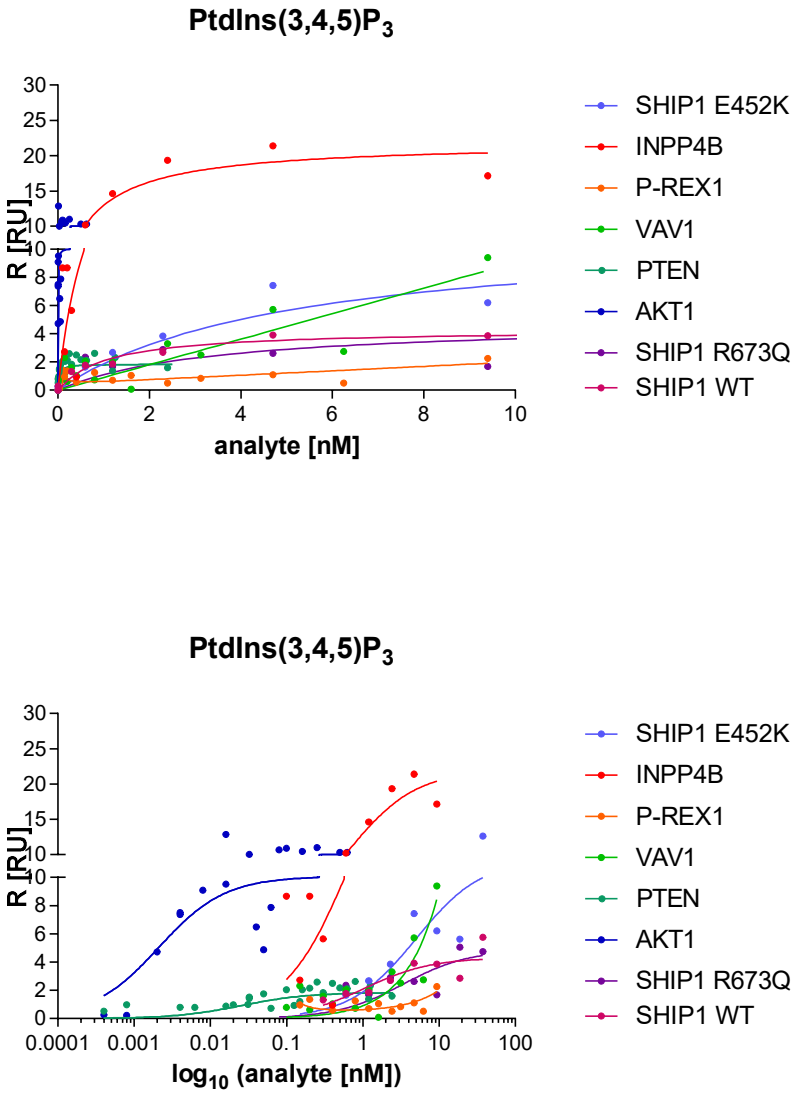

fig. 94: Surface Plasmon Resonance (SPR) analysis of phosphoinositide binding proteins, comparison of PtdIns(3,4,5)P_3 binding. Lipid monolayers containing PtdIns(3,4,5)P_3 or a control surface were used as a ligand and the proteins of choice were used as analytes in appropriate concentration ranges. Measurements were performed at the MASS-1 (Sierra Sensors). The log_{10} representation and the normal x-axis representation is shown n=3, due to clarity reasons error bars are not shown.

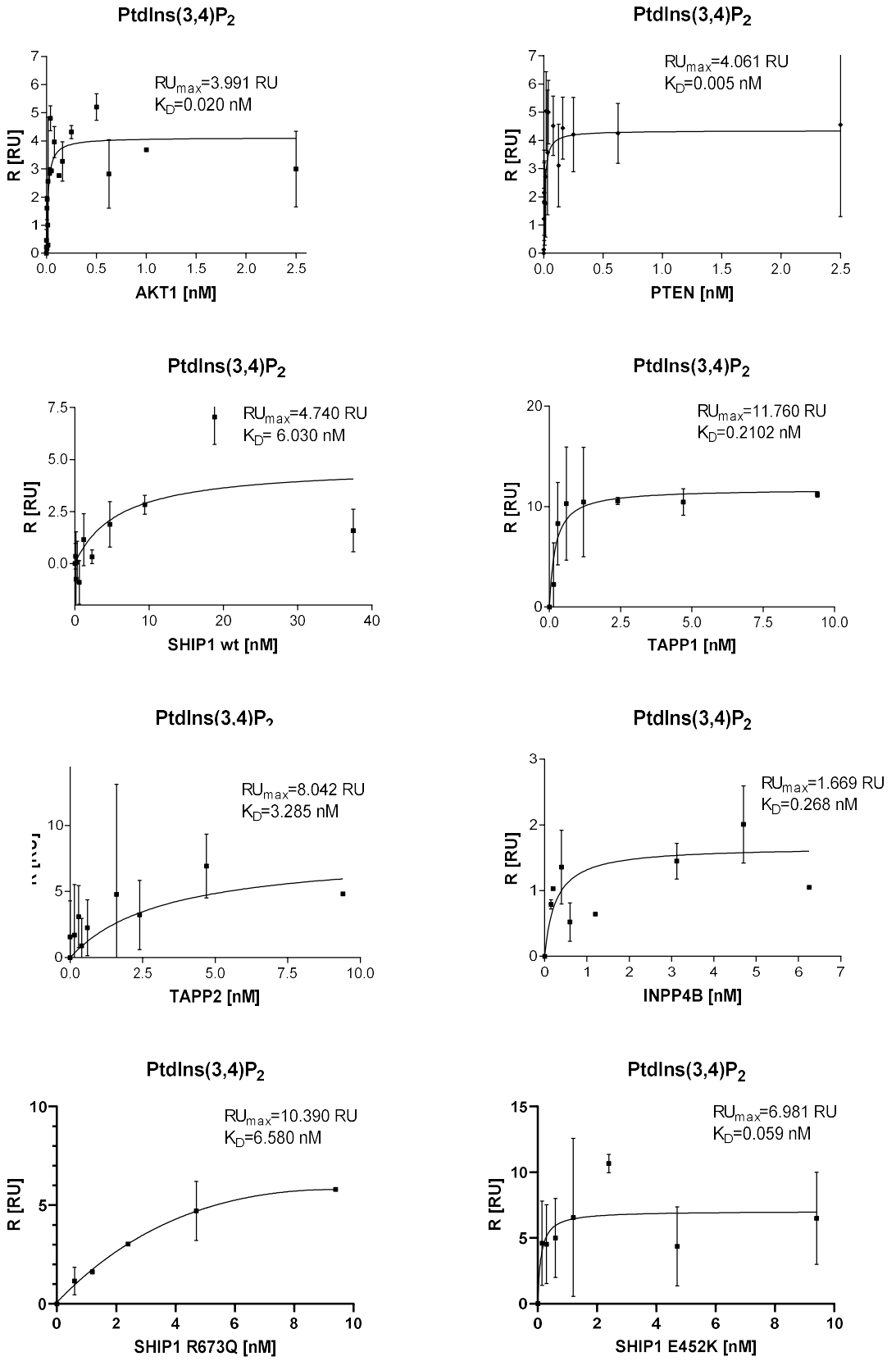

fig. 95: Surface Plasmon Resonance (SPR) analysis of phosphoinositide binding proteins towards PtdIns(3,4)P_2. Lipid monolayers containing PtdIns(3,4)P_2 or a control surface were used as a ligand and the proteins of choice were used as analytes in appropriate concentration ranges. Measurements were performed at the MASS-1 (Sierra Sensors). For calculation of K_D values measured RU values were plotted against the concentration of the analyte and fitted by hyperbolic regression. Error bars indicate standard deviations. n=3.

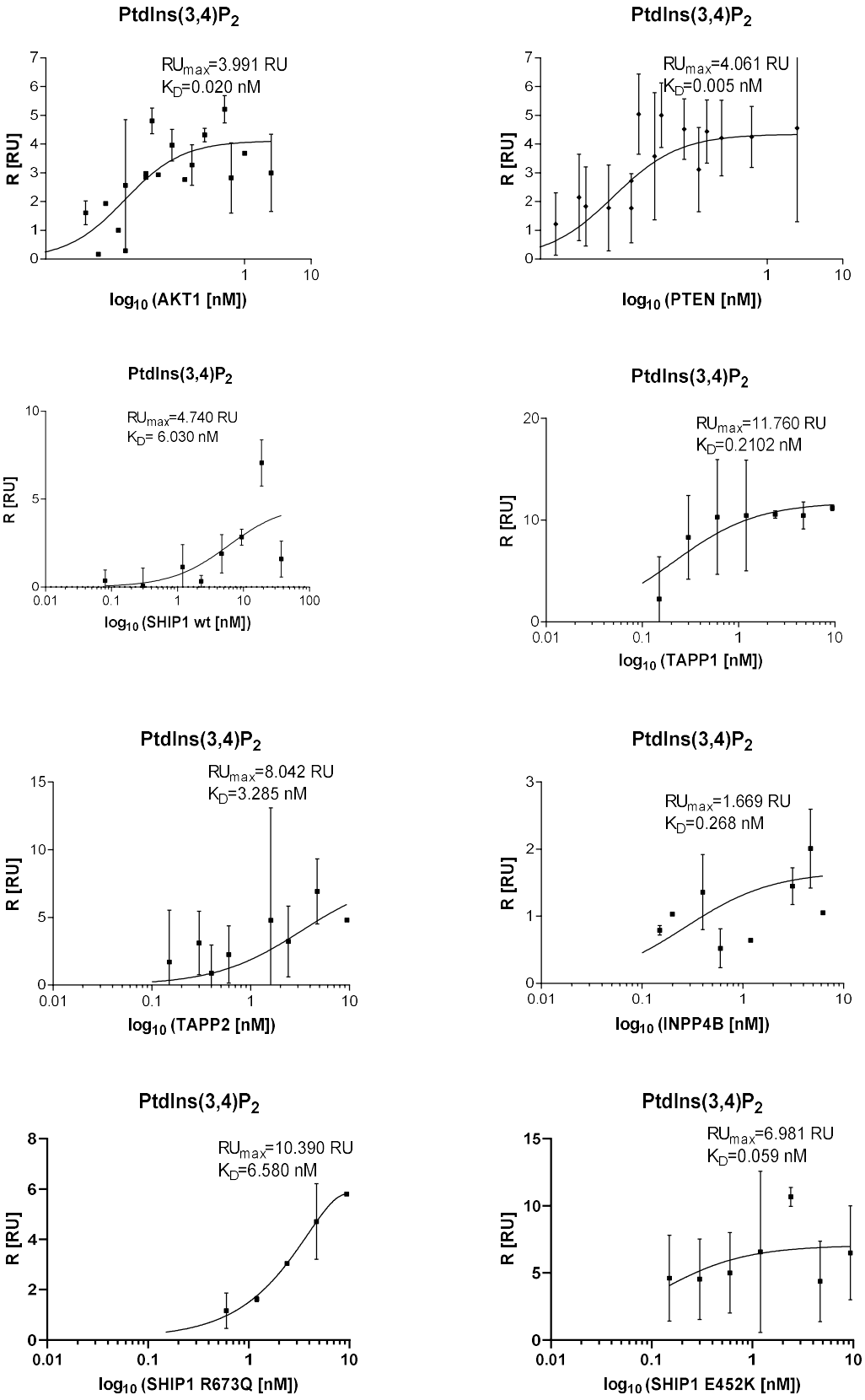

fig. 96: Surface Plasmon Resonance (SPR) analysis of phosphoinositide binding proteins towards PtdIns(3,4)P_2 (log_{10} representation). Lipid monolayers containing PtdIns(3,4)P_2 or a control surface were used as a ligand and the proteins of choice were used as analytes in appropriate concentration ranges. Measurements were performed at the MASS-1 (Sierra Sensors). For calculation of K_D values measured RU values were plotted against the concentration of the analyte and fitted by hyperbolic regression. The log_{10} representation is shown. Error bars indicate standard deviations. n=3 [1041].

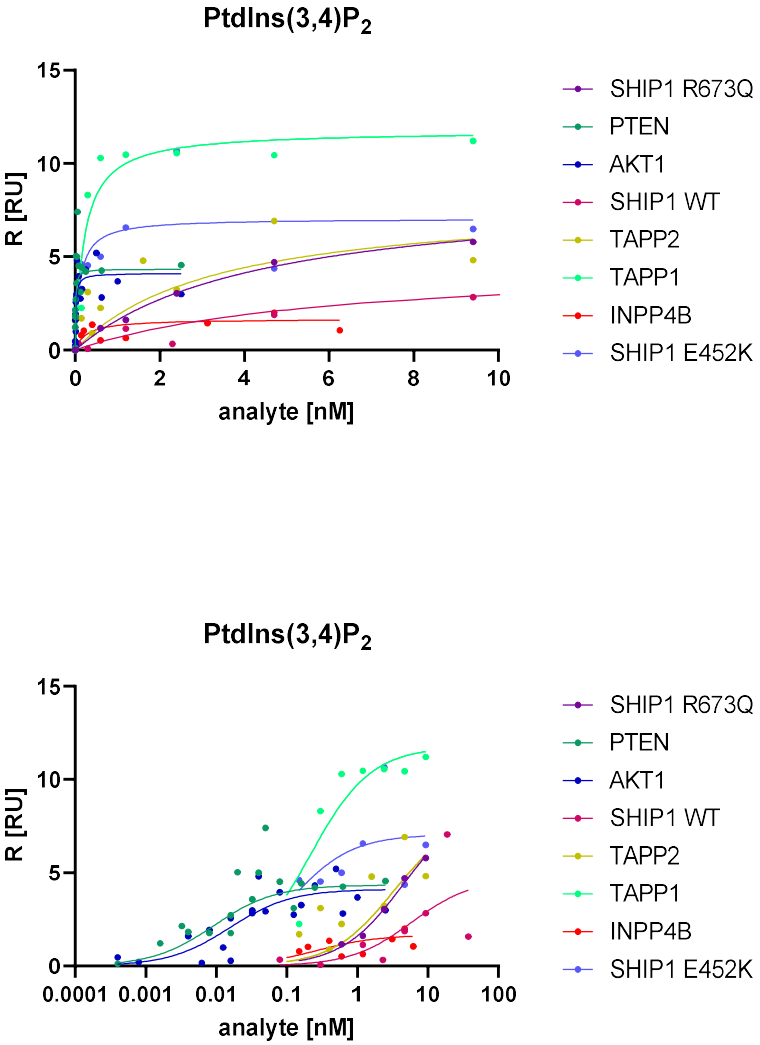

fig. 97: Surface Plasmon Resonance (SPR) analysis of phosphoinositide binding proteins, comparison of PtdIns(3,4)P_2 binding. Lipid monolayers containing PtdIns(3,4)P_2 or a control surface were used as a ligand and the proteins of choice were used as analytes in appropriate concentration ranges. Measurements were performed at the MASS-1 (Sierra Sensors). The $\log_{10}$ representation and the normal x-axis representation is shown n=3, due to clarity reasons error bars are not shown.

Table 13: Surface Plasmon Resonance (SPR) analysis of phosphoinositide binding proteins, overview of measured K_D values towards PtdIns(3,4,5)P_3 and PtdIns(3,4)P_2 . Lipid monolayers containing PtdIns(3,4,5)P_3 or PtdIns(3,4)P_2 or a control surface were used as a ligand and the proteins of choice were used as analytes in appropriate concentration ranges. Measurements were performed at the MASS-1 (Sierra Sensors). For calculation of K_D values measured RU values were plotted against the concentration of the analyte and fitted by hyperbolic regression. Errors indicate standard deviations. n=3 [1041].

	K_D(PtdIns(3,4,5)P_3) [nM]	K_D(PtdIns(3,4)P_2) [nM]
SHIP1 wt	1.070±1.302	6.030±6.455
SHIP1 R673Q	3.390±3.042	6.580±5.156
SHIP1 E452K	5.030±2.842	0.059±0.072
AKT1	0.008±0.003	0.020±0.008
PTEN	0.076±0.060	0.005±0.004
P-REX1	$3.09x10^{10}$±$1.789x10^{9}$	n.d.
INPP4B	0.6921±0.1892	0.2697±0.1621
TAPP1	n.d.	0.2102±0.06261
TAPP2	n.d.	3.285±3.687
VAV1	$15.268x10^{3}$±$1.896x10^{3}$	n.d.

In conclusion, these findings pointed at a possible trapping function of SHIP1 E452K in the case of PtdIns(3,4)P_2 in PTEN deficient tumours (K_D (SHIP1 E452K) around 50 times lower than for the active phosphatase INPP4B).

4.2.2.3. Determination of the membrane/cytosol ratio of phosphoinositide binding protein in H1299 SHIP1 WT, SHIP1 E452K, SHIP1 R673Q and LeGO-approaching the phosphoinositide trapping model in cells

As an approach to access the phosphoinositide trapping model in a cellular context the membrane-to-cytosol ratio of selected phosphoinositide binding proteins was determined in H1299 cells transduced with SHIP1 WT, SHIP1 E452K, R673Q or a LeGO control using differential centrifugation and Western Blot analysis which is shown in **fig. 98**.

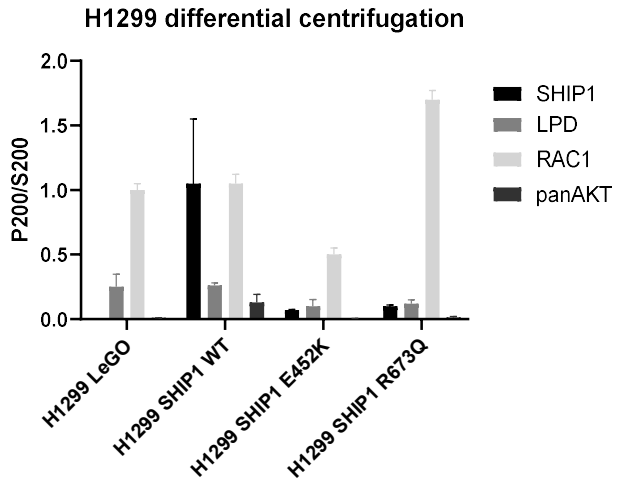

fig. 98: analysis of the membrane-to-cytosol ratio of selected phosphoinositide-binding proteins. H1299 cells were lysed and the membrane (P200) and cytosolic (S200) fractions were separated by differential centrifugation at 200000 g. P200 and S200 were analysed by Western Blot and the P200/S200 ratios were calculated. Error bars indicate standard deviations. n=3

As can be seen SHIP1 WT distributed equally to the membrane and cytosol whereas both SHIP1 mutants showed highly reduced membrane distribution (P200/S200=0.07 for SHIP1 E452K and 0.1 for SHIP1 R673Q) underlining that phosphoinositide binding affinity is not the only variable determining the actual recruitment of SHIP1 proteins to cellular membranes. LPD membrane recruitment was reduced for both SHIP1 E452K and R673Q compared to SHIP1 WT and the LeGO control cells and RAC membrane levels were reduced in H1299 SHIP1 E452K and enhanced in H1299 SHIP1 R673Q. In H1299 SHIP1 WT and LeGO RAC1 was equally distributed over the membrane and cytosol whereas it was enriched in the cytosol in H1299 SHIP1 E452K and enriched in the membrane fraction in H1299 SHIP1 R673Q. panAKT levels were relatively low in the membrane fractions displaying that only phosphorylated AKT is recruited to membranes but in relation to the other cell lines its membrane-fraction was enriched in H1299 SHIP1 WT.
In summary, reflecting the SPR and biochemical data of SHIP1 proteins it should be expected that PtdIns(3,4)P_2 would be enriched in H1299 SHIP1 E452K due to the trapping effect and PtdIns(3,4,5)P_3 levels should be highest in H1299 SHIP1 R673Q (inactive) and H1299 LeGO (no SHIP1) with implications to the PtdIns(3,4)P_2-dependent (RAC1, AKT, LPD) or PtdIns(3,4,5)P_3-dependent (RAC1, AKT) recruitment of phosphoinositide binding proteins. However, this is only poorly reflected in the P200/S200 ratios measured indicating that in the cellular context phosphoinositide binding is more complex than only measuring K_D values in isolation (see discussion section).

4.3. The phosphoinositide binding and catalysis of SHIP1 is dictated by conserved residues of the PH-L, PPase and C2 domain which is reflected at the structural and biochemical level

4.3.1. Computational structure prediction

4.3.1.1. Catalytic domain

4.3.1.1.1. Model building

The structure of the catalytic domain of SHIP1 was not solved at the beginning of the project, however several highly homologous structures of the 5-phosphatase domain belonging to related phosphoinositide-5-phosphatases (i.e. SHIP2) were available in the PDB. Therefore, the SHIP1 catalytic domain was a promising candidate for homology-based modelling.

A model of SHIP1 was built with *Maestro 11* based on homology-modelling (MSA and model building based on MSA and physical constraints) using models 4A9C_A (SHIP2 PPase-C2) or 4A9C_B (SHIP2 PPase-C2 bound to biphenyl 2,3',4,5',6- pentakisphosphate) as a template. This is shown in **fig. 99**.

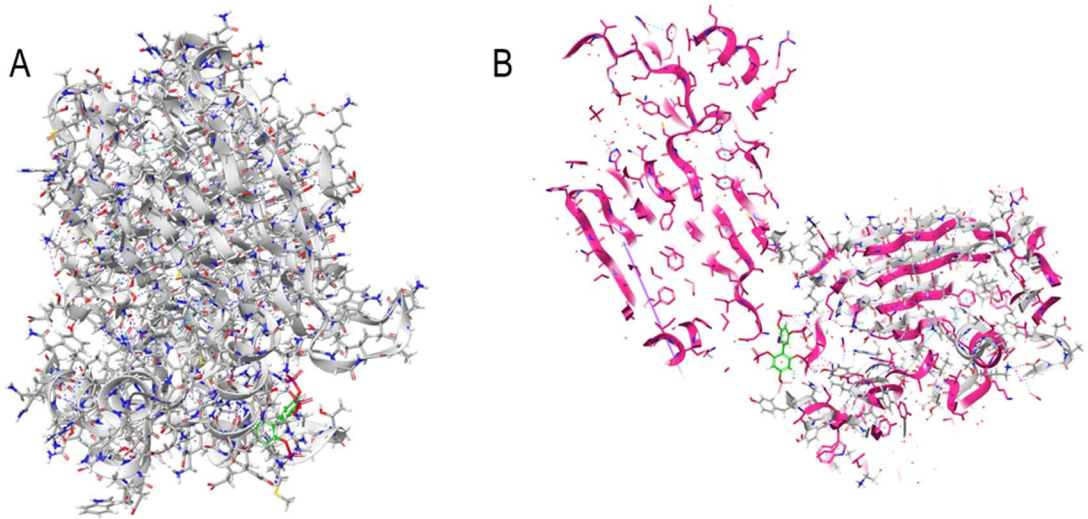

fig. 99: Homology modelling of the SHIP1 catalytic domain, model generation based on 4A9C (SHIP2 PPase-C2). Panel A shows the model generated by *Maestro 11* (light grey) and panel B shows the model superposed to 4A9C (in magenta)

In order to evaluate the generated model some considerations regarding the experimental data of the template structure have to be taken into account as shown in **fig. 100** and discussed below.

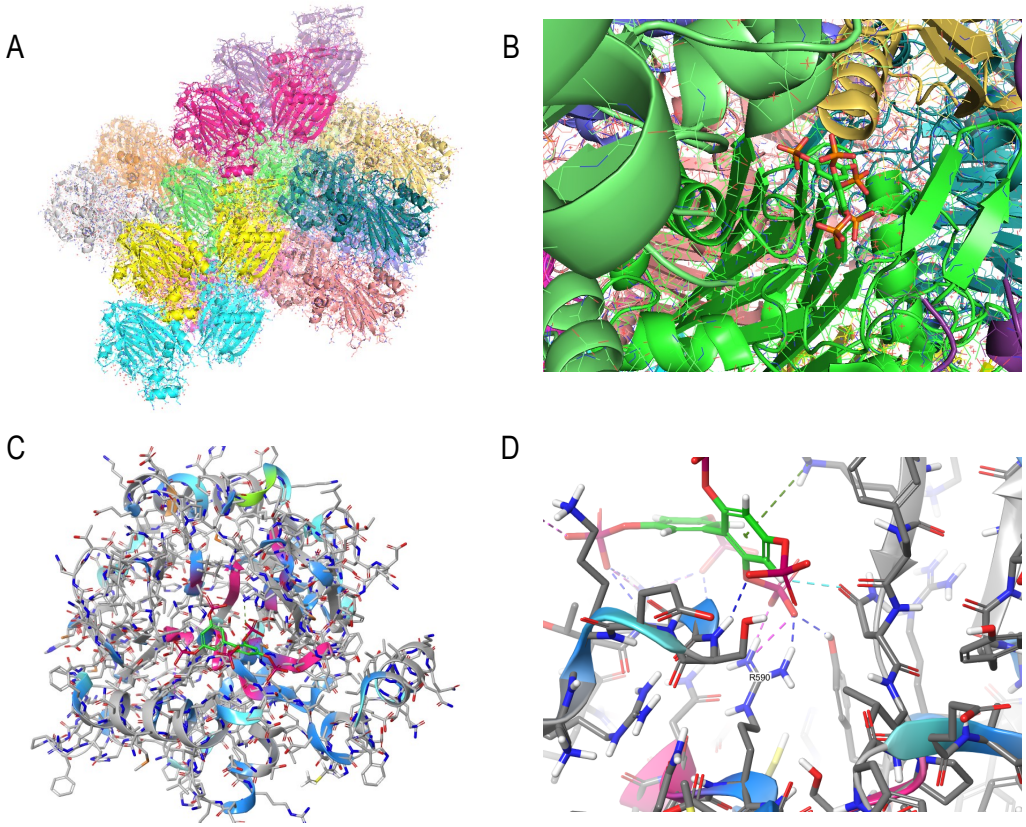

fig. 100: Homology modelling of the SHIP1 catalytic domain, general considerations with regard to the template structure 4A9C. Panel A shows the individual unit cells of the crystal structure of 4A9C and panel B shows a more detailed view regarding the positioning of the ligand in-between the unit cells (generated in Pymol). Panels C and D depict the SHIP1 PPase domain model in light grey. The ligand biphenyl 2,3',4,5',6- pentakisphosphate derived from 4A9C_B is coloured in green, conserved motifs are coloured in magenta and patient-derived mutations are coloured in blue (substitutions), turquoise (silent mutations) or light green (nonsense mutations) (generated in *Maestro 11)*.

As shown for structure 4A9C_B (**fig. 100A/B**) and the respective homology-model of the SHIP1 catalytic domain (**fig. 100C/D**) in the template structure 4A9C_B, the ligand was inserted in-between several bordering unit cells of the crystal which might have influenced its positioning in the final model (i.e. via electrostatic attractions and repulsions or some types of non-covalent contacts with residues from bordering unit cells). Such effects are vital to keep in mind when evaluating protein-ligand interactions. The substrate binding pocket was identified as a loop-rich region. Therefore, it is probably flexible and ligand binding might depend on an induced-fit model rather than some type of rigid binding mode. The conserved motifs (**table 14**) identified in phosphoinositide-5-phosphatases (coloured in magenta) and several of the patient-derived mutations derived from the COSMIC database [619] were in proximity to the ligand, however not making direct contact with the exception of R590. A structural role for the remaining residues can be proposed due to their positioning within the ligand binding pocket or secondary structures comprising residues which directly contact the ligand i.e. by interacting with crucial residues and thus stabilizing their positioning or by dictating the exact positioning of the before-mentioned secondary structures. In addition, the Mg^{2+} ion necessary for catalysis was not co-crystallized in this structure and some residues might be involved in Mg^{2+} binding/catalysis (i.e. D699 or E452).

Table 14: Conserved motifs within the PPase domain of phosphoinositide-5-PPases (according to Zhang et al., 2009) [1042]). Motifs in SHIP1 were identified by Multiple Sequence Alignment.

Conserved motif according to [1042]	**Full motif sequence in SHIP1**	**Starting position of motif in SHIP1**
GDXNXR	GDLNYR	585
PXWXDR	PSWCDR	668
GXQE	GTQE	449
SDHXPV	SDHSPV	698
NXH	(NKH or) NSH[a]	(392 or) 538[a]
TWN	TWN	409

[a] Respectively. In this case, NSH at position 538 is more likely based on the relative order of the motifs in the protein sequence, i.e. it is after GXQE but before PXWXDR.

In addition, the sequence of the SHIP1 catalytic domain was sent to several freely accessible webservers for model building (CPH-models, FFAS-3D, FFAS-03, GENO3D, HHSEARCH, MUSTER, Neff-PPAS, pGenTHREADER, Phyre2, PRC, PROSPECT, RaptorX, SP3, SPARKS-X, Swissmodel). These webservers mainly relied on homology-modelling, in some cases supplemented with threading or *ab initio*/energy-based approaches. Opposed to *Maestro 11* multiple templates were used for model building in most cases. The overall structure of the generated models did not significantly differ and given that the catalytic domain of phosphoinositide-5-phosphatases is highly conserved this was expectable. However, differences were clearly visible in more flexible parts of the protein (i.e. loops) and most importantly, these loops were frequently part of conserved motifs or the substrate binding pocket (not shown). Because of this (and the possible influence of crystal units on each other as discussed above) the results obtained have to be evaluated with a certain amount of uncertainty and care.
A crystal structure of SHIP1 PPase-C2 was deposited into the PDB (PDB 6IBD) during the course of the thesis and was utilized in later parts of the structure analysis (see below).

4.3.1.1.2. Mechanisms of substrate recognition and catalysis based on biphenyl 2,3',4,5',6- pentakisphosphate

Mechanisms of substrate recognition and catalysis of phosphoinositide-5-PPases could be assessed from already solved structures. Corresponding residues of SHIP1 were identified by multiple sequence alignment and structure superposition of SHIP1 with SHIP2 and hINPP5B (**fig. 101** and **fig. 102**).

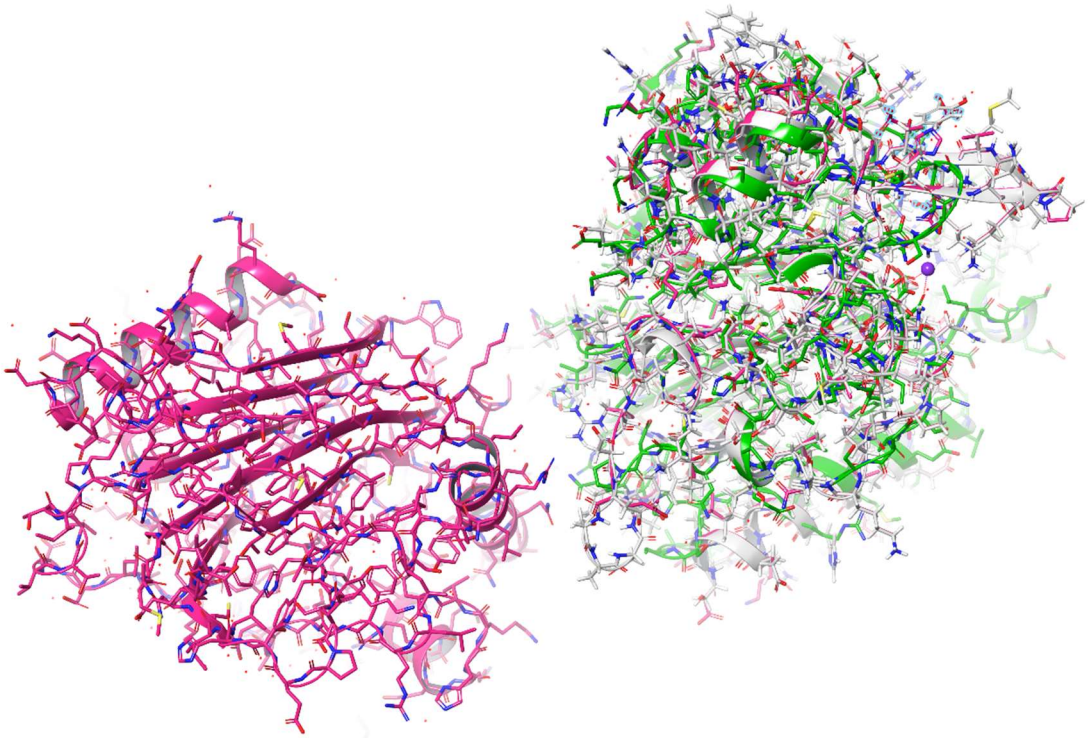

fig. 101: Structure superposition of SHIP1 PPase-C2 (PDB 4A9C), the SHIP1 model of the catalytic domain and INPP5B PPase (PDB 4CMN). SHIP2 PPase-C2 is shown in magenta, the SHIP1 model in light grey and INPP5B PPase is shown in green. The image was generated with *Maestro 11*.

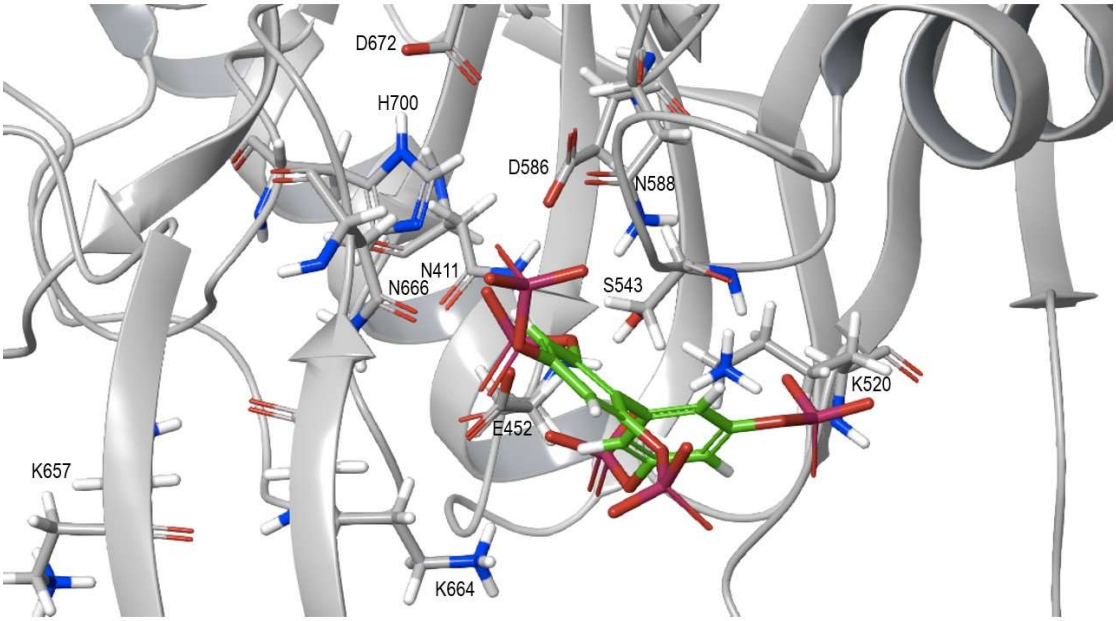

fig. 102: Overview of substrate binding pocket in SHIP1. The SHIP1 model is shown in light grey, residues of interest (based on literature analysis and sequence/structure alignment to SHIP2 and INPP5B, see below and fig. 100) are labelled. The substrate biphenyl 2,3',4,5',6-pentakisphosphate is shown in green. The image was generated with *Maestro 11*.

4.3.1.1.2.1. Substrate recognition

The substrate is recognized by the interaction of its phosphate groups with specific residues within the substrate binding pocket (electrostatic interactions and H-bonds).The 4P is recognized by a highly conserved P4 Interaction Motif (P4IM) consisting of two arginines or lysines, a tyrosine and an asparagine [609]. For the SHIP2 PPase-C2 structure (PDB 4A9C) the respective interactions were analysed by Mills et al. [186] and one could deduce that the P4 in PtdIns(3,4,5)P_3 corresponded to P6 in the synthetic substrate biphenyl 2,3',4,5',6- pentakisphosphate.
By structure and sequence alignment The P4IM of SHIP1 was found to comprise of R590, Y643, N666 and K657 (**fig. 103**).

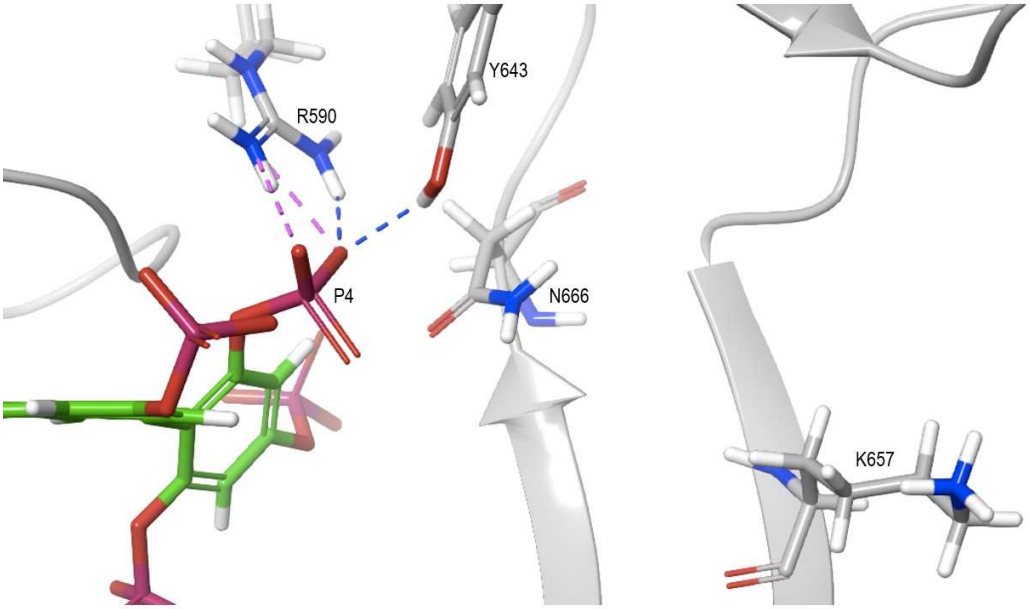

fig. 103: Overview of the 4PIM in SHIP1 based on a model of the SHIP1 catalytic domain built by homology modelling (*Maestro 11*, 4A9C_B was used as template). The protein is shown in light grey and the synthetic substrate biphenyl 2,3',4,5',6- pentakisphosphate is shown in green. The residues comprising the 4PIM are labelled.

By sequence alignment and protein structure alignment the P3 corresponding to the P2 in biphenyl 2,3',4,5',6-pentakisphosphate was found to be recognized by K664 (corresponding to R682 in the SHIP2 structure) (**fig. 103**). In SHIP2 (and propsefully SHIP1) the P3 specificity was explained by the fact that the L4 loop was longer than in other PPases which enabled R682 to recognize the P3 instead of P4. Following P4 binding by N684 (N666 in SHIP1) the L4 loop switched from L4-out to L4-in and two H-bonds between R682 and D613/D615 were released which permitted R682 to contact the P3 [1043]. The P5 (corresponding to the P3´ in biphenyl 2,3',4,5',6-pentakisphosphate) accommodation may be stabilized by K520 and S543 as shown in **fig. 104.**

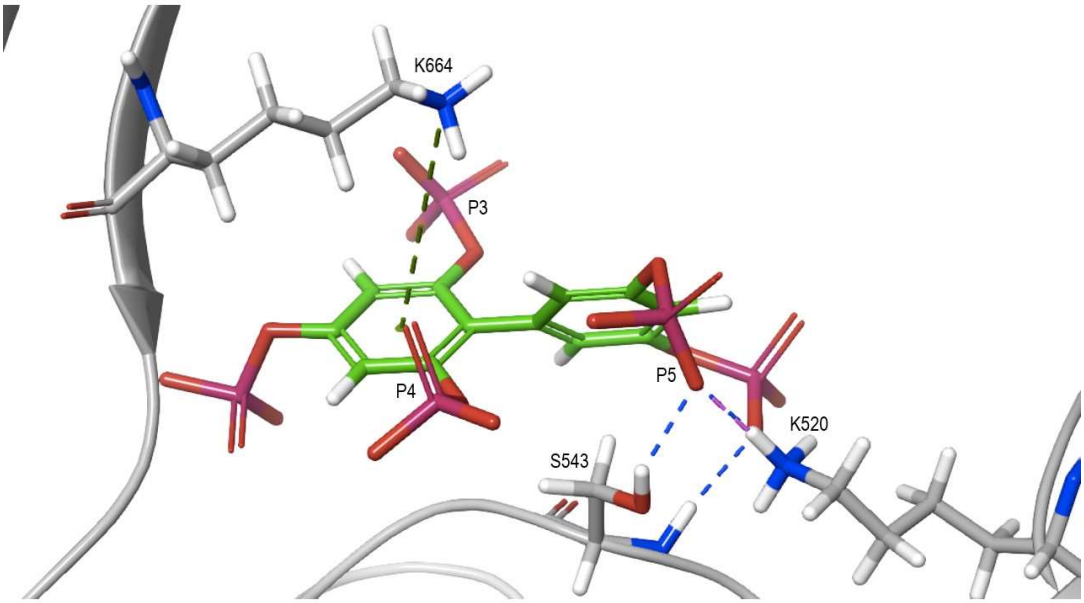

fig. 104: Possible mechanism of the P3 and P5 accommodation in SHIP1 based on a model of the SHIP1 catalytic domain built by homology modelling (*Maestro 11*, 4A9C_B was used as template). The protein is shown in light grey and the synthetic substrate biphenyl 2,3',4,5',6- pentakisphosphate is shown in green. Residues of interest are highlighted in magenta and labelled. H-bonds are indicated as dashed blue lines and ionic interactions as dashed lilac lines, phi-phi stacking is indicated as green dashed lines.

4.3.1.1.2.2. Catalysis

The catalytic mechanism of 5-phosphatases was described earlier for INPP5B. It was shown that catalysis was dependent on Mg^{2+} and was majorly fulfilled by D447 acting first as a base and later on as anacid in its protonated

form [609]. By sequence and structure alignment and under the general consideration that there was no co-crystallization of the template used for modelling of the SHIP1 structure and the Mg^{2+} ion, D586 in SHIP1 was shown to correspond to the acid-base catalyser D447. N449 responsible for stabilizing the activated water molecule equalized N588 in the SHIP1 structure. The histidine residue (H549 in INPP5B and H700 in SHIP1) was observed to be responsible for D5 phosphate interaction and this was stabilized by an aspartate (D524 in INPP5B respectively D672 in SHIP1). E452 (E303 in INPP5B) and N411(N257 in INPP5B) realized the coordination of the Mg^{2+} ion which was modelled from the structure of INPP5B in complex with PtdIns(3,4)P_2 (PDB 4CML) (**fig. 105).**

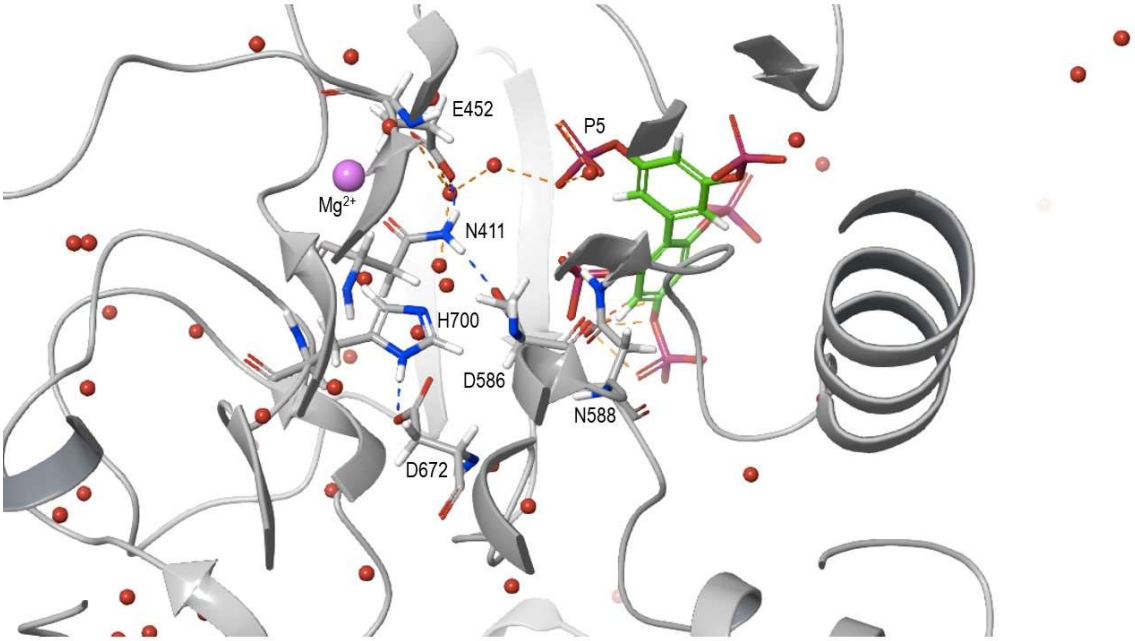

fig. 105: overview on the catalytic mechanism of SHIP1 based on a model of the SHIP1 catalytic domain built by homology modelling *(Maestro 11*, 4A9C_B was used as template). The protein is shown in light grey and the synthetic substrate biphenyl 2,3',4,5',6-pentakisphosphate is shown in green. The Mg^{2+} ion superposed from the structure of INPP5B in complex with PtdIns(3,4)P_2 (PDB 4CML) is shown as a lilac sphere. Residues of interest are labelled. H-bonds are indicated as dashed blue lines and free water molecules as red spheres.

Later in the course of the thesis a structure of SHIP1 co-crystallized with a PO_4^{3-} and a Mg^{2+} ion was published (PDB 6XY7). As can be seen in **fig. 106**, it well reflected the ligand- and co-factor bound state recognized for the SHIP1 model.

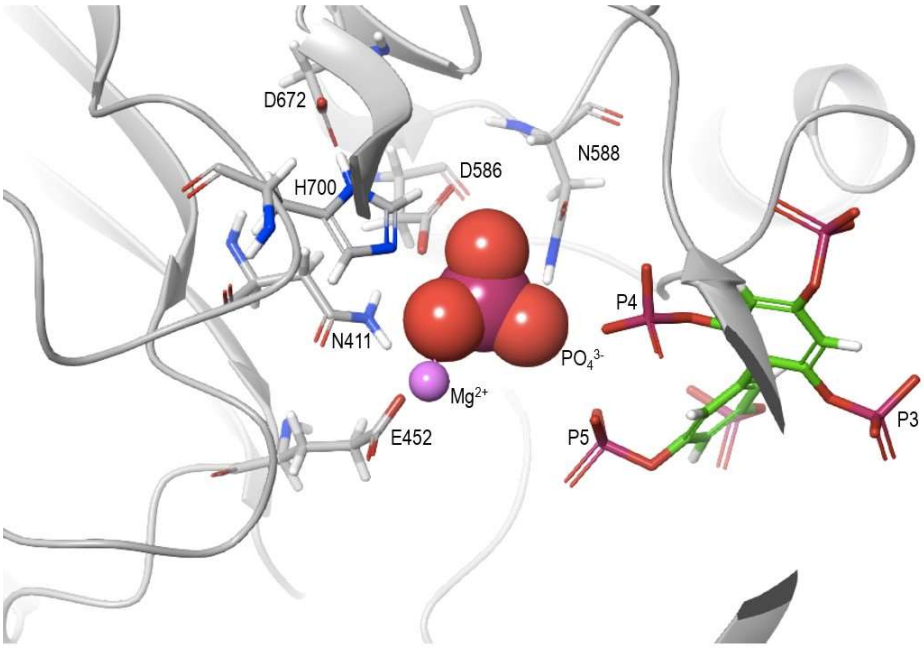

fig. 106: overview on the catalytic mechanism of SHIP1 based on the structure of SHIP1 PPase-C2 co-crystallized with a PO_4^{3-} and a Mg^{2+} ion (PDB 6XY7). The protein is shown in light grey and the synthetic substrate biphenyl 2,3',4,5',6- pentakisphosphate superposed from the SHIP1 model is shown in green. The Mg^{2+} ion is shown as a lilac sphere and the phosphate ion is shown in sphere representation. Residues of interest are labelled.

4.3.1.1.2.3. Mechanisms of substrate recognition and catalysis based on PtdIns(3,4,5)P_3 or Ins(1,3,4,5)P_4

In order to get a more accurate model, it was tried to accommodate the native substrate of SHIP1, PtdIns(3,4,5)P_3 into the substrate binding pocket of the SHIP1 model by docking or structure alignment of ligand bound homologous structures. At this state of the examination a crystal structure of SHIP1 PPase-C2 apo (PDB 6IBD) and bound to PO_4^{3-} and Mg^{2+} (PDB 6XY7) were already deposited in the PDB. The homology model of SHIP1 was compared with 6IBD and 6XY7 by protein structure alignment (**fig. 107**).

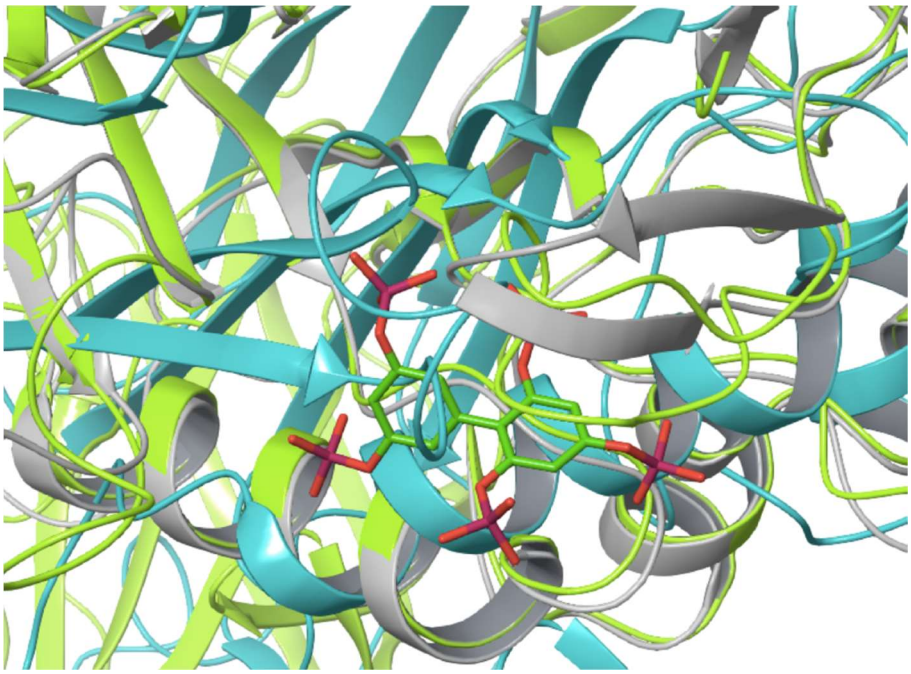

fig. 107: Comparison of the SHIP1 homology model (light grey) with the crystal structure of SHIP1 PPase-C2 apo (PDB 6IBD, green) and bound to PO_4^{3-} and Mg^{2+} (PDB 6XY7, turqouise). Biphenyl 2,3',4,5',6- pentakisphosphate is shown in green. Images were generated with *Maestro 11*.

Especially the loop region defining the substrate binding pocket significantly differed between the three structures which would have implications for the examination of the protein ligand interaction
I chose to use the homology model as it was co-crystallized with a ligand (holoenzyme) whereas 6IBD was crystallized as apoenzyme. Therefore, the model would likely better define loop positions in a ligand bound state. Using 6XY7 would have been an even better option but unfortunately this structure was too compex for docking.
Docking of PtdIns(3,4,5)P_3 would be difficult because of the presence of flexible fatty acid chains. Therefore, in a first approach an alternative strategy was used in order to approximate the SHIP1-PtdIns(3,4,5)P_3 interaction which implicated (1) searching the PDB for homologous holoenzymes, (2) deciding for a structure containing a ligand similar to PtdIns(3,4,5)P_3 which is located within the expected region, (3) manipulating this ligand into PtdIns(3,4,5)P_3 and (4) accommodating the modified ligand into the SHIP1 binding pocket by structural alignment of the model with the chosen template structure.
For the structure search the following sequence was used as a query in the PDB (access 23.01.2019).

input SHIP1 cat aa 403-709 (uniprot Q92835-2)
CAGGGATGAAGTACAACTTGCMITIFIGTWNMGNAPPPKKITSWFLSKGQGKTRDDSADYIPHDIYVIGTQEDPLSEKEWLEILKHSLQEITSV
TFKTVAIHTLWNIRIVVLAKPEHENRISHICTDNVKTGIANTLGNKGAVGVSFMFNGTSLGFVNSHLTSGSEKKLRRNQNYMNILRFLALGDKK
LSPFNITHRFTHLFWFGDLNYRVDLPTWEAETIIQKIKQQQYADLLSHDQLLTERREQKVFLHFEEEEITFAPTYRFERLTRDKYAYTKQKATG
MKYNLPSWCDRVLWKSYPLVHVVCQSYGSTSDIMTSDHSPVFATFE

The structure search resulted in six candidate template structures as listed in **table 15**. The structure alignment of found structures is shown in **fig. 108**.

Table 15: Accommodation of PtdIns(3,4,5)P_3 into the substrate binding pocket of the SHIP model, comparison of candidate template structures. The sequence of SHIP1 PPase (res. 403-709) was used as query in the PDB structure search function in order to define homologous holoenzymes.

ID	Title
4A9C	Crystal structure of human SHIP2 in complex with biphenyl 2,3',4,5',6- pentakisphosphate
3MTC	Crystal Structure of INPP5B in complex with phosphatidylinositol 4-phosphate
4CML	Crystal Structure of INPP5B in complex with Phosphatidylinositol 3,4- bisphosphate
5A7I	Crystal structure of INPP5B in complex with biphenyl 3,3',4,4',5,5'- hexakisphosphate
5A7J	Crystal structure of INPP5B in complex with benzene 1,2,4,5- tetrakisphosphate
1I9Z	CRYSTAL STRUCTURE OF INOSITOL POLYPHOSPHATE 5-PHOSPHATASE DOMAIN (IPP5C) OF SPSYNAPTOJANIN IN COMPLEX WITH INOSITOL (1,4)-BISPHOSPHATE AND CALCIUM ION

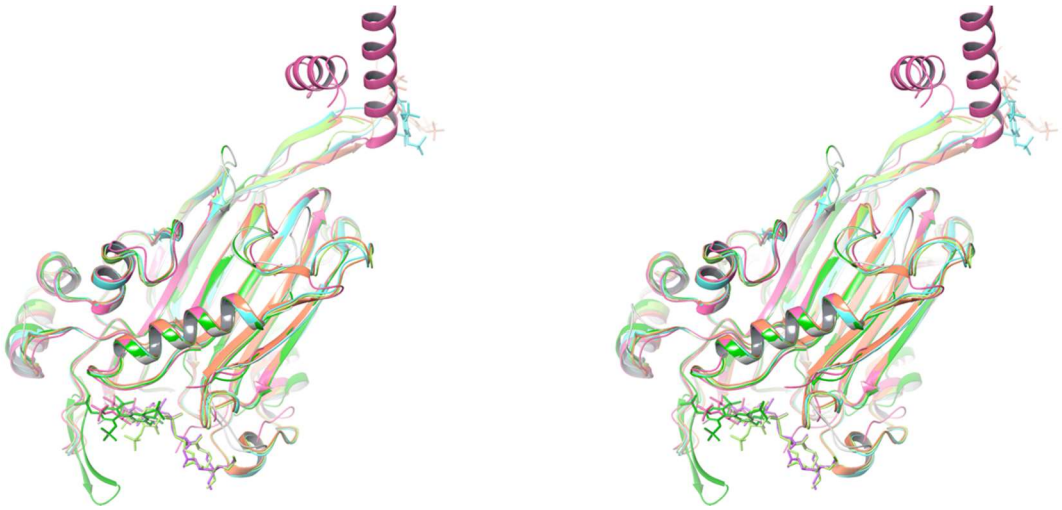

fig. 108: Accommodation of PtdIns(3,4,5)P_3 into the substrate binding pocket of the SHIP model, comparison of candidate template structures. The sequence of SHIP1 PPase (res. 403-709) was used as query in the PDB structure search function in order to define homologous holoenzymes. *Maestro 11* was used for protein structure alignment and image generation. Colour coding is as indicated in table 15.

The two models 5A7J and 1I9Z could not be aligned in correct orientation and were therefore excluded from further examination.
Generally, the assembly of loops within the substrate binding pocket did differ significantly which would impact substrate accommodation and catalysis (see **fig. 109**). However, due to the high percentage of loops in this region the binding pocket could be expected to possess a certain level of flexibility which would hint to a more flexible binding mode according to an induced fit model.

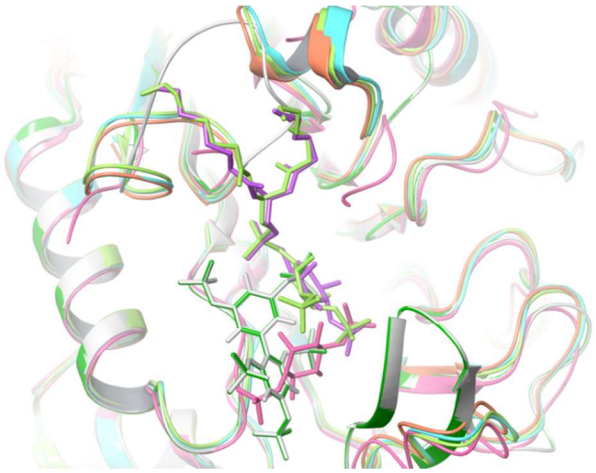

fig. 109: Accommodation of PtdIns(3,4,5)P_3 into the substrate binding pocket of the SHIP model, comparison of candidate template structures; detailed view of the substrate binding pocket. The sequence of SHIP1 PPase (res. 403-709) was used as query in the PDB structure search function in order to define homologous holoenzymes. *Maestro 11* was used for protein structure alignment and image generation. Colour coding is as in table 15.

For the assessment of PtdIns(3,4,5)P_3 binding to SHIP1 the two structures PDBs 4CML and 3MTC were of most value as their respective ligand was most similar to PtdIns(3,4,5)P_3.
Therefore, in the next step PtdIns(3,4)P_2 of 4CML was manipulated into PtdIns(3,4,5)P_3 and subsequently the SHIP1 model was aligned to PDB 4CML. This is depicted in **fig. 110**.

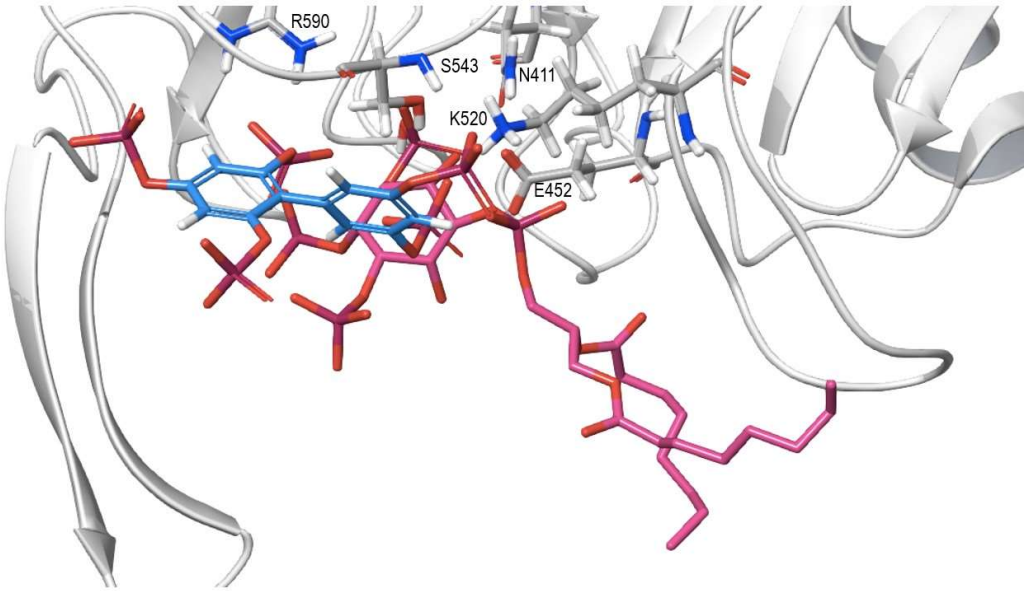

fig. 110: Accommodation of PtdIns(3,4,5)P_3 into the substrate binding pocket of the SHIP model, detailed view of the binding pocket. PtdIns(3,4)P_2 of the Crystal Structure of INPP5B in complex with PtdIns(3,4)P_2 (PDB 4CML) was manipulated to PtdIns(3,4,5)P_3 using *Maestro 11*. Superposition of the SHIP1 model (light grey, biphenyl 2,3',4,5',6- pentakisphosphate is shown in steel blue) and PDB 4CML (only edited substrate =PtdIns(3,4,5)P_3 is shown in magenta).

As depicted some major differences in the orientation of biphenyl 2,3',4,5',6-pentakisphosphate vs. PtdIns(3,4,5)P_3 showed up. This was most likely due to the fact that those substrates were chemically different (FA chains vs. none, two rings vs. one etc.). Also it is of note that the synthetic ligand is not a substrate but inhibitor so it may be not unexpected to bind differently. Next, the interaction between the SHIP1 model and the modelled PtdIns(3,4,5)P_3 was analysed in a similar manner to those performed with BiPh(2,3',4,5',6)P_5. As summarized in **table 16** the results obtained from beforementioned analysis with BiPh(2,3',4,5',6)P_5 were reflected for the PtdIns(3,4,5)P_3 interaction.
As a second approach Ins(1,3,4,5)P_4 was docked into the SHIP1 model using GLIDE and default docking parameters. This is depicted in **fig. 111**.

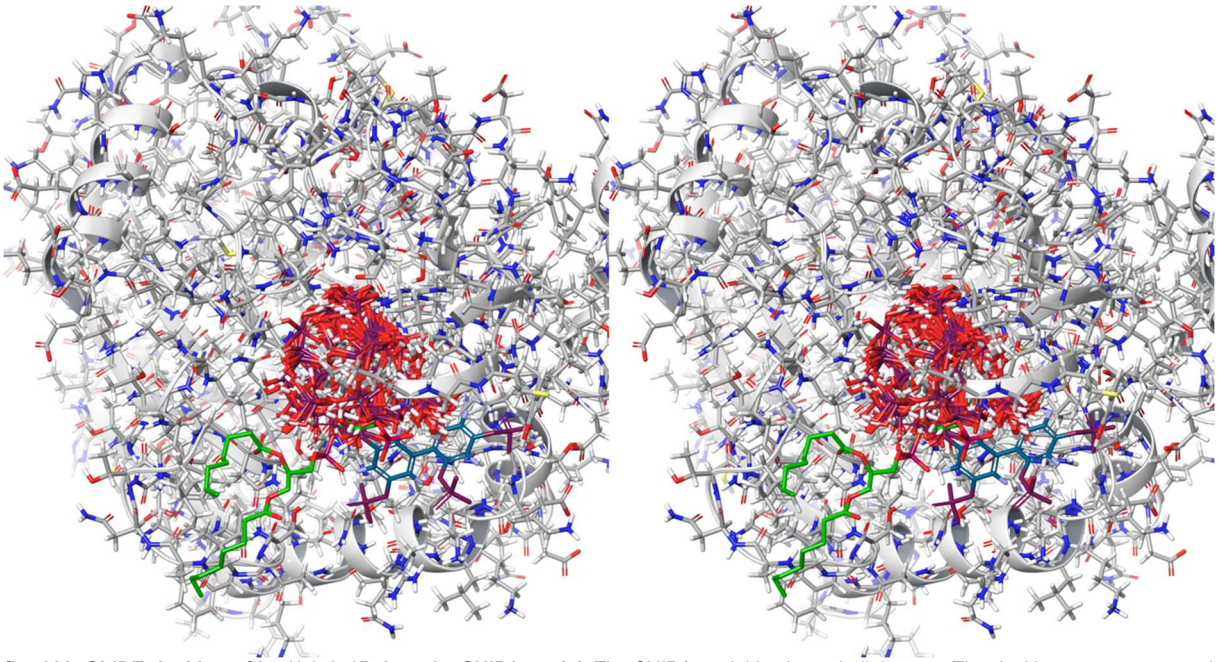

fig. 111: GLIDE-docking of Ins(1,3,4,5)P_4 into the SHIP1 model. The SHIP1 model is shown in light grey. The docking poses generated by GLIDE are shown in magenta, BiPh(2,3',4,5',6)P_5 is shown in steel blue and PtdIns(3,4,5)P_3 is shown in green (see above).

The pose imposing the highest docking score (docking score: -5.773) is shown in **fig. 112** with proposed protein-ligand interaction. For this system the general assignment of interacting residues was as demonstrated for BiPh(2,3',4,5',6)P_5 and PtdIns(3,4,5)P_3 (summarized in **table 16**).

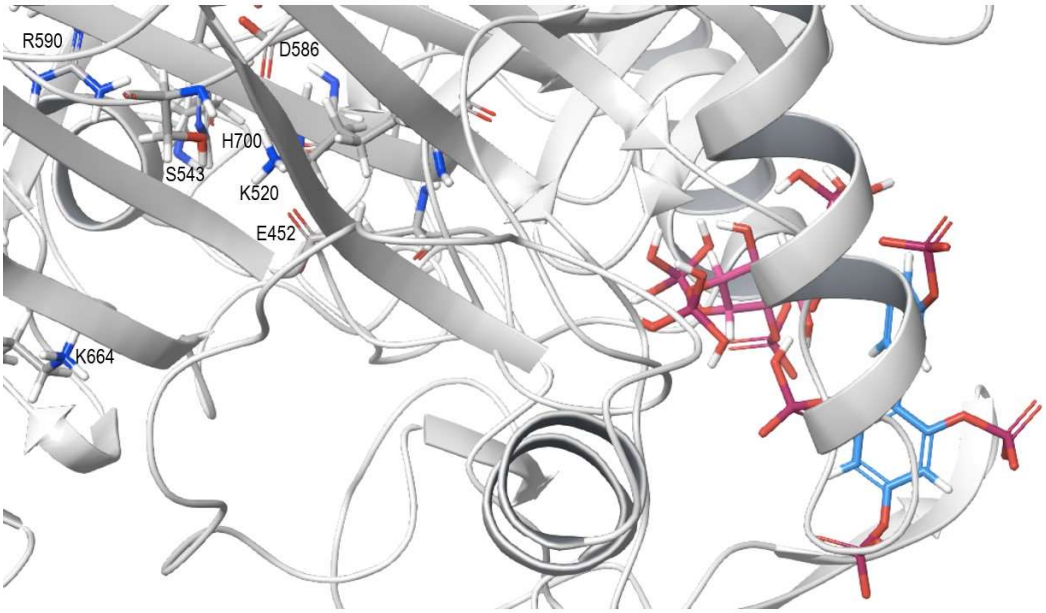

fig. 112: GLIDE Docking of Ins(1,3,4,5)P_4 into the SHIP1 homology model, detailed view of the substrate binding pocket. The SHIP1 model is shown in light grey and the highest ranked docking pose is shown in magenta. BiPh(2,3',4,5',6)P_5 is shown in steel blue. The image was generated in *Maestro 11*.

Summarizing the protein-ligand interaction studies there was an agreement on the general assignment of interacting residues spanning BiPh(2,3',4,5',6)P_5, PtdIns(3,4,5)P_3 and Ins(1,3,4,5)P_4, however, it was not exactly the same. This was not surprising as (1) technical ligand accommodation was performed by different methods and (2) ligands differed on the chemical level. This is summarized in **table 16**.

Table 16: Comparison of ligand-SHIP1 model interaction analysis approaches (details: see text)

	BiPh(2,3',4,5',6)P_5	**PtdIns(3,4,5)P_3**	**Ins(1,3,4,5)P_4**
P1		V643 (main chain)	R644, R647
P2			
P3	K664	K664	K664
P4	R590, Y643, N666, K657	R590, Y643, N666, K657	K664, (N666 and R590 in the surrounding of P4)
P5	K520, S543 (E452, N411, H700, D586, N588, D672 responsible for catalysis)	K520, N588, R590, S543, H700, H540, E452	S543, R590

4.3.1.2. C2 domain

The C2 domain was modelled with Maestro based on PDB 5OKO (SHIP2 PPase-C2).
In their study of the structural evaluation of the PPase and C2 domain of SHIP2 as well as their interface and influence on each other Le Coq et al. found four conserved lysines (K758 R762, K764, K826) based on Multiple Sequence Alignment which were located in the conserved CBL motifs [1044]. The corresponding lysines in the SHIP1 model of the C2 domain were K740, K742, K746 and K806. As shown in **fig. 113** they are all located well to form a putative PtdIns(3,4)P_2 binding pocket.

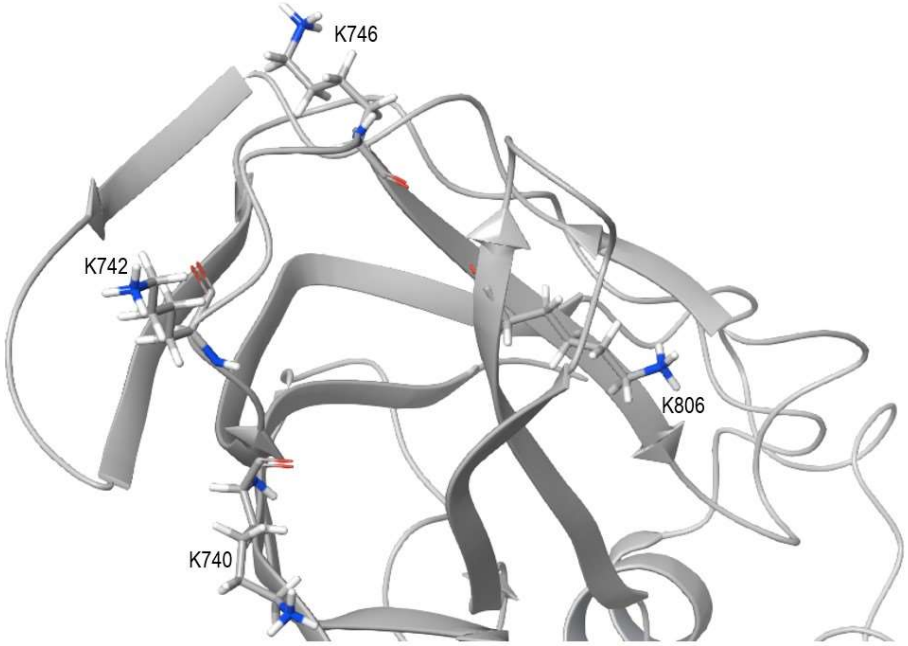

fig. 113: Conserved lysines in the model of SHIP1 C2. The homology model of SHIP1 C2 is shown in light grey. Conserved lysines implicated from structure alignment to SHIP2 [1044] are labelled.

4.3.2. Experimental structure analysis

4.3.2.1. Domain boundaries determination and trial expression of SHIP1 PHL-PPase-C2 constructs in E. coli

The determination of domain boundaries would be the initial step for any experimental structure determination approach and should define which part of a protein would be feasible for crystallization. This is based on (1) similarity to existing structures in the PDB and (2) secondary structure prediction (i.e. long stretches of coil or unstructured regions should be avoided; constructs should not start or end in the middle of a secondary structure element such as an α-helix or a β-sheet). A first domain boundary assessment was performed by Maria Garcia Alai (EMBL, Hamburg) for the construct SHIP1 PHL-PPase-C2_long. The domains PH-L, PPase and C2 were chosen for structure analysis experiments as the structure of SHIP1 PPase-C2 had already been solved (PDB 6IBD) and the PRR was predicted to be unstructured which would be very likely to hinder proper crystallization and data assessment.

PHL-PPase-C2_long (aa 258-854)
INMVSKLSQLTSLLSSIEDKVKALLHEGPESPHRPSLIPPVTFEVKAESLGIPQKMQLKVDVESGKLIIKKSKDGSEDKFYSHKKILQLIKSQKFL
NKLVILVETEKEKILRKEYVFADSKKREGFCQLLQQMKNKHSEQPEPDMITIFIGTWNMGNAPPPKKITSWFLSKGQGKTRDDSADYIPHDIYV
IGTQEDPLSEKEWLEILKHSLQEITSVTFKTVAIHTLWNIRIVVLAKPEHENRISHICTDNVKTGIANTLGNKGAVGVSFMFNGTSLGFVNSHLTS

GSEKKLRRNQNYMNILRFLALGDKKLSPFNITHRFTHLFWFGDLNYRVDLPTWEAETIIQKIKQQQYADLLSHDQLLTERREQKVFLHFEEEEI
TFAPTYRFERLTRDKYAYTKQKATGMKYNLPSWCDRVLWKSYPLVHVVCQSYGSTSDIMTSDHSPVFATFEAGVTSQFVSKNGPGTVDSQ
GQIEFLRCYATLKTKSQTKFYLEFHSSCLESFVKSQEGENEEGSEGELVVKFGETLPKLKPIISDPEYLLDQHILISIKSSDSDESYGEGCIALRL
EATETQLPIYTPLTHHGELTGHFQGEIKLQT

The construct was cloned into the expression vector pETM30 using an *EcoRI/NcoI* strategy. The respective cDNA was synthesized by Integrated DNA technology with the silent mutation c.C2517→T (H839H) to remove an internal *NcoI* cleavage site. An analytical test expression and Ni-NTA purification of the construct was performed at the CSSB Hamburg by Angelica Struve. The construct was transformed into *BL21(DE3)* and an overnight culture was prepared. The main culture of 500 mL LB-Kan was inoculated with the overnight culture and incubated at RT, 150rpm until the OD_{600} was around 0.8-0.9. Expression was then induced with 0.5 mM IPTG for 4 hours at 22°C. After harvesting the bacteria were lysed in lysis buffer (50mM Tris pH8, 250mM NaCl, and 20 mM imidazole plus protease inhibitors and *DNase I*). The lysate was subjected to Ni-NTA beads purification using Running/Wash buffer (50mM Tris pH8, 250mM NaCl, and 20 mM imidazole) and Elution buffer (50mM Tris pH8, 250mM NaCl, and 250 mM imidazole) and analysed by SDS-PAGE and *Coomassie* staining. Fractions A7-A12 indicated a band between 80 and 115 kDa which could be the target protein (expected M_w of tagged protein: 95 kDa) and were verified by Western Blot (anti-His, anti-GST and anti-SHIP1 P290). Unfortunately, it was not possible to reproduce the result neither in an analytical nor a preparative scale and additional trial expressions testing different bacterial strains, expression (temperature and IPTG concentration) and buffer conditions failed to produce sufficient soluble protein in all cases (not shown, trial expressions were partly performed by Philipp Lewe, CSSB Hamburg).
As SHIP1 PHL-PPase-C2_long was not sufficiently soluble in the trial expressions it was hypothesized that domain boundaries might not be optimal. In an attempt to optimize the domain boundaries (leading to SHIP1 PHL-PPase-C2_short, see below) a sequence search was performed at the PDB webserver (date of access: 13.02.2020) using the PHL-PPase-C2_long sequence as query and a wide panel of structures of 5-Phosphatase PPase or PPase-C2 constructs was identified. Following this, a Multiple Sequence Alignment of SHIP2 and SHIP1 structures was performed in Pymol in order to get an overview on conserved parts, similarity and identity. Structures were also aligned at the Cα level This is shown in **fig. 114**.

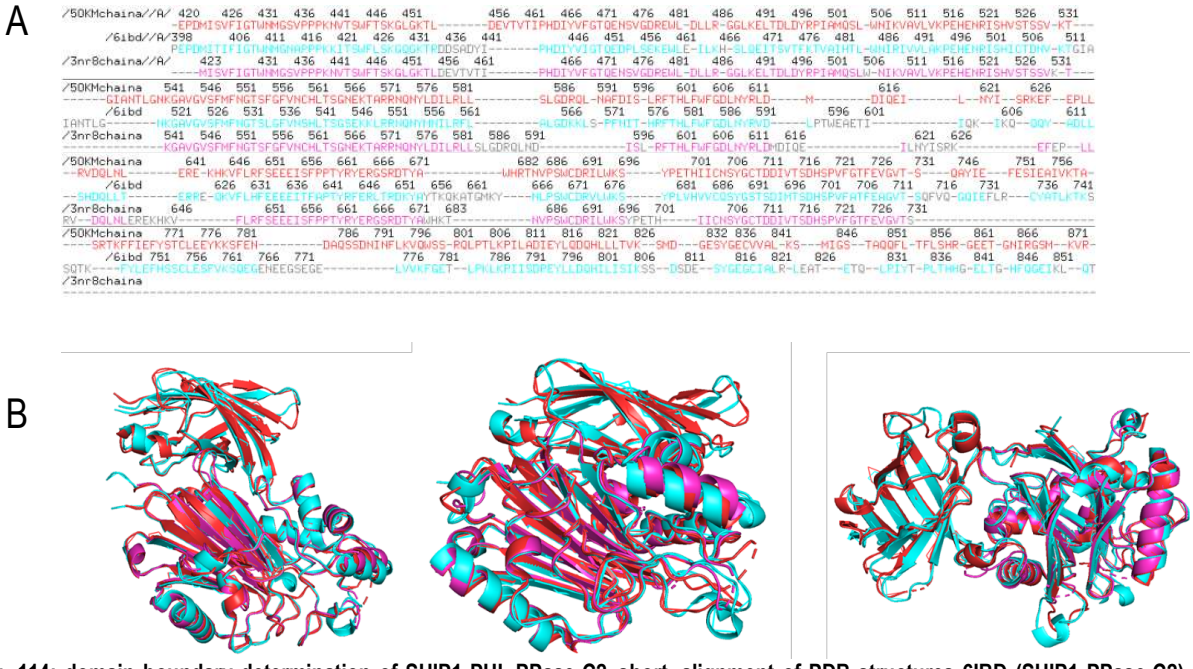

fig. 114: domain boundary determination of SHIP1 PHL-PPase-C2_short, alignment of PDB structures 6IBD (SHIP1 PPase-C2), 3NR8 (SHIP2 PPase) and 5OKM (SHIP2 PPase-C2). Panel A shows the Multiple Sequence Alignment and panel B shows the structure alignment. Alignments and images were generated in Pymol.

As can be seen, the overall structure is very similar in all constructs with conserved secondary structure elements. The end of the last β-sheet in the SHIP1 PPase-C2 structure (6IBD) was defined as Q853 which was nearly identical with the C-terminus of SHIP1 PHL-PPase-C2_long (T854). Therefore, the C-terminal border for the shortened construct PHL-PPase-C2 was left unchanged.

For verification of the left/N-terminal border there was less information available as no highly homologues structures could be find when using the PDB structure search or pBLAST (date of access 13.01.2020). Therefore, the boundary determination was mainly based on the NMR structure of SHIP1 PH-L published by MingLum et al. [608]. In addition, some representative PH domain crystal structures were retrieved from the PDB for a general structure analysis of PH domains (superposition to Cα using Pymol) (**fig. 115**).

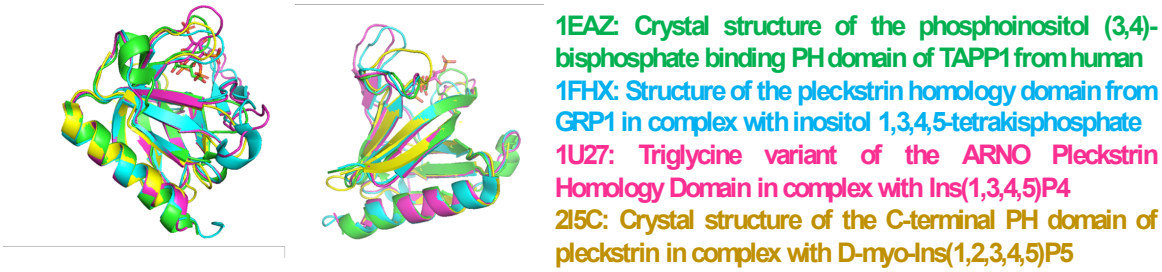

fig. 115: Structure alignment of model PH domain retrieved from the PDB. Alignments and Images were generated in Pymol.

As can be seen, all structures shared the same general domain structure of two beta sheets (3-stranded or 4-stranded) and an α-helix. This was analysed exemplarily in further detail for PDB 1EAZ as depicted in **fig. 116**.

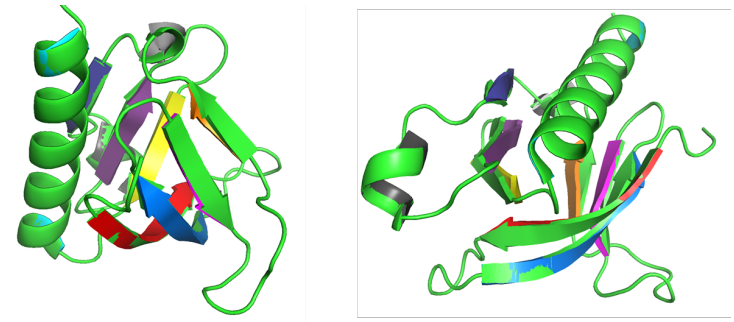

beta1	K194-Q201
beta2	W208-L215
beta3	T219-F223
beta4	R233-P236
turn1	K238-V240
beta5	K242-E245
turn2	Q248-M253
beta6	L257-V261
beta7	T266-Q270
helix1	S273-Q291

fig. 116: analysis of secondary structure elements in PDB 1EAZ. The analysis was performed in Pymol.

As found by *Clustal 2.1.* Multiple Sequence Alignment the conserved secondary structure elements identified in the model PH domains were only moderately conserved in SHIP1 PH-L (**fig. 117**). Therefore, alignment of PH domain structures to SHIP1 was not feasible for N-terminal domain boundary determination

fig. 117: Alignment of model PH-domains with SHIP1 PHL-PPase-C2_long. The Alignment was done using *Clustal 2.1*.. The conserved secondary structure elements found in PH domains are labelled.

Of note, also the PH-L domain of SHIP1 adopts the general fold of the PH domains regardless of the relatively low sequence homology. According to the NMR analysis of Ming-Lum et al. [608], they proposed that aa292-401 (291-400 in Caucasian isoform) would form a closed domain structure. As PHL-PPase-C2_long started at aa258 already it might be possible that those additional amino acids would form some kind of secondary structure. In an attempt to analyse the possible fold of the sequence located between PH-L and SH2 domain (aa 101-291) pBLAST on structural level (PDB) and sequence level (uniprot) was applied (date of access 14.01.2020). However, no results could be obtained from the PDB search. On the sequence level, most homologues were phosphoinositide-5-phosphatases as expectable. Secondary structure prediction of this part of the protein was then performed using PHYRE2 (date of access 13.02.2020) or PSIPRED (date of access 20.03.2020) (**fig. 118** and **fig. 119**).

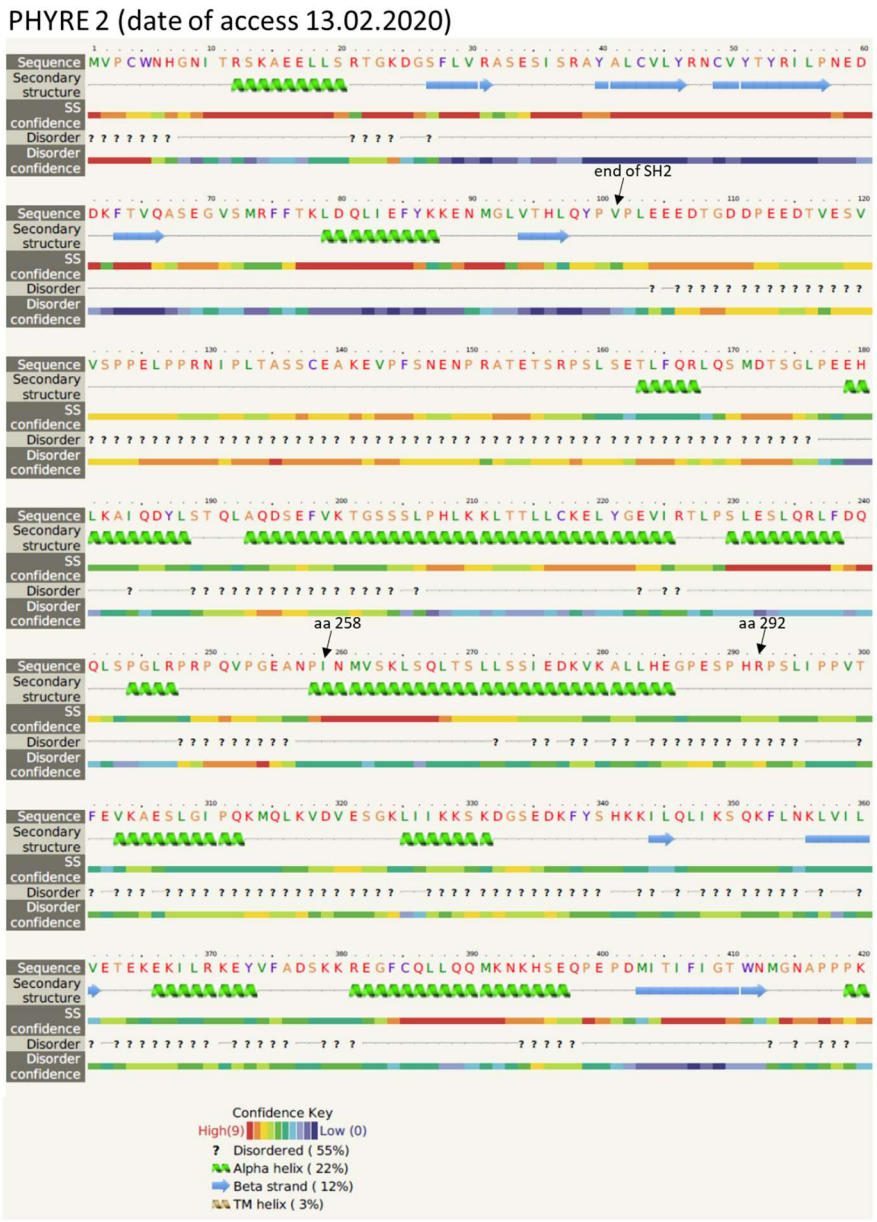

fig. 118: PHYRE secondary structure prediction of SHIP1 aa 101-291.

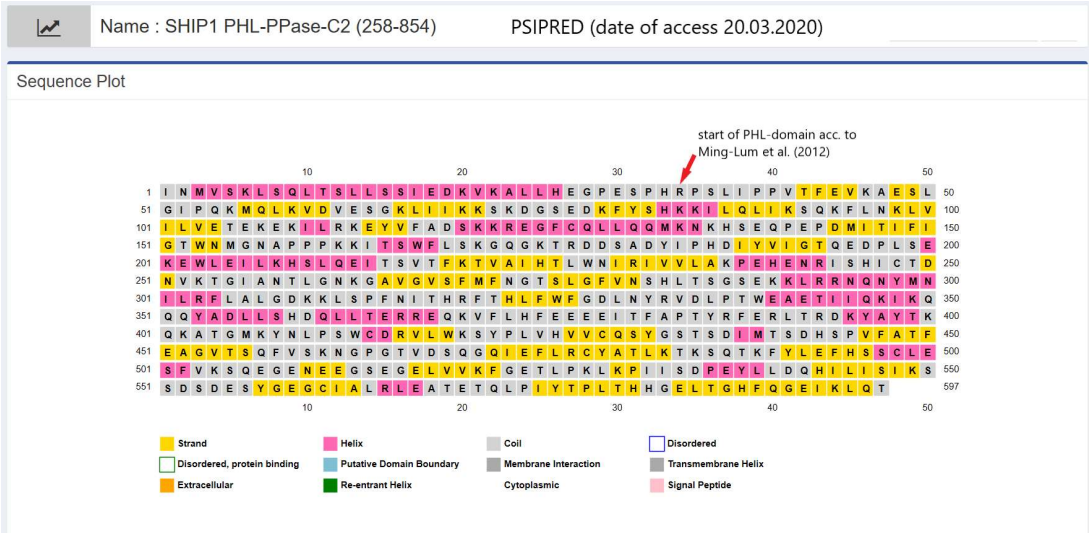

fig. 119: PSIPRED secondary structure prediction of SHIP1 aa 101-291.

According to the secondary structure prediction analysis, there was a helix predicted to start around the beginning of the original construct SHIP1 PHL-PPase-C2_long (aa 258-854) which might be critical. However, in the direct surrounding of res. 291 the structure was predicted as disordered.
Due to the PH-L NMR structure published by MingLum et al. [608] giving certainty that the stretch of aa 291-400 would form a closed structure it was decided to use R291 as the N-terminal boundary for SHIP1 PHL-PPase-C2_short.

SHIP1 PHL-PPase-C2_short (aa 291-854)
RPSLIPPVTFEVKAESLGIPQKMQLKVDVESGKLIIKKSKDGSEDKFYSHKKILQLIKSQKFLNKLVILVETEKEKILRKEYVFADSKKREGFCQL
LQQMKNKHSEQPEPDMITIFIGTWNMGNAPPPKKITSWFLSKGQGKTRDDSADYIPHDIYVIGTQEDPLSEKEWLEILKHSLQEITSVTFKTVAI
HTLWNIRIVVLAKPEHENRISHICTDNVKTGIANTLGNKGAVGVSFMFNGTSLGFVNSHLTSGSEKKLRRNQNYMNILRFLALGDKKLSPFNIT
HRFTHLFWFGDLNYRVDLPTWEAETIIQKIKQQQYADLLSHDQLLTERREQKVFLHFEEEEITFAPTYRFERLTRDKYAYTKQKATGMKYNLP
SWCDRVLWKSYPLVHVVCQSYGSTSDIMTSDHSPVFATFEAGVTSQFVSKNGPGTVDSQGQIEFLRCYATLKTKSQTKFYLEFHSSCLESF
VKSQEGENEEGSEGELVVKFGETLPKLKPIISDPEYLLDQHILISIKSSDSDESYGEGCIALRLEATETQLPIYTPLTHHGELTGHFQGEIKLQT

The construct was cloned into the expression vector pET47b(+) using a *KpnI/NcoI* strategy. However, the trial expressions using different strains, expression and buffer conditions conclusively failed to produce sufficient soluble SHIP1. Of note, although the bacterial expression of SHIP1 FL (see 4.2.2.1.1.) yielded soluble and biologically active protein that was not a suitable strategy as the yield and grade of purity was too low for crystallization or other structure determination approaches.
In summary, it was concluded that *E. coli* might not be the optimal expression system for high yield expression of the relatively complex SHIP1 protein/domain constructs.

4.3.2.2. Trial expression of TwinStrep-SHIP1 FL in H1299 and HEK-293F

Due to the unsucessful expression trials of SHIP1 FL or SHIP1 constructs in a bacterial system it was decided to switch to a mammalian expression system. H1299 cells were chosen as they were easy to culture and showed high overexpression of active HA-tagged SHIP1 when transduced (see 4.2.1.) as well as a high overall yield of protein. In addition to transduction with HA-SHIP1 FL H1299 cells were also transduced with TwinStrep-SHIP1 FL using the same lentiviral transduction protocol. The transduction was verified by FACS (eGFP fluorescence) and Western Blot using SHIP1 P1C1. In addition, TwinStrep-SHIP1 FL was transiently transfected in HEK-293F cells which is a more convenient expression system for producing high densities of protein expressing cells. As depicted in **fig. 120** SHIP1 expression was detected in both systems. With the help of the recombinant SHIP1 standard total SHIP1 amounts were approximated. For SHIP1 in H1299 1000 ng/40 µg lysate (quantified from the Western Blot) would be around 300 µg protein out of one T175 flask (40 µg is approx. 1/100 of a 10 cm dish, multiplied by 3 for a T175 flask) and for SHIP1 in HEK-293F 100 ng/1x10^4 cells was quantified from the Western Blot which would be 300 µg in total for a 30 mL transfection (3x10^7 cells).

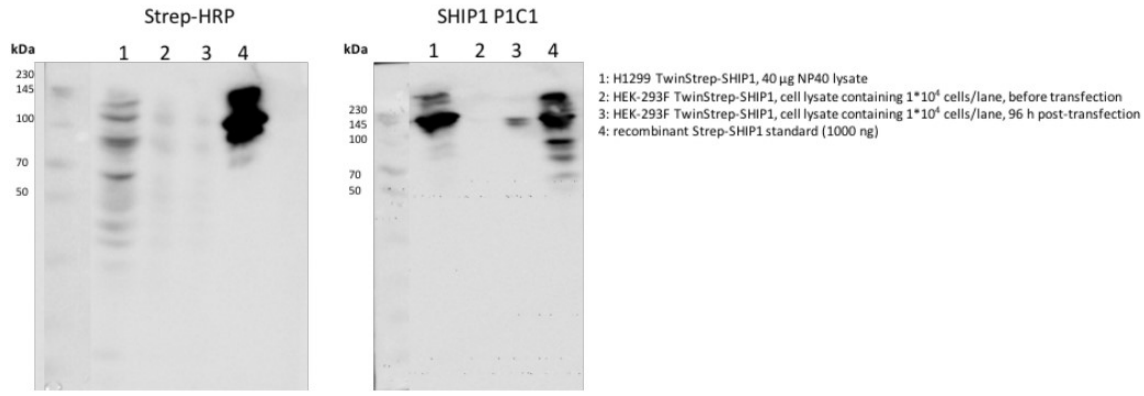

fig. 120: SHIP1 levels in H1299 transduced with pLeGO-iG2-Puro(+)-TwinStrep-SHIP1 FL and HEK-293F cells transfected with pLeGO-iG2-Puro(+)-TwinStrep-SHIP1 FL. Cells were lysed by NP40 lysis (H1299) or ultrasonication (HEK-293F) and blotted with SHIP1 P1C1 or StrepMAB-Classic-HRP. Recombinant Strep-SHIP1 was used to determine the amount of SHIP1 in the cell lysates.

For a trial Strep-purification eight T175-flasks of H1299 TwinStrep-SHIP1 FL were lysed by NP40 lysis and the lysate was diluted 1:10 in buffer W and loaded onto a *Strep-Tactin XT* resin. Unfortunately, no binding of SHIP1 to the resin was observed neither when the contact time between lysate and resin was extended or the lysate was pre-incubated with avidin (not shown). Due to the relatively low Western Blot signal when detecting the Strep tag

compared to SHIP1 it was suspected that the Strep-tag might not be (fully) accessible for binding to the *Strep-Tactin XT* resin.

4.3.3. Biochemical analysis of the mechanisms of phosphoinositide binding and catalysis of SHIP1 FL and SHIP1 phosphoinositide binding domains

4.3.3.1. Cloning and expression of SHIP1 domain constructs

SHIP1 FL was expressed as indicated in 4.2.2.1.1. SHIP1 phosphoinositide domain constructs PH-L, PPase, C2, PH-L-PPase, PPase-C2, PHL-C2 and PHL-PPase-C2 were cloned into pASG-IBA5 using the Stargate cloning system, expressed in *E. coli BL21(DE3)pLysSpREP4,* purified by *Strep-Tactin XT* affinity chromatography and if necessary concentrated by ultrafiltration. The expression was verified by *Coomassie Brilliant Blue* staining and Western Blot analysis using StrepMAB Classic (**fig. 121**).

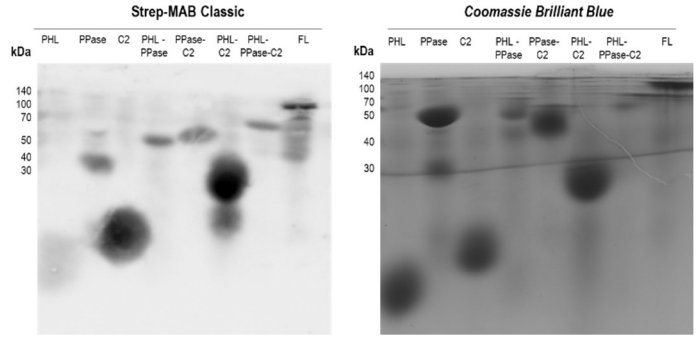

fig. 121: expression and *Strep-Tactin XT* affinity chromatographic purification of SHIP1 phosphoinositide binding domain constructs. SHIP1 phosphoinositide domain constructs PH-L, PPase, C2, PH-L-PPase, PPase-C2, PHL-C2 and PHL-PPase-C2 and SHIP1 FL were cloned into pASG-IBA5 using the Stargate cloning system, expressed in *E. coli BL21(DE3)pLysSpREP4*, purified by *Strep-Tactin XT* affinity chromatography and if necessary concentrated by ultrafiltration. The expression was analysed by Western Blot using StrepMAB Classic and *Coomassie Brilliant Blue* Staining.

4.3.3.2. Analysis of the substrate specificity and catalysis of SHIP1

The substrate specificity of SHIP1 was analysed by MDD-HPLC using water-soluble InsPs instead of PtdInsPs and is already published [573]. The MDD-HPLC measurements were performed by Torsten Wundenberg and Christoph Rehbach and summarized in **fig. 122**. For initial establishment of candidate substrates an IP_x-hydrolysate was used and candidate substrates were then measured separately in order to determine the exact properties of the reactions.

A

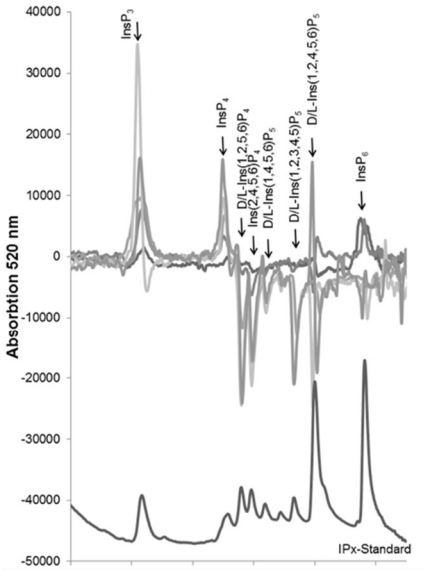

B

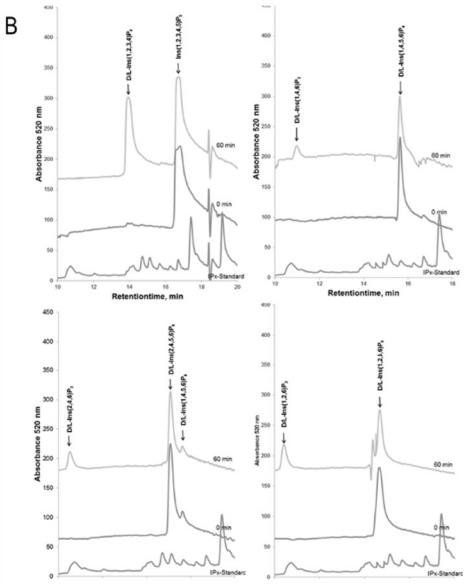

C

Inositol phosphate	specific initial velocity [nmol/min/mg]
5PP-InsP$_5$	NS
4/6PP-InsP$_5$	NS
InsP$_6$	NS
Ins(1,2,3,4,5)P$_5$	372.88
Ins(1,2,3,5,6)P$_5$	NS
Ins(1,2,3,4,6)P$_5$	NS
Ins(2,3,4,5,6)P$_5$	NS
Ins(1,2,4,5,6)P$_5$	NS
Ins(1,3,4,5,6)P$_5$	NS
Ins(3,4,5,6)P$_4$	ND
Ins(1,4,5,6)P$_4$	22.65
Ins(2,4,5,6)P$_4$	39.54
Ins(1,2,5,6)P$_4$	100.37
Ins(2,3,4,5)P$_4$	ND

fig. 122: Determination of the substrate specificity of SHIP1 by MDD-HPLC. Panel A shows the initial identification of SHIP1 substrates using IP$_x$ and panel B shows the verification of identified substrates. Panel C summarizes the enzyme activities for measured inositol phosphates. The MDD-HPLC measurements were performed by Torsten Wundenberg and Christoph Rehbach, adapted from [573].

As can be seen the best substrates were Ins(1,2,3,4,5)P$_5$ and Ins(1,3,4,5)P$_4$ whereas Ins(2,3,4,5)P$_4$, Ins(1,4,5,6)P$_4$ and Ins(2,4,5,6)P$_4$ were weaker substrates. Of note, Ins(2,3,4,5)P$_4$ was a substrate of SHIP1 but not of SHIP2 whereas the remaining substrates were shared substrates of SHIP1 and SHIP2 [571]. Using GLIDE docking the predicted interactions of Ins(1,3,4,5)P$_4$ and Ins(2,3,4,5)P$_4$ with SHIP1 (PDB 6IBD) were compared in order to possibly define critical residues interacting with the P2 which may explain the specificity for Ins(2,3,4,5)P$_4$ and K659 was identified as a candidate interactor (**fig. 123A**). Additionally, it was tried to determine a possible pattern of phosphate groups which would enable one to predict which phosphate positions would favour or hinder the sterical accommodation of an InsP (or PtdInsP) respectively their catalysis and it was found that especially a phosphate moiety at position 6 was a negative predictive marker and a phosphate at positions 1, 3, 4 and 5 and to a weak extend at position 2 were a positive predictive marker (**fig. 123B**).

A

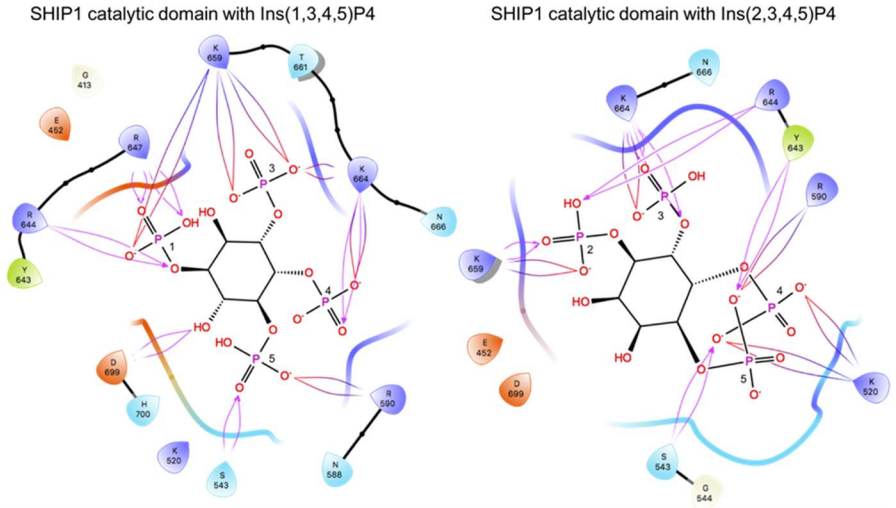

B

phosphate	1	2	3	4	5	6
Ins(1,2,3,4,5)P_5						
Ins(1,3,4,5)P_4						
Ins(2,3,4,5)P_4						
Ins(2,4,5,6)P_4						
Ins(1,4,5,6)P_4						

fig. 123: Determination of the substrate specificity of SHIP1, mechanisms and patterns of substrate accommodation and catalysis. Panel A shows the ligand interaction diagram of GLIDE-docked SHIP1 substrates in SHIP1 PPase-C2 and was generated with *Maestro 11*. Panel B summarizes the presence (green shaded) or absence (red shaded) of phosphate groups in SHIP1 substrates to identify interaction promoting or hindering phosphate moieties, adapted from [573].

The enzyme kinetics of SHIP1 FL towards its most biologically relevant substrate PtdIns(3,4,5)P_3 was analysed using a malachite-green based optical phosphatase assay. The specific activity of SHIP1 was determined for different concentrations of PtdIns(3,4,5)P_3 ranging from 0 to 300 µM and fitted by hyperbolic and sigmoidal regression to determine V_{max} and K_M. As shown in **fig. 124** both regression strategies led to comparable values for V_{max} and K_M, however the regression coefficient was higher for the sigmoidal regression. Sigmoidal enzyme kinetics point to allosteric regression which was described for SHIP1 in a previous paper [614].

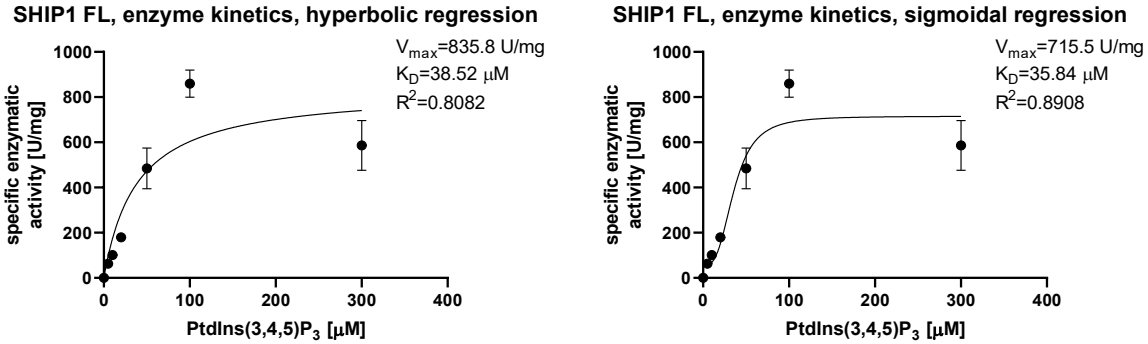

fig. 124: determination of the enzyme kinetics of SHIP1 FL towards PtdIns(3,4,5)P_3. The specific activity of SHIP1 FL was determined for substrate concentrations ranging from 0-300 µM and plotted by hyperbolic or sigmoidal regression to determine the V_{max} and K_M. Error bars indicate standard deviations. n=3.

Further, the enzyme kinetics of the SHIP1 domain constructs bearing the PPase domain (PH-L-PPase, PPase-C2, PHL-PPase-C2 and PPase) were analysed as for the FL protein. This is shown in **fig. 125**.

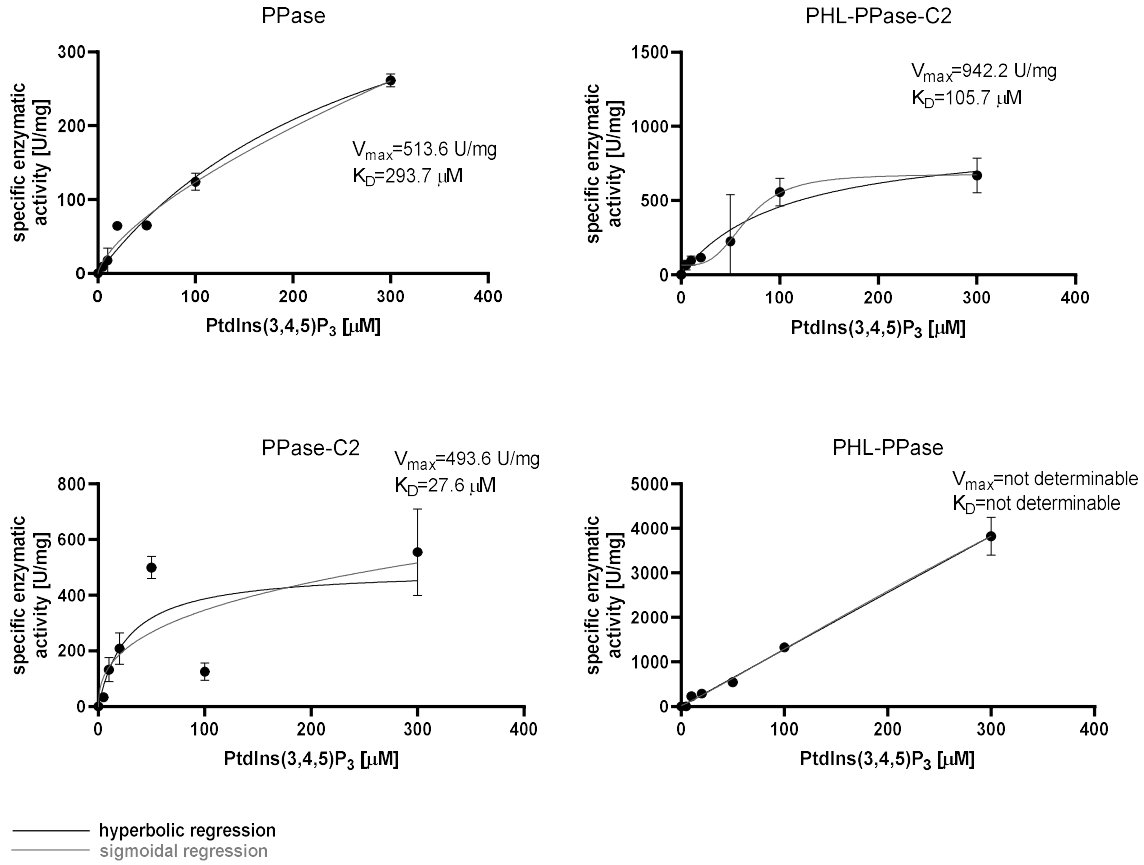

fig. 125: Determination of the enzyme kinetics of SHIP1 PPase, PHL-PPase, PPase-C2 and PHL-PPase-C2. The specific activity of SHIP1 FL was determined for substrate concentrations ranging from 0-300 µM and plotted by hyperbolic or sigmoidal regression to determine the V_{max} and K_M. Error bars indicate standard deviations. n=3.

As shown, catalysis was significantly impaired in PPase and PHL-PPase compared to SHIP1 FL and those constructs bearing the C2 domain. In addition, PPase-C2 and especially PHL-PPase-C2 showed a rather sigmoidal enzyme kinetics as also found in the FL protein.
For the constructs, the turnover number k_{cat} and catalytic efficiency k_{cat}/K_M were calculated in comparison to the FL protein which is depicted in **table 17**. The catalytic efficiency was highest for the FL protein and significantly enhanced in constructs bearing the C2 domain (PPase-C2 and PHL-PPase-C2) compared to the PPase domain alone. Those taken together with the sigmoidal kinetics found in PPase-C2 and PHL-PPase-C2 but not in PPase again verified the function of the C2 domain as an allosteric activator while the PH-L domain might rather negatively influence the SHIP1 catalysis (increased K_M and reduced catalytic efficiency in constructs bearing the PH-L domain compared with equivalents not bearing it).

Table 17: Comparison of the enzyme kinetic parameter (V_{max}, K_M, k_{cat} and k_{cat}/K_M) of SHIP1 FL, PPase, PH-L-PPase, PPase-C2 and PH-L, PPase-C2, n.d.=not determinable

	FL	PPase	PH-L-PPase	PPase-C2	PH-L-PPase-C2
V_{max}	861.2	513.6	n.d.	493.6	942.2
K_M	38.5	293.7	n.d.	27.6	105.7
k_{cat}	0.035	0.021	n.d.	0.020	0.038
k_{cat}/K_M	9010	71	n.d.	723	360

4.3.3.3. Analysis of the phosphoinositide binding of SHIP1

The phosphoinositide-binding of SHIP1 FL was assessed by SPR (4.2.2.2). In the following section the establishment of alternative assay systems with less work and financial expenditure but also less quantitative value (qualitative to semi-quantitative) (PLO, COVA-PIP Array) will be described with the aim to utilize them as complementary binding assays as well as initial screening systems (i.e. for mutant proteins).
The PLO assay is a method to analyse the interaction strength between a protein and a lipid. Lipids of interest are spotted onto a hydrophobic membrane and incubated with the protein of interest. Bound protein of interest is then

detected using an appropriate antibody. For the PLO assay commercially available PIP array strips (Echelon) were used containing phospholipids in concentrations ranging from 1.56 pmol/spot to 100 pmol/spot. To establish the assay, a commercially purchasable positive control (PI(4,5)P2 Grip (PLC-d1-PH)) (Echelon) was used which specifically binds to PtdIns(4,5)P_2. The membrane was blocked for 1 hour at RT in PBS, 0.1% Tween-20, 3% fatty-acid free BSA (blocking buffer) after which PI(4,5)P2 Grip was added at a final concentration of 1 µg/mL in blocking buffer for 1 hour at RT. The membrane was washed 3 times for 5 minutes in PBS, 0.1% Tween-20 (PBS-T) and anti-GST goat polyclonal antibody (Merck) was added in a dilution of 1:2000 (in blocking buffer) for 1 hour at RT. Primary antibody dilution was discarded and the membrane was washed 3 times for 5 minutes in PBS-T. Secondary HRP coupled anti-goat antibody (diluted 1:2000 in blocking buffer) was added and incubated for 1 hour at RT. The membrane was once again washed in PBS-T 3 times for 5 minutes at RT. Signals were detected by chemiluminescence and signal intensity for PtdIns(4,5)P_2 was quantified and normalized to the maximal signal (100 pmol/spot PtdIns(4,5)P_2). Normalized signal intensities were plotted against pmol/spot PtdIns(4,5)P_2 and fitted by hyperbolic regression. The apparent K_D was 31.83 pmol/spot which equalized 6.4 nM ((pmol/spot)/reaction volume in mL, reaction volume was 5 mL). Signals for other phospholipids were significantly weaker or not detectable and most possibly the result of unspecific binding i.e. due to not further optimized assay conditions. Conclusively, the positive control showed the expected results (**fig. 126**).

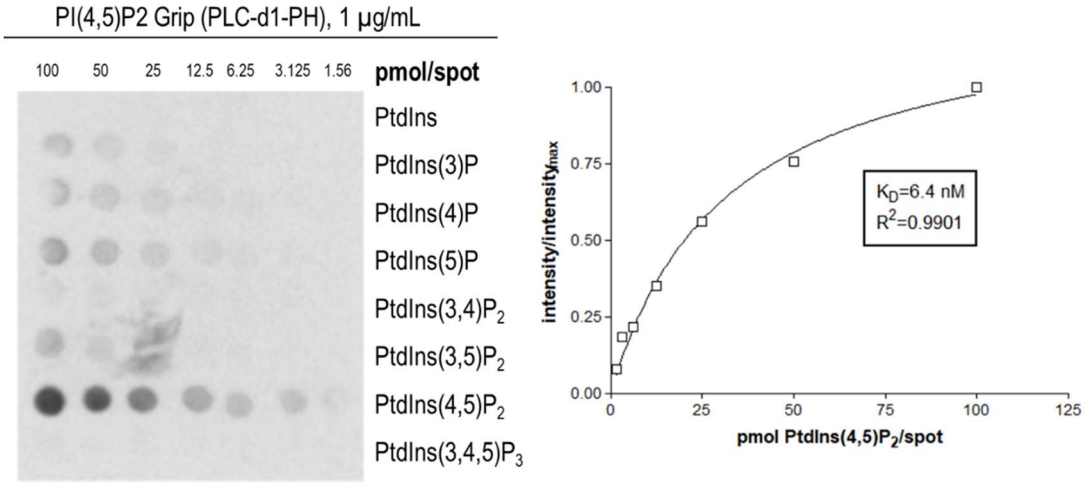

fig. 126: phospholipid overlay assay using PI(4,5)P2 Grip (PLC-d1-PH) (details: see text).

Following the general establishment of the assay, it was aimed to establish the assay system for SHIP1 FL. following the standard assay protocol (see above) and using either StrepMAB Classic-HRP or SHIP1 P1C1 and anti-mouse HRP for detection. As can be seen in **fig. 127** a concentration dependent interaction between SHIP1 and PtdIns(3,4,5)P_3 or PtdIns(3,4)P_2 was verified, however at a low signal to noise ratio and low overall signal intensity especially for PtdIns(3,4,5)P_3 which was expectable given prior examinations which could show that the more hydrophilic the phospholipid was the higher the level of phospholipid passing over from the hydrophobic membrane into the hydrophilic buffer system used and consequently get washed away resulting in reduced signal intensity [1045]. Especially when SHIP1 P1C1 was used for detection some kind of "ring effect" could be observed (high ring-shaped signal at the outer borders of spots) which aggravated quantification. As an alternative it was tried to quantitate only the inner part of the spots to avoid the problems caused by ring effects, however with no differences given the overall result (not shown). Also, several attempts for assay optimization (concentration of SHIP1 FL, buffer composition i.e. concentration of Tween-20, overnight incubation vs. 1 hour incubation of primary antibody, adaption of washing steps) remained without success. Using StrepMAB Classic K_D values of 3.1 pmol/spot (0.62 nM) for PtdIns(3,4)P_2 and 1.3 pmol/spot (0.26 nM) for PtdIns(3,4,5)P_3 were estimated.

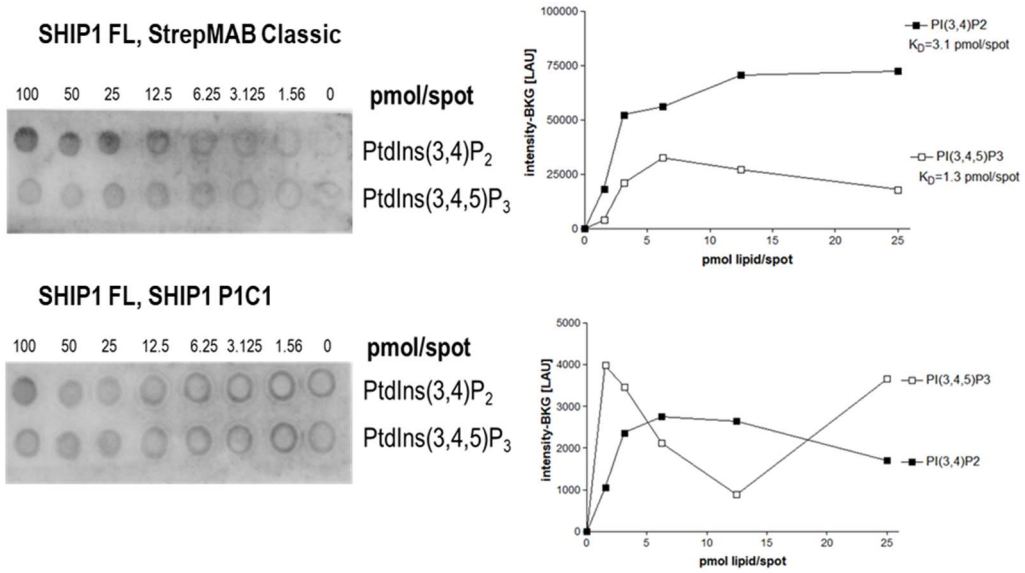

fig. 127: phospholipid overlay assay using SHIP1 FL and either StrepMAB Classic-HRP or SHIP1 P1C1 and anti-mouse HRP for detection (details: see text).

All in all, the PLO system was not found optimal to reliably analyse the interaction of SHIP1 proteins (or Strep tagged phospholipid binding proteins) with phosphoinositides of interest.
As an alternative approach COVA-PIP Array was used. For this assay systems COVA-PIP 96-well plates containing the phosphoinositide of interest absorbed to the bottom of the wells and pre-blocked were purchased from Echelon and the assay establishment was performed using SHIP1 FL in concentrations ranging from 0 to 1.5 µg/mL and a plate containing 20 pmol PtdIns(3,4,5)P_3/well. SHIP1 FL was diluted to 0.5, 1.0 or 1.5 µg/mL in blocking buffer (3% BSA, 0.5% Tween in PBS) and 100 µL/well was pipetted into the Cova-PIP plate and incubated for 1 h at RT and gentle shake. The protein solution was discarded and the plate was washed 3 times for 3 minutes with wash buffer (0.1% Tween-20 in PBS) after which Strep-Mab classic-HRP (1:10000 diluted according to the manufacturer) was added and incubated for 1 h at RT and gentle shake. The plate was washed once with PBS-T as described above and additionally once for 3 minutes with PBS and bound SHIP1 FL was detected by developing the plate for 30 minutes with 100 µL/well TMB in the dark and measuring the absorbance at 650 nm (fig. **128**).

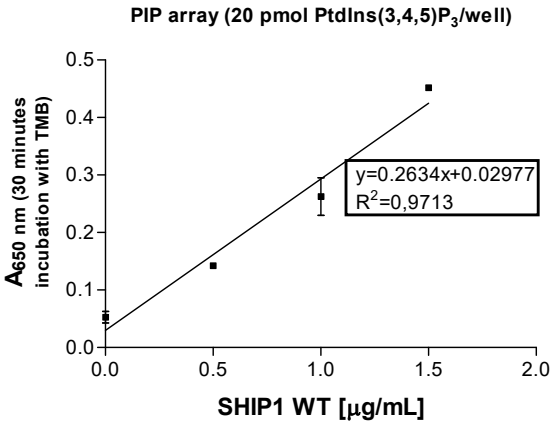

fig. 128: Establishment of the Cova-PIP Array. SHIP1 FL was diluted to 0.5, 1.0 or 1.5 µg/mL in blocking buffer or blocking buffer only was used as negative control and PtdIns(3,4,5)P_3 was constant at 20 pmol/well. The level of bound SHIP1 was detected using StrepMab-Classic HRP and measuring the absorbance at 650 nm after incubation with TMB for 30 minutes. Absorbance values were plotted against the concentration of SHIP1 WT used and analysed by linear regression. Error bars indicate standard deviations. n=2.

As depicted in **fig. 128** the level of SHIP1 bound was proportional to the level of SHIP1 used in the assay with a linear regression coefficient of 0.9713. Especially, this system beared the advantage that signal intensity was homogenous (no ring effects). For the actual assay COVA-PIP Array plates were used coated with PtdIns(3,4,5)P_3 or PtdIns(3,4)P_2 in concentrations ranging from 0 to 100 pmol/spot. Recombinant Strep-SHIP1 FL was diluted to a final concentration of 1 µg/mL in blocking buffer. Measured absorption values at 650 nm were normalized to

absorption at 100 pmol/spot and plotted against the amount of phosphoinositide (**fig. 129-131** and **table 19**). In a final volume of 100 µL 1 pmol phosphoinositide/100 µL is equal to 10 nmol/L or 10 nM and therefore an apparent K_D value of 22.3 nM for PtdIns(3,4,5)P_3 and 22.4 nM for PtdIns(3,4)P_2 was estimated for SHIP1 FL using this system. The K_D values obtained from the three assay systems (SPR, COVA-PIP Array, PLO) for SHIP1 FL are summarized in **table 18**. As can be seen they differed from each other but were all in the nM range. Moreover, for all three assay systems the K_D values of PtdIns(3,4)P_2 and PtdIns(3,4,5)P_3 were similar to each other. All in all, both the COVA-PIP Array and (taken into account the discussed technical constraints) the PLO assay can be seen as valuable (semi-quantitative) screening tools to select proteins for further more quantitative binding assays (such as SPR). However, it has to be taken into account that the COVA- PIP and PLO assay described here were limited as the pre-produced plates only offered a certain range of phosphoinositide amounts which might be problematic for the determination of sub-nM K_D-values

Table 18: comparison of KD values for the interaction of SHIP1 FL with PtdIns(3,4,5)P_3 and PtdIns(3,4)P_2 obtained with COVA-PIP Array, PLO and SPR.

K_D [nM]	PtdIns(3,4,5)P_3	PtdIns(3,4)P_2
COVA-PIP Array	22.3	22.4
PLO	0.26	0.62
SPR	1.07	6.03

Further, the KD values for the SHIP1 phosphoinositide binding domain constructs towards PtdIns(3,4)P_2 and PtdIns(3,4,5)P_3 were determined by COVA-PIP Array assay. This method was chosen due to its relatively low time effort while still providing (semi-)quantitative data in a first approach which can be used for additional more accurate studies such as SPR. The result of the COVA-PIP Array is summarized in **fig. 129-131** and **table 19**.

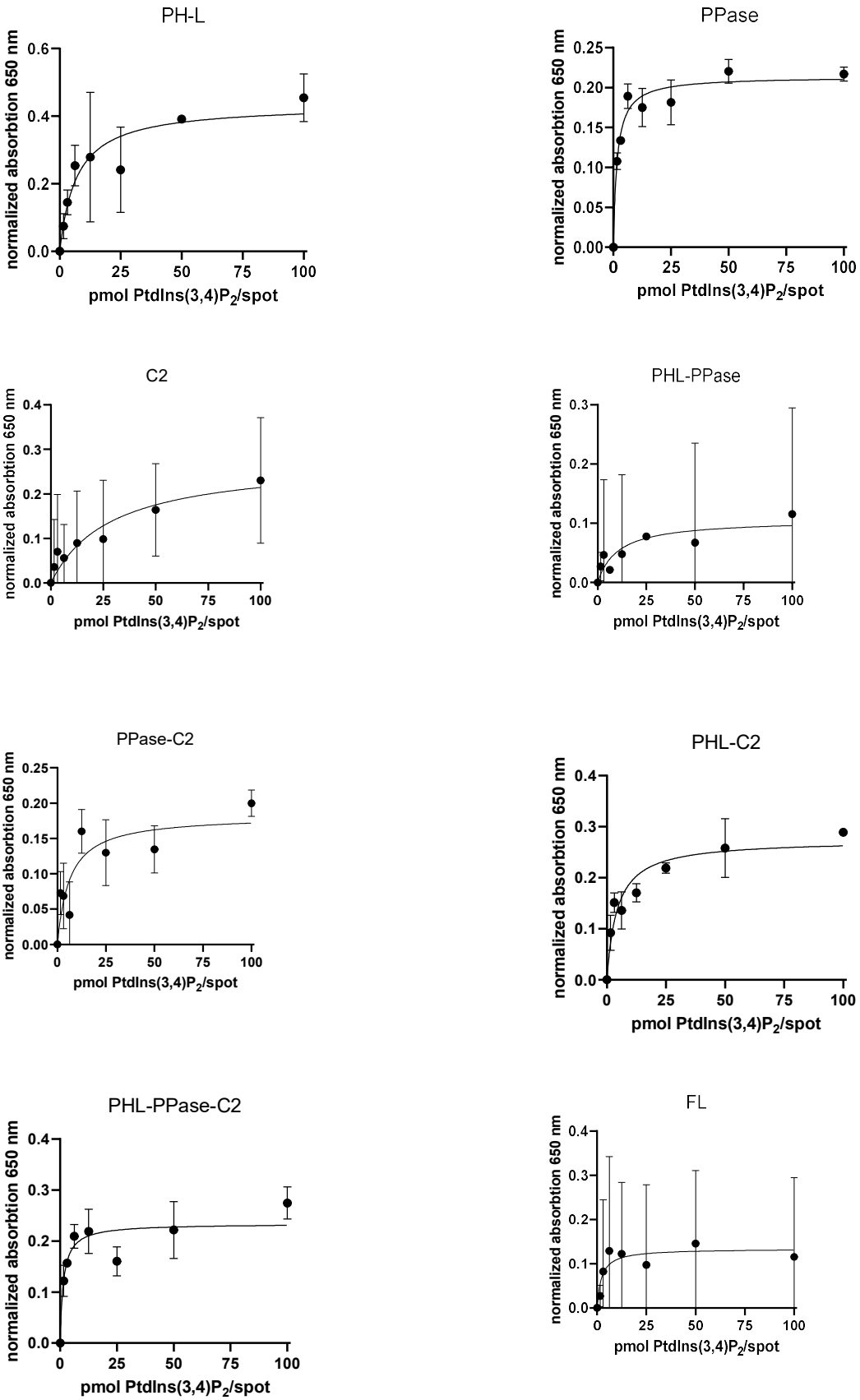

fig. 129: Determination of the K_D values of SHIP1 phosphoinositide domain constructs towards PtdIns(3,4)P_2 by COVA-PIP-Array. For the assay, commercially available 96-well plates coated with PtdIns(3,4)P_2 (Echelon) were used. The assay was performed according to the instructions of the manufacturer. Error bars indicate standard deviations. n=3.

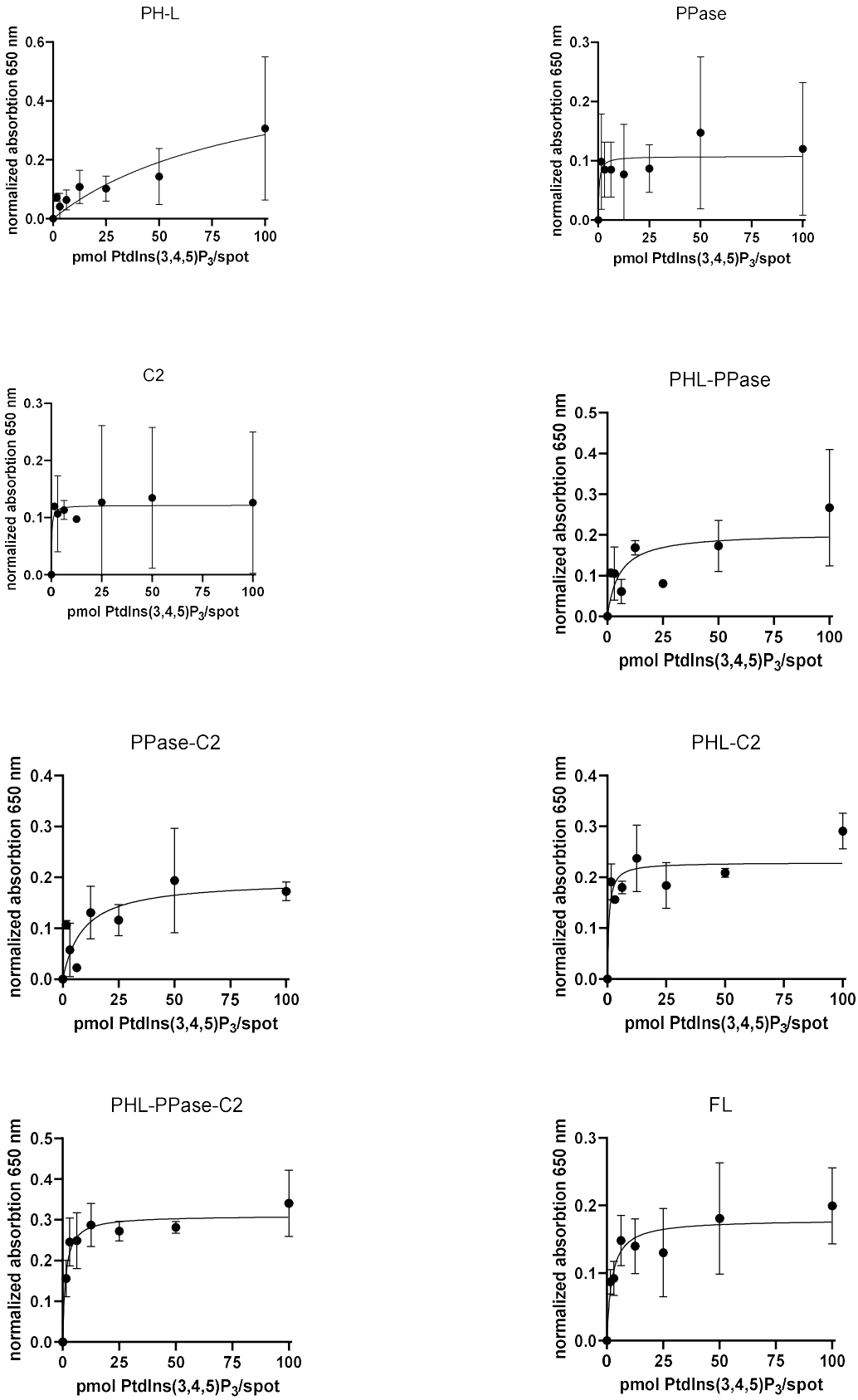

fig. 130 Determination of the K_D values of SHIP1 phosphoinositide domain constructs towards PtdIns(3,4,5)P_3 by COVA-PIP-Array. For the assay, commercially available 96-well plates coated with PtdIns(3,4,5)P_3 (Echelon) were used. The assay was performed according to the instructions of the manufacturer. Error bars indicate standard deviations. n=3.

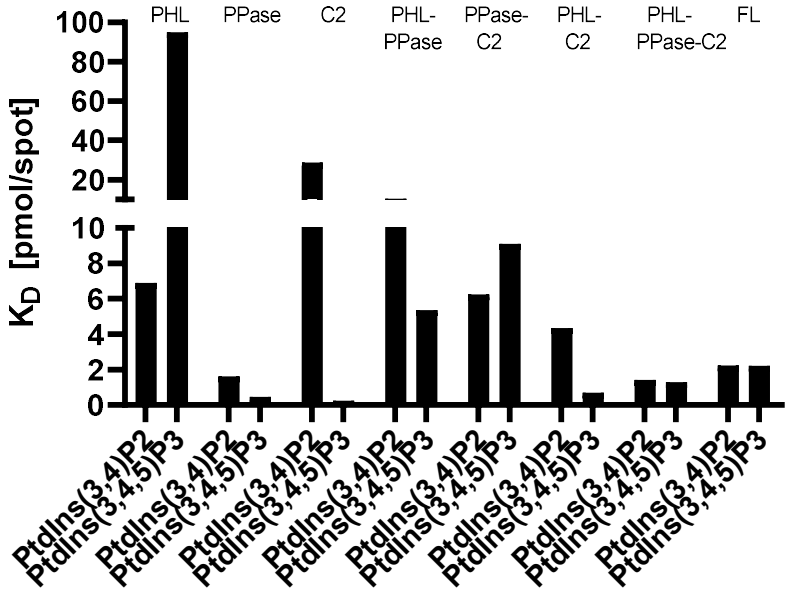

fig. 131: Comparison of the K_D values of SHIP1 phosphoinositide domain constructs and SHIP1 FL towards PtdIns(3,4)P_2 and PtdIns(3,4,5)P3. COVA-PIP-Array was used for the determination of the K_D values. n=3.

Table 19: Comparison of the K_D values of SHIP1 phosphoinositide domain constructs and SHIP1 FL towards PtdIns(3,4)P_2 and PtdIns(3,4,5)P3. For the SHIP1 phosphoinositide domain constructs, COVA-PIP-Array was used for the determination of the K_D values. n=3.

K_D [pmol/spot]	PH-L	PPase	C2	PHL-PPase	PPase-C2	PHL-C2	PHL-PPase-C2	FL
PtdIns(3,4)P_2	6.913	1.604	28.74	10.43	6.246	4.351	1.419	2.24
PtdIns(3,4,5)P_3	95.02	0.459	0.2351	5.364	9.116	0.6908	1.291	2.225

In summary, all constructs showed K_D values in the nM range (<100 pmol/spot). SHIP1 PPase, C2, PHL-PPase and PHL-C2 displayed higher affinity towards PtdIns(3,4,5)P_3 while PH-L and PPase-C2 showed higher affinity towards PtdIns(3,4)P_2 and PHL-PPase-C2 and FL displayed relatively comparable affinities towards PtdIns(3,4)P_2 and PtdIns(3,4,5)P_3. From the data obtained, no general contribution of one domain for the specific binding to only either PtdIns(3,4)P_2 or PtdIns(3,4,5)P_3 could be concluded and to this point, binding to phosphoinositides seems to be highly complex and not coverable by a simple model.

5. Discussion

5.1. SHIP1 is a player in the tumorigenesis of Colorectal Cancer (CRC)

SHIP1, a hematopoietic phosphoinositide-5-PPase was found to be expressed in several carcinoma entities and established carcinoma cell lines. The expression was most prominent in CRC (60% of CRC samples analysed showed high or moderate expression of SHIP1 in a TMA assay [591]). The re-expression of SHIP1 in non-hematopoietic cancer but not healthy tissue led to the hypothesis that SHIP1 might have an (oncogenic) function in carcinoma and with special focus in CRC. In order to analyse the function of SHIP1 in CRC two working approaches were utilized which included (1) overexpression of SHIP1 in the SHIP1 negative CRC line HCT-116 and (2) downregulation (*knock-down* or *knock-out*) of SHIP1 in the SHIP1 positive CRC lines HT-29 and SW-480. The cell lines were generated by lentiviral transduction and verified by Western Blot analysis. On the cellular level, SHIP1 did not significantly affect cell proliferation in 2D- and 3D- (tumoroid) culture but had a cell line dependent effect on cell motility (migration, invasion and chemotaxis). SHIP1 positively affected cell motility in HCT-116 and SW-480 and negatively in HT-29. Cell line dependent effects of SHIP1 on the kinome and signal transduction (MAPK and PI3K/AKT/mTORC1 pathway) were found and with regard to the proteome SHIP1 mostly affected energy metabolism and gene expression (transcription, translation, histones and mRNA splicing). Also, the transduction procedure alone significantly altered the proteome.
In general, several of the observed effects of SHIP1 were found to be associated with traits commonly altered in cancers.
The most obvious aspect speaking for a functional role of SHIP1 in colorectal cancer would be its re-expression in CRC while not found in healthy colorectal tissue. The ectopic expression of SHIP1 in CRC may be due to epigenetic alterations (DNA level), on the RNA level (i.e. via loss of miRs such as miR-155 which mediates repression of SHIP1 in AML [1046]) or on the protein level (i.e. via loss of SHIP1 degrading proteins/mechanisms, for instance in CML SHIP1 is primed for ubiquitination by BCR/ABL/SRC kinase dependent phosphorylation [586], [587]).
Secondly, SHIP1 regulated cell motility (migration, invasion and chemotaxis) in cell culture which would be a critical point for metastasis *in vivo*. Although a direct link of increased chemotaxis in SW-480 SCR vs. SHIP1 KD2 and metastasis in the NSG-mouse model examined could not be found, a weak positive impact of SHIP1 on metastasis was found in a past mouse model (HCT-116 SHIP1 WT vs. LeGO, unpublished) which correlated with increased invasion and migration in HCT-116 SHIP1 WT compared to LeGO control cells *in vitro*. To this point, it has to be taken into account that (1) in the SW-480 model only chemotaxis was examined due to technical limitations which is not exactly based on the same molecular mechanisms than migration and especially invasion (critical for metastasis) and (2) metastasis is a highly complex multi-step process including EMT and shedding of single cells from the primary tumour, invasion through the ECM, extravasation, survival in the blood/lymph flow (protection from mechanical tension etc.), homing and intravasation and colonization (MET, proliferation and generation of the macrometastase). Therefore, increased motility is required but not sufficient for metastasis and one could not directly conclude that more motile cells would automatically show higher metastatic potential. On the signal transduction level, the spatiotemporal accumulation of certain phosphoinositides is strongly correlated to cell motility (i.e. the formation of filopodia, lamellipodia and invadopodia) as several signalling proteins possess phosphoinositide binding domains (see 1.3.). Especially concerning PtdIns(3,4)P_2, the product of the SHIP1 catalysed reaction, there is evidence that it directly links to cell motility. For instance, the lamellipodial protein lamellipodin is recruited to the leading edge by PtdIns(3,4)P_2 and the invadopodial/podosomal adaptor protein TKS5 contains a PtdIns(3)P/PtdIns(3,4)P_2-specific PH domain. Of note, SHIP2 was linked to metastasis in both a positive (NSCLC, mammary carcinoma) and a negative (mammary carcinoma) way [1047] and the differential impact of SHIP1 enzymes on cell motility traits was also reflected for SHIP1 in the CRC models (positive impact in HCT-116 and SW-480 and negative impact in HT-29). Most possibly this can be explained by means of the Two-PIP hypothesis, i.e. SHIP1 could promote PtdIns(3,4)P_2-dependent motility via LPD or reduce PtdIns(3,4,5)P_3-dependent motility via VAV or P-REX.
Thirdly, from the proteome analysis there was evidence that SHIP1 affected cellular metabolism. The metabolic reprogramming is a common trait in cancers and became most prominently featured when the Warburg effect was first described. Newer studies however indicate, that metabolic reprogramming is more complex than once assumed and not necessarily limited to the Warburg effect. In fact, several studies found that the metabolic state of cancer cells was dictated by both the transcriptional program of the tumour cell (via overexpression of oncogenes and downregulation of tumour suppressor proteins) but also by the tumour environment (nutrient and oxygen availability) and the tumour microenvironment (metabolic community of tumour cells and cells of the TME) and therefore, a tumour might be heterogeneous with regard to the metabolic state of the individual tumours and the

metabolic state can change during tumour progression. In their reviews, Fu et al. [1048] and Vaupel and Multhoff [1049] differentiated between two general subpopulations which could co-exist in a tumour. The first subpopulation was marked by a glycolytic metabolic state (Warburg population) with defect or temporarily unfunctional mitochondria and oxidative phosphorylation. For instance, some tumour cells were shown to inherit inactivating mutations in TCA cycle enzymes or loss of Mn-dependent mitochondrial superoxide dismutase leading to the activation of respiratory chain uncoupling proteins (UPCs) and on the other hand, key glycolytic enzymes such as lactate dehydrogenase, enolase or hexokinase 2, lactate transporters (MCTs) and GLUT1 were upregulated transcriptionally or over-activated by key Warburg *upstream* signalling pathways (MAPK/c-MYC and PI3K/AKT/mTORC/HIF1α). The low-activity pyruvate kinase isoform PKM2 was typically predominant over PKM1 in those cells leading to the accumulation of glycolytic intermediates for the biosynthesis of amino acids, nucleotides, lipids or NADPH necessary for rapid cell proliferation and redox balance. Another key point for the preference of aerobic glycolysis over oxidative phosphorylation would be the role of secreted lactate and H^+ which triggered enhanced invasion, metastasis, neo-angiogenesis and immunosuppression in the TME (oncometabolite). The second subpopulation was mainly dependent on oxidative phosphorylation for ATP production and utilized a metabolic symbiosis with cells of the TME, mostly CAFs, termed the reverse Warburg effect. In this scenario, a pseudohypoxic state was induced in the TME by secretion of ROS from the tumour cell. This resulted in defective CAF mitochondria due to the loss of caveolin-1 and a glycolytic phenotype of the CAFs via NF-κB and HIF1α. The metabolites produced in the CAFs (lactate, pyruvate, ketones or fatty acids) were then secreted into the extracellular space by MCTs and uptaken by the tumour cell and used for ATP production via oxidative phosphorylation. Clarifying, those subpopulations are not strictly separated from each other but rather a continuum and, as mentioned beforehand, can merge into each other, a phenomenon termed metabolic plasticity. The preference for one phenotype was shown to depend on the transcriptional/epigenetic programming or stage of the tumour and the extracellular environment. For instance, under nutrient deprivation, tumour cells tended to switch to the Reverse Warburg phenotype to secure sufficient ATP production and it was hypothesized that especially cancer stem cells and early tumour stages displayed higher abundance of the Warburg phenotype to secure rapid proliferation and later-stage tumours marked by an established TME and the potential for a functional metabolic symbiosis were predominantly of the Reverse Warburg phenotype for more efficient ATP production. In the context of phosphoinositide signalling, PtdIns(3,4)P_2 was shown to exert differential effects on cell metabolism depending on its localization within the cell. At the plasma membrane, PtdIns(3,4)P_2 regulates the translocation of GLUT4 to the plasma membrane and glycogen synthesis. As indicated in 1.4.3. SHIP2 regulates glucose homeostasis in insulin-sensitive tissues as it counteracts the AKT dependent translocation of GLUT4 to reduce glucose uptake and the AKT dependent inhibition of GSK3β to reduce glycogen synthesis [592], [593]. *SHIP2*$^{-/-}$ mice are therefore hypersensitive to insulin and display hypoglycaemia and weight loss even under a high-caloric diet and *SHIP2* overexpressing mice are marked by insulin resistance. [594], [595], [596], [597]. Furthermore, PI3KI-dependent effects on GLUT4 and GSK3-β are further reduced by a negative *feedback-loop* comprising the PtdIns(3,4)P_2-dependent recruitment of TAPP1 to the plasma membrane. While at the plasma membrane PtdIns(3,4)P_2 can potentially activate mTORC1 *downstream* of PI3K/AKT due to the Two-PIP-hypothesis, endosomal PtdIns(3,4)P_2 was shown to inhibit mTORC1 in response to nutrient starvation which correlated with reduced levels of G6PDH, glycolysis, pentose phosphate pathway, purine synthesis and mitochondrial biogenesis/ATP generation [1050]. As summarized for SW-480 and for HCT-116 (**fig. 132**) the general metabolic profile of SHIP1 expressing SW-480 cells (SW-480 SCR) showed upregulation of AKT, the key enzyme for inducing the Warburg effect in cancer cells. Also speaking in favour for a Warburg phenotype would be the use of glycolytic intermediates for amino acid synthesis due to upregulation of PHGDH and the upregulation of the gluconeogenesis-involved oxaloacetate malate carrier as well as reduced expression of enzymes of the key mitochondrial pathways Krebs cycle (CS, OAT), β-oxidation (HADHB, ACOT7, ACADVL) and OxPhos (cytochrome C, ubiquinone, ATP-synthase) and mitochondrial ATP-transporter. However, the downregulation of the key enzyme of the pentose phosphate pathway G6PDH and the upregulation of the OxPhos complex NADH-DH and of MTPN would be in favour of a reverse Warburg phenotype. In HCT-116 a Warburg phenotype would be more probable due to the general mitochondrial defect as well as upregulation of LDH, one of the key Warburg enzymes, PHGDH and the key gluconeogenesis enzyme PEPCK but the two glycolysis/gluconeogenesis enzymes PGK1 and G6P-isomerase were downregulated by SHIP1 as well as AKT and MAPK activity was reduced which both are key pathways to uphold the Warburg effect in tumour cells (but may be compensated by other oncogenic pathways such as SRC, PKC). Of note, also the activity of AMPK was reduced by HCT-116 pointing to an energy deficite and a rather catabolic metabolic state. Fourthly, SHIP1 impacted translation, transcription and mRNA processing/splicing as indicated in the proteome analysis. The dysregulation of those features is also common in cancer and could lead to aberrant expression of oncogenes, reduced expression of tumour suppressors or expression of oncogenic alternative splice forms. For

instance, the alternative splice form of RAC1, RAC1b was shown to be constitutively active and expressed in tumour but not in healthy tissue [388].
In the proteome analysis a set of proteins regulated by SHIP1 in SW-480 correlated with an impact on the prognosis of CRC patients. Regarding this point, in some cases those pointed to an oncogene function of SHIP1 while in others they pointed to a tumour suppressor function. Of note, a not insignificant amount of proteins were observed to fulfil dual impacts on the clinical prognosis in cancer patients dependent on cancer type, stage and others. Exemplarily, with regard to enhanced expression of MCM complex subunits in SW-480 SHIP1 KD vs. SCR (MCM 3-7) MCM proteins (helicase proteins involved in DNA replication and cell cycle progression) were found both favourable and unfavourable or no prognostic markers in cancer as summarized by Ju et al. (2020) [1051].
A cell-line dependent effect of SHIP1 on signal transduction was observed. While in HCT-116 SHIP1 expression rather negatively impacted PI3K/AKT/mTORC1 and MAPK signalling in SW-480 and HT-29 SHIP1 rather positively (PI3K/AKT/mTORC) or ambiguously (MAPK) impacted it. This is in accordance with the fact that SW-480 and HT-29 naturally express SHIP1 while HCT-116 does not. Therefore, it is likely to conclude that SW-480 and HT-29 may take advantage and HCT-116 may take disadvantage out of SHIP1 expression (i.e. here with regard of signal transduction). Consistent with this a loss or overgrowth of SHIP1 KD was observed in SW-480 and HT-29 over a longer culturing period.
In the NSG-mouse model SW-480 SHIP1 KD2 mice displayed a prolonged overall survival in comparison to the SW-480 SCR cohort. The findings that the SHIP1 KD was lost in the established tumours (Western Blot analysis of mouse tumours obtained after sacrificing the mice) and that a high portion of the mice had to be sacrificed due to the development of ulci are problematic in this context. However, the loss of the SHIP1 KD during tumour development could also support the hypothesis of SHIP1 as an oncogene in CRC as it can be supposed that SHIP1 might be necessary for full tumour development and SHIP1-negative tumours would die, be overgrown or more easily detected by the immune system before macro-tumours could have developed. A similar effect was also observed in cell culture where the SHIP1 KD was lost over a longer culturing period. At the end of the thesis, a SHIP1 KO was successfully established which would be valuable in future experiments to avoid such problems.
Although from the results obtained there is evidence for a possible oncogenic function of SHIP1 in CRC a cell-line and context-blanket consensus on the role of SHIP1 in this cancer entity could not be concluded As already discussed, phosphoinositide-5-phosphatases do have the potential to act both as a tumour suppressor or an oncogene due to the Two-PIP hypothesis depending on the cell line/context (see 1.4.3.) [84] and the results obtained do fit into this model. In SW-480 and HCT-116 one could propose an oncogenic function of SHIP1 due to its positive effect on cell motility and the *in vivo* data obtained in the NSG-mouse experiment of SW-480 which should be valued strongest. This should be verified in the future using transgenic mice with a colorectal specific overexpression of SHIP1 via the Cre/Lox system and foci assay to determine the oncogenic strength of SHIP1. In contrast, in HT-29 SHIP1 could be proposed to be a tumour suppressor due to its negative effect on cell motility. In further experiments, a rescue of the SHIP1 KD should be established in SW-480 or alternatively a KD/KO of SHIP1 in HCT-116 SHIP1 WT in order to minimize the cell-line dependent differences of the experimental setup used (HCT-116 vs. SW-480/HT-29) and to verify the function of SHIP1 in CRC in a more integrated system.
The obtained results are summarized in **fig. 132** (note that for the kinome data those do not necessarily reflect actual enhanced enzymatic activity due to the PAMGENE principle of computationally matching enhanced phosphorylation status of selected substrate consensus sequences to enhanced activity of the most probably responsible kinase [631]):

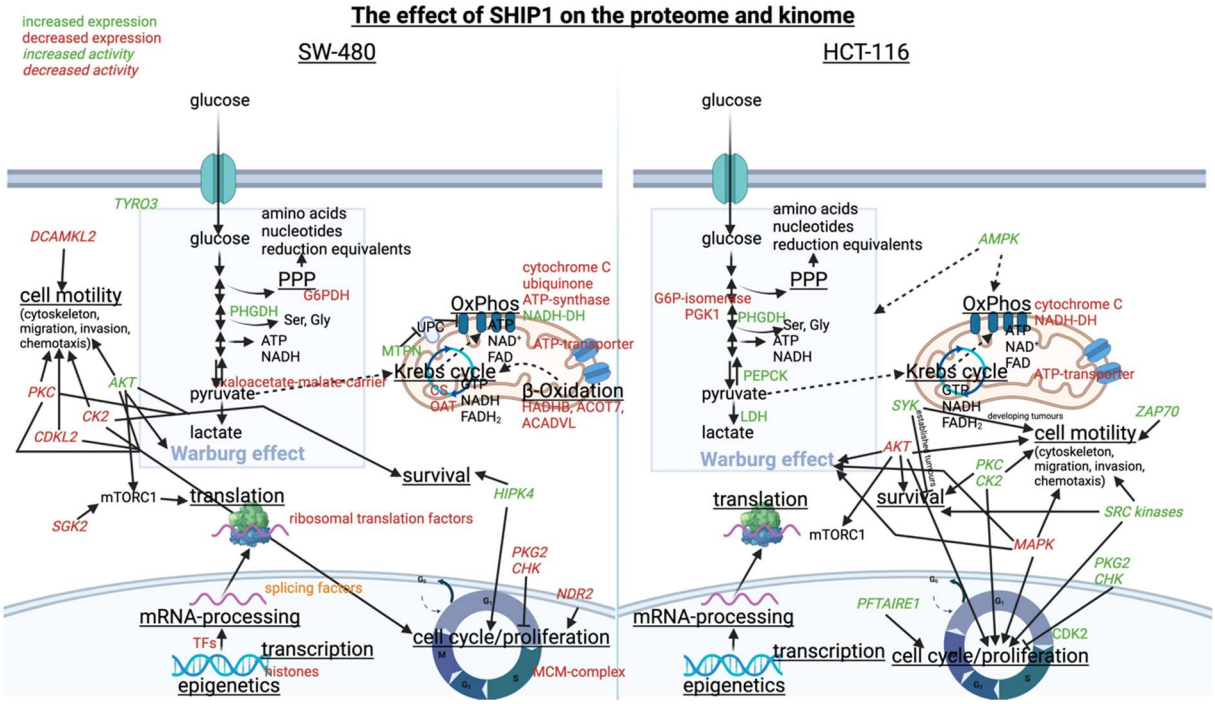

fig. 132: model of SHIP1 regulated pathways in SW-480 and HCT-116.

In HCT-116 the phenotype shifted to increased cell motility (migration and invasion) but no alterations in proliferation and survival were induced by SHIP1 overexpression. The mechanistical analysis pointed to a possible upregulation of cell motility via SRC kinases, ZAP70, PKC and CK2. With respect to cell proliferation, positive (increased activity of PKC, CK2 and PFTAIRE and upregulation of proteins involved in cell cycle progression and DNA replication) and negative (increased activity of CHK, PKG2 and reduced activation of the MAPK and PI3K/AKT/mTORC pathways) consequences of SHIP1 overexpression might balance each other so that the overall impact on cell proliferation would be neglible. A similar explanation can be assumed for cell survival/apoptosis (increased activity of PKC, SYK, SRC kinases and CK2 vs. decreased activity of AKT). Furthermore, from the signalling pathways altered by SHIP1 overexpression, it can be proposed that SHIP1 would impact energy metabolism due to dysregulation of the respiratory chain, mitochondrial transporter, glycolysis and gluconeogenesis and increased activity of AMPK and downregulation of the PI3K/AKT/mTORC pathway and had little direct effect on translation, transcription and mRNA processing (i.e. via SRC kinase members).
In SW-480 increased cell motility (chemotaxis) but no effect on proliferation and survival was observed for SHIP1 expressing cells (SW-480 SCR). With regard to cell motility this might be mostly due to overactivation of the PI3K/AKT/mTORC pathway maybe via TYRO3 or via the TYRO3/FYN cascade. With regard to cell proliferation as for HCT-116 negative (decreased activity of PKC, NDR2, CK2 and CDKL2, decreased levels of MCM complex) and positive (decreased activity of CHK, increased activity of HIPK4 and increased activation of the MAPK (effect of SHIP1 on this pathway not clarified, see also 4.1.4.) and PI3K/AKT/mTORC pathways again possibly via TYRO3 overactivation) of SHIP1 expression may balance each other out and the same can be assumed for cell survival (differential effects of PKA and increased activity of AKT and HIPK4 and decreased activity of PKC and CK2). Furthermore, a strong effect of SHIP1 expression on gene expression (translation, transcription, epigenetics and splicing) was found on the level of the proteome and kinome alike which was less pronounced in HCT-116, as well as alterations in energy metabolism would be expectable.

5.2. Patient-derived SHIP1 mutants of the catalytic domain affect the biochemical and structural properties of SHIP1 as well as its cellular behaviour

A significant portion of SHIP1 ectopically expressed in carcinomas was found to be mutated (5.56% in large intestine carcinomas). This finding was very intriguing as a high mutation rate is a common threat in cancers leading to the generation of oncogenes out of proto-oncogenes or loss/reduced levels or activity of tumour suppressor or DNA repair genes. One could propose that either the SHIP1 mutations found in the patient material would be bystander mutations with no apparent advantage for the tumour cell or they are advantageous mutations which became dominant in the course of the tumour micro-evolution. If so, the patient-derived mutations would have to

have a novel function that allowed it to dominate over SHIP1 WT. To test this, selected patient-derived mutations of the catalytic domain (E452K, R551Q, R577C and R673Q) were analysed for their biochemical properties and behaviour in cell culture (H1299) as well as on a structural level (*in-silico* analysis). The catalytic domain was chosen due to the high density of mutations found in this domain as well as the high level of information available in the literature. The impact of the selected SHIP1 mutations is summarized in **table 20**.

Table 20: summary of the properties and cellular behaviour of SHIP1 WT vs. selected patient-derived SHIP1 mutants of the catalytic domain

SHIP1 WT	SHIP1 E452K	SHIP1 R551Q	SHIP1 R577C	SHIP1 R673Q
protein levels, stability and localization				
½-life time≥24 h membrane/cytosol=1	40% expression of SHIP1 WT	200% expression of SHIP1 WT	140% expression of SHIP1 WT	2-5% expression of SHIP1 WT ½-life time=0.32 h membrane/cytosol=0.1 reduced stability due to enhanced proteasomal degradation
signal transduction (relative to LeGO)				
reduced P-AKT increased P-p44/42-MAPK	reduced P-AKT increased P-p44/42-MAPK	increased P-AKT increased P-p44/42-MAPK	increased P-AKT increased P-p44/42-MAPK	increased P-AKT increased P-p44/42-MAPK
catalytic activity (cellular SHIP1, 20 µM PtdIns(3,4,5)P_3 relative to SHIP1 WT				
	increased	strongly reduced	slightly reduced	no activity
enzyme kinetics (recombinant SHIP1)				
$9x10^3$ L/mol*s catalytic efficiency (Nelson, 2017, unpublished)	20-fold reduced catalytic efficiency (Nelson, 2017, unpublished)			
structural alterations caused by mutation				
	loss of H-bonds w./ N414 and maybe H700 in direct proximity to catalytic/substrate binding site	loss of H-bonds w./ G544 and N588 in direct proximity to catalytic/substrate binding site	loss of interaction w./ the main chains of F522, D566, L564, L569	loss of salt bridges w./ E634 and D617
K_D (binding to PtdIns(3,4,5)P_3)				
1.07 nM	5.03 nM			3.39 nM
K_D (binding to PtdIns(3,4)P_2)				
6.03 nM	0.06 nM candidate trapping mutant in PTEN-deficient tumours			6.58 nM

In conclusion, SHIP1 mutants impacted the enzymatic and binding properties, behaviour in cell culture and intra-protein interactions and therefore it is very likely that they would fulfil specific functions in tumorigenesis, maybe also only in specific stages of it. Regarding the SHIP1 mutant E452K, at first glance there were conflicting findings regarding the catalytic activity of cellular SHIP1 at 20 µM PtdIns(3,4,5)P_3 and the catalytic efficiency determined for recombinant SHIP1. However, it has to be taken into account that those two methods to compare the enzymatic properties of SHIP1 enzymes are different in principal aspects. First, using cellular SHIP1 the actual amount of SHIP1 used in the assay could not be determined *a priori* whereas when using recombinant SHIP1 a fixed enzyme amount was used. As the enzyme activity is correlated with the amount of enzyme used in the assay especially at non-saturated concentrations of the substrate this might be problematic and might not be completely outcalculated by the determination of the specific activity following the Western Blot-based calculation of the SHIP1 amount used in the assay. Secondly, the catalytic activity of cellular SHIP1 was measured at only one substrate concentration whereas the calculation of the enzymatic efficiency of recombinant SHIP1 is based on different substrate concentrations. As dictated by the Michaelis-Menten kinetics the enzyme activity is also dependent on the substrate concentration and relatively low substrate concentrations (well below saturation) can be in part compensated by increasing the amount of SHIP1. Therefore, in theory the increased catalytic activity of cellular SHIP1 E452K could be also explained by higher enzyme levels in the assay. Due to this double insecurity, determining the catalytic efficiency using recombinant SHIP1 would probably be the more accurate method. Another point to consider is the potential difference of cellular vs. recombinant (expressed in *E. coli*) SHIP1 i.e. regarding certain PTMs as well as the technical conditions of SHIP1 isolation (immunoprecipitation by SHIP1 antibody vs. *Strep Tactin* purification) which could potentially impact the catalytic properties of SHIP1 and may be different for SHIP1 WT and different SHIP1 mutants.

SHIP1 mutations E452K and R673Q and SHIP1 WT were mechanistically analysed in the context of a so-called phosphoinositide-trapping model. The phosphoinositide trapping model was reasoned as one possible model to explain oncogenic effects of SHIP1 expression in carcinoma. Ectopic expression of SHIP1 WT or (inactive) SHIP1 mutants would protect phosphoinositides implicated in oncogenic signal transduction (PtdIns(3,4,5)P_3 and

PtdIns(3,4)P_2) from degradation by phosphoinositide phosphatases and leading to their local accumulation. This would then recruit and activate PtdIns(3,4,5)P_3 and/or PtdIns(3,4)P_2 associating effector proteins replacing SHIP1 and in conclusion increasing the amplitude of oncogenic outputs (such as enhanced proliferation, survival and/or migration/invasion) which would favour primary tumour development and/or metastasis of carcinomas. For the model to be fulfilled there has to be K_D (phosphatases) > K_D (SHIP1) > K_D (effector proteins). Moreover, SHIP1 proteins protecting PtdIns(3,4,5)P_3 (substrate) would have to display strongly reduced or no catalytic activity as otherwise PtdIns(3,4,5)P_3 would become degraded instead of trapped. In contrast, with regard to PtdIns(3,4)P_2 SHIP1 proteins could be either active or inactive and trapping of PtdIns(3,4)P_2 by active SHIP1 proteins might be even more efficient as this would enhance the pool of PtdIns(3,4)P_2 in parallel. Moreover, PtdIns(3,4)P_2 was previously described to be an allosteric activator of SHIP1 amplifying the effect of PtdIns(3,4)P_2 accumulation (*feed-forward* loop) [614]. This makes clear that (1) binding and enzymatic properties of SHIP1 proteins, (2) binding (and enzymatic) properties of phosphoinositide phosphatases and (3) binding properties of effector proteins have to be considered when aiming to evaluate the phosphoinositide trapping model in total.
To analyse the phosphoinositide trapping model, SHIP1 WT, selected SHIP1 mutants (SHIP1 E452K, SHIP1 R673Q), phosphoinositide phosphatases (PTEN, INPP4B) and effector proteins (AKT1, TAPP2, P-REX1, TAPP1, TAPP2) were recombinantly expressed in *E. coli* as *Strep* fusion proteins and purified by *Strep Tactin* affinity chromatography. The affinity of purified proteins towards PtdIns(3,4)P_2 and/or PtdIns(3,4,5)P_3 was determined by Surface Plasmon Resonance (SPR) (see 4.2.2.2.).
The discussion should be started with a general reflection of the K_D value within the experimental context.

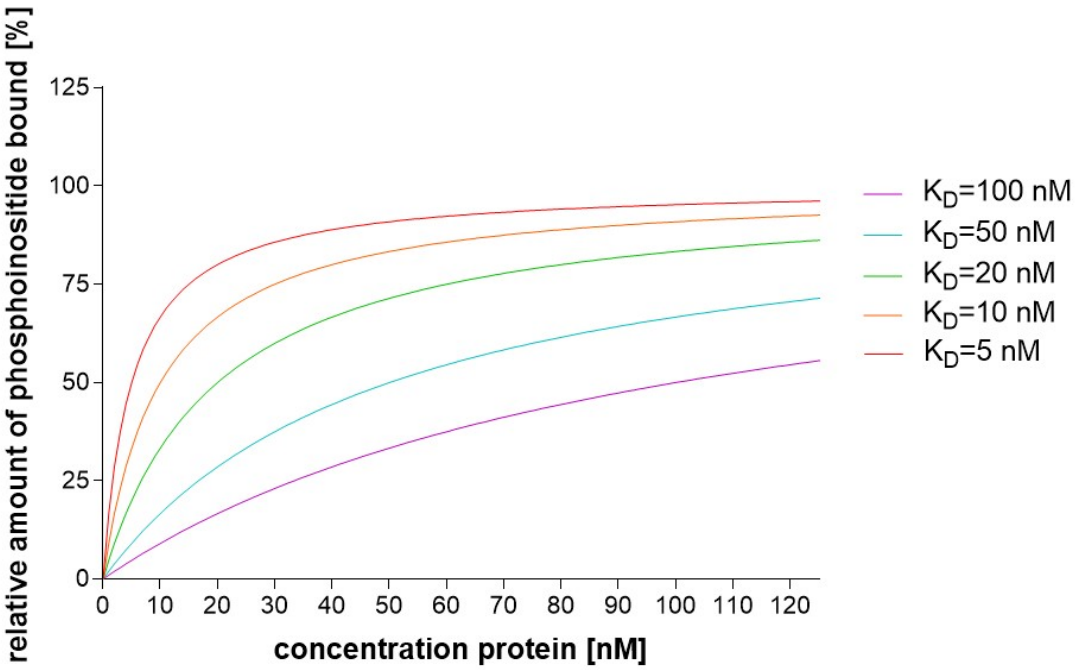

fig. 133: theoretical saturation curves for different K_D values.

As sketched in **fig. 133** the K_D value is a measure to determine the affinity between two binding partners (here is the phosphoinositide the ligand and saturated and the protein the analyte which is titrated) and determines the concentration of given analyte needed to reach the half maximal outcome of the binding assay (half maximal occupation of phosphoinositide). Therefore, the K_D value dictates how much analyte will be bound at a certain concentration of analyte. The formula of the K_D value in general is

$$Y = \frac{Y_{\max} * X}{(K_D + X)} \quad (5)$$

One can then define a fixed relative amount of phosphoinositide occupied Y_0 so that Y=Y_0 becomes a constant and a fixed $Y_{max(0)}$=const. to facilitate and one can further write the K_D value as a product of a constant $K_{D(0)}$ and a factor n>0.

$$Y_0 = \frac{Y_{\max(0)} * X}{(nK_{D(0)} + X)} \quad (6)$$

Hence, the equation will be solved for X.

$$X(n) = \frac{nK_{\mathrm{D}(0)} * Y_0}{Y_{\max(0)} * \left(Y_{\max(0)} - Y_0\right)} (7)$$

The protein concentration needed to occupy a given amount of phosphoinositide (the value of X) is dependent on n as all other factors in the equation are constants (**fig. 134** for an example). So that a protein with K_D value mK_D will have to be present at a concentration of mX_0 to reach Y_0 in comparison to a protein with K_D=K_D(0) and concentration X_0 needed to occupy Y_0.

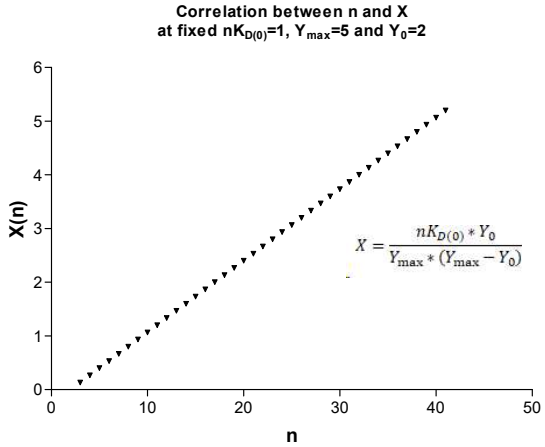

fig. 134: K_D value determination, correlation between n and X at fixed $nK_{D(0)}$=1, Y_{max}=5 and Y_0=2.

One can then define a value for the binding efficiency equal to the catalytic efficiency k_{cat}/K_M with $k_{cat}=V_{max}/[E_0]$ which would be c/K_D with $c=Y_{max(0)}$*a and a being a fixed phosphoinositide concentration, c=const. so that c/K_D~$1/K_D$ meaning the lower the K_D value the higher the binding efficiency.
To further take into consideration the contribution of Y_{max} one can set Y_{max} as a second variable

$$X(Y_{\max}) = \frac{nK_{\mathrm{D}(0)} * Y_0}{Y_{\max} * (Y_{\max} - Y_0)} = \frac{nK_{\mathrm{D}(0)} * Y_0}{Y_{\max}^2 - Y_{\max}Y_0} (8)$$

And one sees that the value of X is proportional to n (or the K_D value) and reversely correlated to Y_{max}. The correlation of X and Y_{max} is exponential and for high Y_{max} $X(Y_{max})$ approaches 0 (**fig. 135**).

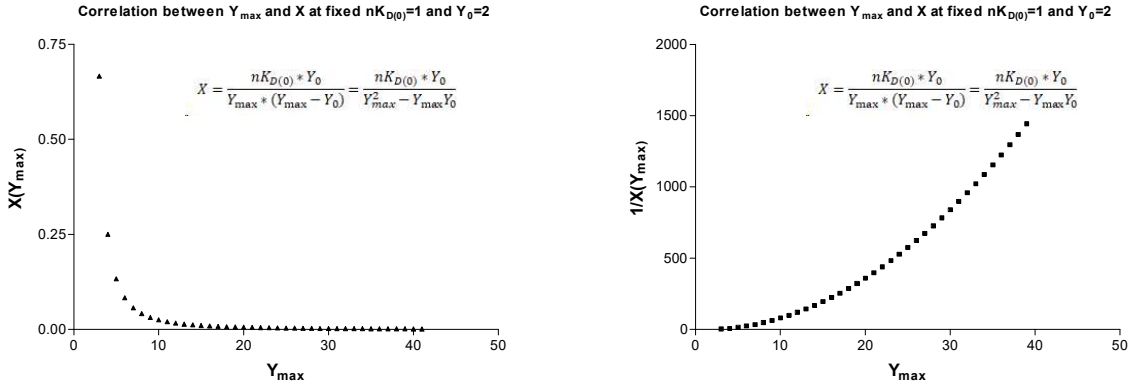

fig. 135: correlation between Y_{max} and X at fixed $nK_{D(0)}$=1 and Y_0=2

If one sets both Y_{max} and n as variables f;n,$Y_{max} \rightarrow X(n,Y_{max})$ is monotonously descending with $\lim_{i\to\infty} f(Y_{\max}, n) = 0$ as the denominator dependent on Y_{max} becomes dominant at high values of Y_{max}, n (exponential vs. linear correlation) (**fig. 136**).

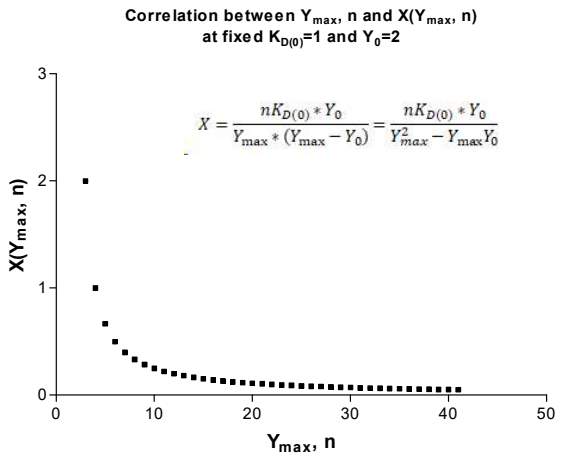

fig. 136: correlation between Y_{max}, n and $X(Y_{max}, n)$ at fixed $nK_{D(0)}$=1 and Y_0=2

In the cellular context of the investigation, one can however assume that such high levels of Y_{max} (which may be measurable in a simplified experimental setting such as an SPR binding assay) will not be present in the local cellular environment of interest as Y_{max} is limited to the local available concentration of phosphoinositide which can be assumed to be negligible with regard to the concentration of the total protein pool (note that all phosphoinositide binding proteins do form a mutually competitive pool further limiting the concentration of phosphoinositide available for each protein) so that one can estimate Y_{max} as constant and limit our evaluation to the consideration of K_D values (see above). Especially for high values of experimental defined Y_{max} this simplification will be paramount for the following discussion of results (see RAC-GEFs).
From the experimental results both RAC-GEFs (VAV1, P-REX1) showed very low affinity towards their cognate binding partner PtdIns(3,4,5)P_3 which is in accordance with previous reports suggesting that further mechanisms might be necessary for the membrane localization of those proteins (i.e. $G_{\beta\gamma}$, protein protein interactions, see also 1.3.2.) [250], [400]. All other proteins showed affinities in the low nM to pM range lying in the field of physiological relevant K_D values for PtdIns(3,4,5)P_3 and PtdIns(3,4)P_2 which was stated to be <200 nM by Lemmon et al. [1052]. Therefore, all those are likely to interact with mentioned phospholipids in cells and to be of relevance in related signalling events. The order of K_D values was as follows:

- P-REX1>>>VAV1>>>SHIP1 E452K=SHIP1 R673Q>SHIP1 WT>INPP4B>>PTEN>>AKT1
  for PtdIns(3,4,5)P_3
- SHIP1 WT=SHIP1 R673Q>TAPP2>>TAPP1=INPP4B>>SHIP1 E452K>AKT1>>PTEN
  for PtdIns(3,4)P_2

These results can be interpreted as follows (summarized in **fig. 138**):

- Binding to PtdIns(3,4,5)P_3: Inactive SHIP1 R673Q which could theoretically realise the trapping in the model showed lower affinity towards PtdIns(3,4,5)P_3 than active phosphatases (SHIP1 WT, INPP4B, PTEN). The K_D values for SHIP1 WT and INPP4B were approximately in the same range and therefore their relative concentrations would very likely determine the relative amount of PtdIns(3,4,5)P_3 bound by each protein (and the relative amounts of PtdIns(3,4)P_2 and PtdIns(3,5)P_2 formed out of their shared substrate PtdIns(3,4,5)P_3). In contrast, the K_D value of PTEN was ~10-fold lower meaning that most PtdIns(3,4,5)P_3 will be occupied by PTEN and PtdIns(4,5)P_2 will be the favoured product. As the K_D value of AKT1 was also ~10-fold lower than that of PTEN however, AKT1 would be able to displace PTEN from PtdIns(3,4,5)P_3 and therefore, a sufficient amount of AKT1 would become activated and enable oncogenic signalling (survival, proliferation and cell growth). Of course, local accumulation of certain proteins over others might influence this equilibrium (see below for an example concerning SHIP1 WT and SHIP1 mutants).
  SHIP1 R673Q showed ~5-fold increased K_D values with regard to SHIP1 WT. As we could assume that the SHIP1 mutations would be either homozygous (100% of SHIP1 mutated) or heterozygous (50% of SHIP1 mutated and 50% SHIP1 wt) two possible scenarios could be hypothesized: (1) homozygous mutation of SHIP1: In this case there would be no competition between SHIP1 R673Q and SHIP1 WT but SHIP1 R673Q would compete with other phosphoinositide-5-phosphatases and (2) heterozygous

mutation of SHIP1: In this scenario there would be equal absolute amounts of both SHIP1 proteins in theory, however in cell culture SHIP1 R673Q displayed strongly decreased protein levels so that the concentration of SHIP1 WT would be potentially higher than that of SHIP1 R673Q in cells. It was also found in H1299 that membrane localization of SHIP1 R673Q was impaired further reducing the local concentration of those mutant in the relevant cellular compartment (the plasma membrane). However, for other model systems or inactive SHIP1 mutants (i.e. SHIP1 R551Q which showed higher expression than SHIP1 WT in H1299) one can hypothesize that the relative levels of SHIP1 WT vs. SHIP1 mutants at the plasma membrane or still further dissected at specific membranous compartments serving as signalling hubs (i.e. lipid rafts) could be different than shown for SHIP1 R673Q and H1299 and likely be dependent on the cell type and cellular context (i.e. protein interaction partners, signalling environment, epigenetic/transcriptional and translational control of protein levels etc.) so that one could assume that in certain cell types or cellular situations and for certain inactive SHIP1 mutants the local concentration of SHIP1 mutants would be sufficient to displace SHIP1 WT if K_D values would be similar.

- Binding to PtdIns(3,4)P_2: SHIP1 E452K might be able to displace INPP4B from PtdIns(3,4)P_2 and itself become replaced by AKT1, therefore exhibiting a trapping effect in the absence of PTEN. As tumour cells often become PTEN deficient in the course of tumour development this mechanism might be of high relevance to amplify PtdIns(3,4)P_2 dependent signalling and therefore promotion of tumorigenesis in those cells (always to be taken into account the Two-PIP hypothesis/context dependent function of PtdIns(3,4)P_2 in cellular signalling). An explanation for the significantly higher affinity of SHIP1 E452K to PtdIns(3,4)P_2 compared to SHIP1 WT came from *in silico* GLIDE docking of Ins(1,3,4)P_3 to the crystal structure of ligand-bound SHIP2 (PDB 4A9C_B) preferred over SHIP1-apo (PDB 6IBD) due to an expected induced fit conformational change of the substrate binding pocket upon ligand binding (see also 4.3.1.) (performed by Johannes Kirchmair, Department of Pharmaceutical Sciences, Division of Pharmaceutical Chemistry, Vienna). The docking propsed the establishment of a novel salt bridge between the K452 and the P4 not present in the WT enzyme which shifted the GLIDE predicted binding energy from -6.857 kcal/mol (SHIP1 WT) to -7.663 kcal/mol (SHIP1 E452K) (**fig.137**) [1041].

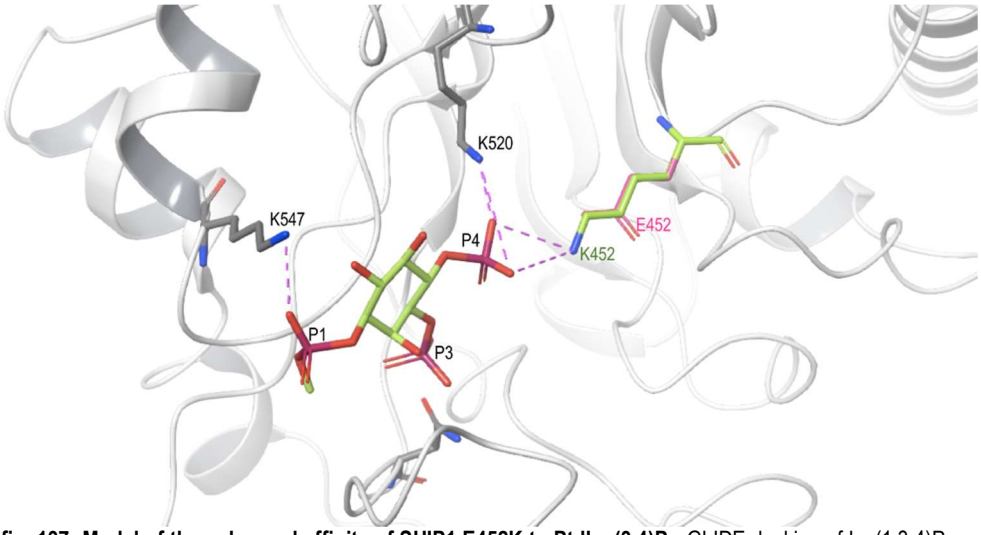

fig. 137: Model of the enhanced affinity of SHIP1 E452K to PtdIns(3,4)P_2. GLIDE docking of Ins(1,3,4)P_3 was performed for the SHIP1 model based on the crystal structure of ligand-bound SHIP2 (PDB 4A9C_B) WT or E452K by Johannes Kirchmair. Salt bridges are shown as lilac dashed lines. The image was done with *Maestro 11*.

- Concerning the isolated binding assays, both RAC-GEFs (P-REX1 and VAV1) showed very low affinity towards PtdIns(3,4,5)P_3, however the measured affinity values do not reflect their actual affinity to the plasma membrane compartment of interest as further factors contribute to plasma membrane recruitment. This is especially observable for mentioned RAC-GEFs but not completely negligible for the other candidate proteins and therefore one must always very critically and carefully evaluate the results of such isolated and simplified affinity studies and should keep in mind that those might not be of high relevance in the actual cellular situation.

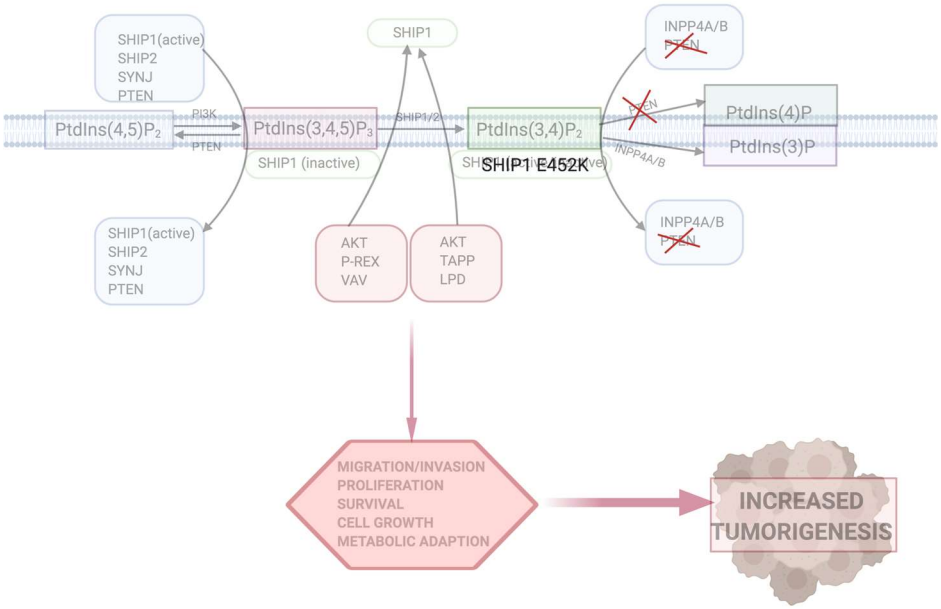

fig. 138: overview of the phosphoinositide trapping model according to the obtained results. In this model, ectopic expression of SHIP1 WT or SHIP1 mutants would protect phosphoinositides implicated in oncogenic signal transduction (PtdIns(3,4,5)P_3 and PtdIns(3,4)P_2) from degradation by phosphoinositide phosphatases (PTEN, INPP4A/B, active SHIP1, SHIP2) thereby increasing their concentration. Accumulation of PtdIns(3,4,5)P_3 and/or PtdIns(3,4)P_2 would then recruit and activate PtdIns(3,4,5)P_3 and/or PtdIns(3,4)P_2 binding effector proteins (AKT, P-REX, VAV, LPD, TAPP) replacing SHIP1 which would stimulate oncogenic outputs such as increased proliferation, survival and/or migration. This would ultimately result in enhanced tumour proliferation and /or metastasis of carcinoma cells. The prerequisite for phosphoinositide trapping would be K_D (phosphatases) > K_D (SHIP1) > K_D (effector proteins). SHIP1 proteins protecting PtdIns(3,4,5)P_3 (substrate) would have to be ideally catalytically dead or exhibit reduced catalytic activity as otherwise PtdIns(3,4,5)P_3 would become degraded instead of trapped. Concerning PtdIns(3,4)P_2 SHIP1 proteins could be either active or inactive and trapping of PtdIns(3,4)P_2 by active SHIP1 proteins might be even more efficient as they would be capable to enhance the pool of PtdIns(3,4)P_2 in parallel. As SHIP1 is allosterically activated by PtdIns(3,4)P_2 this would further enable a *feed-forward* loop amplifying the accumulation of PtdIns(3,4)P_2 and resulting oncogenic signal transduction pathways. The obtained results pointed to a candidate trapping function of SHIP1 E452K in PTEN-deficient tumours with regard to PtdIns(3,4)P_2 [1041].

In addition, it was tried to modulate the phosphoinositide trapping model in cells. For the cellular model H1299 cells were used as they were proven to be PTEN negative [1053]. In the model approach, H1299 cells were transduced with SHIP1 WT, SHIP1 E452K or SHIP1 R673Q or a LeGO control vector and the membrane-to-cytosol ratios of selected PtdIns(3,4,5)P_3 (AKT, RAC1) or PtdIns(3,4)P_2 (AKT, RAC1, LPD) dependent effector proteins and SHIP1 were determined by means of differential centrifugation and Western Blot analysis. In general, the expectations derived from the biochemical measurements were only poorly reflected in the cellular context indicating that in cells membrane recruitment is more complex than just phosphoinositide-binding affinities as will be discussed in more detail below.

1. SHIP1 WT was observed to be equally distributed over the cytosolic and membranous fraction whereas both SHIP1 mutants were shown significantly reduced in the membrane fraction. In contrast, the measured KD values were comparable, respectively the affinity of SHIP1 E452K to PtdIns(3,4)P_2 was even higher than for SHIP1 WT and out of this one would expect similar or even higher membrane recruitment of the SHIP1 mutants to the membrane compared to SHIP1 WT based solely on phosphoinositide binding affinities which was not the case. This illustrates again that membrane recruitment of SHIP1 proteins is also dependent on additional mechanisms such as general membrane lipid binding i.e. via the MIM of the PPase domain, PPIs of the SH2 and PRR domains with membrane-bound proteins such as SHC or GRB2 or alterations in signal transductions which could indirectly alter the membrane recruitment of SHIP1 proteins.
2. From the biochemical analysis one would expect an accumulation of PtdIns(3,4)P_2 and generally PtdIns(3,4)P_2 dependent effector proteins dependent on their binding affinity and (spatio-temporal) levels in H1299 SHIP1 E452K due to the trapping effect and an accumulation of PtdIns(3,4,5)P_3 (and PtdIns(3,4,5)P_3-dependent effector proteins) would be expected in H1299 SHIP1 LeGO and H1299 SHIP1 R673Q due to the lack of active SHIP1 which is not reflected in the results obtained from the differential centrifugation.

a. Membranous AKT was generally low but highest in H1299 SHIP1 WT. It would be however expected that membranous AKT should be lowest in this line due to lowest enrichment of PtdIns(3,4,5)P_3 and PtdIns(3,4)P_2. Out of this contradictory result it has to be assumed that recruitment of AKT is not solely based on phosphoinositide binding as discussed already for SHIP1. Of note, one might expect that the majority of AKT bound to membranes would be phosphorylated which is in contrast to decreased P-AKT levels in H1299 SHIP1 WT.
b. Equal to AKT membranous RAC1 should be lowest in H1299 SHIP1 WT but in reality it is lowest in H1299 SHIP1 E452K, therefore PtdIns(3,4)P_2 may not be critical for RAC1 membrane recruitment in H1299. Intriguingly, RAC1 is most enriched in H1299 SHIP1 R673Q but not in H1299 LeGO where one could assume similar levels of PtdIns(3,4,5)P_3 and they did not significantly differ between H1299 SHIP1 WT and H1299 LeGO although one would expect lower levels of PtdIns(3,4,5)P_3 in H1299 SHIP1 WT. Therefore, if RAC1 membrane recruitment would be promoted by PtdIns(3,4,5)P_3 which is supported minorly by highest membranous RAC1 levels in H1299 SHIP1 R673Q due to the trail of thought above additional mechanisms have to contribute to RAC1 recruitment to membranes. Of note, although membranous RAC1 is similar in H1299 SHIP1 WT and LeGO from the RAC1-GTP-assays active RAC1 levels associated with membrane recruitment of RAC1 were significantly higher in H1299 SHIP1 WT compared to H1299 LeGO.
c. From the biochemical measurements one would expect that membrane recruitment of LPD should be highest in H1299 SHIP1 E452K due to accumulation of PtdIns(3,4)P_2 (note that the K_D value of LPD was not determined due to the fact that LPD could not be cloned into the designated expression vector). In fact, membranous LPD was decreased in H1299 SHIP1 E452K and H1299 SHIP1 R673Q compared to H1299 SHIP1 WT and H1299 LeGO.

Concluding, the cellular modulation of the phosphoinositide trapping model reflects the difficulty to transfer a simplified biochemical model to a more complex cellular context. Apart from the additional mechanisms of membrane recruitment apart from phosphoinositide binding discussed above the most important point in evaluating the value of the phosphoinositide trapping model in a cellular context or the context of tumour development would be in my opinion the spatiotemporal and highly dynamic enrichment of both phosphoinositides and phosphoinositide binding proteins i.e. in specialized compartments such as lipid rafts which is absolutely neglected in the pure phosphoinositide-protein K_D-value determination-based approach presented here. Also, the differential centrifugation does not distinguish between different membrane types (plasma membrane, endosomal membranes etc.) and therefore it would be highly valuable to supplement those initial results with complementary methods such as fluorescence microscopy. For example, in a recent study Hertel et al. presented a multiplexed method to measure the dynamic recruitment of signalling proteins to membrane subcompartments. They applied a reporter construct consisting of the PH domain of PLC specific for PtdIns(4,5)P_2, a plasma membrane targeting signal and a split GFP reporter that is activated upon PtdIns(4,5)P_2 binding (dPlcR) and combined it with a red reporter dInPAkt to successfully detect the spatiotemporally restricted formation of PtdIns(3,4,5)P_3 by the PI3K reaction after stimulation of Cos7 cells with EGF [1054]. However, fluorescence reporter systems were shown in some past studies to be not completely reliable in all cases [1052].

5.2.2. Phosphoinositide levels and subcompartmentalization of the plasma membrane

The relative basal levels of phosphoinositides at the inner leaflet of the plasma membrane were stated to be very low in comparison to scaffolding lipids such as phosphatidyl ethanolamine or phosphatidyl choline and tend to increase rapidly upon stimulation. In unstimulated cells PtdIns(3,4,5)P_3 and PtdIns(3,4)P_2 contributed to 0.0001% of the whole lipid pool [1055]. Upon stimulation of neutrophils with FMLP Stephens et al. found an increase of PtdIns(3,4,5)P_3 from 5 µM to 200 µM peaking at 10 seconds post-stimulation and of PtdIns(3,4)P_2 from 10 µM to 100-200 µM peaking at 17 seconds post-stimulation [1056]. As mentioned above, from studies performed with the PtdIns(4,5)P_2 specific PH domains of PLCδ (K_D 1.7 µM) and pleckstrin (K_D 30 µM) Lemmon et al. stated the critical affinity for specific PtdIns(4,5)P_2-protein interaction to be <10 µM which applied for a critical K_D<200 nM for PtdIns(3,4)P_2 and PtdIns(3,4,5)P_3 due to the relative abundances of those phosphoinositide species in the inner leaflet of the plasma membrane [1052].

Although not well understood due to lack of appropriate methods (i.e. very high-resolution microscopy) it is still common sense to state the presence of membrane compartmentalization in addition to membrane polarization actively uphold by flippases and lipid transporters to allow for the spatiotemporal accumulation of signalling components (lipids, scaffolding and adaptor proteins, signalling proteins etc.) to signalling hubs within membranes [1057]. From indirect measurements it was suspected that membranes do possess the ability of self-organization

and that distinct nanoscale domains would form due to the thermodynamic properties of membrane components (lipids, proteins, sugars) forming a heterogeneous membrane substructure and that the local properties of a membrane would depend on its local composition [1058], [1059], [1060]. The demixing of the membrane would be probably prevented by the actomyosin cytoskeleton scaffolding the membrane subdomains (quenched disorder) [1061], [1062], [1063]. The membrane scaffold was shown to prevent free and fast diffusion of membrane proteins and helps stabilizing certain states. This was termed hop-diffusion as membrane proteins were observed to move fast within their compartment but stay for ms before "hopping" over the cytoskeleton obstacle to a neighbouring one [1064], [1065]. The most obvious of such a scaffolding function are distinct structures such as focal adhesions or lamellipodia and upon experimentally induced actin-depolymerisation it was shown that membranes became more homogenous and larger membrane substructures such as lipid rafts disappeared [1066], [1067], [1068], [1069]. Upon appropriate signals (i.e. receptor activation/dimerization, antigen crosslinking etc.) the established membrane structure gets locally perturbed and membrane nanodomains would aggregate to those larger signalling hub structures mentioned above. Intriguingly, the formation of those higher-ordered structures is both dependent on the basal compartmentalization of the membrane and the stabilizing effect induced by the signalling process which influence each other in a cooperative system. Most importantly, the whole system is a highly dynamic and complex network where all determinants do influence each other [1070], [1071]. Returning to the phosphoinositide trapping model one could therefore hypothesize that certain cellular contexts may bias recruitment of phosphoinositide binding proteins to certain subcompartments/signalling hubs and this can fluctuate over time which makes the discrepancy of the cellular modelling of the phosphoinositide trapping versus the SPR measurements even more expectable.

5.3. Biochemical, biophysical and structural analysis of SHIP1

The focus in this part of the thesis was laid on the three phosphoinositide-binding domains of SHIP1 (PH-L, PPase, C2). Whereas the phosphoinositide binding and catalysis of phosphoinositide-5-phosphatases is quite well understood, there is limited knowledge concerning the PH-L and the C2 domain. On a structural level *in silico* analysis of the PPase and C2 domain was performed for the crystal structure of SHIP1 PPase-C2 (PDB 6IBD) and a model build on the basis of SHIP2 PPase-C2 co-crystallized with the synthetic ligand BiPh-2,3´,4,5´,6-P_5 (PDB 4A9C_B). Regarding the PPase domain presumably critical residues for catalysis and phosphoinositide binding were identified based on the literature available and structure analysis of the interactions of SHIP1/SHIP1 model PPase with BiPh-2,3´,4,5´,6-P_5, and PtdIns(3,4,5)P_3 adapted and modified from the crystal structure of INPP5B co-crystallized with PtdIns(3,4)P_2 (PDB 4CML) or GLIDE-docked Ins(1,3,4,5)P_4. Concerning the C2 domain, LeCoq et al. identified four critical lysines to form a possible PtdIns(3,4)P_2 binding pocket which could be found also in SHIP1 using sequence and structure alignment [1044]. With regard to the PH-L domain MingLum et al. [608] identified that it specifically bound PtdIns(3,4,5)P_3 and they identified two critical lysines (K397 and K370) to be responsible for it. However, to date only an NMR structure of minor quality has been published for this domain [608]. In order to get a better understanding of the phosphoinositide binding of SHIP1 PH-L and the interplay of the three phosphoinositide binding domains in SHIP1 it was therefore aimed to perform a crystal structure analysis of SHIP1 PH-L-PPase-C2 and if possible the FL protein. However, the trials that have been performed so far testing two different constructs of PH-L-PPase-C2 and several strains and expression conditions in *E. coli* beared no sufficient amounts of soluble protein and the same applied for the FL protein. Trial expression of SHIP1 FL in a mammalian cell culture system (transduction of TwinStrep-SHIP1 FL in H1299 or transfection in HEK-293F) beared high expression of SHIP1 in the cell lysate, however an initial test purification using *Strep-Tactin XT* revealed no binding of SHIP1 to the resin possibly due to non-accessibility of the TwinStrep-tag. Another factor which might diminish SHIP1 yields could be its numerous interactions with other proteins, lipids or subcompartments within the cell which is especially problematic when using an intracellular expression system as having done so far. Therefore, in future experiments already in the planning phase other tags or tag localizations as well as the use of a signal sequence for secretion of SHIP1 should be tried. Due to its convernience and potential to upscale it more easily, the HEK-293F system should be preferred over the adherent H1299 system.

On a biochemical level, the substrate specificity of SHIP1 FL was identified using MDD-HPLC and a partly but not complete overlap to that of SHIP2 was found. Especially, Ins(2,3,4,5)P_4 was identified as a unique substrate of SHIP1 but not of SHIP2 and this might be mediated by an interaction of K659 with P2 [571], [573]. By structure analysis and comparison of the phosphate group patterns of SHIP1 substrates phosphate bearing positions promoting (1, 3, 4, 5 and weakly 2) or hindering (6) substrate accommodation were identified. The enzyme kinetics of SHIP1 FL towards PtdIns(3,4,5)P_3 were determined and pointed to a possible allosteric regulation (sigmodal curve) of SHIP1 with a K_M value of 35-38 µM which was in accordance with a previous report [614]; and the K_D values of SHIP1 FL towards PtdIns(3,4,5)P_3 and PtdIns(3,4)P_2 were determined by three different methods (SPR,

PLO, PIP-Array) which gave affinity values in the nM to pM range and comparable tendencies concerning the affinities of PtdIns(3,4)P_2 vs. PtdIns(3,4,5)P_3. Regarding the individual SHIP1 phosphoinositide binding domains the presence of the C2 domain positively and the presence of the PH-L domain rather negatively influenced the catalytic efficiency of SHIP1 and phosphoinositide binding as analysed by COVA-PIP Array was observed to be complex with no obvious contribution of one domain to the specific binding of only PtdIns(3,4,5)P_3 or PtdIns(3,4)P_2. Regarding the sigmoidal fitting of the enzyme kinetics and the found positive influence of the C2 domain on enzymatic efficiency this was in accordance with a previous study by Ong et al. [614] which showed that SHIP1 was allosterically regulated by binding of its product PtdIns(3,4)P_2 to the C2 domain providing a positive *feed-forward* loop. This is of special interest in the context of one study by LeCoq et al. [1043] concerning SHIP2 which identified four conserved lysines residing in the C2 domain (K740, K742, K746 and K806 in SHIP1) that were well situated to form a putative substrate binding pocket and could biochemically accommodate the substrate by ionic interactions. Of note, the L4-out and later on the L4-in conformation of SHIP2 PPase appeared to be stabilized by interactions of the PPase with the C2 domain by means of a mainly hydrophobic interface. Both the PPase and the C2 domain of SHIP2 were shown to interact with membranous PtdSer which was suggested to help in correctly orientating SHIP2 to its membrane-bound substrate PtdIns(3,4,5)P_3 but was negligible when soluble Ins(1,3,4,5)P_4 was used as substrate. The L4-out conformation describes the ordered L4 loop conformation which is realized by an interaction of R682 (K664 in SHIP1) with D613 and D614 which were aligned to D592 and P694 in SHIP1. The L4-out conformation is required for substrate access and by binding of R682 to the P4 it switches to the L4-in conformation which enables catalysis in a closed biochemical milieu. In summary, also SHIP2 was therefore allosterically regulated by the C2 domain which was enhanced in the presence of phospholipid binding (PtdSer) in the context of catalysis taking place at membranes (positioning effect) and a similar effect was also observed for the lipid PPase activity of PTEN and PLCδ1. In SHIP1 it is therefore very likely to propose that the allosteric activation effect of the C2 domain would also be due to (1) stabilizing the L4-out and L4-in loop positions and (2) localizing the PPase domain correctly to the plasma membrane and PtdIns(3,4,5)P_3. In a recent study, K681 of SHIP1 was shown to directly bind to AQX-MN100 and PtdIns(3,4)P_2 and this was disturbed in the K681A mutant [1072]. Also the PH-L domain of SHIP1 was shown to exert such a localizing effect as it was also shown to display phospholipid binding properties and was required for the localized recruitment of SHIP1 to phagocytic cups in macrophages [608] and in SHIP2 the PH-L domain was shown to act as an allosteric activator for PtdIns(3,4,5)P_3 but not for Ins(1,3,4,5)P_4 [1073]. From the already published results concerning the PH-L domain of SHIP1 and the PPase-C2 domains of SHIP1 and SHIP2 several residues in the PH-L and C2 domain were supposed or verified to contribute to phospholipid binding or allosteric activation of SHIP enzymes and to be of biological relevance when mutated. In further studies it would be very interesting to perform mutational studies concerning SHIP1 C2 and the PPase-C2 interface which have been performed so far only for SHIP2. Crystal structure analysis of the SHIP1 PHL-PPase-C2 domain possibly bound to phospholipids which has not been realized yet due to expression problems would reveal valuable insights into the mechanisms of a proposed PHL-PPase interface and the mechanistic relevance of the PH-L domain alone or bound to PtdIns(3,4,5)P_3 on substrate accommodation and catalysis.

The catalytic mechanism and PtdIns(3,4,5)P_3 accommodation in the PPase domain of SHIP1 could be rather well modelled due to the high number of already published structures and publications of related phosphoinositide-5-PPase domains. Recently, a structure of SHIP1 PPase-C2 co-crysatllized with a PO_4^{3-} and a Mg^{2+} ion (PDB 6XY7) was published which related very well to the current understanding of phosphoinositide-5-phosphatase catalysis and it would be very valuable in the future to see if this could be verified by co-crystallization of SHIP1 with a full (synthetic) substrate instead of an isolated phosphate ion. A bunch of recently published structures of SHIP1 PPase-C2 co-crystallized with synthetic compounds was not suitable to evaluate the substrate-PPase interaction as they did not localize to the substrate binding pocket (**fig. 139**).

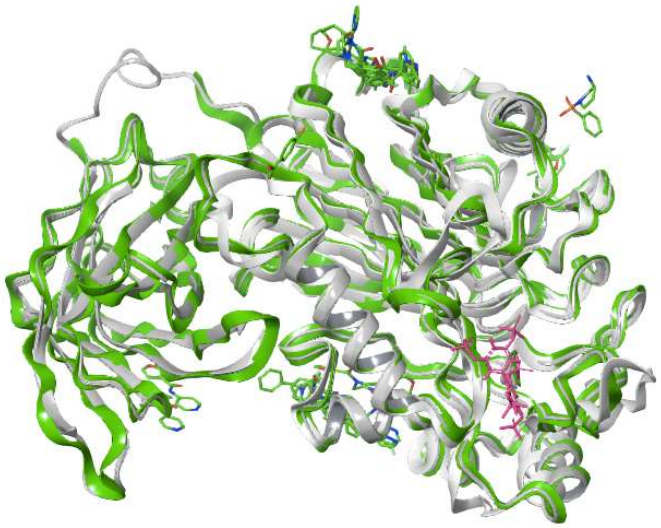

fig. 139: structure alignment of the SHIP1 model with the synthetic substrate BiPh-2,3´,4,5´,6-P_5 with the available crystal structures of SHIP1 PPase-C2 co-crystallized with synthetic compounds. The SHIP1 model is shown in light grey and BiPh-2,3´,4,5´,6-P_5 is shown in magenta. SHIP1 PPase-C2 and the co-crystallized synthetic compounds (SHIP1 apo PDB 6IBD, co-crystallized structures PDBs 5RW3,5RW8,5RW4,5RW9,5RYC,5RX7,5RWO,5RWP,5RWU,5RWS,5RW7,5RWM,5RX0,5RWF,5RY5,5RWT,5RXT,5RWN,5RX6,5RX9,5RW5,5RYI,5RWJ,5RX5,5RXW) are shown in green. The image and structure alignment were done with *Maestro 11*.

The proposed overall model (**fig. 140**) based on published data of the SHIP1 membrane interaction, substrate binding, activation and catalysis would be (1) possible initial or basal contact of SHIP1 PH-L, PPase and C2 with membrane lipids (rather unspecific hydrophobic or ionic interactions as shown for the MIM of SHIP1 PPase), (2) following the PI3K reaction SHIP1 PH-L and PPase would contact PtdIns(3,4,5)P_3, the PH-L domain possibly stabilizes and correctly localizes SHIP1 and the PPase domain converts PtdIns(3,4,5)P_3 to PtdIns(3,4)P_2, (3) in parallel and slightly time-relapsed to the SHIP1 reaction the C2 domain binds to PtdIns(3,4)P_2 either produced directly by the same SHIP1 protein (which might include that SHIP1 has to shift its conformation so that the C2 domain can now localize to the place formerly inhabited by the PPase domain), other SHIP1 proteins or other phosphoinositide-5-PPases in direct proximity to the SHIP1 molecule in focus; and allosteric activation of SHIP1 by the PPase-C2 interface and the additional effect of PtdIns(3,4)P_2 to accelerate the reaction (*feed-forward* loop) takes place and (4) detachment or partial detachment of SHIP1 from the membrane to allow for a new catalysis cycle. For both points 3 and 4 one can argue that both regarding the intramolecular scenario (proposed domain shifting, displacement of the PPase domain by the C2 domain and the PH-L domain by the PPase domain) and the intermolecular scenario (displacement of SHIP1 by terminating PPases such as INPP4B) the affinities of the domains/proteins to PtdIns(3,4,5)P_3 and PtdIns(3,4)P_2 would play a vital role to mediate it with the restrictions discussed already concerning the phosphoinositide trapping model (i.e. effect of the membrane). Partly opposed to this model however, from the affinity data obtained in this thesis for SHIP1 FL and designated SHIP1 phosphoinositide binding domains, no general contribution of one domain for the specific binding to only either PtdIns(3,4)P_2 or PtdIns(3,4,5)P_3 could be concluded and to this point, binding to phosphoinositides seems to be more complex than previously assumed and not coverable by such a simple model. However, the COVA-PIP Array system applied to measure those interactions does have to be handled with care especially as the lipids were presented in an isolated form without a membrane background diluting them which can lead to artefacts. Adding yet another layer of complexity, membrane interaction would be also dependent on protein-protein interaction-mediated membrane contacts of the PRR and SH2 domains. In this context, cooperative binding can sequester the protein to higher levels than expected from individual affinities of the isolated domains due to the concept of avidity. In the future, structural and especially time-resolved measurements as well as further experiments using selected SHIP1 mutants will be required to fully evaluate the mechanisms and dynamics of the phosphoinositide binding and catalysis of SHIP1.

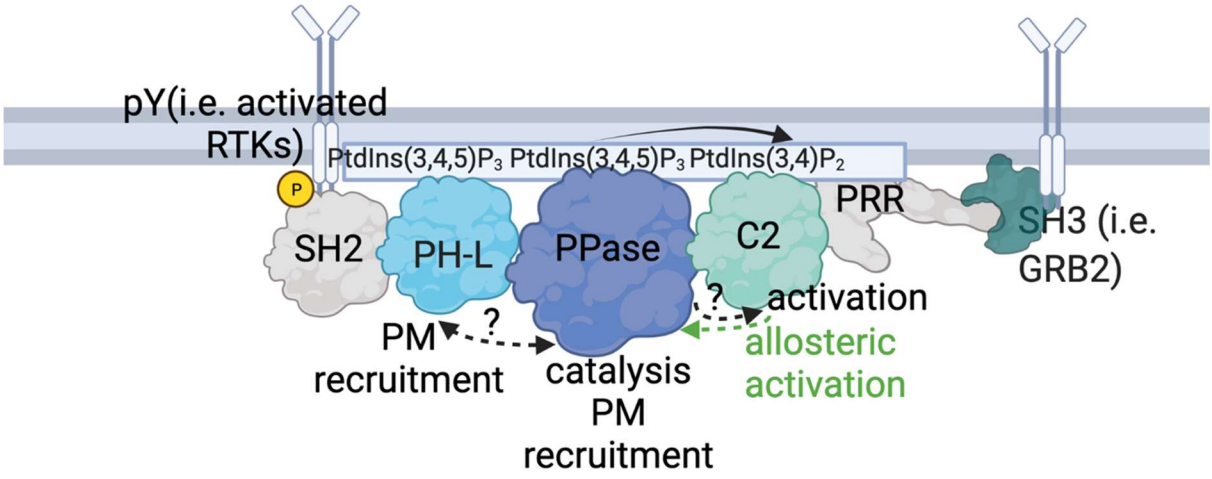

fig. 140: proposed model of membrane accommodation and catalysis of SHIP1. Abbreviations: pY=phosphorylated tyrosine, RTK=receptor tyrosine kinase, SH2=SRC Homology 2, PH-L=Pleckstrin Homology-Like, PPase=Phosphatase domain, PRR=proline rich region, SH3=SRC Homology 3, GRB2=Growth Factor Receptor Bound 2, PM=plasma membrane

6. References

[1] Weinberg, R.A., 2014. The Biology of Cancer., Garland Science, Taylor & Francis Group, New York.
[2] Hanahan, D., Weinberg, R.A., 2011. Hallmarks of cancer: The next generation. Cell, 2011, **144**, 646–674.
[3] Alberts, B., Johnson, A., Lewis, J., Morgan, D.O., et al., 2015. Molecular Biology of The Cell., Garland Science, Taylor & Francis Group, New York.
[4] Cheng, N., Chytil, A., Shyr, Y., Joly, A., Moses, H.L., 2008. Transforming Growth Factor- Signaling-Deficient Fibroblasts Enhance Hepatocyte Growth Factor Signaling in Mammary Carcinoma Cells to Promote Scattering and Invasion. Mol. Cancer Res., 2008, **6**, 1521–1533.
[5] Jiang, B., Liu, L., 2009. *Adv. Cancer Res.*, vol. 102, pp. 19–65.
[6] Yuan, T.L., Cantley, L.C., 2008. PI3K pathway alterations in cancer: variations on a theme. Oncogene, 2008, **27**, 5497–510.
[7] Burkhart, D.L., Sage, J., 2008. Cellular mechanisms of tumour suppression by the retinoblastoma gene. Nat. Rev. Cancer, 2008, **8**, 671–682.
[8] Junttila, M.R., Evan, G.I., 2009. p53--a Jack of all trades but master of none. Nat Rev Cancer, 2009, **9**.
[9] Adams, J.M., Cory, S., 2007. The Bcl-2 apoptotic switch in cancer development and therapy. Oncogene, 2007, **26**, 1324–37.
[10] Lowe, S.W., Cepero, E., Evan, G., 2004. Intrinsic tumour suppression. Nature, 2004, **432**, 307–15.
[11] Evan, G., Littlewood, T., 1998. A matter of life and cell death. Science, 1998, **281**, 1317–22.
[12] Blasco, M.A., 2005. Telomeres and human disease: ageing, cancer and beyond. Nat. Rev. Genet., 2005, **6**, 611–22.
[13] Shay, J.W., Wright, W.E., 2000. Hayflick, his limit, and cellular ageing. Nat. Rev. Mol. Cell Biol., 2000, **1**, 72–6.
[14] Ferrara, N., 2010. Pathways mediating VEGF-independent tumor angiogenesis. Cytokine Growth Factor Rev., 2010, **21**, 21–6.
[15] Mac Gabhann, F., Popel, A.S., 2008. Systems biology of vascular endothelial growth factors. Microcirculation, 2008, **15**, 715–38.
[16] Carmeliet, P., 2005. VEGF as a key mediator of angiogenesis in cancer. Oncology, 2005, **69 Suppl 3**, 4–10.
[17] Qian, B.-Z., Pollard, J.W., 2010. Macrophage diversity enhances tumor progression and metastasis. Cell, 2010, **141**, 39–51.
[18] Zumsteg, A., Christofori, G., 2009. Corrupt policemen: inflammatory cells promote tumor angiogenesis. Curr. Opin. Oncol., 2009, **21**, 60–70.
[19] Murdoch, C., Muthana, M., Coffelt, S.B., Lewis, C.E., 2008. The role of myeloid cells in the promotion of tumour angiogenesis. Nat. Rev. Cancer, 2008, **8**, 618–31.
[20] Hanahan, D., Folkman, J., 1996. Patterns and emerging mechanisms of the angiogenic switch during tumorigenesis. Cell, 1996, **86**, 353–64.
[21] Nagy, J.A., Chang, S.-H., Shih, S.-C., Dvorak, A.M., Dvorak, H.F., 2010. Heterogeneity of the tumor vasculature. Semin. Thromb. Hemost., 2010, **36**, 321–31.
[22] Baluk, P., Hashizume, H., McDonald, D.M., 2005. Cellular abnormalities of blood vessels as targets in cancer. Curr. Opin. Genet. Dev., 2005, **15**, 102–11.
[23] Raica, M., Cimpean, A.M., Ribatti, D., 2009. Angiogenesis in pre-malignant conditions. Eur. J. Cancer, 2009, **45**, 1924–34.
[24] Berx, G., van Roy, F., 2009. Involvement of members of the cadherin superfamily in cancer. Cold Spring Harb. Perspect. Biol., 2009, **1**, a003129.
[25] Cavallaro, U., Christofori, G., 2004. Cell adhesion and signalling by cadherins and Ig-CAMs in cancer. Nat. Rev. Cancer, 2004, **4**, 118–32.
[26] Klymkowsky, M.W., Savagner, P., 2009. Epithelial-mesenchymal transition: a cancer researcher's conceptual friend and foe. Am. J. Pathol., 2009, **174**, 1588–93.
[27] Polyak, K., Weinberg, R.A., 2009. Transitions between epithelial and mesenchymal states: acquisition of malignant and stem cell traits. Nat. Rev. Cancer, 2009, **9**, 265–73.
[28] Thiery, J.P., Acloque, H., Huang, R.Y.J., Nieto, M.A., 2009. Epithelial-mesenchymal transitions in development and disease. Cell, 2009, **139**, 871–90.
[29] Yilmaz, M., Christofori, G., 2009. EMT, the cytoskeleton, and cancer cell invasion. Cancer Metastasis Rev., 2009, **28**, 15–33.
[30] Barrallo-Gimeno, A., Nieto, M.A., 2005. The Snail genes as inducers of cell movement and survival: implications in development and cancer. Development, 2005, **132**, 3151–61.
[31] Schmalhofer, O., Brabletz, S., Brabletz, T., 2009. E-cadherin, beta-catenin, and ZEB1 in malignant progression of cancer. Cancer Metastasis Rev., 2009, **28**, 151–66.
[32] Yang, J., Weinberg, R.A., 2008. Epithelial-mesenchymal transition: at the crossroads of development and tumor metastasis. Dev. Cell, 2008, **14**, 818–29.
[33] Talmadge, J.E., Fidler, I.J., 2010. AACR centennial series: the biology of cancer metastasis: historical perspective. Cancer Res., 2010, **70**, 5649–69.
[34] Fidler, I.J., 2003. The pathogenesis of cancer metastasis: the "seed and soil" hypothesis revisited. Nat. Rev. Cancer, 2003, **3**, 453–8.
[35] Paget, S., 1889. The distribution of secondary growths in cancer of the breast. Lancet, 1889, **1**, 571–573.
[36] Krebs, M.G., Hou, J.-M., Ward, T.H., Blackhall, F.H., Dive, C., 2010. Circulating tumour cells: their utility in cancer management and predicting outcomes. Ther. Adv. Med. Oncol., 2010, **2**, 351–65.
[37] Warburg, O.H., 1930. The Metabolism of Tumours: Investigations from the Kaiser Wilhelm Institute for Biology, Berlin-Dahlem (London, UK: Arnold Constable). 1930.
[38] WARBURG, O., 1956. On respiratory impairment in cancer cells. Science, 1956, **124**, 269–70.
[39] WARBURG, O., 1956. On the origin of cancer cells. Science, 1956, **123**, 309–14.
[40] POTTER, V.R., 1958. The biochemical approach to the cancer problem. Fed. Proc., 1958, **17**, 691–7.
[41] Vander Heiden, M.G., Cantley, L.C., Thompson, C.B., 2009. Understanding the Warburg effect: the metabolic requirements of cell proliferation. Science, 2009, **324**, 1029–33.
[42] Jones, R.G., Thompson, C.B., 2009. Tumor suppressors and cell metabolism: a recipe for cancer growth. Genes Dev., 2009, **23**, 537–48.
[43] DeBerardinis, R.J., Lum, J.J., Hatzivassiliou, G., Thompson, C.B., 2008. The biology of cancer: metabolic reprogramming fuels cell growth and proliferation. Cell Metab., 2008, **7**, 11–20.
[44] Hsu, P.P., Sabatini, D.M., 2008. Cancer cell metabolism: Warburg and beyond. Cell, 2008, **134**, 703–7.
[45] Semenza, G.L., 2010. HIF-1: upstream and downstream of cancer metabolism. Curr. Opin. Genet. Dev., 2010, **20**, 51–6.
[46] Semenza, G.L., 2010. Defining the role of hypoxia-inducible factor 1 in cancer biology and therapeutics. Oncogene, 2010, **29**, 625–34.
[47] Kroemer, G., Pouyssegur, J., 2008. Tumor cell metabolism: cancer's Achilles' heel. Cancer Cell, 2008, **13**, 472–82.
[48] Teng, M.W.L., Swann, J.B., Koebel, C.M., Schreiber, R.D., Smyth, M.J., 2008. Immune-mediated dormancy: an equilibrium with cancer. J. Leukoc. Biol., 2008, **84**, 988–93.
[49] Kim, R., Emi, M., Tanabe, K., 2007. Cancer immunoediting from immune surveillance to immune escape. Immunology, 2007, **121**, 1–14.
[50] Yang, L., Pang, Y., Moses, H.L., 2010. TGF-beta and immune cells: an important regulatory axis in the tumor microenvironment and progression. Trends Immunol., 2010, **31**, 220–7.
[51] Shields, J.D., Kourtis, I.C., Tomei, A.A., Roberts, J.M., Swartz, M.A., 2010. Induction of Lymphoidlike Stroma and Immune Escape by Tumors That Express the Chemokine CCL21. Science (80-.)., 2010, **328**, 749–752.
[52] Mougiakakos, D., Choudhury, A., Lladser, A., Kiessling, R., Johansson, C.C., 2010. Regulatory T cells in cancer. Adv. Cancer Res., 2010, **107**, 57–117.
[53] Ostrand-Rosenberg, S., Sinha, P., 2009. Myeloid-derived suppressor cells: linking inflammation and cancer. J. Immunol., 2009, **182**, 4499–506.
[54] Negrini, S., Gorgoulis, V.G., Halazonetis, T.D., 2010. Genomic instability--an evolving hallmark of cancer. Nat. Rev. Mol. Cell Biol., 2010, **11**, 220–8.

[55] Salk, J.J., Fox, E.J., Loeb, L.A., 2010. Mutational heterogeneity in human cancers: origin and consequences. Annu. Rev. Pathol., 2010, **5**, 51–75.
[56] Kinzler, K.W., Vogelstein, B., 1997. Cancer-susceptibility genes. Gatekeepers and caretakers. Nature, 1997, **386**, 761, 763.
[57] Dvorak, H.F., Underhill, L.H., Dvorak, H.F., 1986. Tumors: wounds that do not heal. Similarities between tumor stroma generation and wound healing. N. Engl. J. Med., 1986, **315**, 1650–9.
[58] Colotta, F., Allavena, P., Sica, A., Garlanda, C., Mantovani, A., 2009. Cancer-related inflammation, the seventh hallmark of cancer: links to genetic instability. Carcinogenesis, 2009, **30**, 1073–1081.
[59] DeNardo, D.G., Andreu, P., Coussens, L.M., 2010. Interactions between lymphocytes and myeloid cells regulate pro- versus anti-tumor immunity. Cancer Metastasis Rev., 2010, **29**, 309–16.
[60] Grivennikov, S.I., Greten, F.R., Karin, M., 2010. Immunity, Inflammation, and Cancer. Cell, 2010, **140**, 883–899.
[61] Karnoub, A.E., Weinberg, R.A., n.d. Chemokine networks and breast cancer metastasis. Breast Dis., n.d., **26**, 75–85.
[62] Hanahan, D., Coussens, L.M., 2012. Accessories to the Crime: Functions of Cells Recruited to the Tumor Microenvironment. Cancer Cell, 2012, **21**, 309–322.
[63] Bunney, T.D., Katan, M., 2010. Phosphoinositide signalling in cancer: beyond PI3K and PTEN. Nat. Rev. Cancer, 2010, **10**, 342–352.
[64] Sasaki, T., Takasuga, S., Sasaki, J., Kofuji, S., et al., 2009. Mammalian phosphoinositide kinases and phosphatases. Prog. Lipid Res., 2009, **48**, 307–43.
[65] Di Paolo, G., De Camilli, P., 2006. Phosphoinositides in cell regulation and membrane dynamics. Nature, 2006, **443**, 651–7.
[66] D'Angelo, G., Vicinanza, M., Di Campli, A., De Matteis, M.A., 2008. The multiple roles of PtdIns(4)P -- not just the precursor of PtdIns(4,5)P2. J. Cell Sci., 2008, **121**, 1955–63.
[67] Katan, M., 2005. New insights into the families of PLC enzymes: looking back and going forward. Biochem. J., 2005, **391**, e7-9.
[68] Katso, R., Okkenhaug, K., Ahmadi, K., White, S., et al., 2001. Cellular function of phosphoinositide 3-kinases: implications for development, homeostasis, and cancer. Annu. Rev. Cell Dev. Biol., 2001, **17**, 615–75.
[69] Engelman, J.A., Luo, J., Cantley, L.C., 2006. The evolution of phosphatidylinositol 3-kinases as regulators of growth and metabolism. Nat. Rev. Genet., 2006, **7**, 606–19.
[70] Michell, R.H., Heath, V.L., Lemmon, M.A., Dove, S.K., 2006. Phosphatidylinositol 3,5-bisphosphate: metabolism and cellular functions. Trends Biochem. Sci., 2006, **31**, 52–63.
[71] Li, H., Marshall, A.J., 2015. Phosphatidylinositol (3,4) bisphosphate-specific phosphatases and effector proteins: A distinct branch of PI3K signaling. Cell. Signal., 2015, **27**, 1789–1798.
[72] Hennessy, B.T., Smith, D.L., Ram, P.T., Lu, Y., Mills, G.B., 2005. Exploiting the PI3K/AKT pathway for cancer drug discovery. Nat Rev Drug Discov, 2005, **4**, 988–1004.
[73] Foster, J.G., Blunt, M.D., Carter, E., Ward, S.G., 2012. Inhibition of PI3K Signaling Spurs New Therapeutic Opportunities in Inflammatory / Autoimmune Diseases and Hematological Malignancies. Pharmacol. Rev., 2012, **64**, 1027–1054.
[74] Manning, B.D., Cantley, L.C., 2007. AKT/PKB Signaling: Navigating Downstream. Cell, 2007, **129**, 1261–1274.
[75] Thorpe, L.M., Yuzugullu, H., Zhao, J.J., 2015. PI3K in cancer: divergent roles of isoforms, modes of activation and therapeutic targeting. Nat. Rev. Cancer, 2015, **15**, 7–24.
[76] Alessi, D.R., Andjelkovic, M., Caudwell, B., Cron, P., et al., 1996. Mechanism of activation of protein kinase B by insulin and IGF-1. EMBO J., 1996, **15**, 6541–51.
[77] Blume-Jensen, P., Hunter, T., 2001. Oncogenic kinase signalling. Nature, 2001, **411**, 355–65.
[78] Lynch, D.K., Ellis, C.A., Edwards, P.A., Hiles, I.D., 1999. Integrin-linked kinase regulates phosphorylation of serine 473 of protein kinase B by an indirect mechanism. Oncogene, 1999, **18**, 8024–32.
[79] Kawakami, Y., Nishimoto, H., Kitaura, J., Maeda-Yamamoto, M., et al., 2004. Protein kinase C betaII regulates Akt phosphorylation on Ser-473 in a cell type- and stimulus-specific fashion. J. Biol. Chem., 2004, **279**, 47720–5.
[80] Sarbassov, D.D., Guertin, D.A., Ali, S.M., Sabatini, D.M., 2005. Phosphorylation and regulation of Akt/PKB by the rictor-mTOR complex. Science (80-.)., 2005, **307**, 1098–1101.
[81] Leslie, N.R., Batty, I.H., Maccario, H., Davidson, L., Downes, C.P., 2008. Understanding PTEN regulation: PIP2, polarity and protein stability. Oncogene, 2008, **27**, 5464–76.
[82] Norris, F.A., Atkins, R.C., Majerus, P.W., 1997. The cDNA Cloning and Characterization of Inositol Polyphosphate 4-Phosphatase Type II: EVIDENCE FOR CONSERVED ALTERNATIVE SPLICING IN THE 4-PHOSPHATASE FAMILY. J. Biol. Chem., 1997, **272**, 23859–23864.
[83] Gewinner, C., Wang, Z.C., Richardson, A., Teruya-Feldstein, J., et al., 2009. Evidence that Inositol Polyphosphate 4-Phosphatase Type II Is a Tumor Suppressor that Inhibits PI3K Signaling. Cancer Cell, 2009, **16**, 115–125.
[84] Kerr, W.G., 2011. Inhibitor and activator: Dual functions for SHIP in immunity and cancer. Ann. N. Y. Acad. Sci., 2011, **1217**, 1–17.
[85] Lien, E.C., Dibble, C.C., Toker, A., 2017. PI3K signaling in cancer: beyond AKT. Curr. Opin. Cell Biol., 2017, **45**, 62–71.
[86] Djordjevic, S., Driscoll, P.C., 2002. Structural insight into substrate specificity and regulatory mechanisms of phosphoinositide 3-kinases. Trends Biochem. Sci., 2002, **27**, 426–432.
[87] Schmid, M.C., Avraamides, C.J., Dippold, H.C., Franco, I., et al., 2011. Receptor Tyrosine Kinases and TLR/IL1Rs Unexpectedly Activate Myeloid Cell PI3Kγ, A Single Convergent Point Promoting Tumor Inflammation and Progression. Cancer Cell, 2011, **19**, 715–727.
[88] Kurig, B., Shymanets, A., Bohnacker, T., Prajwal, et al., 2009. Ras is an indispensable coregulator of the class IB phosphoinositide 3-kinase p87/p110gamma. Proc. Natl. Acad. Sci. U. S. A., 2009, **106**, 20312–7.
[89] Brock, C., Schaefer, M., Reusch, H.P., Czupalla, C., et al., 2003. Roles of G beta gamma in membrane recruitment and activation of p110 gamma/p101 phosphoinositide 3-kinase gamma. J. Cell Biol., 2003, **160**, 89–99.
[90] Stoyanov, B., Volinia, S., Hanck, T., Rubio, I., et al., 1995. Cloning and characterization of a G protein-activated human phosphoinositide-3 kinase. Science, 1995, **269**, 690–3.
[91] Maier, U., Babich, A., Nürnberg, B., 1999. Roles of non-catalytic subunits in gbetagamma-induced activation of class I phosphoinositide 3-kinase isoforms beta and gamma. J. Biol. Chem., 1999, **274**, 29311–7.
[92] Suire, S., Coadwell, J., Ferguson, G.J., Davidson, K., et al., 2005. p84, a New Gβγ-Activated Regulatory Subunit of the Type IB Phosphoinositide 3-Kinase p110γ.vol. 15.
[93] Stephens, L.R., Eguinoa, A., Erdjument-Bromage, H., Lui, M., et al., 1997. The G beta gamma sensitivity of a PI3K is dependent upon a tightly associated adaptor, p101. Cell, 1997, **89**, 105–14.
[94] Songyang, Z., Shoelson, S.E., Chaudhuri, M., Gish, G., et al., 1993. SH2 domains recognize specific phosphopeptide sequences. Cell, 1993, **72**, 767–78.
[95] Engelman, J.A., Jänne, P.A., Mermel, C., Pearlberg, J., et al., 2005. ErbB-3 mediates phosphoinositide 3-kinase activity in gefitinib-sensitive non-small cell lung cancer cell lines. Proc. Natl. Acad. Sci. U. S. A., 2005, **102**, 3788–93.
[96] Engelman, J.A., 2009. Targeting PI3K signalling in cancer: opportunities, challenges and limitations. Nat. Rev. Cancer, 2009, **9**, 550–62.
[97] Rubio, I., Rodriguez-Viciana, P., Downward, J., Wetzker, R., 1997. Interaction of Ras with phosphoinositide 3-kinase gamma. Biochem. J., 1997, 891–5.
[98] Rodriguez-Viciana, P., Warne, P.H., Khwaja, A., Marte, B.M., et al., 1997. Role of phosphoinositide 3-OH kinase in cell transformation and control of the actin cytoskeleton by Ras. Cell, 1997, **89**, 457–467.
[99] Rodriguez-Viciana, P., Warne, P.H., Vanhaesebroeck, B., Waterfield, M.D., Downward, J., 1996. Activation of phosphoinositide 3-kinase by

interaction with Ras and by point mutation. EMBO J., 1996, **15**, 2442–51.
[100] Pacold, M.E., Suire, S., Perisic, O., Lara-Gonzalez, S., et al., 2000. Crystal structure and functional analysis of Ras binding to its effector phosphoinositide 3-kinase gamma. Cell, 2000, **103**, 931–43.
[101] Suire, S., Hawkins, P., Stephens, L., 2002. Activation of phosphoinositide 3-kinase gamma by Ras. Curr. Biol., 2002, **12**, 1068–75.
[102] Rodriguez-Viciana, P., Sabatier, C., McCormick, F., 2004. Signaling specificity by Ras family GTPases is determined by the full spectrum of effectors they regulate. Mol. Cell. Biol., 2004, **24**, 4943–54.
[103] Murphy, G.A., Graham, S.M., Morita, S., Reks, S.E., et al., 2002. Involvement of phosphatidylinositol 3-kinase, but not RalGDS, in TC21/R-Ras2-mediated transformation. J. Biol. Chem., 2002, **277**, 9966–75.
[104] Fritsch, R., de Krijger, I., Fritsch, K., George, R., et al., 2013. RAS and RHO families of GTPases directly regulate distinct phosphoinositide 3-kinase isoforms. Cell, 2013, **153**, 1050–63.
[105] Li, J., Yen, C., Liaw, D., Podsypanina, K., et al., 1997. PTEN, a putative protein tyrosine phosphatase gene mutated in human brain, breast, and prostate cancer. Science, 1997, **275**, 1943–7.
[106] Steck, P.A., Pershouse, M.A., Jasser, S.A., Yung, W.K., et al., 1997. Identification of a candidate tumour suppressor gene, MMAC1, at chromosome 10q23.3 that is mutated in multiple advanced cancers. Nat. Genet., 1997, **15**, 356–62.
[107] Jimenez, C., Jones, D.R., Rodríguez-Viciana, P., Gonzalez-García, A., et al., 1998. Identification and characterization of a new oncogene derived from the regulatory subunit of phosphoinositide 3-kinase. EMBO J., 1998, **17**, 743–53.
[108] Utermark, T., Rao, T., Cheng, H., Wang, Q., et al., 2012. The p110α and p110β isoforms of PI3K play divergent roles in mammary gland development and tumorigenesis. Genes Dev., 2012, **26**, 1573–86.
[109] Yang, J., Cron, P., Good, V.M., Thompson, V., et al., 2002. Crystal structure of an activated Akt/protein kinase B ternary complex with GSK3-peptide and AMP-PNP. Nat. Struct. Biol., 2002, **9**, 940–944.
[110] Vasudevan, K.M., Garraway, L.A., 2010. AKT Signaling in Physiology and Disease. Curr Top Microbiol Immunol., 2010, **347**, 105–133.
[111] Noguchi, M., Ropars, V., Roumestand, C., Suizu, F., 2007. Proto-oncogene TCL1: more than just a coactivator for Akt. FASEB J., 2007, **21**, 2273–84.
[112] Bellacosa, A., Kumar, C.C., Di Cristofano, A., Testa, J.R., 2005. Activation of AKT kinases in cancer: implications for therapeutic targeting. Adv. Cancer Res., 2005, **94**, 29–86.
[113] Franke, T.F., Kaplan, D.R., Cantley, L.C., Toker, A., 1997. Direct regulation of the Akt proto-oncogene product by phosphatidylinositol-3,4-bisphosphate. Science, 1997, **275**, 665–8.
[114] Alessi, D.R., James, S.R., Downes, C.P., Holmes, A.B., et al., 1997. Characterization of a 3-phosphoinositide-dependent protein kinase which phosphorylates and activates protein kinase Balpha. Curr. Biol., 1997, **7**, 261–9.
[115] Stokoe, D., Stephens, L.R., Copeland, T., Gaffney, P.R., et al., 1997. Dual role of phosphatidylinositol-3,4,5-trisphosphate in the activation of protein kinase B. Science, 1997, **277**, 567–70.
[116] Stephens, L., Anderson, K., Stokoe, D., Erdjument-Bromage, H., et al., 1998. Protein kinase B kinases that mediate phosphatidylinositol 3,4,5-trisphosphate-dependent activation of protein kinase B. Science, 1998, **279**, 710–4.
[117] Hresko, R.C., Mueckler, M., 2005. mTOR/RICTOR is the Ser473 kinase for Akt/PKB in 3T3–L1 adipocytes. J Biol Chem, 2005, **280**, 40406–40416.
[118] Lee, S., Comer, F.I., Sasaki, A., McLeod, I.X., et al., 2005. TOR Complex 2 Integrates Cell Movement during Chemotaxis and Signal Relay in Dictyostelium. Mol. Biol. Cell, 2005, **16**.
[119] Williams, M.R., Arthur, J.S., Balendran, A., van der Kaay, J., et al., 2000. The role of 3-phosphoinositide dependent protein kinase 1 in activating AGC kinases defined in embryonic stem cells. Curr. Biol., 2000, **10**, 439–448.
[120] Guertin, D.A., Stevens, D.M., Thoreen, C.C., Burds, A.A., et al., 2006. Ablation in Mice of the mTORC Components raptor, rictor, or mLST8 Reveals that mTORC2 Is Required for Signaling to Akt-FOXO and PKCα, but Not S6K1. Dev. Cell, 2006, **11**, 859–871.
[121] Inoki, K., Li, Y., Zhu, T., Wu, J., Guan, K.-L., 2002. TSC2 is phosphorylated and inhibited by Akt and suppresses mTOR signalling. Nat. Cell Biol., 2002, **4**, 648–57.
[122] Jacinto, E., Facchinetti, V., Liu, D., Soto, N., et al., 2006. SIN1/MIP1 Maintains rictor-mTOR Complex Integrity and Regulates Akt Phosphorylation and Substrate Specificity. Cell, 2006, **127**, 125–137.
[123] Manning, B.D., Tee, A.R., Logsdon, M.N., Blenis, J., Cantley, L.C., 2002. Identification of the tuberous sclerosis complex-2 tumor suppressor gene product tuberin as a target of the phosphoinositide 3-kinase/akt pathway. Mol. Cell, 2002, **10**, 151–62.
[124] Chiang, G.G., Abraham, R.T., 2005. Phosphorylation of mammalian target of rapamycin (mTOR) at Ser-2448 is mediated by p70S6 kinase. J Biol Chem, 2005, **280**, 25485–25490.
[125] Holz, M.K., Blenis, J., 2005. Identification of S6 kinase 1 as a novel mammalian target of rapamycin (mTOR)-phosphorylating kinase. J Biol Chem, 2005, **280**, 26089–26093.
[126] Zhang, H.H., Lipovsky, A.I., Dibble, C.C., Sahin, M., Manning, B.D., 2006. S6K1 regulates GSK3 under conditions of mTOR-dependent feedback inhibition of Akt. Mol. Cell, 2006, **24**, 185–197.
[127] Greer, E.L., Brunet, A., 2005. FOXO transcription factors at the interface between longevity and tumor suppression. Oncogene, 2005, **24**, 7410–7452.
[128] Maira, S.M. et al, 2001. Carboxyl-terminal modulator protein (CTMP), a negative regulator of PKB/Akt and v-Akt at the plasma membrane. Science (80-.)., 2001, **294**, 374–380.
[129] Perrotti, D., Neviani, P., 2013. Targeting A Tumor Suppressor To Suppress Tumor Growth: News and Views on Protein Phosphatase 2A (PP2A) as a Target for Anti- cancer Therapy. Lancet Oncol., 2013, **14**, e229-e38.
[130] Newton, A., Trotman, L., 2014. Turning Off AKT: PHLPP as a Drug Target. Ann Rev Pharmacol Toxicol, 2014, **54**, 537–58.
[131] Li, H., Marshall, A.J., 2015. Phosphatidylinositol (3,4) bisphosphate-specific phosphatases and effector proteins: A distinct branch of PI3K signaling. Cell. Signal., 2015, **27**, 1789–1798.
[132] Allam, A., Marshall, A.J., 2005. Role of the adaptor proteins Bam32, TAPP1 and TAPP2 in lymphocyte activation. Immunol. Lett., 2005, **97**, 7–17.
[133] Dowler, S., Currie, R.A., Campbell, D.G., Deak, M., et al., 2000. Identification of pleckstrin-homology-domain-containing proteins with novel phosphoinositide-binding specificities. Biochem J, 2000, **351**, 19–31.
[134] Manna, D., Albanese, A., Wei, S.P., Cho, W., 2007. Mechanistic basis of differential cellular responses of phosphatidylinositol 3,4-bisphosphate- and phosphatidylinositol 3,4,5-trisphosphate-binding pleckstrin homology domains. J. Biol. Chem., 2007, **282**, 32093–32105.
[135] Marshall, A.J., Krahn, A.K., Ma, K., Duronio, V., Hou, S., 2002. TAPP1 and TAPP2 are targets of phosphatidylinositol 3-kinase signaling in B cells: sustained plasma membrane recruitment triggered by the B-cell antigen receptor. Mol. Cell. Biol., 2002, **22**, 5479–91.
[136] Thomas, C.C., Dowler, S., Deak, M., Alessi, D.R., van Aalten, D.M., 2001. Crystal structure of the phosphatidylinositol 3,4-bisphosphate-binding pleckstrin homology (PH) domain of tandem PH-domain-containing protein 1 (TAPP1): molecular basis of lipid specificity. Biochem. J., 2001, **358**, 287–94.
[137] Zhang, T., Li, H., Cheung, S.M., Costantini, J.L., et al., 2009. Phosphoinositide 3-kinase-regulated adapters in lymphocyte activation. Immunol. Rev., 2009, **232**, 255–272.
[138] Krahn, A.K., Ma, K., Hou, S., Duronio, V., Marshall, A.J., 2004. Two distinct waves of membrane-proximal B cell antigen receptor signaling differentially regulated by Src homology 2-containing inositol polyphosphate 5-phosphatase. J. Immunol., 2004, **172**, 331–9.
[139] Freeburn, R.W., Wright, K.L., Burgess, S.J., Astoul, E., et al., 2002. Evidence That SHIP-1 Contributes to Phosphatidylinositol 3,4,5-Trisphosphate Metabolism in T Lymphocytes and Can Regulate Novel Phosphoinositide 3-Kinase Effectors. J. Immunol., 2002, **169**, 5441–5450.

[140] Kornau, H.C., Schenker, L.T., Kennedy, M.B., Seeburg, P.H., 1995. Domain interaction between NMDA receptor subunits and the postsynaptic density protein PSD-95. Science, 1995, **269**, 1737–40.

[141] Songyang, Z., Fanning, A.S., Fu, C., Xu, J., et al., 1997. Recognition of unique carboxyl-terminal motifs by distinct PDZ domains. Science, 1997, **275**, 73–7.

[142] Kimber, W.A., Deak, M., Prescott, A.R., Alessi, D.R., 2003. Interaction of the protein tyrosine phosphatase PTPL1 with the PtdIns(3,4)P2-binding adaptor protein TAPP1. Biochem. J., 2003, **376**, 525–35.

[143] Hogan, A., Yakubchyk, Y., Chabot, J., Obagi, C., et al., 2004. The phosphoinositol 3,4-bisphosphate-binding protein TAPP1 interacts with syntrophins and regulates actin cytoskeletal organization. J. Biol. Chem., 2004, **279**, 53717–24.

[144] Bompard, G., Puech, C., Prébois, C., Vignon, F., Freiss, G., 2002. Protein-tyrosine phosphatase PTPL1/FAP-1 triggers apoptosis in human breast cancer cells. J. Biol. Chem., 2002, **277**, 47861–9.

[145] Dromard, M., Bompard, G., Glondu-Lassis, M., Puech, C., et al., 2007. The putative tumor suppressor gene PTPN13/PTPL1 induces apoptosis through insulin receptor substrate-1 dephosphorylation. Cancer Res., 2007, **67**, 6806–13.

[146] Li, H., Hou, S., Wu, X., Nandagopal, S., et al., 2013. The Tandem PH Domain-Containing Protein 2 (TAPP2) Regulates Chemokine-Induced Cytoskeletal Reorganization and Malignant B Cell Migration. PLoS One, 2013, **8**, e57809.

[147] Costantini, J.L., Cheung, S.M.S., Hou, S., Li, H., et al., 2009. TAPP2 links phosphoinositide 3-kinase signaling to B-cell adhesion through interaction with the cytoskeletal protein utrophin: expression of a novel cell adhesion-promoting complex in B-cell leukemia. Blood, 2009, **114**, 4703–12.

[148] Del Principe, M.I., Del Poeta, G., Buccisano, F., Maurillo, L., et al., 2006. Clinical significance of ZAP-70 protein expression in B-cell chronic lymphocytic leukemia. Blood, 2006, **108**, 853–61.

[149] Landego, I., Jayachandran, N., Wullschleger, S., Zhang, T., et al., 2012. Interaction of TAPP adapter proteins with phosphatidylinositol (3,4)-bisphosphate regulates B-cell activation and autoantibody production. Eur. J. Immunol., 2012, **42**, 2760–2770.

[150] Wullschleger, S., Wasserman, D.H., Gray, A., Sakamoto, K., Alessi, D.R., 2011. Role of TAPP1 and TAPP2 adaptor binding to PtdIns(3,4)P2 in regulating insulin sensitivity defined by knock-in analysis. Biochem. J., 2011, **434**, 265–74.

[151] Cardone, M.H., Roy, N., Stennicke, H.R., Salvesen, G.S., et al., 1998. Regulation of cell death protease caspase-9 by phosphorylation. Science, 1998, **282**, 1318–21.

[152] Datta, S.R., Katsov, A., Hu, L., Petros, A., et al., 2000. 14-3-3 proteins and survival kinases cooperate to inactivate BAD by BH3 domain phosphorylation. Mol. Cell, 2000, **6**, 41–51.

[153] Datta, S.R., Dudek, H., Tao, X., Masters, S., et al., 1997. Akt phosphorylation of BAD couples survival signals to the cell-intrinsic death machinery. Cell, 1997, **91**, 231–41.

[154] del Peso, L., González-García, M., Page, C., Herrera, R., Nuñez, G., 1997. Interleukin-3-induced phosphorylation of BAD through the protein kinase Akt. Science, 1997, **278**, 687–9.

[155] Frame, S., Cohen, P., 2001. GSK3 takes centre stage more than 20 years after its discovery. Biochem. J., 2001, **359**, 1–16.

[156] Cross, D.A.E., Alessi, D.R., Cohen, P., Andjelkovich, M., Hemmings, B.A., 1995. Inhibition of glycogen synthase kinase-3 by insulin mediated by protein kinase B. Nature, 1995, **378**, 785–789.

[157] Maurer, U., Charvet, C., Wagman, A.S., Dejardin, E., Green, D.R., 2006. Glycogen Synthase Kinase-3 Regulates Mitochondrial Outer Membrane Permeabilization and Apoptosis by Destabilization of MCL-1. Mol. Cell, 2006, **21**, 749–760.

[158] Mayo, L.D., Donner, D.B., 2001. A phosphatidylinositol 3-kinase/Akt pathway promotes translocation of Mdm2 from the cytoplasm to the nucleus. Proc. Natl. Acad. Sci. U. S. A., 2001, **98**, 11598–603.

[159] Zhou, B.P., Liao, Y., Xia, W., Zou, Y., et al., 2001. HER-2/neu induces p53 ubiquitination via Akt-mediated MDM2 phosphorylation. Nat. Cell Biol., 2001, **3**, 973–82.

[160] Tran, H., Brunet, A., Griffith, E.C., Greenberg, M.E., 2003. The many forks in FOXO's road. Sci. STKE, 2003, **2003**, RE5.

[161] Dijkers, P.F., Birkenkamp, K.U., Lam, E.W.-F., Thomas, N.S.B., et al., 2002. FKHR-L1 can act as a critical effector of cell death induced by cytokine withdrawal. J. Cell Biol., 2002, **156**, 531–542.

[162] Brunet, A., Bonni, A., Zigmond, M.J., Lin, M.Z., et al., 1999. Akt promotes cell survival by phosphorylating and inhibiting a Forkhead transcription factor. Cell, 1999, **96**, 857–68.

[163] Du, K., Montminy, M., 1998. CREB is a regulatory target for the protein kinase Akt/PKB. J. Biol. Chem., 1998, **273**, 32377–9.

[164] Arcinas, M., Heckman, C.A., Mehew, J.W., Boxer, L.M., 2001. Molecular mechanisms of transcriptional control of bcl-2 and c-myc in follicular and transformed lymphoma. Cancer Res., 2001, **61**, 5202–6.

[165] Wang, J.M., Chao, J.R., Chen, W., Kuo, M.L., et al., 1999. The antiapoptotic gene mcl-1 is up-regulated by the phosphatidylinositol 3-kinase/Akt signaling pathway through a transcription factor complex containing CREB. Mol. Cell. Biol., 1999, **19**, 6195–206.

[166] Nidai Ozes, O., Mayo, L.D., Gustin, J.A., Pfeffer, S.R., et al., 1999. NF-kappaB activation by tumour necrosis factor requires the Akt serine-threonine kinase. Nature, 1999, **401**, 82–85.

[167] Shishodia, S., Aggarwal, B.B., 2004. Nuclear factor-kappaB activation mediates cellular transformation, proliferation, invasion angiogenesis and metastasis of cancer. Cancer Treat. Res., 2004, **119**, 139–73.

[168] Bhaskar, P.T., Hay, N., 2007. The Two TORCs and Akt. Dev. Cell, 2007, **12**, 487–502.

[169] Vander Haar, E., Lee, S.-I., Bandhakavi, S., Griffin, T.J., Kim, D.-H., 2007. Insulin signalling to mTOR mediated by the Akt/PKB substrate PRAS40. Nat. Cell Biol., 2007, **9**, 316–23.

[170] Hara, K., Maruki, Y., Long, X., Yoshino, K., et al., 2002. Raptor, a binding partner of target of rapamycin (TOR) mediates TOR Action. Cell, 2002, **110**, 177–189.

[171] Kim, D.-H., Sarbassov, D.D., Ali, S.M., Latek, R.R., et al., 2003. GbetaL, a positive regulator of the rapamycin-sensitive pathway required for the nutrient-sensitive interaction between raptor and mTOR. Mol. Cell, 2003, **11**, 859–904.

[172] Loewith, R., Jacinto, E., Wullschleger, S., Lorberg, A., et al., 2002. Two TOR complexes, only one of which is rapamycin sensitive, have distinct roles in cell growth control. Mol. Cell, 2002, **10**, 457–468.

[173] Sancak, Y., Thoreen, C.C., Peterson, T.R., Lindquist, R.A., et al., 2007. PRAS40 Is an Insulin- Regulated Inhibitor of the mTORC1 Protein Kinase. Mol. Cell, 2007, **25**, 903–915.

[174] Kim, D.-H., Sarbassov, D.D., Ali, S.M., King, J.E., et al., 2002. mTOR Interacts with Raptor to Form a Nutrient-Sensitive Complex that Signals to the Cell Growth Machinery. Cell, 2002, **110**, 163–175.

[175] Schalm, S.S., Fingar, D.C., Sabatini, D.M., Blenis, J., 2003. TOS Motif-Mediated Raptor Binding Regulates 4E–BP1 Multisite Phosphorylation and Function. Curr. Biol., 2003, **13**, 797–806.

[176] Guertin, D.A., Sabatini, D.M., 2007. Defining the Role of mTOR in Cancer. Cancer Cell, 2007, **12**, 9–22.

[177] Peterson, R.T., Beal, P.A., Comb, M.J., Schreiber, S.L., 2000. FKBP12-rapamycin-associated protein (FRAP) autophosphorylates at serine 2481 under translationally repressive conditions. J. Biol. Chem., 2000, **275**, 7416–7423.

[178] Takahashi, T., Hara, K., Inoue, H., Kawa, Y., et al., 2000. Carboxyl-terminal region conserved among phosphoinositide-kinase-related kinases is indispensable for mTOR function in vivo and in vitro. Genes Cells. Genes Cells, 2000, **5**, 765–775.

[179] Dames, S.A., Mulet, J.M., Rathgeb-Szabo, K., Hall, M.N., Grzesiek, S., 2005. The solution structure of the FATC domain of the protein kinase target of rapamycin suggests a role for redox-dependent structural and cellular stability. J. Biol. Chem., 2005, **280**, 20558–20564.

[180] Sarbassov, D.D., Sabatini, D.M., 2005. Redox regulation of the nutrient-sensitive raptor-mTOR pathway and complex. J. Biol. Chem., 2005, **280**, 39505–39509.

[181] Gingras, A.C., Kennedy, S.G., O'Leary, M.A., Sonenberg, N., Hay, N., 1998. 4E–BP1, a repressor of mRNA translation, is phosphorylated and inactivated by the Akt(PKB) signaling pathway. Genes Dev., 1998, **12**, 502–513.

[182] Ma, L., Chen, Z., Erdjument-Bromage, H., Tempst, P., Pandolfi, P.P., 2005. Phosphorylation and functional inactivation of TSC2 by Erk implications for tuberous sclerosis and cancer pathogenesis. Cell, 2005, **121**, 179–193.

[183] Hay, N., Sonenberg, N., 2004. Upstream and downstream of mTOR. Genes Dev., 2004, **18**, 1926–1945.

[184] Li, Y., Inoki, K., Vacratsis, P., Guan, K.L., 2003. The p38 and MK2 kinase cascade phosphorylates tuberin, the tuberous sclerosis 2 gene product, and enhances its interaction with 14–3-3. J. Biol. Chem., 2003, **278**, 13663–13671.

[185] Manning, B.D., Cantley, L.C., 2003. Rheb fills a GAP between TSC and TOR. Trends Biochem. Sci., 2003, **28**, 573–6.

[186] Mills, S.J., Persson, C., Cozier, G., Thomas, M.P., et al., 2012. A synthetic polyphosphoinositide headgroup surrogate in complex with SHIP2 provides a rationale for drug discovery. ACS Chem. Biol., 2012, **7**, 822–828.

[187] Hsu, Y.C., Chern, J.J., Cai, Y., Liu, M., Choi, K.W., 2007. Drosophila TCTP is essential for growth and proliferation through regulation of dRheb GTPase. Nature, 2007, **445**, 785–788.

[188] Kovacina, K.S., Park, G.Y., Bae, S.S., Guzzetta, A.W., et al., 2003. Identification of a proline-rich Akt substrate as a 14–3-3 binding partner. J. Biol. Chem., 2003, **278**, 10189–10194.

[189] Nobukuni, T., Joaquin, M., Roccio, M., Dann, S.G., et al., 2005. Amino acids mediate mTOR/raptor signaling through activation of class 3 phosphatidylinositol 3OH-kinase. Proc. Natl. Acad. Sci. USA, 2005, **102**, 14238–14243.

[190] Smith, E.M., Finn, S.G., Tee, A.R., Browne, G.J., Proud, C.G., 2005. The tuberous sclerosis protein TSC2 is not required for the regulation of the mammalian target of rapamycin by amino acids and certain cellular stresses. J. Biol. Chem., 2005, **280**, 18717–18727.

[191] Sofer, A., Lei, K., Johannessen, C.M., Ellisen, L.W., 2005. Regulation of mTOR and cell growth in response to energy stress by REDD1. Mol Cell Biol, 2005, **25**, 5834–5845.

[192] Sarbassov, D., Ali, S.M., Sabatini, D.M., 2005. Growing roles for the mTOR pathway. Curr. Opin. Cell Biol., 2005, **17**, 596–603.

[193] Wullschleger, S., Loewith, R., Hall, M.N., 2006. TOR signaling in growth and metabolism. Cell, 2006, **124**, 471–484.

[194] Dorrello, N.V., Peschiaroli, A., Guardavaccaro, D., Colburn, N.H., et al., 2006. S6K1- and bTRCP-mediated degradation of PDCD4 promotes protein translation and cell growth. Science (80-.)., 2006, **314**, 467–471.

[195] Ruggero, D., Montanaro, L., Ma, L., Xu, W., et al., 2004. The translation factor eIF-4E promotes tumor formation and cooperates with c-Myc in lymphomagenesis. Nat Med, 2004, **10**, 484–486.

[196] Lazaris-Karatzas, A., Montine, K.S., Sonenberg, N., 1990. Malignant transformation by a eukaryotic initiation factor subunit that binds to mRNA 5' cap. Nature, 1990, **345**, 544–547.

[197] Lazaris-Karatzas, A., Sonenberg, N., 1992. The mRNA 5' cap-binding protein, eIF-4E, cooperates with v-myc or E1A in the transformation of primary rodent fibroblasts. Mol. Cell. Biol., 1992, **12**, 1234–8.

[198] Liang, J., Zubovitz, J., Petrocelli, T., Kotchetkov, R., et al., 2002. PKB/Akt phosphorylates p27, impairs nuclear import of p27 and opposes p27-mediated G1 arrest. Nat. Med., 2002, **8**, 1153–60.

[199] Medema, R.H., Kops, G.J., Bos, J.L., Burgering, B.M., 2000. AFX-like Forkhead transcription factors mediate cell-cycle regulation by Ras and PKB through p27kip1. Nature, 2000, **404**, 782–7.

[200] Welcker, M., Singer, J., Loeb, K.R., Grim, J., et al., 2003. Multisite phosphorylation by Cdk2 and GSK3 controls cyclin E degradation. Mol. Cell, 2003, **12**, 381–92.

[201] Wei, W., Jin, J., Schlisio, S., Harper, J.W., Kaelin, W.G., 2005. The v-Jun point mutation allows c-Jun to escape GSK3-dependent recognition and destruction by the Fbw7 ubiquitin ligase. Cancer Cell, 2005, **8**, 25–33.

[202] Yeh, E., Cunningham, M., Arnold, H., Chasse, D., et al., 2004. A signalling pathway controlling c-Myc degradation that impacts oncogenic transformation of human cells. Nat. Cell Biol., 2004, **6**, 308–318.

[203] Diehl, J.A., Cheng, M., Roussel, M.F., Sherr, C.J., 1998. Glycogen synthase kinase-3beta regulates cyclin D1 proteolysis and subcellular localization. Genes Dev., 1998, **12**, 3499–511.

[204] Mamane, Y., Petroulakis, E., Rong, L., Yoshida, K., et al., 2004. eIF4E--from translation to transformation. Oncogene, 2004, **23**, 3172–9.

[205] King, F.W., Skeen, J., Hay, N., Shtivelman, E., 2004. Inhibition of Chk1 by activated PKB/Akt. Cell Cycle, 2004, **3**, 634–7.

[206] Puc, J., Keniry, M., Li, H.S., Pandita, T.K., et al., 2005. Lack of PTEN sequesters CHK1 and initiates genetic instability. Cancer Cell, 2005, **7**, 193–204.

[207] Berx, G., Raspé, E., Christofori, G., Thiery, J.P., Sleeman, J.P., 2007. Pre-EMTing metastasis? Recapitulation of morphogenetic processes in cancer. Clin. Exp. Metastasis, 2007, **24**, 587–97.

[208] Condeelis, J., Singer, R.H., Segall, J.E., 2005. The great escape: when cancer cells hijack the genes for chemotaxis and motility. Annu. Rev. Cell Dev. Biol., 2005, **21**, 695–718.

[209] Machesky, L.M., 2008. Lamellipodia and filopodia in metastasis and invasion. FEBS Lett., 2008, **582**, 2102–2111.

[210] Chen, W.T., 1996. Proteases associated with invadopodia, and their role in degradation of extracellular matrix. Enzyme Protein, 1996, **49**, 59–71.

[211] Buccione, R., Orth, J.D., McNiven, M.A., 2004. Foot and mouth: podosomes, invadopodia and circular dorsal ruffles. Nat. Rev. Mol. Cell Biol., 2004, **5**, 647–57.

[212] Chen, W.-T., 1989. Proteolytic activity of specialized surface protrusions formed at rosette contact sites of transformed cells. J. Exp. Zool., 1989, **251**, 167–185.

[213] Nürnberg, A., Kitzing, T., Grosse, R., 2011. Nucleating actin for invasion. Nat. Rev. Cancer, 2011, **11**, 177–87.

[214] Hoshino, D., Branch, K.M., Weaver, A.M., 2013. Signaling inputs to invadopodia and podosomes. J. Cell Sci., 2013, **126**, 2979–89.

[215] Faix, J., Rottner, K., 2006. The making of filopodia. Curr. Opin. Cell Biol., 2006, **18**, 18–25.

[216] Petrie, R.J., Doyle, A.D., Yamada, K.M., 2009. Random versus directionally persistent cell migration. Nat. Rev. Mol. Cell Biol., 2009, **10**, 538–49.

[217] Etienne-Manneville, S., Hall, A., 2002. Rho GTPases in cell biology. Nature, 2002, **420**, 629–35.

[218] Gupton, S.L., Gertler, F.B., 2007. Filopodia: the fingers that do the walking. Sci. STKE, 2007, **2007**, re5.

[219] Hashimoto, Y., Parsons, M., Adams, J.C., 2007. Dual actin-bundling and protein kinase C-binding activities of fascin regulate carcinoma cell migration downstream of Rac and contribute to metastasis. Mol. Biol. Cell, 2007, **18**, 4591–602.

[220] Hashimoto, Y., Skacel, M., Lavery, I.C., Mukherjee, A.L., et al., 2006. Prognostic significance of fascin expression in advanced colorectal cancer: an immunohistochemical study of colorectal adenomas and adenocarcinomas. BMC Cancer, 2006, **6**, 241.

[221] Vignjevic, D., Kojima, S., Aratyn, Y., Danciu, O., et al., 2006. Role of fascin in filopodial protrusion. J. Cell Biol., 2006, **174**, 863–875.

[222] Vignjevic, D., Montagnac, G., 2008. Reorganisation of the dendritic actin network during cancer cell migration and invasion. Semin. Cancer Biol., 2008, **18**, 12–22.

[223] Hashimoto, Y., Shimada, Y., Kawamura, J., Yamasaki, S., Imamura, M., 2004. The prognostic relevance of fascin expression in human gastric carcinoma. Oncology, 2004, **67**, 262–270.

[224] Hashimoto, Y., Ito, T., Inoue, H., Okumura, T., et al., 2005. Prognostic significance of fascin overexpression in human esophageal squamous cell carcinoma. Clin. Cancer Res., 2005, **11**, 2597–2605.

[225] Pelosi, G., Pastorino, U., Pasini, F., Maissoneuve, P., et al., 2003. Independent prognostic value of fascin immunoreactivity in stage I nonsmall cell lung cancer. Br. J. Cancer, 2003, **88**, 537–547.

[226] Rodriguez-Pinilla, S.M., Sarrió, D., Honrado, E., Hardisson, D., et al., 2006. Prognostic Significance of Basal-Like Phenotype and Fascin Expression in Node-Negative Invasive Breast Carcinomas. Clin. Cancer Res., 2006, **12**, 1533–1539.

[227] Lee, T.K., Poon, R.T.P., Man, K., Guan, X.-Y., et al., 2007. Fascin over-expression is associated with aggressiveness of oral squamous cell carcinoma. Cancer Lett., 2007, **254**, 308–315.

[228] Hu, W., McCrea, P.D., Deavers, M., Kavanagh, J.J., et al., 2000. Increased expression of fascin, motility associated protein, in cell cultures derived from ovarian cancer and in borderline and carcinomatous ovarian tumors. Clin. Exp. Metastasis, 2000, **18**, 83–8.

[229] Condeelis, J., Segall, J.E., 2003. Intravital imaging of cell movement in tumours. Nat. Rev. Cancer, 2003, **3**, 921–30.

[230] Krause, M., Gautreau, A., 2014. Steering cell migration: lamellipodium dynamics and the regulation of directional persistence. Nat. Rev. Mol. Cell Biol., 2014, **15**, 577–590.

[231] Yamaguchi, H., Condeelis, J., 2007. Regulation of the actin cytoskeleton in cancer cell migration and invasion. Biochim. Biophys. Acta - Mol. Cell Res., 2007, **1773**, 642–652.

[232] Caldieri, G., Ayala, I., Attanasio, F., Buccione, R., 2009. Chapter 1 Cell and Molecular Biology of Invadopodia. Int. Rev. Cell Mol. Biol., 2009, **275**, 1–34.

[233] Bompard, G., Caron, E., 2004. Regulation of WASP/WAVE proteins: making a long story short. J. Cell Biol., 2004, **166**, 957–62.

[234] Mizutani, K., Miki, H., He, H., Maruta, H., Takenawa, T., 2002. Essential Role of Neural Wiskott-Aldrich Syndrome Protein in Podosome Formation and Degradation of Extracellular Matrix in src-transformed Fibroblasts. CANCER Res., 2002, **62**, 669–674.

[235] Lorenz, M., Yamaguchi, H., Wang, Y., Singer, R.H., Condeelis, J., 2004. Imaging sites of N-wasp activity in lamellipodia and invadopodia of carcinoma cells. Curr. Biol., 2004, **14**, 697–703.

[236] Yamaguchi, H., Lorenz, M., Kempiak, S., Sarmiento, C., et al., 2005. Molecular mechanisms of invadopodium formation: the role of the N-WASP-Arp2/3 complex pathway and cofilin. J. Cell Biol., 2005, **168**, 441–52.

[237] Nakahara, H., Otani, T., Sasaki, T., Miura, Y., et al., 2003. Involvement of Cdc42 and Rac small G proteins in invadopodia formation of RPMI7951 cells. Genes Cells, 2003, **8**, 1019–27.

[238] Baldassarre, M., Ayala, I., Beznoussenko, G., Giacchetti, G., et al., 2006. Actin dynamics at sites of extracellular matrix degradation. Eur. J. Cell Biol., 2006, **85**, 1217–31.

[239] Chen, Z., Borek, D., Padrick, S.B., Gomez, T.S., et al., 2010. Structure and control of the actin regulatory WAVE complex. Nature, 2010, **468**, 533–8.

[240] Steffen, A., Ladwein, M., Dimchev, G.A., Hein, A., et al., 2013. Rac function is crucial for cell migration but is not required for spreading and focal adhesion formation. J. Cell Sci., 2013, **126**, 4572–88.

[241] Kobayashi, K., Kuroda, S., Fukata, M., Nakamura, T., et al., 1998. p140Sra-1 (specifically Rac1-associated protein) is a novel specific target for Rac1 small GTPase. J. Biol. Chem., 1998, **273**, 291–5.

[242] Lebensohn, A.M., Kirschner, M.W., 2009. Activation of the WAVE complex by coincident signals controls actin assembly. Mol. Cell, 2009, **36**, 512–24.

[243] Stovold, C.F., Millard, T.H., Machesky, L.M., 2005. Inclusion of Scar/WAVE3 in a similar complex to Scar/WAVE1 and 2. BMC Cell Biol., 2005, **6**, 11.

[244] Hirao, N., Sato, S., Gotoh, T., Maruoka, M., et al., 2006. NESH (Abi-3) is present in the Abi/WAVE complex but does not promote c-Abl-mediated phosphorylation. FEBS Lett., 2006, **580**, 6464–70.

[245] Innocenti, M., Zucconi, A., Disanza, A., Frittoli, E., et al., 2004. Abi1 is essential for the formation and activation of a WAVE2 signalling complex. Nat. Cell Biol., 2004, **6**, 319–27.

[246] Eden, S., Rohatgi, R., Podtelejnikov, A. V., Mann, M., Kirschner, M.W., 2002. Mechanism of regulation of WAVE1-induced actin nucleation by Rac1 and Nck. Nature, 2002, **418**, 790–793.

[247] Gautreau, A., Ho, H.H., Li, J., Steen, H., et al., 2004. Purification and architecture of the ubiquitous Wave complex. Proc. Natl. Acad. Sci. U. S. A., 2004, **101**, 4379–83.

[248] Derivery, E., Lombard, B., Loew, D., Gautreau, A., 2009. The Wave complex is intrinsically inactive. Cell Motil. Cytoskeleton, 2009, **66**, 777–90.

[249] Ismail, A.M., Padrick, S.B., Chen, B., Umetani, J., Rosen, M.K., 2009. The WAVE regulatory complex is inhibited. Nat. Struct. Mol. Biol., 2009, **16**, 561–3.

[250] Campa, C.C., Ciraolo, E., Ghigo, A., Germena, G., Hirsch, E., 2015. Crossroads of PI3K and Rac pathways. Small GTPases, 2015, **6**, 71–80.

[251] Leng, Y., Zhang, J., Badour, K., Arpaia, E., et al., 2005. Abelson-interactor-1 promotes WAVE2 membrane translocation and Abelson-mediated tyrosine phosphorylation required for WAVE2 activation. Proc. Natl. Acad. Sci., 2005, **102**, 1098–1103.

[252] Sossey-Alaoui, K., Li, X., Cowell, J.K., 2007. c-Abl-mediated phosphorylation of WAVE3 is required for lamellipodia formation and cell migration. J. Biol. Chem., 2007, **282**, 26257–65.

[253] Stuart, J.R., Gonzalez, F.H., Kawai, H., Yuan, Z.-M., 2006. c-Abl interacts with the WAVE2 signaling complex to induce membrane ruffling and cell spreading. J. Biol. Chem., 2006, **281**, 31290–7.

[254] Chen, B., Brinkmann, K., Chen, Z., Pak, C.W., et al., 2014. The WAVE regulatory complex links diverse receptors to the actin cytoskeleton. Cell, 2014, **156**, 195–207.

[255] Krause, M., Leslie, J.D., Stewart, M., Lafuente, E.M., et al., 2004. Lamellipodin, an Ena/VASP ligand, is implicated in the regulation of lamellipodial dynamics. Dev. Cell, 2004, **7**, 571–83.

[256] Law, A.-L., Vehlow, A., Kotini, M., Dodgson, L., et al., 2013. Lamellipodin and the Scar/WAVE complex cooperate to promote cell migration in vivo. J. Cell Biol., 2013, **203**.

[257] Endris, V., Haussmann, L., Buss, E., Bacon, C., et al., 2011. SrGAP3 interacts with lamellipodin at the cell membrane and regulates Rac-dependent cellular protrusions. J. Cell Sci., 2011, **124**, 3941–55.

[258] Quinn, C.C., Pfeil, D.S., Chen, E., Stovall, E.L., et al., 2006. UNC-6/netrin and SLT-1/slit guidance cues orient axon outgrowth mediated by MIG-10/RIAM/lamellipodin. Curr. Biol., 2006, **16**, 845–53.

[259] Smith, K., Humphreys, D., Hume, P.J., Koronakis, V., 2010. Enteropathogenic Escherichia coli Recruits the Cellular Inositol Phosphatase SHIP2 to Regulate Actin-Pedestal Formation. Cell Host Microbe, 2010, **7**, 13–24.

[260] Humphreys, D., Liu, T., Davidson, A.C., Hume, P.J., Koronakis, V., 2012. The Drosophila Arf1 homologue Arf79F is essential for lamellipodium formation. J. Cell Sci., 2012, **125**, 5630–5.

[261] Boulay, P.-L., Cotton, M., Melançon, P., Claing, A., 2008. ADP-ribosylation factor 1 controls the activation of the phosphatidylinositol 3-kinase pathway to regulate epidermal growth factor-dependent growth and migration of breast cancer cells. J. Biol. Chem., 2008, **283**, 36425–34.

[262] Zhang, J., Neal, J., Lian, G., Hu, J., et al., 2013. Filamin A regulates neuronal migration through brefeldin A-inhibited guanine exchange factor 2-dependent Arf1 activation. J. Neurosci., 2013, **33**, 15735–46.

[263] Hashimoto, S., Onodera, Y., Hashimoto, A., Tanaka, M., et al., 2004. Requirement for Arf6 in breast cancer invasive activities. Proc. Natl. Acad. Sci. U. S. A., 2004, **101**, 6647–52.

[264] Hoover, H., Muralidharan-Chari, V., Tague, S., D'Souza-Schorey, C., 2005. *Methods Enzymol.*, vol. 404, pp. 134–147.

[265] Palacios, F., Price, L., Schweitzer, J., Collard, J.G., D'Souza-Schorey, C., 2001. An essential role for ARF6-regulated membrane traffic in adherens junction turnover and epithelial cell migration. EMBO J., 2001, **20**, 4973–4986.

[266] Santy, L.C., Frank, S.R., Casanova, J.E., 2001. Expression and analysis of ARNO and ARNO mutants and their effects on ADP-ribosylation factor (ARF)-mediated actin cytoskeletal rearrangements. Methods Enzym., 2001, **329**, 256–264.

[267] Tague, S.E., Muralidharan, V., D'Souza-Schorey, C., 2004. ADP-ribosylation factor 6 regulates tumor cell invasion through the activation of the MEK/ERK signaling pathway. Proc. Natl. Acad. Sci., 2004, **101**, 9671–9676.

[268] Humphreys, D., Davidson, A.C., Hume, P.J., Makin, L.E., Koronakis, V., 2013. Arf6 coordinates actin assembly through the WAVE complex, a mechanism usurped by Salmonella to invade host cells. Proc. Natl. Acad. Sci., 2013, **110**, 16880–16885.

[269] Ridley, A.J., 2011. Life at the leading edge. Cell, 2011, **145**, 1012–22.

[270] Campellone, K.G., Welch, M.D., 2010. A nucleator arms race: cellular control of actin assembly. Nat. Rev. Mol. Cell Biol., 2010, **11**, 237–51.

[271] Bear, J.E., Svitkina, T.M., Krause, M., Schafer, D.A., et al., 2002. Antagonism between Ena/VASP proteins and actin filament capping regulates fibroblast motility. Cell, 2002, **109**, 509–21.

[272] Barzik, M., Kotova, T.I., Higgs, H.N., Hazelwood, L., et al., 2005. Ena/VASP proteins enhance actin polymerization in the presence of barbed end capping proteins. J. Biol. Chem., 2005, **280**, 28653–62.

[273] Pasic, L., Kotova, T., Schafer, D.A., 2008. Ena/VASP proteins capture actin filament barbed ends. J. Biol. Chem., 2008, **283**, 9814–9.

[274] Breitsprecher, D., Kiesewetter, A.K., Linkner, J., Vinzenz, M., et al., 2011. Molecular mechanism of Ena/VASP-mediated actin-filament elongation. EMBO J., 2011, **30**, 456–67.

[275] Breitsprecher, D., Kiesewetter, A.K., Linkner, J., Urbanke, C., et al., 2008. Clustering of VASP actively drives processive, WH2 domain-mediated actin filament elongation. EMBO J., 2008, **27**, 2943–54.

[276] Hansen, S.D., Mullins, R.D., 2010. VASP is a processive actin polymerase that requires monomeric actin for barbed end association. J. Cell Biol., 2010, **191**, 571–84.

[277] Block, J., Breitsprecher, D., Kühn, S., Winterhoff, M., et al., 2012. FMNL2 drives actin-based protrusion and migration downstream of Cdc42. Curr. Biol., 2012, **22**, 1005–12.

[278] Pellegrin, S., Mellor, H., 2005. The Rho Family GTPase Rif Induces Filopodia through mDia2. Curr. Biol., 2005, **15**, 129–133.

[279] Schirenbeck, A., Bretschneider, T., Arasada, R., Schleicher, M., Faix, J., 2005. The Diaphanous-related formin dDia2 is required for the formation and maintenance of filopodia. Nat. Cell Biol., 2005, **7**, 619–25.

[280] Lebrand, C., Dent, E.W., Strasser, G.A., Lanier, L.M., et al., 2004. Critical role of Ena/VASP proteins for filopodia formation in neurons and in function downstream of netrin-1. Neuron, 2004, **42**, 37–49.

[281] Yang, C., Czech, L., Gerboth, S., Kojima, S., et al., 2007. Novel roles of formin mDia2 in lamellipodia and filopodia formation in motile cells. PLoS Biol., 2007, **5**, e317.

[282] Rottner, K., Behrendt, B., Small, J. V, Wehland, J., 1999. VASP dynamics during lamellipodia protrusion. Nat. Cell Biol., 1999, **1**, 321–2.

[283] Reinhard, M., Halbrugge, M., Scheer1, U., Wiegand2, C., et al., 1992. The 46/50 kDa phosphoprotein VASP purified from human platelets is a novel protein associated with actin filaments and focal contacts. EMBO J., 1992, **1**, 2063–2070.

[284] Gertler, F.B., Niebuhr, K., Reinhard, M., Wehland, J., Soriano, P., 1996. Mena, a relative of VASP and Drosophila Enabled, is implicated in the control of microfilament dynamics. Cell, 1996, **87**, 227–39.

[285] Di Modugno, F., Mottolese, M., Di Benedetto, A., Conidi, A., et al., 2006. The Cytoskeleton Regulatory Protein hMena (ENAH) Is Overexpressed in Human Benign Breast Lesions with High Risk of Transformation and Human Epidermal Growth Factor Receptor-2-Positive/Hormonal Receptor-Negative Tumors. Clin. Cancer Res., 2006, **12**, 1470–1478.

[286] Di Modugno, F., DeMonte, L., Balsamo, M., Bronzi, G., et al., 2007. Molecular cloning of hMena (ENAH) and its splice variant hMena+11a: epidermal growth factor increases their expression and stimulates hMena+ 11a phosphorylation in breast cancer cell lines. Cancer Res., 2007, **67**, 2657–2665.

[287] Astolfi, A., Landuzzi, L., Nicoletti, G., De Giovanni, C., et al., 2005. Gene Expression Analysis of Immune-Mediated Arrest of Tumorigenesis in a Transgenic Mouse Model of HER-2/neu-Positive Basal-Like Mammary Carcinoma. Am. J. Pathol., 2005, **166**, 1205–1216.

[288] Wang, W., Goswami, S., Lapidus, K., Wells, A.L., et al., 2004. Identification and Testing of a Gene Expression Signature of Invasive Carcinoma Cells within Primary Mammary Tumors. Cancer Res., 2004, **64**, 8585–8594.

[289] Skoble, J., Auerbuch, V., Goley, E.D., Welch, M.D., Portnoy, D.A., 2001. Pivotal role of VASP in Arp2/3 complex–mediated actin nucleation, actin branch-formation, and Listeria monocytogenes motility. J. Cell Biol., 2001, **108912**, 21–9525.

[290] Goley, E.D., Welch, M.D., 2006. The ARP2/3 complex: an actin nucleator comes of age. Nat. Rev. Mol. Cell Biol., 2006, **7**, 713–26.

[291] Baldassarre, M., Pompeo, A., Beznoussenko, G., Castaldi, C., et al., 2003. Dynamin participates in focal extracellular matrix degradation by invasive cells. Mol. Biol. Cell, 2003, **14**, 1074–84.

[292] Otsubo, T., Iwaya, K., Mukai, Y., Mizokami, Y., et al., 2004. Involvement of Arp2/3 complex in the process of colorectal carcinogenesis. Mod. Pathol., 2004, **17**, 461–467.

[293] Semba, S., Iwaya, K., Matsubayashi, J., Serizawa, H., et al., 2006. Coexpression of Actin-Related Protein 2 and Wiskott-Aldrich Syndrome Family Verproline-Homologous Protein 2 in Adenocarcinoma of the Lung. Clin. Cancer Res., 2006, **12**, 2449–2454.

[294] Yanagawa, R., Furukawa, Y., Tsunoda, T., Kitahara, O., et al., 2001. Genome-wide screening of genes showing altered expression in liver metastases of human colorectal cancers by cDNA microarray. Neoplasia, 2001, **3**, 395–401.

[295] Kurisu, S., Suetsugu, S., Yamazaki, D., Yamaguchi, H., Takenawa, T., 2005. Rac-WAVE2 signaling is involved in the invasive and metastatic phenotypes of murine melanoma cells. Oncogene, 2005, **24**, 1309–1319.

[296] Ichetovkin, I., Grant, W., Condeelis, J., 2002. Cofilin produces newly polymerized actin filaments that are preferred for dendritic nucleation by the Arp2/3 complex. Curr. Biol., 2002, **12**, 79–84.

[297] Chen, Q., Pollard, T.D., 2013. Actin filament severing by cofilin dismantles actin patches and produces mother filaments for new patches. Curr. Biol., 2013, **23**, 1154–62.

[298] Wagner, A.R., Luan, Q., Liu, S.-L., Nolen, B.J., 2013. Dip1 Defines a Class of Arp2/3 Complex Activators that Function without Preformed Actin Filaments. Curr. Biol., 2013, **23**, 1990–1998.

[299] Liu, S.L., Needham, K.M., May, J.R., Nolen, B.J., 2011. Mechanism of a concentration-dependent switch between activation and inhibition of Arp2/3 complex by coronin. J Biol Chem, 2011, **286**, 17039–17046.

[300] Humphries, C.L., Balcer, H.I., D'Agostino, J.L., Winsor, B., et al., 2002. Direct regulation of Arp2/3 complex activity and function by the actin binding protein coronin. J. Cell Biol., 2002, **159**, 993–1004.

[301] Cai, L., Makhov, A.M., Schafer, D.A., Bear, J.E., 2008. Coronin 1B antagonizes cortactin and remodels Arp2/3-containing actin branches in lamellipodia. Cell, 2008, **134**, 828–42.

[302] Cai, L., Holoweckyj, N., Schaller, M.D., Bear, J.E., 2005. Phosphorylation of Coronin 1B by Protein Kinase C Regulates Interaction with Arp2/3 and Cell Motility. J. Biol. Chem., 2005, **280**, 31913–31923.

[303] Williams, H.C., 2012. Role of coronin 1B in PDGFinduced migration of vascular smooth muscle cells. Circ. Res., 2012, **111**, 56–65.

[304] Rocca, D.L., Martin, S., Jenkins, E.L., Hanley, J.G., 2008. Inhibition of Arp2/3-mediated actin polymerization by PICK1 regulates neuronal morphology and AMPA receptor endocytosis. Nat. Cell Biol., 2008, **10**, 259–271.

[305] Maritzen, T., Zech, T., Schmidt, M.R., Krause, E., et al., 2012. Gadkin negatively regulates cell spreading and motility via sequestration of the actin-nucleating ARP2/3 complex. Proc. Natl. Acad. Sci., 2012, **109**, 10382–10387.

[306] Dang, I., Gorelik, R., Sousa-Blin, C., Derivery, E., et al., 2013. Inhibitory signalling to the Arp2/3 complex steers cell migration. Nature, 2013, **503**, 281–4.

[307] Law, A.-L., Vehlow, A., Kotini, M., Dodgson, L., et al., 2013. Lamellipodin and the Scar/WAVE complex cooperate to promote cell migration in vivo. J. Cell Biol., 2013, **203**, 673–89.

[308] Michael, M., Vehlow, A., Navarro, C., Krause, M., 2010. c-Abl, Lamellipodin, and Ena/VASP Proteins Cooperate in Dorsal Ruffling of Fibroblasts and Axonal Morphogenesis. Curr. Biol., 2010, **20**, 783–791.

[309] Bamburg, J.R., 1999. Proteins of the ADF/cofilin family: essential regulators of actin dynamics. Annu. Rev. Cell Dev. Biol., 1999, **15**, 185–230.
[310] Okano, I., Hiraoka, J., Otera, H., Nunoue, K., et al., 1995. Identification and characterization of a novel family of serine/threonine kinases containing two N-terminal LIM motifs. J. Biol. Chem., 1995, **270**, 31321–30.
[311] Yang, N., Higuchi, O., Ohashi, K., Nagata, K., et al., 1998. Cofilin phosphorylation by LIM-kinase 1 and its role in Rac-mediated actin reorganization. Nature, 1998, **393**, 809–12.
[312] Toshima, J., Toshima, J.Y., Amano, T., Yang, N., et al., 2001. Cofilin phosphorylation by protein kinase testicular protein kinase 1 and its role in integrin-mediated actin reorganization and focal adhesion formation. Mol. Biol. Cell, 2001, **12**, 1131–45.
[313] Mizuno, K., Okano, I., Ohashi, K., Nunoue, K., et al., 1994. Identification of a human cDNA encoding a novel protein kinase with two repeats of the LIM/double zinc finger motif. Oncogene, 1994, **9**, 1605–12.
[314] Yonezawa, N., Homma, Y., Yahara, I., Sakai, H., Nishida, E., 1991. A short sequence responsible for both phosphoinositide binding and actin binding activities of cofilin. J. Biol. Chem., 1991, **266**, 17218–21.
[315] Yonezawa, N., Nishida, E., Iida, K., Yahara, I., Sakai, H., 1990. Inhibition of the interactions of cofilin, destrin, and deoxyribonuclease I with actin by phosphoinositides. J. Biol. Chem., 1990, **265**, 8382–6.
[316] Mouneimne, G., Soon, L., DesMarais, V., Sidani, M., et al., 2004. Phospholipase C and cofilin are required for carcinoma cell directionality in response to EGF stimulation. J. Cell Biol., 2004, **166**, 697–708.
[317] Niwa, R., Nagata-Ohashi, K., Takeichi, M., Mizuno, K., Uemura, T., 2002. Control of actin reorganization by Slingshot, a family of phosphatases that dephosphorylate ADF/cofilin. Cell, 2002, **108**, 233–46.
[318] Meberg, P.J., Ono, S., Minamide, L.S., Takahashi, M., Bamburg, J.R., 1998. Actin depolymerizing factor and cofilin phosphorylation dynamics: Response to signals that regulate neurite extension. Cell Motil. Cytoskeleton, 1998, **39**, 172–190.
[319] Ambach, A., Saunus, J., Konstandin, M., Wesselborg, S., et al., 2000. The serine phosphatases PP1 and PP2A associate with and activate the actin-binding protein cofilin in human T lymphocytes. Eur. J. Immunol., 2000, **30**, 3422–31.
[320] Gohla, A., Birkenfeld, J., Bokoch, G.M., 2005. Chronophin, a novel HAD-type serine protein phosphatase, regulates cofilin-dependent actin dynamics. Nat. Cell Biol., 2005, **7**, 21–29.
[321] Ghosh, M., Song, X., Mouneimne, G., Sidani, M., et al., 2004. Cofilin promotes actin polymerization and defines the direction of cell motility. Science, 2004, **304**, 743–6.
[322] Hotulainen, P., Paunola, E., Vartiainen, M.K., Lappalainen, P., 2005. Actin-depolymerizing factor and cofilin-1 play overlapping roles in promoting rapid F-actin depolymerization in mammalian nonmuscle cells. Mol. Biol. Cell, 2005, **16**, 649–64.
[323] Zebda, N., Bernard, O., Bailly, M., Welti, S., et al., 2000. Phosphorylation of ADF/cofilin abolishes EGF-induced actin nucleation at the leading edge and subsequent lamellipod extension. J Cell Biol , 151 pp. 1119-1128. , 2000.
[324] Weaver, A.M., Karginov, A. V, Kinley, A.W., Weed, S.A., et al., 2001. Cortactin promotes and stabilizes Arp2/3-induced actin filament network formation. Curr. Biol., 2001, **11**, 370–4.
[325] Bowden, E.T., Barth, M., Thomas, D., Glazer, R.I., Mueller, S.C., 1999. An invasion-related complex of cortactin, paxillin and PKCμ associates with invadopodia at sites of extracellular matrix degradation. Oncogene, 1999, **18**, 4440–4449.
[326] Bryce, N.S., Clark, E.S., Leysath, J.L., Currie, J.D., et al., 2005. Cortactin promotes cell motility by enhancing lamellipodial persistence. Curr. Biol., 2005, **15**, 1276–1285.
[327] Kempiak, S.J., Yamaguchi, H., Sarmiento, C., Sidani, M., et al., 2004. An N-WASP mediated pathway for localized activation of actin polymerization which is regulated by cortactin. J Biol Chem, 2004.
[328] Uruno, T., Liu, J., Zhang, P., Fan Yx, Y., et al., 2001. Activation of Arp2/3 complex-mediated actin polymerization by cortactin. Nat. Cell Biol., 2001, **3**, 259–66.
[329] Schuuring, E., 1995. The involvement of the chromosome 11q13 region in human malignancies: cyclin D1 and EMS1 are two new candidate oncogenes--a review. Gene, 1995, **159**, 83–96.
[330] Bringuier, P.P., Tamimi, Y., Schuuring, E., Schalken, J., 1996. Expression of cyclin D1 and EMS1 in bladder tumours; relationship with chromosome 11q13 amplification. Oncogene, 1996, **12**, 1747–53.
[331] Daly, R., 2004. Cortactin signalling and dynamic actin networks. Biochem J, 2004, **382**, 13–25.
[332] Brandman, O., Meyer, T., 2008. Feedback loops shape cellular signals in space and time. Science, 2008, **322**, 390–5.
[333] Danuser, G., Allard, J., Mogilner, A., 2013. Mathematical modeling of eukaryotic cell migration: insights beyond experiments. Annu. Rev. Cell Dev. Biol., 2013, **29**, 501–28.
[334] Castro-Castro, A., Ojeda, V., Barreira, M., Sauzeau, V., et al., 2011. Coronin 1A promotes a cytoskeletal-based feedback loop that facilitates Rac1 translocation and activation. EMBO J., 2011, **30**, 3913–27.
[335] Liang, Y., Niederstrasser, H., Edwards, M., Jackson, C.E., Cooper, J.A., 2009. Distinct roles for CARMIL isoforms in cell migration. Mol. Biol. Cell, 2009, **20**, 5290–305.
[336] Fujiwara, I., Remmert, K., Hammer, J.A., 2010. Direct Observation of the Uncapping of Capping Protein-capped Actin Filaments by CARMIL Homology Domain 3. J. Biol. Chem., 2010, **285**, 2707–2720.
[337] Lai, F.P.L., Szczodrak, M., Oelkers, J.M., Ladwein, M., et al., 2009. Cortactin promotes migration and platelet-derived growth factor-induced actin reorganization by signaling to Rho-GTPases. Mol. Biol. Cell, 2009, **20**, 3209–23.
[338] Garcia Arguinzonis, M.I., Galler, A.B., Walter, U., Reinhard, M., Simm, A., 2002. Increased spreading, Rac/ p21-activated kinase (PAK) activity, and compromised cell motility in cells deficient in vasodilator-stimulated phosphoprotein (VASP). J Biol Chem, 2002, **277**, 45604–45610.
[339] Weiner, O.D., Neilsen, P.O., Prestwich, G.D., Kirschner, M.W., et al., 2002. A PtdInsP3- and Rho GTPase-mediated positive feedback loop regulates neutrophil polarity. Nat. Cell Biol., 2002, **4**, 509–513.
[340] Pankov, R., Endo, Y., Even-Ram, S., Araki, M., et al., 2005. A Rac switch regulates random versus directionally persistent cell migration. J. Cell Biol., 2005, **170**, 793–802.
[341] Soderling, S.H., Binns, K.L., Wayman, G.A., Davee, S.M., et al., 2002. The WRP component of the WAVE-1 complex attenuates Rac-mediated signalling. Nat. Cell Biol., 2002, **4**, 970–5.
[342] Linder, S., 2007. The matrix corroded: podosomes and invadopodia in extracellular matrix degradation. Trends Cell Biol., 2007, **17**, 107–117.
[343] Chen, W.T., Kelly, T., 2003. Seprase complexes in cellular invasiveness. Cancer Metastasis Rev., 2003, **22**, 259–269.
[344] Ghersi, G., Dong, H., Goldstein, L.A., Yeh, Y., et al., 2002. Regulation of fibroblast migration on collagenous matrix by a cell surface peptidase complex. J. Biol. Chem., 2002, **277**, 29231–41.
[345] Seals, D.F., Courtneidge, S.A., 2003. The ADAMs family of metalloproteases: multidomain proteins with multiple functions. Genes Dev., 2003, **17**, 7–30.
[346] Artym, V.V., Zhang, Y., Seillier-Moiseiwitsch, F., Yamada, K.M., Mueller, S.C., 2006. Dynamic interactions of cortactin and membrane type 1 matrix metalloproteinase at invadopodia: defining the stages of invadopodia formation and function. Cancer Res., 2006, **66**, 3034–3043.
[347] Gimona, M., Buccione, R., 2006. Adhesions that mediate invasion. Int. J. Biochem. Cell Biol., 2006, **38**, 1875–1892.
[348] Fujiwara, T., Oda, K., Yokota, S., Takatsuki, A., Ikehara, Y., 1988. Brefeldin A causes disassembly of the Golgi complex and accumulation of secretory proteins in the endoplasmic reticulum. J. Biol. Chem., 1988, **263**, 18545–18552.
[349] Caldieri, G., Giacchetti, G., Beznoussenko, G., Attanasio, F., et al., 2009. Invadopodia biogenesis is regulated by caveolin-mediated modulation of membrane cholesterol levels. J. Cell. Mol. Med. In Press. J. Cell. Mol. Med. Press, 2009.
[350] Sakurai-Yageta, M., Recchi, C., Le Dez, G., Sibarita, J.-B., et al., 2008. The interaction of IQGAP1 with the exocyst complex is required for tumor

cell invasion downstream of Cdc42 and RhoA. J. Cell Biol., 2008, **181**, 985–998.
[351] Hsu, S.-C., TerBush, D., Abraham, M., Guo, W., 2004. The exocyst complex in polarized exocytosis. Int. Rev. Cytol., 2004, **233**, 243–65.
[352] Steffen, A., Le Dez, G., Poincloux, R., Recchi, C., et al., 2008. MT1-MMP-dependent invasion is regulated by TI-VAMP/VAMP7. Curr. Biol., 2008, **18**, 926–31.
[353] Bustelo, X.R., Sauzeau, V., Berenjeno, I.M., 2007. GTP-binding proteins of the Rho/Rac family: regulation, effectors and functions in vivo. Bioessays, 2007, **29**, 356–70.
[354] Raftopoulou, M., Hall, A., 2004. Cell migration: Rho GTPases lead the way. Dev. Biol., 2004, **265**, 23–32.
[355] Nobes, C.D., Hall, A., 1995. Rho, rac, and cdc42 GTPases regulate the assembly of multimolecular focal complexes associated with actin stress fibers, lamellipodia, and filopodia. Cell, 1995, **81**, 53–62.
[356] Ridley, A.J., Hall, A., 1992. The small GTP-binding protein rho regulates the assembly of focal adhesions and actin stress fibers in response to growth factors. Cell, 1992, **70**, 389–99.
[357] Ridley, A.J., Paterson, H.F., Johnston, C.L., Diekmann, D., Hall, A., 1992. The small GTP-binding protein rac regulates growth factor-induced membrane ruffling. Cell, 1992, **70**, 401–10.
[358] Orgaz, J.L., Herraiz, C., Sanz-Moreno, V., 2014. Rho GTPases modulate malignant transformation of tumor cells. Small GTPases, 2014, **5**, e29019.
[359] Sadok, A., Marshall, C.J., 2014. Rho GTPases: Masters of cell migration. Small GTPases, 2014, **5**, e983878.
[360] Jaffe, A.B., Hall, A., 2005. RHO GTPASES: Biochemistry and Biology. Annu. Rev. Cell Dev. Biol., 2005, **21**, 247–269.
[361] Schaefer, A., Reinhard, N.R., Hordijk, P.L., 2014. Toward understanding RhoGTPase speci fi city : structure , function and local activation. Small GTPases, 2014, **5**, 1–11.
[362] Hodge, R.G., Ridley, A.J., 2016. Regulating Rho GTPases and their regulators. Nat. Rev. Mol. Cell Biol., 2016, **17**, 496–510.
[363] Wennerberg, K., Rossman, K.L., Der, C.J., 2005. The Ras superfamily at a glance. J. Cell Sci., 2005, **118**, 843–6.
[364] Wittinghofer, A., Vetter, I.R., 2011. Structure-function relationships of the G domain, a canonical switch motif. Annu. Rev. Biochem., 2011, **80**, 943–71.
[365] Vetter, I.R., Wittinghofer, A., 2001. The guanine nucleotide-binding switch in three dimensions. Science, 2001, **294**, 1299–304.
[366] Lenzen, C., Cool, R.H., Prinz, H., Kuhlmann, J., Wittinghofer, A., 1998. Kinetic analysis by fluorescence of the interaction between Ras and the catalytic domain of the guanine nucleotide exchange factor Cdc25Mm. Biochemistry, 1998, **37**, 7420–30.
[367] Bos, J., Rehmann, H., Wittinghofer, A., 2007. GEFs and GAPs : Critical Elements in the Control of Small G Proteins. Cell, 2007, 865–877.
[368] Cherfils, J., Zeghouf, M., 2013. Regulation of small GTPases by GEFs, GAPs, and GDIs. Physiol. Rev., 2013, **93**, 269–309.
[369] Moon, S.Y., Zheng, Y., 2003. Rho GTPase-activating proteins in cell regulation. Trends Cell Biol., 2003, **13**, 13–22.
[370] DerMardirossian, C., Bokoch, G.M., 2005. GDIs: Central regulatory molecules in Rho GTPase activation. Trends Cell Biol., 2005, **15**, 356–363.
[371] Molnár, G., Dagher, M.C., Geiszt, M., Settleman, J., Ligeti, E., 2001. Role of prenylation in the interaction of Rho-family small GTPases with GTPase activating proteins. Biochemistry, 2001, **40**, 10542–9.
[372] Garcia-Mata, R., Boulter, E., Burridge, K., 2011. The "invisible hand": regulation of RHO GTPases by RHOGDIs. Nat. Rev. Mol. Cell Biol., 2011, **12**, 493–504.
[373] Katayama, M., Kawata, M., Yoshida, Y., Horiuchi, H., et al., 1991. The posttranslationally modified C-terminal structure of bovine aortic smooth muscle rhoA p21. J. Biol. Chem., 1991, **266**, 12639–45.
[374] Adamson, P., Marshall, C.J., Hall, A., Tilbrook, P.A., 1992. Post-translational modifications of p21rho proteins. J. Biol. Chem., 1992, **267**, 20033–8.
[375] Michaelson, D., Silletti, J., Murphy, G., D'Eustachio, P., et al., 2001. Differential localization of Rho GTPases in live cells: regulation by hypervariable regions and RhoGDI binding. J. Cell Biol., 2001, **152**, 111–26.
[376] Wang, D.-A., Sebti, S.M., 2005. Palmitoylated cysteine 192 is required for RhoB tumor-suppressive and apoptotic activities. J. Biol. Chem., 2005, **280**, 19243–9.
[377] Pérez-Sala, D., Boya, P., Ramos, I., Herrera, M., Stamatakis, K., 2009. The C-Terminal Sequence of RhoB Directs Protein Degradation through an Endo-Lysosomal Pathway. PLoS One, 2009, **4**, e8117.
[378] Berzat, A.C., Buss, J.E., Chenette, E.J., Weinbaum, C.A., et al., 2005. Transforming Activity of the Rho Family GTPase, Wrch-1, a Wnt-regulated Cdc42 Homolog, Is Dependent on a Novel Carboxyl-terminal Palmitoylation Motif. J. Biol. Chem., 2005, **280**, 33055–33065.
[379] Chenette, E.J., Mitin, N.Y., Der, C.J., 2006. Multiple sequence elements facilitate Chp Rho GTPase subcellular location, membrane association, and transforming activity. Mol. Biol. Cell, 2006, **17**, 3108–21.
[380] Navarro-Lérida, I., Sánchez-Perales, S., Calvo, M., Rentero, C., et al., 2012. A palmitoylation switch mechanism regulates Rac1 function and membrane organization. EMBO J., 2012, **31**, 534–51.
[381] Hornbeck, P. V, Zhang, B., Murray, B., Kornhauser, J.M., et al., 2015. PhosphoSitePlus, 2014: mutations, PTMs and recalibrations. Nucleic Acids Res., 2015, **43**, D512-20.
[382] Castillo-Lluva, S., Tatham, M.H., Jones, R.C., Jaffray, E.G., et al., 2010. SUMOylation of the GTPase Rac1 is required for optimal cell migration. Nat. Cell Biol., 2010, **12**, 1078–1085.
[383] Kamai, T., Yamanishi, T., Shirataki, H., Takagi, K., et al., 2004. Overexpression of RhoA, Rac1, and Cdc42 GTPases Is Associated with Progression in Testicular Cancer. Clin. Cancer Res., 2004, **10**.
[384] Fritz, G., Brachetti, C., Bahlmann, F., Schmidt, M., Kaina, B., 2002. Rho GTPases in human breast tumours: expression and mutation analyses and correlation with clinical parameters. Br. J. Cancer, 2002, **87**, 635–644.
[385] Engers, R., Ziegler, S., Mueller, M., Walter, A., et al., 2007. Prognostic relevance of increased Rac GTPase expression in prostate carcinomas. Endocr. Relat. Cancer, 2007, **14**, 245–56.
[386] Ji, J., Feng, X., Shi, M., Cai, Q., et al., 2015. Rac1 is correlated with aggressiveness and a potential therapeutic target for gastric cancer. Int. J. Oncol., 2015, **46**, 1343–53.
[387] Pan, Y., Bi, F., Liu, N., Xue, Y., et al., 2004. Expression of seven main Rho family members in gastric carcinoma. Biochem. Biophys. Res. Commun., 2004, **315**, 686–691.
[388] Schnelzer, A., Prechtel, D., Knaus, U., Dehne, K., et al., 2000. Rac1 in human breast cancer: overexpression, mutation analysis, and characterization of a new isoform, Rac1b. Oncogene, 2000, **19**, 3013–3020.
[389] Matos, P., Collard, J.G., Jordan, P., 2003. Tumor-related alternatively spliced Rac1b is not regulated by Rho-GDP dissociation inhibitors and exhibits selective downstream signaling. J. Biol. Chem., 2003, **278**, 50442–8.
[390] Zhou, C., Licciulli, S., Avila, J.L., Cho, M., et al., 2013. The Rac1 splice form Rac1b promotes K-ras-induced lung tumorigenesis. Oncogene, 2013, **32**, 903–909.
[391] Hodis, E., Watson, I.R., Kryukov, G. V, Arold, S.T., et al., 2012. A landscape of driver mutations in melanoma. Cell, 2012, **150**, 251–63.
[392] Krauthammer, M., Kong, Y., Ha, B.H., Evans, P., et al., 2012. Exome sequencing identifies recurrent somatic RAC1 mutations in melanoma. Nat. Genet., 2012, **44**, 1006–1014.
[393] Davis, M.J., Ha, B.H., Holman, E.C., Halaban, R., et al., 2013. RAC1P29S is a spontaneously activating cancer-associated GTPase. Proc. Natl. Acad. Sci. U. S. A., 2013, **110**, 912–7.
[394] Kawazu, M., Ueno, T., Kontani, K., Ogita, Y., et al., 2013. Transforming mutations of RAC guanosine triphosphatases in human cancers. Proc. Natl. Acad. Sci. U. S. A., 2013, **110**, 3029–34.
[395] Vigil, D., Cherfils, J., Rossman, K.L., Der, C.J., 2010. Ras superfamily GEFs and GAPs: validated and tractable targets for cancer therapy? Nat.

Rev. Cancer, 2010, **10**, 842–857.
[396] Barrio-Real, L., Kazanietz, M.G., 2012. Rho GEFs and Cancer: Linking Gene Expression and Metastatic Dissemination. Sci. Signal., 2012, **5**.
[397] Cook, D.R., Rossman, K.L., Der, C.J., 2014. Rho guanine nucleotide exchange factors: regulators of Rho GTPase activity in development and disease. Oncogene, 2014, **33**, 4021–4035.
[398] Porter, A.P., Papaioannou, A., Malliri, A., 2016. Deregulation of Rho GTPases in cancer. Small GTPases, 2016, **1248**, 1–16.
[399] Welch, H.C.E., Coadwell, W.J., Stephens, L.R., Hawkins, P.T., 2003. Phosphoinositide 3-kinase-dependent activation of Rac. FEBS Lett., 2003, **546**, 93–97.
[400] Ziemba, B.P., Pilling, C., Calleja, V., Larijani, B., Falke, J.J., 2013. The PH Domain of Phosphoinositide-Dependent Kinase-1 Exhibits a Novel, Phospho-Regulated Monomer–Dimer Equilibrium with Important Implications for Kinase Domain Activation: Single-Molecule and Ensemble Studies. Biochemistry, 2013, **52**, 4820–4829.
[401] Rossman, K.L., Der, C.J., Sondek, J., 2005. GEF means go: turning on RHO GTPases with guanine nucleotide-exchange factors. Nat. Rev. Mol. Cell Biol., 2005, **6**, 167–80.
[402] Meller, N., Irani-Tehrani, M., Ratnikov, B.I., Paschal, B.M., Schwartz, M.A., 2004. The novel Cdc42 guanine nucleotide exchange factor, zizimin1, dimerizes via the Cdc42-binding CZH2 domain. J. Biol. Chem., 2004, **279**, 37470–6.
[403] Meller, N., Merlot, S., Guda, C., 2005. CZH proteins: a new family of Rho-GEFs. J. Cell Sci., 2005, **118**, 4937–46.
[404] Brugnera, E., Haney, L., Grimsley, C., Lu, M., et al., 2002. Unconventional Rac-GEF activity is mediated through the Dock180-ELMO complex. Nat. Cell Biol., 2002, **4**, 574–82.
[405] Fields, A.P., Justilien, V., 2010. The guanine nucleotide exchange factor (GEF) Ect2 is an oncogene in human cancer. Adv. Enzyme Regul., 2010, **50**, 190–200.
[406] Wu, D., Asiedu, M., Wei, Q., 2009. Myosin-interacting guanine exchange factor (MyoGEF) regulates the invasion activity of MDA-MB-231 breast cancer cells through activation of RhoA and RhoC. Oncogene, 2009, **28**, 2219–2230.
[407] Ahn, S.-J., Chung, K.-W., Lee, R.-A., Park, I.-A., et al., 2003. Overexpression of betaPix-a in human breast cancer tissues. Cancer Lett., 2003, **193**, 99–107.
[408] Hornstein, I., Pikarsky, E., Groysman, M., Amir, G., et al., 2003. The haematopoietic specific signal transducer Vav1 is expressed in a subset of human neuroblastomas. J. Pathol., 2003, **199**, 526–533.
[409] Adam, L., Martin, T.A., Mansel, R.E., Jiang, W.G., et al., 2001. Tiam1 Overexpression Potentiates Heregulin-induced Lymphoid Enhancer Factor-1/beta -Catenin Nuclear Signaling in Breast Cancer Cells by Modulating the Intercellular Stability. J. Biol. Chem., 2001, **276**, 28443–28450.
[410] Qin, J., Xie, Y., Wang, B., Hoshino, M., et al., 2009. Upregulation of PIP3-dependent Rac exchanger 1 (P-Rex1) promotes prostate cancer metastasis. Oncogene, 2009, **28**, 1853–1863.
[411] Berger, M.F., Hodis, E., Heffernan, T.P., Deribe, Y.L., et al., 2012. Melanoma genome sequencing reveals frequent PREX2 mutations. Nature, 2012, **485**, 502–6.
[412] Adam, L., Vadlamudi, R.K., McCrea, P., Kumar, R., 2001. Tiam1 overexpression potentiates heregulin-induced lymphoid enhancer factor-1/beta -catenin nuclear signaling in breast cancer cells by modulating the intercellular stability. J. Biol. Chem., 2001, **276**, 28443–50.
[413] Zhong, D., Li, Y., Peng, Q., Zhou, J., et al., 2009. Expression of Tiam1 and VEGF-C correlates with lymphangiogenesis in human colorectal carcinoma. Cancer Biol. Ther., 2009, **8**, 689–695.
[414] Vaughan, L., Tan, C.-T., Chapman, A., Nonaka, D., et al., 2015. HUWE1 Ubiquitylates and Degrades the RAC Activator TIAM1 Promoting Cell-Cell Adhesion Disassembly, Migration, and Invasion. Cell Rep., 2015, **10**, 88–102.
[415] Malliri, A., van der Kammen, R.A., Clark, K., van der Valk, M., et al., 2002. Mice deficient in the Rac activator Tiam1 are resistant to Ras-induced skin tumours. Nature, 2002, **417**, 867–871.
[416] Malliri, A., Rygiel, T.P., van der Kammen, R.A., Song, J.-Y., et al., 2006. The rac activator Tiam1 is a Wnt-responsive gene that modifies intestinal tumor development. J. Biol. Chem., 2006, **281**, 543–8.
[417] Lindsay, C.R., Lawn, S., Campbell, A.D., Faller, W.J., et al., 2011. P-Rex1 is required for efficient melanoblast migration and melanoma metastasis. Nat. Commun., 2011, **2**, 555.
[418] Lissanu Deribe, Y., Shi, Y., Rai, K., Nezi, L., et al., 2016. Truncating PREX2 mutations activate its GEF activity and alter gene expression regulation in NRAS-mutant melanoma. Proc. Natl. Acad. Sci. U. S. A., 2016, **113**, E1296-305.
[419] Kawasaki, Y., Tsuji, S., Muroya, K., Furukawa, S., et al., 2009. The adenomatous polyposis coli-associated exchange factors Asef and Asef2 are required for adenoma formation in ApcMin/+mice. EMBO Rep., 2009, **10**, 1355–1362.
[420] Chang, K.H., Sanchez-Aguilera, A., Shen, S., Sengupta, A., et al., 2012. Vav3 collaborates with p190-BCR-ABL in lymphoid progenitor leukemogenesis, proliferation, and survival. Blood, 2012, **120**.
[421] Menacho-Márquez, M., García-Escudero, R., Ojeda, V., Abad, A., et al., 2013. The Rho Exchange Factors Vav2 and Vav3 Favor Skin Tumor Initiation and Promotion by Engaging Extracellular Signaling Loops. PLoS Biol., 2013, **11**, e1001615.
[422] Rossman, K.L., Worthylake, D.K., Snyder, J.T., Siderovski, D.P., et al., 2002. A crystallographic view of interactions between Dbs and Cdc42: PH domain-assisted guanine nucleotide exchange. EMBO J., 2002, **21**, 1315–26.
[423] Rossman, K.L., Cheng, L., Mahon, G.M., Rojas, R.J., et al., 2003. Multifunctional Roles for the PH Domain of Dbs in Regulating Rho GTPase Activation. J. Biol. Chem., 2003, **278**, 18393–18400.
[424] Ferguson, K.M., Lemmon, M.A., Schlessinger, J., Sigler, P.B., 1995. Structure of the high affinity complex of inositol trisphosphate with a phospholipase C pleckstrin homology domain. Cell, 1995, **83**, 1037–46.
[425] Snyder, J.T., Rossman, K.L., Baumeister, M.A., Pruitt, W.M., et al., 2001. Quantitative analysis of the effect of phosphoinositide interactions on the function of Dbl family proteins. J. Biol. Chem., 2001, **276**, 45868–75.
[426] Chen, R.H., Corbalan-Garcia, S., Bar-Sagi, D., 1997. The role of the PH domain in the signal-dependent membrane targeting of Sos. EMBO J., 1997, **16**, 1351–9.
[427] Baumeister, M.A., Martinu, L., Rossman, K.L., Sondek, J., et al., 2003. Loss of phosphatidylinositol 3-phosphate binding by the C-terminal Tiam-1 pleckstrin homology domain prevents in vivo Rac1 activation without affecting membrane targeting. J. Biol. Chem., 2003, **278**, 11457–64.
[428] Russo, C., Gao, Y., Mancini, P., Vanni, C., et al., 2001. Modulation of oncogenic DBL activity by phosphoinositol phosphate binding to pleckstrin homology domain. J. Biol. Chem., 2001, **276**, 19524–31.
[429] Welch, H.C.E., Coadwell, W.J., Ellson, C.D., Ferguson, G.J., et al., 2002. P-Rex1, a PtdIns(3,4,5)P3- and Gbetagamma-regulated guanine-nucleotide exchange factor for Rac. Cell, 2002, **108**, 809–21.
[430] Vanni, C., Parodi, A., Mancini, P., Visco, V., et al., 2004. Phosphorylation-independent membrane relocalization of ezrin following association with Dbl in vivo. Oncogene, 2004, **23**, 4098–106.
[431] Bellanger, J.M., Astier, C., Sardet, C., Ohta, Y., et al., 2000. The Rac1- and RhoG-specific GEF domain of Trio targets filamin to remodel cytoskeletal actin. Nat. Cell Biol., 2000, **2**, 888–92.
[432] Seipel, K., O'Brien, S.P., Iannotti, E., Medley, Q.G., Streuli, M., 2001. Tara, a novel F-actin binding protein, associates with the Trio guanine nucleotide exchange factor and regulates actin cytoskeletal organization. J. Cell Sci., 2001, **114**, 389–99.
[433] Bustelo, X.R., 2000. Regulatory and signaling properties of the Vav family. Mol. Cell. Biol., 2000, **20**, 1461–77.
[434] Katzav, S., 1995. Vav: Captain Hook for signal transduction? Crit. Rev. Oncog., 1995, **6**, 87–97.
[435] Hornstein, I., Alcover, A., Katzav, S., 2004. Vav proteins, masters of the world of cytoskeleton organization. Cell. Signal., 2004, **16**, 1–11.
[436] Llorca, O., Arias-Palomo, E., Zugaza, J.L., Bustelo, X.R., 2005. Global conformational rearrangements during the activation of the GDP/GTP

exchange factor Vav3. EMBO J., 2005, **24**, 1330–40.
[437] Aghazadeh, B., Lowry, W.E., Huang, X.Y., Rosen, M.K., 2000. Structural basis for relief of autoinhibition of the Dbl homology domain of proto-oncogene Vav by tyrosine phosphorylation. Cell, 2000, **102**, 625–33.
[438] Han, J., Luby-Phelps, K., Das, B., Shu, X., et al., 1998. Role of substrates and products of PI 3-kinase in regulating activation of Rac-related guanosine triphosphatases by Vav. Science, 1998, **279**, 558–60.
[439] Schuebel, K.E., Movilla, N., Rosa, J.L., Bustelo, X.R., 1998. Phosphorylation-dependent and constitutive activation of Rho proteins by wild-type and oncogenic Vav-2. EMBO J., 1998, **17**, 6608–21.
[440] Welch, H.C.E., 2015. Regulation and function of P-Rex family Rac-GEFs. Small GTPases, 2015, **6**, 49–70.
[441] Donald, S., Hill, K., Lecureuil, C., Barnouin, R., et al., 2004. P-Rex2, a new guanine-nucleotide exchange factor for Rac. FEBS Lett., 2004, **572**, 172–176.
[442] Hill, K., Welch, H.C.E., 2006. *Methods Enzymol.*, vol. 406, pp. 26–41.
[443] Wang, Z., Dong, X., Li, Z., Smith, J.D., Wu, D., 2008. Lack of a significant role of P-Rex1, a major regulator of macrophage Rac1 activation and chemotaxis, in atherogenesis. Prostaglandins Other Lipid Mediat., 2008, **87**, 9–13.
[444] Aslan, J.E., Spencer, A.M., Loren, C.P., Pang, J., et al., 2011. Characterization of the Rac guanine nucleotide exchange factor P-Rex1 in platelets. J. Mol. Signal., 2011, **6**, 11.
[445] Qian, F., Le Breton, G.C., Chen, J., Deng, J., et al., 2012. Role for the guanine nucleotide exchange factor phosphatidylinositol-3,4,5-trisphosphate-dependent rac exchanger 1 in platelet secretion and aggregation. Arterioscler. Thromb. Vasc. Biol., 2012, **32**, 768–77.
[446] Carretero-Ortega, J., Walsh, C.T., Hernández-García, R., Reyes-Cruz, G., et al., 2010. Phosphatidylinositol 3,4,5-triphosphate-dependent Rac exchanger 1 (P-Rex-1), a guanine nucleotide exchange factor for Rac, mediates angiogenic responses to stromal cell-derived factor-1/chemokine stromal cell derived factor-1 (SDF-1/CXCL-12) linked to Rac activation, endothelial cell migration, and in vitro angiogenesis. Mol. Pharmacol., 2010, **77**, 435–42.
[447] Yoshizawa, M., Kawauchi, T., Sone, M., Nishimura, Y. V, et al., 2005. Involvement of a Rac Activator, P-Rex1, in Neurotrophin-Derived Signaling and Neuronal Migration. J. Neurosci., 2005, **25**, 4406–4419.
[448] Hodakoski, C., Hopkins, B.D., Barrows, D., Mense, S.M., et al., 2014. Regulation of PTEN inhibition by the pleckstrin homology domain of P-REX2 during insulin signaling and glucose homeostasis. Proc. Natl. Acad. Sci. U. S. A., 2014, **111**, 155–60.
[449] Donald, S., Humby, T., Fyfe, I., Segonds-Pichon, A., et al., 2008. P-Rex2 regulates Purkinje cell dendrite morphology and motor coordination. Proc. Natl. Acad. Sci. U. S. A., 2008, **105**, 4483–8.
[450] Rosenfeldt, H., Vázquez-Prado, J., Gutkind, J.S., 2004. P-REX2, a novel PI-3-kinase sensitive Rac exchange factor. FEBS Lett., 2004, **572**, 167–171.
[451] Rynkiewicz, N.K., Liu, H.-J., Balamatsias, D., Mitchell, C.A., 2012. INPP4A/INPP4B and P-Rex proteins: Related but different? Adv. Biol. Regul., 2012, **52**, 265–279.
[452] Hill, K., Krugmann, S., Andrews, S.R., Coadwell, W.J., et al., 2005. Regulation of P-Rex1 by Phosphatidylinositol (3,4,5)-Trisphosphate and Gβγ Subunits. J. Biol. Chem., 2005, **280**, 4166–4173.
[453] Urano, D., Nakata, A., Mizuno, N., Tago, K., Itoh, H., 2008. Domain–domain interaction of P-Rex1 is essential for the activation and inhibition by G protein βγ subunits and PKA. Cell. Signal., 2008, **20**, 1545–1554.
[454] Barber, M.A., Donald, S., Thelen, S., Anderson, K.E., et al., 2007. Membrane Translocation of P-Rex1 Is Mediated by G Protein beta Subunits and Phosphoinositide 3-Kinase. J. Biol. Chem., 2007, **282**, 29967–29976.
[455] Zhao, T., Nalbant, P., Hoshino, M., Dong, X., et al., 2007. Signaling requirements for translocation of P-Rex1, a key Rac2 exchange factor involved in chemoattractant-stimulated human neutrophil function. J. Leukoc. Biol., 2007, **81**, 1127–1136.
[456] Sosa, M.S., Lopez-Haber, C., Yang, C., Wang, H., et al., 2010. Identification of the Rac-GEF P-Rex1 as an Essential Mediator of ErbB Signaling in Breast Cancer. Mol. Cell, 2010, **40**, 877–892.
[457] Barber, M.A., Hendrickx, A., Beullens, M., Ceulemans, H., et al., 2012. The guanine-nucleotide-exchange factor P-Rex1 is activated by protein phosphatase 1α. Biochem. J., 2012, **443**, 173–183.
[458] Hendrickx, A., Beullens, M., Ceulemans, H., Den Abt, T., et al., 2009. Docking Motif-Guided Mapping of the Interactome of Protein Phosphatase-1. Chem. Biol., 2009, **16**, 365–371.
[459] Mayeenuddin, L.H., Garrison, J.C., 2006. Phosphorylation of P-Rex1 by the Cyclic AMP-dependent Protein Kinase Inhibits the Phosphatidylinositiol (3,4,5)-Trisphosphate and Gbeta -mediated Regulation of Its Activity. J. Biol. Chem., 2006, **281**, 1921–1928.
[460] Wertheimer, E., Gutierrez-Uzquiza, A., Rosemblit, C., Lopez-Haber, C., et al., 2012. Rac signaling in breast cancer: A tale of GEFs and GAPs. Cell Signal, 2012, **24**, 353–362.
[461] Wong, C.-Y.A., Wuriyanghan, H., Xie, Y., Lin, M.-F., et al., 2011. Epigenetic regulation of phosphatidylinositol 3,4,5-triphosphate-dependent Rac exchanger 1 gene expression in prostate cancer cells. J. Biol. Chem., 2011, **286**, 25813–22.
[462] Guo, B., Liu, L., Yao, J., Ma, R., et al., 2014. miR-338-3p Suppresses Gastric Cancer Progression through a PTEN-AKT Axis by Targeting P-REX2a. Mol. Cancer Res., 2014, **12**, 313–321.
[463] Chen, X., Pan, M., Han, L., Lu, H., et al., 2013. miR-338-3p suppresses neuroblastoma proliferation, invasion and migration through targeting PREX2a. FEBS Lett., 2013, **587**, 3729–3737.
[464] Fine, B., Hodakoski, C., Koujak, S., Su, T., et al., 2009. Activation of the PI3K Pathway in Cancer Through Inhibition of PTEN by Exchange Factor P-REX2a. Science (80-.)., 2009, **325**, 1261–1265.
[465] Côté, J.-F., Vuori, K., 2002. Identification of an evolutionarily conserved superfamily of DOCK180-related proteins with guanine nucleotide exchange activity. J. Cell Sci., 2002, **115**, 4901–13.
[466] Meller, N., Irani-Tehrani, M., Kiosses, W.B., Del Pozo, M.A., Schwartz, M.A., 2002. Zizimin1, a novel Cdc42 activator, reveals a new GEF domain for Rho proteins. Nat. Cell Biol., 2002, **4**, 639–647.
[467] Namekata, K., Enokido, Y., Iwasawa, K., Kimura, H., 2004. MOCA induces membrane spreading by activating Rac1. J. Biol. Chem., 2004, **279**, 14331–7.
[468] Sanui, T., Inayoshi, A., Noda, M., Iwata, E., et al., 2003. DOCK2 regulates Rac activation and cytoskeletal reorganization through interaction with ELMO1. Blood, 2003, **102**, 2948–50.
[469] Yajnik, V., Paulding, C., Sordella, R., McClatchey, A.I., et al., 2003. DOCK4, a GTPase activator, is disrupted during tumorigenesis. Cell, 2003, **112**, 673–84.
[470] Nishikimi, A., Meller, N., Uekawa, N., Isobe, K., et al., 2005. Zizimin2: a novel, DOCK180-related Cdc42 guanine nucleotide exchange factor expressed predominantly in lymphocytes. FEBS Lett., 2005, **579**, 1039–46.
[471] Gumienny, T.L., Brugnera, E., Tosello-Trampont, A.C., Kinchen, J.M., et al., 2001. CED-12/ELMO, a novel member of the CrkII/Dock180/Rac pathway, is required for phagocytosis and cell migration. Cell, 2001, **107**, 27–41.
[472] Horvitz, H.R., Reddien, P.W., 2000. CED-2/CrkII and CED-10/Rac control phagocytosis and cell migration in Caenorhabditis elegans. Nat. Cell Biol., 2000, **2**, 131–136.
[473] Horvitz, H.R., Wu, Y.-C., 1998. C. elegans phagocytosis and cell-migration protein CED-5 is similar to human DOCK180. Nature, 1998, **392**, 501–504.
[474] Wu, Y.C., Tsai, M.C., Cheng, L.C., Chou, C.J., Weng, N.Y., 2001. C. elegans CED-12 acts in the conserved crkII/DOCK180/Rac pathway to control cell migration and cell corpse engulfment. Dev. Cell, 2001, **1**, 491–502.

[475] Zhou, Z., Caron, E., Hartwieg, E., Hall, A., Horvitz, H.R., 2001. The C. elegans PH domain protein CED-12 regulates cytoskeletal reorganization via a Rho/Rac GTPase signaling pathway. Dev. Cell, 2001, **1**, 477–89.

[476] Grimsley, C.M., Kinchen, J.M., Tosello-Trampont, A.-C., Brugnera, E., et al., 2004. Dock180 and ELMO1 proteins cooperate to promote evolutionarily conserved Rac-dependent cell migration. J. Biol. Chem., 2004, **279**, 6087–97.

[477] Buday, L., Wunderlich, L., Tamás, P., 2002. The Nck family of adapter proteins: regulators of actin cytoskeleton. Cell. Signal., 2002, **14**, 723–31.

[478] Hasegawa, H., Kiyokawa, E., Tanaka, S., Nagashima, K., et al., 1996. DOCK180, a major CRK-binding protein, alters cell morphology upon translocation to the cell membrane. Mol. Cell. Biol., 1996, **16**, 1770–6.

[479] Côté, J.F., Vuori, K., 2007. GEF what? Dock180 and related proteins help Rac to polarize cells in new ways. Trends Cell Biol., 2007, **17**, 383–393.

[480] Lu, M., Kinchen, J.M., Rossman, K.L., Grimsley, C., et al., 2004. PH domain of ELMO functions in trans to regulate Rac activation via Dock180. Nat. Struct. Mol. Biol., 2004, **11**, 756–62.

[481] Lu, M., Ravichandran, K.S., 2006. Dock180-ELMO cooperation in Rac activation. Methods Enzymol., 2006, **406**, 388–402.

[482] Lu, M., Kinchen, J.M., Rossman, K.L., Grimsley, C., et al., 2005. A Steric-inhibition model for regulation of nucleotide exchange via the Dock180 family of GEFs. Curr. Biol., 2005, **15**, 371–7.

[483] Katoh, H., Negishi, M., 2003. RhoG activates Rac1 by direct interaction with the Dock180-binding protein Elmo. Nature, 2003, **424**, 461–4.

[484] deBakker, C.D., Haney, L.B., Kinchen, J.M., Grimsley, C., et al., 2004. Phagocytosis of apoptotic cells is regulated by a UNC-73/TRIO-MIG-2/RhoG signaling module and armadillo repeats of CED-12/ELMO. Curr. Biol., 2004, **14**, 2208–16.

[485] Côté, J.-F., Motoyama, A.B., Bush, J.A., Vuori, K., 2005. A novel and evolutionarily conserved PtdIns(3,4,5)P3-binding domain is necessary for DOCK180 signalling. Nat. Cell Biol., 2005, **7**, 797–807.

[486] Franca-Koh, J., Kamimura, Y., Devreotes, P.N., 2007. Leading-edge research: PtdIns(3,4,5)P3 and directed migration. Nat. Cell Biol., 2007, **9**, 15–17.

[487] Steck, P.A., Pershouse, M.A., Jasser, S.A., Yung, W.K., et al., 1997. Identification of a candidate tumour suppressor gene, MMAC1, at chromosome 10q23.3 that is mutated in multiple advanced cancers. Nat. Genet., 1997, **15**, 356–62.

[488] Li, D.M., Sun, H., 1997. TEP1, encoded by a candidate tumor suppressor locus, is a novel protein tyrosine phosphatase regulated by transforming growth factor beta. Cancer Res., 1997, **57**, 2124–9.

[489] Wang, X., Jiang, X., 2008. PTEN: a default gate-keeping tumor suppressor with a versatile tail. Cell Res., 2008, **18**, 807–816.

[490] Maehama, T., Dixon, J.E., 1998. The tumor suppressor, PTEN/MMAC1, dephosphorylates the lipid second messenger, phosphatidylinositol 3,4,5-trisphosphate. J. Biol. Chem., 1998, **273**, 13375–8.

[491] Shen, W.H., Balajee, A.S., Wang, J., Wu, H., et al., 2007. Essential role for nuclear PTEN in maintaining chromosomal integrity. Cell, 2007, **128**, 157–70.

[492] Ali, I.U., Schriml, L.M., Dean, M., 1999. Mutational spectra of PTEN/MMAC1 gene: a tumor suppressor with lipid phosphatase activity. J. Natl. Cancer Inst., 1999, **91**, 1922–32.

[493] Sansal, I., Sellers, W.R., 2004. The biology and clinical relevance of the PTEN tumor suppressor pathway. J. Clin. Oncol., 2004, **22**, 2954–2963.

[494] Marsh, D.J., Dahia, P.L.M., Zheng, Z., Liaw, D., et al., 1997. Germline mutations in PTEN are present in Bannayan-Zonana syndrome. Nat. Genet., 1997, **16**, 333–334.

[495] Liaw, D., Marsh, D.J., Li, J., Dahia, P.L.M., et al., 1997. Germline mutations of the PTEN gene in Cowden disease, an inherited breast and thyroid cancer syndrome. Nat. Genet., 1997, **16**, 64–67.

[496] Song, M.S., Salmena, L., Pandolfi, P.P., 2012. The functions and regulation of the PTEN tumour suppressor. Nat Rev Mol Cell Biol, 2012, **13**, 283–296.

[497] Myers, M.P., Stolarov, J.P., Eng, C., Li, J., et al., 1997. P-TEN, the tumor suppressor from human chromosome 10q23, is a dual-specificity phosphatase. Proc. Natl. Acad. Sci. U. S. A., 1997, **94**, 9052–7.

[498] Lee, J.O., Yang, H., Georgescu, M.M., Cristofano, A. Di, et al., 1999. Crystal structure of the PTEN tumor suppressor: Implications for its phosphoinositide phosphatase activity and membrane association. Cell, 1999, **99**, 323–334.

[499] Myers, M.P., Pass, I., Batty, I.H., Van der Kaay, J., et al., 1998. The lipid phosphatase activity of PTEN is critical for its tumor supressor function. Proc. Natl. Acad. Sci. U. S. A., 1998, **95**, 13513–8.

[500] Gildea, J.J., Herlevsen, M., Harding, M.A., Gulding, K.M., et al., 2004. PTEN can inhibit in vitro organotypic and in vivo orthotopic invasion of human bladder cancer cells even in the absence of its lipid phosphatase activity. Oncogene, 2004, **23**, 6788–97.

[501] Das, S., Dixon, J.E., Cho, W., 2003. Membrane-binding and activation mechanism of PTEN. Proc. Natl. Acad. Sci., 2003, **100**, 7491–7496.

[502] Redfern, R.E., Redfern, D., Furgason, M.L.M., Munson, M., et al., 2008. PTEN phosphatase selectively binds phosphoinositides and undergoes structural changes. Biochemistry, 2008, **47**, 2162–71.

[503] Campbell, R.B., Liu, F., Ross, A.H., 2003. Allosteric Activation of PTEN Phosphatase by Phosphatidylinositol 4,5-Bisphosphate. J. Biol. Chem., 2003, **278**, 33617–33620.

[504] McCONNACHIE, G., PASS, I., WALKER, S.M., DOWNES, C.P., 2003. Interfacial kinetic analysis of the tumour suppressor phosphatase, PTEN: evidence for activation by anionic phospholipids. Biochem. J., 2003, **371**, 947–955.

[505] Iijima, M., Huang, Y.E., Luo, H.R., Vazquez, F., Devreotes, P.N., 2004. Novel Mechanism of PTEN Regulation by Its Phosphatidylinositol 4,5-Bisphosphate Binding Motif Is Critical for Chemotaxis. J. Biol. Chem., 2004, **279**, 16606–16613.

[506] Walker, S.M., Leslie, N.R., Perera, N.M., Batty, I.H., Downes, C.P., 2004. The tumour-suppressor function of PTEN requires an N-terminal lipid-binding motif. Biochem. J., 2004, **379**, 301–7.

[507] Georgescu, M.M., Kirsch, K.H., Akagi, T., Shishido, T., Hanafusa, H., 1999. The tumor-suppressor activity of PTEN is regulated by its carboxyl-terminal region. Proc. Natl. Acad. Sci. U. S. A., 1999, **96**, 10182–7.

[508] Hollander, M.C., Blumenthal, G.M., Dennis, P. a, 2011. PTEN loss in the continuum of common cancers, rare syndromes and mouse models. Nat. Rev. Cancer, 2011, **11**, 289–301.

[509] Lu, J., Jeong, H.-W., Jeong, H., Kong, N., et al., 2009. Stem cell factor SALL4 represses the transcriptions of PTEN and SALL1 through an epigenetic repressor complex. PLoS One, 2009, **4**, e5577.

[510] Stambolic, V., MacPherson, D., Sas, D., Lin, Y., et al., 2001. Regulation of PTEN transcription by p53. Mol. Cell, 2001, **8**, 317–25.

[511] Patel, L., Pass, I., Coxon, P., Downes, C.P., et al., 2001. Tumor suppressor and anti-inflammatory actions of PPARgamma agonists are mediated via upregulation of PTEN. Curr. Biol., 2001, **11**, 764–8.

[512] Escrivà, M., Peiró, S., Herranz, N., Villagrasa, P., et al., 2008. Repression of PTEN phosphatase by Snail1 transcriptional factor during gamma radiation-induced apoptosis. Mol. Cell. Biol., 2008, **28**, 1528–40.

[513] Hettinger, K., Vikhanskaya, F., Poh, M.K., Lee, M.K., et al., 2007. c-Jun promotes cellular survival by suppression of PTEN. Cell Death Differ., 2007, **14**, 218–29.

[514] Bartel, D.P., 2009. MicroRNAs: Target Recognition and Regulatory Functions. Cell, 2009, **136**, 215–233.

[515] Xiao, C., Srinivasan, L., Calado, D.P., Patterson, H.C., et al., 2008. Lymphoproliferative disease and autoimmunity in mice with increased miR-17-92 expression in lymphocytes. Nat. Immunol., 2008, **9**, 405–14.

[516] Olive, V., Bennett, M.J., Walker, J.C., Ma, C., et al., 2009. miR-19 is a key oncogenic component of mir-17-92. Genes Dev., 2009, **23**, 2839–2849.

[517] Mavrakis, K.J., Wolfe, A.L., Oricchio, E., Palomero, T., et al., 2010. Genome-wide RNA-mediated interference screen identifies miR-19 targets in Notch-induced T-cell acute lymphoblastic leukaemia. Nat. Cell Biol., 2010, **12**, 372–9.

[518] Meng, F., Henson, R., Wehbe-Janek, H., Ghoshal, K., et al., 2007. MicroRNA-21 regulates expression of the PTEN tumor suppressor gene in

human hepatocellular cancer. Gastroenterology, 2007, **133**, 647–58.
[519] Ma, X., Kumar, M., Choudhury, S.N., Becker Buscaglia, L.E., et al., 2011. Loss of the miR-21 allele elevates the expression of its target genes and reduces tumorigenesis. Proc. Natl. Acad. Sci. U. S. A., 2011, **108**, 10144–9.
[520] Poliseno, L., Salmena, L., Zhang, J., Carver, B., et al., 2010. A coding-independent function of gene and pseudogene mRNAs regulates tumour biology. Nature, 2010, **465**, 1033–1038.
[521] Salmena, L., Poliseno, L., Tay, Y., Kats, L., Pandolfi, P.P., 2011. A ceRNA hypothesis: the Rosetta Stone of a hidden RNA language? Cell, 2011, **146**, 353–8.
[522] Al-Khouri, A.M., Ma, Y., Togo, S.H., Williams, S., Mustelin, T., 2005. Cooperative phosphorylation of the tumor suppressor phosphatase and tensin homologue (PTEN) by casein kinases and glycogen synthase kinase 3beta. J. Biol. Chem., 2005, **280**, 35195–202.
[523] Xu, D., Yao, Y., Jiang, X., Lu, L., Dai, W., 2010. Regulation of PTEN Stability and Activity by Plk3. J. Biol. Chem., 2010, **285**, 39935–39942.
[524] Rabinovsky, R., Pochanard, P., McNear, C., Brachmann, S.M., et al., 2009. p85 Associates with unphosphorylated PTEN and the PTEN-associated complex. Mol. Cell. Biol., 2009, **29**, 5377–88.
[525] Vazquez, F., Grossman, S.R., Takahashi, Y., Rokas, M. V, et al., 2001. Phosphorylation of the PTEN tail acts as an inhibitory switch by preventing its recruitment into a protein complex. J. Biol. Chem., 2001, **276**, 48627–30.
[526] Trotman, L.C., Wang, X., Alimonti, A., Chen, Z., et al., 2007. Ubiquitination Regulates PTEN Nuclear Import and Tumor Suppression. Cell, 2007, **128**, 141–156.
[527] Lee, S.-R., Yang, K.-S., Kwon, J., Lee, C., et al., 2002. Reversible Inactivation of the Tumor Suppressor PTEN by H2O2. J. Biol. Chem., 2002, **277**, 20336–20342.
[528] Silva, A., Yunes, J.A., Cardoso, B.A., Martins, L.R., et al., 2008. PTEN posttranslational inactivation and hyperactivation of the PI3K/Akt pathway sustain primary T cell leukemia viability. J. Clin. Invest., 2008, **118**, 3762–74.
[529] Molina, J.R., Agarwal, N.K., Morales, F.C., Hayashi, Y., et al., 2012. PTEN, NHERF1 and PHLPP form a tumor suppressor network that is disabled in glioblastoma. Oncogene, 2012, **31**, 1264–74.
[530] Takahashi, Y., Morales, F.C., Kreimann, E.L., Georgescu, M.-M., 2006. PTEN tumor suppressor associates with NHERF proteins to attenuate PDGF receptor signaling. EMBO J., 2006, **25**, 910–20.
[531] Wu, X., Hepner, K., Castelino-Prabhu, S., Do, D., et al., 2000. Evidence for regulation of the PTEN tumor suppressor by a membrane-localized multi-PDZ domain containing scaffold protein MAGI-2. Proc. Natl. Acad. Sci. U. S. A., 2000, **97**, 4233–8.
[532] Li, Z., Dong, X., Wang, Z., Liu, W., et al., 2005. Regulation of PTEN by Rho small GTPases. Nat. Cell Biol., 2005, **7**, 399–404.
[533] Chagpar, R.B., Links, P.H., Pastor, M.C., Furber, L.A., et al., 2010. Direct positive regulation of PTEN by the p85 subunit of phosphatidylinositol 3-kinase. Proc. Natl. Acad. Sci. U. S. A., 2010, **107**, 5471–6.
[534] Freeman, D.J., Li, A.G., Wei, G., Li, H.-H., et al., 2003. PTEN tumor suppressor regulates p53 protein levels and activity through phosphatase-dependent and -independent mechanisms. Cancer Cell, 2003, **3**, 117–30.
[535] Tang, Y., Eng, C., 2006. PTEN autoregulates its expression by stabilization of p53 in a phosphatase-independent manner. Cancer Res., 2006, **66**, 736–42.
[536] Li, A.G., Piluso, L.G., Cai, X., Wei, G., et al., 2006. Mechanistic insights into maintenance of high p53 acetylation by PTEN. Mol. Cell, 2006, **23**, 575–87.
[537] Oren, M., 2003. Decision making by p53: life, death and cancer. Cell Death Differ., 2003, **10**, 431–442.
[538] Brooks, C.L., Gu, W., 2006. p53 Ubiquitination: Mdm2 and Beyond. Mol. Cell, 2006, **21**, 307–315.
[539] Stambolic, V., Suzuki, A., de la Pompa, J.L., Brothers, G.M., et al., 1998. Negative regulation of PKB/Akt-dependent cell survival by the tumor suppressor PTEN. Cell, 1998, **95**, 29–39.
[540] Trotman, L.C., Niki, M., Dotan, Z.A., Koutcher, J.A., et al., 2003. Pten dose dictates cancer progression in the prostate. PLoS Biol., 2003, **1**, E59.
[541] Puc, J., Keniry, M., Li, H.S., Pandita, T.K., et al., 2005. Lack of PTEN sequesters CHK1 and initiates genetic instability. Cancer Cell, 2005, **7**, 193–204.
[542] Salmena, L., Carracedo, A., Pandolfi, P.P., 2008. Tenets of PTEN Tumor Suppression. Cell, 2008, **133**, 403–414.
[543] Chen, Z., Trotman, L.C., Shaffer, D., Lin, H.-K., et al., 2005. Crucial role of p53-dependent cellular senescence in suppression of Pten-deficient tumorigenesis. Nature, 2005, **436**, 725–30.
[544] Norris, F.A., Majerus, P.W., 1994. Hydrolysis of phosphatidylinositol 3,4-bisphosphate by inositol polyphosphate 4-phosphatase isolated by affinity elution chromatography. J. Biol. Chem., 1994, **269**, 8716–20.
[545] Ivetac, I., Munday, A.D., Kisseleva, M. V, Zhang, X.-M., et al., 2005. The type Ialpha inositol polyphosphate 4-phosphatase generates and terminates phosphoinositide 3-kinase signals on endosomes and the plasma membrane. Mol. Biol. Cell, 2005, **16**, 2218–33.
[546] Ferron, M., Vacher, J., 2006. Characterization of the murine Inpp4b gene and identification of a novel isoform. Gene, 2006, **376**, 152–61.
[547] Ivetac, I., Gurung, R., Hakim, S., Horan, K.A., et al., 2009. Regulation of PI(3)K/Akt signalling and cellular transformation by inositol polyphosphate 4-phosphatase-1. EMBO Rep., 2009, **10**, 487–93.
[548] Rogers, S., Wells, R., Rechsteiner, M., 1986. Amino acid sequences common to rapidly degraded proteins: the PEST hypothesis. Science, 1986, **234**, 364–8.
[549] Wang, K.K., Villalobo, A., Roufogalis, B.D., 1989. Calmodulin-binding proteins as calpain substrates. Biochem. J., 1989, **262**, 693–706.
[550] Hiebert, S.W., Lutterbach, B., Amann, J., 2001. Role of co-repressors in transcriptional repression mediated by the t(8;21), t(16;21), t(12;21), and inv(16) fusion proteins. Curr. Opin. Hematol., 2001, **8**, 197–200.
[551] Hug, B.A., Lee, S.Y.D., Kinsler, E.L., Zhang, J., Lazar, M.A., 2002. Cooperative function of Aml1-ETO corepressor recruitment domains in the expansion of primary bone marrow cells. Cancer Res., 2002, **62**, 2906–12.
[552] Liu, Y., Cheney, M.D., Gaudet, J.J., Chruszcz, M., et al., 2006. The tetramer structure of the Nervy homology two domain, NHR2, is critical for AML1/ETO's activity. Cancer Cell, 2006, **9**, 249–260.
[553] Lopez, S.M., Hodgson, M.C., Packianathan, C., Bingol-Ozakpinar, O., et al., 2013. Determinants of the tumor suppressor INPP4B protein and lipid phosphatase activities. Biochem. Biophys. Res. Commun., 2013, **440**, 277–82.
[554] Nystuen, A., Legare, M.E., Shultz, L.D., Frankel, W.N., 2001. A null mutation in inositol polyphosphate 4-phosphatase type I causes selective neuronal loss in weeble mutant mice. Neuron, 2001, **32**, 203–12.
[555] Sasaki, J., Kofuji, S., Itoh, R., Momiyama, T., et al., 2010. The PtdIns(3,4)P(2) phosphatase INPP4A is a suppressor of excitotoxic neuronal death. Nature, 2010, **465**, 497–501.
[556] Sachs, A.J., David, S.A., Haider, N.B., Nystuen, A.M., 2009. Patterned neuroprotection in the Inpp4a(wbl) mutant mouse cerebellum correlates with the expression of Eaat4. PLoS One, 2009, **4**, e8270.
[557] Li, H., Marshall, A.J., 2015. Phosphatidylinositol (3,4) bisphosphate-specific phosphatases and effector proteins: A distinct branch of PI3K signaling. Cell. Signal., 2015, **27**, 1789–1798.
[558] Woolley, J.F., Dzneladze, I., Salmena, L., 2015. Phosphoinositide signaling in cancer: INPP4B Akt(s) out. Trends Mol. Med., 2015, **21**, 530–532.
[559] Chen, H., Li, H., Chen, Q., 2016. INPP4B reverses docetaxel resistance and epithelial-to-mesenchymal transition via the PI3K/Akt signaling pathway in prostate cancer. Biochem. Biophys. Res. Commun., 2016, **477**, 467–472.
[560] Perez-Lorenzo, R., Gill, K.Z., Shen, C.-H., Zhao, F.X., et al., 2014. A Tumor Suppressor Function for the Lipid Phosphatase INPP4B in Melanocytic Neoplasms. J. Invest. Dermatol., 2014, **134**, 1359–1368.
[561] Gasser, J.A., Inuzuka, H., Lau, A.W., Wei, W., et al., 2014. SGK3 mediates INPP4B-dependent PI3K signaling in breast cancer. Mol. Cell, 2014,

56, 595–607.
[562] Dzneladze, I., He, R., Woolley, J.F., Son, M.H., et al., 2015. INPP4B overexpression is associated with poor clinical outcome and therapy resistance in acute myeloid leukemia. Leukemia, 2015, **29**, 1485–1495.
[563] Rijal, S., Fleming, S., Cummings, N., Rynkiewicz, N.K., et al., 2015. Inositol polyphosphate 4-phosphatase II (INPP4B) is associated with chemoresistance and poor outcome in AML. Blood, 2015, **125**, 2815–24.
[564] Damen, J.E., Liu, L., Rosten, P., Humphries, R.K., et al., 1996. The 145-kDa protein induced to associate with Shc by multiple cytokines is an inositol tetraphosphate and phosphatidylinositol 3,4,5-triphosphate 5-phosphatase. Proc. Natl. Acad. Sci. U. S. A., 1996, **93**, 1689–93.
[565] Kavanaugh, W.M., Pot, D.A., Chin, S.M., Deuter-Reinhard, M., et al., 1996. Multiple forms of an inositol polyphosphate 5-phosphatase form signaling complexes with Shc and Grb2. Curr. Biol., 1996, **6**, 438–45.
[566] Lioubin, M.N., Algate, P.A., Tsai, S., Carlberg, K., et al., 1996. p150Ship, a signal transduction molecule with inositol polyphosphate-5-phosphatase activity. Genes Dev., 1996, **10**, 1084–95.
[567] Ware, M., Rosten, P., Damen, J., Liu, L., et al., 1996. Cloning and characterization of human SHIP, the 145-kD inositol 5- phosphatase that associates with SHC after cytokine stimulation. Blood, 1996, **88**.
[568] Condé, C., Gloire, G., Piette, J., 2011. Enzymatic and non-enzymatic activities of SHIP-1 in signal transduction and cancer. Biochem. Pharmacol., 2011, **82**, 1320–1334.
[569] Liu, L., Damen, J.E., Cutler, R.L., Krystal, G., 1994. Multiple cytokines stimulate the binding of a common 145-kilodalton protein to Shc at the Grb2 recognition site of Shc. Mol. Cell. Biol., 1994, **14**, 6926–35.
[570] Pesesse, X., Moreau, C., Drayer, A.L., Woscholski, R., et al., 1998. The SH2 domain containing inositol 5-phosphatase SHIP2 displays phosphatidylinositol 3,4,5-trisphosphate and inositol 1,3,4,5-tetrakisphosphate 5-phosphatase activity. FEBS Lett., 1998, **437**, 301–3.
[571] Chi, Y., Zhou, B., Wang, W.-Q., Chung, S.-K., et al., 2004. Comparative mechanistic and substrate specificity study of inositol polyphosphate 5-phosphatase Schizosaccharomyces pombe Synaptojanin and SHIP2. J. Biol. Chem., 2004, **279**, 44987–95.
[572] Taylor, V., Wong, M., Brandts, C., Reilly, L., et al., 2000. 5' phospholipid phosphatase SHIP-2 causes protein kinase B inactivation and cell cycle arrest in glioblastoma cells. Mol. Cell. Biol., 2000, **20**, 6860–71.
[573] Nelson, N., Wundenberg, T., Lin, H., Rehbach, C., et al., 2020. Characterization of the substrate specificity of the inositol 5-phosphatase SHIP1. Biochem. Biophys. Res. Commun., 2020, **524**, 366–370.
[574] Fernandes, S., Iyer, S., Kerr, W.G., 2013. Role of SHIP1 in cancer and mucosal inflammation. Ann. N. Y. Acad. Sci., 2013, **1280**, 6–10.
[575] Helgason, C.D., Damen, J.E., Rosten, P., Grewal, R., et al., 1998. Targeted dysruption of SHIP leads to hematopoietic pertubations lung pathology, and a shortened life span. Genes Dev., 1998, **12**, 1610.
[576] Oh, S.-Y., Zheng, T., Bailey, M.L., Barber, D.L., et al., 2007. Src homology 2 domain-containing inositol 5-phosphatase 1 deficiency leads to a spontaneous allergic inflammation in the murine lung. J. Allergy Clin. Immunol., 2007, **119**, 123–31.
[577] Mcnagny, K.M., Blanchet, M.-R., Zbytnuik, L., Krystal, G., et al., 2009. SHIP1 Is a Repressor of Mast Cell Hyperplasia, Cytokine Production, and Allergic Inflammation In Vivo. J Immunol Ref., 2009, **183**, 228–236.
[578] Takeshita, S., Namba, N., Zhao, J.J., Jiang, Y., et al., 2002. SHIP-deficient mice are severely osteoporotic due to increased numbers of hyper-resorptive osteoclasts. Nat. Med., 2002, **8**, 943–9.
[579] Liu, Q., Sasaki, T., Kozieradzki, I., Wakeham, A., et al., 1999. SHIP is a negative regulator of growth factor receptor-mediated PKB/Akt activation and myeloid cell survival. Genes Dev., 1999, **13**, 786–91.
[580] Maeda, K., Mehta, H., Drevets, D.A., Coggeshall, K.M., 2010. IL-6 increases B-cell IgG production in a feed-forward proinflammatory mechanism to skew hematopoiesis and elevate myeloid production. Blood, 2010, **115**.
[581] Ghansah, T., Paraiso, K.H.T., Highfill, S., Desponts, C., et al., 2004. Expansion of Myeloid Suppressor Cells in SHIP-Deficient Mice Represses Allogeneic T Cell Responses. J. Immunol., 2004, **173**.
[582] Collazo, M.M., Wood, D., Paraiso, K.H.T., Lund, E., et al., 2009. SHIP limits immunoregulatory capacity in the T-cell compartment. Blood, 2009, **113**, 2934–44.
[583] Kashiwada, M., Cattoretti, G., McKeag, L., Rouse, T., et al., 2006. Downstream of tyrosine kinases-1 and Src homology 2-containing inositol 5'-phosphatase are required for regulation of CD4+CD25+ T cell development. J. Immunol., 2006, **176**, 3958–65.
[584] Helgason, C.D., Antonchuk, J., Bodner, C., Humphries, R.K., 2003. Homeostasis and regeneration of the hematopoietic stem cell pool are altered in SHIP-deficient mice. Blood, 2003, **102**.
[585] Desponts, C., Hazen, A.L., H, Paraiso, K., Kerr, W.G., 2006. SHIP deficiency enhances HSC proliferation and survival but compromises homing and repopulation. Blood, 2006, **107**, 4338–4345.
[586] Ruschmann, J., Ho, V., Antignano, F., Kuroda, E., et al., 2010. Tyrosine phosphorylation of SHIP promotes its proteasomal degradation. Exp. Hematol., 2010, **38**, 392-402.e1.
[587] Sattler, M., Verma, S., Byrne, C.H., Shrikhande, G., et al., 1999. BCR/ABL directly inhibits expression of SHIP, an SH2-containing polyinositol-5-phosphatase involved in the regulation of hematopoiesis. Mol. Cell. Biol., 1999, **19**, 7473–80.
[588] Luo, J.-M., Yoshida, H., Komura, S., Ohishi, N., et al., 2003. Possible dominant-negative mutation of the SHIP gene in acute myeloid leukemia. Leukemia, 2003, **17**, 1–8.
[589] Luo, J.-M., Liu, Z.-L., Hao, H.-L., Wang, F.-X., et al., 2004. Mutation analysis of SHIP gene in acute leukemia. Zhongguo shi yan xue ye xue za zhi, 2004, **12**, 420–6.
[590] Lo, T.C.T., Barnhill, L.M., Kim, Y., Nakae, E.A., et al., 2009. Inactivation of SHIP1 in T-cell acute lymphoblastic leukemia due to mutation and extensive alternative splicing. Leuk. Res., 2009, **33**, 1562–6.
[591] Schaks, M., Allgoewer, K., Nelson, N., Ehm, P., et al., 2020. Ectopic Expression of Hematopoietic SHIP1 in Human Colorectal Cancer. Biomedicines, 2020, **8**, 215.
[592] Wada, T., Sasaoka, T., Funaki, M., Hori, H., et al., 2001. Overexpression of SH2-containing inositol phosphatase 2 results in negative regulation of insulin-induced metabolic actions in 3T3-L1 adipocytes via its 5'-phosphatase catalytic activity. Mol. Cell. Biol., 2001, **21**, 1633–46.
[593] Sasaoka, T., Hori, H., Wada, T., Ishiki, M., et al., 2001. SH2-containing inositol phosphatase 2 negatively regulates insulin-induced glycogen synthesis in L6 myotubes. Diabetologia, 2001, **44**, 1258–67.
[594] Clément, S., Krause, U., Desmedt, F., Tanti, J.-F., et al., 2001. The lipid phosphatase SHIP2 controls insulin sensitivity. Nature, 2001, **409**, 92–97.
[595] Clément, S., Krause, U., Desmedt, F., Tanti, J.-F., et al., 2004. corrigendum: The lipid phosphatase SHIP2 controls insulin sensitivity. Nature, 2004, **431**, 878–878.
[596] Sleeman, M.W., Wortley, K.E., Lai, K.-M. V, Gowen, L.C., et al., 2005. Absence of the lipid phosphatase SHIP2 confers resistance to dietary obesity. Nat. Med., 2005, **11**, 199–205.
[597] Kagawa, S., Soeda, Y., Ishihara, H., Oya, T., et al., 2008. Impact of Transgenic Overexpression of SH2-Containing Inositol 5'-Phosphatase 2 on Glucose Metabolism and Insulin Signaling in Mice. Endocrinology, 2008, **149**, 642–650.
[598] Prasad, N.K., Tandon, M., Badve, S., Snyder, P.W., Nakshatri, H., 2008. Phosphoinositol phosphatase SHIP2 promotes cancer development and metastasis coupled with alterations in EGF receptor turnover. Carcinogenesis, 2008, **29**, 25–34.
[599] Sumie, S., Kawaguchi, T., Komuta, M., Kuromatsu, R., et al., 2007. Significance of glucose intolerance and SHIP2 expression in hepatocellular carcinoma patients with HCV infection. Oncol. Rep., 2007, **18**, 545–52.
[600] Franke, T.F., Kaplan, D.R., Cantley, L.C., Toker, A., 1997. Direct regulation of the Akt proto-oncogene product by phosphatidylinositol-3,4-bisphosphate. Science, 1997, **275**, 665–8.

[601] Hamilton, M.J., Ho, V.W., Kuroda, E., Ruschmann, J., et al., 2011. Role of SHIP in cancer. Exp. Hematol., 2011, **39**, 2–13.

[602] Daigle, I., Yousefi, S., Colonna, M., Green, D., Simon, H., 2002. Death receptors bind SHP-1 and block cytokine-induced anti-apoptotic signaling in neutrophils. Nat Med, 2002, **8**, 61–7.

[603] Liu, Q., Oliveira-Dos-Santos, A.J., Mariathasan, S., Bouchard, D., et al., 1998. The inositol polyphosphate 5-phosphatase ship is a crucial negative regulator of B cell antigen receptor signaling. J. Exp. Med., 1998, **188**, 1333–42.

[604] Pearse, R.N., Kawabe, T., Bolland, S., Guinamard, R., et al., 1999. SHIP recruitment attenuates Fc gamma RIIB-induced B cell apoptosis. Immunity, 1999, **10**, 753–60.

[605] Osborne, M.A., Zenner, G., Lubinus, M., Zhang, X., et al., 1996. The inositol 5'-phosphatase SHIP binds to immunoreceptor signaling motifs and responds to high affinity IgE receptor aggregation. J. Biol. Chem., 1996, **271**, 29271–8.

[606] Brauweiler, A.M., Tamir, I., Cambier, J.C., 2000. Bilevel control of B-cell activation by the inositol 5-phosphatase SHIP. Immunol. Rev., 2000, **176**, 69–74.

[607] Robson, J., Davidson, D., Veillette, A., 2004. Inhibition of the Jun N-terminal protein kinase pathway by SHIP-1, a lipid phosphatase that interacts with the adaptor molecule Dok-3. Mol Cell Biol, 2004, **24**, 2332–43.

[608] Ming-Lum, a., Shojania, S., So, E., McCarrell, E., et al., 2012. A pleckstrin homology-related domain in SHIP1 mediates membrane localization during Fc receptor-induced phagocytosis. FASEB J., 2012, **26**, 3163–3177.

[609] Hsu, F.S., Mao, Y., 2015. The structure of phosphoinositide phosphatases: Insights into substrate specificity and catalysis. Biochim. Biophys. Acta - Mol. Cell Biol. Lipids, 2015, **1851**, 698–710.

[610] Whisstock, J.C., Wiradjaja, F., Waters, J.E., Gurung, R., 2002. The structure and function of catalytic domains within inositol polyphosphate 5-phosphatases. IUBMB Life, 2002, **53**, 15–23.

[611] Tsujishita, Y., Guo, S., Stolz, L.E., York, J.D., et al., 2001. Specificity determinants in phosphoinositide dephosphorylation: crystal structure of an archetypal inositol polyphosphate 5-phosphatase. Cell, 2001, **105**, 379–89.

[612] Tsutakawa, S.E., Shin, D.S., Mol, C.D., Izumi, T., et al., 2013. Conserved structural chemistry for incision activity in structurally non-homologous apurinic/apyrimidinic endonuclease APE1 and endonuclease IV DNA repair enzymes. J. Biol. Chem., 2013, **288**, 8445–55.

[613] Trésaugues, L., Silvander, C., Flodin, S., Welin, M., et al., 2014. Structural basis for phosphoinositide substrate recognition, catalysis, and membrane interactions in human inositol polyphosphate 5-phosphatases. Structure, 2014, **22**, 744–755.

[614] Ong, C.J., Ming-Lum, A., Nodwell, M., Ghanipour, A., et al., 2007. Small-molecule agonists of SHIP1 inhibit the phosphoinositide 3-kinase pathway in hematopoietic cells. Blood, 2007, **110**, 1942–9.

[615] Lucas, D.M., Rohrschneider, L.R., 1999. A Novel Spliced Form of SH2-Containing Inositol Phosphatase Is Expressed During Myeloid Development. Blood, 1999, **93**.

[616] Tu, Z., Ninos, J., Ma, Z., Wang, J., et al., 2001. Embryonic and hematopoietic stem cells express a novel SH2-containing inositol 50-phos- phatase isoform that partners with the Grb2 adapter protein. Blood, 2001, **98**, 2028–38.

[617] Rohrschneider, L.R., Custodio, J.M., Anderson, T.A., Miller, C.P., Gu, H., 2005. The intron 5/6 promoter region of the ship1 gene regulates expression in stem/progenitor cells of the mouse embryo. Dev. Biol., 2005, **283**, 503–21.

[618] Weber, K., Bartsch, U., Stocking, C., Fehse, B., 2008. A multicolor panel of novel lentiviral "gene ontology" (LeGO) vectors for functional gene analysis. Mol. Ther., 2008, **16**, 698–706.

[619] Tate, J.G., Bamford, S., Jubb, H.C., Sondka, Z., et al., 2019. COSMIC: The Catalogue Of Somatic Mutations In Cancer. Nucleic Acids Res., 2019, **47**, D941–D947.

[620] Bartha, Á., Győrffy, B., 2020. TNMplot.com: a web tool for the comparison of gene expression in normal, tumor and metastatic tissues. BioRxiv, 2020, 2020.11.10.376228.

[621] Chandrashekar, D.S., Bashel, B., Balasubramanya, S.A.H., Creighton, C.J., et al., 2017. UALCAN: A Portal for Facilitating Tumor Subgroup Gene Expression and Survival Analyses. Neoplasia (United States), 2017, **19**, 649–658.

[622] Shinawi, T., Hill, V.K., Krex, D., Schackert, G., et al., 2013. DNA methylation profiles of long- and short-term glioblastoma survivors. Epigenetics, 2013, **8**, 149–156.

[623] Men, C., Chai, H., Song, X., Li, Y., et al., 2017. Identification of DNA methylation associated gene signatures in endometrial cancer via integrated analysis of dna methylation and gene expression systematically. J. Gynecol. Oncol., 2017, **28**, 1–13.

[624] Edmondson, R., Broglie, J.J., Adcock, A.F., Yang, L., 2014. Three-dimensional cell culture systems and their applications in drug discovery and cell-based biosensors. Assay Drug Dev. Technol., 2014, **12**, 207–218.

[625] Fukushima, N., Ishii, I., Contos, J.J., Weiner, J.A., Chun, J., 2001. Lysophospholipid receptors. Annu. Rev. Pharmacol. Toxicol., 2001, **41**, 507–534.

[626] Ishii, I., Fukushima, N., Ye, X., Chun, J., 2004. Lysophospholipid receptors: signaling and biology. Annu. Rev. Biochem., 2004, **73**, 321–54.

[627] Choi, J.W., Herr, D.R., Noguchi, K., Yung, Y.C., et al., 2010. LPA receptors: subtypes and biological actions. Annu. Rev. Pharmacol. Toxicol., 2010, **50**, 157–86.

[628] van Meeteren, L.A., Ruurs, P., Stortelers, C., Bouwman, P., et al., 2006. Autotaxin, a Secreted Lysophospholipase D, Is Essential for Blood Vessel Formation during Development. Mol. Cell. Biol., 2006, **26**, 5015–5022.

[629] Tanaka, M., Okudaira, S., Kishi, Y., Ohkawa, R., et al., 2006. Autotaxin Stabilizes Blood Vessels and Is Required for Embryonic Vasculature by Producing Lysophosphatidic Acid. J. Biol. Chem., 2006, **281**, 25822–25830.

[630] Lappano, R., Maggiolini, M., 2011. G protein-coupled receptors: novel targets for drug discovery in cancer. Nat. Rev. Drug Discov., 2011, **10**, 47–60.

[631] N.d. Pamgene - Pamgene n.d.

[632] Reinhardt, H.C., Yaffe, M.B., 2009. Kinases that control the cell cycle in response to DNA damage: Chk1, Chk2, and MK2. Curr. Opin. Cell Biol., 2009, **21**, 245–255.

[633] Kang, J.-H., 2014. Protein Kinase C (PKC) Isozymes and Cancer. New J. Sci., 2014, **2014**, 1–36.

[634] Gorin, M.A., Pan, Q., 2009. Protein kinase Cε: An oncogene and emerging tumor biomarker. Mol. Cancer, 2009, **8**, 9.

[635] Cenni, V., Döppler, H., Sonnenburg, E.D., Maraldi, N., et al., 2002. Regulation of novel protein kinase C ε by phosphorylation. Biochem. J., 2002, **363**, 537–545.

[636] Xu, T.R., He, G., Dobson, K., England, K., Rumsby, M., 2007. Phosphorylation at Ser729 specifies a Golgi localisation for protein kinase C epsilon (PKCε) in 3T3 fibroblasts. Cell. Signal., 2007, **19**, 1986–1995.

[637] Totoń, E., Ignatowicz, E., Skrzeczkowska, K., Rybczyńska, M., 2011. Protein kinase Ce as a cancer marker and target for anticancer therapy.

[638] Browning, D.D., Kwon, I.K., Wang, R., 2010. CGMP-dependent protein kinases as potential targets for colon cancer prevention and treatment. Future Med. Chem., 2010, **2**, 65–80.

[639] Rappaport, J.A., Waldman, S.A., 2018. The guanylate cyclase C-cGMP signaling axis opposes intestinal epithelial injury and neoplasia. Front. Oncol., 2018, **8**.

[640] Li, N., Lee, K., Xi, Y., Zhu, B., et al., 2015. Phosphodiesterase 10A: A novel target for selective inhibition of colon tumor cell growth and β-catenin-dependent TCF transcriptional activity. Oncogene, 2015, **34**, 1499–1509.

[641] Lee, K., Piazza, G.A., 2017. The interaction between the Wnt/β-catenin signaling cascade and PKG activation in cancer. J. Biomed. Res., 2017, **31**, 189–196.

[642] Lin, S., Wang, J., Wang, L., Wen, J., et al., 2017. Phosphodiesterase-5 inhibition suppresses colonic inflammation-induced tumorigenesis via

blocking the recruitment of MDSC. Am. J. Cancer Res., 2017, **7**, 41–52.
[643] Whitt, J.D., Li, N., Tinsley, H.N., Chen, X., et al., 2012. A novel sulindac derivative that potently suppresses colon tumor cell growth by inhibiting cGMP phosphodiesterase and β-catenin transcriptional activity. Cancer Prev. Res., 2012, **5**, 822–833.
[644] Basu, N., Bhandari, R., Natarajan, V.T., Visweswariah, S.S., 2009. Cross Talk between Receptor Guanylyl Cyclase C and c-src Tyrosine Kinase Regulates Colon Cancer Cell Cytostasis. Mol. Cell. Biol., 2009, **29**, 5277–5289.
[645] Danaee, H., Kalebic, T., Wyant, T., Fassan, M., et al., 2017. Consistent expression of guanylyl cyclase-C in primary and metastatic gastrointestinal cancers. PLoS One, 2017, **12**.
[646] Zhang, L., Zhou, W., Velculescu, V.E., Kern, S.E., et al., 1997. Gene expression profiles in normal and cancer cells. Science (80-.)., 1997, **276**, 1268–1272.
[647] Cohen, M., Hawkins, J., Witte, D., 1998. Guanylin mRNA expression in human intestine and colorectal adenocarcinoma. Lab Invest, 1998, **78**, 101–8.
[648] Shailubhai, K., Yu, H., Karunanandaa, K., Wang, J., et al., 2000. Uroguanylin treatment suppresses polyp formation in the Apc(Min/+) mouse and induces apoptosis in human colon adenocarcinoma cells via cyclic GMP. Cancer Res., 2000, **60**, 5151–7.
[649] Steinbrecher, K.A., Tuohy, T.M.F., Heppner Goss, K., Scott, M.C., et al., 2000. Expression of guanylin is downregulated in mouse and human intestinal adenomas. Biochem. Biophys. Res. Commun., 2000, **273**, 225–230.
[650] Wilson, C., Lin, J.E., Li, P., Snook, A.E., et al., 2014. The paracrine hormone for the GUCY2C tumor suppressor, guanylin, is universally lost in colorectal cancer. Cancer Epidemiol. Biomarkers Prev., 2014, **23**, 2328–2337.
[651] Cagir, B., Gelmann, A., Park, J., Fava, T., et al., 1999. Guanylyl cyclase C messenger RNA is a biomarker for recurrent stage II colorectal cancer. Ann. Intern. Med., 1999, **131**, 805–812.
[652] Carrithers, S.L., Barber, M.T., Biswas, S., Parkinson, S.J., et al., 1996. Guanylyl cyclase C is a selective marker for metastatic colorectal tumors in human extraintestinal tissues. Proc. Natl. Acad. Sci. U. S. A., 1996, **93**, 14827–14832.
[653] Litchfield, D.W., 2003. Protein kinase CK2: Structure, regulation and role in cellular decisions of life and death. Biochem. J., 2003, **369**, 1–15.
[654] Olsten, M.E.K., Litchfield, D.W., 2004. *Biochem. Cell Biol.*, vol. 82, Biochem Cell Biol, pp. 681–693.
[655] Faust, R.A., Tawfic, S., Davis, A.T., Bubash, L.A., Ahmed, K., 2000. Antisense oligonucleotides against protein kinase CK2-α inhibit growth of squamous cell carcinoma of the head and neck in vitro. Head Neck, 2000, **22**, 341–346.
[656] Stalter, G., Siemer, S., Becht, E., Ziegler, M., et al., 1994. Asymmetric expression of protein kinase CK2 subunits in human kidney tumors. Biochem. Biophys. Res. Commun., 1994, **202**, 141–147.
[657] Landesman-Bollag, E., Romieu-Mourez, R., Song, D.H., Sonenshein, G.E., et al., 2001. Protein kinase CK2 in mammary gland tumorigenesis. Oncogene, 2001, **20**, 3247–3257.
[658] Daya-Makin, M., Sanghera, J.S., Mogentale, T.L., Lipp, M., et al., 1994. Activation of a Tumor-associated Protein Kinase (p40TAK) and Casein Kinase 2 in Human Squamous Cell Carcinomas and Adenocarcinomas of the Lung. Cancer Res., 1994, **54**.
[659] Yenice, S., Davis, A.T., Goueli, S.A., Akdas, A., et al., 1994. Nuclear casein kinase 2 (CK-2) activity in human normal, benign hyperplastic, and cancerous prostate. Prostate, 1994, **24**, 11–16.
[660] Seldin, D.C., Leder, P., 1995. Casein kinase IIα transgene-induced murine lymphoma: Relation to theileriosis in cattle. Science (80-.)., 1995, **267**, 894–897.
[661] Kelliher, M.A., Seldin, D.C., Leder, P., 1996. Tal-1 induces T cell acute lymphoblastic leukemia accelerated by casein kinase IIα. EMBO J., 1996, **15**, 5160–5166.
[662] Landesman-Bollag, E. Channavajhala, P., Cardiff, R., 1998. p53 deficiency and misexpression of protein kinase CK2α collaborate in the development of thymic lymphomas in mice. Oncogene, 1998, **16**, 2965–2974.
[663] Scaglioni, P.P., Yung, T.M., Cai, L.F., Erdjument-Bromage, H., et al., 2006. A CK2-Dependent Mechanism for Degradation of the PML Tumor Suppressor. Cell, 2006, **126**, 269–283.
[664] Torres, J., Pulido, R., 2001. The tumor suppressor PTEN is phosphorylated by the protein kinase CK2 at its C terminus. Implications for PTEN stability to proteasome-mediated degradation. J. Biol. Chem., 2001, **276**, 993–998.
[665] Keller, D.M., Lu, H., 2002. p53 serine 392 phosphorylation increases after UV through induction of the assembly of the CK2·hSPT16·SSRP1 complex. J. Biol. Chem., 2002, **277**, 50206–50213.
[666] Channavajhala, P., Seldin, D.C., 2002. Functional interaction of protein kinase CK2 and c-Myc in lymphomagenesis. Oncogene, 2002, **21**, 5280–5288.
[667] Oelgeschläger, M., Krieg, J., Lüscher-Firzlaff, J.M., Lüscher, B., 1995. Casein kinase II phosphorylation site mutations in c-Myb affect DNA binding and transcriptional cooperativity with NF-M. Mol. Cell. Biol., 1995, **15**, 5966–5974.
[668] Lin, A., Frost, J., Deng, T., Smeal, T., et al., 1992. Casein kinase II is a negative regulator of c-Jun DNA binding and AP-1 activity. Cell, 1992, **70**, 777–789.
[669] Eddy, S.F., Guo, S., Demicco, E.G., Romieu-Mourez, R., et al., 2005. Inducible IκB kinase/IκB kinase ε expression is induced by CK2 and promotes aberrant nuclear factor-κB activation in breast cancer cells. Cancer Res., 2005, **65**, 11375–11383.
[670] Dessauge, F., Lizundia, R., Langsley, G., 2005. *Parasitology*, vol. 130, Cambridge University Press, pp. S37–S44.
[671] Seldin, D.C., Landesman-Bollag, E., Farago, M., Currier, N., et al., 2005. CK2 as a positive regulator of Wnt signalling and tumourigenesis. Mol. Cell. Biochem., 2005, **274**, 63–67.
[672] Bousset, K., Henriksson, M., Lüscher-Firzlaff, J., Litchfield, D., Lüscher, B., 1993. Identification of casein kinase II phosphorylation sites in Max: effects on DNA-binding kinetics of Max homo- and Myc/Max heterodimers. Oncogene, 1993, **8**, 3211–20.
[673] Romieu-Mourez, R., Landesman-Bollag, E., Seldin, D., Sonenshein, G., 2002. Protein kinase CK2 promotes aberrant activation of nuclear factor-kappaB, transformed phenotype, and survival of breast cancer cells. Cancer Res., 2002, **62**, 6770–8.
[674] Di Maira, G., Salvi, M., Arrigoni, G., Marin, O., et al., 2005. Protein kinase CK2 phosphorylates and upregulates Akt/PKB. Cell Death Differ., 2005, **12**, 668–677.
[675] Tözsér, J., Bagossi, P., Zahuczky, G., Specht, S.I., et al., 2003. Effect of caspase cleavage-site phosphorylation on proteolysis. Biochem. J., 2003, **372**, 137–143.
[676] Izeradjene, K., Douglas, L., Delaney, A., Houghton, J.A., 2005. Casein kinase II (CK2) enhances death-inducing signaling complex (DISC) activity in TRAIL-induced apoptosis in human colon carcinoma cell lines. Oncogene, 2005, **24**, 2050–2058.
[677] Izeradjene, K., Douglas, L., Delaney, A., Houghton, J.A., 2004. Influence of casein kinase II in tumor necrosis factor-related apoptosis-inducing ligand-induced apoptosis in human rhabdomyosarcoma cells. Clin. Cancer Res., 2004, **10**, 6650–6660.
[678] Yamane, K., Kinsella, T.J., 2005. Casein kinase 2 regulates both apoptosis and the cell cycle following DNA damage induced by 6-thioguanine. Clin. Cancer Res., 2005, **11**, 2355–2363.
[679] Yamane, K., Kinsella, T.J., 2005. CK2 inhibits apoptosis and changes its cellular localization following ionizing radiation. Cancer Res., 2005, **65**, 4362–4367.
[680] Hardie, D.G., Ross, F.A., Hawley, S.A., 2012. AMPK: A nutrient and energy sensor that maintains energy homeostasis. Nat. Rev. Mol. Cell Biol., 2012, **13**, 251–262.
[681] Lin, S.C., Hardie, D.G., 2018. AMPK: Sensing Glucose as well as Cellular Energy Status. Cell Metab., 2018, **27**, 299–313.
[682] Ross, F.A., MacKintosh, C., Hardie, D.G., 2016. AMP-activated protein kinase: a cellular energy sensor that comes in 12 flavours. FEBS J., 2016, 2987–3001.

[683] Vara-Ciruelos, D., Russell, F.M., Grahame Hardie, D., 2019. The strange case of AMPK and cancer: Dr Jekyll or Mr Hyde? Open Biol., 2019, **9**.

[684] Hardie, D.G., Hawley, S.A., 2001. AMP-activated protein kinase: The energy charge hypothesis revisited. BioEssays, 2001, **23**, 1112–1119.

[685] Chen, L., Jiao, Z.H., Zheng, L.S., Zhang, Y.Y., et al., 2009. Structural insight into the autoinhibition mechanism of AMP-activated protein kinase. Nature, 2009, **459**, 1146–1149.

[686] Xin, F.J., Wang, J., Zhao, R.Q., Wang, Z.X., Wu, J.W., 2013. Coordinated regulation of AMPK activity by multiple elements in the α-subunit. Cell Res., 2013, **23**, 1237–1240.

[687] Hawley, S.A., Selbert, M.A., Goldstein, E.G., Edelman, A.M., et al., 1995. 5'-AMP activates the AMP-activated protein kinase cascade, and Ca2+/calmodulin activates the calmodulin-dependent protein kinase I cascade, via three independent mechanisms. J. Biol. Chem., 1995, **270**, 27186–27191.

[688] Ross, F.A., Jensen, T.E., Hardie, D.G., 2016. Differential regulation by AMP and ADP of AMPK complexes containing different γ subunit isoforms. Biochem. J., 2016, **473**, 189–199.

[689] Davies, S.P., Helps, N.R., Cohen, P.T.W., Hardie, D.G., 1995. 5'-AMP inhibits dephosphorylation, as well as promoting phosphorylation, of the AMP-activated protein kinase. Studies using bacterially expressed human protein phosphatase-2Cα and native bovine protein phosphatase-2Ac. FEBS Lett., 1995, **377**, 421–425.

[690] Hawley, S.A., Pan, D.A., Mustard, K.J., Ross, L., et al., 2005. Calmodulin-dependent protein kinase kinase-β is an alternative upstream kinase for AMP-activated protein kinase. Cell Metab., 2005, **2**, 9–19.

[691] Woods, A., Dickerson, K., Heath, R., Hong, S.P., et al., 2005. Ca2+/calmodulin-dependent protein kinase kinase-β acts upstream of AMP-activated protein kinase in mammalian cells. Cell Metab., 2005, **2**, 21–33.

[692] Hurley, R.L., Anderson, K.A., Franzone, J.M., Kemp, B.E., et al., 2005. The Ca2+/calmodulin-dependent protein kinase kinases are AMP-activated protein kinase kinases. J. Biol. Chem., 2005, **280**, 29060–29066.

[693] Zhang, C.S., Hawley, S.A., Zong, Y., Li, M., et al., 2017. Fructose-1,6-bisphosphate and aldolase mediate glucose sensing by AMPK. Nature, 2017, **548**, 112–116.

[694] Pehmøller, C., Treebak, J.T., Birk, J.B., Chen, S., et al., 2009. Genetic disruption of AMPK signaling abolishes both contraction- and insulin-stimulated TBC1D1 phosphorylation and 14-3-3 binding in mouse skeletal muscle. Am. J. Physiol. - Endocrinol. Metab., 2009, **297**.

[695] McGee, S.L., Van Denderen, B.J.W., Howlett, K.F., Mollica, J., et al., 2008. AMP-activated protein kinase regulates GLUT4 transcription by phosphorylating histone deacetylase 5. Diabetes, 2008, **57**, 860–867.

[696] Mihaylova, M.M., Vasquez, D.S., Ravnskjaer, K., Denechaud, P.D., et al., 2011. Class IIa histone deacetylases are hormone-activated regulators of FOXO and mammalian glucose homeostasis. Cell, 2011, **145**, 607–621.

[697] Barnes, K., Ingram, J.C., Porras, O.H., Barros, L.F., et al., 2002. Activation of GLUT1 by metabolic and osmotic stress: potential involvement of AMP-activated protein kinase (AMPK). J. Cell Sci., 2002, **115**, 2433 LP – 2442.

[698] Wu, N., Zheng, B., Shaywitz, A., Dagon, Y., et al., 2013. AMPK-Dependent Degradation of TXNIP upon Energy Stress Leads to Enhanced Glucose Uptake via GLUT1. Mol. Cell, 2013, **49**, 1167–1175.

[699] Rider, M.H., Bertrand, L., Vertommen, D., Michels, P.A., et al., 2004. 6-Phosphofructo-2-kinase/fructose-2,6-bisphosphatase: Head-to-head with a bifunctional enzyme that controls glycolysis. Biochem. J., 2004, **381**, 561–579.

[700] Marsin, A.S., Bouzin, C., Bertrand, L., Hue, L., 2002. The stimulation of glycolysis by hypoxia in activated monocytes is mediated by AMP-activated protein kinase and inducible 6-phosphofructo-2-kinase. J. Biol. Chem., 2002, **277**, 30778–30783.

[701] Marsin, A.S., Bertrand, L., Rider, M.H., Deprez, J., et al., 2000. Phosphorylation and activation of heart PFK-2 by AMPK has a role in the stimulation of glycolysis during ischaemia. Curr. Biol., 2000, **10**, 1247–1255.

[702] Merrill, G.F., Kurth, E.J., Hardie, D.G., Winder, W.W., 1997. AICA riboside increases AMP-activated protein kinase, fatty acid oxidation, and glucose uptake in rat muscle. Am. J. Physiol. - Endocrinol. Metab., 1997, **273**.

[703] Zong, H., Ren, J.M., Young, L.H., Pypaert, M., et al., 2002. AMP kinase is required for mitochondrial biogenesis in skeletal muscle in response to chronic energy deprivation. Proc. Natl. Acad. Sci. U. S. A., 2002, **99**, 15983–15987.

[704] Cantó, C., Gerhart-Hines, Z., Feige, J.N., Lagouge, M., et al., 2009. AMPK regulates energy expenditure by modulating NAD + metabolism and SIRT1 activity. Nature, 2009, **458**, 1056–1060.

[705] Egan, D.F., Shackelford, D.B., Mihaylova, M.M., Gelino, S., et al., 2011. Phosphorylation of ULK1 (hATG1) by AMP-activated protein kinase connects energy sensing to mitophagy. Science (80-.)., 2011, **331**, 456–461.

[706] Kim, J., Kundu, M., Viollet, B., Guan, K.L., 2011. AMPK and mTOR regulate autophagy through direct phosphorylation of Ulk1. Nat. Cell Biol., 2011, **13**, 132–141.

[707] Shiloh, R., Gilad, Y., Ber, Y., Eisenstein, M., et al., 2018. Non-canonical activation of DAPK2 by AMPK constitutes a new pathway linking metabolic stress to autophagy. Nat. Commun., 2018, **9**.

[708] Hardie, D.G., 2018. Keeping the home fires burning † : AMP-activated protein kinase. J. R. Soc. Interface, 2018, **15**.

[709] Toyama, E.Q., Herzig, S., Courchet, J., Lewis, T.L., et al., 2016. Metabolism: AMP-activated protein kinase mediates mitochondrial fission in response to energy stress. Science (80-.)., 2016, **351**, 275–281.

[710] Lantier, L., Fentz, J., Mounier, R., Leclerc, J., et al., 2014. AMPK controls exercise endurance, mitochondrial oxidative capacity, and skeletal muscle integrity. FASEB J., 2014, **28**, 3211–3224.

[711] O'Neill, H.M., Maarbjerg, S.J., Crane, J.D., Jeppesen, J., et al., 2011. AMP-activated protein kinase (AMPK) β1β2 muscle null mice reveal an essential role for AMPK in maintaining mitochondrial content and glucose uptake during exercise. Proc. Natl. Acad. Sci. U. S. A., 2011, **108**, 16092–16097.

[712] Carling, D., Zammit, V.A., Hardie, D.G., 1987. A common bicyclic protein kinase cascade inactivates the regulatory enzymes of fatty acid and cholesterol biosynthesis. FEBS Lett., 1987, **223**, 217–222.

[713] Grahame Hardie, D., Carling, D., T.R. Sim, A., 1989. The AMP-activated protein kinase: a multisubstrate regulator of lipid metabolism. Trends Biochem. Sci., 1989, **14**, 20–23.

[714] Li, Y., Xu, S., Mihaylova, M.M., Zheng, B., et al., 2011. AMPK phosphorylates and inhibits SREBP activity to attenuate hepatic steatosis and atherosclerosis in diet-induced insulin-resistant mice. Cell Metab., 2011, **13**, 376–388.

[715] Kawaguchi, T., Osatomi, K., Yamashita, H., Kabashima, T., Uyeda, K., 2002. Mechanism for fatty acid "sparing" effect on glucose-induced transcription: Regulation of carbohydrate-responsive element-binding protein by AMP-activated protein kinase. J. Biol. Chem., 2002, **277**, 3829–3835.

[716] Bultot, L., Guigas, B., Von Wilamowitz-Moellendorff, A., Maisin, L., et al., 2012. AMP-activated protein kinase phosphorylates and inactivates liver glycogen synthase. Biochem. J., 2012, **443**, 193–203.

[717] Jørgensen, S.B., Nielsen, J.N., Birk, J.B., Olsen, G.S., et al., 2004. The α2-5' AMP-activated protein kinase is a site 2 glycogen synthase kinase in skeletal muscle and is responsive to glucose loading. Diabetes, 2004, **53**, 3074–3081.

[718] Saxton, R.A., Sabatini, D.M., 2017. mTOR Signaling in Growth, Metabolism, and Disease. Cell, 2017, **168**, 960–976.

[719] Qian, X., Li, X., Tan, L., Lee, J.H., et al., 2018. Conversion of prps hexamer to monomer by AMPK-mediated phosphorylation inhibits nucleotide synthesis in response to energy stress. Cancer Discov., 2018, **8**, 94–107.

[720] Wang, X., Li, W., Williams, M., Terada, N., et al., 2001. Regulation of elongation factor 2 kinase by p90RSK1 and p70 S6 kinase. EMBO J., 2001, **20**, 4370–4379.

[721] Browne, G.J., Proud, C.G., 2004. A Novel mTOR-Regulated Phosphorylation Site in Elongation Factor 2 Kinase Modulates the Activity of the

Kinase and Its Binding to Calmodulin. Mol. Cell. Biol., 2004, **24**, 2986–2997.
[722] Jones, R.G., Plas, D.R., Kubek, S., Buzzai, M., et al., 2005. AMP-activated protein kinase induces a p53-dependent metabolic checkpoint. Mol. Cell, 2005, **18**, 283–293.
[723] Imamura, K., Ogura, T., Kishimoto, A., Kaminishi, M., Esumi, H., 2001. Cell cycle regulation via p53 phosphorylation by a 5'-AMP activated protein kinase activator, 5-aminoimidazole-4-carboxamide-1-β-D-ribofuranoside, in a human hepatocellular carcinoma cell line. Biochem. Biophys. Res. Commun., 2001, **287**, 562–567.
[724] Viollet, B., Athea, Y., Mounier, R., Guigas, B., et al., 2009. AMPK: Lessons from transgenic and knockout animals. Front. Biosci., 2009, **14**, 19–44.
[725] Rolf, J., Zarrouk, M., Finlay, D.K., Foretz, M., et al., 2013. AMPKα1: A glucose sensor that controls CD8 T-cell memory. Eur. J. Immunol., 2013, **43**, 889–896.
[726] Adams, J.M., Harris, A.W., Pinkert, C.A., Corcoran, L.M., et al., 1985. The c-myc oncogene driven by immunoglobulin enhancers induces lymphoid malignancy in transgenic mice. Nature, 1985, **318**, 533–538.
[727] Vara-Ciruelos, D., Dandapani, M., Russell, F.M., Grzes, K.M., et al., 2019. Phenformin, But Not Metformin, Delays Development of T Cell Acute Lymphoblastic Leukemia/Lymphoma via Cell-Autonomous AMPK Activation. Cell Rep., 2019, **27**, 690-698.e4.
[728] Pineda, C.T., Ramanathan, S., Fon Tacer, K., Weon, J.L., et al., 2015. Degradation of AMPK by a cancer-specific ubiquitin ligase. Cell, 2015, **160**, 715–728.
[729] Vila, I.K., Yao, Y., Kim, G., Xia, W., et al., 2017. A UBE2O-AMPKα2 Axis that Promotes Tumor Initiation and Progression Offers Opportunities for Therapy. Cancer Cell, 2017, **31**, 208–224.
[730] Kishton, R.J., Barnes, C.E., Nichols, A.G., Cohen, S., et al., 2016. AMPK Is Essential to Balance Glycolysis and Mitochondrial Metabolism to Control T-ALL Cell Stress and Survival. Cell Metab., 2016, **23**, 649–662.
[731] Saito, Y., Chapple, R.H., Lin, A., Kitano, A., Nakada, D., 2015. AMPK Protects Leukemia-Initiating Cells in Myeloid Leukemias from Metabolic Stress in the Bone Marrow. Cell Stem Cell, 2015, **17**, 585–596.
[732] Jeon, S.M., Chandel, N.S., Hay, N., 2012. AMPK regulates NADPH homeostasis to promote tumour cell survival during energy stress. Nature, 2012, **485**, 661–665.
[733] Liu, L., Ulbrich, J., Müller, J., Wüstefeld, T., et al., 2012. Deregulated MYC expression induces dependence upon AMPK-related kinase 5. Nature, 2012, **483**, 608–612.
[734] Shackelford, D.B., Abt, E., Gerken, L., Vasquez, D.S., et al., 2013. LKB1 Inactivation Dictates Therapeutic Response of Non-Small Cell Lung Cancer to the Metabolism Drug Phenformin. Cancer Cell, 2013, **23**, 143–158.
[735] Eichner, L.J., Brun, S.N., Herzig, S., Young, N.P., et al., 2019. Genetic Analysis Reveals AMPK Is Required to Support Tumor Growth in Murine Kras-Dependent Lung Cancer Models. Cell Metab., 2019, **29**, 285-302.e7.
[736] Shu, F., Lv, S., Qin, Y., Ma, X., et al., 2007. Functional characterization of human PFTK1 as a cyclin-dependent kinase. Proc. Natl. Acad. Sci. U. S. A., 2007, **104**, 9248–9253.
[737] Jiang, M., Gao, Y., Yang, T., Zhu, X., Chen, J., 2009. Cyclin Y, a novel membrane-associated cyclin, interacts with PFTK1. FEBS Lett., 2009, **583**, 2171–2178.
[738] Li, S., Jiang, M., Wang, W., Chen, J., 2014. 14-3-3 Binding to Cyclin y contributes to cyclin Y/CDK14 association. Acta Biochim. Biophys. Sin. (Shanghai)., 2014, **46**, 299–304.
[739] Li, S., Song, W., Jiang, M., Zeng, L., et al., 2014. Phosphorylation of cyclin y by CDK14 induces its ubiquitination and degradation. FEBS Lett., 2014, **588**, 1989–1996.
[740] Yang, T., Chen, J.Y., 2001. Identification and cellular localization of human PFTAIRE1. Gene, 2001, **267**, 165–172.
[741] Wang, X., Jia, Y., Fei, C., Song, X., Li, L., 2016. Activation/proliferation-associated protein 2 (Caprin-2) positively regulates CDK14/cyclin Y-mediated lipoprotein. J. Biol. Chem., 2016, **291**, 26427–26434.
[742] Davidson, G., Shen, J., Huang, Y.L., Su, Y., et al., 2009. Cell Cycle Control of Wnt Receptor Activation. Dev. Cell, 2009, **17**, 788–799.
[743] Leung, W.K.C., Ching, A.K.K., Wong, N., 2011. Phosphorylation of Caldesmon by PFTAIRE1 kinase promotes actin binding and formation of stress fibers. Mol. Cell. Biochem., 2011, **350**, 201–206.
[744] Leung, W.K.C., Ching, A.K.K., Chan, A.W.H., Poon, T.C.W., et al., 2011. A novel interplay between oncogenic PFTK1 protein kinase and tumor suppressor TAGLN2 in the control of liver cancer cell motility. Oncogene, 2011, **30**, 4464–4475.
[745] Liu, M.H., Shi, S.M., Li, K., Chen, E.Q., 2016. Knockdown of PFTK1 expression by RNAi inhibits the proliferation and invasion of human non-small lung adenocarcinoma cells. Oncol. Res., 2016, **24**, 181–187.
[746] Gu, X., Wang, Y., Wang, H., Ni, Q., et al., 2015. Upregulated PFTK1 promotes tumor cell proliferation, migration, and invasion in breast cancer. Med. Oncol., 2015, **32**.
[747] Yang, L., Zhu, J., Huang, H., Yang, Q., et al., 2015. PFTK1 promotes gastric cancer progression by regulating proliferation, migration and invasion. PLoS One, 2015, **10**.
[748] Zhang, W., Liu, R., Tang, C., Xi, Q., et al., 2016. PFTK1 regulates cell proliferation, migration and invasion in epithelial ovarian cancer. Int. J. Biol. Macromol., 2016, **85**, 405–416.
[749] Cao, L., Zhou, J., Zhang, J., Wu, S., et al., 2015. Cyclin-dependent kinase 5 decreases in gastric cancer and its nuclear accumulation suppresses gastric tumorigenesis. Clin. Cancer Res., 2015, **21**, 1419–1428.
[750] Zhu, J., Liu, C., Liu, F., Wang, Y., Zhu, M., 2016. Knockdown of PFTAIRE protein kinase 1 (PFTK1) inhibits proliferation, invasion, and EMT in colon cancer cells. Oncol. Res., 2016, **24**, 137–144.
[751] Mao, Y., Jia, Y., Zhu, H., Wang, W., et al., 2017. High expression of PFTK1 in cancer cells predicts poor prognosis in colorectal cancer. Mol. Med. Rep., 2017, **16**, 224–230.
[752] Tu, J., Zhao, Z., Xu, M., Chen, M., et al., 2019. LINC00707 contributes to hepatocellular carcinoma progression via sponging miR-206 to increase CDK14. J. Cell. Physiol., 2019, **234**, 10615–10624.
[753] Li, Q., Zhou, L., Wang, M., Wang, N., et al., 2018. MicroRNA-613 impedes the proliferation and invasion of glioma cells by targeting cyclin-dependent kinase 14. Biomed. Pharmacother., 2018, **98**, 636–642.
[754] Li, Y., Zhai, Y., Song, Q., Zhang, H., et al., 2018. Genome-Wide association study identifies a new locus at 7q21.13 associated with hepatitis b virus–Related hepatocellular carcinoma. Clin. Cancer Res., 2018, **24**, 906–915.
[755] Zhen, Y., Nan, Y., Guo, S., Zhang, L., et al., 2019. Knockdown of NEAT1 repressed the malignant progression of glioma through sponging miR-107 and inhibiting CDK14. J. Cell. Physiol., 2019, **234**, 10671–10679.
[756] Sun, Y., Zhu, Q., Yang, W., Shan, Y., et al., 2019. LncRNA H19/miR-194/PFTK1 axis modulates the cell proliferation and migration of pancreatic cancer. J. Cell. Biochem., 2019, **120**, 3874–3886.
[757] Yang, J., Zhu, H., Jin, Y., Song, Y., 2018. MiR-431 inhibits cell proliferation and induces cell apoptosis by targeting CDK14 in pancreatic cancer. Eur. Rev. Med. Pharmacol. Sci., 2018, **22**, 4493–4499.
[758] Ji, Q., Xu, X., Li, L., Goodman, S.B., et al., 2017. miR-216a inhibits osteosarcoma cell proliferation, invasion and metastasis by targeting CDK14. Cell Death Dis., 2017, **8**, e3103–e3103.
[759] Gu, Z., Hou, Z., Zheng, L., Wang, X., et al., 2018. Long noncoding RNA LINC00858 promotes osteosarcoma through regulating miR-139-CDK14 axis. Biochem. Biophys. Res. Commun., 2018, **503**, 1134–1140.
[760] Dai, J., Xu, L., Hu, X., Han, G., et al., 2018. Long noncoding RNA OIP5-AS1 accelerates CDK14 expression to promote osteosarcoma tumorigenesis via targeting miR-223. Biomed. Pharmacother., 2018, **106**, 1441–1447.

[761] Li, J., Shao, W., Feng, H., 2019. MiR-542-3p, a microRNA targeting CDK14, suppresses cell proliferation, invasiveness, and tumorigenesis of epithelial ovarian cancer. Biomed. Pharmacother., 2019, **110**, 850–856.

[762] Jin, B., Jin, H., Wu, H.B., Xu, J.J., Li, B., 2018. Long non-coding RNA SNHG15 promotes CDK14 expression via miR-486 to accelerate non-small cell lung cancer cells progression and metastasis. J. Cell. Physiol., 2018, **233**, 7164–7172.

[763] Imawari, Y., Mimoto, R., Hirooka, S., Morikawa, T., et al., 2018. Downregulation of dual-specificity tyrosine-regulated kinase 2 promotes tumor cell proliferation and invasion by enhancing cyclin-dependent kinase 14 expression in breast cancer. Cancer Sci., 2018, **109**, 363–372.

[764] Yu, S., Sun, L., Jiao, Y., Lee, L.T.O., 2018. The role of G protein-coupled receptor kinases in cancer. Int. J. Biol. Sci., 2018, **14**, 189–203.

[765] Brenninkmeijer, C.B.A.P., Price, S.A., López Bernal, A., Phaneuf, S., 1999. Expression of G-protein-coupled receptor kinases in pregnant term and non-pregnant human myometrium. J. Endocrinol., 1999, **162**, 401–408.

[766] Chen, K., Fu, C., Chen, C., Liu, L., et al., 2014. Role of GRK4 in the regulation of arterial AT1 receptor in hypertension. Hypertension, 2014, **63**, 289–296.

[767] Villar, V.A.M., Jones, J.E., Armando, I., Palmes-Saloma, C., et al., 2009. G protein-coupled receptor kinase 4 (GRK4) regulates the phosphorylation and function of the dopamine D3 receptor. J. Biol. Chem., 2009, **284**, 21425–21434.

[768] King, D.W., Steinmetz, R., Wagoner, H.A., Hannon, T.S., et al., 2003. Differential Expression of GRK Isoforms in Nonmalignant and Malignant Human Granulosa Cells. Endocrine, 2003, **22**, 135–141.

[769] McCoy, C.E., Macdonald, A., Morrice, N.A., Campbell, D.G., et al., 2007. Identification of novel phosphorylation sites in MSK1 by precursor ion scanning MS. Biochem. J., 2007, **402**, 491–501.

[770] Reyskens, K.M.S.E., Arthur, J.S.C., 2016. Emerging roles of the mitogen and stress activated kinases MSK1 and MSK2. Front. Cell Dev. Biol., 2016, **4**, 56.

[771] Gaertner, T.R., Kolodziej, S.J., Wang, D., Kobayashi, R., et al., 2004. Comparative Analyses of the Three-dimensional Structures and Enzymatic Properties of α, β, γ, and δ Isoforms of Ca 2+-Calmodulin-dependent Protein Kinase II. J. Biol. Chem., 2004, **279**, 12484–12494.

[772] Lisman, J., Yasuda, R., Raghavachari, S., 2012. Mechanisms of CaMKII action in long-term potentiation. Nat. Rev. Neurosci., 2012, **13**, 169–182.

[773] Rokita, A.G., Anderson, M.E., 2012. New therapeutic targets in cardiology: Arrhythmias and Ca2+/calmodulin- dependent kinase II (CaMKII). Circulation, 2012, **126**, 2125–2139.

[774] Meyer, T., Hanson, P.I., Stryer, L., Schulman, H., 1992. Calmodulin trapping by calcium-calmodulin-dependent protein kinase. Science (80-.)., 1992, **256**, 1199–1202.

[775] Erickson, J.R., Joiner, M. ling A., Guan, X., Kutschke, W., et al., 2008. A Dynamic Pathway for Calcium-Independent Activation of CaMKII by Methionine Oxidation. Cell, 2008, **133**, 462–474.

[776] Gutierrez, D.A., Fernandez-Tenorio, M., Ogrodnik, J., Niggli, E., 2013. NO-dependent Ca MKII activation during β-adrenergic stimulation of cardiac muscle. Cardiovasc. Res., 2013, **100**, 392–401.

[777] Orrenius, S., Zhivotovsky, B., Nicotera, P., 2003. Regulation of cell death: The calcium-apoptosis link. Nat. Rev. Mol. Cell Biol., 2003, **4**, 552–565.

[778] Nowycky, M.C., Thomas, A.P., 2002. Intracellular calcium signaling. J. Cell Sci., 2002, **115**, 3715–3716.

[779] Griffith, W.H., Jasek, M.C., Bain, S.H., Murchison, D., 2000. Modification of ion channels and calcium homeostasis of basal forebrain neurons during aging. Behav. Brain Res., 2000, **115**, 219–233.

[780] Britschgi, A., Bill, A., Brinkhaus, H., Rothwell, C., et al., 2013. Calcium-activated chloride channel ANO1 promotes breast cancer progression by activating EGFR and CAMK signaling. Proc. Natl. Acad. Sci. U. S. A., 2013, **110**.

[781] Wang, T., Guo, S., Liu, Z., Wu, L., et al., 2014. CAMK2N1 inhibits prostate cancer progression through androgen receptor-dependent signaling. Oncotarget, 2014, **5**, 10293–10306.

[782] Wang, C., Li, N., Liu, X., Zheng, Y., Cao, X., 2008. A novel endogenous human CaMKII inhibitory protein suppresses tumor growth by inducing cell cycle arrest via p27 stabilization. J. Biol. Chem., 2008, **283**, 11565–11574.

[783] Duan, S., Yao, Z., Hou, D., Wu, Z., et al., 2007. Phosphorylation of Pirh2 by Calmodulin-dependent kinase II impairs its ability to ubiquitinate p53. EMBO J., 2007, **26**, 3062–3074.

[784] Yuan, K., Chung, L.W.K., Siegal, G.P., Zayzafoon, M., 2007. α-CaMKII controls the growth of human osteosarcoma by regulating cell cycle progression. Lab. Investig., 2007, **87**, 938–950.

[785] Si, J., Collins, S.J., 2008. Activated Ca2+/calmodulin-dependent protein kinase IIγ is a critical regulator of myeloid leukemia cell proliferation. Cancer Res., 2008, **68**, 3733–3742.

[786] Li, N., Wang, C., Wu, Y., Liu, X., Cao, X., 2009. Ca2+/calmodulin-dependent protein kinase II promotes cell cycle progression by directly activating MEK1 and subsequently modulating p27 phosphorylation. J. Biol. Chem., 2009, **284**, 3021–3027.

[787] Glover-Collins, K., Thompson, M.E., 2008. Nuclear export of BRCA1 occurs during early S phase and is calcium-dependent. Cell. Signal., 2008, **20**, 958–968.

[788] Hoffman, A., Carpenter, H., Kahl, R., Watt, L.F., et al., 2014. Dephosphorylation of CaMKII at T253 controls the metaphase-anaphase transition. Cell. Signal., 2014, **26**, 748–756.

[789] Hart, M.R., Su, H.Y., Broka, D., Goverdhan, A., Schroeder, J.A., 2013. Inactive ERBB receptors cooperate with reactive oxygen species to suppress cancer progression. Mol. Ther., 2013, **21**, 1996–2007.

[790] Cohen, M.H., Kokhlin, O.W., 2009. Mechanisms of prostate cancer cell survival after inhibition of AR expression. J. Cell. Biochem., 2009, **106**, 363–371.

[791] Daft, P.G., Yuan, K., Warram, J.M., Klein, M.J., et al., 2013. Alpha-CaMKII plays a critical role in determining the aggressive behavior of human osteosarcoma. Mol. Cancer Res., 2013, **11**, 349–359.

[792] Bourguignon, L.Y.W., Gilad, E., Brightman, A., Diedrich, F., Singleton, P., 2006. Hyaluronan-CD44 interaction with leukemia-associated RhoGEF and epidermal growth factor receptor promotes Rho/Ras co-activation, phospholipase Cε-Ca2+ signaling, and cytoskeleton modification in head and neck squamous cell carcinoma cells. J. Biol. Chem., 2006, **281**, 14026–14040.

[793] Takabatake, S., Ohtsuka, S., Sugawara, T., Hatano, N., et al., 2019. Regulation of Ca 2+ /calmodulin-dependent protein kinase kinase β by cAMP signaling. Biochim. Biophys. Acta - Gen. Subj., 2019, **1863**, 672–680.

[794] Melander Gradin, H., Marklund, U., Larsson, N., Chatila, T.A., Gullberg, M., 1997. Regulation of microtubule dynamics by Ca2+/calmodulin-dependent kinase IV/Gr-dependent phosphorylation of oncoprotein 18. Mol. Cell. Biol., 1997, **17**, 3459–3467.

[795] Takai, N., Miyazaki, T., Nishida, M., Nasu, K., Miyakawa, I., 2002. Ca2+/calmodulin-dependent protein kinase IV expression in epithelial ovarian cancer. Cancer Lett., 2002, **183**, 185–193.

[796] Sapio, L., Di Maiolo, F., Illiano, M., Esposito, A., et al., 2014. Targeting protein kinase a in cancer therapy: An update. EXCLI J., 2014, **13**, 843–855.

[797] Cooper, D.M.F., 2005. *Biochem. Soc. Trans.*, vol. 33, Biochem Soc Trans, pp. 1319–1322.

[798] Cooper, D.M.F., 2003. Regulation and organization of adenylyl cyclases and cAMP. Biochem. J., 2003, **375**, 517–529.

[799] Zhong, H., SuYang, H., Erdjument-Bromage, H., Tempst, P., Ghosh, S., 1997. The transcriptional activity of NF-κB is regulated by the IκB-associated PKAc subunit through a cyclic AMP-independent mechanism. Cell, 1997, **89**, 413–424.

[800] Dulin, N.O., Niu, J., Browning, D.D., Ye, R.D., Voyno-Yasenetskaya, T., 2001. Cyclic AMP-independent Activation of Protein Kinase A by Vasoactive Peptides. J. Biol. Chem., 2001, **276**, 20827–20830.

[801] Zhang, W., Qin, C., Zhao, J., Wang, X., 2004. Phospholipase D alpha 1-derived phosphatidic acid interacts with ABI1 phosphatase 2C and regulates abscisic acid signaling. Proc. Natl. Acad. Sci. U. S. A., 2004, **101**, 9508–13.

[802] Yang, H., Lee, C.J., Zhang, L., Sans, M.D., Simeone, D.M., 2008. Regulation of transforming growth factor β-induced responses by protein kinase A in pancreatic acinar cells. Am. J. Physiol. - Gastrointest. Liver Physiol., 2008, **295**.

[803] Naviglio, S., Di Gesto, D., Illiano, F., Chiosi, E., et al., 2010. Leptin potentiates antiproliferative action of cAMP elevation via protein kinase A down-regulation in breast cancer cells. J. Cell. Physiol., 2010, **225**, 801–809.

[804] Rivas, M., Santisteban, P., 2003. *Mol. Cell. Endocrinol.*, vol. 213, Elsevier Ireland Ltd, pp. 31–45.

[805] Mantovani, G., Bondioni, S., Lania, A.G., Rodolfo, M., et al., 2008. High expression of PKA regulatory subunit 1A protein is related to proliferation of human melanoma cells. Oncogene, 2008, **27**, 1834–1843.

[806] Wu, K.J., Mattioli, M., Morse, H.C., Dalla-Favera, R., 2002. c-MYC activates protein kinase A (PKA) by direct transcriptional activation of the PKA catalytic subunit beta (PKA-Cβ) gene. Oncogene, 2002, **21**, 7872–7882.

[807] Howe, A.K., 2004. Regulation of actin-based cell migration by cAMP/PKA. Biochim. Biophys. Acta - Mol. Cell Res., 2004, **1692**, 159–174.

[808] Jiang, P., Enomoto, A., Takahashi, M., 2009. Cell biology of the movement of breast cancer cells: Intracellular signalling and the actin cytoskeleton. Cancer Lett., 2009, **284**, 122–130.

[809] McKenzie, A.J., Campbell, S.L., Howe, A.K., 2011. Protein kinase a activity and anchoring are required for ovarian cancer cell migration and invasion. PLoS One, 2011, **6**, 26552.

[810] Shaikh, D., Zhou, Q., Chen, T., Ibe, J.C.F., et al., 2012. CAMP-dependent protein kinase is essential for hypoxia-mediated epithelial-mesenchymal transition, migration, and invasion in lung cancer cells. Cell. Signal., 2012, **24**, 2396–2406.

[811] Di Cristofano, A., 2017. *Curr. Top. Dev. Biol.*, vol. 123, Academic Press Inc., pp. 49–71.

[812] Kobayashi, T., Cohen, P., 1999. Activation of serum- and glucocorticoid-regulated protein kinase by agonists that activate phosphatidylinositide 3-kinase is mediated by 3-phosphoinositide-dependent protein kinase-1 (PDK1) and PDK2. Biochem. J., 1999, **339**, 319–328.

[813] Pao, A.C., Bhargava, A., Di Sole, F., Quigley, R., et al., 2010. Expression and role of serum and glucocorticoid-regulated kinase 2 in the regulation of Na+/H+ exchanger 3 in the mammalian kidney. Am. J. Physiol. - Ren. Physiol., 2010, **299**, F1496.

[814] Webster, M.K., Goya, L., Ge, Y., Maiyar, A.C., Firestone, G.L., 1993. Characterization of sgk, a novel member of the serine/threonine protein kinase gene family which is transcriptionally induced by glucocorticoids and serum. Mol. Cell. Biol., 1993, **13**, 2031–2040.

[815] Mizuno, H., Nishida, E., 2001. The ERK MAP kinase pathway mediates induction of SGK (serum- and glucocorticoid-inducible kinase) by growth factors. Genes to Cells, 2001, **6**, 261–268.

[816] Náray-Fejes-Tóth, A., Canessa, C., Cleaveland, E.S., Aldrich, G., Fejes-Tóth, G., 1999. sgk Is an aldosterone-induced kinase in the renal collecting duct. Effects on epithelial Na+ channels. J. Biol. Chem., 1999, **274**, 16973–16978.

[817] Fagerli, U.M., Ullrich, K., Stühmer, T., Holien, T., et al., 2011. Serum/glucocorticoid-regulated kinase 1 (SGK1) is a prominent target gene of the transcriptional response to cytokines in multiple myeloma and supports the growth of myeloma cells. Oncogene, 2011, **30**, 3198–3206.

[818] Waldegger, S., Barth, P., Raber, G., Lang, F., 1997. Cloning and characterization of a putative human serine/threonine protein kinase transcriptionally modified during anisotonic and isotonic alterations of cell volume. Proc. Natl. Acad. Sci. U. S. A., 1997, **94**, 4440–4445.

[819] Leong, M.L.L., Maiyar, A.C., Kim, B., O'Keeffe, B.A., Firestone, G.L., 2003. Expression of the serum- and glucocorticoid-inducible protein kinase, Sgk, is a cell survival response to multiple types of environmental stress stimuli in mammary epithelial cells. J. Biol. Chem., 2003, **278**, 5871–5882.

[820] Brickley, D.R., Mikosz, C.A., Hagan, C.R., Conzen, S.D., 2002. Ubiquitin modification of serum and glucocorticoid-induced protein kinase-1 (SGK-1). J. Biol. Chem., 2002, **277**, 43064–43070.

[821] Bogusz, A.M., Brickley, D.R., Pew, T., Conzen, S.D., 2006. A novel N-terminal hydrophobic motif mediates constitutive degradation of serum- and glucocorticoidinduced kinase-1 by the ubiquitin-proteasome pathway. FEBS J., 2006, **273**, 2913–2928.

[822] Park, J., Leong, M.L.L., Buse, P., Maiyar, A.C., et al., 1999. Serum and glucocorticoid-inducible kinase (SGK) is a target of the PI 3-kinase-stimulated signaling pathway. EMBO J., 1999, **18**, 3024–3033.

[823] García-Martínez, J.M., Alessi, D.R., 2008. mTOR complex 2 (mTORC2) controls hydrophobic motif phosphorylation and activation of serum- and glucocorticoid-induced protein kinase 1 (SGK1). Biochem. J., 2008, **416**, 375–385.

[824] Calleja, V., Alcor, D., Laguerre, M., Park, J., et al., 2007. Intramolecular and intermolecular interactions of protein kinase B define its activation in vivo. PLoS Biol., 2007, **5**, 780–791.

[825] Milburn, C.C., Deak, M., Kelly, S.M., Price, N.C., et al., 2003. Binding of phosphatidylinositol 3,4,5-trisphosphate to the pleckstrin homology domain of protein kinase B induces a conformational change. Biochem. J., 2003, **375**, 531–538.

[826] Biondi, R.M., Kieloch, A., Currie, R.A., Deak, M., Alessi, D.R., 2001. The PIF-binding pocket in PDK1 is essential for activation of S6K and SGK, but not PKB. EMBO J., 2001, **20**, 4380–4390.

[827] Collins, B.J., Deak, M., Arthur, J.S.C., Armit, L.J., Alessi, D.R., 2003. In vivo role of the PIF-binding docking site of PDK1 defined by knock-in mutation. EMBO J., 2003, **22**, 4202–4211.

[828] Eirew, P., Steif, A., Khattra, J., Ha, G., et al., 2015. Dynamics of genomic clones in breast cancer patient xenografts at single-cell resolution. Nature, 2015, **518**, 422–426.

[829] Sahoo, S., Brickley, D.R., Kocherginsky, M., Conzen, S.D., 2005. Coordinate expression of the PI3-kinase downstream effectors serum and glucocorticoid-induced kinase (SGK-1) and Akt-1 in human breast cancer. Eur. J. Cancer, 2005, **41**, 2754–2759.

[830] Nasir, O., Wang, K., Föller, M., Gu, S., et al., 2009. Relative resistance of SGK1 knockout mice against chemical carcinogenesis. IUBMB Life, 2009, **61**, 768–776.

[831] Heikamp, E.B., Patel, C.H., Collins, S., Waickman, A., et al., 2014. The AGC kinase SGK1 regulates T H 1 and T H 2 differentiation downstream of the mTORC2 complex. Nat. Immunol., 2014, **15**, 457–464.

[832] Liu, M., Chen, L., Chan, T.H.M., Wang, J., et al., 2012. Serum and glucocorticoid kinase 3 at 8q13.1 promotes cell proliferation and survival in hepatocellular carcinoma. Hepatology, 2012, **55**, 1754–1765.

[833] Brunet, A., Park, J., Tran, H., Hu, L.S., et al., 2001. Protein Kinase SGK Mediates Survival Signals by Phosphorylating the Forkhead Transcription Factor FKHRL1 (FOXO3a). Mol. Cell. Biol., 2001, **21**, 952–965.

[834] Burchfield, J.G., Lennard, A.J., Narasimhan, S., Hughes, W.E., et al., 2004. Akt mediates insulin-stimulated phosphorylation of Ndrg2: Evidence for cross-talk with protein kinase C θ. J. Biol. Chem., 2004, **279**, 18623–18632.

[835] Castel, P., Ellis, H., Bago, R., Toska, E., et al., 2016. PDK1-SGK1 Signaling Sustains AKT-Independent mTORC1 Activation and Confers Resistance to PI3Kα Inhibition. Cancer Cell, 2016, **30**, 229–242.

[836] Sommer, E.M., Dry, H., Cross, D., Guichard, S., et al., 2013. Elevated SGK1 predicts resistance of breast cancer cells to Akt inhibitors. Biochem. J., 2013, **452**, 499–508.

[837] Bago, R., Sommer, E., Castel, P., Crafter, C., et al., 2016. The hVps34- <scp>SGK</scp> 3 pathway alleviates sustained PI3K/Akt inhibition by stimulating <scp>mTORC</scp> 1 and tumour growth. EMBO J., 2016, **35**, 1902–1922.

[838] Boehmer, C., Okur, F., Setiawan, I., Bröer, S., Lang, F., 2003. Properties and regulation of glutamine transporter SN1 by protein kinases SGK and PKB. Biochem. Biophys. Res. Commun., 2003, **306**, 156–162.

[839] Caohuy, H., Yang, Q., Eudy, Y., Ha, T.A., et al., 2014. Activation of 3-phosphoinositide-dependent kinase 1 (PDK1) and serum- And glucocorticoid-induced protein kinase 1 (SGK1) by short-chain sphingolipid C4-ceramide rescues the trafficking defect of &x25b5;F508-cystic fibrosis transmembrane conductance regulator (&x25b5;F508-CFTR). J. Biol. Chem., 2014, **289**, 35953–35968.

[840] Lee, I.H., Dinudom, A., Sanchez-Perez, A., Kumar, S., Cook, D.I., 2007. Akt mediates the effect of insulin on epithelial sodium channels by inhibiting Nedd4-2. J. Biol. Chem., 2007, **282**, 29866–29873.

[841] Shisheva, A., 2012. *Curr. Top. Microbiol. Immunol.*, vol. 362, Curr Top Microbiol Immunol, pp. 127–162.

[842] Berwick, D.C., Dell, G.C., Welsh, G.I., Heesom, K.J., et al., 2004. Protein kinase B phosphorylation of PIKfyve regulates the trafficking of GLUT4 vesicles. J. Cell Sci., 2004, **117**, 5985–5993.

[843] Murray, J.T., Cummings, L.A., Bloomberg, G.B., Cohen, P., 2005. Identification of different specificity requirements between SGK1 and PKBα. FEBS Lett., 2005, **579**, 991–994.

[844] Murray, J.T., Campbell, D.G., Morrice, N., Auld, G.C., et al., 2004. Exploitation of KESTREL to identify NDRG family members as physiological substrates for SGK1 and GSK3. Biochem. J., 2004, **384**, 477–488.

[845] Sandu, C., Artunc, F., Palmada, M., Rexhepaj, R., et al., 2006. Impaired intestinal NHE3 activity in the PDK1 hypomorphic mouse. Am. J. Physiol. - Gastrointest. Liver Physiol., 2006, **291**.

[846] Lu, M., Wang, J., Jones, K.T., Ives, H.E., et al., 2010. mTOR complex-2 activates ENaC by phosphorylating SGK1. J. Am. Soc. Nephrol., 2010, **21**, 811–818.

[847] Ehmer, U., Sage, J., 2016. Control of proliferation and cancer growth by the hippo signaling pathway. Mol. Cancer Res., 2016, **14**, 127–140.

[848] Nishio, M., Otsubo, K., Maehama, T., Mimori, K., Suzuki, A., 2013. Capturing the mammalian hippo: Elucidating its role in cancer. Cancer Sci., 2013, **104**, 1271–1277.

[849] Harvey, K.F., Pfleger, C.M., Hariharan, I.K., 2003. The Drosophila Mst ortholog, hippo, restricts growth and cell proliferation and promotes apoptosis. Cell, 2003, **114**, 457–467.

[850] Bhat, K.P.L., Salazar, K.L., Balasubramaniyan, V., Wani, K., et al., 2011. The transcriptional coactivator TAZ regulates mesenchymal differentiation in malignant glioma. Genes Dev., 2011, **25**, 2594–2609.

[851] Wang, Y., Dong, Q., Zhang, Q., Li, Z., et al., 2010. Overexpression of yes-associated protein contributes to progression and poor prognosis of non-small-cell lung cancer. Cancer Sci., 2010, **101**, 1279–1285.

[852] Yimlamai, D., Christodoulou, C., Galli, G.G., Yanger, K., et al., 2014. Hippo pathway activity influences liver cell fate. Cell, 2014, **157**, 1324–1338.

[853] Hergovich, A., 2016. The Roles of NDR Protein Kinases in Hippo Signalling. Genes (Basel)., 2016, **7**, 21.

[854] Hergovich, A., Kohler, R.S., Schmitz, D., Vichalkovski, A., et al., 2009. The MST1 and hMOB1 Tumor Suppressors Control Human Centrosome Duplication by Regulating NDR Kinase Phosphorylation. Curr. Biol., 2009, **19**, 1692–1702.

[855] Cornils, H., Stegert, M.R., Hergovich, A., Hynx, D., et al., 2010. Ablation of the Kinase NDR1 Predisposes Mice to the Development of T Cell Lymphoma. Sci. Signal., 2010, **3**.

[856] Vichalkovski, A., Gresko, E., Cornils, H., Hergovich, A., et al., 2008. NDR Kinase Is Activated by RASSF1A/MST1 in Response to Fas Receptor Stimulation and Promotes Apoptosis. Curr. Biol., 2008, **18**, 1889–1895.

[857] Chiba, S., Ikeda, M., Katsunuma, K., Ohashi, K., Mizuno, K., 2009. MST2- and Furry-Mediated Activation of NDR1 Kinase Is Critical for Precise Alignment of Mitotic Chromosomes. Curr. Biol., 2009, **19**, 675–681.

[858] Cornils, H., Kohler, R.S., Hergovich, A., Hemmings, B.A., 2011. Human NDR Kinases Control G1/S Cell Cycle Transition by Directly Regulating p21 Stability. Mol. Cell. Biol., 2011, **31**, 1382–1395.

[859] Zhang, L., Tang, F., Terracciano, L., Hynx, D., et al., 2015. NDR functions as a physiological YAP1 kinase in the intestinal epithelium. Curr. Biol., 2015, **25**, 296–305.

[860] Reiner, O., Coquelle, F.M., Peter, B., Levy, T., et al., 2006. The evolving doublecortin (DCX) superfamily. BMC Genomics, 2006, **7**.

[861] N.d. DCLK2 - Serine/threonine-protein kinase DCLK2 - Homo sapiens (Human) - DCLK2 gene & protein n.d.

[862] Meyerson, M., Enders, G.H., Wu, C.L., Su, L.K., et al., 1992. A family of human cdc2-related protein kinases. EMBO J., 1992, **11**, 2909–2917.

[863] Sassa, T., Gomi, H., Itohara, S., 2004. Postnatal expression of Cdkl2 in mouse brain revealed by LacZ inserted into the Cdkl2 locus. Cell Tissue Res., 2004, **315**, 147–156.

[864] Gomi, H., Sassa, T., Thompson, R.F., Itohara, S., 2010. Involvement of cyclin-dependent kinase-like 2 in cognitive function required for contextual and spatial learning in mice. Front. Behav. Neurosci., 2010, **4**.

[865] Fang, C.L., Uen, Y.H., Chen, H.K., Hseu, Y.C., et al., 2018. Loss of cyclin-dependent kinase-like 2 predicts poor prognosis in gastric cancer, and its overexpression suppresses cells growth and invasion. Cancer Med., 2018, **7**, 2993–3002.

[866] Li, L., Liu, C., Amato, R.J., Chang, J.T., et al., 2014. CDKL2 promotes epithelial-mesenchymal transition and breast cancer progression. Oncotarget, 2014, **5**, 10840–10853.

[867] Vincent, S., Settleman, J., 1997. The PRK2 kinase is a potential effector target of both Rho and Rac GTPases and regulates actin cytoskeletal organization. Mol. Cell. Biol., 1997, **17**, 2247–2256.

[868] Cryns, V.L., Byun, Y., Rana, A., Mellor, H., et al., 1997. Specific proteolysis of the kinase protein kinase C-related kinase 2 by caspase-3 during apoptosis. Identification by a novel, small pool expression cloning strategy. J. Biol. Chem., 1997, **272**, 29449–29453.

[869] Takahashi, M., Mukai, H., Toshimori, M., Miyamoto, M., Ono, Y., 1998. Proteolytic activation of PKN by caspase-3 or related protease during apoptosis. Proc. Natl. Acad. Sci. U. S. A., 1998, **95**, 11566–11571.

[870] Lim, W.G., Chen, X., Liu, J. ping, Tan, B.J., et al., 2008. The C-terminus of PRK2/PKNγ is required for optimal activation by RhoA in a GTP-dependent manner. Arch. Biochem. Biophys., 2008, **479**, 170–178.

[871] Lachmann, S., Jevons, A., De Rycker, M., Casamassima, A., et al., 2011. Regulatory Domain Selectivity in the Cell-Type Specific PKN-Dependence of Cell Migration. PLoS One, 2011, **6**, e21732.

[872] Calautti, E., Grossi, M., Mammucari, C., Aoyama, Y., et al., 2002. Fyn tyrosine kinase is a downstream mediator of Rho/PRK2 function in keratinocyte cell-cell adhesion. J. Cell Biol., 2002, **156**, 137–148.

[873] Koh, H., Lee, K.H., Kim, D., Kim, S., et al., 2000. Inhibition of Akt and its anti-apoptotic activities by tumor necrosis factor-induced protein kinase C-related kinase 2 (PRK2) cleavage. J. Biol. Chem., 2000, **275**, 34451–34458.

[874] Schmidt, A., Durgan, J., Magalhaes, A., Hall, A., 2007. Rho GTPases regulate PRK2/PKN2 to control entry into mitosis and exit from cytokinesis. EMBO J., 2007, **26**, 1624–1636.

[875] Liu, W., Li, J., Song, Y.S., Li, Y., et al., 2017. Cdk5 links with DNA damage response and cancer. Mol. Cancer, 2017, **16**, 60.

[876] Odajima, J., Wills, Z.P., Ndassa, Y.M., Terunuma, M., et al., 2011. Cyclin E Constrains Cdk5 Activity to Regulate Synaptic Plasticity and Memory Formation. Dev. Cell, 2011, **21**, 655–668.

[877] Modi, P.K., Komaravelli, N., Singh, N., Sharma, P., 2012. Interplay between MEK-ERK signaling, cyclin D1, and cyclin-dependent kinase 5 regulates cell cycle reentry and apoptosis of neurons. Mol. Biol. Cell, 2012, **23**, 3722–3730.

[878] Wei, K., Ye, Z., Li, Z., Dang, Y., et al., 2016. An immunohistochemical study of cyclin-dependent kinase 5 (CDK5) expression in non-small cell lung cancer (NSCLC) and small cell lung cancer (SCLC): A possible prognostic biomarker. World J. Surg. Oncol., 2016, **14**, 34.

[879] Daval, M., Gurlo, T., Costes, S., Huang, C.J., Butler, P.C., 2011. Cyclin-dependent kinase 5 promotes pancreatic β-cell survival via Fak-Akt signaling pathways. Diabetes, 2011, **60**, 1186–1197.

[880] Lin, H., Chen, M.C., Chiu, C.Y., Song, Y.M., Lin, S.Y., 2007. Cdk5 regulates STAT3 activation and cell proliferation in medullary thyroid carcinoma cells. J. Biol. Chem., 2007, **282**, 2776–2784.

[881] Hsu, F.N., Chen, M.C., Chiang, M.C., Lin, E., et al., 2011. Regulation of androgen receptor and prostate cancer growth by cyclin-dependent kinase 5. J. Biol. Chem., 2011, **286**, 33141–33149.

[882] Sun, S.S., Zhou, X., Huang, Y.Y., Kong, L.P., et al., 2015. Targeting STAT3/miR-21 axis inhibits epithelial-mesenchymal transition via regulating CDK5 in head and neck squamous cell carcinoma. Mol. Cancer, 2015, **14**, 213.

[883] Ehrlich, S.M., Liebl, J., Ardelt, M.A., Lehr, T., et al., 2015. Targeting cyclin dependent kinase 5 in hepatocellular carcinoma - A novel therapeutic approach. J. Hepatol., 2015, **63**, 102–113.

[884] Feldmann, G., Mishra, A., Hong, S.M., Bisht, S., et al., 2010. Inhibiting the cyclin-dependent kinase CDK5 blocks pancreatic cancer formation and progression through the suppression of Ras-Ral signaling. Cancer Res., 2010, **70**, 4460–4469.

[885] Courapied, S., Sellier, H.L., De Carné Trécesson, S., Vigneron, A., et al., 2010. The cdk5 kinase regulates the STAT3 transcription factor to prevent DNA damage upon topoisomerase I inhibition. J. Biol. Chem., 2010, **285**, 26765–26778.

[886] Abraham, J., Lemmers, B., Hande, M.P., Moynahan, M.E., et al., 2003. Eme1 is involved in DNA damage processing and maintenance of genomic stability in mammalian cells. EMBO J., 2003, **22**, 6137–6147.

[887] Tian, B., Yang, Q., Mao, Z., 2009. Phosphorylation of ATM by Cdk5 mediates DNA damage signalling and regulates neuronal death. Nat. Cell Biol., 2009, **11**, 211–218.

[888] Huang, E., Qu, D., Zhang, Y., Venderova, K., et al., 2010. The role of Cdk5-mediated apurinic/apyrimidinic endonuclease 1 phosphorylation in neuronal death. Nat. Cell Biol., 2010, **12**, 563–571.

[889] Arai, S., Matsushita, A., Du, K., Yagi, K., et al., 2007. Novel homeodomain-interacting protein kinase family member, HIPK4, phosphorylates human p53 at serine 9. FEBS Lett., 2007, **581**, 5649–5657.

[890] Van Der Laden, J., Soppa, U., Becker, W., 2015. Effect of tyrosine autophosphorylation on catalytic activity and subcellular localisation of homeodomain-interacting protein kinases (HIPK). Cell Commun. Signal., 2015, **13**, 3–3.

[891] Vaandrager, A.B., Hogema, B.M., Edixhoven, M., Van den Burg, C.M.M., et al., 2003. Autophosphorylation of cGMP-dependent protein kinase type II. J. Biol. Chem., 2003, **278**, 28651–28658.

[892] Stitt, T.N., Conn, G., Goret, M., Lai, C., et al., 1995. The anticoagulation factor protein S and its relative, Gas6, are ligands for the Tyro 3/Axl family of receptor tyrosine kinases. Cell, 1995, **80**, 661–670.

[893] Taylor, I.C.A., Roy, S., Yaswen, P., Stampfer, M.R., Varmus, H.E., 1995. Mouse mammary tumors express elevated levels of RNA encoding the murine homolog of SKY, a putative receptor tyrosine kinase. J. Biol. Chem., 1995, **270**, 6872–6880.

[894] Uehara, S., Fukuzawa, Y., Matuyama, T., Gotoh, K., 2017. Role of Tyro3, Axl, and Mer Receptors and Their Ligands (Gas6, and Protein S) in Patients with Hepatocellular Carcinoma. J. Cancer Ther., 2017, **08**, 112–130.

[895] Pierce, A., Bliesner, B., Xu, M., Nielsen-Preiss, S., et al., 2008. Axl and Tyro3 modulate female reproduction by influencing gonadotropin-releasing hormone neuron survival and migration. Mol. Endocrinol., 2008, **22**, 2481–2495.

[896] Qin, A., Qian, W., 2018. MicroRNA-7 inhibits colorectal cancer cell proliferation, migration and invasion via TYRO3 and phosphoinositide 3-kinase/protein B kinase/mammalian target of rapamycin pathway suppression. Int. J. Mol. Med., 2018, **42**, 2503–2514.

[897] Vouri, M., An, Q., Pilkington, G., Hafizi, S., 2016. Hetero-interaction amongst Tyro3 and Axl receptor tyrosine kinases diversifies cancer signalling. Eur. J. Cancer, 2016, **69**, 42.

[898] Brown, J.E., Krodel, M., Pazos, M., Lai, C., Prieto, A.L., 2012. Cross-phosphorylation, signaling and proliferative functions of the Tyro3 and Axl receptors in Rat2 cells. PLoS One, 2012, **7**.

[899] Heiring, C., Dahlbäck, B., Muller, Y.A., 2004. Ligand recognition and homophilic interactions in Tyro3: Structural insights into the Axl/Tyro3 receptor tyrosine kinase family. J. Biol. Chem., 2004, **279**, 6952–6958.

[900] Angelillo-Scherrer, A., Burnier, L., Flores, N., Savi, P., et al., 2005. Role of Gas6 receptors in platelet signaling during thrombus stabilization and implications for antithrombotic therapy. J. Clin. Invest., 2005, **115**, 237–246.

[901] Lan, Z., Wu, H., Li, W., Wu, S., et al., 2000. Transforming activity of receptor tyrosine kinase tyro3 is mediated, at least in part, by the PI3 kinase-signaling pathway. Blood, 2000, **95**, 633–638.

[902] Zhu, Y.Z., Wang, W., Xian, N., Wu, B., 2016. Inhibition of TYRO3/Akt signaling participates in hypoxic injury in hippocampal neurons. Neural Regen. Res., 2016, **11**, 752–757.

[903] Guo, H., Barrett, T.M., Zhong, Z., Fernndez, J.A., et al., 2011. Protein S blocks the extrinsic apoptotic cascade in tissue plasminogen activator/N-methyl D-aspartate-treated neurons via Tyro3-Akt-FKHRL1 signaling pathway. Mol. Neurodegener., 2011, **6**.

[904] Zhong, Z., Wang, Y., Guo, H., Sagare, A., et al., 2010. Protein S protects neurons from excitotoxic injury by activating the TAM receptor tyro3-phosphatidylinositol 3-kinase-Akt pathway through its sex hormone-binding globulin-like region. J. Neurosci., 2010, **30**, 15521–15534.

[905] Zhu, D., Wang, Y., Singh, I., Bell, R.D., et al., 2010. Protein S controls hypoxic/ischemic blood-brain barrier disruption through the TAM receptor Tyro3 and sphingosine 1-phosphate receptor. Blood, 2010, **115**, 4963–4972.

[906] Miyamoto, Y., Torii, T., Takada, S., Ohno, N., et al., 2015. Involvement of the Tyro3 receptor and its intracellular partner Fyn signaling in Schwann cell myelination. Mol. Biol. Cell, 2015, **26**, 3489–3503.

[907] Linger, R.M.A., Keating, A.K., Earp, H.S., Graham, D.K., 2010. Taking aim at Mer and Axl receptor tyrosine kinases as novel therapeutic targets in solid tumors. Expert Opin. Ther. Targets, 2010, **14**, 1073–1090.

[908] Akkermann, R., Aprico, A., Perera, A.A., Bujalka, H., et al., 2017. The TAM receptor Tyro3 regulates myelination in the central nervous system. Glia, 2017, **65**, 581–591.

[909] Ekyalongo, R., Mukohara, T., Funakoshi, Y., Tomioka, H., et al., 2014. TYRO3 as a potential therapeutic target in breast cancer. Anticancer Res., 2014, **34**, 3337–45.

[910] Duan, Y., Wong, W., Chua, S.C., Wee, H.L., et al., 2016. Overexpression of Tyro3 and its implications on hepatocellular carcinoma progression. Int. J. Oncol., 2016, **48**, 358–366.

[911] Salemi, L.M., Maitland, M.E.R., McTavish, C.J., Schild-Poulter, C., 2017. Cell signalling pathway regulation by RanBPM: Molecular insights and disease implications. Open Biol., 2017, **7**.

[912] Graham, D.K., Deryckere, D., Davies, K.D., Earp, H.S., 2014. The TAM family: Phosphatidylserine-sensing receptor tyrosine kinases gone awry in cancer. Nat. Rev. Cancer, 2014, **14**, 769–785.

[913] Wang, Y., Shi, J., Chai, K., Ying, X., Zhou, B., 2013. The Role of Snail in EMT and Tumorigenesis. Curr. Cancer Drug Targets, 2013, **13**, 963–972.

[914] Tsai, S.-J., Chien, C.-W., Chen, S.-Y., Lin, S.-C., et al., 2018. *Cancer Res.*, vol. 78, American Association for Cancer Research (AACR), pp. 2488–2488.

[915] Schmitz, R., Valls, A.F., Yerbes, R., Richter, S. von, et al., 2016. TAM receptors Tyro3 and Mer as novel targets in colorectal cancer. Oncotarget, 2016, **7**, 56355–56370.

[916] Schmidt, T., Ben-Batalla, I., Schultze, A., Loges, S., 2012. Macrophage-tumor crosstalk: Role of TAMR tyrosine kinase receptors and of their ligands. Cell. Mol. Life Sci., 2012, **69**, 1391–1414.

[917] Loges, S., Schmidt, T., Tjwa, M., Van Geyte, K., et al., 2010. Malignant cells fuel tumor growth by educating infiltrating leukocytes to produce the mitogen Gas6. Blood, 2010, **115**, 2264–2273.

[918] Ubil, E., Caskey, L., Holtzhausen, A., Hunter, D., et al., 2018. Tumor-secreted Pros1 inhibits macrophage M1 polarization to reduce antitumor immune response. J. Clin. Invest., 2018, **128**, 2356–2369.

[919] Polvi, A., Armstrong, E., Lai, G., Lemke, G., et al., 1993. The human TYROS gene and pseudogene are located in chromosome 15q14-q25. Gene, 1993, **134**, 289–293.

[920] Ohashi, K., Mizuno, K., Kuma, K., Miyata, T., Nakamura, T., 1994. Cloning of the cDNA for a novel receptor tyrosine kinase, Sky, predominantly expressed in brain. Oncogene, 1994, **9**, 699–705.

[921] Dai, W., Pan, H., Hassanain, H., Gupta, S., Murphy, M.J., 1994. Molecular cloning of a novel receptor tyrosine kinase, tif, highly expressed in human ovary and testis. Oncogene, 1994, **9**, 975–9.

[922] Avilla, E., Guarino, V., Visciano, C., Liotti, F., et al., 2011. Activation of TYRO3/AXL tyrosine kinase receptors in thyroid cancer. Cancer Res., 2011, **71**, 1792–1804.

[923] Eryildiz, F., Tyner, J.W., 2016. *Cancer Res.*, vol. 76, American Association for Cancer Research (AACR), pp. 1265–1265.

[924] Dantas-Barbosa, C., Lesluyes, T., Le Loarer, F., Chibon, F., et al., 2017. Expression and role of TYRO3 and AXL as potential therapeutical targets in leiomyosarcoma. Br. J. Cancer, 2017, **117**, 1787–1797.

[925] Lee, C., 2015. Overexpression of Tyro3 receptor tyrosine kinase leads to the acquisition of taxol resistance in ovarian cancer cells. Mol. Med. Rep., 2015, **12**, 1485–1492.

[926] Kabir, T.D., Ganda, C., Brown, R.M., Beveridge, D.J., et al., 2018. A microRNA-7/growth arrest specific 6/TYRO3 axis regulates the growth and invasiveness of sorafenib-resistant cells in human hepatocellular carcinoma. Hepatology, 2018, **67**, 216–231.

[927] Zhu, S., Wurdak, H., Wang, Y., Galkin, A., et al., 2009. A genomic screen identifies TYRO3 as a MITF regulator in melanoma. Proc. Natl. Acad. Sci. U. S. A., 2009, **106**, 17025–17030.

[928] Demarest, S.J., Gardner, J., Vendel, M.C., Ailor, E., et al., 2013. Evaluation of Tyro3 expression, Gas6-mediated akt phosphorylation, and the impact of anti-Tyro3 antibodies in melanoma cell lines. Biochemistry, 2013, **52**, 3102–3118.

[929] Chien, C.W., Hou, P.C., Wu, H.C., Chang, Y.L., et al., 2016. Targeting TYRO3 inhibits epithelial-mesenchymal transition and increases drug sensitivity in colon cancer. Oncogene, 2016, **35**, 5872–5881.

[930] Lai, C., Gore, M., Lemke, G., 1994. Structure, expression, and activity of Tyro 3, a neural adhesion-related receptor tyrosine kinase. Oncogene, 1994, **9**.

[931] Thomson, S., Petti, F., Sujka-Kwok, I., Mercado, P., et al., 2011. A systems view of epithelial-mesenchymal transition signaling states. Clin. Exp. Metastasis, 2011, **28**, 137–155.

[932] Kim, N.Y., Lee, H.Y., Lee, C., 2015. Metformin targets Axl and Tyro3 receptor tyrosine kinases to inhibit cell proliferation and overcome chemoresistance in ovarian cancer cells. Int. J. Oncol., 2015, **47**, 353–360.

[933] Alexander, P.B., Chen, R., Gong, C., Yuan, L., et al., 2017. Distinct receptor tyrosine kinase subsets mediate anti-HER2 drug resistance in breast cancer. J. Biol. Chem., 2017, **292**, 748–759.

[934] Goel, R.K., Lukong, K.E., 2016. Understanding the cellular roles of Fyn-related kinase (FRK): implications in cancer biology. Cancer Metastasis Rev., 2016, **35**, 179–199.

[935] Lechner, K.S., Neurath, M.F., Weigmann, B., 2020. Role of the IL-2 inducible tyrosine kinase ITK and its inhibitors in disease pathogenesis. J. Mol. Med., 2020, **98**, 1385–1395.

[936] Carson, C.C., Moschos, S.J., Edmiston, S.N., Darr, D.B., et al., 2015. IL2 inducible T-cell kinase, a novel therapeutic target in Melanoma. Clin. Cancer Res., 2015, **21**, 2167–2176.

[937] Manning, G., Whyte, D.B., Martinez, R., Hunter, T., Sudarsanam, S., 2002. The protein kinase complement of the human genome. Science (80-.)., 2002, **298**, 1912–1934.

[938] Thomas, S.M., Brugge, J.S., 1997. Cellular functions regulated by SRC family kinases. Annu. Rev. Cell Dev. Biol., 1997, **13**, 513–609.

[939] Frame, M.C., 2002. Src in cancer: Deregulation and consequences for cell behaviour. Biochim. Biophys. Acta - Rev. Cancer, 2002, **1602**, 114–130.

[940] Sen, B., Johnson, F.M., 2011. Regulation of Src Family Kinases in Human Cancers. J. Signal Transduct., 2011, **2011**, 14.

[941] Parsons, S.J., Parsons, J.T., 2004. Src family kinases, key regulators of signal transduction. Oncogene, 2004, **23**, 7906–7909.

[942] Meyer, T., Xu, L.H., Chang, J., Lui, E.T., et al., 2003. Breast cancer cell line proliferation blocked by the Src-related Rak tyrosine kinase. Int. J. Cancer, 2003, **104**, 139–146.

[943] Brown, M.T., Cooper, J.A., 1996. Regulation, substrates and functions of src. Biochim. Biophys. Acta - Rev. Cancer, 1996, **1287**, 121–149.

[944] Yeatman, T.J., 2004. A renaissance for SRC. Nat. Rev. Cancer, 2004, **4**, 470–480.

[945] Roskoski, R., 2004. Src protein-tyrosine kinase structure and regulation. Biochem. Biophys. Res. Commun., 2004, **324**, 1155–1164.

[946] Parsons, J.T., Weber, M.J., 1989. Genetics of src: structure and functional organization of a protein tyrosine kinase. Curr. Top. Microbiol. Immunol., 1989, **147**, 79–127.

[947] Serfas, M.S., Tyner, A.L., 2002. *Oncol. Res.*, vol. 13, Cognizant Communication Corporation, pp. 409–419.

[948] Anneren, C., Lindholm, C., Kriz, V., Welsh, M., 2005. The FRK / RAK-SHB Signaling Cascade: A Versatile Signal- Transduction Pathway that Regulates Cell Survival, Differentiation and Proliferation. Curr. Mol. Med., 2005, **3**, 313–324.

[949] Gonfloni, S., Weijland, A., Kretzschmar, J., Superti-Furga, G., 2000. Crosstalk between the catalytic and regulatory domains allows bidirectional regulation of Src. Nat. Struct. Biol., 2000, **7**, 281–286.

[950] Okada, M., Nakagawa, H., 1989. A protein tyrosine kinase involved in regulation of pp60c-src function. J Biol Chem, 1989, **264**, 20886–93.

[951] Cooper, J.A., Gould, K.L., Cartwright, C.A., Hunter, T., 1986. Tyr527 is phosphorylated in pp60c-src: Implications for regulation. Science (80-.)., 1986, **231**, 1431–1434.

[952] Zrihan-Licht, S., Lim, J., Keydar, I., Sliwkowski, M.X., et al., 1997. Association of Csk-homologous kinase (CHK) (formerly MATK) with HER- 2/ErbB-2 in breast cancer cells. J. Biol. Chem., 1997, **272**, 1856–1863.

[953] Ingley, E., 2008. Src family kinases: Regulation of their activities, levels and identification of new pathways. Biochim. Biophys. Acta - Proteins Proteomics, 2008, **1784**, 56–65.

[954] Oneyama, C., Hikita, T., Enya, K., Dobenecker, M.W., et al., 2008. The Lipid Raft-Anchored Adaptor Protein Cbp Controls the Oncogenic Potential of c-Src. Mol. Cell, 2008, **30**, 426–436.

[955] Walter, A.O., Peng, Z.Y., Cartwright, C.A., 1999. The Shp-2 tyrosine phosphatase activates the Src tyrosine kinase by a non-enzymatic mechanism. Oncogene, 1999, **18**, 1911–1920.

[956] Arregui, C.O., Balsamo, J., Lilien, J., 1998. Impaired integrin-mediated adhesion and signaling in fibroblasts expressing a dominant, negative mutant PTP1B. J. Cell Biol., 1998, **143**, 861–873.

[957] Chappel, J., Ross, F.P., Abu-Amer, Y., Shaw, A., Teitelbaum, S.L., 1997. 1,25-dihydroxyvitamin D3 regulates pp60(c-src) activity and expression of a pp60(c-src) activating phosphatase. J. Cell. Biochem., 1997, **67**, 432–438.

[958] Somani, A.K., Bignon, J.S., Mills, G.B., Siminovitch, K.A., Branch, D.R., 1997. Src kinase activity is regulated by the SHP-1 protein-tyrosine phosphatase. J. Biol. Chem., 1997, **272**, 21113–21119.

[959] Bromann, P.A., Korkaya, H., Courtneidge, S.A., 2004. The interplay between Src family kinases and receptor tyrosine kinases. Oncogene, 2004, **23**, 7957–7968.

[960] Abram, C.L., Courtneidge, S.A., 2000. Src family tyrosine kinases and growth factor signaling. Exp. Cell Res., 2000, **254**, 1–13.

[961] Ishizawar, R., Parsons, S.J., 2004. C-Src and cooperating partners in human cancer. Cancer Cell, 2004, **6**, 209–214.

[962] Johns, T.G., Perera, R.M., Vernes, S.C., Vitali, A.A., et al., 2007. The efficacy of epidermal growth factor receptor-specific antibodies against glioma xenografts is influenced by receptor levels, activation status, and heterodimerization. Clin. Cancer Res., 2007, **13**, 1911–1925.

[963] Biscardi, J.S., Tice, D.A., Parsons, S.J., 1999. C-Src, receptor tyrosine kinases, and human cancer. Adv. Cancer Res., 1999, **76**, 117–119.

[964] Kaplan, K.B., Swedlow, J.R., Varmus, H.E., Morgan, D.O., 1992. Association of p60(c-src) with endosomal membranes in mammalian fibroblasts. J. Cell Biol., 1992, **118**, 321–333.

[965] David-Pfeuty, T., Nouvian-Dooghe, Y., 1990. Immunolocalization of the cellular src protein in interphase and mitotic NIH c-src overexpresser cells. J. Cell Biol., 1990, **111**, 3097–3116.

[966] Verbeek, B.S., Vroom, T.M., Adriaansen-Slot, S.S., Ottenhoff-Kalff, A.E., et al., 1996. c-Src protein expression is increased in human breast cancer. An immunohistochemical and biochemical analysis. J. Pathol., 1996, **180**, 383–388.

[967] Neel, H., Gondran, P., Weil, D., Dautry, F., 1995. Regulation of pre-mRNA processing by src. Curr. Biol., 1995, **5**, 413–422.

[968] Barnekow, A., Jahn, R., Schartl, M., 1990. Synaptophysin: a substrate for the protein tyrosine kinase pp60c-src in intact synaptic vesicles. Oncogene, 1990, **5**, 1019–24.

[969] Onofri, F., Giovedì, S., Vaccaro, P., Czernik, A.J., et al., 1997. Synapsin I interacts with c-Src and stimulates its tyrosine kinase activity. Proc. Natl. Acad. Sci. U. S. A., 1997, **94**, 12168–12173.

[970] Foster-Barber, A., Bishop, J.M., 1998. Src interacts with dynamin and synapsin in neuronal cells. Proc. Natl. Acad. Sci. U. S. A., 1998, **95**, 4673–4677.

[971] Au-Yeung, B.B., Shah, N.H., Shen, L., Weiss, A., 2018. ZAP-70 in Signaling, Biology, and Disease. Annu. Rev. Immunol., 2018, **36**, 127–156.

[972] Iwashima, M., Irving, B.A., Van Oers, N.S.C., Chan, A.C., Weiss, A., 2014. Sequential interactions of the TCR with two distinct cytoplasmic tyrosine kinases. J. Immunol., 2014, **193**, 4279–4282.

[973] Chan, A.C., Irving, B.A., Fraser, J.D., Weiss, A., 1991. The ζ chain is associated with a tyrosine kinase and upon T-cell antigen receptor stimulation associates with ZAP-70, a 70-kDa tyrosine phosphoprotein. Proc. Natl. Acad. Sci. U. S. A., 1991, **88**, 9166–9170.

[974] Deindl, S., Kadlecek, T.A., Brdicka, T., Cao, X., et al., 2007. Structural Basis for the Inhibition of Tyrosine Kinase Activity of ZAP-70. Cell, 2007, **129**, 735–746.

[975] Yan, Q., Barros, T., Visperas, P.R., Deindl, S., et al., 2013. Structural Basis for Activation of ZAP-70 by Phosphorylation of the SH2-Kinase Linker. Mol. Cell. Biol., 2013, **33**, 2188–2201.

[976] Mikhailik, A., Ford, B., Keller, J., Chen, Y., et al., 2007. A Phosphatase Activity of Sts-1 Contributes to the Suppression of TCR Signaling. Mol. Cell, 2007, **27**, 486–497.

[977] San Luis, B., Sondgeroth, B., Nassar, N., Carpino, N., 2011. Sts-2 is a phosphatase that negatively regulates Zeta-associated Protein (ZAP)-70 and T cell receptor signaling pathways. J. Biol. Chem., 2011, **286**, 15943–15954.

[978] Carpino, N., Turner, S., Mekala, D., Takahashi, Y., et al., 2004. Regulation of ZAP-70 Activation and TCR Signaling by Two Related Proteins, Sts-1 and Sts-2. Immunity, 2004, **20**, 37–46.

[979] Zhang, W., Sloan-Lancaster, J., Kitchen, J., Trible, R.P., Samelson, L.E., 1998. LAT: The ZAP-70 tyrosine kinase substrate that links T cell receptor to cellular activation. Cell, 1998, **92**, 83–92.

[980] Wardenburg, J.B., Fu, C., Jackman, J.K., Flotow, H., et al., 1996. Phosphorylation of SLP-76 by the ZAP-70 protein-tyrosine kinase is required for T-cell receptor function. J. Biol. Chem., 1996, **271**, 19641–19644.

[981] Isakov, N., Wange, R.L., Watts, J.D., Aebersold, R., Samelson, L.E., 1996. Purification and characterization of human ZAP-70 protein-tyrosine kinase from a baculovirus expression system. J. Biol. Chem., 1996, **271**, 15753–15761.

[982] Deng, Y., Alicea-Velázquez, N.L., Bannwarth, L., Lehtonen, S.I., et al., 2014. Global analysis of human nonreceptor tyrosine kinase specificity using high-density peptide microarrays. J. Proteome Res., 2014, **13**, 4339–4346.

[983] Xue, L., Wang, W.H., Iliuk, A., Hu, L., et al., 2012. Sensitive kinase assay linked with phosphoproteomics for identifying direct kinase substrates. Proc. Natl. Acad. Sci. U. S. A., 2012, **109**, 5615–5620.

[984] Schmitz, R., Baumann, G., Gram, H., 1996. Catalytic specificity of phosphotyrosine kinases Blk, Lyn, c-Src and Syk as assessed by phage display. J. Mol. Biol., 1996, **260**, 664–677.

[985] Brdicka, T., Kadlecek, T.A., Roose, J.P., Pastuszak, A.W., Weiss, A., 2005. Intramolecular Regulatory Switch in ZAP-70: Analogy with Receptor Tyrosine Kinases. Mol. Cell. Biol., 2005, **25**, 4924–4933.

[986] Levin, S.E., Zhang, C., Kadlecek, T.A., Shokat, K.M., Weiss, A., 2008. Inhibition of ZAP-70 kinase activity via an analog-sensitive allele blocks T cell receptor and CD28 superagonist signaling. J. Biol. Chem., 2008, **283**, 15419–15430.

[987] Qian, D., Mollenauer, M.N., Weiss, A., 1996. Dominant-negative Zeta-associated protein 70 inhibits T cell antigen receptor signaling. J. Exp. Med., 1996, **183**, 611–620.

[988] Chakraborty, A.K., Weiss, A., 2014. Insights into the initiation of TCR signaling. Nat. Immunol., 2014, **15**, 798–807.

[989] Thill, P.A., Weiss, A., Chakraborty, A.K., 2016. Phosphorylation of a Tyrosine Residue on Zap70 by Lck and Its Subsequent Binding via an SH2 Domain May Be a Key Gatekeeper of T Cell Receptor Signaling In Vivo . Mol. Cell. Biol., 2016, **36**, 2396–2402.

[990] Wu, J., Zhao, Q., Kurosaki, T., Weiss, A., 1997. The Vav binding site (Y315) in ZAP-70 is critical for antigen receptor- mediated signal transduction. J. Exp. Med., 1997, **185**, 1877–1882.

[991] Au-Yeung, B.B., Levin, S.E., Zhang, C., Hsu, L.-Y., et al., 2010. A genetically selective inhibitor demonstrates a function for the kinase Zap70 in regulatory T cells independent of its catalytic activity. Nat. Immunol., 2010, **11**, 1085–1092.

[992] Braiman, A., Isakov, N., 2015. The role of Crk adaptor proteins in T-cell adhesion and migration. Front. Immunol., 2015, **6**.

[993] KOBAYASHI, T., NAKAMURA, S. -i, TANIGUCHI, T., YAMAMURA, H., 1990. Purification and characterization of a cytosolic protein-tyrosine kinase from porcine spleen. Eur. J. Biochem., 1990, **188**, 535–540.

[994] Zioncheck, T.F., Harrison, M.L., Geahlen, R.L., 1986. Purification and characterization of a protein-tyrosine kinase from bovine thymus. J Biol Chem, 1986, **261**, 15637–15643.

[995] Sada, K., Takano, T., Yanagi, S., Yamamura, H., 2001. Structure and function of Syk protein-tyrosine kinase. J. Biochem., 2001, **130**, 177–186.

[996] Mócsai, A., Ruland, J., Tybulewicz, V.L.J., 2010. The SYK tyrosine kinase: A crucial player in diverse biological functions. Nat. Rev. Immunol., 2010, **10**, 387–402.

[997] Abram, C.L., Lowell, C.A., 2007. The expanding role for ITAM-based signaling pathways in immune cells. Sci. STKE, 2007, **2007**.

[998] Geahlen, R.L., 2009. Syk and pTyr'd: Signaling through the B cell antigen receptor. Biochim. Biophys. Acta - Mol. Cell Res., 2009, **1793**, 1115–1127.

[999] Yanagi, S., Inatome, R., Takano, T., Yamamura, H., 2001. Syk expression and novel function in a wide variety of tissues. Biochem. Biophys. Res. Commun., 2001, **288**, 495–498.

[1000] Coopman, P.J., Mueller, S.C., 2006. The Syk tyrosine kinase: A new negative regulator in tumor growth and progression. Cancer Lett., 2006, **241**, 159–173.

[1001] Krisenko, M.O., Geahlen, R.L., 2015. Calling in SYK: SYK's dual role as a tumor promoter and tumor suppressor in cancer. Biochim. Biophys. Acta - Mol. Cell Res., 2015, **1853**, 254–263.

[1002] Baudot, A.D., Jeandel, P.Y., Mouska, X., Maurer, U., et al., 2009. The tyrosine kinase Syk regulates the survival of chronic lymphocytic leukemia B cells through PKC and proteasome-dependent regulation of Mcl-1 expression. Oncogene, 2009, **28**, 3261–3273.

[1003] Rickert, R.C., 2013. New insights into pre-BCR and BCR signalling with relevance to B cell malignancies. Nat. Rev. Immunol., 2013, **13**, 578–591.

[1004] Gobessi, S., Laurenti, L., Longo, P.G., Carsetti, L., et al., 2009. Inhibition of constitutive and BCR-induced Syk activation downregulates Mcl-1 and induces apoptosis in chronic lymphocytic leukemia B cells. Leukemia, 2009, **23**, 686–697.

[1005] Singh, A., Greninger, P., Rhodes, D., Koopman, L., et al., 2009. A Gene Expression Signature Associated with "K-Ras Addiction" Reveals Regulators of EMT and Tumor Cell Survival. Cancer Cell, 2009, **15**, 489–500.

[1006] Zhang, J., Benavente, C.A., McEvoy, J., Flores-Otero, J., et al., 2012. A novel retinoblastoma therapy from genomic and epigenetic analyses. Nature, 2012, **481**, 329–334.

[1007] Shin, G., Kang, T.-W., Yang, S., Baek, S.-J., et al., 2011. GENT: Gene Expression Database of Normal and Tumor Tissues. Cancer Inform., 2011, **10**, CIN.S7226.

[1008] Luangdilok, S., Box, C., Patterson, L., Court, W., et al., 2007. Syk tyrosine kinase is linked to cell motility and progression in squamous cell carcinomas of the head and neck. Cancer Res., 2007, **67**, 7907–7916.

[1009] Goodman, P.A., Wood, C.M., Vassilev, A., Mao, C., Uckun, F.M., 2001. Spleen tyrosine kinase (Syk) deficiency in childhood pro-B cell acute

lymphoblastic leukemia. Oncogene, 2001, **20**, 3969–3978.
[1010] Layton, T., Stalens, C., Gunderson, F., Goodison, S., Silletti, S., 2009. Syk tyrosine kinase acts as a pancreatic adenocarcinoma tumor suppressor by regulating cellular growth and invasion. Am. J. Pathol., 2009, **175**, 2625–2636.
[1011] Hoeller, C., Thallinger, C., Pratscher, B., Bister, M.D., et al., 2005. The non-receptor-associated tyrosine kinase syk is a regulator of metastatic behavior in human melanoma cells. J. Invest. Dermatol., 2005, **124**, 1293–1299.
[1012] Muthusamy, V., Duraisamy, S., Bradbury, C.M., Hobbs, C., et al., 2006. Epigenetic silencing of novel tumor suppressors in malignant melanoma. Cancer Res., 2006, **66**, 11187–11193.
[1013] Yang, Z., Huo, L., Chen, H., Ni, B., et al., 2013. Hypermethylation and prognostic implication of Syk gene in human colorectal cancer. Med. Oncol., 2013, **30**.
[1014] Yuan, Y., Wang, J., Li, J., Wang, L., et al., 2006. Frequent epigenetic inactivation of Spleen tyrosine kinase gene in human hepatocellular carcinoma. Clin. Cancer Res., 2006, **12**, 6687–6695.
[1015] Sung, Y.M., Xu, X., Sun, J., Mueller, D., et al., 2009. Tumor suppressor function of Syk in human MCF10A in vitro and normal mouse mammary epithelium in vivo. PLoS One, 2009, **4**.
[1016] Latour, S., Chow, L.M.L., Veillette, A., 1996. Differential intrinsic enzymatic activity of Syk and Zap-70 protein- tyrosine kinases. J. Biol. Chem., 1996, **271**, 22782–22790.
[1017] Hong, J., Yuan, Y., Wang, J., Liao, Y., et al., 2014. Expression of variant isoforms of the tyrosine kinase syk determines the prognosis of hepatocellular carcinoma. Cancer Res., 2014, **74**, 1845–1856.
[1018] Prinos, P., Garneau, D., Lucier, J.F., Gendron, D., et al., 2011. Alternative splicing of SYK regulates mitosis and cell survival. Nat. Struct. Mol. Biol., 2011, **18**, 673–679.
[1019] Wendler, F., 2018. The LMTK-family of kinases: Emerging important players in cell physiology and disease pathogenesis. Biochim. Biophys. Acta - Mol. Basis Dis., 2018.
[1020] Nixon, A., Jia, Y., White, C., Bradbury, N.A., 2013. Determination of the membrane topology of lemur tyrosine kinase 2 (LMTK2) by fluorescence protease protection. Am. J. Physiol. - Cell Physiol., 2013, **304**.
[1021] Wang, H., Brautigan, D.L., 2002. A novel transmembrane Ser/Thr kinase complexes with protein phosphatase-1 and inhibitor-2. J. Biol. Chem., 2002, **277**, 49605–49612.
[1022] Gundry, C., Marco, S., Rainero, E., Miller, B., et al., 2017. Phosphorylation of Rab-coupling protein by LMTK3 controls Rab14-dependent EphA2 trafficking to promote cell:cell repulsion. Nat. Commun., 2017, **8**.
[1023] Shi, H., Wu, J., Ji, M., Zhou, Q., et al., 2013. Serum lemur tyrosine kinase 3 expression in colorectal cancer patients predicts cancer progression and prognosis. Med. Oncol., 2013, **30**.
[1024] Stebbing, J., Filipovic, A., Lit, L.C., Blighe, K., et al., 2013. LMTK3 is implicated in endocrine resistance via multiple signaling pathways. Oncogene, 2013, **32**, 3371–3380.
[1025] Puri, C., Chibalina, M. V., Arden, S.D., Kruppa, A.J., et al., 2010. Overexpression of myosin VI in prostate cancer cells enhances PSA and VEGF secretion, but has no effect on endocytosis. Oncogene, 2010, **29**, 188–200.
[1026] Inoue, T., Kon, T., Ohkura, R., Yamakawa, H., et al., 2008. BREK/LMTK2 is a myosin VI-binding protein involved in endosomal membrane trafficking. Genes to Cells, 2008, **13**, 483–495.
[1027] Manser, C., Vagnoni, A., Guillot, F., Davies, J., Miller, C.C.J., 2012. Cdk5/p35 phosphorylates lemur tyrosine kinase-2 to regulate protein phosphatase-1C phosphorylation and activity. J. Neurochem., 2012, **121**, 343–348.
[1028] Shah, K., Bradbury, N.A., 2015. Lemur tyrosine kinase 2, a novel target in prostate cancer therapy. Oncotarget, 2015, **6**, 14233–14246.
[1029] Stebbing, J., Filipovic, A., Ellis, I.O., Green, A.R., et al., 2012. LMTK3 expression in breast cancer: Association with tumor phenotype and clinical outcome. Breast Cancer Res. Treat., 2012, **132**, 537–544.
[1030] Zhao, G., Guo, J., Li, D., Jia, C., et al., 2013. MicroRNA-34a suppresses cell proliferation by targeting lmtk3 in human breast cancer mcf-7 cell line. DNA Cell Biol., 2013, **32**, 699–707.
[1031] Asano, T., Sato, S., Yoshimoto, N., Endo, Y., et al., 2014. High expression of LMTK3 is an independent factor indicating a poor prognosis in estrogen receptor α-positive breast cancer patients. Jpn. J. Clin. Oncol., 2014, **44**, 889–897.
[1032] Lu, L., Yuan, X., Zhang, Q., Zhang, H., Shen, B., 2017. LMTK3 knockdown retards cell growth and invasion and promotes apoptosis in thyroid cancer. Mol. Med. Rep., 2017, **15**, 2015–2022.
[1033] Xu, Y., Zhang, H., Lit, L.C., Grothey, A., et al., 2014. The kinase LMTK3 promotes invasion in breast cancer through GRB2-mediated induction of integrin β1. Sci. Signal., 2014, **7**.
[1034] Xu, Y., Zhang, H., Nguyen, V.T.M., Angelopoulos, N., et al., 2015. LMTK3 Represses Tumor Suppressor-like Genes through Chromatin Remodeling in Breast Cancer. Cell Rep., 2015, **12**, 837–849.
[1035] Gomez-Rodriguez, J., Kraus, Z.J., Schwartzberg, P.L., 2011. Tec family kinases Itk and Rlk/Txk in T lymphocytes: Cross-regulation of cytokine production and T-cell fates. FEBS J., 2011, **278**, 1980–1989.
[1036] Gao, Y., Zhou, J., Li, J., 2021. Discoidin domain receptors orchestrate cancer progression: A focus on cancer therapies. Cancer Sci., 2021, **112**, 962–969.
[1037] Uhlén, M. et al., 2015. Proteomics. Tissue-based map of the human proteome. Science (80-.)., 2015, **347**.
[1038] Li, Z., Wang, J., Zhou, T., Ye, X., 2016. Establishment of a colorectal cancer nude mouse visualization model of HIF-1α overexpression. Oncol. Lett., 2016, **11**, 2725–2732.
[1039] Schumacher, U., Adam, E., 1997. Lectin histochemical HPA-binding pattern of human breast and colon cancers is associated with metastases formation in severe combined immunodeficient mice. Histochem. J., 1997, **29**, 677–684.
[1040] Brooks, R., Fuhler, G.M., Iyer, S., Smith, M.J., et al., 2010. SHIP1 inhibition increases immunoregulatory capacity and triggers apoptosis of hematopoietic cancer cells. J. Immunol., 2010, **184**, 3582–3589.
[1041] Nelson, N., Razeto, A., Gilardi, A., Grättinger, M., et al., 2021. AKT1 and PTEN show the highest affinities among phosphoinositide binding proteins for the second messengers PtdIns(3,4,5)P3 and PtdIns(3,4)P2. Biochem. Biophys. Res. Commun., 2021, **568**, 110–115.
[1042] Zhang, Y., Wavreille, A.S., Kunys, A.R., Pei, D., 2009. The SH2 domains of inositol polyphosphate 5-phosphatases SHIP1 and SHIP2 have similar ligand specificity but different binding kinetics. Biochemistry, 2009, **48**, 11075–11083.
[1043] Le Coq, J., Camacho-Artacho, M., Velázquez, J.V., Santiveri, C.M., et al., 2017. Structural basis for interdomain communication in SHIP2 providing high phosphatase activity. Elife, 2017, **6**.
[1044] Coq, J. Le, Camacho-Artacho, M., Velázquez, J.V., Santiveri, C.M., et al., 2017. Structural basis for interdomain communication in SHIP2 providing high phosphatase activity. Elife, 2017, **6**.
[1045] Narayan, K., Lemmon, M.A., 2006. Determining Selectivity of Phosphoinositide-Binding Domains. Methods, 2006, **39**, 122–133.
[1046] O'Connell, R.M., Chaudhuri, A.A., Rao, D.S., Baltimore, D., 2009. Inositol phosphatase SHIP1 is a primary target of miR-155. Proc. Natl. Acad. Sci., 2009, **106**, 7113–7118.
[1047] Gozzelino, L., De Santis, M.C., Gulluni, F., Hirsch, E., Martini, M., 2020. PI(3,4)P2 Signaling in Cancer and Metabolism. Front. Oncol., 2020, **10**, 360.
[1048] Fu, Y., Liu, S., Yin, S., Niu, W., et al., 2017. The reverse Warburg effect is likely to be an Achilles' heel of cancer that can be exploited for cancer therapy. Oncotarget, 2017, **8**, 57813–57825.
[1049] Vaupel, P., Multhoff, G., 2020. Revisiting the Warburg effect: historical dogma versus current understanding. J Physiol., 2020.

[1050] Frezza, C., 2020. Metabolism and cancer: the future is now. Br. J. Cancer, 2020, **122**, 133–135.
[1051] Yu, S., Wang, G., Shi, Y., Xu, H., et al., 2020. MCMs in Cancer: Prognostic Potential and Mechanisms. Anal. Cell. Pathol., 2020, **2020**.
[1052] LEMMON, M.A., FERGUSON, K.M., 2000. Signal-dependent membrane targeting by pleckstrin homology (PH) domains. Biochem. J., 2000, **350**, 1–18.
[1053] Soria, J.-C., Lee, H.-Y., Lee, J.I., Wang, L., et al., 2002. Lack of PTEN Expression in Non-Small Cell Lung Cancer Could Be Related to Promoter Methylation. Clin. Cancer Res., 2002, **8**, 1178 LP – 1184.
[1054] Hertel, F., Li, S., Chen, M., Pott, L., et al., 2020. Fluorescent biosensors for multiplexed imaging of phosphoinositide dynamics. ACS Chem. Biol., 2020, **15**, 33–38.
[1055] Lemmon, M.A., 2008. Membrane recognition by phospholipid-binding domains. Nat. Rev. Mol. Cell Biol., 2008, **9**, 99–111.
[1056] Stephens, L.R., Jackson, T.R., Hawkins, P.T., 1993. Agonist-stimulated synthesis of phosphatidylinositol(3,4,5)-trisphosphate. A new intracellular signalling system? BBA - Mol. Cell Res., 1993, **1179**, 27–75.
[1057] Schmick, M., Bastiaens, P.I.H., 2014. The Interdependence of Membrane Shape and Cellular Signal Processing. Cell, 2014, **156**, 1132–1138.
[1058] Almeida, P.F.F., Pokorny, A., Hinderliter, A., 2005. Thermodynamics of membrane domains. Biochim. Biophys. Acta - Biomembr., 2005, **1720**, 1–13.
[1059] Baumgart, T., Capraro, B.R., Zhu, C., Das, S.L., 2011. Thermodynamics and Mechanics of Membrane Curvature Generation and Sensing by Proteins and Lipids. Http://dx.doi.org/10.1146/annurev.physchem.012809.103450, 2011, **62**, 483–506.
[1060] Simons, K., Gerl, M.J., 2010. Revitalizing membrane rafts: new tools and insights. Nat. Rev. Mol. Cell Biol. 2010 1110, 2010, **11**, 688–699.
[1061] Machta, B.B., Papanikolaou, S., Sethna, J.P., Veatch, S.L., 2011. Minimal Model of Plasma Membrane Heterogeneity Requires Coupling Cortical Actin to Criticality. Biophys. J., 2011, **100**, 1668–1677.
[1062] Ehrig, J., Petrov, E.P., Schwille, P., 2011. Near-Critical Fluctuations and Cytoskeleton-Assisted Phase Separation Lead to Subdiffusion in Cell Membranes. Biophys. J., 2011, **100**, 80–89.
[1063] Speck, T., Vink, R.L.C., 2012. Random pinning limits the size of membrane adhesion domains. Phys. Rev. E, 2012, **86**, 031923.
[1064] Sako, Y., Kusumi, A., 1995. Barriers for lateral diffusion of transferrin receptor in the plasma membrane as characterized by receptor dragging by laser tweezers: fence versus tether. J. Cell Biol., 1995, **129**, 1559.
[1065] Suzuki, K., Ritchie, K., Kajikawa, E., Fujiwara, T., Kusumi, A., 2005. Rapid Hop Diffusion of a G-Protein-Coupled Receptor in the Plasma Membrane as Revealed by Single-Molecule Techniques. Biophys. J., 2005, **88**, 3659–3680.
[1066] Mueller, V., Ringemann, C., Honigmann, A., Schwarzmann, G., et al., 2011. STED Nanoscopy Reveals Molecular Details of Cholesterol- and Cytoskeleton-Modulated Lipid Interactions in Living Cells. Biophys. J., 2011, **101**, 1651–1660.
[1067] Andrade, D.M., Clausen, M.P., Keller, J., Mueller, V., et al., 2015. Cortical actin networks induce spatio-temporal confinement of phospholipids in the plasma membrane – a minimally invasive investigation by STED-FCS. Sci. Reports 2015 51, 2015, **5**, 1–12.
[1068] Lenne, P.-F., Wawrezinieck, L., Conchonaud, F., Wurtz, O., et al., 2006. Dynamic molecular confinement in the plasma membrane by microdomains and the cytoskeleton meshwork. EMBO J., 2006, **25**, 3245–3256.
[1069] Huang, H., Simsek, M.F., Jin, W., Pralle, A., 2015. Effect of Receptor Dimerization on Membrane Lipid Raft Structure Continuously Quantified on Single Cells by Camera Based Fluorescence Correlation Spectroscopy. PLoS One, 2015, **10**, e0121777.
[1070] Honigmann, A., Pralle, A., 2016. Compartmentalization of the Cell Membrane. J. Mol. Biol., 2016, **428**, 4739–4748.
[1071] Hanzal-Bayer, M.F., Hancock, J.F., 2007. Lipid rafts and membrane traffic. FEBS Lett., 2007, **581**, 2098–2104.
[1072] Chamberlain, T.C., Cheung, S.T., Yoon, J.S.J., Ming-Lum, A., et al., 2020. Interleukin-10 and Small Molecule SHIP1 Allosteric Regulators Trigger Anti-inflammatory Effects through SHIP1/STAT3 Complexes. IScience, 2020, **23**, 101433.
[1073] Le Coq, J., López Navajas, P., Rodrigo Martin, B., Alfonso, C., Lietha, D., 2021. A new layer of phosphoinositide-mediated allosteric regulation uncovered for SHIP2. FASEB J., 2021, **35**, 1–12.

Anhang

Auflistung der Gefahrstoffe nach GHS

1,4-Dithiothreitol	GHS07, H302, H315, H319, P264, P280, P270, P301+P310, P302+P352, P330, P332+P313
2-Mercaptoethanol	GHS06, GHS08, GHS05, GHS09, H301+H331, H310, H315, H317, H318, H373, H410, P261, P280, P301+P310+P330, P302+P352+P310, P305+P351+P338+P310, P403+P223
2-Propanol	GHS07, GHS02, H225, H319, H336, P210, P233, P240, P305+P351+P338, P403+P235
Aceton	GHS02, GHS07, H225, H319, H336, EUH066, P210, P233, P305+P351+P338
Acrylamid	GHS08, GHS06, H301, H312, H332, H315, H319, H317, H340, H350, H361f, H372, H312+H332, P201, P280, P302+P352, P304+P340, P305+P351+P338, P308+P313
Ampicillin Natrium	GHS08, H334, H317, P280, P261, P301+P352, P342+P311
Chloramphenicol	GHS08, H351, H361d, P308+P313
Chloroform	GHS06, GHS08, H302, H315, H319, H331, H336, H351, H361d, H372, P201, P261, P304+P340+P311, P305+P351+P338, P308+P313, P403+P223
Diethylether	GHS07, GHS02, H224, H302, H336, EUH019, EUH066, P210, P240, P403+P235, P243
Ethanol	GHS02, H225, P210
Ethidiumbromid	GHS06, GHS08, H302, H330, H341, P260, P301+P312, P304+P340, P308+P313, P310, P450
Imidazol	GHS05, GHS07, GHS08, H302, H314, H360d, P260, P280, P301+P330+P331, P303+P361+P353, P305+P351+P338, P308+P313
Kaliumhydroxid	GHS05, GHS07, H290, H302, H314, , P280, P301+P330+P331, P305+P351+P338, P308+P310
Kanamycin Sulfat	GHS08, H372, H360, P308+P313, P314, P281, P260, P202, P201
Methanol	GHS08, GHS06, GHS02, H225, H331, H311, H301, H370, P210, P233, P280, P302+P352, P304+P340, P308+P310, P403+P235
Natriumazid	GHS09, GHS06, GHS08, H300+H310, H373, H410, EUH032, P273, P280, P301+P310, P302+P352, P310, P280, P405
Natriumhydroxid	GHS05, H290, H302, H314, P280, P301+P330+P331, P305+P351+P338, P308+P310
Natriumorthovanadat	GHS07, H302+H312+H332, P280
Natrumfluorid	GHS06, H301, H315, H319, P302+P352, P305+P351+P338, P308+P310
NP-40	GHS07, H315, H319, P302+P352, P305+P351+P338
Penicillin/Streptomycin	GHS08, H317, H334, H361, P302+P352, P304+P340, P201, P260, P333+P313, P261
Salzsäure	GHS07, GHS05, H290, H314, H335, P260, P280, P303+P361+P353, P304+P340+P310, P305+P351+P338
Staurosporine	GHS08, H340, H350, P201, P308+P313
TEMED	GHS07, GHS02, GHS05, H225, H302+H332, H314, P210, P280, P301+P330+P331, P303+P351+P338, P310
Trichloressigsäure	GHS09, GHS05, H314, H410, P273, P280, P303+P361+P353, P304+P340, P310, P305+P351+P338, P391
Triton X-100	GHS05, GHS07, GHS09, H302, H318, H411, P280, P301+P312+P330, P305+P351+P338+P310

Auflistung der verwendeten KMR-Substanzen, Kat. I und II

Cas-Nummer	Stoffname (IUPAC)	Verfahren und eingetzte Menge	Kategorie (I oder II)
1239-45-8	3,8-Diamino -1-ethyl-6-phenylphenantridiniumbromid (Ethidiumbromid)	Agarose-Gelelektrophorese, 0.5 µL/Gel (10 mg/mL), Σ25 µL	M3
79-06-1	Acrylamid/Bisacrylamid	SDS-Polyacrylamid-Gelelektrophorese, 15 mL/Gel (30%ige Lösung), Σ1500 mL	K2M2RF3
7786-81-4	NiSO4	Ni-NTA-Affinitätschromatographie, 100 mM Lösung, 5 mL	K1M3R2

Hinweise zur Entsorgung

GVO-enthaltende Materialien wurden autoklaviert und entsorgt. Methanol, Acrylamid, Ethidiumbromid und Säuren und Laugen wurden gesondert entsorgt

Hiermit versichere ich an Eides statt, die vorliegende Dissertation selbst verfasst und keine anderen als die angegebenen Hilfsmittel benutzt zu haben. Die eingereichte schriftliche Fassung entspricht der auf dem elektronischen Speichermedium. Ich versichere, dass diese Dissertation nicht in einem früheren Promotionsverfahren eingereicht wurde.

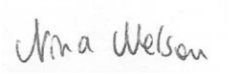

Datum, Unterschrift